

1-1-1993

## Studies of the friction and wetting behavior of polymer surfaces with controlled surface structures/

Timothy G. Bee  
*University of Massachusetts Amherst*

Follow this and additional works at: [https://scholarworks.umass.edu/dissertations\\_1](https://scholarworks.umass.edu/dissertations_1)

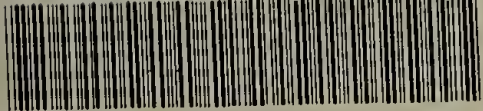
---

### Recommended Citation

Bee, Timothy G., "Studies of the friction and wetting behavior of polymer surfaces with controlled surface structures/" (1993). *Doctoral Dissertations 1896 - February 2014*. 814.  
<https://doi.org/10.7275/z7jg-3966> [https://scholarworks.umass.edu/dissertations\\_1/814](https://scholarworks.umass.edu/dissertations_1/814)

This Open Access Dissertation is brought to you for free and open access by ScholarWorks@UMass Amherst. It has been accepted for inclusion in Doctoral Dissertations 1896 - February 2014 by an authorized administrator of ScholarWorks@UMass Amherst. For more information, please contact [scholarworks@library.umass.edu](mailto:scholarworks@library.umass.edu).





312066011094709



STUDIES OF THE FRICTION AND WETTING BEHAVIOR OF  
POLYMER SURFACES WITH CONTROLLED SURFACE STRUCTURES

A Dissertation Presented

by

TIMOTHY G. BEE

Submitted to the Graduate School of the  
University of Massachusetts in partial fulfillment  
of the requirements for the degree of

DOCTOR OF PHILOSOPHY

May 1993

Department of Polymer Science and Engineering

© Copyright by Timothy G. Bee 1993

All Rights Reserved



STUDIES OF THE FRICTION AND WETTING BEHAVIOR OF  
POLYMER SURFACES WITH CONTROLLED SURFACE STRUCTURES

A Dissertation Presented

by

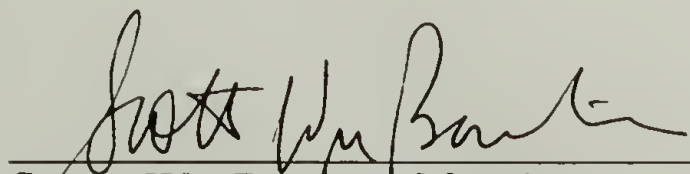
TIMOTHY G. BEE

Approved as to style and content by:



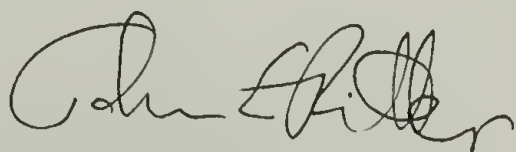
---

Thomas J. McCarthy, Chair



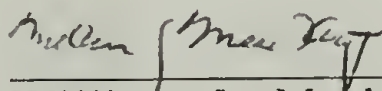
---

Scott W. Barton, Member



---

John E. Ritter, Member



---

William J. Macknight, Department Head  
Polymer Science and Engineering

## ACKNOWLEDGEMENTS

First, I would like to thank my advisor, Tom McCarthy, for his help and support for the past five years. Not only did I learn a great deal of science from Tom, but I also learned a lot about managing an effective research program through his example. His dedication, enthusiasm and personal interest in my education (in both Science and English) motivated me in my research and made graduate school a fulfilling experience. Thanks also go to Professors Scott Barton and John Ritter for their helpful suggestions concerning my research, thesis and scientific education.

Working in the McCarthy group was boat loads of fun from the very beginning due to the people who have been in the group over the past five years. So, thanks go to Jack, Rick, Cady, Dave, Elisa, Bob B., Joan, Damo, Brant, Katrina, Eric, Bob F., Anthony, Raul, Juha and especially the other two "kids" in the group, Molly and Nicole, for their part in making it enjoyable to go into the lab everyday and for their contributions to my research. I also want to acknowledge Jay Dias, a former group member, for helpful discussions concerning PCTFE surface chemistry.

For great times outside of the lab, I want to thank Scott, the only other Parrot-Head in the department and the Running Radicals; Gregg, Jeff, Howard and Chris.

Finally, I want to thank my parents for their love and support throughout my life. Most importantly, I have to thank Susie for all of her help, understanding (especially during the last six months of this endeavor) and love.



## ABSTRACT

### STUDIES OF THE FRICTION AND WETTING BEHAVIOR OF POLYMER SURFACES WITH CONTROLLED SURFACE STRUCTURES

MAY 1993

TIMOTHY G. BEE, B.S. CHEM., UNIVERSITY OF MICHIGAN

Ph. D., UNIVERSITY OF MASSACHUSETTS

Directed by: Professor Thomas J. McCarthy

Reaction of poly(chlorotrifluoroethylene) (PCTFE) with trimethyl 4-lithioorthobutyrate and hydrolysis produces a surface containing carboxylic acids (PCTFE-CO<sub>2</sub>H). The advancing water contact angle ( $\Theta_A$ ) varies from  $\sim 56^\circ$  at low pH to  $\sim 30^\circ$  at high pH. The receding water contact angle ( $\Theta_R$ ) is  $0^\circ$  at all pH values. PCTFE-CO<sub>2</sub>H could be reduced to the alcohol, creating a less hydrophilic surface ( $\Theta_A/\Theta_R = 62^\circ/22^\circ$ ) or converted to the *n*-octyl ester, rendering a hydrophobic surface ( $\Theta_A/\Theta_R = 99^\circ/47^\circ$ ).

PCTFE reacts with acetaldehyde 3-lithiopropyl ethyl acetal at  $-78 - -15^\circ\text{C}$  to introduce the acetal into the outer  $\sim 30 - 1000 \text{ \AA}$  of the surface (PCTFE-PEAA). Hydrolysis produces a hydrophilic ( $\Theta_A/\Theta_R = 67^\circ/17^\circ$ ), alcohol-functionalized surface (PCTFE-OH) which was derivatized to prepare a series of linear hydrocarbon and fluorocarbon ester surfaces. Reactions with multifunctional reagents produced crosslinked surfaces. Gravimetric, XPS, ATR-IR and contact angles results are consistent with the proposed surface structures and high reaction yields. Water contact angles on the hydrocarbon

ester surfaces range from  $82^{\circ}/46^{\circ}$  (acetate) to  $108^{\circ}/90^{\circ}$  (stearate), while those on the fluorocarbon esters range from  $92^{\circ}/51^{\circ}$  (trifluoroacetate) to  $120^{\circ}/69^{\circ}$  (perfluorodecanoate). Hexadecane contact angles and XPS results show that the stearate and perfluorodecanoate esters form ordered surfaces. Friction properties of these modified surfaces were also investigated. The effects of varying the ester chain length, crosslinking the surface and varying the modification depth were studied. Contrary to expectations, the perfluorinated surfaces exhibited greater friction than their hydrocarbon analogs. The results show that chemical interactions at the sliding interface have little influence on friction and that it is the deformation behavior of the polymer near the interface that dictates the magnitude of the energy losses.

Mixed surfaces were prepared to study the effect of surface composition on wetting. Randomly mixed hydroxyl/hydrocarbon ester surfaces were prepared by kinetic control of the esterification of PCTFE-OH, while compositionally similar, patchy surfaces were prepared by kinetic control of the hydrolysis of PCTFE-Esters. Esterification of the alcohol groups in these two sets of mixed surfaces was utilized to prepare the corresponding hydrocarbon ester/fluorocarbon ester mixed surfaces. As expected, greater contact angle hysteresis was observed on the patchy surfaces.



# TABLE OF CONTENTS

	<u>Page</u>
ACKNOWLEDGMENTS.....	iv
ABSTRACT.....	v
LIST OF TABLES .....	xii
LIST OF FIGURES .....	xiv
LIST OF SCHEMES.....	xxvi
Chapter	
I. INTRODUCTION .....	1
Polymer Surface Modification.....	1
Introduction.....	1
Poly(chlorotrifluoroethylene)/Organolithium Surface Chemistry.....	6
Surface Analytical Techniques .....	11
Contact Angle.....	11
X-ray photoelectron Spectroscopy (XPS).....	28
Attenuated Total Reflectance Infrared Spectroscopy (ATR-IR).....	36
References and Notes.....	41
II. PREPARATION OF A REACTIVE CARBOXYLIC ACID FUNCTIONALIZED SURFACE.....	47
Introduction.....	47
Experimental .....	50
General.....	50
Trimethyl 4-lithioorthobutyrate (LiTMOB).....	51

Reaction of LiTMOB with PCTFE Film (PCTFE-TMOB).....	5 2
Oxidation of PCTFE-TMOB .....	5 2
Hydrolysis of PCTFE-TMOB (PCTFE-CO <sub>2</sub> H).....	5 3
Labelling of PCTFE-CO <sub>2</sub> H with Thallium.....	5 3
Acid Catalyzed Esterification of PCTFE-CO <sub>2</sub> H (PCTFE-CO <sub>2</sub> Oct <sup>A</sup> ).....	5 3
Esterification of PCTFE-CO <sub>2</sub> H via the Acid Chloride (PCTFE-CO <sub>2</sub> Oct <sup>B</sup> ) .....	5 4
Esterification of PCTFE-CO <sub>2</sub> H via the Imidazolid (PCTFE-CO <sub>2</sub> Oct <sup>C</sup> ).....	5 4
Reduction of PCTFE-CO <sub>2</sub> H (PCTFE-OH <sup>*</sup> ) .....	5 4
Labelling of PCTFE-OH with Heptafluorobutyryl Chloride (PCTFE-OHFB <sup>*</sup> ).....	5 5
Results and Discussion.....	5 5
Initial Modification (PCTFE-TMOB).....	5 5
Hydrolysis of PCTFE-TMOB (PCTFE-CO <sub>2</sub> H).....	6 6
Reactivity of PCTFE-CO <sub>2</sub> H (Esterification and Reduction).....	7 3
Conclusions and Future Work Suggestions.....	7 6
References and Notes.....	7 9
III. PREPARATION OF MODIFIED POLY(CHLOROTRIFLUOROETHYLENE) SURFACES FOR FRICTION STUDIES .....	8 2
Introduction.....	8 2
Experimental.....	8 6
General.....	8 6
Acetaldehyde 3-lithiopropyl Ethyl Acetal (LiPEAA).....	8 8
Procedure 1.....	8 8
Procedure 2.....	8 8
Reaction of LiPEAA with PCTFE Film (PCTFE-PEAA) .....	8 9



Hydrolysis of PCTFE-PEAA (PCTFE-OH) .....	8 9
Reaction of PCTFE-OH with Acetyl Chloride (PCTFE-OAc).....	9 0
Reaction of PCTFE-OH with Butyryl Chloride (PCTFE-OBu).....	9 0
Reaction of PCTFE-OH with Decanoyl Chloride (PCTFE-ODec) .....	9 1
Reaction of PCTFE-OH with Stearoyl Chloride (PCTFE-OSear).....	9 1
Reaction of PCTFE-OH with Trifluoroacetic Anhydride (PCTFE-OTFAc).....	9 2
Reaction of PCTFE-OH with Heptafluorobutyryl Chloride (PCTFE-OHFB).....	9 2
Preparation of Perfluorodecanoyl Chloride (PFDecCl).....	9 2
Reaction of PCTFE-OH with PFDecCl (PCTFE-OPFDec) .....	9 3
Reaction of PCTFE-OH with Adipoyl Chloride (PCTFE-O <sub>2</sub> Adip) .....	9 3
Reaction of PCTFE-OH with 1,3,5-Benzene- tricarboxyl Trichloride (PCTFE-O <sub>3</sub> Benz).....	9 4
Oxidation of Modified Film Samples.....	9 4
Results and Discussion.....	9 5
Initial Modification (PCTFE-PEAA).....	9 5
Hydrolysis of PCTFE-PEAA (PCTFE-OH) .....	1 1 0
Esterification of PCTFE-OH.....	1 1 6
Conclusions and Future Work Suggestions.....	1 3 9
References and Notes.....	1 4 2
IV. FRICTION STUDIES OF SURFACE MODIFIED POLYMER FILMS .....	1 4 6
Introduction.....	1 4 6
Polymer Friction .....	1 4 7
Introduction.....	1 4 7
Deformation Friction .....	1 4 8
Adhesive Friction .....	1 4 9

Countersurfaces.....	1 5 2
Normal Load .....	1 5 2
Sliding Speed.....	1 5 5
Ambient Temperature .....	1 5 7
Summary.....	1 5 7
Experimental .....	1 5 8
Results and Discussion.....	1 6 1
Friction Behavior of Unmodified Poly(chlorotrifluoroethylene).....	1 6 1
Friction Behavior of Modified Poly(chlorotrifluoroethylene) Surfaces.....	1 6 8
Conclusions and Future Work Suggestions.....	1 8 8
References and Notes.....	1 8 9
V. PREPARATION AND WETTING BEHAVIOR OF HETEROGENEOUS SURFACES.....	1 9 4
Introduction.....	1 9 4
Experimental .....	1 9 7
General.....	1 9 7
Catalyzed Esterifications of PCTFE-OH (PCTFE-OBu <sup>t</sup> , PCTFE-ODec, PCTFE-OS <sup>t</sup> ear, PCTFE-OTFAc, PCTFE-OHFB, and PCTFE-OPFDec).....	1 9 8
Uncatalyzed Esterifications of PCTFE-OH (PCTFE-OBu <sup>t</sup> , PCTFE-ODec, PCTFE-OS <sup>t</sup> ear, and PCTFE-OHFB).....	1 9 8
Acid Catalyzed Methanolysis of PCTFE-Esters .....	1 9 9
Base Catalyzed Hydrolysis/Methanolysis of PCTFE-Esters.....	1 9 9
Results and Discussion.....	1 9 9
Kinetics of the Esterification of PCTFE-OH.....	2 0 6
Pyridine Catalyzed Esterifications.....	2 0 6
Uncatalyzed Esterifications .....	2 2 0



Competitive Esterification of Heptafluorobutyryl Chloride and Butyryl Chloride with PCTFE-OH .....	234
Kinetics of the Hydrolysis/Methanolysis of PCTFE-Esters .....	235
Acid Catalyzed Methanolysis.....	238
Base Catalyzed Hydrolysis/Methanolysis.....	240
Wetting Behavior of Mixed Surfaces as a Function of Surface Composition.....	263
Conclusions and Future Work Suggestions.....	282
References and Notes.....	286
APPENDIX: DATA TABLES FOR CHAPTER V.....	288
BIBLIOGRAPHY .....	299

## LIST OF TABLES

Table	Page
2.1. Water contact angle data ( $\Theta_A/\Theta_R$ ) for modified PCTFE surfaces.....	56
2.2. XPS atomic composition data for modified PCTFE surfaces.....	60
3.1. Water contact angle data ( $\Theta_A/\Theta_R$ ) for modified surfaces used in friction studies.....	97
3.2. XPS atomic composition data for PCTFE-PEAA and PCTFE-OH used in friction studies.....	100
3.3. Gravimetric thicknesses ( $\text{\AA}$ ) for modified surfaces.....	115
3.4. XPS atomic composition data for hydrocarbon and crosslinked ester surfaces used in friction studies.....	121
3.5. XPS atomic composition data for fluorocarbon ester surfaces used in friction studies.....	122
3.6. Hexadecane contact angle data for model substrates and PCTFE modified surfaces.....	128
3.7. Methylene asymmetric and symmetric stretching infrared peak positions in hydrocarbons.....	131
4.1. Qualitative changes in coefficient of friction, $\mu$ , with changes in normal load and sliding speed.....	187
5.1. Characterization results for the homogeneous modified PCTFE surfaces used in this study.....	205
5.2. Contact angles ( $\Theta_A/\Theta_R$ ) of the basic hydrolysis solutions on the modified PCTFE surfaces.....	237

5.3. XPS and contact angle results for the acid catalyzed methanolysis of the modified PCTFE surfaces.....	239
---	-----



## LIST OF FIGURES

Figure	Page
1.1. Measurement of advancing (top) and receding (bottom) contact angles.....	1 6
1.2. Variable angle XPS.....	3 2
2.1. XPS survey spectra (75° takeoff angle) of: (a) PCTFE, (b) PCTFE-TMOB (-78 °C) and (c) PCTFE-TMOB (-17 °C).....	5 7
2.2. XPS C1s spectra (75° takeoff angle) of: (a) PCTFE, (b) PCTFE-TMOB (-78 °C) and (c) PCTFE-TMOB (-17 °C).....	5 8
2.3. Surface structure of PCTFE-TMOB.....	6 1
2.4. ATR-IR spectra of: (a) PCTFE-TMOB (-78 °C), (b) PCTFE-TMOB (-51 °C) and (c) PCTFE-TMOB (-17 °C).....	6 2
2.5. UV-vis spectrum of PCTFE-TMOB (-17 °C).....	6 3
2.6. Modified layer thickness as a function of modification temperature.....	6 4
2.7. XPS survey and C1s spectra of oxidized PCTFE-TMOB.....	6 5
2.8. XPS labelling of PCTFE-CO <sub>2</sub> H with thallium.....	6 8
2.9. ATR-IR spectra of: (a) PCTFE-CO <sub>2</sub> H, (b) PCTFE-CO <sub>2</sub> Oct <sup>ABC</sup> and (c) PCTFE-OH*.....	7 0
2.10. XPS C1s spectra of: (a) PCTFE-TMOB, (b) PCTFE-CO <sub>2</sub> H, (c) PCTFE-CO <sub>2</sub> Oct <sup>ABC</sup> , (d) PCTFE-OH* and (e) PCTFE-OHFB*.....	7 1

2.11. $\Theta_A$ dependence on probe fluid pH (buffered aqueous solutions).....	72
3.1. XPS survey spectra (75° takeoff angle) of: (a) PCTFE, (b) PCTFE-PEAA (-78 °C) and (c) PCTFE-PEAA (-15 °C).....	98
3.2. XPS C1s spectra (75° takeoff angle) of: (a) PCTFE, (b) PCTFE-PEAA (-78 °C) and (c) PCTFE-PEAA (-15 °C).....	99
3.3. Surface structure of PCTFE-PEAA.....	101
3.4. ATR-IR spectra of: (a) PCTFE-PEAA (-78 °C), (b) PCTFE-PEAA (-53 °C) and (c) PCTFE-PEAA (-15 °C).....	103
3.5. UV-vis spectra of PCTFE-PEAA (-78, -67, -27 and -15 °C from low to high absorbance).....	104
3.6. Modified layer thickness as a function of modification temperature.....	105
3.7. XPS survey and C1s spectra of oxidized PCTFE-PEAA (prepared at -15 °C).....	106
3.8. Proposed physical structure of surface-modified PCTFE.....	109
3.9. ATR-IR spectra of the hydrolysis product of PCTFE-PEAA (-15 °C) as a function of solvent composition (methanol:water): (a) (100:0), (b) (50:50) and (c) (0:100).....	111
3.10. ATR-IR spectrum of PCTFE-OH (-15 °C initial modification).....	113
3.11. XPS C1s spectra (75° takeoff angle) of: (a)PCTFE-OH, (b) PCTFE-OBu <sub>t</sub> , (c) PCTFE-ODec and (d) PCTFE-OS <sub>t</sub> ear.....	114
3.12. XPS O1s spectra (75° takeoff angle) of: (a) PCTFE-OH and (b) PCTFE-OBu <sub>t</sub> .....	122

3.13. XPS C1s spectra of PCTFE-OHFB: (a) 15° takeoff angle and (b) 75° takeoff angle.....	126
3.14. XPS C1s spectra of PCTFE-OPFDec: (a) 15° takeoff angle and (b) 75° takeoff angle.....	127
3.15. Schematic of: (a) PCTFE-ODec, (b) PCTFE-OSTear, (c) PCTFE-OHFB and (d) PCTFE-OPFDec modified ester surfaces.....	130
3.16. ATR-IR spectrum of PCTFE-OBuT (-15 °C initial modification).....	132
3.17. ATR-IR spectrum of PCTFE-ODec (-15 °C initial modification).....	132
3.18. ATR-IR spectrum of PCTFE-OSTear (-15 °C initial modification).....	133
3.19. ATR-IR spectrum of PCTFE-OHFB (-15 °C initial modification).....	134
3.20. ATR-IR spectrum of PCTFE-OPFDec (-15 °C initial modification).....	134
3.21. ATR-IR spectrum of PCTFE-O <sub>2</sub> Adip (-15 °C initial modification).....	136
3.22. ATR-IR spectrum of PCTFE-O <sub>3</sub> Benz (-15 °C initial modification).....	136
3.23. ATR-IR spectrum of PCTFE-ODec: (a) -78 °C initial modification and (b) -60 °C initial modification.....	137
3.24. ATR-IR spectrum of PCTFE-OPFDec: (a) -78 °C initial modification and (b) -60 °C initial modification.....	137
4.1. Instrument to measure coefficient of friction of polymer films.....	160



4.2.	Coefficient of friction of virgin PCTFE sliding PET: (a) fresh PCTFE sliding on fresh PET (first 100 runs), (b) fresh PCTFE sliding on used PET (next 15 runs) and (c) used PCTFE sliding on fresh PET (last 10 runs).....	162
4.3.	Interferometric surface profile of PET countersurface measured perpendicular to the sliding direction.....	164
4.4.	Measurement of contact angle anisotropy on friction surfaces.....	165
4.5.	Friction of PCTFE measured in controlled atmospheres.....	167
4.6.	Coefficient of friction of modified polymer surfaces (-78 °C initial modification).....	170
4.7.	Coefficient of friction of: (a) hydrocarbon esters (-78 °C initial modification) and (b) fluorocarbon esters (-78 °C initial modification).....	173
4.8.	Coefficient of friction of: (a) hydro- and perfluoroacetate esters (-78 °C initial modification), (b) hydro- and perfluorobutyrate esters (-78 °C initial modification) and (c) hydro- and perfluorodecanoate esters (-78 °C initial modification).....	175
4.9.	Raw friction data for PCTFE-PEAA as a function of modification temperature.....	176
4.10.	XPS survey spectrum (15° takeoff angle) of PET after sliding against PCTFE-PEAA (-15 °C modification).....	178
4.11.	Coefficient of friction of PCTFE-OH as a function of the initial modification temperature.....	180

4.12. Coefficient of friction of PCTFE-O <sub>2</sub> Adip as a function of the initial modification temperature.....	180
4.13. Coefficient of friction of PCTFE-O <sub>3</sub> Benz as a function of the initial modification temperature.....	181
4.14. Coefficient of friction of PCTFE-OS <sub>tear</sub> as a function of the initial modification temperature.....	182
4.15. Coefficient of friction of PCTFE-OB <sub>ut</sub> as a function of the initial modification temperature.....	183
4.16. Coefficient of friction of PCTFE-OH <sub>FB</sub> as a function of the initial modification temperature.....	183
4.17. Coefficient of friction of PCTFE-OD <sub>ec</sub> as a function of the initial modification temperature.....	184
4.18. Coefficient of friction of PCTFE-OP <sub>FDec</sub> as a function of the initial modification temperature.....	185
4.19. XPS survey and C1s spectra (15° takeoff angle) of PET countersurface after sliding against: (a) PCTFE-OH (-15 °C initial modification) (b) PCTFE-OD <sub>ec</sub> (-15 °C initial modification) and (c) PCTFE-OP <sub>FDec</sub> (-15 °C initial modification).....	186
5.1. Preparation of mixed hydroxyl/ester and mixed ester/ester surfaces.....	196
5.2. Formation of: (a) random and (b) patchy mixed surfaces.....	204
5.3. XPS results for pyridine catalyzed esterification kinetics with heptafluorobutyryl chloride.....	207

5.4.	Contact angle results for pyridine catalyzed esterification kinetics with heptafluorobutyryl chloride. Water contact angles after initial reaction (circles) and hexadecane contact angles after labelling with butyryl chloride (squares).....	207
5.5.	Calculated XPS C/F ratio as a function of surface composition for mixed heptafluorobutyrate/hydrocarbon ester surfaces.....	209
5.6.	XPS results for pyridine catalyzed esterification kinetics with butyryl chloride.....	210
5.7.	(a) Water, (b) methylene iodide and (c) hexadecane contact angle results for pyridine catalyzed esterification kinetics with butyryl chloride.....	212
5.8.	XPS results for pyridine catalyzed esterification kinetics with decanoyl chloride.....	214
5.9.	Contact angle results for pyridine catalyzed esterification kinetics with decanoyl chloride. Water contact angles after initial reaction (circles) and hexadecane contact angles after labelling with heptafluorobutyryl chloride (squares).....	214
5.10.	XPS results for pyridine catalyzed esterification kinetics with stearoyl chloride.....	216
5.11.	Contact angle results for pyridine catalyzed esterification kinetics with stearoyl chloride. (a) Water (circles) and hexadecane (triangles) contact angles after initial reaction and (b) hexadecane contact angles after labelling with heptafluorobutyryl chloride.....	217
5.12.	Rate of pyridine catalyzed esterifications of PCTFE-OH.....	219



5.13. XPS results for uncatalyzed esterification kinetics with heptafluorobutyryl chloride.....	221
5.14. Contact angle results for uncatalyzed esterification kinetics with heptafluorobutyryl chloride. Water contact angles after initial reaction (circles) and hexadecane contact angles after labelling with butyryl chloride (squares).....	221
5.15. XPS results for uncatalyzed esterification kinetics with butyryl chloride. (a) 15° takeoff angle and (b) 75° takeoff angle.....	223
5.16. Water contact angle results for uncatalyzed esterification kinetics for butyryl chloride after initial reaction.....	224
5.17. (a) Advancing and (b) receding hexadecane contact angle results for uncatalyzed esterification kinetics with butyryl chloride after labelling with perfluorinated reagents.....	226
5.18. XPS results for uncatalyzed esterification kinetics with decanoyl chloride.....	227
5.19. Contact angle results for uncatalyzed esterification kinetics with decanoyl chloride. Water contact angles after initial reaction (circles) and hexadecane contact angles after labelling with heptafluorobutyryl chloride (squares).....	228
5.20. XPS results for uncatalyzed esterification kinetics with stearoyl chloride.....	229
5.21. Contact angle results for uncatalyzed esterification kinetics with stearoyl chloride. (a) Water (circles) and hexadecane (triangles) contact angles after initial reaction and (b) hexadecane contact angles after labelling with heptafluorobutyryl chloride.....	231
5.22. Rate of uncatalyzed esterification of PCTFE-OH.....	233

5.23. XPS results for competitive reactions of butyryl chloride and heptafluorobutyryl chloride with PCTFE-OH.....	234
5.24 XPS results for base catalyzed aqueous hydrolysis of PCTFE-OHFB as a function of temperature (The points at 0 represent no reaction not 0 °C.).....	242
5.25. Contact angle results for base catalyzed aqueous hydrolysis of PCTFE-OHFB as a function of temperature (The points at 0 represent no reaction not 0 °C.). Water contact angles after initial reaction (circles) and hexadecane contact angles after labelling with butyryl chloride (squares).....	242
5.26. XPS results for the base catalyzed hydrolysis of PCTFE-OBu (25:75 methanol:water).....	244
5.27. Contact angle results for the base catalyzed hydrolysis of PCTFE-OBu (25:75 methanol:water). Water contact angles after hydrolysis (circles) and hexadecane contact angles after labelling with heptafluorobutyryl chloride (squares).....	245
5.28. XPS results for the base catalyzed hydrolysis of PCTFE-OBu (0:100 methanol:water).....	247
5.29. Contact angle results for the base catalyzed hydrolysis of PCTFE-OBu (0:100 methanol:water). Water contact angles after hydrolysis (circles) and hexadecane contact angles after labelling with heptafluorobutyryl chloride (squares).....	247
5.30. XPS results for the base catalyzed hydrolysis of PCTFE-ODec (100:0 methanol:water).....	248

5.31. Contact angle results for the base catalyzed hydrolysis of PCTFE-ODec (100:0 methanol:water). Water contact angles after hydrolysis (circles) and hexadecane contact angles after labelling with heptafluorobutyryl chloride (squares).....	249
5.32. XPS results for the base catalyzed hydrolysis of PCTFE-ODec (75:25 methanol:water).....	251
5.33. Contact angle results for the base catalyzed hydrolysis of PCTFE-ODec (75:25 methanol:water). Water contact angles after hydrolysis (circles) and hexadecane contact angles after labelling with heptafluorobutyryl chloride (squares).....	251
5.34. XPS results for the base catalyzed hydrolysis of PCTFE-ODec (50:50 methanol:water).....	253
5.35. Contact angle results for the base catalyzed hydrolysis of PCTFE-ODec (50:50 methanol:water). Water contact angles after hydrolysis (circles) and hexadecane contact angles after labelling with heptafluorobutyryl chloride (squares).....	254
5.36. XPS results for the base catalyzed hydrolysis of PCTFE-OSTear (100:0 methanol:water).....	256
5.37. Contact angle results for the base catalyzed hydrolysis of PCTFE-OSTear (100:0 methanol:water). Water contact angles after hydrolysis (circles) and hexadecane contact angles after labelling with heptafluorobutyryl chloride (squares).....	256
5.38. XPS results for the base catalyzed hydrolysis of PCTFE-OSTear (75:25 methanol:water).....	259



5.39. Contact angle results for the base catalyzed hydrolysis of PCTFE-OSTear (75:25 methanol:water). Water contact angles after hydrolysis (circles) and hexadecane contact angles after labelling with heptafluorobutyryl chloride (squares).....	259
5.40. Kinetics of the base catalyzed hydrolysis of PCTFE-OBu as a function of solvent composition.....	260
5.41. Kinetics of the base catalyzed hydrolysis of PCTFE-ODec as a function of solvent composition.....	261
5.42. Kinetics of the base catalyzed hydrolysis of PCTFE-OSTear as a function of solvent composition.....	261
5.43. Kinetics of the base catalyzed methanolysis (100:0 methanol:water) of: (a) PCTFE-ODec and (b) PCTFE-OSTear.....	262
5.44. Cosine of the water contact angles as a function of surface composition for the mixed PCTFE-OH/OBu surfaces prepared by kinetic control of the esterification of PCTFE-OH with butyryl chloride.....	264
5.45. Cosine of the water contact angles as a function of surface composition for the mixed PCTFE-OH/ODec surfaces prepared by kinetic control of the esterification of PCTFE-OH with decanoyl chloride.....	265
5.46. Cosine of the water contact angles as a function of surface composition for the mixed PCTFE-OH/OSTear surfaces prepared by kinetic control of the esterification of PCTFE-OH with stearoyl chloride.....	265

5.47. Cosine of the water contact angles as a function of surface composition for the mixed PCTFE-OH/OBut surfaces prepared by kinetic control of the hydrolyses of PCTFE-OBut. ....	268
5.48. Cosine of the water contact angles as a function of surface composition for the mixed PCTFE-OH/ODec surfaces prepared by kinetic control of the hydrolyses of PCTFE-ODec. ....	270
5.49. Cosine of the water contact angles as a function of surface composition for the mixed PCTFE-OH/OSTear surfaces prepared by kinetic control of the hydrolyses of PCTFE-OSTear. ....	271
5.50. Cosine of the hexadecane contact angles as a function of surface composition for the mixed PCTFE-OSTear/OHFB surfaces prepared by sequential esterifications of PCTFE-OH. ....	273
5.51. Cosine of the hexadecane contact angles as a function of surface composition for the mixed PCTFE-ODec/OHFB surfaces prepared by sequential esterifications of PCTFE-OH. ....	274
5.52. Cosine of the hexadecane contact angles as a function of surface composition for the mixed PCTFE-OBut/OHFB surfaces prepared by sequential esterifications PCTFE-OH. ....	276
5.53. Cosine of the hexadecane contact angles as a function of surface composition for the mixed PCTFE-OBut/OTFAc surfaces prepared by sequential esterifications of PCTFE-OH. ....	278
5.54. Cosine of the hexadecane contact angles as a function of surface composition for the mixed PCTFE-OBut/OPFDec surfaces prepared by sequential esterifications of PCTFE-OH. ....	278

- 5.55. Cosine of the hexadecane contact angles as a function of surface composition for the mixed PCTFE-OSTear/OHFB surfaces prepared by the hydrolyses/re-esterification of PCTFE-OSTear.....281
- 5.56. Cosine of the hexadecane contact angles as a function of surface composition for the mixed PCTFE-ODec/OHFB surfaces prepared by the hydrolyses/re-esterification of PCTFE-ODec.....281
- 5.57. Cosine of the hexadecane contact angles as a function of surface composition for the mixed PCTFE-OBu/OHFB surfaces prepared by the hydrolyses/re-esterification of PCTFE-OBu.....282



## LIST OF SCHEMES

Scheme	Page
1.1. Proposed mechanism of the reaction of organo-lithium reagents with PCTFE.....	8
2.1. Reaction of PCTFE with LiTMOB.....	55
2.2. Oxidative removal of PCTFE-TMOB modified layer.....	65
2.3. Hydrolysis of PCTFE-TMOB and further modifications of PCTFE-CO <sub>2</sub> H.....	67
3.1. Introduction of alcohol groups into the surface of PCTFE.....	95
3.2. Reaction of PCTFE with LiPEAA.....	96
3.3. Oxidative removal of modified layer.....	106
3.4. Esterifications of PCTFE-OH.....	117
4.1. Surface modifications of PCTFE.....	169

# CHAPTER I

## INTRODUCTION

### Polymer Surface Modification

#### Introduction

The functional group chemistry at a surface plays an important role in a number of physical properties; adhesion, friction, wetting and biocompatibility are examples.<sup>1</sup> Thus, a number of researchers have investigated various methods of modifying the structure of polymer surfaces<sup>2</sup> in order to control these phenomena, without changing the bulk material properties. These methods include polymer grafting,<sup>3,4</sup> flame treatment,<sup>5</sup> plasma treatment,<sup>6,7</sup> corona discharge treatment,<sup>8,9</sup> chemical reduction<sup>10,11</sup> and chemical oxidation.<sup>12,13</sup> Many of these procedures have been successfully used in industry to modify a wide variety of polymers (i.e. polycarbonate, polyethylene, polypropylene, polystyrene and poly(tetrafluoroethylene)). These modification techniques, however, can be harsh and uncontrolled in nature and often result in a surface which is crosslinked, topographically changed and/or chemically heterogeneous.<sup>2</sup> It is thus difficult to relate changes in the microscopic surface structure resulting from these modifications to changes in macroscopic properties, like wetting and friction. Hence, little advancement has been made in the understanding of surface structure-property relationships.

A principal reason for this lack of progress can be attributed to a deficiency in substrates suitable for these types of studies. The ideal substrate for molecular level characterization of surface phenomena is one in which a unique functional group exists in a well defined layer at the polymer surface. The bulk of the polymer beneath this modified layer should remain unchanged in chemistry and in physical properties. It would be desirable, for comparative purposes, to be able to vary the thickness of this modified layer and the identity of the functional group. With these factors in mind, it is necessary to develop techniques for functionalizing polymer surfaces in order to produce materials whose surface structures are known at the molecular level. Once these materials have been exhaustively characterized, surface structure-property correlations can be made.

Research in the McCarthy group has focused on modifying polymer surfaces in a controlled manner. This research program utilizes relatively (compared to the modifications mentioned above) nondestructive techniques to introduce a variety of specific functional groups into the surfaces of polymer films. The objective of this research is to learn how to predict particular properties with knowledge of the surface chemical structure, as well as to impart desired properties by introducing specific functional groups into the polymer surface in specific locations, densities and patterns. The first stage of this research is the development of surface modification techniques to prepare suitable substrates like those discussed above. Chemically resistant polymer films, (poly(ether ether ketone) (PEEK),<sup>14</sup> poly(tetrafluoroethylene) (PTFE),<sup>15</sup> poly(vinylidene fluoride) (PVF2),<sup>16</sup> poly(tetrafluoroethylene-co-hexafluoropropylene)



(FEP)<sup>17</sup> and poly(chlorotrifluoroethylene) (PCTFE)<sup>18-21</sup>) were chosen for study for a variety of reasons.<sup>18,19</sup> The most important of these reasons is that a versatile functional group can be introduced into the surfaces of these inert materials under brutal conditions and then transformed by a number of relatively mild reaction which do not affect the bulk of the material. Thus, a series of polymer samples that differ solely in their surface chemistry can be prepared to investigate the properties mentioned. An additional goal of this research program concerns the relationship between the reactivity of an organic functional group in a surface and its environment. In polymer solids, the environment surrounding a functional group can be controlled by choice of reaction temperature and/or solvent. Both of these variables play a role in determining the degree of mobility of the functional group and its vulnerability to attack by reagents in solution. Under many circumstances, functional groups confined to a surface may exhibit significantly different reactivities than those that are in solution due to attenuation of solvation forces and/or steric constraints at the solid/solution interface.

This research group has found that in the surface modification of polymers at the solid/solution interface several factors need to be considered when trying to control the surface selectivity of the reaction and the structures of the resulting interfaces. These factors have been discussed in detail<sup>22</sup> with a number of examples and will be briefly reviewed here. The unreacted polymer in contact with the reactive solution will interact with the solvent and reagent(s) to varying extents. This interaction ranges along a continuum from the polymer not being wet by the solvent to being highly swollen or

even dissolved by the solvent. Solvent mixtures add complexity to the system as the polymer may interact more strongly with one solvent than another. Reagents likely partition between the polymer and the solution to varying extents depending on their relative solubilities in the two phases. Thus, the interfacial region where reaction takes place will vary from sharp to diffuse, affecting the thickness of the modified layer and the distribution of the newly introduced functional groups in that layer. The reaction temperature can also affect the diffuseness of this interface. Higher temperatures increase polymer chain mobility and affect the solvent polymer interactions to different extents. Upon reaction the structure of the polymer/solution interface changes and a new set of reaction conditions results. The product polymer surface can interact more strongly with the solvent and reagents than the unmodified polymer leading to deeply modified surfaces or in the extreme case corrosion and/or dissolution of the modified layer. If the product polymer-solution interactions are unfavorable, autoinhibition results where the modified surface layer acts as a barrier preventing reagent from reaching the underlying virgin material. In addition to how the modification affects the polymer-solution interactions, the specific chemistry that occurs can affect the modified surface structure. Crosslinking will prevent dissolution of the modified layer. In cases where the product polymer-solution interactions are strong a thick modified layer will result. If the crosslink density is high enough, autoinhibition may result. In modifications that cleave polymers at the surface, chain ends will be important features. Finally, the structure of the modified layer once isolated from solvent and

reagents may be very different from the modified polymer in contact with the solution. The compatability (or lack thereof) of functional groups in the near surface regions and the disparity between interfacial free energies may cause reorganization of the surface during rinsing procedures and solvent removal. This surface reconstruction would likely segregate the surface components and concentrate specific functional groups at the polymer/ambient interface.

This dissertation describes fundamental studies investigating the role surface structure plays in determining surface reactivity, wetting and friction behavior. This research has utilized surface modification techniques developed for PCTFE to prepare model substrates with well-defined surface structures. These surface modified polymer samples have been thoroughly characterized, using an array of analytical techniques, so that correlations between surface structure and the surface phenomena mentioned above can be made.

At this point it is necessary to define surface structure as it pertains to the studies described in this thesis. When discussing modified polymer surfaces it is essential to think in terms of the three dimensional structure of the modified layer. Very few polymer surface modifications restrict themselves to the outer atomic layer of the material (the "true" surface). Most proceed tens or even thousands of angstroms into the substrate polymer, producing relatively thick, modified layers. Throughout this thesis the terms in or into the surface (rather than on or onto) will be used to emphasize the three dimensional nature of these surface layers.



The important variables to consider when characterizing the structure of the modified layer are: (1) the roughnesses of the modified polymer/air and the modified polymer/unmodified polymer interfaces, (2) the thickness of the layer, (3) the identity and distribution of the functional groups in both the x-y plane parallel to the surface and in the z-direction perpendicular to the surface, (4) any preferred orientation of these functional groups, (5) the morphology of the modified layer (crystalline or amorphous) and (6) the viscoelastic properties of the modified surface layer as determined by these new functional groups and morphologies.

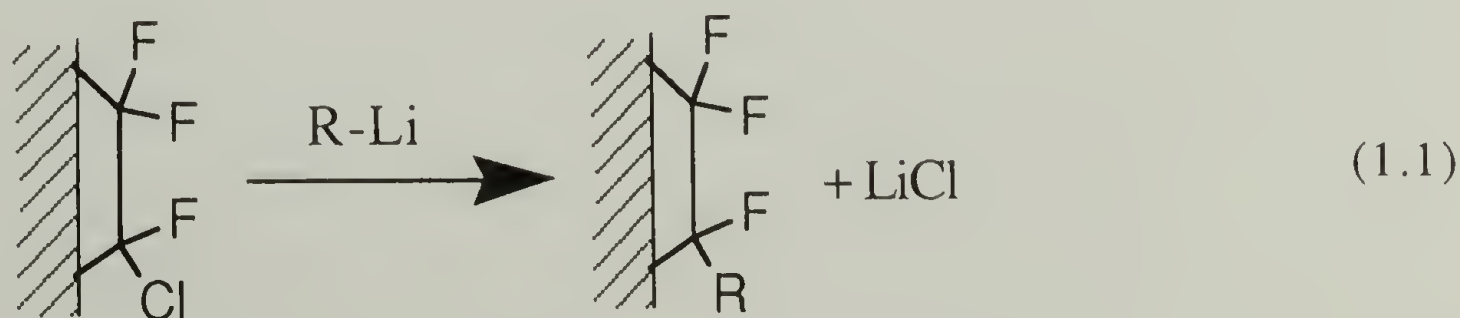
The remaining sections of this introduction present an overview of the surface modification of PCTFE with organolithium reagents. Specifically, this discussion will be concerned with the effects of reaction temperature, solvent composition and modification reagent on the surface structure. In addition, the surface analytical techniques utilized in this thesis will be reviewed in sufficient detail that the unfamiliar reader can understand their application toward the characterization of the surfaces prepared and used in these studies. Each of these techniques yields different types information regarding the polymer surface composition. When used in combination they provide a powerful tool for elucidating the structure of the modified layer.

### Poly(chlorotrifluoroethylene)/Organolithium Surface Chemistry

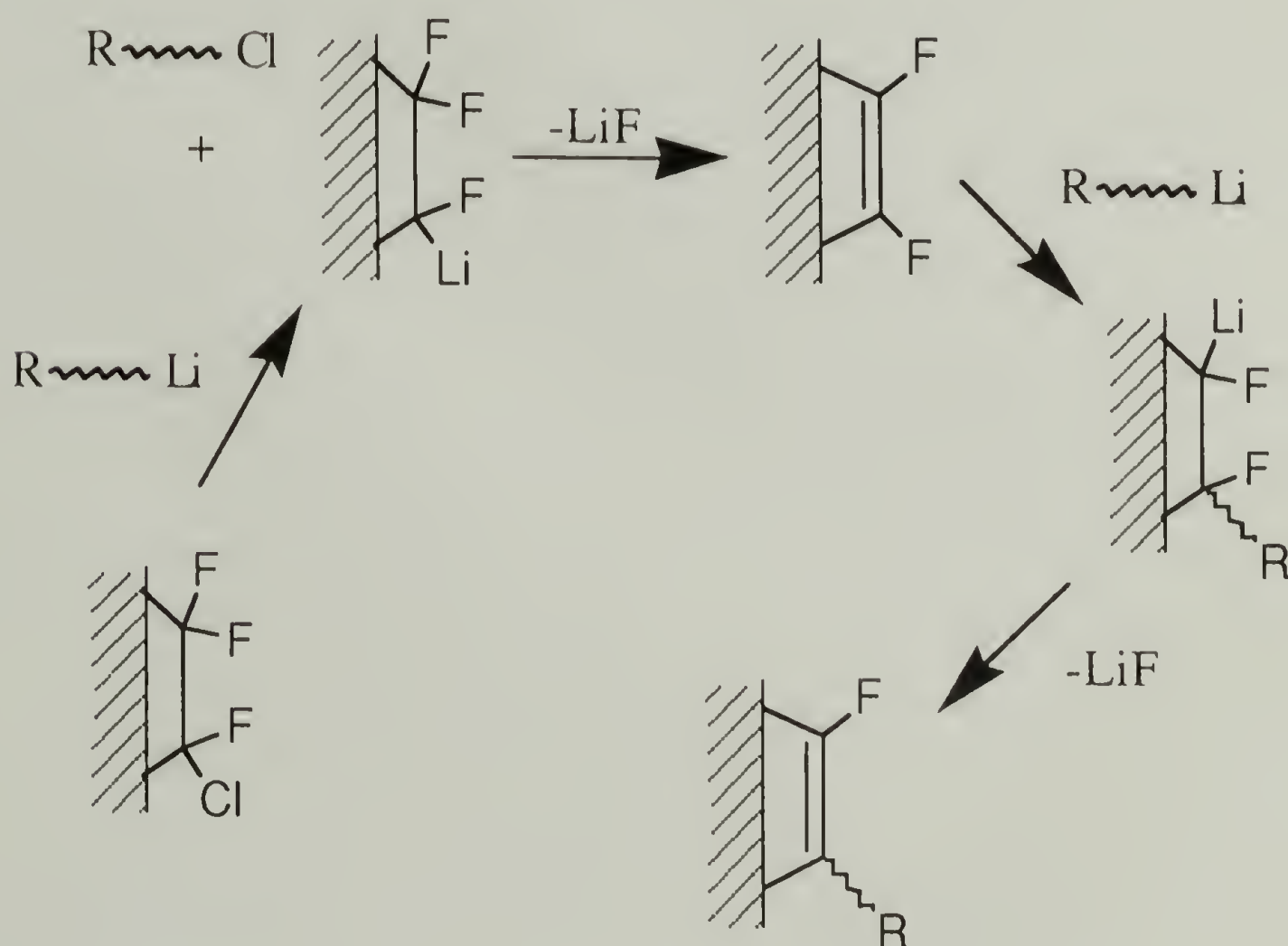
The poly(chlorotrifluoroethylene) (PCTFE) used in this study was purchased from Allied-Signal as Aclar 33C and is actually a terpolymer consisting of primarily chlorotrifluoroethylene with small

amounts of tetrafluoroethylene and vinylidene fluoride. This material is a flexible thermoplastic film (0.005 inches thick) with high optical transparency and is principally used for military and pharmaceutical packaging applications. The polymer exhibits good mechanical properties from -240 - 200 °C, is inert to most chemicals and oxididants, has very low permeability to water and other gases and exhibits excellent electrical properties. It has a crystalline melting temperature of 202 - 204 °C and a glass transition temperature of 58 - 65 °C. The density of this material reflects its crystalline content and varies from  $d = 2.10$  (45% crystallinity) to  $d = 2.13$  (65%) depending on its thermal history. The refractive index of PCTFE is 1.435.<sup>23</sup>

Although PCTFE is inert to most chemicals, it has been found to react with a variety of organometallic reagents. Danielson *et al.*<sup>24</sup> studied the reaction of alkyl- and aryllithium reagents with PCTFE powder for use as packing materials in high performance liquid chromatography columns. The conditions employed in these modifications were such that the polymer was extensively modified with no apparent surface selectivity. However, their proposed product polymer (Equation 1.1) is not consistent with the formation of a golden-brown material upon reaction.



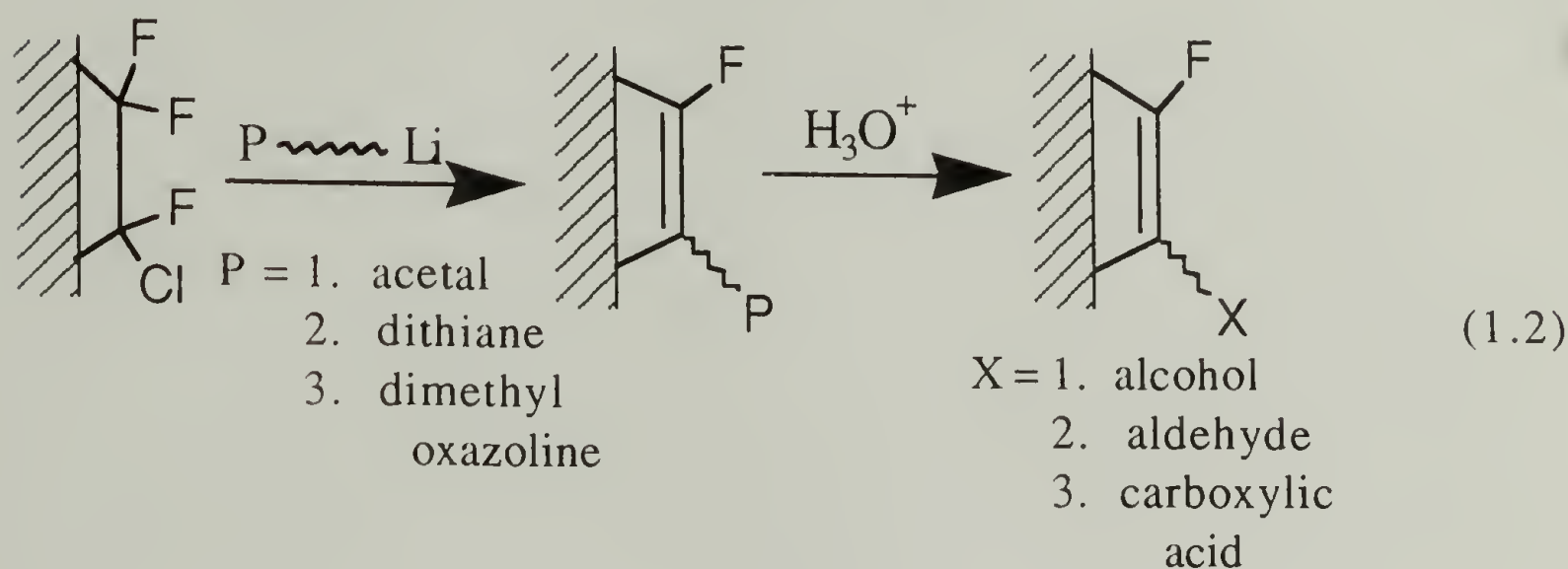
This research prompted Dias and McCarthy to reinvestigate these reactions with PCTFE powder and oligomeric oils, under less severe conditions, in order to determine the reaction mechanism, products and potential as surface modifications.<sup>18,20</sup> Their results showed that after reacting PCTFE with methyllithium (or phenyllithium), the methyl (or phenyl) group was added to the polymer backbone along with a considerable degree of unsaturation. Also observed was the production of methyl chloride (or chlorobenzene) and lithium fluoride. From these results they proposed the mechanism for these reactions shown in Scheme 1.1.



**Scheme 1.1.** Proposed mechanism of the reaction of organolithium reagents with PCTFE.



Once this reaction had been studied in detail, it was extended to introduce alcohols, aldehydes and carboxylic acids into the PCTFE surface.<sup>19,20</sup> Their strategy utilized the reaction of PCTFE with organolithium reagents containing the appropriate protected functional groups as shown in Equation 1.2.



Their results showed that the depth of the initial reaction is dependent on the temperature of the reaction, the solvent used and the structure of the lithium reagent. Higher reaction temperatures increase surface mobility resulting in thicker modified layers. For example, reactions of PCTFE with acetaldehyde 3-lithiopropyl ethyl acetal (LiPEAA) carried out in 50:50 THF/heptane at -78 and -20 °C for 60 min produced 50 Å and 1000 Å thick modified layers, respectively. Solvents which wet and/or swell the polymer to greater extents increase the diffuseness of the polymer/solution interface increasing modified layer thicknesses. The reaction of PCTFE with 2-lithio-1,3-dithiane (LiDT) in 20:80 THF/heptane at -20 °C results in a 25 Å thick modified layer. Increasing the THF/heptane ratio to 90:10 (THF swells PCTFE) increases the modification depth to 70 Å. The large difference in the modified

layer thickness for these two reagents (compare the -20 °C results for each reagent above) is the result of the different manner in which the product polymer surface interacts with the reaction solution. PCTFE-DT does not interact extensively with the solution resulting in autoinhibition and relatively thin modified layers. On the other hand, PCTFE-PEAA appears to interact strongly with the solution as no autoinhibition is observed, resulting in deeply modified surfaces.

The hydrolytic deprotection of these functional groups (and others from similar modifications) was not facile and a variety of conditions were attempted and optimized.<sup>20</sup> In general, it was found necessary to use a combination of water, an organic solvent (typically acetone or methanol) to lower the interfacial free energy and an organic acid catalyst. The exact ratio of organic solvent to water was found to be important and appears to be a tradeoff between the surface tension of the solution and its reflux temperature.

The reactivities of these functionalized surfaces were assessed in detail using standard solution conditions for organic functional group transformations. PCTFE-OH, the alcohol functionalized surface derived from PCTFE-PEAA proved to be reactive and extremely versatile.<sup>21</sup> PCTFE-OH was found to react with a wide variety of acid chlorides to give the corresponding surface-confined esters. The tosylate of PCTFE-OH was prepared via reaction with *p*-toluenesulfonyl chloride and reacted with chloride, bromide and cyanide ions in good yield. Reaction of PCTFE-OH with isocyanates produces the expected urethanes. Oxidation of PCTFE-OH with dicyclohexyl carbodiimide, Me<sub>2</sub>SO and anhydrous phosphoric acid

yields the aldehyde and with pyridinium dichromate in DMF yields the carboxylic acid. It was also found in these studies that di- and poly-functional reagents tend to react multiply with PCTFE-OH to produced cross-linked surfaces.

## Surface Analytical Techniques

### Contact Angle

The measurement of the contact angle that a liquid droplet makes with a solid surface yields information on the outermost few angstroms of the solid.<sup>25</sup> From a very simple and inexpensive measurement, knowledge of the surface energetics, surface roughness and surface chemical heterogeneity is obtained.

The contact angle was first associated with the surface energetics of the solid and the liquid by Young<sup>26</sup> in 1805 and later put on thermodynamic footing by Gibbs<sup>27</sup> in 1878. A change in the area of a drop of liquid resting on a solid surface is accompanied by a change in Gibbs free energy,  $G$ , of the system:

$$dG = \gamma^{SL}dA_{SL} + \gamma^{SV}dA_{SV} + \gamma^{LV}dA_{LV} \quad (1.3)$$

where  $\gamma^{SL}$  is the surface free energy of the solid-liquid interface,  $\gamma^{SV}$  is the surface free energy of the solid-vapor interface,  $\gamma^{LV}$  is the surface free energy of the liquid-vapor interface and the  $dA_i$ 's are the associated changes in area of each interface. The surface free energy is defined to be the work required to create a unit area of an interface.  $\gamma$  is often also called the surface tension, which is the work



necessary to stretch an existing surface. In a liquid, stretching a surface also creates new surface, so surface tension and surface free energy are equivalent. A solid, on the other hand, can be stretched without creating more surface. Thus, there is a change in the surface tension, but not the surface free energy and these two terms are not equivalent. Throughout this discussion these expressions will be used interchangeably due to past conventions, but it is emphasized that what is really meant is surface free energy. The free energy of a solid surface newly formed in a vacuum is  $\gamma^{S^{\circ}}$ . The same surface in equilibrium with a vapor has a free energy  $\gamma^{SV}$ , where  $\gamma^{SV} < \gamma^{S^{\circ}}$  and the difference is defined as the spreading pressure,  $\pi$ , of the vapor on the solid surface. For low energy surfaces like polymers, adsorption of the liquid vapor on the solid is small (especially true for non-volatile liquids), so  $\pi$  is small and can be neglected for all practical purposes, i.e.  $\gamma^{SV} = \gamma^{S^{\circ}}$  in the following discussions.

Returning to Equation 1.3, simple geometry yields:

$$dA_{SV} = -dA_{SL} \text{ and } dA_{LV} = dA_{SL}\cos\Theta \quad (1.4)$$

where  $\Theta$  is the contact angle at the S/L/V interface. Combining equations 1.3 and 1.4:

$$dG = (\gamma^{SL} - \gamma^{SV} + \gamma^{LV}\cos\Theta)dA_{SL} \quad (1.5)$$

From this relation a spreading coefficient,  $S$ , can be defined as  $S = -dG/dA_{SL}$ .

When  $S > 0$  the liquid spreads spontaneously over the solid, decreasing  $\Theta$ .

When  $S < 0$  the liquid contracts, increasing  $\Theta$ .

When  $S = 0$  the system is at equilibrium and

$$\gamma^{SV} - \gamma^{SL} = \gamma^{LV} \cos \Theta \quad (1.6)$$

Equation 1.6 is known as Young's equation.

From these beginnings the literature has been filled with experimental studies of contact angles of a variety of liquids on a number of solids.<sup>28</sup> Usually,  $\gamma^{LV}$  is known from a separate measurement, however  $\gamma^{SV}$  and  $\gamma^{SL}$  cannot be determined from other experiments, so  $\Theta$  can only be used to calculate the difference between  $\gamma^{SV}$  and  $\gamma^{SL}$  from Young's equation. This difference is useful in experiments involving a particular solid-liquid pair, but it would be desirable to obtain  $\gamma^{SV}$  and  $\gamma^{SL}$  independently in order to improve the understanding of interfacial interactions and surface free energy of solids.

In order to obtain information about the solid surface free energy, Zisman developed the concept of the critical surface tension,  $\gamma^C$ .<sup>33</sup> To determine  $\gamma^C$  the cosines of the contact angle for a series of homologous liquids on a given solid are plotted versus the liquid surface tensions. The critical surface tension is given by the intercept at  $\cos \Theta = 1$  and is defined as the surface tension of that liquid which could just totally spread on the solid surface. This method yields an empirical value of the surface free energy of the

solid and can be related to the solid surface constitution. Small changes in the outermost atomic layer of the solid are reflected by significant changes in  $\gamma^C$ . The correlation of  $\gamma^C$  with  $\gamma^{SV}$  works well when the critical surface tension is determined for an apolar solid using a series of apolar liquids that interact only through van der Waal's forces, such as hydrocarbons. In these cases a linear relationship is observed between  $\cos \Theta$  and the liquid surface tensions. When hydrogen bonding and other polar interactions are involved, deviations from linearity are observed and  $\gamma^C$  tends to underestimate  $\gamma^{SV}$ .<sup>31</sup>

The difficulties associated with using  $\gamma^C$  to estimate  $\gamma^{SV}$  have led a number of researchers<sup>34-38</sup> to center their efforts on using the concept of additivity of energy to break  $\gamma^{SV}$ ,  $\gamma^{LV}$  and  $\gamma^{SL}$  into polar and apolar components. van Oss *et al.*<sup>38</sup> recently developed a relationship that they designate as the Complete Young Equation:

$$(1 + \cos \Theta)\gamma_{TOT}^L = 2((\gamma_d^S \gamma_d^L)^{1/2} + (\gamma_+^S \gamma_-^L)^{1/2} + (\gamma_-^S \gamma_+^L)^{1/2}) \quad (1.7)$$

where the superscripts L and S refer to the liquid-vapor and the solid-vapor interfaces, respectively;  $\gamma_+^i$  and  $\gamma_-^i$  are the constituent electron-acceptor and electron-donor parameters, respectively, of the polar component of the surface tension,  $\gamma_p^i = 2(\gamma_+^i \gamma_-^i)^{1/2}$ ;  $\gamma_d^i$  is the apolar component of the surface tension and the total surface tension is  $\gamma_{TOT}^i = \gamma_d^i + \gamma_p^i$ . The total interfacial free energy,  $\gamma_{TOT}^{SL}$ , can be determined from:



$$\gamma^{SL}_{TOT} = \gamma^{SL}_d + \gamma^{SL}_p \quad (1.8)$$

$$\text{where } \gamma^{SL}_d = ((\gamma^S_d)^{1/2} - (\gamma^L_d)^{1/2})^2 \quad (1.9)$$

$$\text{and } \gamma^{SL}_p = 2((\gamma^S_+ \gamma^S_-)^{1/2} + (\gamma^L_+ \gamma^L_-)^{1/2} - (\gamma^S_+ \gamma^L_-)^{1/2} - (\gamma^S_- \gamma^L_+)^{1/2}) \quad (1.10)$$

If the contact angle is determined using a liquid with not only known total surface tension,  $\gamma^{L}_{TOT}$ , but also its  $\gamma^L_d$  component and its  $\gamma^L_+$  and  $\gamma^L_-$  parameters, there are still three independently variable unknowns that compose  $\gamma^S_{TOT}$ , i.e.  $\gamma^S_d$ ,  $\gamma^S_+$  and  $\gamma^S_-$ . Thus, a single contact angle measurement still cannot characterize the solid surface. However, if contact angles are measured with three different, completely characterized, liquids (of which two must be polar and hydrogen-bonding) on a particular solid (in order to be able to solve three equations for three unknowns) the surface tension properties of the solid can be completely characterized. Experimental results using these relations accurately predict the contact angles measured on a number of polar and apolar solid surfaces with a variety of polar and apolar liquids. Also, these derivations explain the deviation from linearity in determinations of  $\gamma^C$  when either the solid is polar or the liquids used in the measurement are polar.

All of the equations discussed above are based on a number of assumptions that predict only one intrinsic contact angle,  $\Theta_o$ , for a given liquid-solid pair independent of how that angle is measured. These assumptions are: (1) the solid is sufficiently rigid that it does not deform during the measurement; (2) the solid surface is smooth; (3) the solid is chemically homogeneous; (4) the liquid does not penetrate into or swell the solid; (5) the surface functional groups do not reorganize in response to changes in the environment during the

measurement and (6) no adsorption of impurities from the probe fluid, reaction with the probe fluid or extraction of substances in the solid by the probe fluid takes place at the solid-liquid interface. The first assumption is generally valid for polymers with the exception of some low modulus solids ( $<10^5$  dyn/cm<sup>2</sup>) such as aqueous gels and will not be discussed here. It is sufficient to say that contact angle measurements made on these types of materials do result in vertical displacement of the solid/liquid/vapor interface.<sup>39</sup> In most practical situations it is found that one or more of the remainder of these assumptions is not applicable. Thus, observed contact angles depend on whether the angle was measured as the solid/liquid contact area increases (the advancing contact angle,  $\Theta_A$ ) or decreases (the receding contact angle,  $\Theta_R$ ) as shown in Figure 1.1 and on the time scale of the measurement.

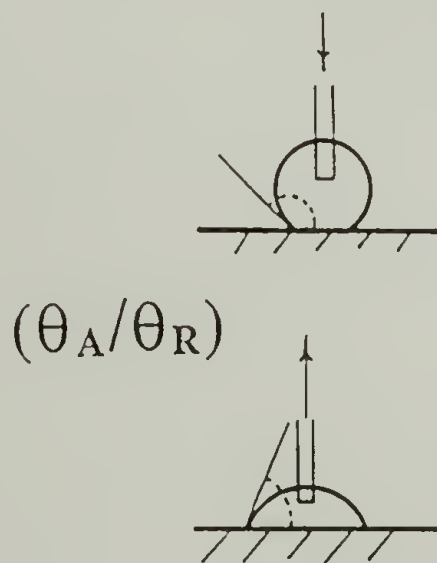


**Figure 1.1.** Measurement of advancing (top) and receding (bottom) contact angles.

In general (there are exceptions, especially when assumption 6 above is involved),  $\Theta_A > \Theta_0 > \Theta_R$  and the difference between  $\Theta_A$  and

$\Theta_R$  is termed the contact angle hysteresis. Andrade<sup>32</sup> has broken contact angle hysteresis into two categories: (1) thermodynamic hysteresis, where the hysteresis is reproducible for a number of contact angle measurements made with the same liquid on the same area of the solid and (2) kinetic hysteresis, where the hysteresis changes with the number of repeat measurements. Thermodynamic hysteresis is generally based on the concept of a number of metastable states separated by energy barriers that prevent attainment of the true contact angle (see below) and is associated with surface roughness and chemical heterogeneities. Kinetic hysteresis is usually time dependent and can be associated with breakdowns in assumptions 4 - 6 above which lead to changes in any or all of  $\gamma^{SL}$ ,  $\gamma^{SV}$  and  $\gamma^{LV}$ . It is often observed that when kinetic hysteresis is involved,  $\Theta_A$  approaches  $\Theta_R$  with each successive measurement. Examples of both types of hysteresis will be discussed below.

The effect of surface roughness on contact angle was first addressed by Wenzel,<sup>30</sup> who derived the following relationship between the intrinsic contact angle,  $\Theta_0$ , and the observed contact angle,  $\Theta'$ :

$$\cos \Theta' = r \cos \Theta_0 \quad (1.11)$$

$r$  is known as Wenzel's roughness ratio and is defined as  $r = A'/A$ , where  $A$  is the apparent surface area of a plane having the same macroscopic dimensions and  $A'$  is the true surface area taking into account peaks and valleys. This treatment predicts that roughening of a surface with an intrinsic contact angle greater than  $90^\circ$  will



increase the observed contact angle and will decrease the observed angle for surfaces with  $\Theta_0 < 90^\circ$ . However, this derivation is rather crude and does not consider the existence of metastable states of the surface induced by roughness and gives no insight into hysteresis.

Johnson and Dettre<sup>30,41</sup> analyzed the effect of surface roughness on contact angle hysteresis through an intuitively simple model. Their model consists of a drop of liquid on a surface of concentric grooves. The intrinsic contact angle that the liquid makes with an equivalent smooth surface is  $\Theta_0$ . They further assume that the volume of the drop is constant and that gravitational forces are absent. This latter condition implies that the free surface of the liquid will always be a section of a sphere. The observed angle,  $\Theta$ , for a particular configuration of the droplet measured with respect to the macroscopic horizontal is given by:

$$\Theta = \Theta_0 + \alpha \quad (1.12)$$

where  $\alpha$  is the angle of inclination of the surface at the liquid-solid contact line. Furthermore, the maximum and minimum observable contact angles are:

$$\Theta_{\max} = \Theta_0 + \alpha_{\max} \quad (1.13)$$

and

$$\Theta_{\min} = \Theta_0 - \alpha_{\max} \quad (1.14)$$

The above conditions place geometrical constraints on the system that limit the position of the edge of the drop to only two

locations in each groove where the drop can have the required volume and contact angle while maintaining its spherical shape. Thus, only a finite number of drop configurations is possible, each with its own macroscopic contact angle. The stability of each configuration is determined by its free energy and the difference in the free energy between each metastable state determines the size of the energy barrier between them. If the free energy of the system is plotted versus the contact angle, a set of metastable states is observed with a global minimum at the angle calculated from Wenzel's equation ( $\Theta'$ ) and maxima at  $\Theta_{\max}$  and  $\Theta_{\min}$ . The metastable configurations are separated by energy barriers that are greatest at  $\Theta'$  and approach zero at  $\Theta_{\max}$  and  $\Theta_{\min}$ . The experimentally observed contact angles depend on the amount of mechanical energy possessed by the drop. If the vibrational energy of a drop is greater than the energy barrier between two metastable configurations, the drop will move to the lower energy state decreasing the hysteresis. The ability of the drop to overcome energy barriers is the drop energy,  $E_d$ . It is nearly impossible to eliminate vibrations during contact angle measurements, so  $E_d$  never equals zero and consequently,  $\Theta_{\max}$  and  $\Theta_{\min}$  are never observed. As  $E_d$  increases, contact angle hysteresis decreases. If the height of the energy barrier between metastable states for particular values of  $r$  and  $\Theta_0$  is plotted versus  $\Theta$  along with  $E_d$  (which is independent of  $\Theta$ ) the intersection of the two curves yields  $\Theta_A$  and  $\Theta_R$  for each  $E_d$ . Johnson and Dettre have calculated families of hysteresis curves for  $\Theta_0 = 120^\circ$  and  $\Theta_0 = 45^\circ$  and different values of  $E_d$  as a function of the roughness ratio,  $r$ . Their results show that increasing surface

roughness increases advancing contact angles and decreases receding contact angles. Also, increasing the energy of the drop decreases the observed hysteresis such that both  $\Theta_A$  and  $\Theta_R$  approach  $\Theta'$ .

While this is a very simple model, many of the conclusions derived from the above discussions can be applied to real surfaces. The effect of going from a circular-groove model to a real surface consisting of random hills and valleys introduces more possible configurations and lowers the energy barrier between them. However, the qualitative behavior observed in both systems will be the same. The contact angle behavior described by Johnson and Dettre has been experimentally tested by a number of investigators<sup>42-44</sup> on several different rough surfaces with several different probe fluids. In all cases it was observed that as the surface roughness increased the advancing contact angle increased and the receding contact angle decreased.

It has also been observed that if the surface is very rough two different situations arise depending on the value of  $\Theta_0$ . If  $\Theta_0 < 90^\circ$  there is a critical roughness above which the liquid will spread spontaneously over the surface due to capillary forces. This critical roughness is reached when  $r = 1/\cos \Theta_0$ .<sup>30</sup> This wicking behavior has been observed in measurements of the contact angle of methanol on paraffin wax where the advancing contact angle initially increased with roughness until  $r$  exceeded 1.2 - 1.4 at which point a decrease in  $\Theta_A$  was measured.<sup>45</sup> For this system  $\Theta_0 = 42^\circ$ , so the critical roughness for wicking is predicted to be  $r = 1.35$  in agreement with the observed behavior.



Liquids with  $\Theta_o > 90^\circ$  may not be able to penetrate into the crevices of very rough surfaces. The observed macroscopic contact angle behavior results from a composite interface that consists of the solid surface under study and air trapped in the voids between the solid and the liquid drop. Cassie and Baxter<sup>46</sup> derived an equation for composite interfaces analogous to Wenzel's for surface roughness:

$$\cos \Theta' = Q_1 \cos \Theta_o - Q_2 \quad (1.15)$$

where  $Q_1 = A_{SL}/A$  and  $Q_2 = A_{LV}^c/A$ . The area  $A_{LV}^c$  refers to the area of the liquid-air interface under the drop. Equation 1.15 reduces to Wenzel's equation when  $Q_2 = 0$ . If Wenzel's and Cassie and Baxter's equations are used to plot the observed contact angle,  $\Theta'$ , as a function of the roughness ratio, their intersection yields the critical point at which a composite surface is formed. The major effect of going from a noncomposite to a composite surface is a significant reduction in the magnitude of the energy barriers between metastable states. Thus, both the advancing and receding contact angles approach the angle predicted by equation 1.15 and a reduction in hysteresis is observed. Experimental support for these discussions is provided by measurements of water contact angles on roughened paraffin and fluorocarbon waxes<sup>42</sup> and on plasma treated poly(tetrafluoroethylene).<sup>44</sup> For both of these systems it was observed that the transition from a noncomposite to a composite interface was accompanied by an increase in the receding contact angles to values near those of  $\Theta_A$  creating highly hydrophobic surfaces.

Heterogeneities in the functional groups in a surface can also cause contact angle hysteresis. The affect of surface heterogeneity on the contact angle was first addressed by Cassie,<sup>47</sup> who derived the following relationship for the observed equilibrium contact angle,  $\Theta'$ :

$$\cos \Theta' = Q_1 \cos \Theta_1 + Q_2 \cos \Theta_2 \quad (1.16)$$

where  $Q_1$  is the fraction of the surface area with contact angle  $\Theta_1$  and  $Q_2$  is the fraction with the angle  $\Theta_2$ . The derivation that led to this result assumed that the surface is composed of well-separated and distinct patches that are large compared to molecular dimensions. Using this assumption the work of adhesion between each type of patch and the liquid drop was averaged to produce the final result. Recently, Israelachvili and Gee<sup>48</sup> developed an equilibrium model that is applicable when the heterogeneities are on the order of molecular dimensions. For patches of this size, it is necessary to average the polarizabilities, dipole moments or surface charges of the two regions. Doing so results in the following relation which replaces Cassie's equation whenever the size of chemically heterogeneous patches approach molecular dimensions:

$$(1 + \cos \Theta')^2 = Q_1(1 + \cos \Theta_1)^2 + Q_2(1 + \cos \Theta_2)^2 \quad (1.17)$$

A comparison of equations 1.16 and 1.17 shows that for molecular sized patches, the Cassie equation predicts a larger contact angle than that obtained by the analysis of Israelachvili and Gee.

Neither of the analyses mentioned above pertain to dynamic contact angle measurements and neither address the issue of hysteresis caused by heterogeneities. Consider a surface that is composed of islands with intrinsically high contact angles superimposed on a continuous area with low contact angles. As a drop advances over such a surface, the edge of the liquid becomes pinned at the boundaries of the low surface energy (non-wetting) islands because of the energy barrier involved in moving the drop from the low to the high contact angle region. As a drop recedes from a heterogeneous surface, the edge of the liquid again becomes pinned at the boundary due to the same type of energy barrier. It has been suggested<sup>49</sup> that the advancing contact angle is associated with the low surface energy regions, while the receding contact angle can be correlated with the high surface energy areas, producing contact angle hysteresis. Johnson and Dettre<sup>30,50</sup> used these ideas to formulate a model consisting of concentric circular regions of alternating intrinsic contact angles,  $\Theta_1$  and  $\Theta_2$ , with  $\Theta_1 > \Theta_2$ , where the size of each region is large compared to molecular dimensions, but small compared to the size of the liquid drop. As with rough surfaces, chemical heterogeneities lead to a large number of metastable states accessible to the system and their analysis follows a similar course. The global minimum in the plot of free energy as a function of contact angle is given by Cassie's equation for equilibrium contact angles on heterogeneous surfaces. The maximum and minimum observable angles are  $\Theta_1$  and  $\Theta_2$ , respectively and the energy barriers are greatest at  $\Theta'$  and approach zero at  $\Theta_1$  and  $\Theta_2$ . Analogous to the analysis for surface roughness, the observed



advancing and receding contact angles are the result of a balance between the energy of the drop and the free energy barriers of the surface. Their analysis shows that as the vibrational energy of the liquid increases or the size of the surface heterogeneities decreases, the contact angle hysteresis decreases as both the advancing and receding contact angles approach the result predicted by equation 1.16. If the size of the patches approaches molecular dimensions the analysis of Israelachvili and Gee<sup>48</sup> predicts that the hysteresis will disappear and the equilibrium contact angle will be given by equation 1.17. If the energy of the drop is small or the heterogeneities are large, the advancing contact angle approaches  $\Theta_1$  and the receding angle approaches  $\Theta_2$ . Based on this model Johnson and Dettre<sup>30</sup> have drawn several qualitative conclusions that are pertinent to the evaluation of experimental data:

1. Advancing angles are more reproducible on predominantly low energy surfaces, while receding angles are more reproducible on high energy surfaces.

2. Advancing (receding) contact angles alone cannot fully characterize a heterogeneous surface, as both 10 and 90 % surface coverage by high (low) contact angle patches give approximately the same advancing (receding) contact angles, but very different receding (advancing) angles.

3. The advancing angle is a measure of the wettability of the low energy portion of the surface and the receding angle is more indicative of the high energy surface fraction.

Again, as in the analysis of roughened surfaces, the random heterogeneity of a real surface increases the number of metastable

configurations and decreases the energy barriers compared to the model, but the qualitative conclusions of the model should be applicable to real surfaces. A number of experimental studies of surfaces composed of wetting and non-wetting regions support these conclusions.<sup>43</sup> Most of these studies have involved partial monolayers of long chain amphiphiles, such as stearic acid or octadecylamine on glass or other inorganic surfaces using a variety of probe liquids. The results show that the advancing contact angle typically reaches its maximum value at less than 50 % surface coverage, while the receding contact angle remains low at low surface coverages and gradually increases to its maximum value when complete coverage is attained.

As discussed above both surface roughness and heterogeneity can cause significant contact angle hysteresis. However, experimental results suggest that the major cause of hysteresis is surface heterogeneity, as intentionally roughening surfaces only increases hysteresis by a few degrees. Analyses of the model systems indicate that the size of the energy barriers between the metastable states is the same for rugosities and heterogeneities of similar magnitude. Differences in the amount of hysteresis caused by each effect can be assigned to the greater possible hysteresis on heterogeneous surfaces. For heterogeneous surfaces, the maximum possible hysteresis is  $\Theta_1 - \Theta_2$ , which can be greater than  $100^\circ$ . Thus, even when the energy barriers separating the metastable states are small, the observed hysteresis can still be quite large. For rough surfaces, the maximum hysteresis is  $2\alpha_{\max}$ , which is usually less than  $10^\circ$  for polymer surfaces that have not been intentionally

roughened. Thus, even relatively large energy barriers do not result in significant hysteresis.

As discussed above, surface roughness and chemical heterogeneities give rise to thermodynamic hysteresis that can be associated with metastable configurations of the drop on the solid surface. Other major causes of hysteresis are associated with kinetic effects related to the ability of the liquid to penetrate into the solid, reorientation of the surface functional groups, or adsorption, reaction or extraction taking place at the solid-liquid interface.

If the liquid used as the probe fluid can penetrate into the solid surface considerable hysteresis is observed. The advancing angle is measured as the drop moves over the dry solid surface, while the receding angle is measured on a composite surface in which the voids between the molecules of the solid are saturated with the probe fluid. Thus, in the measurement of the receding contact angle, the liquid is interacting with a surface that is compositionally similar to itself, resulting in a much lower contact angle. If  $\Theta_A$  is measured on an area that had previously been in contact with the probe fluid (such that the same type of composite surface mentioned above exists) it will have a much lower value than that measured on the "dry" surface and a decrease in the hysteresis will be observed. Penetration may be due to specific interactions of the probe fluid with the solid and/or entropically driven diffusion in response to the infinite concentration gradient initially present. Timmons and Zisman<sup>51</sup> studied the role of molecular size and volume of the liquid on contact angle hysteresis. Their results show hysteresis can be related to the molecular volume of the liquid. The observed



hysteresis was small for liquids with molecular volumes greater than 125 cm<sup>3</sup>/g-mole and relatively large for liquids with small molecular volumes such as water (18 cm<sup>3</sup>/g-mole) that can readily penetrate into even well-packed surfaces.

Reorientation of the functional groups at the solid-liquid interface has also been suggested as a possible cause of contact angle hysteresis.<sup>52</sup> The functional groups of polymer surfaces are likely quite mobile and can easily change their conformation in response to the environment to lower interfacial free energies. Thus, the advancing contact angle is a measure of the functional groups initially present at the solid-air interface that possess one set of values for  $\gamma^{SL}$  and  $\gamma^{SV}$ . Once the liquid is in contact with the solid, the functional groups at the surface may reorganize to lower the solid-liquid interfacial free energy creating a new solid surface with different values of  $\gamma^{SL}$  and  $\gamma^{SV}$ . The receding contact angle is indicative of the functional groups present at the new solid surface interface after this reorientation.

Adsorption of components of the liquid drop to the solid-liquid interface, reaction of the probe fluid with the solid and extraction of low molecular weight portions of the solid by the liquid all cause contact angle hysteresis. It is easily imagined that each of these processes can cause changes in  $\gamma^{SL}$ ,  $\gamma^{SV}$  and/or  $\gamma^{LV}$  from the initial values that are characterized by the advancing contact angle measurement to the final values measured by the receding contact angle. The amount of hysteresis that is observed depends on the time scale of each of these processes in relation to the time scale of the measurement. A particularly interesting example of the effects

of adsorption on hysteresis is the spreading of aqueous solutions of amphiphiles on inorganic substrates.<sup>33</sup> The advancing contact angle of such a solution is low because of the high surface energy of the inorganic surface and the low surface-solution interfacial free energy. During the measurement molecules of amphiphile adsorb to the inorganic surface forming a close-packed hydrophobic monolayer. When the liquid is withdrawn from this monolayer the resulting receding contact angle is observed to be considerably higher than the initial value of  $\Theta_A$ .

From all of the above discussions it is obvious that a number of variables are involved in determining the wetting behavior of liquid on any given solid surface. Thus, correct interpretation of the results can be quite difficult. However, contact angle measurements can provide a wealth of information, especially when used in combination with other surface analytical techniques like those discussed below.

### X-ray photoelectron Spectroscopy (XPS)

Since its introduction XPS (often referred to as Electron Spectroscopy for Chemical Analysis (ESCA)) has become one of the most useful techniques for polymer surface analysis. It not only provides qualitative information concerning the functional groups present at a surface, but also their relative amounts.

The physical basis for the analysis is the photoelectric effect, where a beam of monoenergetic soft x-rays is focused on the sample, ejecting core shell electrons. While the x-ray beam passes deep into

the sample, the emitted electrons can only escape through the outer few tens of angstroms without losing their kinetic energy from inelastic collisions, thus, the technique is surface sensitive. The number of electrons emitted are then counted as a function of their energy. Each element has a unique set of core electrons so an elemental analysis is obtained. In addition, since the energy of core states is influenced by energy levels of the valence states, different functional groups give slightly different results. Thus, some specific functional group information is recorded. Quantitative information is calculated from peak areas and atomic sensitivity factors obtained from samples with known composition.

When a sample is irradiated with light of frequency,  $\nu$ , electrons are emitted with a specific kinetic energy,  $E_{KE}$ . The binding energy,  $E_{BE}$ , of the electron to its original element can then be calculated:

$$E_{BE} = h\nu - E_{KE} \quad (1.18)$$

where  $h$  is Planck's constant. Some additional terms must be added due to sample charging,  $SC$ , and the loss of kinetic energy observed as the electron moves through the detector,  $\phi$ , (the spectrophotometer work function):

$$E_{BE} = h\nu - E_{KE} - SC - \phi \quad (1.19)$$

The results reported in this work are not corrected for sample charging.



Typical binding energies for core shell photoelectrons fall in the range of 0 - 1000 eV. Thus, photon sources must produce light with an energy greater than 1000 eV or the soft x-ray range. Generally, a heated filament is used to produce electrons which are accelerated to a target anode over a potential of up to 20 kV. Impingement of the high energy electrons on the target results in the production of x-rays characteristic of the anode material. Common anode materials are magnesium, aluminum, titanium and chromium whose  $K_{\alpha}$  x-rays have energies of 1254, 1487, 4510, and 5417 eV respectively. Although the titanium and chromium x-rays have sufficient energy to eject electrons that lie in deeper core shells and can escape from deeper within the sample, only magnesium and aluminum anodes were used in this work due to their narrower line widths and their lower energy, which decreases sample damage.

The intensity of electrons detected from a particular element in a homogeneous, infinitely thick sample is the result of a number of factors which may be summarized by the following:

$$N_{i,k} = I_0 \rho_i \sigma_{i,k} \lambda_{i,k} T_{i,k} \quad (1.20)$$

where  $N_{i,k}$  is the measured peak area for the  $k$ th shell of element  $i$ ,  $I_0$  is the x-ray flux,  $\rho_i$  is the volume density of element  $i$  in the surface under study (the information desired in an XPS experiment),  $\sigma_{i,k}$  is the photoionization cross-section (the probability for photoionization),  $\lambda_{i,k}$  is the electron mean free path in the material and  $T_{i,k}$  is the instrument transmission function (the number of electrons counted compared with the number that enter the

detector).  $\sigma$ ,  $\lambda$  and  $T$  are all kinetic energy dependent and as such, are different for each element.

Each of the terms from equation 1.20 may be calculated or measured independently. However, the precision in doing so is not particularly high. Thus, quantitative information is typically obtained by calibrating the particular instrument with appropriate materials and the use of atomic sensitivity factors,  $S_{i,k}$ . From equation 1.20:

$$\rho_i = N_{i,k}/I_0\sigma_{i,k}\lambda_{i,k}T_{i,k} = N_{i,k}/S_{i,k} \quad (1.21)$$

Generally, F1s electrons are assigned a value of  $S=1.00$  and all other sensitivity factors are related to that value by measuring relative intensities of samples of known surface composition through the relation:

$$C_j = \frac{\rho_j}{\sum \rho_i} = \frac{N_j/S_j}{\sum (N_i/S_i)} \quad (1.22)$$

Where  $C_j$  is the atomic concentration of element  $j$ . Typical calibration materials used in this work are poly(tetrafluoroethylene), poly(chlorotrifluoroethylene) and poly(ethylene terephthalate). Measuring relative concentrations through Equation 1.22 as opposed to calculating  $\rho_i$  directly has two main advantages: (1) it is not necessary to know the exact x-ray flux, which usually decreases over the lifetime of the anode and (2) the ratios of the mean free paths

vary little from sample to sample even though the mean free paths themselves are highly material-dependent.

XPS has also been found to be useful in depth profiling samples which have a surface excess of one material over another. Typical examples<sup>53</sup> appear in studies of polymer blends,<sup>55</sup> block copolymers,<sup>56,57</sup> polymer adsorption,<sup>58</sup> Langmuir-Blodgett films,<sup>59,60</sup> self-assembled monolayers<sup>61,62</sup> and chemical surface modifications.<sup>63</sup> The method used is known as variable angle XPS and involves varying the takeoff angle ( $\Theta_T$ ) between the sample surface and the detector. Electrons emerging from similar vertical depths within the sample must travel through more material to reach the detector as  $\Theta_T$  decreases (Figure 1.2).

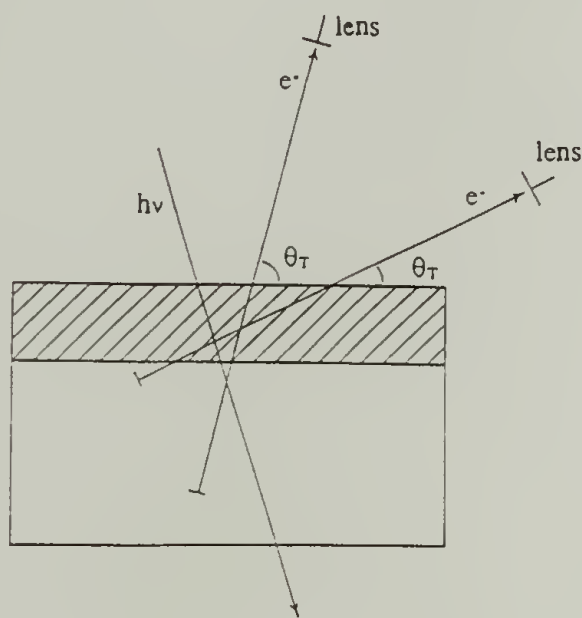


**Figure 1.2.** Variable angle XPS.

Thus, at small angles fewer electrons can escape from the deeper regions without losing their kinetic energy before reaching the detector, increasing the surface sensitivity of the technique. The



number of electrons,  $dN$ , detected from any differential depth,  $dZ$ , may be expressed as:

$$\begin{aligned} dN &= I_0 \rho \sigma T (e^{-Z/\lambda \sin \Theta_T}) dZ \\ &= k (e^{-Z/\lambda \sin \Theta_T}) dZ \end{aligned} \quad (1.23)$$

Simply integrating from 0 to a thickness,  $t$ , will provide the total number of electrons detected from that surface layer:

$$N = k \lambda \sin \Theta_T (1 - e^{-t/\lambda \sin \Theta_T}) \quad (1.24)$$

Of course, equation 1.24 reduces to equation 1.20 when  $t = \infty$  and  $\Theta_T = 90^\circ$ . This relationship implies that for a takeoff angle of  $75^\circ$ , 64.5% of the signal observed comes from  $t = \lambda$ , while 95.5% comes from  $t = 3\lambda$  and at  $15^\circ$ , 64.5% comes from  $t = 0.27\lambda$  and 95.5% from  $t = 0.80\lambda$ . Thus, 56% of the  $75^\circ$  spectrum is made up of information contained in the  $15^\circ$  spectrum. For surface modified samples, it is simple to assume a uniform overlayer of thickness,  $t_A$ , on an infinite matrix as is also shown in Figure 1.2. The intensity of the signal from region A,  $N_A$ , and from region B,  $N_B$ , may be expressed as:

$$N_A = k_A \lambda_A \sin \Theta_T (1 - e^{-t_A/\lambda_A \sin \Theta_T}) \quad (1.25)$$

$$N_B = k_B \lambda_B \sin \Theta_T (e^{-t_A/\lambda_B \sin \Theta_T}) \quad (1.26)$$

provided that the mean free path of the electrons generated in region B is the same in both A and B. To find  $t_A$ , one simply needs to

ratio the experimentally determined peak intensities (taking into account differences in cross-sections, volume densities and throughput functions for the two regions) and have a knowledge of the inelastic mean free paths.

Values for inelastic mean free paths have been obtained experimentally via a number of different overlayer techniques. In these techniques one measures the change in signal from the substrate as a function of the thickness of the overlayer. Overlayers have been deposited by Langmuir-Blodgett techniques,<sup>59,60</sup> molecular self-assembly<sup>62</sup> and vapor phase methods.<sup>64,65</sup> Inelastic mean free paths have also been calculated from experimentally determined peak intensities of standard materials and published photoionization cross-sections.<sup>66</sup> Values for  $\lambda$  in organic materials range from the relatively low values reported by Clark *et al.* (from poly(paraxylylene) overlayers on gold)<sup>64,65</sup> to the higher values of Gedman *et al.* (calculated from photoionization cross-sections),<sup>66</sup> Laibinis *et al.* (from self-assembled monolayers on metals)<sup>63</sup> and Clark *et al.*,<sup>59</sup> and Andrade *et al.*<sup>60</sup> (Langmuir-Blodgett overlayer methods). The proper values for  $\lambda$  remain somewhat controversial and likely are highly material-dependent.

Recently Ashley and coworkers<sup>67</sup> developed a theoretical model for calculating inelastic mean free paths in organic materials. Their calculations take into account differences in the electron density of different substances and differences in the kinetic energy of electrons originating from different elements.

$$\lambda = \frac{M}{\rho n} E_K / (13.6 \ln(E_K) - 17.6 - 1400/E_K) \quad (1.27)$$

where  $M$  is the molecular weight of the molecule or repeat unit,  $\rho$  is the density of the material,  $n$  the number of valence electrons in the repeat unit and  $E_K$  the electron kinetic energy in eV. For PCTFE this equation yields values of  $\lambda$  for carbon of 23.8 Å for Al  $K_\alpha$  x-rays and 20.1 Å for Mg  $K_\alpha$  x-rays. Throughout this dissertation a value of  $\lambda = 14$  Å for carbon, as determined by Clark *et al.*<sup>64,65</sup> for poly(paraxylylene) overlayers on gold with Mg  $K_\alpha$  x-rays (the only excitation source used in this dissertation for quantitative depth profiling), is used. This result was chosen because it is the most consistent experimental value of  $\lambda$  to date for electrons traveling through amorphous polymers. From the earlier discussion this value can be used to calculate that a 15° takeoff angle assays the outer 10 Å and a 75° takeoff angle assays the outer 42 Å.

Further information of the identity and concentration of functional groups present in a modified polymer surface may be obtained in XPS analysis through the use of derivatization reactions. Derivatization is often necessary because surface modifications often introduce a wide variety of functional groups. In many cases particular peaks in an XP spectrum may correspond to more than one type of functional group. The identity of the functional groups that are present may be ascertained by treating the material with a reagent which selectively reacts with a specific functional group and which contains an XPS label which is easily observed and hopefully may be quantified. A great deal of work has been published in which XPS derivatization techniques have been used and discussed<sup>68,69</sup>. Ideally XPS labelling reactions should be functional



group specific, proceed quantitatively throughout the XPS sampling depth, introduce an element which has a high sensitivity for detection and is unique to that surface, and proceed under reasonably mild conditions.

From these discussions it has been shown that XPS is likely the single most useful technique in polymer surface analysis. The method has been used extensively in this work to identify the presence of different functional groups in a modified surface, the extent of modification and in some cases the depth of modification.

#### Attenuated Total Reflectance Infrared Spectroscopy (ATR-IR)

In order to obtain information more conventional to organic chemists, ATR-IR was utilized to record infrared spectra of the modified surfaces prepared in this thesis. Spectra were obtained on an IBM 38 FTIR at 4 cm<sup>-1</sup> resolution fitted with a micro-ATR accessory. The internal reflectance element (IRE) used was a 10x5x1mm Germanium ( $n = 4.0$ ) single crystal with an entrance angle of 45°. The IRE was cleaned before use by gently rubbing with a cotton-tipped applicator wetted with methylene chloride. Spectra were acquired by clamping the film sample tightly to both sides of the IRE and ratioed against a background of the IRE to calculate transmittance. Experimental difficulty is mainly associated with reproducing the contact between the sample and the IRE. Thus, quantitative information is difficult to reproduce, but qualitative results are excellent, provided the modified layer is thick enough.

The theoretical background behind ATR spectroscopy has been well developed by Harrick<sup>70</sup> and others.<sup>71,72</sup> The technique is based

on the phenomenon that when light strikes an interface between optically denser and rarer media above a certain angle (the critical angle,  $\Theta_c$ ), it is totally reflected. The critical angle can be calculated from:

$$\Theta_c = \sin^{-1} n_{21} \quad (1.28)$$

where  $n_{21} = n_2/n_1$  and  $n_2$  is the refractive index of the rarer medium and  $n_1$  is the refractive index of the denser medium through which the light propagates. For total internal reflection, the electric field amplitude at the interface, but in the rarer medium, may be expressed for unit incoming  $\parallel$  and  $\perp$  polarization as:

$$E_{y0} = \frac{2\cos\Theta}{(1-n_{21}^2)^{1/2}} \quad (1.29)$$

$$E_{x0} = 2 \frac{(\sin^2\Theta - n_{21}^2)^{1/2}\cos\Theta}{(1-n_{21}^2)^{1/2}[(1+n_{21}^2)\sin^2\Theta - n_{21}^2]^{1/2}} \quad (1.30)$$

$$E_{z0} = \frac{2\sin\Theta\cos\Theta}{(1-n_{21}^2)^{1/2}[(1+n_{21}^2)\sin^2\Theta - n_{21}^2]^{1/2}} \quad (1.31)$$

Where the coordinate system is defined as a right-handed system where  $x$  lies along the propagation direction and positive  $z$  is normal to the surface into the rarer medium.  $E_{y0}$  represents the electric field amplitude for perpendicular polarization while parallel polarization is given by:

$$E_{\parallel} = (|E_{x0}|^2 + |E_{z0}|^2)^{1/2} \quad (1.32)$$

An important result of these equations is that at the reflecting interface E fields exist in all spatial directions. Thus, unlike in normal transmission spectroscopy, where E fields only exist perpendicular to the direction of propagation and dipoles oriented parallel to the propagating direction do not absorb energy, in reflection spectroscopy dipoles will absorb energy regardless of their orientation.

It follows from these equations that an electromagnetic field exists in the rarer medium whose amplitude decreases exponentially from the surface:

$$E = E_0 e^{-z/d_p} \quad (1.33)$$

The depth of penetration,  $d_p$ , is defined as the distance where the electric field falls to  $1/e$  of its original value and may be expressed as:

$$d_p = \frac{\lambda_1}{2\pi(\sin^2\Theta - n_2^2)^{1/2}} \quad (1.34)$$

where  $\lambda_1$  is the wavelength of light in the denser medium. Inserting values for  $n_1$  (germanium,  $n = 4.0$ ),  $n_2$  (PCTFE,  $n = 1.43$ ) and  $\Theta = 45^\circ$  yields  $d_p = 0.2609 \lambda_1$  or  $0.87 \mu\text{m}$  at  $3000 \text{ cm}^{-1}$  and  $1.74 \mu\text{m}$  at  $1500 \text{ cm}^{-1}$ .

In the presence of an absorbing rarer medium the reflectivity drops to less than 100% due to the interaction of the electric field



with the material. The reflection loss due to this interaction does not follow a simple relation, but may be calculated rigorously with a computer. A simplifying assumption may be made which yields more physical insight into the interaction of the penetrating field with the absorbing medium. When the interaction is weak (where the absorption loss is less than 10% per reflection) the strength of the interaction can be expressed as an effective thickness,  $d_e$ , which represents the actual thickness of a film that would give the same absorption in a transmission measurement as the absorption obtained from a single reflection measurement (the spectra recorded in this dissertation utilized 10 reflections).

The effective thicknesses can be expressed as:

$$d_e = \frac{n_{21}}{\cos\Theta} \int E^2 dz \quad (1.35)$$

where  $E = E_0 e^{-z/d_p}$ .

For materials whose thickness is much greater than the penetration depth of the evanescent field, integrating from 0 to  $\infty$  yields:

$$d_e = \frac{n_{21} E_0^2 d_p}{2 \cos\Theta} \quad (1.36)$$

The net effect of all these factors is to give an increase in the effective thickness with a decrease in  $\Theta$ , an increase in  $n_{21}$  and an increase in  $\lambda$ . The  $1/\cos\Theta$  term is to account for the change in sample area with  $\Theta$ . Upon substituting the appropriate expressions for  $d_p$

and  $E_0^2$  the effective thicknesses for perpendicular and parallel polarizations in a semi-infinite, bulk sample are:

$$d_{e\perp} = \frac{\lambda_1 n_{21} \cos \Theta}{\pi(1 - n_{21}^2)(\sin^2 \Theta - n_{21}^2)^{1/2}} \quad (1.37)$$

$$d_{e\parallel} = \frac{\lambda_1 n_{21} \cos \Theta (2 \sin^2 \Theta - n_{21}^2)}{\pi(1 - n_{21}^2)[(1 + n_{21}^2) \sin^2 \Theta - n_{21}^2](\sin^2 \Theta - n_{21}^2)^{1/2}} \quad (1.38)$$

From these expressions, it is seen that  $d_e$  is different for the two polarizations, being greater for parallel polarized light.

Inserting values for  $n_1$  (germanium,  $n = 4.0$ ),  $n_2$  (PCTFE,  $n = 1.43$ ) and  $\Theta = 45^\circ$ , these two equations reduce to:

$$d_{e\perp} = 0.1512\lambda_1 \quad (1.39)$$

$$d_{e\parallel} = 0.3024\lambda_1 \quad (1.40)$$

Thus at  $3000 \text{ cm}^{-1}$   $d_{e\perp}$  and  $d_{e\parallel}$  are  $0.50 \text{ }\mu\text{m}$  and  $1.0 \text{ }\mu\text{m}$ , respectively, while at  $1500 \text{ cm}^{-1}$  the effective thicknesses are  $1.01 \text{ }\mu\text{m}$  and  $2.02 \text{ }\mu\text{m}$ , respectively. Thus, for two bands which have equal intensity in a transmission spectrum, the longer wavelength band will be more intense in an internal reflection spectrum when the thickness of the sample is large.

For surface modified samples, three media are involved: (1) the IRE, with refractive index  $n_1$ , (2) the modified layer, with refractive index  $n_2$  and (3) the bulk polymer with refractive index  $n_3$ . If the modified layer thicknesses,  $t$ , is much less than the

penetration depth, the electric field can be assumed to be relatively constant throughout the modified layer (this assumption is valid to within a few percent when  $2\pi t/\lambda_1 < 0.1$ , i.e.  $t < 800 \text{ \AA}$  when  $\lambda_1 = 2000 \text{ cm}^{-1}$ ). Thus,

$$d_e = \frac{n_{21}E_0^2t}{\cos\Theta} \quad (1.41)$$

Expressions similar to Equations 1.37 and 1.38 can be derived for this set of conditions that show that the electric fields in the modified layer are controlled by the IRE and the bulk unreacted polymer, rather than by the thin modified layer. The important result of these equations is that the effective thickness measured for the surface modified layer is proportional to the thickness of the modified layer, rather than the depth of penetration. The consequence of this result is that, unlike the bulk material, the absorption bands from thin modified layers are not relatively stronger at longer wavelengths and thus internal reflection spectra of these layers will closely resemble those of transmission spectra.

### References and Notes

- (1) For a review see Clark, D.T. and Feast, W.J. *Polymer Surfaces*, Wiley-Interscience: New York, 1978.
- (2) For a review of polymer surface modifications see Ward, W.J. and McCarthy, T.J. In *Encyclopedia of Polymer Science and Engineering*, 2nd ed.; Supplement, Wiley: New York, 1989, pp.674 - 689.
- (3) Oster, G. and Shibata, O. *J. Polym. Sci.*, **1957**, 26, 233.



- (4) Yamamoto, F. and Yamakawa, S. *J. Polym. Sci.: Polym. Phys. Ed.*, **1979**, *17*, 1581.
- (5) Briggs, D.; Brewis, D.M. and Konieczko, M.B. *J. Mat. Sci.*, **1979**, *14*, 1344.
- (6) Clark, D.T. and Wilson, R. *J. Polym. Sci.: Polym. Chem. Ed.*, **1983**, *21*, 837.
- (7) Collins, G.C.S.; Lowe, A.C. and Nicholas, D. *Eur. Polym. J.*, **1973**, *9*, 1173.
- (8) Rossman, K. *J. Polym. Sci.*, **1956**, *19*, 141.
- (9) Amouroux, J.; Goldman, M. and Revoil, M.F. *J. Polym. Sci.: Polym. Chem. Ed.*, **1982**, *20*, 1373.
- (10) Dwight, D.W. and Riggs, W.M. *J. Colloid Interface Sci.*, **1974**, *47*, 650.
- (11) Barker, D.J.; Brewis, D.M. and Dahm, R.H. *J. Materials. Sci.*, **1979**, *14*, 749.
- (12) Rasmussen, J.R.; Stedronsky, E.R. and Whitesides, G.M. *J. Am. Chem. Soc.* **1977**, *99*, 4736.
- (13) Baszkin, A. and Ter-Minassian-Saraga, L. *J. Polym. Sci.: Part C*, **1971**, 243.
- (14) Franchina, N.L. and McCarthy, T.J. *Macromolecules*, **1991**, *24*, 3045.
- (15) Costello, C.A. and McCarthy, T.J. *Macromolecules*, **1987**, *20*, 2819.
- (16) (a) Brennan, J.V. and McCarthy, T.J. *Polym. Prepr. (Am. Chem. Soc., Div. Polym. Chem.)* **1987**, *29(2)*, 338. (b) Brennan, J.V. and McCarthy, T.J. *Polym. Prepr. (Am. Chem. Soc., Div. Polym. Chem.)* **1989**, *30(2)*, 152.
- (17) Bening, R.C. and McCarthy, T.J. *Macromolecules* **1990**, *23*, 2648.
- (18) Dias, A.J. and McCarthy, T.J. *Macromolecules* **1985**, *18*, 1826.

- (19) Dias, A.J. and McCarthy, T.J. *Macromolecules* **1987**, *20*, 2068.
- (20) Dias, A.J. Ph.D. dissertation, University of Massachusetts, 1987.
- (21) Lee, K.-W. and McCarthy, T.J. *Macromolecules* **1988**, *21*, 3353.
- (22) Kolb, B.U.; Patton, P.A.. and McCarthy, T.J. *Macromolecules* **1990**, *23*, 366.
- (23) **Aclar Technical Data**, Allied-Signal Chemical Corp. Morristown, New Jersey.
- (24) Danielson, N.D.; Taylor, R.T.; Huth, J.A.; Siergiej, R.W.; Galloway, J.G. and Paperman, J.B. *Ind. Eng. Chem. Prod. Res. Dev.*, **1983**, *22*, 303.
- (25) Langmuir, I. *J. Am. Chem. Soc.* **1916**, *38*, 2221.
- (26) Young, T. (a) *Phil. Trans.*, **1805**, *95*, 65 and (b) *Phil. Trans.*, **1805**, *95*, 82.
- (27) Gibbs, J.W. *The Collected Works of J. Willard Gibbs, Volume 1, Thermodynamics*, Yale University Press: New Haven, 1928.
- (28) For reviews see references 29 - 32. Also, see reference 38 and references therein.
- (29) Fowkes, F.M.. Ed. *Contact Angle, Wettability and Adhesion*, Advances in Chemistry Series, No. 43, American Chemical Society: Washington, D.C. 1964.
- (30) Johnson, R.E., Jr. and Dettre, R. H. In *Surface and Colloid Science*, Vol 2, Matijevic, E., Ed., Wiley-Interscience: New York, 1969.
- (31) Cherry, B.W. *Polymer Surfaces*, Cambridge University Press: Cambridge, Great Britain, 1981.
- (32) Andrade, J.D., Ed. *Surface and Intefacial Aspects of Biomedical Polymers, vol. 1: Surface Chemistry and Physics*; Plenum: New York, 1985.
- (33) See Zisman in reference 29 pp. 1 - 51 for general discussions.

- (34) Girifalco, L.A. and Good, R.J. *J. Phys. Chem.*, **1957**, 61, 904.
- (35) Fowkes, F.M. *Ind. Eng. Chem.*, **1964**, 56, 40.
- (36) Owens, D.K. and Wendt, R.C. *J. Appl. Poly. Sci.*, **1969**, 13, 1741.
- (37) Wu, S. *J. Adhesion*, **1973**, 5, 39.
- (38) van Oss, D.J.; Good, R.J. and Chaudhury, M.K. *Langmuir*, **1988**, 4, 884.
- (39) Andrade, J.D.; King, R.N.; Gregonis, D.E. and Coleman, J. *Poly. Sci. Symp*, **1979**, 66, 313.
- (40) Wenzel, R.N. *Ind. Eng. Chem.*, **1936**, 28, 988.
- (41) See Johnson, R.E., Jr. and Dettre, R.H. in reference 29 pp. 112 - 135.
- (42) See Johnson, R.E., Jr. and Dettre, R.H. in reference 29 pp. 136 - 144 and references therein.
- (43) See reference 30 and references therein.
- (44) Mora, M.; Occhiello, E. and Garbassi, F. *Langmuir*, **1989**, 5, 872.
- (45) Bartell, F.E. and Shepard, J.W. *J. Phys. Chem.*, **1953**, 57, 458.
- (46) Cassie, A.B.D. and Baxter, S. *Trans. Faraday Soc.*, **1944**, 40, 546.
- (47) Cassie, A.B.D. *Disc. Faraday Soc.*, **1948**, 3, 11.
- (48) Israelachvili, J.N. and Gee, M.L. *Langmuir*, **1989**, 5, 288.
- (49) Pease, D.C. *J. Phys. Chem.*, **1945**, 49, 107.
- (50) Johnson, R.E., Jr. and Dettre, R.H. *J. Phys. Chem.*, **1964**, 68, 1744.
- (51) Timmons, C.O. and Zisman, W.A. *J. Colloid Interface Sci.*, **1966**, 165.
- (52) Langmuir, I. *Science*, **1938**, 87, 493.



- (53) A review of XPS is provided by references 32 and 54 with a number of examples.
- (54) Clark, D.T. and Feast, W.J., *J. Macromol. Sci.-Revs. Macromon. Chem.*, **1975**, *12*, 191.
- (55) (a) Schmidt, J.J.; Gardella, J.A., Jr. and Salvati, L., Jr. *Macromolecules*, **1989**, *22*, 4489. (b) Clark, M.B., Jr.; Burkhardt, C.A. and Gardella, J.A., Jr. *Macromolecules*, **1989**, *22*, 4495.
- (56) Thomas, H.R. and O'Malley, J.J., *Macromolecules*, **1979**, *12*, 323.
- (57) O'Malley, J.J.; Thomas, H.R. and Lee, G.M., *Macromolecules*, **1979**, *12*, 996.
- (58) Parsonage, E.; Tirrell, M.; Watanabe, H. and Nuzzo, R.G. *Macromolecules* **1991**, *24*, 1987.
- (59) Clark, D.T., Fok, Y.C.T. and Roberts *J. Electron Spectr.*, **1981**, *22*, 173.
- (60) Hall, S.M., Andrade, J.D., Ma, S.M. and King, R.N. *J. Electron Spectr.*, **1979**, *17*, 181.
- (61) Troughton, E.B., Bain, C.D., Whitesides, G.M., Nuzzo, R.G., Allara, D.L. and Porter, M.D. *Langmuir*, **1988**, *4*, 365.
- (62) Laibinis, P.E.; Bain, C.D. and Whitesides, G.M. *J. Phys. Chem.*, **1991**, *95*, 7017.
- (63) See references 2, 14 - 22, 32 and 54.
- (64) Clark, D.T., Thomas, H.R. and Shuttleworth, D. *J. Polym. Sci., Polym. Lett.*, **1978**, *16*, 465.
- (65) Clark, D.T. and Thomas, H.R. *J. Polym. Sci., Chem.*, **1977**, *15*, 2843.
- (66) Cadman, P., Gossedge, G. and Scott, J.D. *J. Electron Spectr.*, **1978**, *13*, 1.

- (67) Ashley, J.C. *IEEE Trans. Nucl. Sci.*, **1980**, NS-27, 1454.
- (68) Riggs, W. and Dwight, D.J. *J. Electron Spectr.*, **1974**, 5, 447.
- (69) Miller, D.R. and Nikolaos, A.P. *J. Macromol Sci.-Rev. Macromol. Chem and Phys.*, **1986**, C26(1), 33.
- (70) Harrick, N.J. *Internal Reflection Spectroscopy*, Wiley Interscience: New York, **1967**.
- (71) Mirabella, F.M. Jr. *Applied Spectroscopy Reviews*, **1985**, 21(1&2), 45.
- (72) Muller, G., Abraham, K. and Schaldach, M. *Applied Optics*, **1981**, 20(7), 1182.

## CHAPTER II

# PREPARATION OF A REACTIVE CARBOXYLIC ACID FUNCTIONALIZED SURFACE

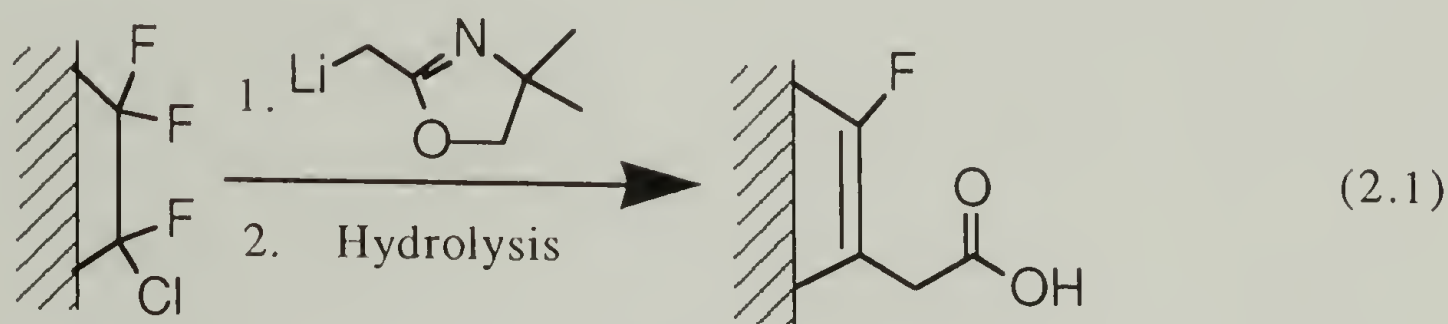
### Introduction

Carboxylic acid functionalized polymer surfaces have been prepared and extensively studied over the past 15 years.<sup>1-10</sup> The techniques used to conduct these surface modifications are typically chemical oxidations, corona discharge or plasma treatments. There are a number of inherent problems with these modified surfaces if one wishes to correlate surface structures with surface properties. For example, these modifications often introduce additional functionality (usually alcohols and ketones) other than carboxylic acids into the surface. These "impure" surfaces make characterization of further derivatives difficult and assignments of changes in surface properties to a particular change in surface chemistry impossible. In addition, most of these modifications are corrosive, resulting in a surface that is highly pitted, again, making surface structure-property correlations tenuous.

Previous work in the McCarthy research group has investigated the preparation of carboxylic acid-functionalized surfaces by a number of methods.<sup>7-12</sup> Some of these involve multistep syntheses<sup>11,12</sup> yielding surfaces containing a multitude of functional groups like those mentioned above. One method,<sup>10</sup> results in a

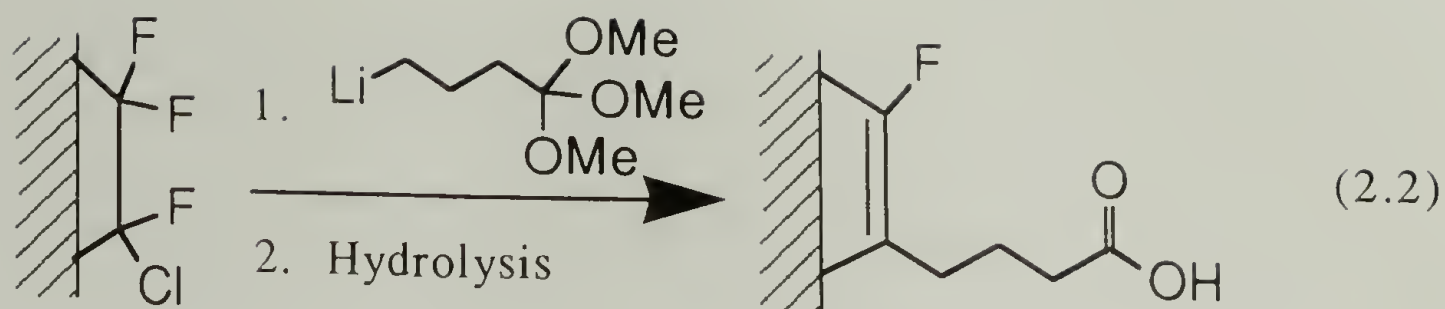


surface which contains a very low density of carboxylic acids (approximately 1  $\text{-CO}_2\text{H}$  for every 12 - 16 repeat units) in a thinly modified layer ( $<10 \text{ \AA}$ ) making characterization of further modifications difficult. This modification is also limited because the modified layer thickness cannot be varied. A direct method of preparing densely functionalized acid surfaces with controlled thicknesses was attempted through PCTFE-organolithium chemistry using 4,4-dimethyloxazoline as the acid protecting group (Equation 2.1).<sup>7,8</sup>



This particular modification has not proven to be as useful for further transformations as hoped. The subsequent deprotection proceeds in high yield (75 - 90 %), but is not quantitative under a wide variety of conditions. Furthermore, a number of esterification reactions attempted on the acid resulted in either no observable products or very low yields ( $<30 \%$ ). A consistent explanation for this low reactivity is that the acid group is separated from the polymer backbone by only a single methylene unit, placing a steric constraint at the reactive site.

In this work an alternative preparation of an acid-functionalized PCTFE surface is presented (Equation 2.2).



Trimethyl 4-lithioorthobutyrate has been chosen as the surface modification reagent for four reasons: (1) the corresponding bromoorthoester is commercially available facilitating the synthesis of the lithium reagent, (2) orthoesters are often used as protecting groups for acids and are easily hydrolyzed to the corresponding acid,<sup>13</sup> (3) the depth of the reaction may be varied by simply changing the reaction temperature<sup>7</sup> and (4) it is anticipated that the three carbon spacer between the polymer backbone and the functional group will make the surface more reactive to traditional carboxylic acid chemistry. A PCTFE hydroxyl surface which also contains a three carbon spacer has been shown to undergo a number of transformations familiar to solution organic chemistry.<sup>14</sup>

The objectives of this work are: (1) to confirm that the orthoester functionality can be added to the PCTFE surface and to study the modification depth as a function of reaction temperature, (2) to prove that the orthoester can be hydrolyzed to the acid in high yield and (3) to show that this carboxylic acid surface is reactive.

## Experimental

### General

PCTFE film (5-mil from Allied Aclar 33C) was extracted in refluxing dichloromethane for 2 h and dried (0.05 mm, room temp., >24 h). Films for gravimetric analysis were dried (0.05 mm, 70 °C) for three days. Heptane (Aldrich) was distilled under nitrogen from calcium hydride. Tetrahydrofuran (THF) (Aldrich, anhydrous) was distilled under nitrogen from sodium/benzophenone. Trimethyl 4-bromoorthobutyrate (BrTMOB) (Aldrich) was distilled under vacuum (trap-to-trap) from potassium carbonate and stored under nitrogen over potassium carbonate. *tert*-Butyllithium (*t*-BuLi) (Aldrich, 1.7 M in pentane) was standardized by titration with biphenylmethanol in THF at -78 °C.<sup>15</sup> Potassium chlorate (Alfa) was used as received. Thallous ethoxide (Aldrich) was filtered through a 0.5 µm PTFE filter under nitrogen immediately before use. Ethanol was distilled under nitrogen from magnesium turnings. Thionyl chloride, 1-octanol and heptafluorobutyryl chloride (HFBC) (all Aldrich) were distilled (trap-to-trap) and stored under nitrogen. *p*-Toluenesulfonic acid monohydrate (Aldrich) was dehydrated by azeotropic distillation of the water with benzene and recrystallized from benzene. Methanol, dichloromethane (both Fisher, HPLC Grade), THF (Aldrich) and water (house distilled, redistilled with a Gilmont Still) used as wash solvents were sparged with nitrogen. Other reagents were obtained from Aldrich and used as received. X-ray photoelectron spectra (XPS) were obtained with a Perkin Elmer-Physical Electronics 5100 with Mg K<sub>α</sub> excitation (400 W, 15.0 kV).



Binding energies shown are not corrected for sample charging. Spectra were routinely recorded at two takeoff angles ( $\Theta_T$ ):  $15^\circ$  and  $75^\circ$  (measured between the film surface plane and the analyzer).<sup>16</sup> XPS atomic composition data were determined using sensitivity factors obtained from measurements made on samples of known surface composition: F1s, 1.00; C1s, 0.225; O1s, 0.620; N1s, 0.392 and Cl2p, 0.655. Attenuated Total Reflectance Infrared (ATR-IR) spectra were obtained on an IBM 38 FTIR at  $4\text{ cm}^{-1}$  resolution using a  $10\times5\times1\text{ mm}$  germanium internal reflection element with an entrance angle of  $45^\circ$ . UV-vis spectra were acquired on a Perkin Elmer Lambda 2 optics bench and data manipulated with an IBM PS/2 using Perkin Elmer PECSS UV-vis software. Spectra were recorded using an unreacted sample of PCTFE as the reference. Gravimetric measurements were made on a Cahn 29 Automatic Electrobalance. Dynamic advancing ( $\Theta_A$ ) and receding ( $\Theta_R$ ) contact angles were measured with a Ramé-Hart telescopic goniometer as the probe fluid was added to ( $\Theta_A$ ) and removed from ( $\Theta_R$ ) the sample surface with a Gilmont syringe fitted with a 24 gauge flat-tipped needle. Results are reported as  $\Theta_A/\Theta_R$ . Probe fluids used were water purified as described above or buffered pH solutions prepared by a published procedure<sup>18</sup> and adjusted to the desired pH utilizing a Fisher 825MP pH meter.

#### Trimethyl 4-lithioorthobutyrate (LiTMOB)

BrTMOB (3.05 g, 13.4 mmol) was added via syringe to a dried nitrogen-purged reaction flask containing a glass-coated magnetic stir bar. Heptane (46 mL) was added and the solution cooled to

-78 °C (a small amount of BrTMOB precipitates from the solution at this temperature). *t*-BuLi (1.7 M, 7.8 mL, 13.3 mmol) in heptane (32 mL), also at -78 °C, was then added slowly to the BrTMOB solution via cannula. The mixture was stirred at this temperature for 15 min and then placed in a -20 °C bath for 30 min. The resulting white suspension was then cooled to -78 °C and THF (86 mL, also at -78 °C) was added to dissolve the precipitate. (Notebook T5P39)

#### Reaction of LiTMOB with PCTFE Film (PCTFE-TMOB)

A nitrogen-purged Schlenk tube containing PCTFE film was equilibrated to the desired reaction temperature. (Reactions were conducted at temperatures of -78, -67, -51, -26, and -17 °C.) A solution of LiTMOB in heptane/THF (prepared as described above) at the same temperature was then added via cannula to cover the film. After 30 min the reagent solution was removed and the film was washed with methanol (1x at the reaction temperature), methanol (3x), H<sub>2</sub>O (3x), methanol (3x) and then dichloromethane (3x) and dried (0.05 mm, >24 h). Films for gravimetric analysis were dried more extensively (0.05 mm, 70 °C, 3 days). (Notebook T5P39)

#### Oxidation of PCTFE-TMOB

PCTFE-TMOB films were placed in a solution of 1.0 g of KClO<sub>3</sub> in 50 mL of concentrated H<sub>2</sub>SO<sub>4</sub> for 2 h. The films were then removed, rinsed with distilled water, soaked in distilled water for 2 h, in methanol for 2 h, in dichloromethane for 1 h and dried (0.05 mm, 70 °C, 3 days). (Notebook T5P125)

### Hydrolysis of PCTFE-TMOB (PCTFE-CO<sub>2</sub>H)

To a nitrogen-purged, jacketed (for reflux) Schlenk tube containing PCTFE-TMOB (prepared at -17 °C) film and PTFE boiling chips a solution of CF<sub>3</sub>CO<sub>2</sub>H:acetone:H<sub>2</sub>O (5:20:80 mL) was added via cannula. The reaction mixture was then heated to reflux. After 24 h, the solution was removed and the film was washed with H<sub>2</sub>O (3x), methanol (3x) and then dichloromethane (3x) and dried (0.05 mm, >24 h). (Notebook T5P65)

### Labelling of PCTFE-CO<sub>2</sub>H with Thallium

PCTFE-CO<sub>2</sub>H was immersed in neat thallos ethoxide at room temperature in a nitrogen-purged glove bag for 2 min, soaked in ethanol for 2 h and then washed with ethanol (3x) and dried (0.05 mm, >24 h). (Notebook T5P77)

### Acid Catalyzed Esterification of PCTFE-CO<sub>2</sub>H (PCTFE-CO<sub>2</sub>Oct<sup>A</sup>)

To a nitrogen-purged, jacketed Schlenk tube containing PCTFE-CO<sub>2</sub>H film, PTFE boiling chips and 1.0 g of *p*-toluenesulfonic acid, 20 mL of THF was added followed by 5 mL of 1-octanol. The reaction mixture was then heated to reflux. After 24 h, the solution was removed and the film was washed with THF (5x), H<sub>2</sub>O (5x), methanol (3x) and then dichloromethane (3x) and dried (0.05 mm, >24 h). (Notebook T6P21)



#### Esterification of PCTFE-CO<sub>2</sub>H via the Acid Chloride (PCTFE-CO<sub>2</sub>Oct<sup>B</sup>)

To a nitrogen-purged Schlenk tube containing PCTFE-CO<sub>2</sub>H film, 25 mL of THF was added followed by 3 mL of thionyl chloride. After 24 h at room temperature, the solution was removed and 20 mL of THF was added followed by 5 mL of 1-octanol. The reaction was allowed to proceed for 24 h and the film was washed with THF (5x), methanol (3x) and then dichloromethane (3x) and dried (0.05 mm, >24 h). (Notebook T6P37)

#### Esterification of PCTFE-CO<sub>2</sub>H via the Imidazolid (PCTFE-CO<sub>2</sub>Oct<sup>C</sup>)

To a nitrogen-purged Schlenk tube containing PCTFE-CO<sub>2</sub>H film 1.0 g of carbonyldiimidazole (CDI) was added in a glove box. THF (25 mL) was then added and the solution brought to reflux. After 24 h, the CDI solution was removed via cannula and 25 mL of THF was added followed by 5 mL of 1-octanol. After 40 h at reflux, the solution was removed and the film was washed with THF (5x), methanol (3x) and then dichloromethane (3x) and dried (0.05 mm, >24 h). (Notebook T6P61)

#### Reduction of PCTFE-CO<sub>2</sub>H (PCTFE-OH\*)

To a nitrogen-purged Schlenk tube containing PCTFE-CO<sub>2</sub>H film 25 mL of BH<sub>3</sub>·THF (1.0 M in THF) was added. The film was allowed to react for 24 h at room temperature under nitrogen and then washed with THF (5x) and H<sub>2</sub>O (5x). The film was then soaked in a solution of CH<sub>3</sub>CO<sub>2</sub>H:THF (5:20 mL) for 24 h and washed with THF (5x), H<sub>2</sub>O (5x), methanol (3x) and then dichloromethane (3x) and dried (0.05 mm, >24 h). (Notebook T5P113)

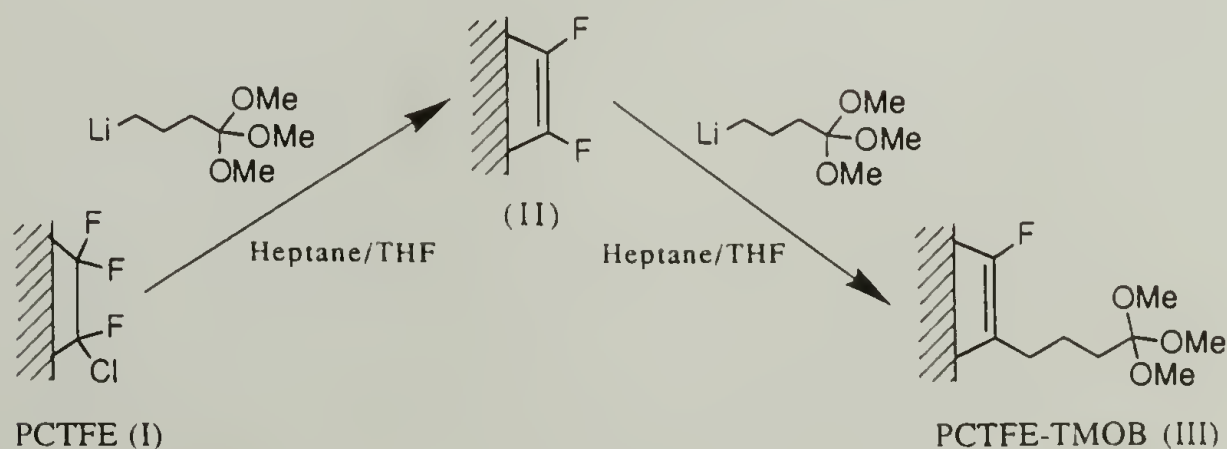
## Labelling of PCTFE-OH with Heptafluorobutyryl Chloride (PCTFE-OHFB\*)

To a nitrogen-purged Schlenk tube containing PCTFE-OH film, 25 mL of THF was added followed by 1.1 mL of HFBC. The film was allowed to react for 24 h under nitrogen and then washed with THF (5x) and then dichloromethane (3x) and dried (0.05 mm, >24 h). (Notebook T6P5)

## Results and Discussion

### Initial Modification (PCTFE-TMOB)

The mechanism and the temperature, solvent and alkyllithium structure dependencies of the reaction of PCTFE film with organolithium reagents have been described in detail.<sup>7,19-21</sup> The protected-carboxylic acid-containing lithium reagent, trimethyl 4-lithioorthobutyrate (LiTMOB) is conveniently prepared by lithium-halogen exchange between BrTMOB and *tert*-butyllithium in heptane and is soluble in THF/heptane mixtures. PCTFE film reacts with LiTMOB in THF/heptane (50:50) by the reduction-addition-elimination reaction described in Scheme 2.1. This solvent ratio



**Scheme 2.1.** Reaction of PCTFE with LiTMOB.

was chosen in order to make comparisons with other PCTFE-organolithium modifications.<sup>7</sup> One of the objectives of this research was to control the modified layer thickness by varying the reaction temperature in this initial modification. Thus, the reaction was run at five different temperatures (-78, -67, -51, -26 and -17 °C) for 30 min and the effects on the modified layer assessed. Water contact angle analysis of the reacted film samples (Table 2.1) indicates that a more hydrophilic surface has been produced. PCTFE is a hydrophobic material and as such exhibits high water contact angles (104°/77°). Upon introduction of the relatively polar trimethyl orthobutyrate group the contact angles decrease (73°-78°/48°-49°). These results are essentially independent of reaction temperature suggesting that the surface structure accessible to contact angle measurements is the same for each modification temperature.

**Table 2.1.** Water contact angle data ( $\Theta_A/\Theta_R$ ) for modified PCTFE surfaces.

<u>Surface</u>	<u><math>\Theta_A/\Theta_R</math></u>
PCTFE	104°/77°
PCTFE-TMOB (-78 °C)	76/49
PCTFE-TMOB (-67 °C)	77/49
PCTFE-TMOB (-51 °C)	78/48
PCTFE-TMOB (-26 °C)	76/49
PCTFE-TMOB (-17 °C)	73/48
PCTFE-CO <sub>2</sub> H	55/0
PCTFE-CO <sub>2</sub> Oct <sup>A</sup>	98/47
PCTFE-CO <sub>2</sub> Oct <sup>B</sup>	100/45
PCTFE-CO <sub>2</sub> Oct <sup>C</sup>	98/49
PCTFE-OH*	62/22
PCTFE-OHFB*	89/47



Information concerning the modified surface structure may be obtained from the XPS spectra. Figures 2.1 and 2.2 show XPS survey and C1s spectra for PCTFE and PCTFE-TMOB prepared at -78 and -17 °C (75° takeoff angle). In agreement with the chemistry depicted in Scheme 2.1, the survey spectra of the reacted films indicate a decrease in fluorine and chlorine intensity (chlorine is almost completely removed at -17 °C), an increase in carbon intensity and the incorporation of oxygen into the film surface.

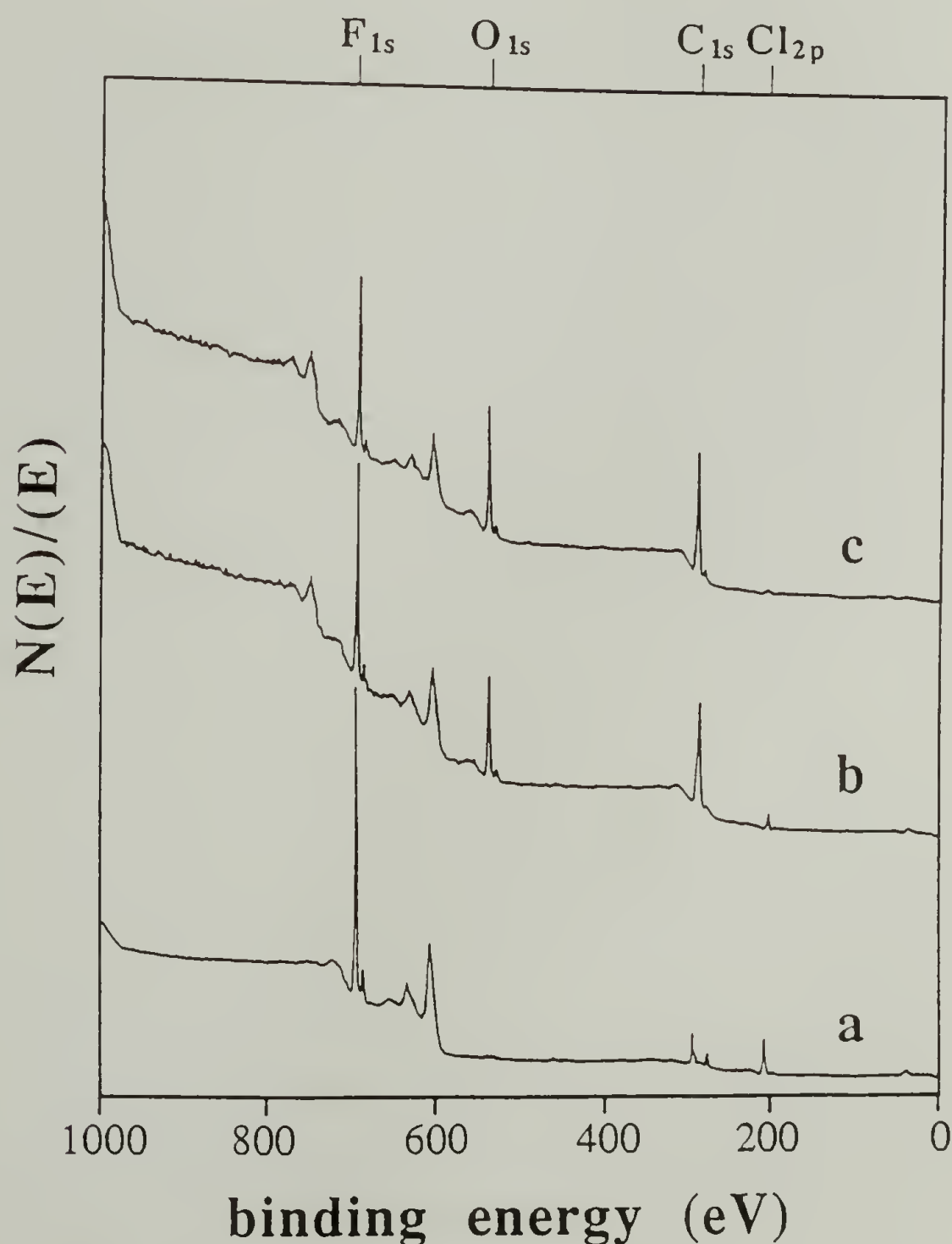


**Figure 2.1.** XPS survey spectra (75° takeoff angle) of: (a) PCTFE, (b) PCTFE-TMOB (-78 °C) and (c) PCTFE-TMOB (-17 °C).

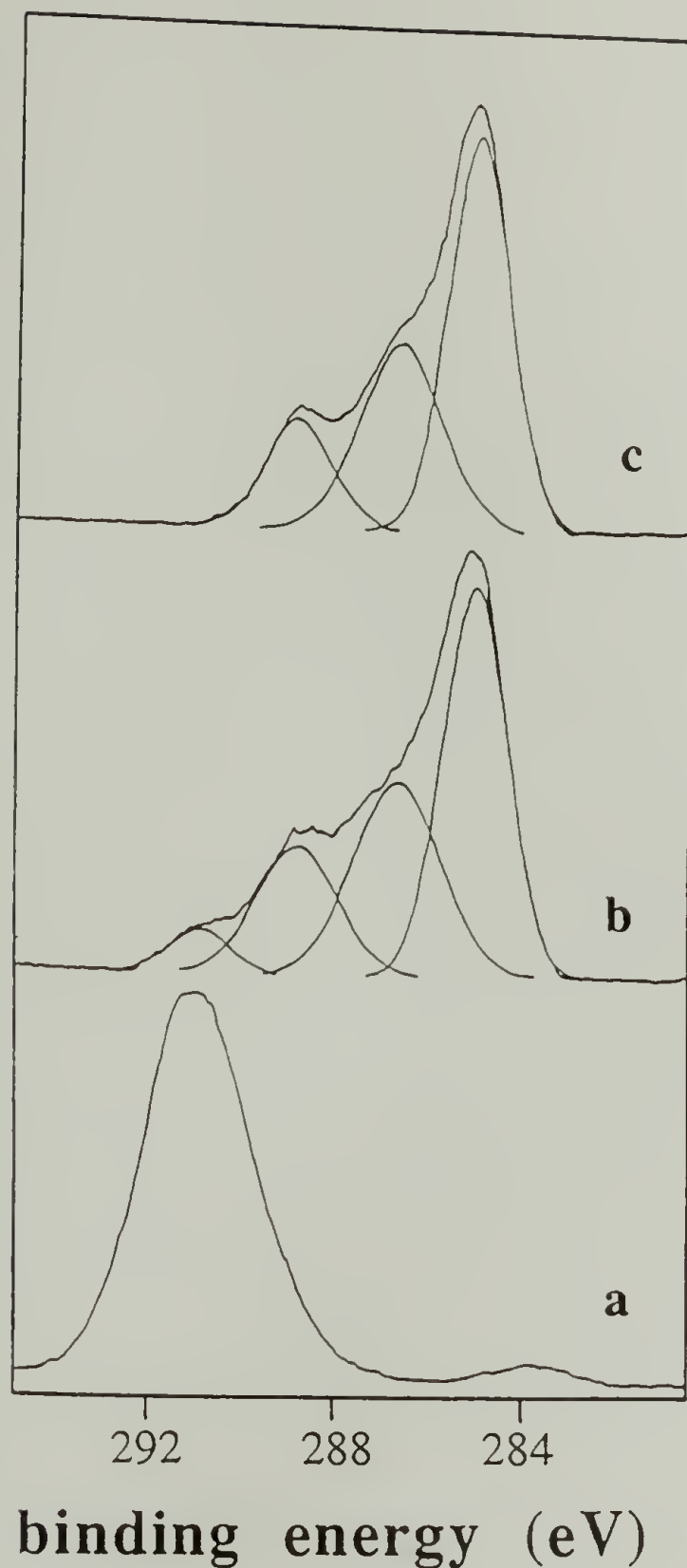


**Figure 2.2.** XPS C1s spectra ( $75^\circ$  takeoff angle) of: (a) PCTFE, (b) PCTFE-TMOB ( $-78^\circ\text{C}$ ) and (c) PCTFE-TMOB ( $-17^\circ\text{C}$ ).

The C1s spectra of the  $-78^\circ\text{C}$  and  $-17^\circ\text{C}$  reacted samples (Figures 2.2b and c, respectively) are shown curve-fitted with four and three peaks, respectively. The highest binding energy peak in the spectrum of the sample prepared at  $-78^\circ\text{C}$  is due to unreacted PCTFE. By comparing the measured areas of the peaks arising from modified

and unmodified material and assuming that a non-corrosive reaction front proceeds parallel to the film surface (The absence of virgin PCTFE in the outer 10 Å, as indicated by the 15° takeoff angle spectra, supports this assumption<sup>16</sup>), a modified layer thickness of ~25 Å is calculated.<sup>22</sup> This high binding energy peak is not present in the spectrum of the sample prepared at -17 °C indicating that the reaction has proceeded entirely through the C1s region XPS sampling depth (~40 Å) at this temperature. The three peaks in the spectrum of the sample prepared at -17 °C and the analogous peaks from the -78 °C sample are, in order of decreasing binding energy, due to the carbon bonded with three oxygens, the carbon bonded to one oxygen or one fluorine and the carbon bonded to only carbon or hydrogen.

A more quantitative assessment of the reaction (Scheme 2.1) can be made through analysis of the XPS atomic composition data (Table 2.2). The predicted stoichiometry for the product of a quantitative reaction is C<sub>9</sub>FO<sub>3</sub>. The observed stoichiometry of PCTFE-TMOB prepared at -17 °C is C<sub>9</sub>F<sub>1.4</sub>O<sub>2.5</sub> (15° takeoff angle) and C<sub>9</sub>F<sub>1.4</sub>O<sub>2.4</sub> (75° takeoff angle). A small amount of chlorine is also observed, more at the higher takeoff angle. This is due to unreacted PCTFE below the modified layer, although no unreacted PCTFE is observed in the C1s spectrum (Figure 2.2c). The mean free path of Cl2p photoelectrons is longer than that of C1s photoelectrons<sup>23</sup> (because of its higher kinetic energy, 1070 eV vs. 950 eV), thus, the Cl2p photoelectrons originate from deeper within the sample than the C1s photoelectrons. In order to minimize discrepancies in the stoichiometry calculations discussed here and throughout the remainder of this chapter, the presence of chlorine is ignored and the 15° takeoff angle data are used.



**Table 2.2.** XPS atomic composition data for modified PCTFE surfaces.

<u>Surface</u>	<u>Θ<sub>T</sub></u>	<u>Experimental</u>				<u>Calculated<sup>a</sup></u>		
		<u>C</u>	<u>F</u>	<u>O</u>	<u>Cl</u>	<u>C</u>	<u>F</u>	<u>O</u>
PCTFE-TMOB (-78 °C)	15	66.2	17.1	15.6	1.1	67.9	10.7	21.4
	75	65.2	17.1	14.7	3.0			
PCTFE-TMOB (-67 °C)	15	66.2	15.8	17.2	0.8			
	75	67.0	14.9	16.6	1.6			
PCTFE-TMOB (-51 °C)	15	66.2	16.0	17.0	0.9			
	75	66.5	14.9	16.4	2.2			
PCTFE-TMOB (-26 °C)	15	67.9	12.7	18.7	0.8			
	75	68.2	12.3	17.7	1.8			
PCTFE-TMOB (-17 °C)	15	69.2	10.9	19.5	0.4			
	75	69.3	10.8	18.6	1.4			
PCTFE-CO <sub>2</sub> H	15	65.6	13.4	19.4	1.6	65.0	15.0	20.0
	75	62.5	15.8	16.7	5.1			
PCTFE-CO <sub>2</sub> Oct <sup>A</sup>	15	82.8	5.3	11.5	0.5	80.0	8.6	11.4
	75	79.0	7.8	12.1	1.2			
PCTFE-CO <sub>2</sub> Oct <sup>B</sup>	15	82.4	4.7	12.0	0.9			
	75	79.3	6.2	12.7	1.7			
PCTFE-CO <sub>2</sub> Oct <sup>C</sup>	15	82.8	4.6	10.5	0.5 <sup>b</sup>			
	75	78.4	6.4	11.8	1.6 <sup>b</sup>			
PCTFE-OH*	15	72.5	12.3	13.7	1.5	72.2	16.7	11.1
	75	70.4	13.0	12.5	4.1			
PCTFE-OHFB*	15	54.1	32.1	12.3	1.4	50.0	40.5	9.4
	75	57.3	27.2	12.2	3.4			

<sup>a</sup>Calculated atomic compositions are based on a surface structure where four of the five polymer repeat units contains the functionality of interest with the fifth being a difluorolefin. (See text for details.)

<sup>b</sup>PCTFE-Oct<sup>C</sup> also contains 1.5% and 1.8% nitrogen at 15° and 75° takeoff angles, respectively.

The high fluorine content and the low oxygen content are inconsistent with a quantitative reaction yield, but consistent with a structure consisting of ~80% trimethyl orthobutyrate-functionalized

repeat units and ~20% difluoroolefins (Figure 2.3). This structure predicts a stoichiometry of  $C_{38}F_6O_{12}$  and the observed composition is  $C_{38}F_{6.0}O_{10.7}$ . These calculations indicate that the organolithium reagent reacts with the PCTFE in quantitative yield to produce the difluoroolefin (II) (Scheme 2.1) and the subsequent reaction with this difluoroolefin proceeds in ~80% yield to produce a modified surface containing four protected carboxylic acids per five original PCTFE repeat units. Similar results have been observed in the reaction of PCTFE with lithiopropyl ethyl acetaldehyde acetal and can likely be attributed steric factors.<sup>14</sup>

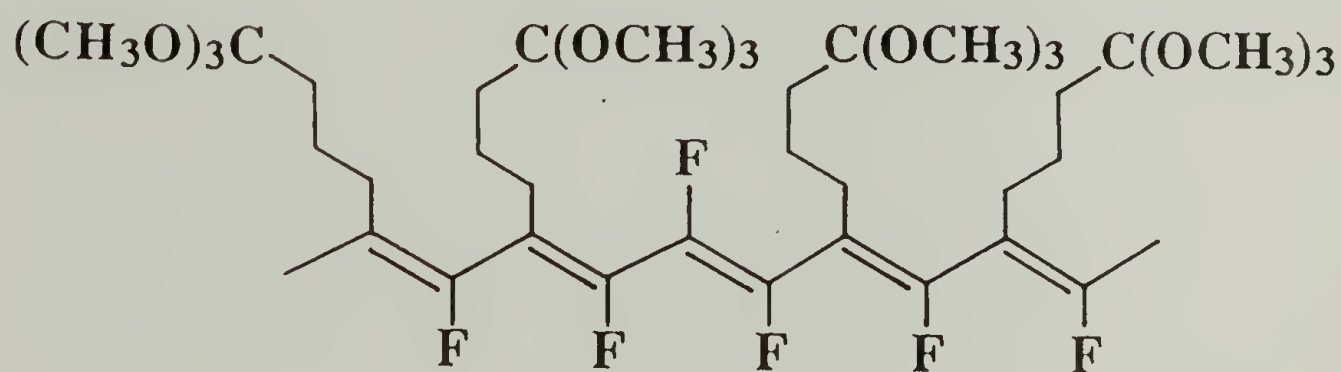


**Figure 2.3.** Surface structure of PCTFE-TMOB. (See text for details.)

For the deeper modified surfaces ATR-IR becomes more informative for qualitative analysis. Figure 2.4 shows ATR-IR spectra for modifications conducted at -78, -51 and -17 °C. As the modification temperature is increased, peaks arising from the orthobutyrate group become more pronounced. The absorbance at  $1740\text{ cm}^{-1}$  from the orthoester<sup>24</sup> increases in intensity, as do the peaks from the C-H stretching vibrations ( $2980\text{-}2840\text{ cm}^{-1}$ ) and the C-H bending modes ( $1460\text{-}1360\text{ cm}^{-1}$ ). The intensity of the absorbances for the -17 °C modified sample indicates that the

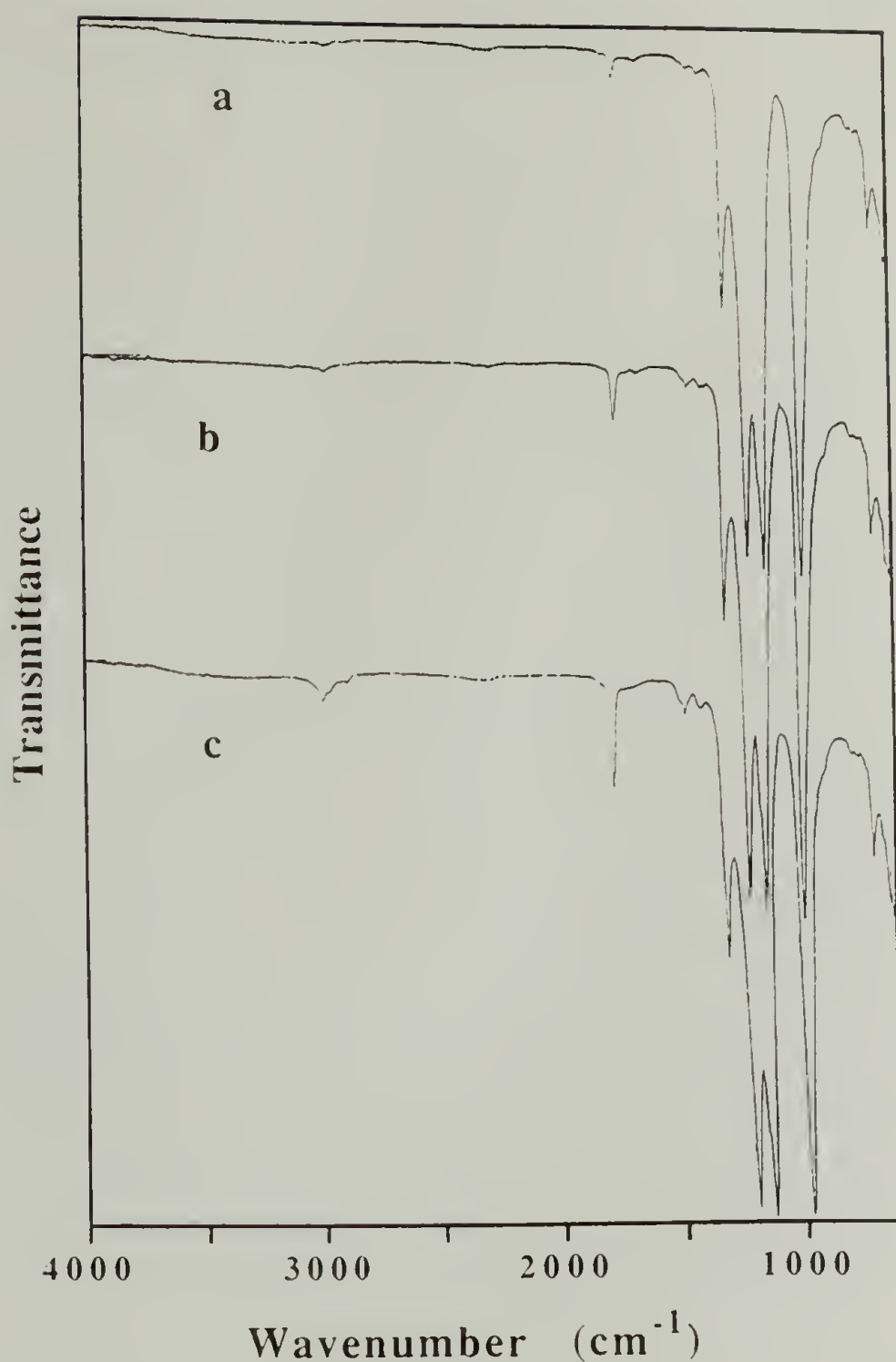


**Figure 2.4.** ATR-IR spectra of: (a) PCTFE-TMOB (-78 °C), (b) PCTFE-TMOB (-51 °C) and (c) PCTFE-TMOB (-17 °C).

reaction has proceeded on the order of one to two hundred angstroms into the film at this temperature. Subsequent chemistry with PCTFE-TMOB described in this work was conducted with samples prepared with an initial modification temperature of -17 °C to facilitate infrared analysis. It is assumed that for the less deeply modified surfaces the chemistry proceeds in a similar fashion.



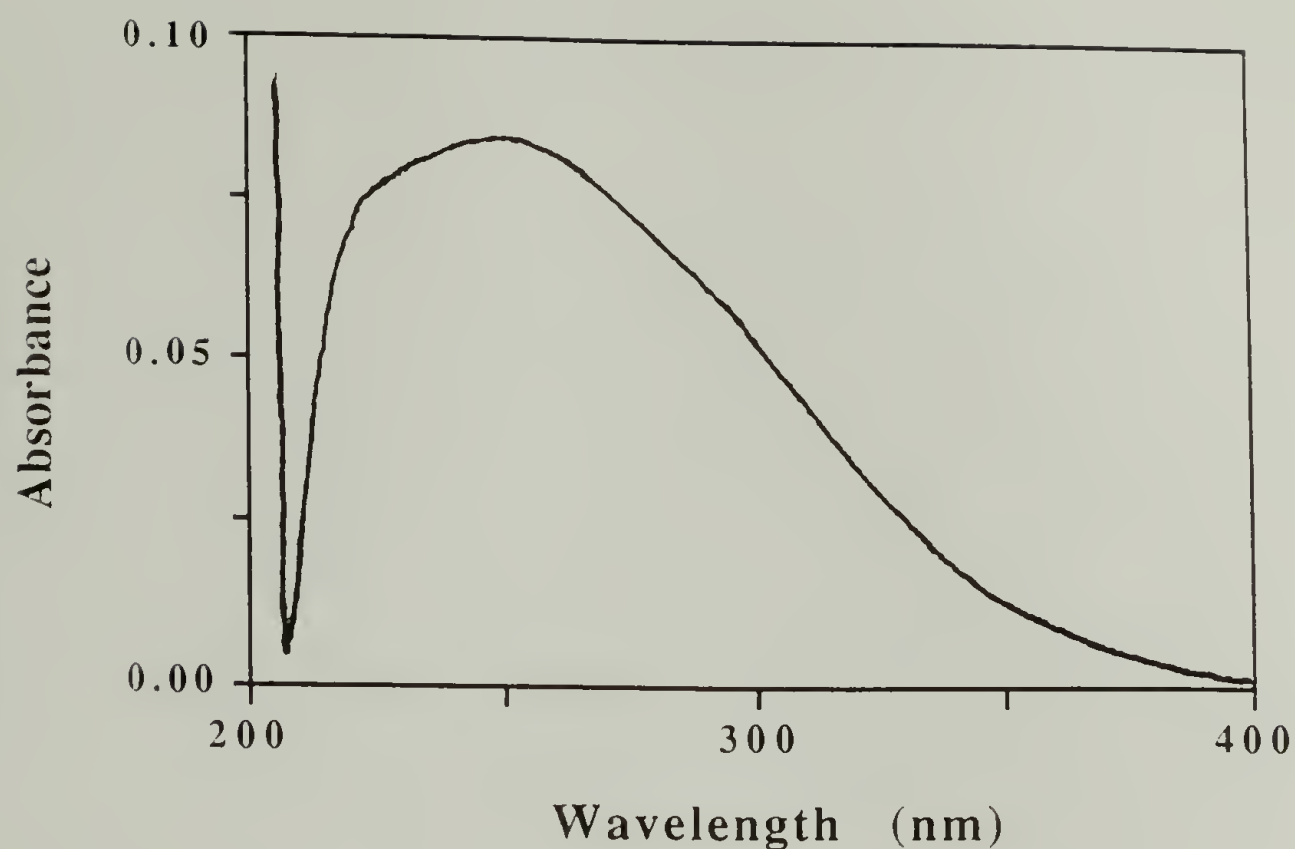
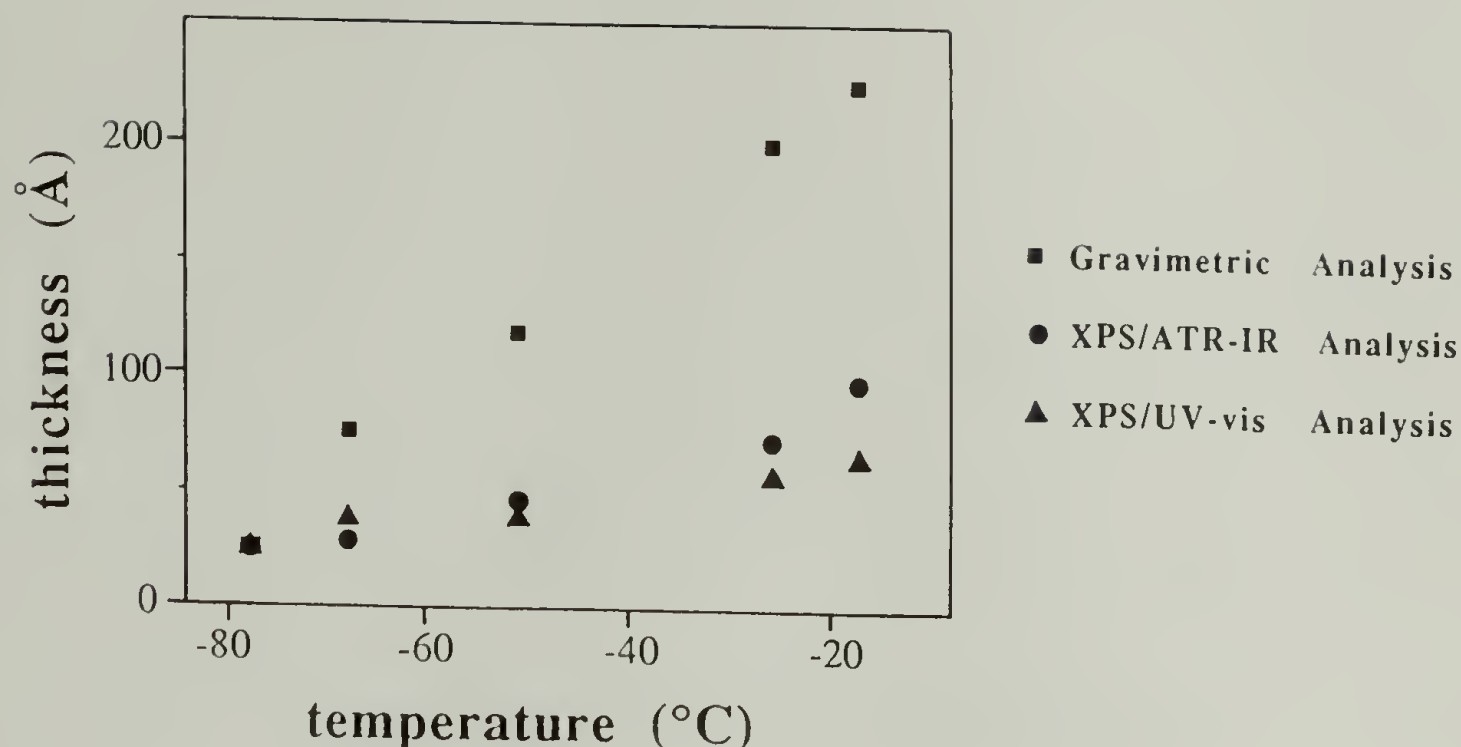


Figure 2.5. UV-vis spectrum of PCTFE-TMOB (-17 °C).

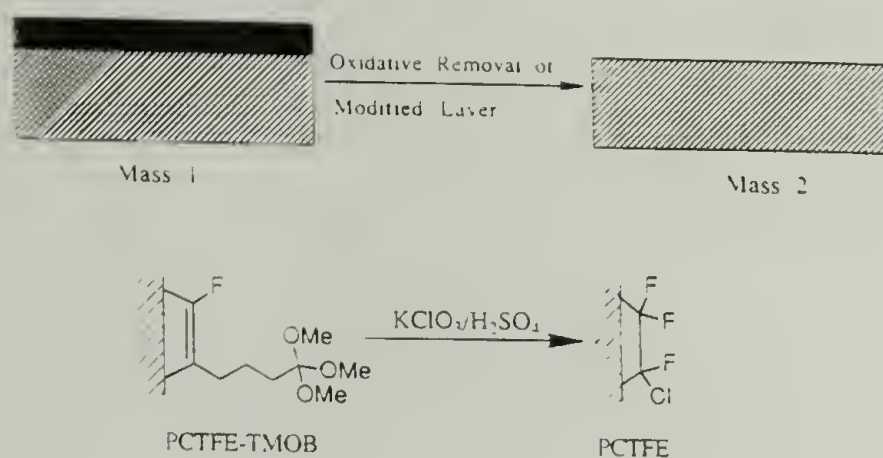
UV-vis transmission spectra (Figure 2.5) of the reacted film samples show the presence of a broad absorption peak beginning at 210 nm and tailing to 390 nm with a maximum at 245 nm, the intensity of which increases with increasing modification temperature. This UV absorbance confirms the conjugation introduced into the polymer backbone as a result of the modification. These UV-vis results provide a convenient method of estimating the depth of modification for the higher temperature reactions. Using the value of 25 Å (as calculated above from the XPS C1s spectrum) for the thickness of the modified layer in the sample prepared at -78 °C, an extinction coefficient of 731 Å/a.u. can be calculated from the absorbance value at 245 nm. Assuming that a Beer's Law relationship is followed, this extinction coefficient can be used to calculate modified layer thicknesses from absorbance values.



**Figure 2.6.** Modified layer thickness as a function of modification temperature. (See text for details.)

The results as a function of reaction temperature are plotted in Figure 2.6. Similar calculations can be made from the ATR-IR spectra using the absorbance at  $1740\text{ cm}^{-1}$  (the extinction coefficient is  $1196\text{ Å/a.u.}$ ). These results are also plotted in Figure 2.6.

Another estimate of reaction depth can be made by oxidatively removing the modified layer with a strong oxidizing agent (Scheme 2.2). XPS, ATR-IR and UV-vis spectra after oxidation with  $\text{KClO}_3/\text{H}_2\text{SO}_4$  are all essentially identical to PCTFE. A small amount of oxygen is present in the XPS spectra (Figure 2.7) due to carboxylic acid groups which remain at the chain termini as a result of the oxidation.<sup>10</sup> Control reactions on unmodified PCTFE show no changes by any technique. Thus, this oxidation removes all of the modified layer from the film surface leaving the virgin material underneath intact.



**Scheme 2.2.** Oxidative removal of PCTFE-TMOB modified layer.

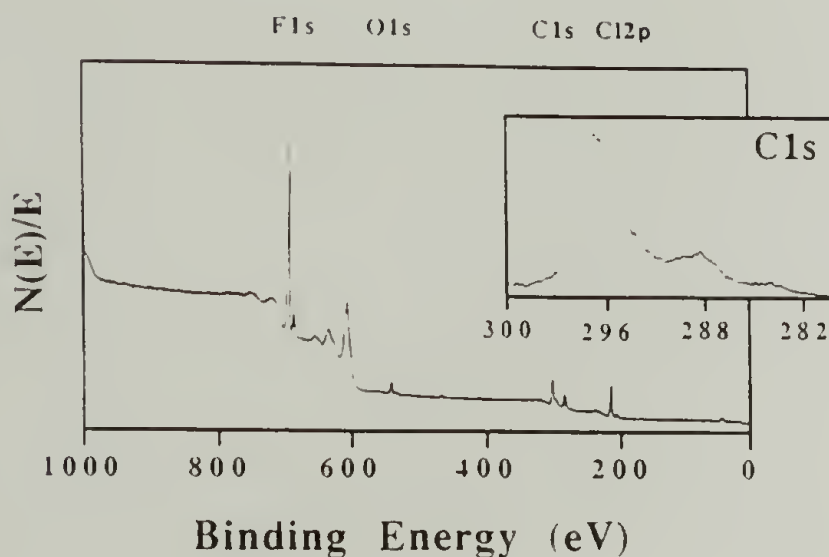


**Figure 2.7.** XPS survey and C1s spectra of oxidized PCTFE-TMOB.

From measurement of the mass lost upon oxidation, the surface area of the film sample and an assumed density of the modified layer ( $2 \text{ g/cm}^3$  - slightly less than that of PCTFE), an average modified layer thickness is calculated. These thickness values are also plotted versus reaction temperature in Figure 2.6. Differences between these modified layer thicknesses and those calculated from the

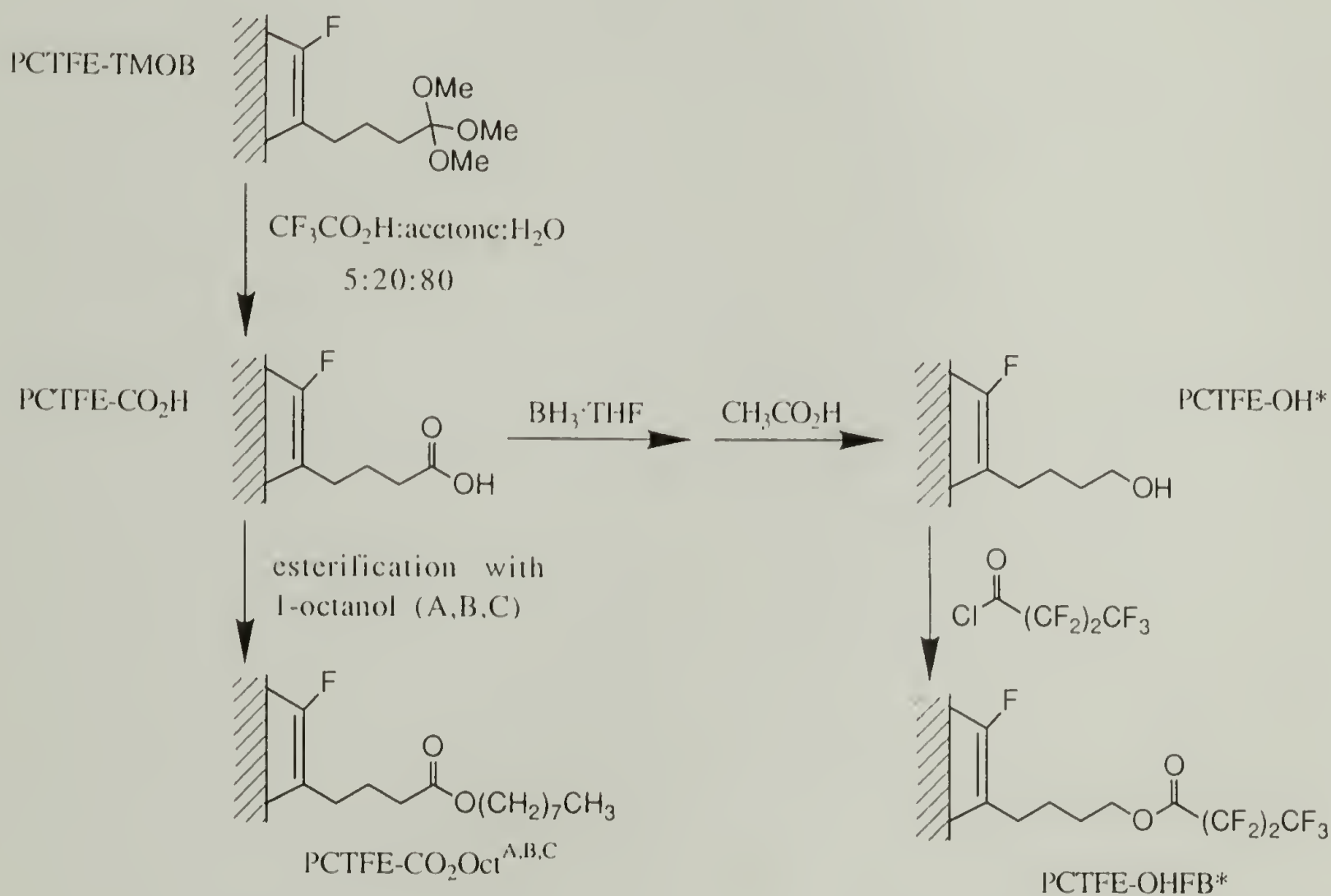


XPS/UV-vis and XPS/ATR-IR data are likely due to a number of factors. The accuracy of the latter two calculations depends on the validity of a number of assumptions: (1) the reaction is non-corrosive and gives a sharp interface that is parallel to the film surface (no modified material is present beneath the XPS sampling depth), (2) the mean free path of C1s photoelectrons is the same in this material as it is in the material in which it was measured<sup>17</sup> and (3) Beer's Law is valid in this solid. The gravimetric results are likely overestimates: unreacted PCTFE (low molecular weight segments of chains between modified blocks and/or crystalline regions unaffected by the modification) is likely removed on oxidation, increasing the mass loss. The convergence of these results at low temperatures (thinner modified layers) implicates the Beer's Law assumption and the loss of unreacted PCTFE mass as the important factors causing the differences. Based on XPS results for the intermediate reaction temperatures and for further functional group transformations, it is believed that the XPS/UV-vis and XPS/ATR-IR results provide more realistic thickness estimates (ranging from ~25 Å at -78 °C to ~100 Å at -17 °C) while the gravimetric method provides an upper bound. Regardless, both methods reveal a reaction temperature-dependent modified layer thickness.

#### Hydrolysis of PCTFE-TMOB (PCTFE-CO<sub>2</sub>H)

A range of conditions for hydrolysis of the orthoester were screened; each involved an acid catalyst, water and an organic solvent to lower the interfacial free energy between the solution and

the solid polymer film. The hydrolysis was followed by labelling the carboxylic acid groups for XPS analysis with thallium (see below) and by monitoring changes in the ATR-IR spectra and water contact angles. The solutions used were mixtures of HCl/H<sub>2</sub>O/methanol, HCl/H<sub>2</sub>O/THF, CF<sub>3</sub>CO<sub>2</sub>H/H<sub>2</sub>O/THF and CF<sub>3</sub>CO<sub>2</sub>H/H<sub>2</sub>O/acetone with the latter in a 5:80:20 (CF<sub>3</sub>CO<sub>2</sub>H:H<sub>2</sub>O:acetone) ratio proving to completely hydrolyze the orthoester (Scheme 2.3).



- A. *p*-toluenesulfonic acid catalyzed
- B. through the intermediate acid chloride (thionyl chloride)
- C. through the intermediate acyl imidazolide (carbonyldiimidazole)

**Scheme 2.3.** Hydrolysis of PCTFE-TMOB and further modifications of PCTFE-CO<sub>2</sub>H.

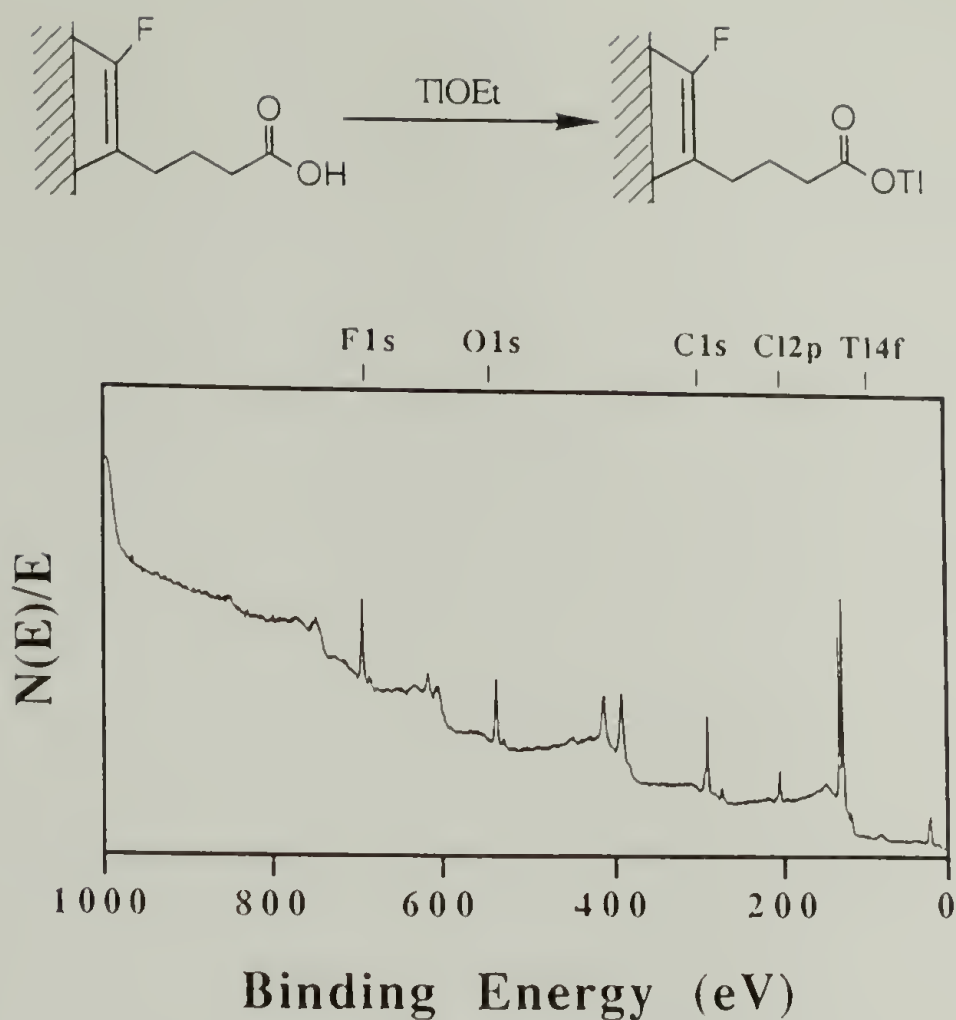


**Figure 2.8.** XPS labelling of PCTFE-CO<sub>2</sub>H with thallium.

Thallous ethoxide was chosen for XPS labelling because: (1) it reacts selectively with acidic functionality and (2) thallium has a large XPS atomic sensitivity factor (6.150 for Tl4f photoelectrons versus for 0.225 for C1s photoelectrons), facilitating detection. The XPS survey spectrum after treatment with neat thallous ethoxide (Figure 2.8) shows pronounced peaks for the Tl4f and the Tl4d photoelectrons at 120 eV and 395 eV respectively. The atomic composition of this surface (C<sub>26</sub>O<sub>6.4</sub>F<sub>4.2</sub>Cl<sub>5.6</sub>Tl<sub>5.9</sub> based on 15° takeoff angle data and C<sub>26</sub>O<sub>6.8</sub>F<sub>5.7</sub>Cl<sub>5.1</sub>Tl<sub>2.3</sub> based of the 75° takeoff angle data) shows that there is more thallium present than would be expected (C<sub>26</sub>O<sub>8.0</sub>F<sub>6.0</sub>Cl<sub>0.0</sub>Tl<sub>4.0</sub>) and a significant amount of chlorine. A consistent explanation for this result is reaction of the ethoxide ion



with the virgin PCTFE lying underneath the modified layer, depositing insoluble  $\text{TiCl}_4$  at the film surface. Virgin PCTFE, PCTFE-TMOB and unsuccessfully hydrolyzed samples do not show any evidence of reaction with the thallous ethoxide. It is likely that the relatively polar acid surface facilitates transport of the ethoxide to the unreacted PCTFE.

The ATR-IR spectrum of PCTFE- $\text{CO}_2\text{H}$  (Figure 2.9a - compare with Figure 2.4c, page 62) indicates the disappearance of the orthoester ( $1740\text{ cm}^{-1}$ ) and the appearance of the carboxylic acid ( $1710\text{ cm}^{-1}$ ). The small peak at  $1782\text{ cm}^{-1}$  in the acid surface can be assigned to  $\alpha$ -fluoroketone resulting from hydrolysis of the difluoroolefin. Figure 2.10 (a and b) compares the  $\text{C1s}$  XPS spectra of PCTFE-TMOB and PCTFE- $\text{CO}_2\text{H}$ . The spectrum of PCTFE- $\text{CO}_2\text{H}$  exhibits a high binding energy peak which is assigned to the carbonyl carbon of the carboxylic acid. The middle binding energy region assigned to carbons bonded to one oxygen (assigned to the three methoxy groups of the orthoester) or one fluorine decreases in intensity after hydrolysis as expected. The observed stoichiometry of PCTFE- $\text{CO}_2\text{H}$  (Table 2.2, page 60) is  $\text{C}_{26}\text{O}_{7.7}\text{F}_{5.3}$  based on the  $15^\circ$  takeoff angle data and  $\text{C}_{26}\text{O}_{6.9}\text{F}_{6.6}$  based on the  $75^\circ$  data. The theoretical value (based on the proposed structure of the PCTFE-TMOB surface (Figure 2.3)) is  $\text{C}_{26}\text{O}_8\text{F}_6$ .

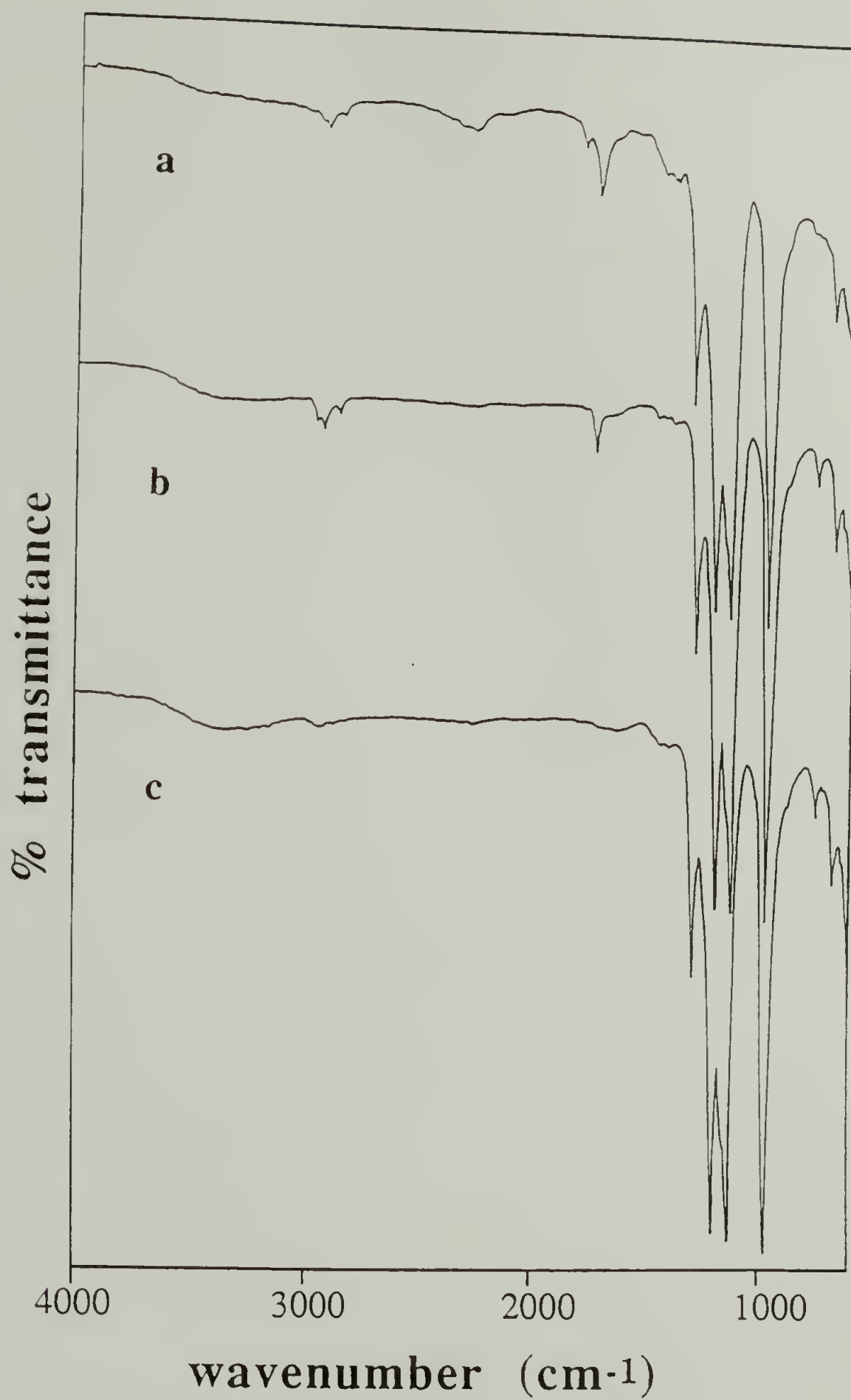


**Figure 2.9.** ATR-IR spectra of: (a) PCTFE-CO<sub>2</sub>H, (b) PCTFE-CO<sub>2</sub>Oct<sup>ABC</sup> and (c) PCTFE-OH\*.



**Figure 2.10.** XPS C1s spectra of: (a) PCTFE-TMOB, (b) PCTFE-CO<sub>2</sub>H, (c) PCTFE-CO<sub>2</sub>Oct<sup>ABC</sup>, (d) PCTFE-OH\* and (e) PCTFE-OHFB\*.

Upon deprotection, water contact angles ( $\Theta_A/\Theta_R=55^\circ/0^\circ$ ) indicate that a very hydrophilic surface has been produced. These values are identical to those of polyethylene carboxylic acid (PE-CO<sub>2</sub>H).<sup>2-6</sup> The pH dependence of the advancing contact angle for PCTFE-CO<sub>2</sub>H as well as PCTFE, PCTFE-TMOB and PCTFE-OH\* (see below) was measured using buffered pH solutions; the data is displayed in Figure 2.11. The results reported here for contact angle



titrations of PCTFE-CO<sub>2</sub>H follow those of PE-CO<sub>2</sub>H. Advancing contact angles are independent of pH until pH~6 and then decrease gradually to  $\Theta_A = 30^\circ$  at pH>10 (receding contact angles are 0 at all pH values). With the highly basic probe fluids the liquid drop spontaneously spreads across the acidic film surface.  $\Theta_A$  (and also  $\Theta_R$ , although not shown) is independent of pH for the other three surfaces. The break in the "titration" curve indicates that the surface-confined acids have pKa's ranging from ~6 - ~10, which is higher than would be expected based on analysis of polybasic acids in solution. This increased difficulty in ionizing carboxylic acids at the solid/solution interface has been attributed to a lower average dielectric constant at the interface.<sup>3,6</sup> It is reasonable to expect that creating a negative charge is more difficult in a medium composed of polymer and water (where ionization takes place) than in solution where solvation can take place. (The reader is referred to references 3 and 6 for a full discussion of contact angle measurements on ionizable surfaces.)

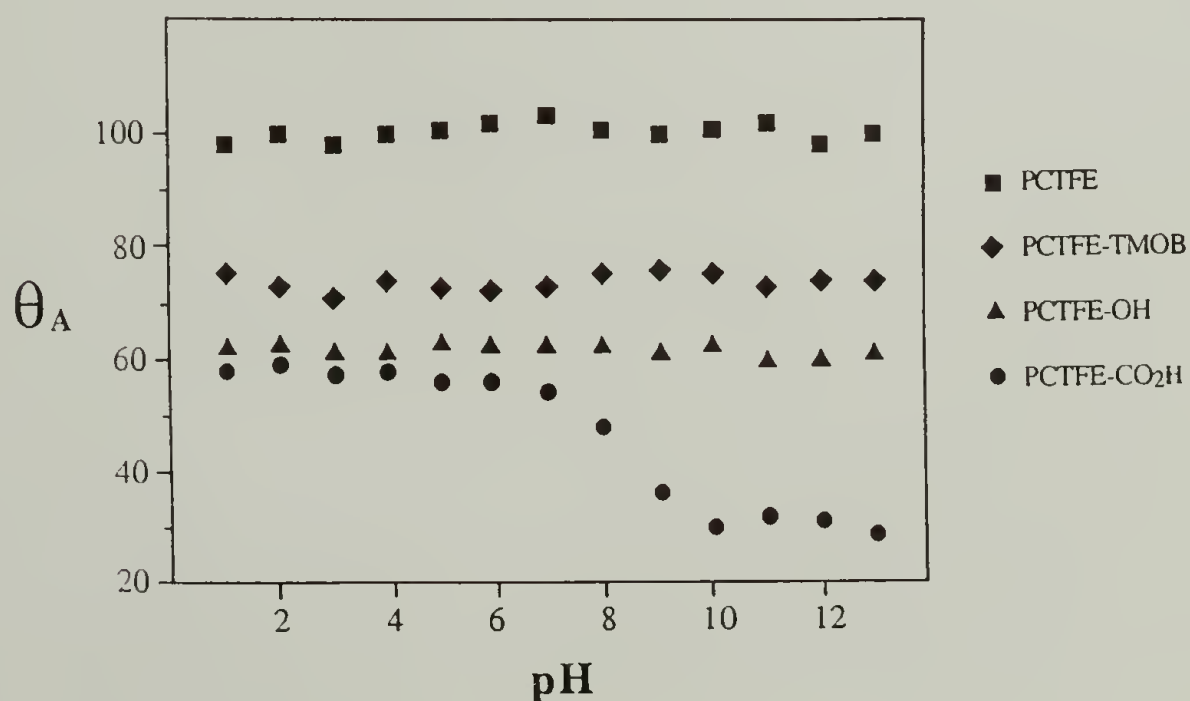


**Figure 2.11.**  $\Theta_A$  dependence on probe fluid pH (buffered aqueous solutions).

### Reactivity of PCTFE-CO<sub>2</sub>H (Esterification and Reduction)

The reactivity of PCTFE-CO<sub>2</sub>H was assessed by esterification reactions using 1-octanol (PCTFE-CO<sub>2</sub>Oct<sup>A,B,C</sup>) and reduction with BH<sub>3</sub>·THF to yield the alcohol (PCTFE-OH\*) (Scheme 2.3, page 67). 1-Octanol was chosen as the alcohol for esterification for analytical reasons. Upon esterification the long hydrocarbon chain should induce significant changes in the water contact angle, XPS and ATR-IR. The *n*-octyl ester was prepared using three different esterification procedures: (1) Fisher esterification using *p*-toluenesulfonic acid as a catalyst (PCTFE-CO<sub>2</sub>Oct<sup>A</sup>), (2) preparation of the acid chloride using thionyl chloride followed by reaction with 1-octanol (PCTFE-CO<sub>2</sub>Oct<sup>B</sup>) and (3) preparation of the acyl imidazolidine using carbonyldiimidazole followed by reaction with 1-octanol (PCTFE-CO<sub>2</sub>Oct<sup>C</sup>). Water contact angle data for the three ester surfaces are given in Table 2.1 (page 56) and indicate the formation of indistinguishable, hydrophobic surfaces ( $\Theta_A/\Theta_R = 98-100^\circ/45-49^\circ$ ). XPS and ATR-IR spectra of the three esters are essentially identical. Figure 2.9b (page 70) shows the ATR-IR spectrum for PCTFE-CO<sub>2</sub>Oct<sup>A</sup>. The carbonyl peak has shifted from 1710 cm<sup>-1</sup> for the acid to 1736 cm<sup>-1</sup> for the ester. The XPS C1s spectrum of this surface (Figure 2.10c, page 71) shows an increase in the intensity of the low binding energy peak (assigned to carbons bonded to hydrogen) relative to the high binding energy carbonyl peak. XPS atomic composition data (Table 2.2, page 60) agree with the expected results, indicating a high yield for these reactions. The predicted stoichiometry for PCTFE-CO<sub>2</sub>Oct is C<sub>58</sub>O<sub>8</sub>F<sub>6</sub>; observed values based on 15° takeoff angle data are C<sub>58</sub>O<sub>8</sub>F<sub>3.7</sub> (PCTFE-CO<sub>2</sub>Oct<sup>A</sup>), C<sub>58</sub>O<sub>8.4</sub>F<sub>3.3</sub>

(PCTFE-CO<sub>2</sub>Oct<sup>B</sup>) and C<sub>58</sub>O<sub>7.4</sub>F<sub>3.2</sub> (PCTFE-CO<sub>2</sub>Oct<sup>C</sup>). The low measured fluorine concentrations indicate that the 12-carbon ester groups lie above the polymer backbone, inhibiting the escape of the F1s photoelectrons. Compositions based on 75° takeoff angle data are, respectively for PCTFE-CO<sub>2</sub>Oct<sup>A,B,C</sup>, C<sub>58</sub>O<sub>3.9</sub>F<sub>5.7</sub>, C<sub>58</sub>O<sub>9.2</sub>F<sub>4.5</sub> and C<sub>58</sub>O<sub>8.7</sub>F<sub>4.7</sub>. XPS also indicates the presence of a small amount of nitrogen in PCTFE-CO<sub>2</sub>Oct<sup>C</sup> (1.5% and 1.8% for 15° and 75° takeoff angles, respectively) that is likely due to incomplete esterification.

The esterification of PCTFE-CO<sub>2</sub>H with 2,2,3,3,4,4,4-heptafluoro-1-butanol was also attempted with acid catalysis and through the intermediate acid chloride. This reagent was also chosen to investigate the reactivity of PCTFE-CO<sub>2</sub>H for analytical reasons. One would expect a large increase in the concentration of fluorine in the surface and in the water contact angles if the reaction were successful. The conditions for both of these reactions were the same as those used for the esterification with 1-octanol discussed above. However, after two attempts with each of these procedures, the analytical results showed that little esterification had occurred. The contact angles increased only slightly (from 55°/0° for PCTFE-CO<sub>2</sub>H to 70°/15°) while the fluorine content in the XPS was unchanged. The reasons for this low reactivity were not investigated, but may be the result of low nucleophilicity of the alcohol due to the strong electron-withdrawing ability of the fluorines.

Reduction of PCTFE-CO<sub>2</sub>H to PCTFE-OH\* using 1.0 M BH<sub>3</sub>·THF in THF was monitored by following the disappearance of the carbonyl peak in the infrared spectrum. After 12 h of reaction, the carbonyl absorbance is absent and a broad O-H stretching band



(3100 - 3600  $\text{cm}^{-1}$ ) is observed (Figure 2.9c, page 70). The XPS C1s spectrum of the reduced surface shows that the high binding carbon peak is completely removed (Figure 2.10d, page 71). The main peak does have a shoulder on the high binding energy side for the carbon attached to the hydroxyl group and the carbons attached to a single fluorine in the polymer backbone. The water contact angles ( $\Theta_A/\Theta_R=62^\circ/22^\circ$ ) are consistent with an alcohol-containing surface; PCTFE-OH produced by an alternative procedure exhibits  $\Theta_A/\Theta_R=67^\circ/17^\circ$ .<sup>14,25</sup> The predicted composition for PCTFE-OH\* is  $\text{C}_{26}\text{O}_4\text{F}_5$ ; the observed stoichiometry based on data in Table 2.2 (page 60) is  $\text{C}_{26}\text{O}_{4.9}\text{F}_{4.4}$  ( $15^\circ$  takeoff angle) and  $\text{C}_{26}\text{O}_{4.6}\text{F}_{4.8}$  ( $75^\circ$  takeoff angle). PCTFE-OH\* reacts with heptafluorobutyryl chloride to yield the expected fluoroester, PCTFE-OHFB\* (Scheme 2.3, page 67). As anticipated, water contact angles indicate the formation of a hydrophobic surface ( $\Theta_A/\Theta_R=89^\circ/47^\circ$ ). The ATR-IR spectrum shows an absorbance at 1782  $\text{cm}^{-1}$  typical of esters fluorinated at the  $\alpha$ -carbon. The C1s XPS spectrum of the heptafluorobutyrate surface (Figure 2.10e, page 71) shows high binding energy photoelectron peaks arising from  $\text{CF}_3$ ,  $\text{CF}_2$  and carbonyl carbons. The predicted atomic composition for PCTFE-OHFB\* is  $\text{C}_{42}\text{O}_8\text{F}_{33}$ ; the measured stoichiometry is  $\text{C}_{42}\text{O}_{9.5}\text{F}_{24.9}$  ( $15^\circ$  takeoff angle) and  $\text{C}_{42}\text{O}_{8.9}\text{F}_{19.9}$  ( $75^\circ$  takeoff angle). The difference between the predicted and measured stoichiometry can be attributed to two factors: (1) incomplete reduction of the carboxylic acid to the alcohol and/or (2) incomplete reaction of the heptafluorobutyryl chloride with the surface alcohol groups. The fact that heptafluorobutyryl chloride reacts in quantitative yield with similar alcohol containing surfaces,<sup>14,25</sup> points

to incomplete reduction as the cause of the difference between the predicted and measured atomic compositions.

### Conclusions and Future Work Suggestions

PCTFE film reacts with LiTMOB to incorporate the trimethyl orthobutyrate group into the polymer surface. The modified surface layer has been postulated to contain four orthoesters for every five polymer repeat units with the fifth being a difluoroolefin. The depth of modification ranges from ~25 to ~100 Å and may be controlled by varying the reaction temperature. It is also likely that the modification depth may be increased by increasing the THF:heptane ratio as has been done in other PCTFE/organolithium surface modifications.<sup>7</sup>

Once the modified surface is prepared, the orthoester can be quantitatively hydrolyzed to the acid in a refluxing solution of trifluoroacetic acid, water and acetone. ATR-IR spectra show a peak shift from 1740 cm<sup>-1</sup> for the orthoester to 1710 cm<sup>-1</sup> for the acid. The acid surface can then be labelled for XPS analysis by reaction with thallous ethoxide. The carboxylic acid surface exhibits extremely low water contact angles and the acid groups may be "titrated" by measuring contact angles as a function of the probe fluid pH.

The reactivity of the acid was investigated by studying the esterification with 1-octanol conducted under three sets of conditions and the reduction to the corresponding alcohol (and subsequent

reaction with heptafluorobutyryl chloride). Contact angle results are consistent with the predicted product surfaces. The high reactivity of this carboxylic acid surface was confirmed by monitoring changes in the carbonyl region of the ATR-IR spectra and by comparing the measured XPS atomic compositions with those predicted based on the proposed structure of PCTFE-TMOB.

Future research could use the surface modifications developed in this work to study the reactivity and wettability of carboxylic acid groups at the solid/solution interface analogous to studies of PE-CO<sub>2</sub>H and its derivatives.<sup>2-6</sup> However, this type of study PCTFE-CO<sub>2</sub>H offers few advantages over PE-CO<sub>2</sub>H and it is doubtful that any significant improvement in understanding would result from such an investigation. Alternatively, the chemistry developed here could be utilized in current studies of the effect of polymer surface structure on adhesion<sup>26</sup> and friction.<sup>27</sup> This carboxylic acid modified PCTFE surface has a higher surface energy than the materials used in these studies, but the same bulk polymer. As such, it would compliment results obtained on *n*-butyl<sup>26</sup> and alcohol (and its derivatives)<sup>26,27</sup> modified PCTFE surfaces.

The most potential for further application of this surface modification lies in its use as a means of preparing well-controlled substrates utilized in the study of polymer adsorption. Most of the current polymer adsorption studies employ inorganic substrates that are easily contaminated by adventitious matter, chemically heterogeneous, not well-characterized and possess surface chemistries that vary from sample to sample. The role of chemical architecture of the polymer chain and that of the solvent in



determining the structure of the adsorbed layer are currently undergoing intense study.<sup>28</sup> The current level of understanding of these factors has progressed to the point that investigation of the function of the substrate surface chemistry in the adsorption process is now essential. The modified surfaces developed here would be ideal for such a study. Reactions (and subsequent adsorptions) could be conducted on polymer films for XPS and contact angle analysis or on polymer powders<sup>19</sup> for increased surface area to measure the amount of adsorbed polymer. The interaction energy between the substrate and the adsorbing polymer segment can be varied by simple derivatization of the modified surface (i.e. reduction of PCTFE-CO<sub>2</sub>H to the corresponding alcohol or esterification with methanol, ethanol, *n*-butanol, etc.). Preliminary studies have been conducted on the adsorption of poly(styrene-*b*-4-hydroxybutene) from solution to PCTFE-CO<sub>2</sub>H and PCTFE-OH\* film.<sup>27</sup> Results show that the block copolymer adsorbs to PCTFE-CO<sub>2</sub>H (exhibiting a high affinity isotherm) under conditions where it does not adsorb to virgin PCTFE (polystyrene homopolymer does adsorb to the PCTFE-CO<sub>2</sub>H). A further level of sophistication would be to prepare solutions containing varying compositions of trimethyl 4-lithioorthobutyrate and *n*-butyl lithium (via lithium-halogen exchange with the corresponding alkyl bromides) for reaction with PCTFE. Subsequent deprotection would produce mixed carboxylic acid/methyl surfaces with varying compositions. Adsorption studies on these substrates may show that a critical level of polar functionality at a surface must be present for adsorption to occur (which may vary with the molecular weight of the adsorbing polymer) and that the structure of

the adsorbed layer is dependent on the surface site density of the polar functional groups.

### References and Notes

- (1) For reviews see: (a) Clark, D.T. and Feast, W.J. "Polymer Surfaces", Wiley-Interscience: New York, 1978, pp. 213 - 234. and (b) Ward, W.J. and McCarthy, T.J. In *Encyclopedia of Polymer Science and Engineering*, 2nd ed.; Supplement, Wiley: New York, 1989, pp.674 - 689.
- (2) Rasmussen, J.R.; Stedronsky, E.R. and Whitesides, G.M. *J. Am. Chem. Soc.* **1977**, 99, 4736.
- (3) Holmes-Farley, S.R.; Reamey, R.H.; McCarthy, T.J.; Deutch, J. and Whitesides, G.M. *Langmuir*, **1985**, 1, 725.
- (4) Holmes-Farley, S.R. and Whitesides, G.M. *Langmuir*, **1987**, 3, 62.
- (5) Holmes-Farley, S.R.; Nuzzo, R.G.; McCarthy, T.J. and Whitesides, G.M. *Langmuir*, **1987**, 3, 799.
- (6) Holmes-Farley, S.R.; Bain, C.D. and Whitesides, G.M. *Langmuir*, **1988**, 4, 921.
- (7) Dias, A.J. and McCarthy, T.J. *Macromolecules* **1987**, 20, 2068.
- (8) Dias, A.J. Ph.D. dissertation, University of Massachusetts, 1987.
- (10) Shoichet, M.S. and McCarthy, T.J. *Macromolecules* **1991**, 24, 982.
- (11) (a) Brennan, J.V. and McCarthy, T.J. *Polym. Prepr. (Am. Chem. Soc., Div. Polym. Chem.)* **1987**, 29(2), 338. (b) Brennan, J.V. and McCarthy, T.J. *Polym. Prepr. (Am. Chem. Soc., Div. Polym. Chem.)* **1989**, 30(2), 152.
- (12) Bening, R.C. and McCarthy, T.J. *Macromolecules* **1990**, 23, 2648.

- (13) March, J. "Advanced Organic Chemistry", Wiley-Interscience: New York, 1985, pp. 329 - 331 and references therein.
- (14) Lee, K.-W. and McCarthy, T.J. *Macromolecules* **1988**, *21*, 3353.
- (15) Juaristi, E.; Martinez-Richa, A.; Garcia-Rivera, A. and Cruz-Sanchez, J.S. *J. Org. Chem.* **1983**, *43*, 2603.
- (16) For a takeoff angle of  $75^\circ$  64.5% of the signal observed comes from a depth,  $t = \lambda$  while 95.5% comes from  $t = 3\lambda$  and at  $15^\circ$  64.5% comes from  $t = 0.27\lambda$  and 95.5% from  $t = 0.80\lambda$ . Where  $\lambda$  is the photoelectron's mean free path. (For C1s photoelectrons  $\lambda = 14 \text{ \AA}$ .<sup>17</sup>)
- (17) This value was measured in poly(*p*-xylylene): Clark, D.T. and Thomas, H.R. *J. Polym. Sci. Polym. Chem. Ed.* **1977**, *15*, 2843.
- (18) Kolthoff, I.M.; Sandel, E.B.; Meehan, E.J.; Bruckenstein, S. *Quantitative Chemical Analysis*, 4th ed.; MacMillan: Toronto, 1969.
- (19) Dias, A.J. and McCarthy, T.J. *Macromolecules* **1985**, *18*, 1826.
- (20) Kolb, B.U.; Patton, P.A.. and McCarthy, T.J. *Macromolecules* **1990**, *23*, 366.
- (21) A review of the results presented in references 7, 18 and 19 is presented in Chapter I of this dissertation.
- (22) See Chapter I of this dissertation for a discussion of these calculations.
- (23) Andrade, J.D., Ed. *Surface and Intefacial Aspects of Biomedical Polymers, vol. 1: Surface Chemistry and Physics*; Plenum: New York, 1985.
- (24) Casy, G.; Furber, M.; Richardson, K.A.; Stephenson, G.R.; Taylor, R.J.K. *Tetrahedron*, **1986**, *21*, 5849.
- (25) See Chapters III and V of this dissertation.
- (26) Fleming, R.J. and McCarthy, T.J. results to be published.



- (27) See Chapter IV of this dissertation.
- (28) For general discussion see: (1) Parsonage, E.; Tirrell, M.; Watanabe, H. and Nuzzo, R.G. *Macromolecules* **1991**, *24*, 1987. (2) Evers, O.A.; Scheutjens, J.M.H.M. and Fleer, G.J. *J. Chem. Soc. Faraday Trans.* **1990**, *86*(9), 1333. (3) Guzonas, D.A.; Boils, D.; Tripp, C.P. and Hair, M.L. *Macromolecules* **1992**, *25*, 2434.
- (29) Kendall, E.W. and McCarthy, T.J. results to be published.

## CHAPTER III

# PREPARATION OF MODIFIED POLY(CHLOROTRIFLUOROETHYLENE) SURFACES FOR FRICTION STUDIES

### Introduction

In the past a great deal of both theoretical and experimental work has been done in the area of polymer friction.<sup>1</sup> Most of the work thus far has been concerned with relating the coefficient of friction,  $\mu$ , to bulk material properties and with the changes polymers undergo during sliding. A number of workers<sup>2</sup> have studied the effects of changes in load, temperature, atmosphere, nominal surface area, sliding speed and surface roughness. Their results have shown that polymers do not follow Amontons' laws as  $\mu$  is found to be somewhat dependent on each of these variables. The causes for these deviations can be attributed to the viscoelastic behavior of organic polymers. One study<sup>3</sup> has shown very good correlations between changes in  $\mu$  with temperature and similar changes in combinations of material constants such as Young's modulus and  $\tan \delta$ . Despite the vast amount of research in polymer tribology, very few studies have been done which look at the specific surface interactions influencing polymer friction. One set of experiments<sup>4</sup> illustrated a direct relationship between the work of adhesion, as determined by contact angle measurements and  $\mu$  in polymer

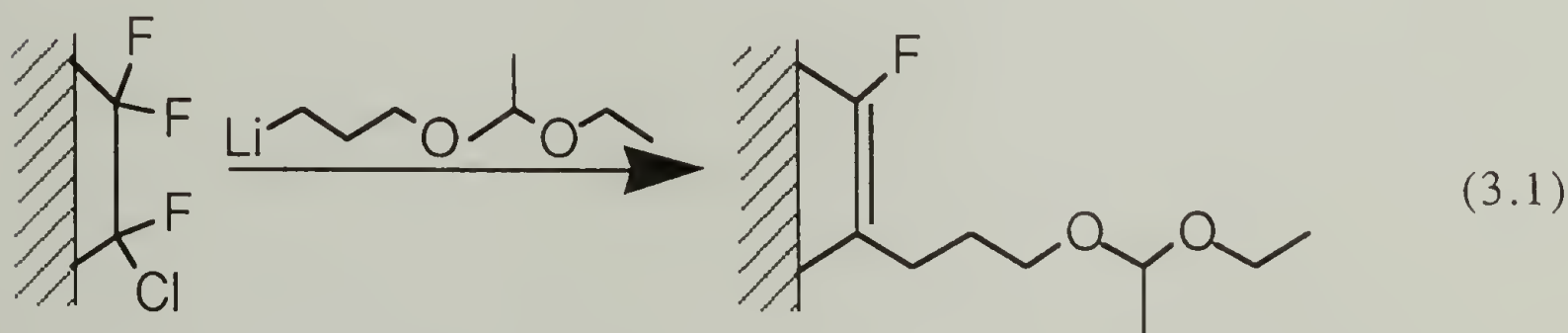
friction. Additionally, the frictional properties of polymers which were surface modified by reaction with  $\text{Br}_2$ ,  $\text{Cl}_2$ ,  $\text{F}_2$  gases, plasma treatments and chemical oxidations have been studied.<sup>5</sup> These surface treatments modify the frictional behavior but are relatively destructive in nature, and due to the heterogeneity of functional groups introduced, have not been well characterized. Thus, a correlation between the observed changes in friction and a specific change in surface structure is impossible.

McCarthy and coworkers have undertaken a research program utilizing relatively nondestructive techniques to introduce a variety of specific functional groups into the surfaces of polymer films in a controlled manner.<sup>6-11</sup> The long range goal of this work is the understanding of surface structure-property relationships i.e. wettability, adhesion and friction. Chemically resistant polymer films (poly(ether ether ketone) (PEEK), polytetrafluoroethylene (PTFE), polyvinylidene fluoride (PVF2), poly(tetrafluoroethylene-*co*-hexafluoropropylene) (FEP) and poly(chlorotrifluoroethylene) (PCTFE)) have been chosen as substrates for a variety of reasons. The most important of which is that a versatile functional group can be introduced into these surfaces under stringent conditions, then further reacted under relatively mild conditions which do not affect the bulk of the material. Thus, a series of polymer samples differing solely in their surface chemistry can be prepared and then utilized to investigate the properties mentioned. Changes in the wettability of modified materials have been used as a qualitative analytical tool to monitor surface reactions and other surface phenomena such as surface reconstruction, molecular self-assembly and

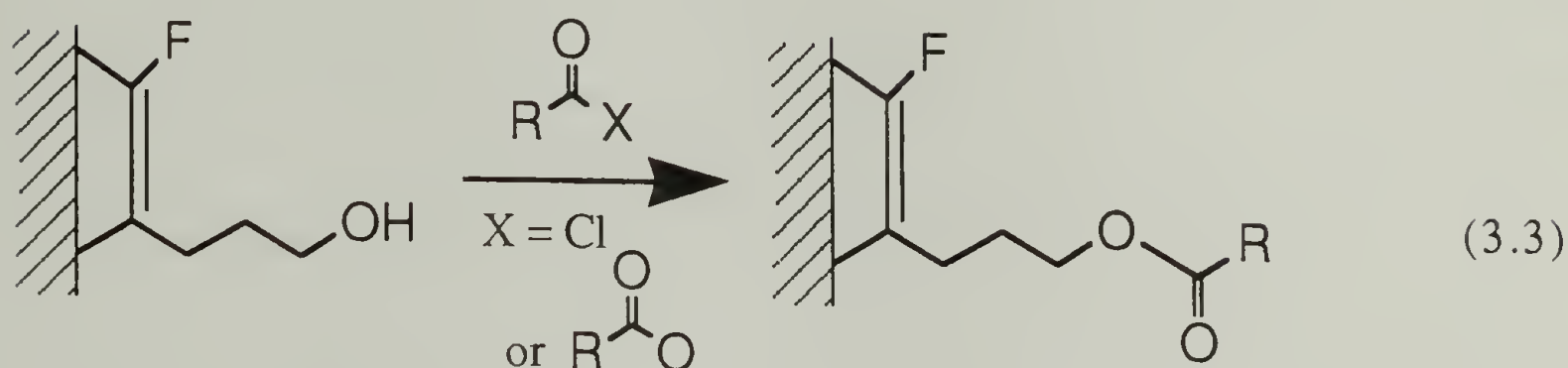
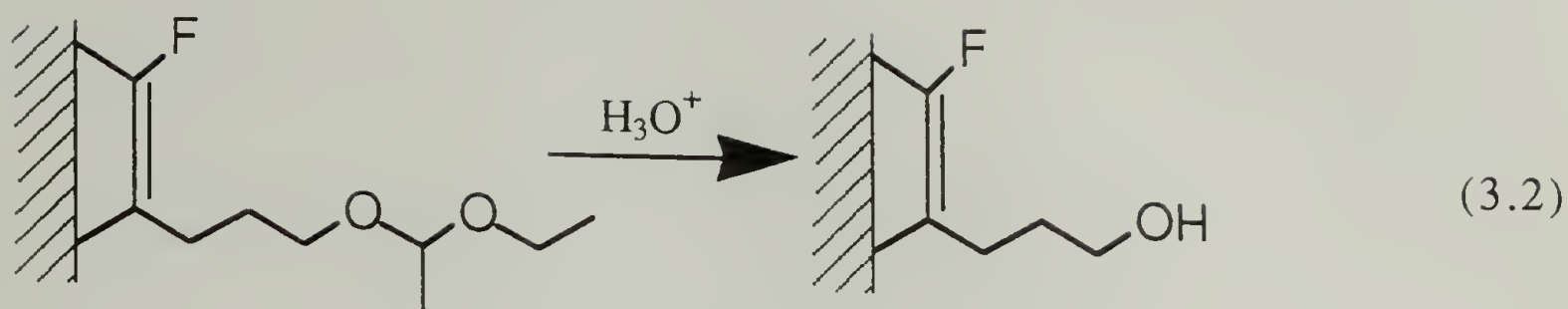


biocompatibility.<sup>6-16</sup> Other than wettability there has been little research concerned with influencing a specific surface property through well-controlled changes in surface chemistry. One example is the adhesion of a modified PCTFE surface containing triethoxy silane functionality to glass.<sup>17</sup> The understanding of and the ability to manipulate and characterize surface chemistry at the functional group level has now progressed to the point where an attempt to correlate surface structure and frictional behavior can be made.

In this research, the friction of chemically surface modified polychlorotrifluoroethylene (PCTFE) has been chosen for study. The surface modification chemistry developed for this substrate has been shown to be highly versatile.<sup>11</sup> The chemistry of the initial modification (Equation 3.1), to introduce the protected alcohol, is clean and well characterized,<sup>10</sup> although it may introduce some topographical changes in the surface. The depth of the reaction may be controlled by choice of time, temperature, solvent composition or alkyllithium concentration. In this dissertation, reaction temperature has been varied to control modified layer thicknesses.



The subsequent deprotection reaction (Equation 3.2) and further modifications proceed in high yield (Equation 3.3). The modifications do not alter the relatively inert substrate polymer, are also clean and



easily characterized, yet mild in comparison to the initial modification. It is assumed that any gross physical changes in the polymer surface take place only in the initial modification. Thus, any changes in friction behavior observed after further modification are due solely to the presence of different organic functional groups placed at the surface. Finally, reaction with multifunctional reagents can be utilized to crosslink the surface region, effecting a change in the surface modulus. The broad objective of the research presented in this chapter is to prepare a series of surface modified polymer film samples with well controlled and understood surface structures suitable for friction studies. Specifically, an acetal, an alcohol, a series of hydrocarbon and fluorocarbon ester surfaces with differing tail lengths and crosslinked surfaces, all with controlled modified layer thicknesses in the range of tens to thousands of angstroms were prepared and thoroughly characterized. Studies of the friction behavior of these samples are discussed in the following chapter.

## Experimental

### General

PCTFE film (5-mil Aclar 33C, Allied) was extracted in refluxing dichloromethane for 2 h and dried (0.05 mm, room temp., >24 h). Films for gravimetric analysis were dried (0.05 mm, 70 °C) for three days. Heptane (Aldrich) was distilled under nitrogen from calcium hydride. Benzene (Aldrich) and tetrahydrofuran (THF) (Aldrich, anhydrous) were distilled under nitrogen from sodium/benzophenone. 3-Bromo-1-propanol (Aldrich) was distilled under vacuum (5 mm, 60 - 64 °C) from potassium carbonate. Ethyl vinyl ether (Aldrich) was distilled (trap-to-trap) from calcium hydride immediately before use. Acetaldehyde 3-bromopropyl ethyl acetal (BrPEAA) was synthesized according to a previously described procedure.<sup>10</sup> *tert*-Butyllithium (*t*-BuLi) (Aldrich, 1.7 M in pentane) was standardized by titration with biphenylmethanol in THF at -78 °C.<sup>18</sup> Potassium chlorate was purchased from Alfa and used as received. Pyridine (Aldrich) was distilled under nitrogen from calcium hydride. Acetyl chloride and butyryl chloride (both Aldrich) were distilled and stored under nitrogen. Adipoyl chloride, decanoyl chloride and stearoyl chloride (all Aldrich) were vacuum distilled and stored under nitrogen. Trifluoroacetic anhydride and heptafluorobutyryl chloride (both Aldrich) were distilled (trap-to-trap) and stored under nitrogen. Perfluorodecanoic acid (Aldrich) was used as received. Methanol, dichloromethane (both Fisher, HPLC Grade), THF (Aldrich) and water (house distilled, redistilled with a



Gilmont Still) used as wash solvents were sparged with nitrogen. Other reagents were obtained from Aldrich and used as received. X-ray photoelectron spectra (XPS) were obtained with a Perkin Elmer-Physical Electronics 5100 with Mg  $K_{\alpha}$  excitation (400 W, 15.0 kV). Binding energies shown are not corrected for sample charging. Spectra were routinely recorded at two takeoff angles ( $\Theta_T$ ): 15° and 75° (measured between the film surface plane and the analyzer).<sup>19</sup> XPS atomic composition data were determined using sensitivity factors obtained from measurements made on samples of known surface composition: F1s, 1.00; C1s, 0.225; O1s, 0.620 and Cl2p, 0.655. Attenuated Total Reflectance Infrared (ATR-IR) spectra were obtained on an IBM 38 FTIR at 4 cm<sup>-1</sup> resolution using a 10x5x1 mm germanium internal reflection element with an entrance angle of 45°. UV-vis spectra were acquired on a Perkin Elmer Lambda 2 optics bench and data manipulated with an IBM PS/2 using Perkin Elmer PECSS UV-vis software. Spectra were recorded using an unreacted sample of PCTFE as the reference. Gravimetric measurements were made on a Cahn 29 Automatic Electrobalance. Dynamic advancing ( $\Theta_A$ ) and receding ( $\Theta_R$ ) contact angles were measured with a Ramé-Hart telescopic goniometer as the probe fluid was added to ( $\Theta_A$ ) and removed from ( $\Theta_R$ ) the sample surface with a Gilmont syringe fitted with a 24 gauge flat-tipped needle. Results are reported as  $\Theta_A/\Theta_R$ . Probe fluids used were water purified as described above or hexadecane vacuum distilled from calcium hydride and stored under nitrogen.

### Acetaldehyde 3-Lithiopropyl Ethyl Acetal (LiPEAA)

The synthesis of this reagent was accomplished using either of two procedures which give essentially identical modified surfaces (by all analytical techniques used in this study). However, the second procedure was found to yield more reproducible results and has the added advantage of indicating to the researcher that the organolithium reagent of interest has been formed in sufficient quantity to effectively modify the PCTFE surface before proceeding.

Procedure 1. BrPEAA (2.8 g, 13.3 mmol) was added via syringe to a dried nitrogen-purged reaction flask containing a glass-coated magnetic stir bar. Heptane (43 mL) was added and the solution cooled to -78 °C. *t*-BuLi (1.7 M, 7.7 mL, 13.1 mmol) in heptane (28 mL), also at -78 °C, was then added slowly to the BrPEAA solution via cannula. The mixture was stirred at this temperature for 30 min then placed in a -20 °C bath for 45 min. The resulting white suspension was then cooled to -78 °C and THF (79 mL, also at -78 °C) was added to dissolve the precipitate. (Notebook T3P13)

Procedure 2. BrPEAA (2.8 g, 13.3 mmol) was added via syringe to a dried nitrogen-purged reaction flask containing a glass-coated magnetic stir bar. Heptane (43 mL) was added and the solution cooled to -78 °C. *t*-BuLi (1.7 M, 7.9 mL, 13.4 mmol) in heptane (28 mL), also at -78 °C, was then added slowly to the BrPEAA solution via cannula. The mixture was stirred at this temperature for 30 min then placed in a -20 °C bath for 45 min. The resulting white suspension was then cooled to -78 °C and THF (79 mL, also at -78 °C)

was added to dissolve the suspension; yielding a clear, yellow solution. The yellow color is likely due to a complex between the excess *t*-BuLi and THF. The solution temperature was then allowed to gradually increase until the excess *t*-BuLi reacted with the THF solvent as indicated by the disappearance of the yellow color. (Notebook T7P43)

#### Reaction of LiPEAA with PCTFE Film (PCTFE-PEAA)

A nitrogen-purged Schlenk tube containing PCTFE film was equilibrated to the desired reaction temperature. (Reactions were conducted at temperatures of -78, -67, -60, -53, -27, and -15 °C.) A solution of LiPEAA in heptane/THF (prepared as described above) at the same temperature was then added via cannula to cover the film. After 30 min the reagent solution was removed and the film washed with methanol (1x at the reaction temperature), methanol (3x), H<sub>2</sub>O (3x), methanol (3x) and then dichloromethane (3x) and dried (0.05 mm, >24 h). Films for gravimetric analysis were dried more extensively (0.05 mm, 70 °C, 3 days). (Notebook T3P13, T4P87, T4P97, T4P127, T4P133, T4P141, T6P81, T7P43 and T7P117)

#### Hydrolysis of PCTFE-PEAA (PCTFE-OH)

PCTFE-OH was originally prepared from PCTFE-PEAA as reported previously<sup>11</sup> (3 h at reflux in a 30:65:5 solution of H<sub>2</sub>O:methanol:concentrated HCl), but it was subsequently discovered that these conditions dissolved the modified layer as it reacted (See the results and discussion of this chapter for details.). Thus, an alternate hydrolysis procedure was developed.



To a nitrogen-purged, jacketed (for reflux) Schlenk tube containing PCTFE-PEAA (prepared at -78, -60 or -15 °C) film and PTFE boiling chips, a solution of H<sub>2</sub>O:concentrated HCl (95:5 mL) was added via cannula. The reaction mixture was then heated to reflux. After 30 min the solution was removed and the film washed with H<sub>2</sub>O (3x), methanol (3x) and then dichloromethane (3x) and dried (0.05 mm, >24 h). (Notebook T6P91 and T7P71)

#### Reaction of PCTFE-OH with Acetyl Chloride (PCTFE-OAc)

To a nitrogen-purged Schlenk tube containing the PCTFE-OH film (initial modification temperature of -78 °C), 50 mL of THF was added followed by 1-2 mL of pyridine (12.4 - 24.8 mmole) and 1.24 mL of acetyl chloride (17.5 mmole). The films were allowed to react for 24 h under nitrogen at room temperature and then washed with THF (5x), H<sub>2</sub>O (5x); soaked in THF for >24 h; washed with THF (3x), soaked in H<sub>2</sub>O overnight (>16 h); washed with H<sub>2</sub>O (3x), methanol (5x) and then dichloromethane (5x) and dried (0.05 mm, room temp., >3 days). (Notebook T4P25 and T6P93)

#### Reaction of PCTFE-OH with Butyryl Chloride (PCTFE-OBu)

To a nitrogen-purged Schlenk tube containing the PCTFE-OH film (initial modification temperatures of -78, -60 or -15 °C), 50 mL of THF was added followed by 1-2 mL of pyridine (12.4 - 24.8 mmole) and 1.82 mL of butyryl chloride (17.5 mmole). The films were allowed to react for 24 h under nitrogen at room temperature and then washed with THF (5x), H<sub>2</sub>O (5x); soaked in THF for >24 h; washed with THF (3x); soaked in H<sub>2</sub>O overnight (>16 h); washed with

H<sub>2</sub>O (3x), methanol (5x) and then dichloromethane (5x) and dried (0.05 mm, room temp., >3 days). (Notebook T6P107, T7P85 and T7P131)

#### Reaction of PCTFE-OH with Decanoyl Chloride (PCTFE-ODec)

To a nitrogen-purged Schlenk tube containing the PCTFE-OH film (initial modification temperature of -78, -60 or -15 °C), 50 mL of THF was added followed by 1-2 mL of pyridine (12.4 - 24.8 mmole) and 3.63 mL of decanoyl chloride (17.5 mmole). The films were allowed to react for 24 h under nitrogen at room temperature and then washed with THF (5x), H<sub>2</sub>O (5x); soaked in THF for >24 h; washed with THF (3x); soaked in H<sub>2</sub>O overnight (>16 h); washed with H<sub>2</sub>O (3x), methanol (5x) and then dichloromethane (5x) and dried (0.05 mm, room temp., >3 days). (Notebook T6115, T7P99 and T7P135)

#### Reaction of PCTFE-OH with Stearoyl Chloride (PCTFE-OStear)

To a nitrogen-purged Schlenk tube containing the PCTFE-OH film (initial modification temperature of -78, -60 or -15 °C), 50 mL of THF was added followed by 1-2 mL of pyridine (12.4 - 24.8 mmole) and 5.91 mL of stearoyl chloride (17.5 mmole). The films were allowed to react for 24 h under nitrogen at room temperature and then washed with THF (5x), H<sub>2</sub>O (5x); soaked in THF for >24 h; washed with THF (3x); soaked in H<sub>2</sub>O overnight (>16 h); washed with H<sub>2</sub>O (3x), methanol (5x) and then dichloromethane (5x) and dried (0.05 mm, room temp., >3 days). (Notebook T6P121, T7P109 and T7P139)

#### Reaction of PCTFE-OH with Trifluoroacetic Anhydride (PCTFE-OTFAc)

To a nitrogen-purged Schlenk tube containing the PCTFE-OH film (initial modification temperature of  $-78\text{ }^{\circ}\text{C}$ ), 50 mL of THF was added followed by 1-2 mL of pyridine (12.4 - 24.8 mmole) and 2.47 mL of trifluoroacetic anhydride (17.5 mmole). The films were allowed to react for 24 hours under nitrogen and then washed with THF (5x), methanol (5x) and then dichloromethane (5x) and dried (0.05 mm, room temp., >3 days). (Notebook T4P45 and T6P99)

#### Reaction of PCTFE-OH with Heptafluorobutyryl Chloride (PCTFE-OHFB)

To a nitrogen-purged Schlenk tube containing the PCTFE-OH film (initial modification temperature of  $-78$ ,  $-60$  or  $-15\text{ }^{\circ}\text{C}$ ), 50 mL of THF was added followed by 2.61 mL of heptafluorobutyryl chloride (17.5 mmole). The films were allowed to react for 24 h under nitrogen and then washed with THF (5x), methanol (5x) and then dichloromethane (5x) and dried (0.05 mm, room temp., >3 days). (Notebook T6P109, T7P89 and T7P127)

#### Preparation of Perfluorodecanoyl Chloride (PFDecCl)

Perfluorodecanoic acid (10 g, 19.5 mmol) was added to a nitrogen-purged 100 mL 3-necked round bottom flask containing a magnetic stir bar. The flask was then purged with nitrogen and  $\text{PCl}_5$  (4.1 g, 19.7 mmol) added. After a couple of minutes at room temperature, reaction between the two solids began to occur as evidenced by the formation of an oily liquid. After 1 h, the liquid was separated from any solid that remained and transferred via



cannula to a 50 mL round bottom flask under nitrogen. Benzene (15 mL) was then added and the flask stored in a refrigerator overnight during which time crystals of PFDecCl formed. The benzene was then removed via cannula under nitrogen and fresh benzene added. The mixture was then heated above the melting point of the crystals ( $\sim 28$  °C) and allowed to recrystallize in the refrigerator. This recrystallization procedure was repeated three additional times. The final benzene wash was then removed and the crystals dissolved in  $\sim 50$  mL of THF for preparation of PCTFE-OPFDec. (Notebook T6P123 and T7P1113)

#### Reaction of PCTFE-OH with PFDecCl (PCTFE-OPFDec)

To a nitrogen-purged Schlenk tube containing the PCTFE-OH film (initial modification temperature of -78, -60 or -15 °C), 15 mL of the PFDecCl/THF solution from above was added; followed by 35 mL of THF. The films were allowed to react for 24 hours under nitrogen and then washed with THF (5x), methanol (5x); soaked in THF >24 h; washed with THF (3x), methanol (3x) and then dichloromethane (5x) and dried (0.05 mm, room temp., >3 days). (Notebook T6P127, T7P115 and T7P141)

#### Reaction of PCTFE-OH with Adipoyl Chloride (PCTFE-O<sub>2</sub>Adip)

To a nitrogen-purged Schlenk tube containing the PCTFE-OH film (initial modification temperature of -78 or -15 °C), 50 mL of THF was added followed by 3 mL of pyridine (12.4 - 24.8 mmole) and 2.54 mL of adipoyl chloride (37.2 mmole). The films were allowed to react for 24 h under nitrogen at room temperature and then washed

with THF (5x), methanol (5x) (the -78 °C surface) or H<sub>2</sub>O (5x) (the -15 °C surface); soaked in THF for >24 h; washed with THF (3x); soaked in H<sub>2</sub>O overnight (>16 h); washed with H<sub>2</sub>O (3x), methanol (5x) and then dichloromethane (5x) and dried (0.05 mm, room temp., >3 days). (Notebook T7P53 and T7P83)

#### Reaction of PCTFE-OH with 1,3,5-Benzenetricarbonyl Trichloride (PCTFE-O<sub>3</sub>Benz)

To a nitrogen-purged Schlenk tube containing the PCTFE-OH film (initial modification temperature of -78 or -15 °C) and 1,3,5-benzenetricarbonyl trichloride (4.65 g, 17.5 mmol), 50 mL of THF was added followed by ~5 mL of pyridine (~62 mmole). The films were allowed to react for 24 h under nitrogen at room temperature and then washed with THF (5x), methanol (5x) (the -78 °C surface) or H<sub>2</sub>O (5x) (the -15 °C surface); soaked in THF for >24 h; washed with THF (3x); soaked in H<sub>2</sub>O overnight (>16 h); washed with H<sub>2</sub>O (3x), methanol (5x) and then dichloromethane (5x) and dried (0.05 mm, room temp., >3 days). (Notebook T7P49 and T7P93)

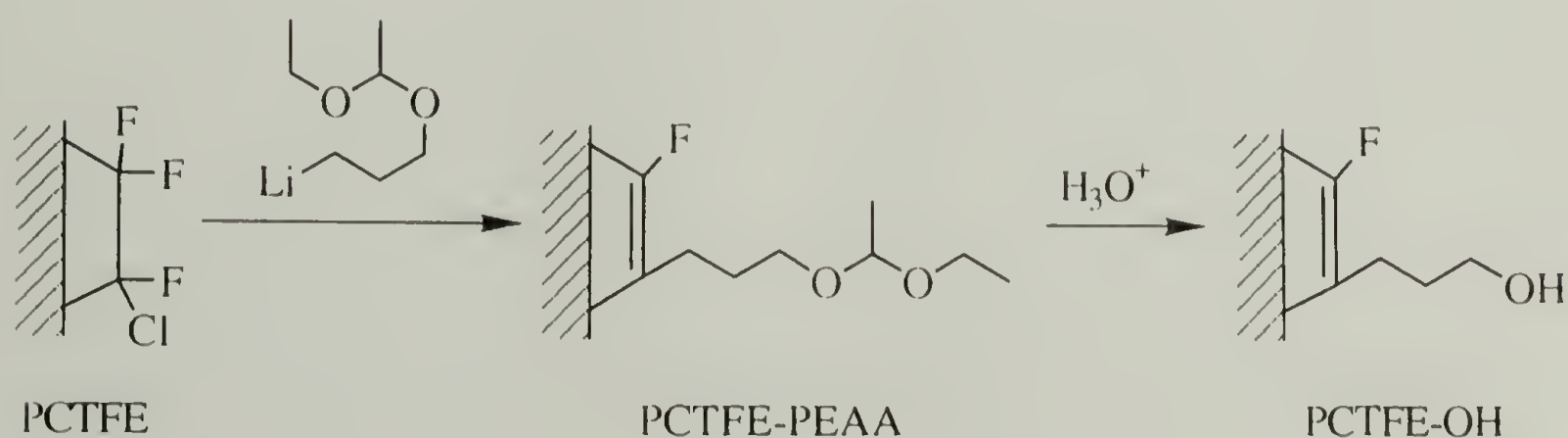
#### Oxidation of Modified Film Samples

Surface modified film samples were placed in a solution of 1.0 g of KClO<sub>3</sub> in 50 mL of concentrated H<sub>2</sub>SO<sub>4</sub> for 2 h (PCTFE-OPFDec samples required 8 h oxidations). The films were then removed from the oxidizing solution, rinsed with distilled water, soaked in distilled water for 2 h, in methanol for 2 h, in dichloromethane for 1 h and dried (0.05 mm, 70 °C, 3 days). (Notebook T3P47)

## Results and Discussion

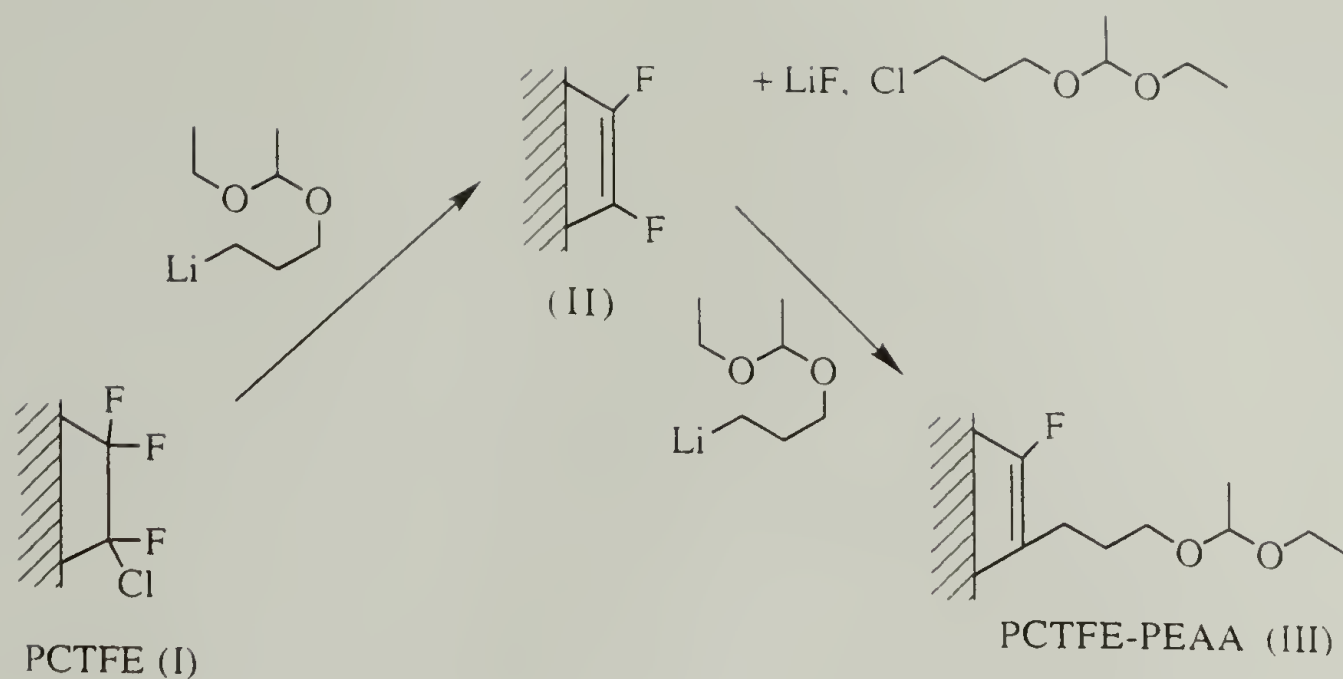
### Initial Modification (PCTFE-PEAA)

The strategy utilized to introduce hydroxyl groups into the surface of poly(chlorotrifluoroethylene) (PCTFE) is shown in Scheme 3.1. The initial modification uses an organolithium reagent (acetaldehyde 3-lithiopropyl ethyl acetal (LiPEAA)) containing a hydroxyl group protected as an acetal. The depth of the initial modification can be controlled by four factors: temperature, time, solvent composition and reagent concentration.<sup>10</sup> The acetal may then be converted to the desired alcohol by hydrolysis in aqueous acid. The preparation and characterization of these two surfaces has been discussed previously.<sup>10,11</sup> However, as a prerequisite to preparing modified surfaces for friction studies, it was necessary to duplicate and add to much of the earlier work. From this replicate study, an improved understanding of the processes involved in these modifications has evolved.



**Scheme 3.1.** Introduction of alcohol groups into the surface of PCTFE.





**Scheme 3.2.** Reaction of PCTFE with LiPEAA.

PCTFE reacts with LiPEAA in THF/heptane (50:50) at -78 to -15 °C by the reduction-elimination-addition reaction shown in Scheme 3.2. This solvent ratio was chosen in order to make comparisons with other PCTFE-organolithium surface modifications.<sup>10,21</sup> One of the objectives of this research was to prepare surfaces for friction studies with varying modified layer thicknesses. Thus, the dependence of modified layer thickness on reaction temperature (-78, -67, -60, -53, -27 and -15 °C) was studied in detail. After reaction, gravimetric analysis indicates a small weight loss, more so at the higher modification temperatures (5 - 90  $\mu\text{g}$  for  $\sim 3\text{ cm}^2$  films at reaction temperatures from -78 - -15 °C); however, a small weight gain would be expected based on the chemistry depicted in Scheme 3.2. These results indicate that this reaction is slightly corrosive. It is thought that the modified surface layer is somewhat soluble in the reaction medium and dissolves as the reaction progresses, although this process has not been studied in

detail.<sup>10</sup> However, visual inspection and SEM of the modified films show no differences from virgin PCTFE: both samples appear flat. Water contact angle data (Table 3.1) indicate, as expected, that upon introduction of the relatively polar acetal group, a more hydrophilic surface is produced. The increase in contact angle hysteresis (the difference between  $\Theta_A$  and  $\Theta_R$ ) with increasing modification temperature ( $\Theta_A/\Theta_R = 77^\circ/46^\circ$  for a  $-78^\circ\text{C}$  reaction and  $88^\circ/37^\circ$  for a  $-15^\circ\text{C}$  reaction) indicates a small increase in surface roughness,<sup>22</sup> as would be expected for a slightly corrosive reaction.

**Table 3.1.** Water contact angle data ( $\Theta_A/\Theta_R$ ) for modified surfaces used in friction studies.

	<u>Initial Modification Temperature</u>		
<u>Surface</u>	<u><math>-78^\circ\text{C}</math></u>	<u><math>-60^\circ\text{C}</math></u>	<u><math>-15^\circ\text{C}</math></u>
PCTFE		104°/77°	
PCTFE-PEAA	77/46	79/44	88/37
PCTFE-OH	67/17	---	69/12
PCTFE-OAc	82/46	---	---
PCTFE-OBu	89/54	91/49	93/40
PCTFE-ODec	106/57	110/55	117/47
PCTFE-OSTear	108/90	111/90	117/90
PCTFE-OTFAc	92/51	---	---
PCTFE-OHFB	107/68	107/69	112/60
PCTFE-OPFDec	120/69	123/69	126/64
PCTFE-O <sub>2</sub> Adip	81/35	---	79/30
PCTFE-O <sub>3</sub> Benz	80/52	---	47/12

Figures 3.1 and 3.2 show XPS survey and C1s spectra of PCTFE and PCTFE-PEAA prepared at -78 and -15 °C (75° takeoff angle). As expected, the PCTFE-PEAA survey spectra (Figure 3.1) show a decrease in the intensity of fluorine and chlorine (chlorine is completely removed from the XPS sampling region at -15 °C), an increase in the amount of carbon and the incorporation of a significant amount of oxygen into the surface of the film. The C1s spectrum of the surface reacted at -78 °C (Figure 3.2b) shows a decrease in the intensity of the high binding energy peak at 295 eV assigned to unmodified PCTFE, and the emergence of a lower binding energy peak containing a high binding energy shoulder.

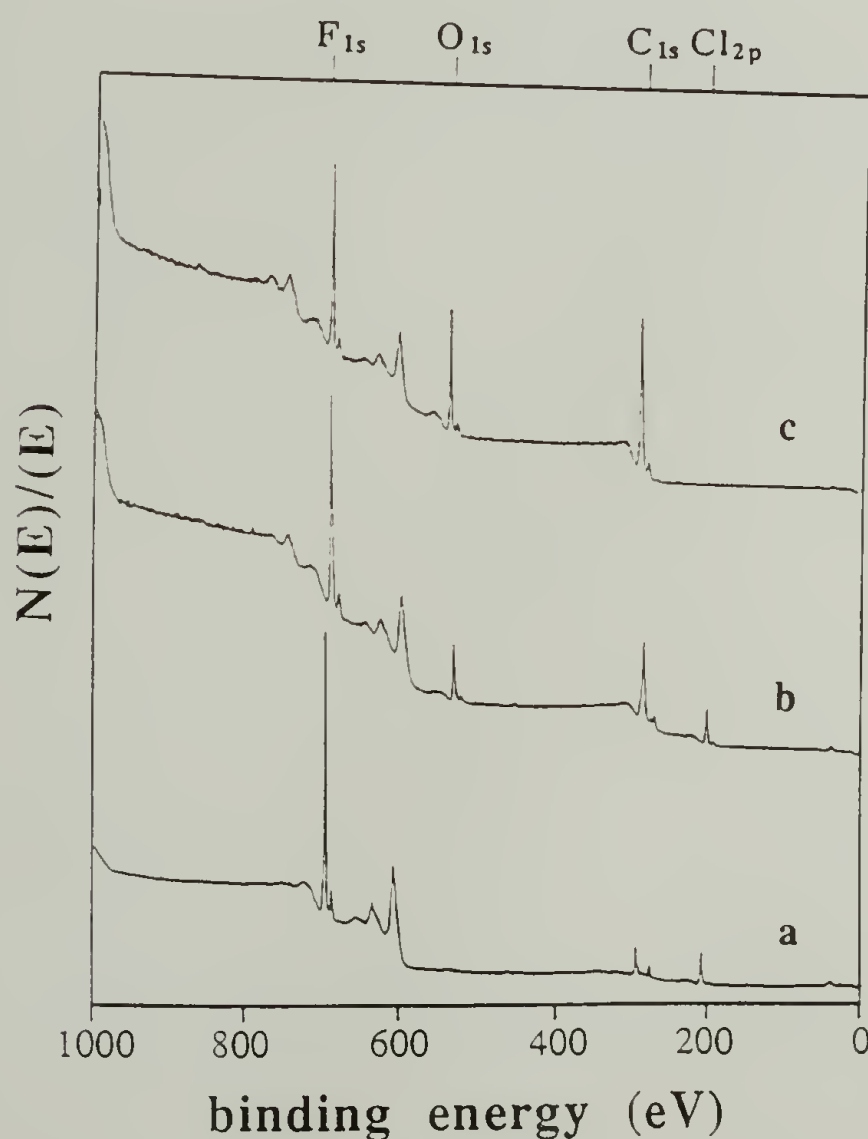


**Figure 3.1.** XPS survey spectra (75° takeoff angle) of: (a) PCTFE, (b) PCTFE-PEAA (-78 °C) and (c) PCTFE-PEAA (-15 °C).



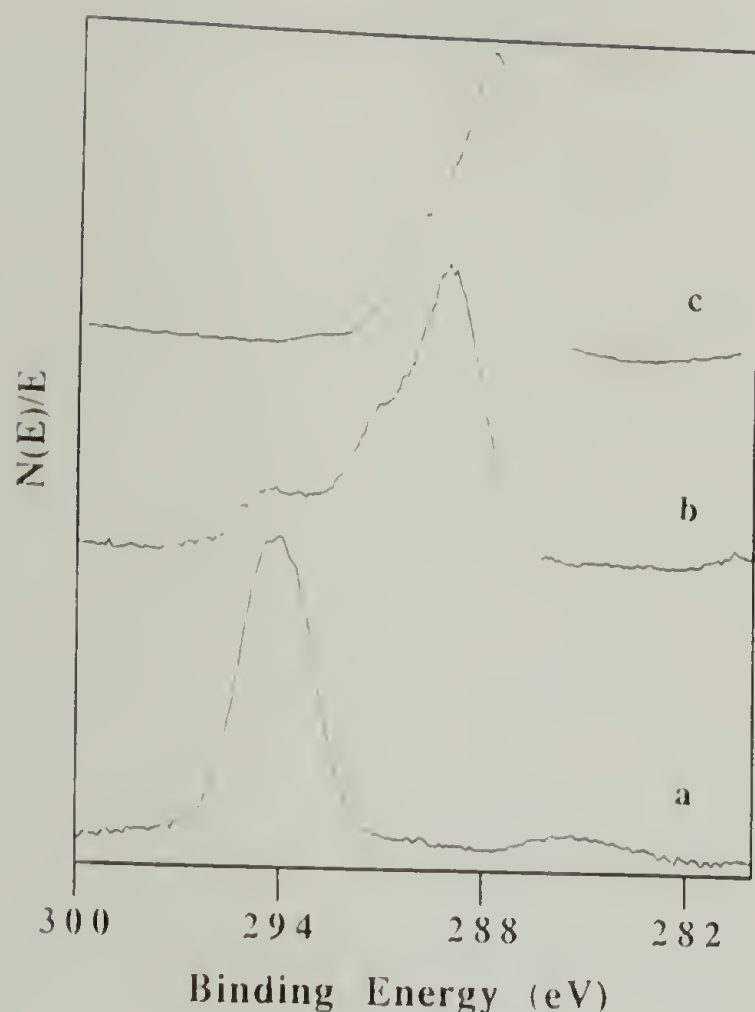


**Figure 3.2.** XPS C1s spectra (75° takeoff angle) of: (a) PCTFE, (b) PCTFE-PEAA (-78 °C) and (c) PCTFE-PEAA (-15 °C).

Assuming that the modified polymer is present as a uniformly thick overlayer (The absence of virgin PCTFE in the outer 10 Å, as indicated by the 15° takeoff angle spectra,<sup>19</sup> supports this assumption.), the relative peak areas of modified to unmodified material can be used calculate a modified layer thickness of ~30 Å.<sup>23</sup> The absence of this peak in the spectrum of the film reacted at -15 °C (and the absence of chlorine in the survey spectrum) indicates that the reaction has proceeded entirely through the XPS sampling depth (~54 Å using a mean free path of 18 Å for Cl2p photoelectrons) at this temperature. The complex peak in the spectrum of the sample prepared at -15 °C and the analogous peak from the -78 °C sample

consists of a low binding energy main peak due to carbons bonded only to hydrogen or other carbons and a high binding shoulder assigned to carbons bonded to one or two oxygens or one fluorine as expected based on the structure of the modified repeat unit (Scheme 3.2).

**Table 3.2.** XPS atomic composition data for PCTFE-PEAA and PCTFE-OH used in friction studies.

<u>Surface</u>		<u>Experimental</u>					<u>Calculated<sup>a</sup></u>		
		<u>Θ<sub>T</sub></u>	<u>C</u>	<u>F</u>	<u>O</u>	<u>Cl</u>	<u>C</u>	<u>F</u>	<u>O</u>
PCTFE-PEAA	-78 °C	15	73.1	13.0	13.4	0.5	73.1	11.5	15.4
		75	68.7	17.1	11.4	2.9			
	-60	15	73.3	12.0	14.5	0.2			
		75	71.1	15.0	12.1	1.8			
	-15	15	74.6	10.1	15.1	0.3			
		75	75.1	11.2	13.2	0.2			
PCTFE-OH	-78 °C	15	68.4	18.8	11.2	1.6	68.8	18.8	12.5
		75	61.4	22.8	10.9	4.8			
	-15	15	68.2	18.8	12.5	0.4			
		75	67.5	18.8	12.5	1.2			

<sup>a</sup>Calculated atomic compositions are based on a surface structure where four of the five polymer repeat units contain the functionality of interest with the fifth being a difluorolefin. (See text for details.)

Analysis of the XPS atomic composition data (Table 3.2) yields a more quantitative interpretation of the modified surface structure. The stoichiometry for a modified surface consisting only of acetal containing repeat units is predicted to be C<sub>9</sub>F<sub>1</sub>O<sub>2</sub>. The observed stoichiometries of PCTFE-PEAA prepared at -15 °C are C<sub>9</sub>F<sub>1.2</sub>O<sub>1.8</sub> (15° takeoff angle) and C<sub>9</sub>F<sub>1.3</sub>O<sub>1.6</sub> (75° takeoff angle). The high fluorine

content and low oxygen content in the experimentally measured values are inconsistent with those predicted based on a quantitative reaction yield and counter to what would be expected from sample contamination or oxidation. It has been proposed<sup>11</sup> that the modified structure is one consisting of ~80% acetal-functionalized repeat units and ~20% difluoroolefins (Figure 3.3). The stoichiometry of this structure is  $C_{38}F_6O_8$ . The observed composition is  $C_{38}F_{5.1}O_{7.7}$  ( $15^\circ$  takeoff angle) and  $C_{38}F_{5.7}O_{6.8}$  ( $75^\circ$  takeoff angle).

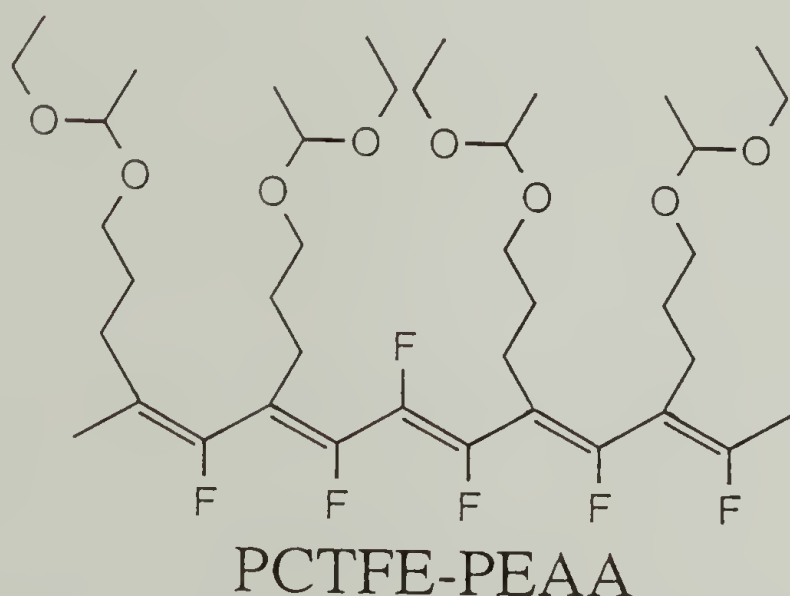


**Figure 3.3.** Surface structure of PCTFE-PEAA. (See text for details.)

The validity of the proposed structure is supported by the agreement between experimentally determined atomic composition ratios and those calculated based on this structure for a number of modified surfaces prepared from PCTFE-PEAA.<sup>11</sup> This structure has been rationalized by proposing that the first step in Scheme 3.2 (formation of the difluoroolefin) proceeds quantitatively, while the second step (introduction of the acetal moiety) proceeds in 80% yield. Similar results have been observed in other reactions of organolithium



reagents with PCTFE and have been attributed to steric factors.<sup>11,21</sup> The stoichiometries calculated from the 15° takeoff angle data (Table 3.2) for the PCTFE-PEAA surfaces prepared at -78 °C ( $C_{38}F_{6.8}O_{7.0}$ ) and -60 °C ( $C_{38}F_{6.2}O_{7.5}$ ) are also in good agreement with that calculated for the proposed surface structure (more so for the sample prepared at -60 °C). The 75° takeoff angle data (Table 3.2) for both of these modification temperatures show a significant amount of chlorine (2.9% and 1.8% at -78 and -60 °C respectively) indicating that thinner modified layer have been prepared at these lower reaction temperatures (As expected, the data indicate that the surface prepared at -78 °C is the thinner of the two).

For the more deeply modified surfaces, ATR-IR becomes a more information rich technique for qualitative analysis. Figure 3.4 shows ATR-IR spectra for modifications conducted at -78, -53 and -15 °C. The -78 °C modification introduces few features into the ATR-IR sampling region due to its shallow modification depth. The appearance of a small amount of absorbance is observed in the C-H stretching ( $3000 - 2840\text{ cm}^{-1}$ ) and bending ( $1500 - 1320\text{ cm}^{-1}$ ) regions of this spectrum, as well as a weak, broad peak at  $1675\text{ cm}^{-1}$  which is assigned to the unsaturation in the modified polymer backbone. The breadth of this peak in the latter region indicates the presence of a range of conjugation lengths. As the reaction temperature is increased to -53 °C, the C-H stretching region becomes more pronounced and distinct peaks are observed for the methyl and methylene symmetric and asymmetric stretching vibrations. Also, the absorbance in the C-H bending region and that due to the C=C double bonds increase in intensity and a small shoulder is observed

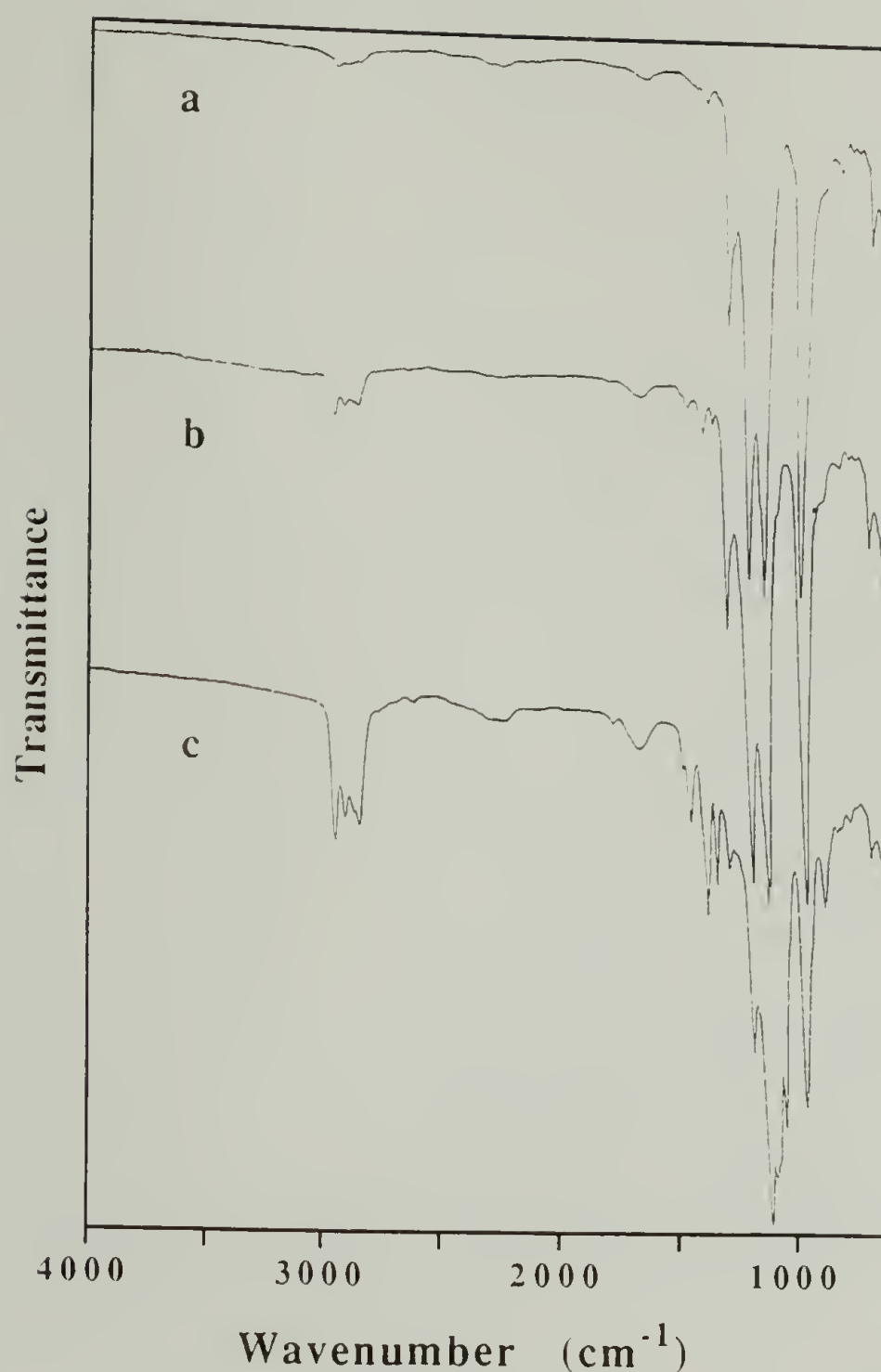


**Figure 3.4.** ATR-IR spectra of: (a) PCTFE-PEAA (-78 °C), (b) PCTFE-PEAA (-53 °C) and (c) PCTFE-PEAA (-15 °C).

on the low frequency side of the  $\text{-CF}_2\text{-}$  symmetric stretching peak ( $1127\text{ cm}^{-1}$ ), which is assigned to the C-O-C asymmetric stretching vibration. When the reaction temperature is  $-15\text{ }^{\circ}\text{C}$ , a significant amount of absorbance with the same pattern as the spectrum of acetaldehyde 3-bromopropyl ethyl acetal, is measured. The C-H stretching and bending regions are well developed as is the peak assigned to the unsaturated, modified polymer backbone

(1675  $\text{cm}^{-1}$ ). Additionally, the intensities of the C-O-C stretching peaks (1120 - 1020  $\text{cm}^{-1}$ ) are now very strong. The intensity of absorption indicates, that at a temperature of -15 °C, the modification depth is on the order of thousands of angstroms.

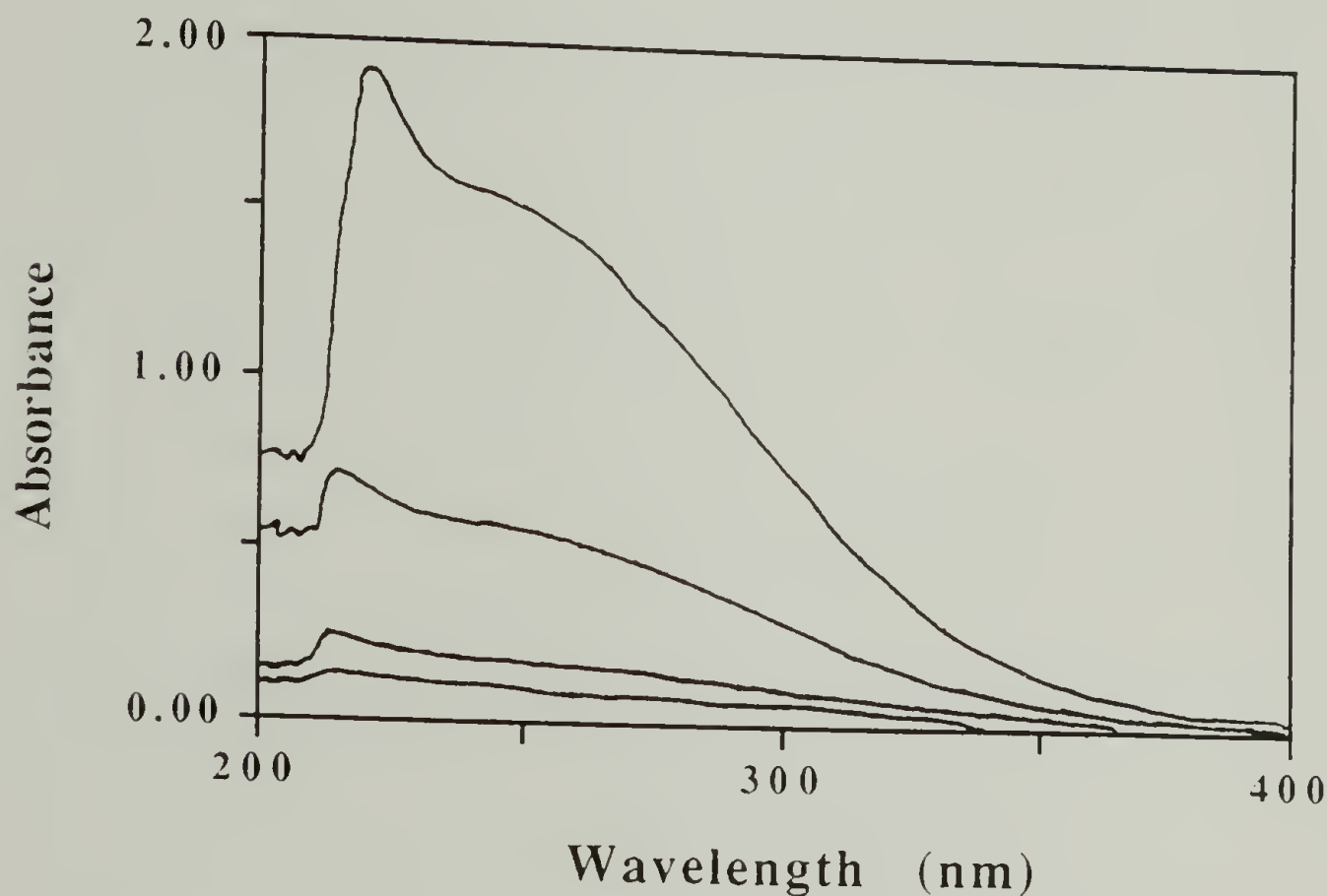


**Figure 3.5.** UV-vis spectra of PCTFE-PEAA (-78, -67, -27 and -15 °C from low to high absorbance).

Figure 3.5 shows UV-vis transmission spectra for samples reacted at a number of temperatures. The UV absorbance in the PCTFE-PEAA films arises from the conjugation introduced into the polymer backbone as a result of the modification. It is readily observed that the absorbance increases as the reaction temperature is increased. This increased absorbance can be attributed to an increase in the number of the absorbing moieties, which translates into an increase in the thickness of the modified layer. These results



provide a convenient method of estimating the depth of modification for the higher temperature reactions. Using the value of 30 Å (as calculated above from the XPS C1s spectrum) for the thickness of the modified layer in the sample prepared at -78 °C, an extinction coefficient of 920 Å/a.u. can be calculated from the absorbance value at 270 nm. Assuming that a Beer's Law relationship is followed, this extinction coefficient can be used to calculate modified layer thicknesses from absorbance values. These thicknesses as a function of reaction temperature are plotted in Figure 3.6.

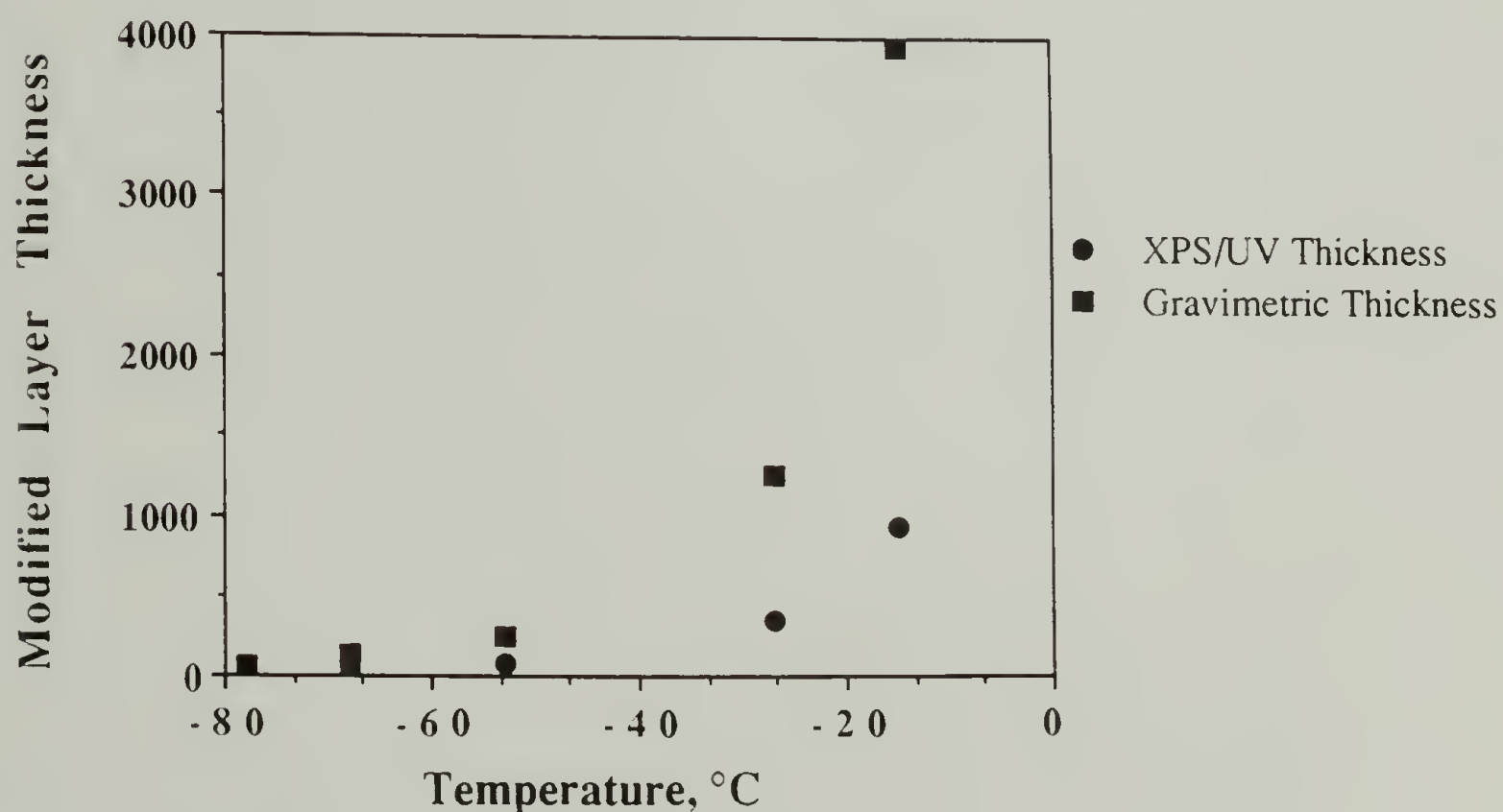
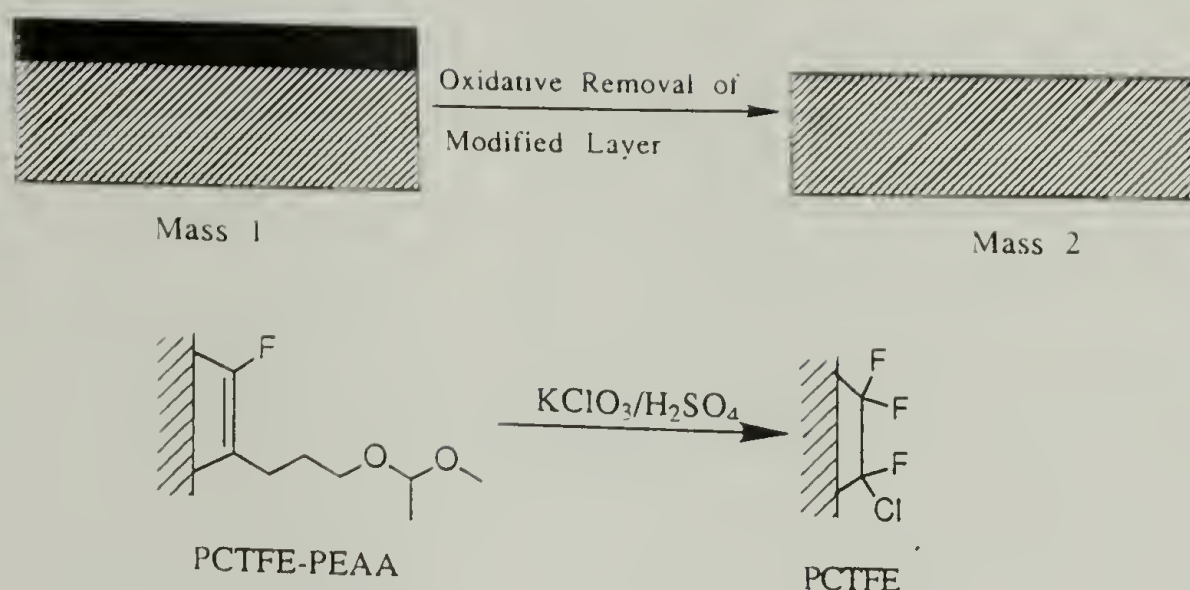
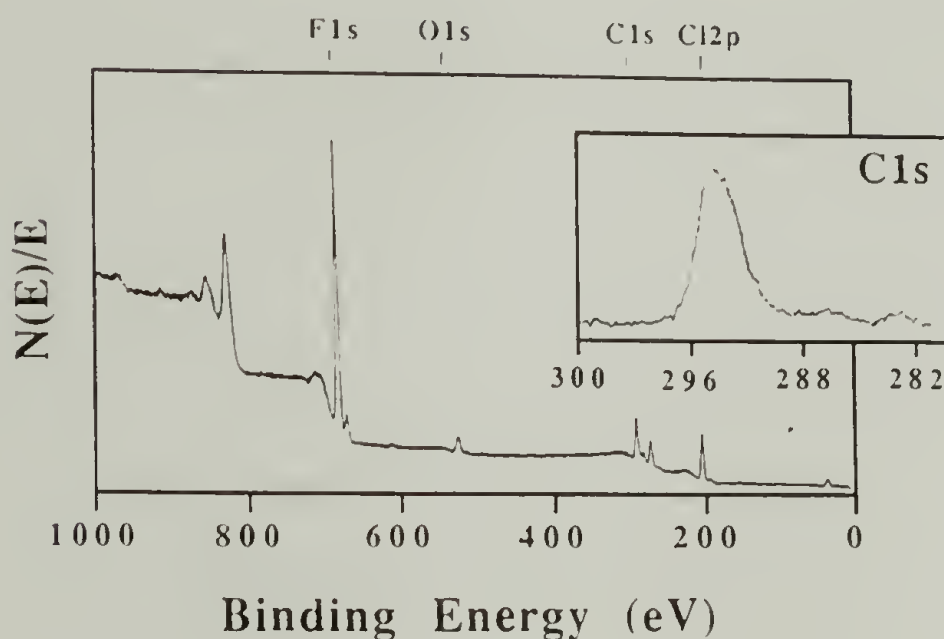


Figure 3.6. Modified layer thickness as a function of modification temperature. (See text for details.)



**Scheme 3.3.** Oxidative removal of modified layer.



**Figure 3.7.** XPS survey and C1s spectra of oxidized PCTFE-PEAA (prepared at  $-15^{\circ}\text{C}$ ).

A different estimate of the modified layer thickness can be made by oxidatively removing the modified layer (as shown in Scheme 3.3). From measurement of the resulting weight loss, the known film surface area and an assumed density for the modified layer ( $2 \text{ g/cm}^3$  - slightly less than that of PCTFE), a modified layer thickness may be calculated. Figure 3.7 shows the XPS spectra ( $15^{\circ}$  takeoff angle) of PCTFE-PEAA (prepared at  $-15^{\circ}\text{C}$ ) after oxidation

with  $\text{KClO}_3/\text{H}_2\text{SO}_4$ . As can be seen, the original PCTFE is almost completely recovered. The small amount of oxygen present is likely due to carboxylic acid groups which remain attached to the surface as a result of the oxidation.<sup>25</sup> ATR-IR and UV-vis spectra of the same sample are also essentially identical to virgin PCTFE. Control reactions on unmodified PCTFE show no changes by any technique. Thus, this oxidation removes all of the modified layer from the surface of the film while not affecting the virgin material underneath. These thickness values are also plotted versus reaction temperature in Figure 3.6. Differences between these results and those obtained from the XPS/UV-vis absorbance data are likely due to a number of factors. The XPS/UV-vis results depend on the validity of Beer's Law in this solid and a modified layer thickness calculated from the XPS C1s spectral data of the sample modified at  $-78\text{ }^\circ\text{C}$ . The accuracy of the XPS calculated thickness depends on two assumptions: (1) the surface modification is non-corrosive and gives a sharp interface that is parallel to the film surface (no unmodified PCTFE is present beneath the depth sampled by XPS) and (2) the mean free path of the C1s photoelectrons in the modified surface layer is the same as it is in the material in which it was measured.<sup>20</sup> As discussed earlier, gravimetric measurements (and to some extent, the contact angle data) made after the initial modification indicate that this reaction is somewhat corrosive in nature. Also, in kinetics experiments for the reaction conducted at  $-78\text{ }^\circ\text{C}$ ,<sup>10</sup> no changes were observed in the XPS spectra after 5 min of reaction, while the absorbances in the UV-vis and ATR-IR spectra continued to increase in intensity even after 60 min. These results indicate that a



significant amount of reaction was occurring beyond the XPS sampling depth. Thus, the interface between modified and unmodified PCTFE is likely diffuse, resulting in an unknown amount of modified polymer below the XPS sampling depth. Hence, the XPS calculated modified layer thickness for the sample reacted at  $-78\text{ }^{\circ}\text{C}$  underestimates the amount of reacted material. The gravimetric measurements likely overestimate the thickness of the modified layer. Unreacted PCTFE (low molecular segments of chains between modified blocks and/or crystalline regions unaffected by the modification) is likely removed in the oxidation, increasing the mass loss.

Although these may be rough estimates of the modified layer thickness, they do provide insight into the interface structure of the modified film sample and are useful for comparison with other PCTFE/organolithium surface modifications and with further modifications of this acetal surface (see below). From the initial gravimetric data, the water contact angles and these thickness estimates, it is proposed that the physical structure of the modified film looks somewhat like that shown in Figure 3.8. After modification, the surface of the film is slightly roughened and there is a somewhat diffuse boundary layer between the modified (which contains crystalline regions of unreacted PCTFE) and unmodified regions. It is also interesting to compare the modified thicknesses reported here with those estimated for PCTFE modified with trimethyl orthobutyrate functionality (see Chapter II of this dissertation). It is observed that at all reaction temperatures the acetal modified layer is much thicker than that of the orthoester and

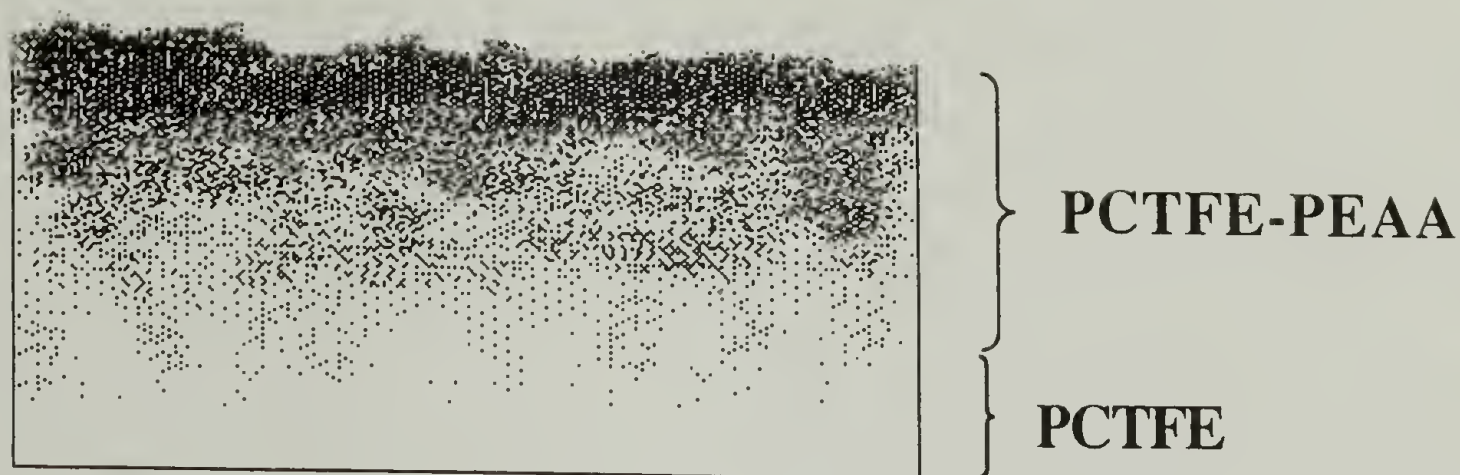


**Figure 3.8.** Proposed physical structure of surface-modified PCTFE.

that this difference becomes more pronounced at the higher reaction temperatures. These differences lie in the manner in which the product polymer surface interacts with the reagent and with the reaction solution.<sup>26</sup> The data indicate that the acetal-containing modified surface interacts more strongly with the organolithium reagent and/or is swollen to a greater extent by the solvent than the unreacted polymer resulting in a thick modified layer. For the orthoester surface, these interactions are of similar magnitude for both the unreacted and product polymer surfaces yielding modified layer thicknesses in the range of  $\sim 25 - 100 \text{ \AA}$ . In other PCTFE/organolithium reactions,<sup>10,26,27</sup> the product surface interacts with the reagent and/or the solvent to a lesser extent than the unmodified polymer resulting in autoinhibition and much thinner modified layers ( $\sim 10 - 50 \text{ \AA}$ ).

### Hydrolysis of PCTFE-PEAA (PCTFE-OH)

The acetal, PCTFE-PEAA, can be hydrolyzed to the corresponding alcohol, PCTFE-OH, (Scheme 3.1, page 95) using refluxing, aqueous HCl for 30 min. Early work was done on thinly modified surfaces (prepared from samples initially modified at  $-78^{\circ}\text{C}$ ) by reacting PCTFE-PEAA in a refluxing solution of aqueous/methanolic HCl for 3 h, as described previously.<sup>11</sup> However, upon closer examination of the resulting product surface using the more deeply modified samples (prepared from samples initially modified at  $-15^{\circ}\text{C}$ ), it was discovered that these conditions dissolved the modified layer as it reacted. Thus, it was necessary to reascertain the appropriate hydrolysis conditions in order to obtain the thickest possible alcohol modified surface, while at the same time maintaining complete deprotection of the acetal.

Figure 3.9 shows ATR-IR spectra for a series of hydrolyses conducted in refluxing, acidic solutions of varying methanol:water ratios for 3 h. The spectrum of the sample hydrolyzed in pure methanol (Figure 3.9a) displays a broad hydrogen-bonded O-H band ( $3330\text{ cm}^{-1}$ ), the methylene C-H stretching bands ( $2990 - 2830\text{ cm}^{-1}$ ) and a shoulder on the low frequency side of the  $\text{CF}_2$  symmetric stretching peak ( $1127\text{ cm}^{-1}$ ), which is assigned to the C-O stretching vibration. Also, it is observed that the peak assigned to the C=C double bond stretching ( $1675\text{ cm}^{-1}$ ) in the modified polymer backbone has decreased in intensity (Compare with Figure 3.4c, page 103). This result, along with the unexpectedly low methylene and C-O absorbances (based on the intensity of the peaks in the spectrum of deeply modified PCTFE-PEAA) indicates that a significant amount



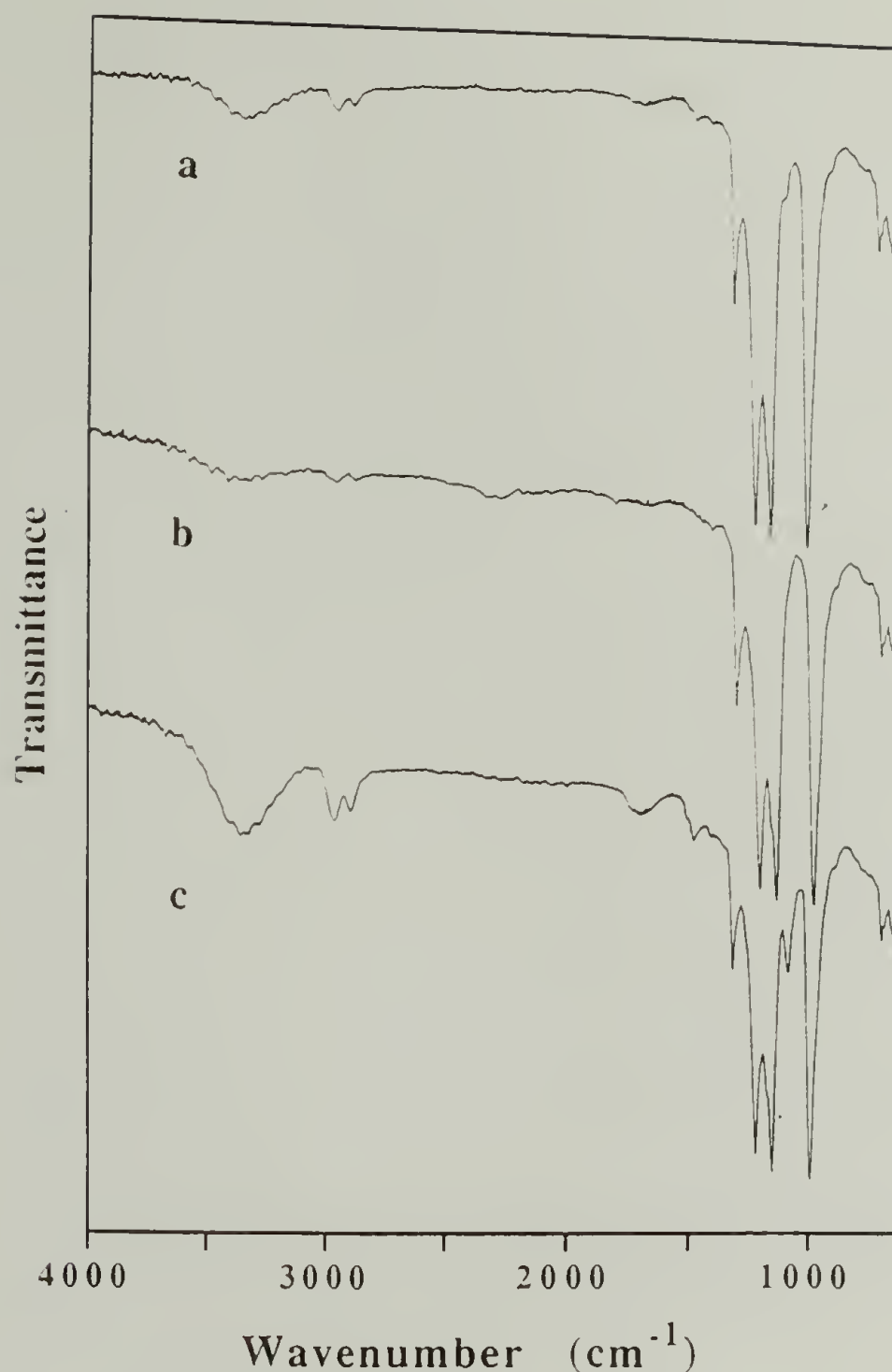


**Figure 3.9.** ATR-IR spectra of the hydrolysis product of PCTFE-PEAA (-15 °C) as a function of solvent composition (methanol:water): (a) (100:0), (b) (50:50) and (c) (0:100).

of dissolution of the product surface has occurred during the hydrolysis. When the hydrolysis solution composition is changed to 50% aqueous methanol (Figure 3.9b) the product alcohol surface has almost completely dissolved. There are two factors that determine the extent of dissolution of the modified layer: (1) the rate of hydrolysis (The faster the modified polymer is produced, the faster it

can dissolve.) and (2) the solubility of the modified polymer in the reaction solvent, which depends on the solvent composition and the reaction temperature. It would be expected that at the same temperature pure methanol would be a better solvent for PCTFE-OH than 50% aqueous methanol<sup>28</sup> and would wet the film better, increasing the rate of reaction.<sup>29</sup> However, these reactions were conducted at the boiling points of the respective solvents which may lead to a higher relative solubility of PCTFE-OH in aqueous methanol and/or may result in an increase in the hydrolysis rate over that in pure methanol. The ATR-IR spectrum of a film sample hydrolyzed in aqueous HCl (no methanol) is displayed in Figure 3.9c. Under these conditions very little of the product surface has dissolved. The intensities of the peaks assigned to the hydroxyl and methylene stretching and the unsaturated backbone are strong and there is now a distinct peak at  $1060\text{ cm}^{-1}$  from the C-O stretching vibration. Once a suitable hydrolysis solvent was determined, the intensity of this C-O stretching peak was used to optimize the reaction time. The conditions ultimately arrived at involved refluxing the film sample in aqueous HCl for 30 min, resulting in the ATR-IR spectrum shown in Figure 3.10.

Upon deprotection the water contact angles ( $\Theta_A/\Theta_R = 67^\circ/17^\circ$  and  $69^\circ/12^\circ$  for surfaces initially modified at  $-78$  and  $-15^\circ\text{C}$  respectively, Table 3.1, page 97) decrease as expected for a more polar, hydrophilic surface. As with PCTFE-PEAA, it is observed that the contact angle hysteresis increases with an increase in the initial modification temperature, indicating a small increase in surface roughness.

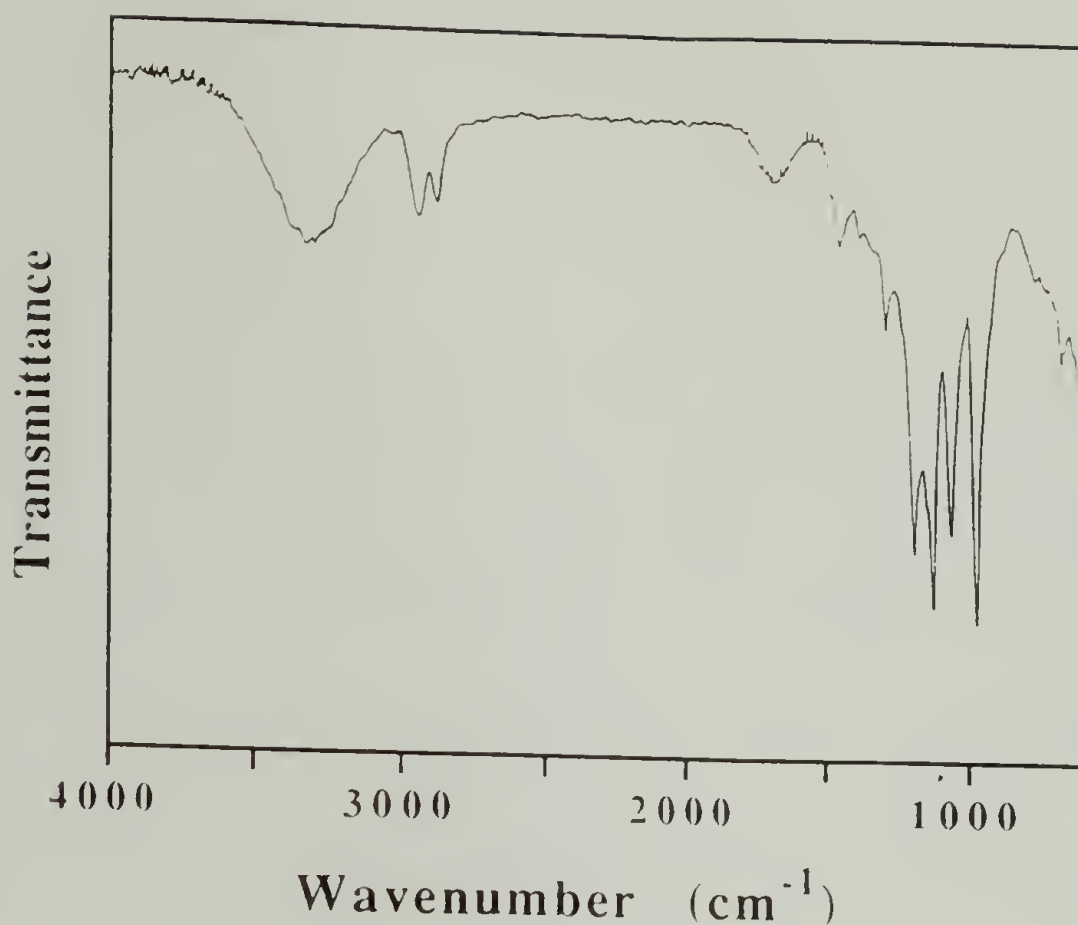


**Figure 3.10.** ATR-IR spectrum of PCTFE-OH (-15 °C initial modification).

The XPS C1s spectrum of PCTFE-OH, initially modified at -15 °C, (75° takeoff angle) shown in Figure 3.11a, is consistent with deprotection. In the acetal-functionalized repeat unit, four of the nine carbons are bonded to electronegative elements (one carbon is also bonded to two oxygens). As discussed above, photoelectrons emitted from these carbons make up the high binding energy shoulder in the C1s spectrum of PCTFE-PEAA (Figure 3.2c, page 99). In the alcohol-functionalized surface, only two of the five carbons are bonded to an electronegative element (none are bonded to two). Thus, it would be expected that after hydrolysis the intensity of the high binding energy shoulder would decrease relative to the main peak, as is observed (Compare Figures 3.11a and 3.2c).



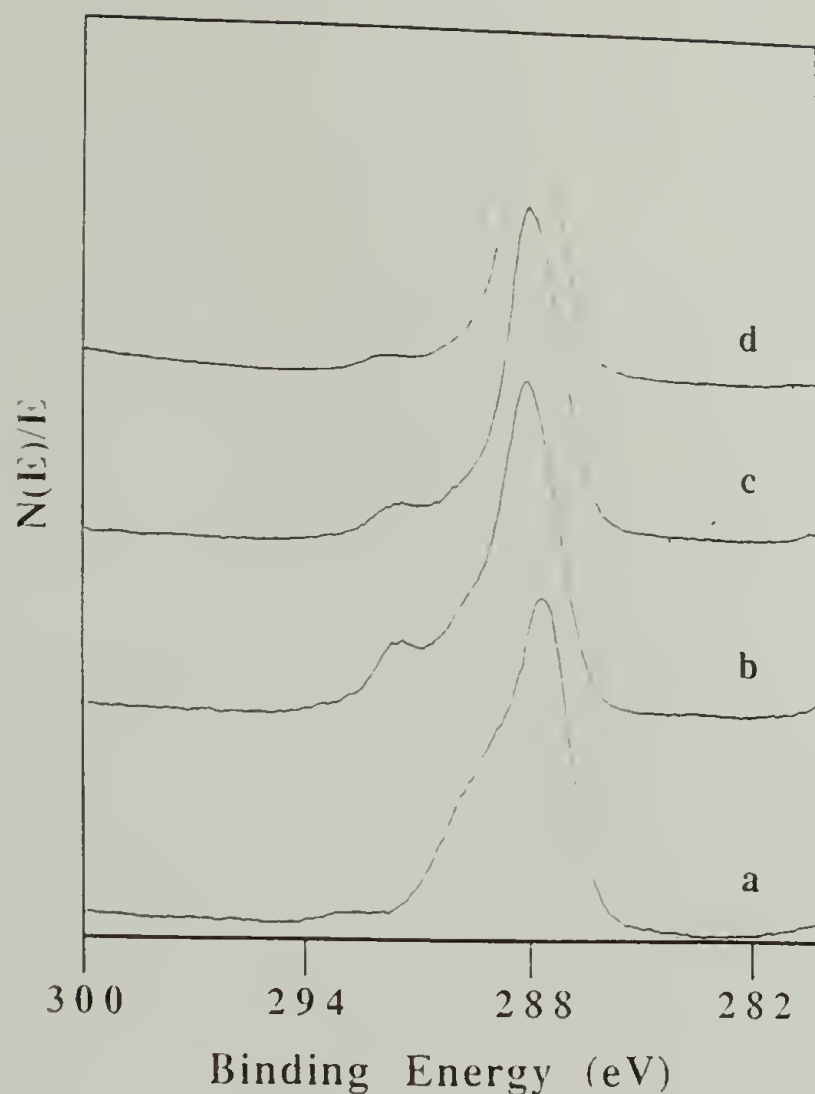


**Figure 3.11.** XPS C1s spectra (75° takeoff angle) of: (a) PCTFE-OH, (b) PCTFE-OBuT, (c) PCTFE-ODec and (d) PCTFE-OSTear.

The 15° takeoff angle C1s spectra of this PCTFE-OH surface (-15 °C initial modification) and of the sample initially modified at -78 °C are essentially identical to the one shown in Figure 3.11a (As expected, the -78 °C, 75° takeoff angle spectrum contains a high binding energy peak from unreacted PCTFE). After deprotection, the experimental atomic composition data (Table 3.2, page 100) for the sample initially modified at -15 °C yields stoichiometries of  $C_{22}F_{6.1}O_{4.0}$  and  $C_{22}F_{6.1}O_{4.1}$  (15° and 75° takeoff angles, respectively) and the 15° takeoff angle data for the sample initially modified at -78 °C yields  $C_{22}F_{6.0}O_{3.6}$ .

The predicted stoichiometry for a modified polymer composed of 80% hydroxyl-functionalized repeat units and 20% difluoroolefins is

$C_{22}F_6O_4$ . The 75° takeoff angle data for the sample initially modified at -78 °C contains a significant amount of chlorine (4.8%), which is consistent with the results obtained from the initial modification.

A gravimetric estimate of the modified layer thickness, similar to those discussed above for PCTFE-PEAA, was made on the PCTFE-OH sample initially modified at -15 °C. This result is shown in Table 3.3 along with a predicted thickness which was derived from the experimental gravimetric thickness of the original acetal surface. The good agreement between these two values indicates that the deprotection reaction has proceeded in high yield and that no significant dissolution of the modified layer has occurred.

**Table 3.3.** Gravimetric thicknesses (Å) for modified surfaces.

<u>Surface</u>	<u>Initial UV Abs.</u>	<u>Experimental</u>	<u>Calculated</u>
PCTFE-PEAA, -60 °C	0.10	360	---
-15	1.02	3,960	---
PCTFE-OH, -15 °C	1.20	2,800	2,480
PCTFE-OBu <sub>t</sub> , -60 °C	0.10	355	360
-15	1.31	3,740	3,960
PCTFE-ODec, -60 °C	0.093	640	520
-15	0.97	5230	5,730
PCTFE-OS <sub>t</sub> ear, -60 °C	0.12	430	730
-15	1.02	4,850	8,100
PCTFE-OHFB, -60 °C	0.099	660	600
-15	1.06	4,500	6,620
PCTFE-OPFDec, -60 °C	0.097	1,020	1,160
-15	1.17	13,940	12,960
PCTFE-O <sub>2</sub> Adip, -15 °C	1.52	3,700	3,640
PCTFE-O <sub>3</sub> Benz, -15 °C	1.01	2,650	3,600

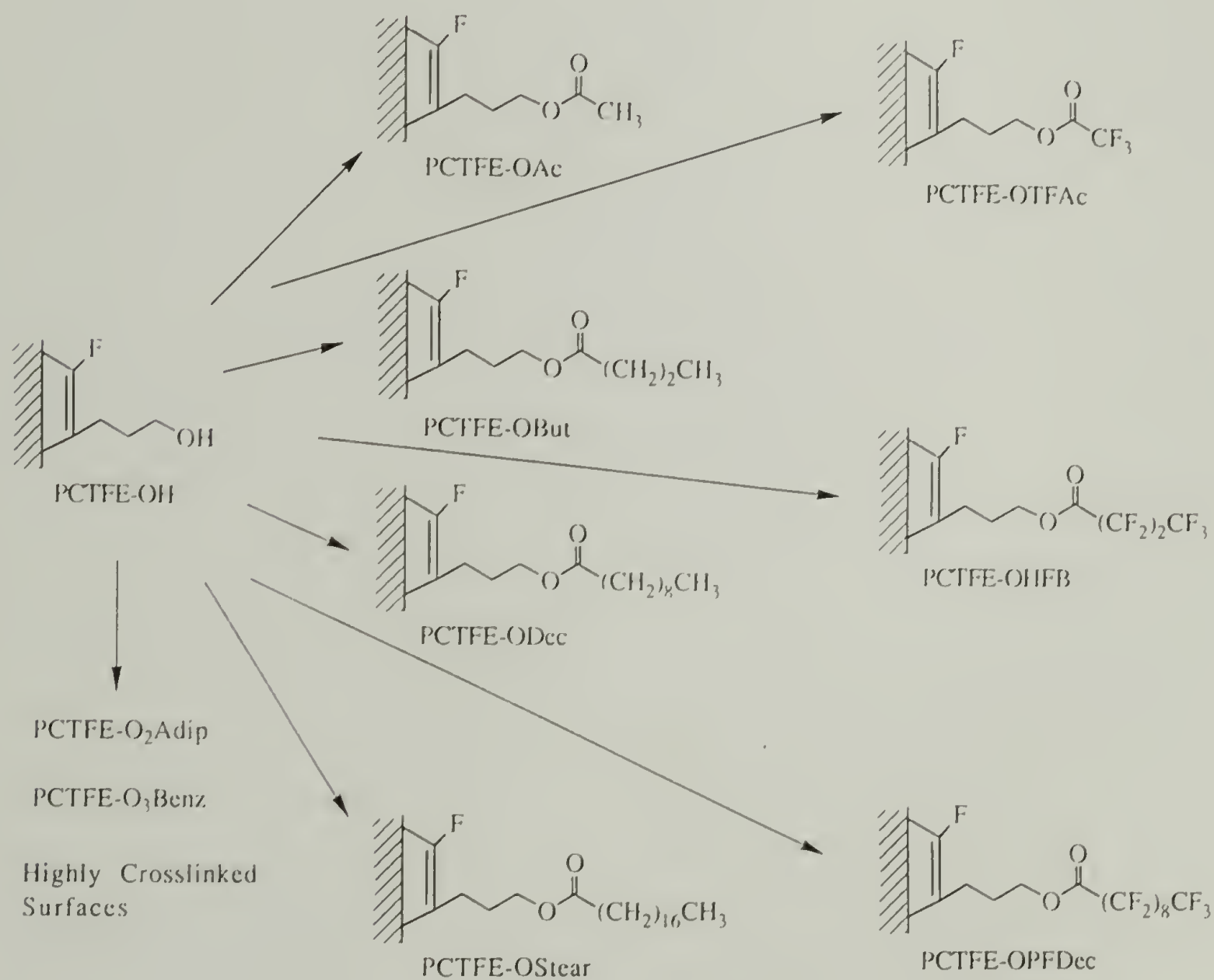
### Esterification of PCTFE-OH

Once the alcohol surface is prepared, a number of different ester surfaces are easily synthesized. Scheme 3.4 shows how further reaction with acid chlorides or acid anhydrides can produce a series of polymer films with varied surface chemistries. The ester surfaces prepared from samples initially modified at  $-78$  and  $-60$  °C are unchanged in appearance from unmodified PCTFE, PCTFE-PEAA and PCTFE-OH. The esters prepared from samples initially modified at  $-15$  °C (including PCTFE-PEAA and PCTFE-OH, though not mentioned above) possess an iridescent sheen, similar to what is observed when oil spreads on water. The thick stearate surface (PCTFE-OStear) is also slightly hazy, indicating the possible formation of microcrystalline regions in the modified material. Results for the characterization of these surfaces are discussed below.

Although not shown in Scheme 3.4, the esterification of PCTFE-OH (initially modified at  $-78$  °C) with pivaloyl chloride was also attempted. The conditions and the isolation procedure used for this reaction were the same as those for the preparation of PCTFE-OBu<sub>t</sub>. Analysis of the resulting product surface showed a significant amount of phosphorous in both the  $15^\circ$  (3%) and  $75^\circ$  (2%) takeoff angle spectra. Acid chlorides are often synthesized from the carboxylic acid and phosphorous pentachloride. A product of this reaction is phosphoryl chloride ( $\text{POCl}_3$ ) which is highly reactive towards alcohols. Since the total number of hydroxyl groups in the surfaces is so small and the reactivity of  $\text{POCl}_3$  is so high, even a low concentration of  $\text{POCl}_3$  in pivaloyl chloride will result in the surface containing a high fraction of phosphate esters. It appears from the



XPS results that after a simple distillation the commercial (Aldrich) pivaloyl chloride remains tainted with this impurity. Unfortunately, pivaloyl chloride (b.p. 105 - 106 °C) and POCl<sub>3</sub> (b.p. 105.8 °C) have very similar boiling points. Thus, it is likely to be difficult to completely remove POCl<sub>3</sub> from pivaloyl chloride even by a fractional distillation. For these reasons, further attempts at this esterification were abandoned.



Scheme 3.4. Esterifications of PCTFE-OH.

Shown in Table 3.1 (page 97) are results for dynamic water contact angles on the modified surfaces. It is reassuring that the measurements yield the expected trends. Upon esterification the contact angles increase dramatically. For both the hydrocarbon esters and the fluorocarbon esters the contact angles increase as the alkyl chain length increases due to the hydrophobic nature of the tail group. Also, in all cases the fluorocarbon esters exhibit higher contact angles than their hydrocarbon analogs, as expected.<sup>30</sup> Three interesting results on the structure of these modified surfaces were obtained from this contact angle data. First, as for PCTFE-PEAA and PCTFE-OH, the contact angle hysteresis increases with an increase in the temperature of the initial modification for all of the modified surfaces. Again, this result indicates that the initial modification is somewhat corrosive causing an increase in surface roughness with increasing reaction temperature. It should be noted that it is predicted<sup>22</sup> that when  $\Theta > 90^\circ$  increasing the surface roughness increases  $\Theta$ , while for  $\Theta < 90^\circ$  an increase in roughness leads to a decrease in  $\Theta$ . The data reported here exhibit these trends (For PCTFE-OStear,  $\Theta_R = 90^\circ$  and is independent of surface roughness.). The second interesting result arises from a comparison of the contact angles of the stearate (PCTFE-OStear) surface with those of the decanoate (PCTFE-ODec) and perfluorodecanoate (PCTFE-OPFDec) surfaces. PCTFE-OStear ( $\Theta_A/\Theta_R = 108-117^\circ/90^\circ$ ) and PCTFE-ODec ( $\Theta_A/\Theta_R = 106-117^\circ/57-47^\circ$ ) have similar advancing water contact angles that are significantly lower than those of PCTFE-OPFDec ( $\Theta_A/\Theta_R = 120-126^\circ/69-64^\circ$ ). The advancing water contact angle is indicative of the non-polar functionality present at the film/air

interface.<sup>31</sup> As expected,  $\Theta_A$  is significantly higher for the perfluorinated long ester (PCTFE-OPFDec) than for the hydrocarbon ester surfaces.<sup>30</sup> The similar value of  $\Theta_A$  for PCTFE-ODec and PCTFE-OSTear indicates that the functionality exposed at the interface is essentially the same for these two surfaces. (Contact angles measured using hexadecane as the probe fluid show that differences do exist, see below.) The receding water contact angle reflects how the probe fluid interacts with the surface after it has been in contact with water. It is thus a measure of the polar functionality present at the film/water interface. (As a result of the measurement, rearrangement of the functional groups at the interface may cause differences in the surface conformation of the polymer at the film/air and film/water interfaces.<sup>32</sup>) The receding contact angle data for these three surfaces indicate that the C<sub>17</sub> chain of PCTFE-OSTear "hides" the polar ester functionality much more efficiently than the C<sub>9</sub> chain of either PCTFE-ODec or PCTFE-OPFDec. This result suggests that the ester functional group is buried at least 5 Å (the region accessible to water contact angle analysis<sup>33</sup>) below the interface by the hydrocarbon tail. Finally, the differences in the results obtained between the two different samples (initially modified at -78 and -15 °C) of each of the crosslinked surfaces (PCTFE-O<sub>2</sub>Adip and PCTFE-O<sub>3</sub>Benz) need to be explained. It has been shown that adipoyl chloride tends to react multiply with PCTFE-OH to form a crosslinked surface.<sup>11</sup> However, some small percentage of the acid chloride functional groups remain unreacted, resulting in a surface composed of mostly diester and some half ester/half acid chloride. A similar result would be expected for



1,3,5-benzenetricarbonyl trichloride. These rogue acid chloride moieties are available for reaction with any nucleophiles present in the wash solvents. The esterifications conducted on the samples initially modified at  $-78\text{ }^{\circ}\text{C}$  were washed with methanol and thus contain a small amount of methyl ester functionality. Those conducted on the samples initially modified at  $-15\text{ }^{\circ}\text{C}$  were washed with water and thus contain a small number of carboxylic acid groups. The differences in these two procedures are manifested in the water contact angle results - the surfaces containing the acidic functionality having depressed water contact angles (Table 3.1, page 97). As a whole, these contact angle results suggest that a number of different modifications have been successfully completed to yield a series of surfaces with varying surface energies.

In order to more fully characterize these surfaces, XPS was utilized to give both qualitative and quantitative information about the modified layers. The experimental atomic compositions for these surfaces are reported in Tables 3.4 and 3.5 and are in good agreement with the calculated compositions (also in Tables 3.4 and 3.5) based on the structure of the modified surface shown in Figure 3.3 (page 101) and quantitative reaction yields. As expected, all of these ester surfaces show an increase in the width of the O1s photoelectron peak due to the introduction of the carbonyl oxygen as displayed in Figure 3.12 for PCTFE-OBu.

**Table 3.4.** XPS atomic composition data for hydrocarbon and crosslinked ester surfaces used in friction studies.

<u>Surface</u>		<u>Experimental</u>					<u>Calculated<sup>a</sup></u>		
		<u>Q<sub>T</sub></u>	<u>C</u>	<u>F</u>	<u>O</u>	<u>Cl</u>	<u>C</u>	<u>F</u>	<u>O</u>
PCTFE-OAc	-78 °C	15	63.1	17.0	18.3	1.6	68.2	13.6	14.3
		75	61.0	18.2	17.3	3.5			
PCTFE-OBu <sub>t</sub>	-78 °C	15	71.9	12.3	15.0	0.8	73.1	11.5	15.4
		75	70.7	13.3	14.8	1.1			
	-60	15	73.3	11.1	15.1	0.5			
		75	71.0	13.1	14.7	1.3			
	-15	15	74.0	8.8	17.1	0.2			
		75	72.2	10.5	17.1	0.3			
	-78 °C	15	84.1	5.6	10.0	0.3			
		75	78.8	8.9	11.2	1.1			
	-60	15	85.8	4.7	9.2	0.3			
		75	81.0	7.5	10.9	0.7			
	-15	15	86.8	3.7	9.4	0.2			
		75	82.7	6.1	11.0	0.2			
PCTFE-OS <sub>t</sub> ear	-78 °C	15	92.8	2.7	3.9	0.5	87.0	5.6	7.4
		75	85.3	6.4	7.6	0.8			
	-60	15	89.3	4.4	6.0	0.3			
		75	87.3	5.0	7.2	0.5			
	-15	15	93.5	2.2	4.2	0.1			
		75	88.6	3.8	7.5	0.2			
PCTFE-O <sub>2</sub> Adip	-78 °C	15	61.3	21.1	15.0	2.6	70.8	12.5	16.7
		75	58.2	23.0	13.9	4.9			
		15	71.2	10.0	18.0	0.7			
		75	70.7	10.4	18.5	0.4			
	-78 °C	15	68.7	11.7	18.7	0.9			
		75	63.6	15.5	17.3	3.6			
PCTFE-O <sub>3</sub> Benz	-15	15	67.2	12.3	20.2	0.4	70.8	12.5	16.7
		75	67.9	11.7	20.0	0.4			

<sup>a</sup>Calculated atomic compositions are based on a surface structure where four of the five polymer repeat units contain the functionality of interest with the fifth being a difluorolefin. (See text for details.)

**Table 3.5.** XPS atomic composition data for fluorocarbon ester surfaces used in friction studies.

<u>Surface</u>		<u><math>\Theta_T</math></u>	<u>Experimental</u>				<u>Calculated<sup>a</sup></u>		
			<u>C</u>	<u>F</u>	<u>O</u>	<u>Cl</u>	<u>C</u>	<u>F</u>	<u>O</u>
PCTFE-OTFAc	-78 °C	15	53.8	30.0	14.8	1.4	53.6	32.1	14.3
		75	52.2	30.8	13.0	4.0			
PCTFE-OHFB	-78 °C	15	46.1	43.1	10.1	0.7	47.5	42.5	10.0
		75	48.5	40.7	9.1	1.6			
	-60	15	47.0	43.5	9.3	0.2			
		75	50.0	40.3	9.0	0.7			
	-15	15	46.9	43.8	9.2	0.1			
		75	49.7	40.7	9.4	0.2			
PCTFE-OPFDec	-78 °C	15	43.5	50.5	5.6	0.4	40.8	54.0	5.3
		75	44.6	48.4	6.1	0.9			
	-60	15	39.5	56.3	4.0	0.2			
		75	44.0	50.4	5.0	0.6			
	-15	15	40.0	56.6	3.3	0.2			
		75	43.9	51.5	4.7	0.0			

<sup>a</sup>Calculated atomic compositions are based on a surface structure where four of the five polymer repeat units contain the functionality of interest with the fifth being a difluorolefin. (See text for details.)

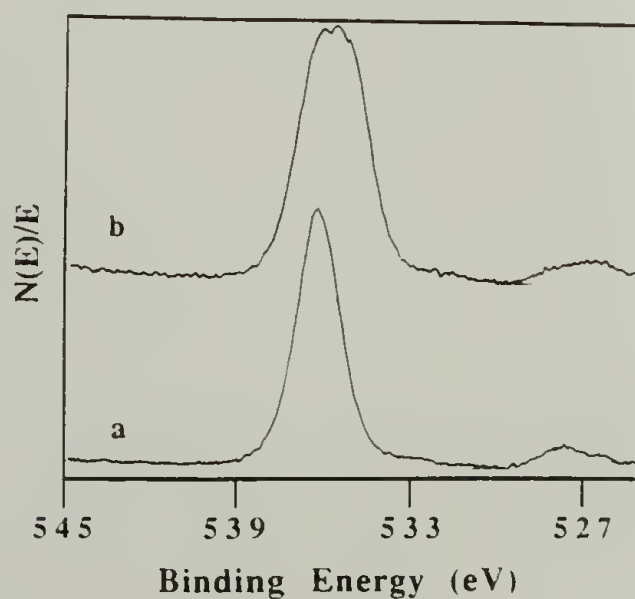


**Figure 3.12.** XPS O1s spectra (75° takeoff angle) of: (a) PCTFE-OH and (b) PCTFE-OBuT.



Figures 3.11b - d (page 114) display the C1s spectra of the butyrate (PCTFE-OBu), decanoate (PCTFE-ODec) and stearate (PCTFE-OSear) modified surfaces (75° takeoff angle, -15 °C initial modification), respectively. These spectra all consist of a high binding energy peak at 292 eV, assigned to the carbonyl carbon of the ester and a large peak at 288 eV, assigned to the carbons in the hydrocarbon tail, the propyl spacer between the main chain and the ester, and the polymer backbone. As anticipated, the relative intensity of the carbonyl peak decreases as the length of the hydrocarbon tail increases from C<sub>3</sub> (butyrate) to C<sub>9</sub> (decanoate) to C<sub>17</sub> (stearate). The 15° takeoff angle C1s spectra for PCTFE-OBu initially modified at -78, -60 and -15 °C are indistinguishable from the one displayed in Figure 3.11b. However, as expected based on the results obtained for PCTFE-PEAA (PCTFE-PEAA and PCTFE-OBu have the same number of carbons, oxygens and fluorines), the 75° spectra for the two less deeply reacted samples contain a higher binding energy peak from the virgin PCTFE beneath the modified layer. The 75° takeoff angle C1s spectra for PCTFE-ODec and PCTFE-OSear initially modified at -78 and -60 °C are identical in appearance to those shown in Figures in 3.11c and 3.11d, respectively. In the 15° takeoff angle spectra of these two esters (all initial modification temperatures) the intensity of the carbonyl peak is significantly reduced relative to that of the main peak (the carbonyl peak is almost absent from the PCTFE-OSear 15° spectra).

The quantitative XPS results agree with the qualitative features discussed above and are consistent with high reaction yields and the structure of the modified polymer depicted in Figure 3.3 (page 101).

The predicted stoichiometry of PCTFE-OBuT is  $C_{38}F_6O_8$ . The observed values (Table 3.4) based on the  $15^\circ$  takeoff angle data for the samples initially modified at  $-78$  and  $-60^\circ C$  are  $C_{38}F_{6.5}O_{7.9}$  and  $C_{38}F_{5.8}O_{7.8}$ , respectively. The stoichiometries for the sample initially modified at  $-15^\circ C$  are  $C_{38}F_{4.5}O_{8.8}$  and  $C_{38}F_{5.5}O_{9.0}$  ( $15^\circ$  and  $75^\circ$  takeoff angles, respectively). The expected stoichiometries of PCTFE-ODec and PCTFE-OSTear are  $C_{62}F_6O_8$  and  $C_{94}F_6O_8$ , respectively. For the samples initially modified at  $-15^\circ C$ , the experimental compositions for PCTFE-ODec ( $15^\circ$  and  $75^\circ$  takeoff angle data, respectively) are  $C_{62}F_{2.6}O_{6.7}$  and  $C_{62}F_{4.6}O_{8.2}$ , while those for PCTFE-OSTear are  $C_{94}F_{2.2}O_{4.2}$  and  $C_{94}F_{3.6}O_{7.1}$ . The PCTFE-ODec and PCTFE-OSTear samples prepared from films initially modified at  $-78$  and  $-60^\circ C$  show results similar to those reported above (Table 3.2). The low measured fluorine and oxygen concentrations in the  $15^\circ$  takeoff angle data, along with the qualitative features of the C1s spectra discussed earlier, suggest that the two longer chain esters are ordered, to some degree, at the surface with their hydrocarbon tails located at the film/air interface. For PCTFE-ODec, the  $75^\circ$  takeoff angle composition is in much better agreement with the predicted value. The good agreement in the oxygen concentration, while the fluorine content remains low, may indicate that the carbonyl group is located closer to the surface than the polymer backbone or may simply reflect the fact that the mean free path of F1s photoelectrons is shorter than that of O1s photoelectrons.<sup>34</sup> The large discrepancy between the measured and the predicted compositions for PCTFE-OSTear, in both the  $15^\circ$  and  $75^\circ$  takeoff angle data, reflect the greater length of the tail group of this ester and suggests the existence of a



significant amount of order at the surface (see below for further discussion).

The predicted stoichiometries for the heptafluorobutyrate (PCTFE-OHFB) and perfluorodecanoate (PCTFE-OPFDec) surfaces are  $C_{38}F_{34}O_8$  and  $C_{62}F_{82}O_8$ , respectively. The  $15^\circ$  and  $75^\circ$  takeoff angle experimental results based on samples initially modified at  $-15^\circ\text{C}$  (Table 3.5) (initial modification temperatures of  $-78$  and  $-60^\circ\text{C}$  provide similar results) are respectively, for PCTFE-OHFB:  $C_{38}F_{35.5}O_{7.5}$  and  $C_{38}F_{31.1}O_{7.2}$ , and for PCTFE-OPFDec:  $C_{62}F_{87.7}O_{5.1}$  and  $C_{62}F_{72.7}O_{6.6}$ . The high fluorine concentrations in the  $15^\circ$  takeoff angle compositions of each sample indicate that these esters are also somewhat ordered at the surface, with their fluorocarbon tails located at the film/air interface.

Figures 3.13 and 3.14 show the XPS C1s spectra of PCTFE-OHFB and PCTFE-OPFDec surfaces ( $15^\circ$  and  $75^\circ$  takeoff angle spectra for samples initially modified at  $-15^\circ\text{C}$ ). The spectra of the samples initially modified at  $-78$  and  $-60^\circ\text{C}$  are essentially identical to those displayed here. Both sets of spectra are complex and contain principally four overlapping peaks which can be assigned (in order of decreasing binding energy) to: (1) the trifluoromethyl carbon, (2) the difluoromethylene carbons, (3) the carbonyl carbon and (4) the methylene (from the propyl spacer) and backbone carbons present (Scheme 3.4). As expected, in the  $75^\circ$  takeoff angle spectrum of PCTFE-OHFB (Figure 3.13b) the peaks from these functional groups are present in roughly a 1:3:1:5 ratio. Conversely, the perfluorodecanoate surface is mostly difluoromethylene and its  $75^\circ$  takeoff angle spectrum exhibits one large peak assigned to these



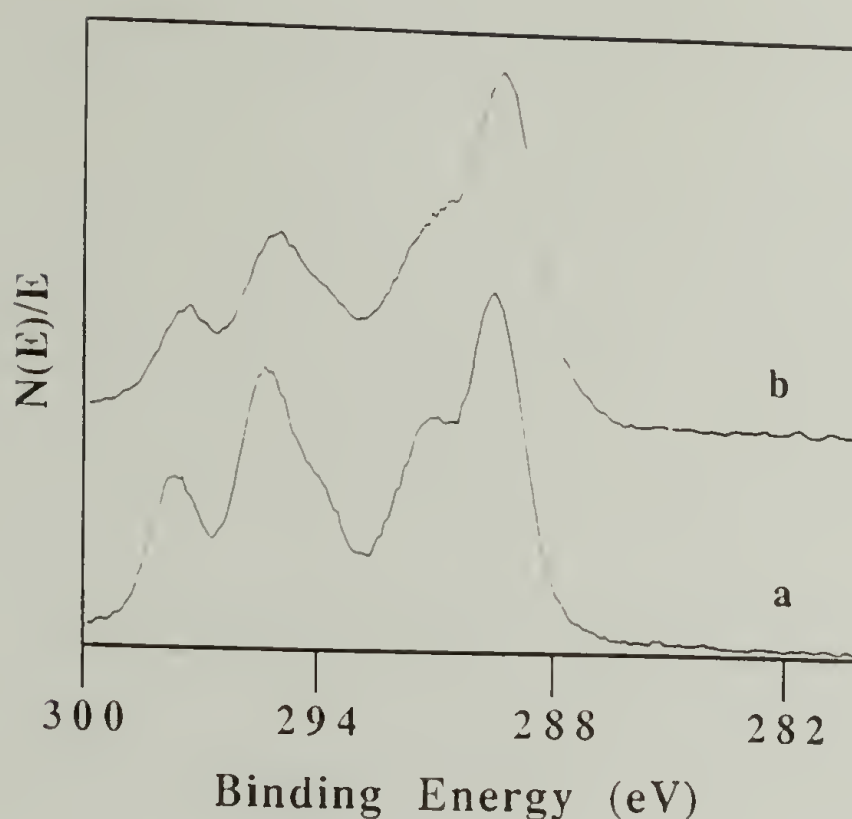


**Figure 3.13.** XPS C1s spectra of PCTFE-OHFB: (a) 15° takeoff angle and (b) 75° takeoff angle.

carbons with a small, high binding energy shoulder due to the trifluoromethyl group at the end of the chain and a small, broad peak on the low binding energy side from the remaining carbons. For both surfaces, it is evident from a comparison between the 15° and the 75° takeoff angle spectra of the relative intensities of the fluorocarbon and hydrocarbon peaks, that the fluorocarbon tails are located at the film surface, supporting the atomic composition data. In the 15° spectrum of PCTFE-OPFDec (Figure 3.14a) the peak from the trifluoromethyl carbon is significantly more pronounced than that in the 75° spectrum, where it is barely observed. This difference indicates that the trifluoromethyl group is likely located directly at the film/air interface, which implies that a significant amount of order must be present at the surface of these samples.

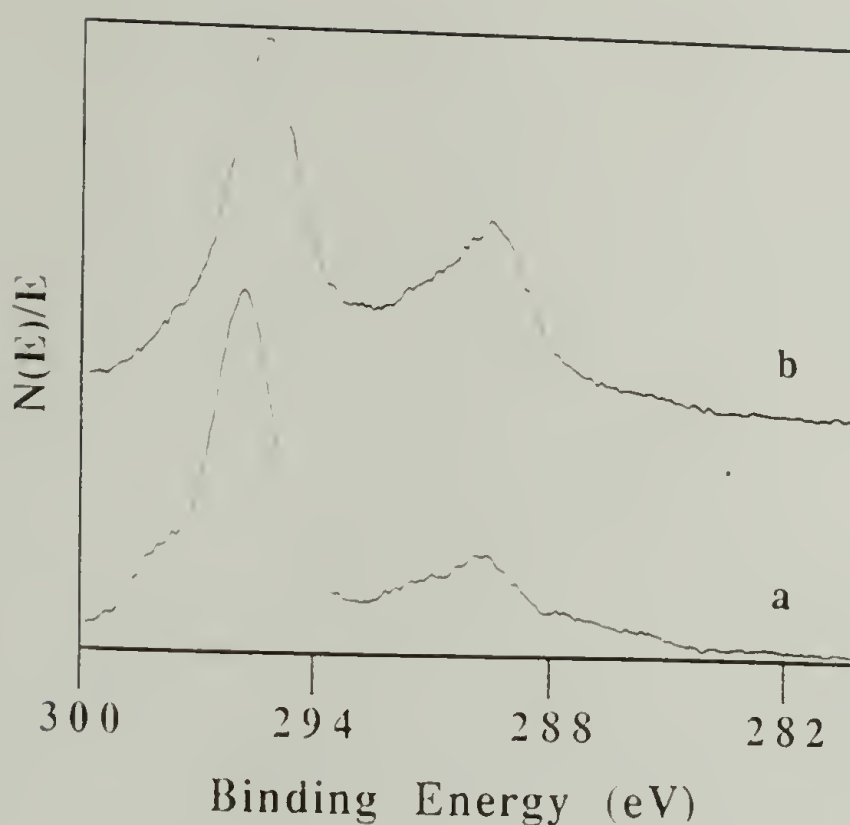


**Figure 3.14.** XPS C1s spectra of PCTFE-OPFDec: (a) 15° takeoff angle and (b) 75° takeoff angle.

The presence of methyl or trifluormethyl groups at the solid/air interface has often been distinguished from a surface comprised of methylene or difluoromethylene groups by measurement of hexadecane contact angles. It has been shown<sup>35</sup> that surfaces which present a close-packed array of methyl groups to this probe fluid exhibit higher hexadecane contact angles and have a significantly lower surface energy than surfaces consisting of predominantly methylene units. Hexadecane spontaneously spreads ( $\Theta = 0^\circ$ ) on polyethylene,<sup>30</sup> a surface that contains only methylene groups. The same is true for the analogous fluorinated groups,<sup>36</sup> except that hexadecane does not spread on polytetrafluoroethylene ( $\Theta = 46^\circ$ )<sup>30</sup> due to the higher interfacial free energy between the hydrocarbon liquid and the oleophobic fluoropolymer. Table 3.6 contains hexadecane contact angle data for PCTFE-ODec, PCTFE-

OStear, PCTFE-OHFB and PCTFE-OPFDec, surfaces which the XPS data suggest may be ordered and/or expose a significant fraction of methyl or trifluoromethyl groups at the surface. Also in Table 3.6, are values for measurements made on octadecanethiol adsorbed to gold<sup>35</sup> and perfluorodecanoic and perfluorolauric acids adsorbed to platinum,<sup>36</sup> two systems which have been shown to be highly oriented close-packed monolayers containing only methyl and trifluoromethyl groups at the monolayer/air interface. These results confirm the proposed ordering (based on the XPS results discussed above) of these ester groups at the modified polymer surface. The hexadecane contact angles of PCTFE-OStear ( $\Theta = 42^\circ$ ) and PCTFE-OPFDec ( $\Theta = 71^\circ$ ) approach those of the pure methyl ( $\Theta = 48^\circ$ ) and pure trifluoromethyl ( $\Theta = 78^\circ$ ) surfaces (the result for PCTFE-OPFDec is nearly identical to that obtained for perfluorodecanoic acid monolayers). From these results and those from the XPS spectra,

**Table 3.6.** Hexadecane contact angle data for model substrates and PCTFE modified surfaces.

<u>Surface</u>	<u>Hexadecane Contact Angle</u>
Polyethylene	0°
Polytetrafluoroethylene	48
Octadecanethiol monolayers	48
Perfluorodecanoic acid monolayer	72
Perfluorolauric acid monolayer	78
PCTFE-OBu	10/0
PCTFE-ODec	10/0
PCTFE-OStear	42/35
PCTFE-OHFB	60/40
PCTFE-OPFDec	71/55



structures like those shown in Figure 3.15 (b and d) are proposed for these modified surfaces. In these structures, the alkyl tails exist in an ordered layer above the ester functional group and the polymer backbone. (There may be some chain tilt in these systems, as has been described for a number of ordered monolayers,<sup>35</sup> but this was not investigated.) The value for the hexadecane contact angle on PCTFE-OHFB ( $\Theta = 60^\circ$ ), suggests that a significant fraction of the surface of this sample also contains trifluoromethyl groups at the interface (Figure 3.15c). These contact angle results for PCTFE-ODec imply that the surface is comprised of predominantly methylene units. As stated above, the XPS results show that a significant portion of the outer  $\sim 10$  Å of this sample contains the hydrocarbon tail, while the ester functional group and the polymer backbone are buried beneath this region. Thus, a surface structure like that shown in Figure 3.15a is proposed, where there is a significant amount of disorder present in the layer composed of the alkyl tails. The reason the stearate esters form an oriented layer at the surface while the decanoate esters do not, is that the C<sub>9</sub> ester tail does not contain enough methylene units to provide the enthalpy needed from van der Waal's interactions to overcome the entropy of disorder. In comparing the ability of PCTFE-OPFDec to "crystallize" at the surface over that of PCTFE-ODec it is well documented<sup>37</sup> that linear perfluorocarbon compounds have higher melting points than their hydrocarbon analogs due to their more streamlined molecular shapes and stiffer chains both of which allow them to pack more efficiently in a crystal lattice.

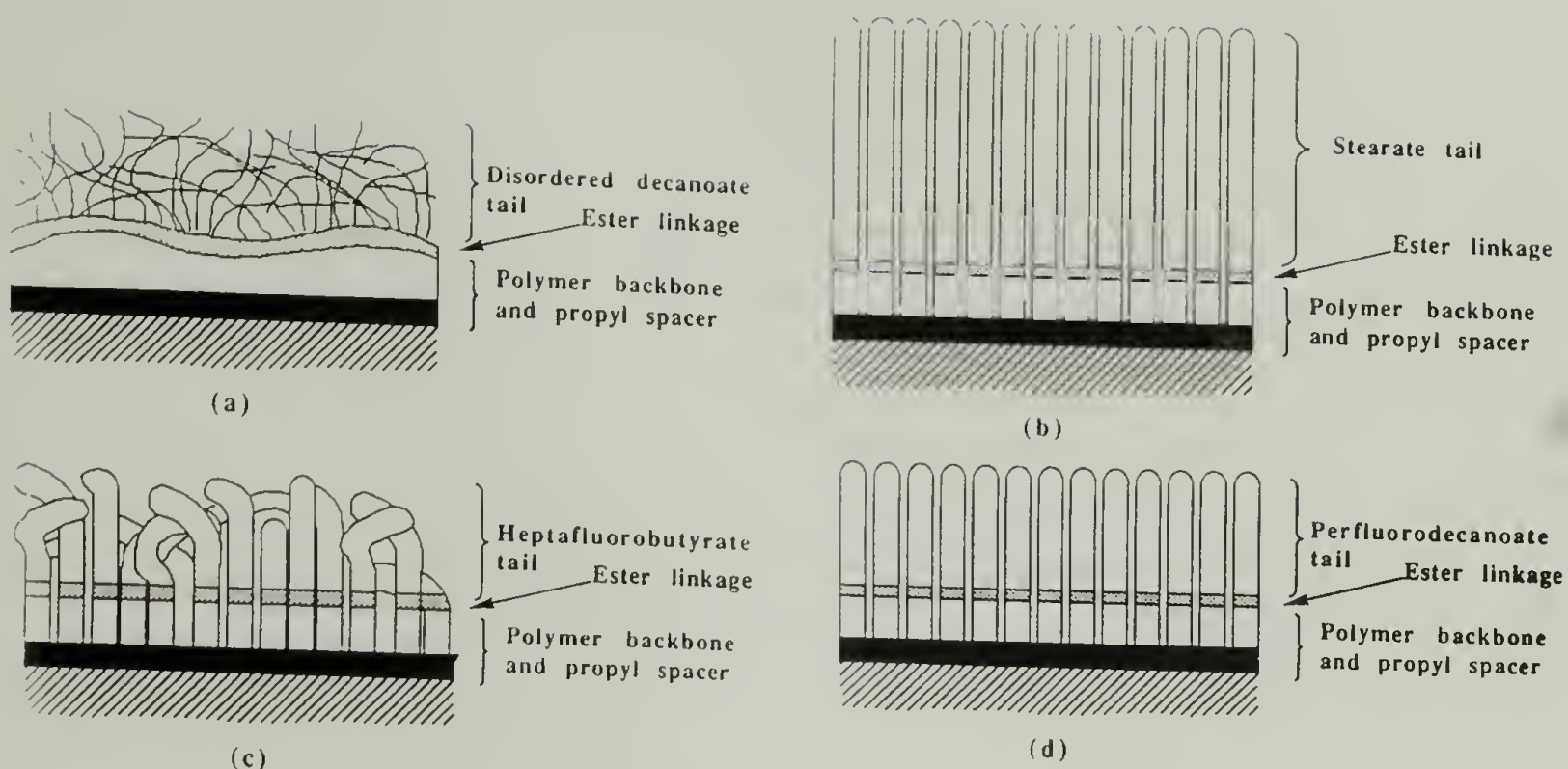


**Figure 3.15.** Schematic of: (a) PCTFE-ODec, (b) PCTFE-OStear, (c) PCTFE-OHFB and (d) PCTFE-OPFDec modified ester surfaces.

The ATR-IR spectra for the deeply modified ester surfaces (-15 °C initial modification) are shown in Figures 3.16 - 3.22. These spectra indicate complete reaction of the hydroxyl group (disappearance of the O-H band at  $3300\text{ cm}^{-1}$  - compare with Figure 3.10, page 113) and as expected peaks assigned to the C-O stretching vibrations ( $1300 - 1000\text{ cm}^{-1}$ ) appear, along with carbonyl bands for the hydrocarbon esters at  $1736$ ,  $1739$  and  $1740\text{ cm}^{-1}$  (PCTFE-OBuT, PCTFE-ODec and PCTFE-OStear, respectively), for the two crosslinked esters at  $1734$  and  $1731\text{ cm}^{-1}$  (PCTFE-O<sub>2</sub>Adip and PCTFE-O<sub>3</sub>Benz, respectively) and for the two fluorocarbon esters at  $1783$  and  $1784\text{ cm}^{-1}$  (PCTFE-OHFB and PCTFE-OPFDec, respectively). Also evident on the low frequency side of the carbonyl peak (either as a broad shoulder or as a distinct peak) is the absorbance assigned to the conjugation in the polymer backbone (see above). In general,

these modified surfaces are so thick that the peaks due to unmodified PCTFE (1288, 1193, 1127 and 970  $\text{cm}^{-1}$ ) beneath the ester surface layer are significantly reduced in intensity or absent from these spectra.

The spectra for the hydrocarbon esters (Figures 3.16 - 3.18) show peaks which can be assigned to the methyl asymmetric stretching ( $\sim 2960 \text{ cm}^{-1}$ ). As expected, these spectra also display an increase in intensity of the methylene asymmetric ( $\sim 2930 \text{ cm}^{-1}$ ) and symmetric ( $\sim 2875 \text{ cm}^{-1}$ ) stretching peaks and the methylene bending peaks (scissoring at  $1465 \text{ cm}^{-1}$  and rocking at  $722 \text{ cm}^{-1}$ ) with an increase in the alkyl chain length. The series of bands from  $1350 - 1215 \text{ cm}^{-1}$  in the spectrum of PCTFE-OStear (Figure 3.18) are characteristic of solids of long chain esters.<sup>38</sup> The peak positions of the methylene asymmetric,  $\nu_{\text{as}}$ , and symmetric,  $\nu_{\text{s}}$ , absorbances can also be used to check for the existence of any order in PCTFE-ODec and PCTFE-OStear (Table 3.7). In hydrocarbon liquids and amorphous solids, the peak positions of  $\nu_{\text{as}}$  and  $\nu_{\text{s}}$  are at  $2924$  and  $2855 \text{ cm}^{-1}$ , respectively. In hydrocarbon crystals, these same peaks are found at  $2918$  and  $2851 \text{ cm}^{-1}$ .<sup>39</sup> The data in Table 3.7 indicate that the hydrocarbon chains in PCTFE-ODec are disordered while those in PCTFE-OStear exhibit a significant amount of order.

**Table 3.7.** Methylene asymmetric and symmetric stretching infrared peak positions in hydrocarbons.

		<u>Vibrational Mode</u>	
		$\nu_{\text{as}}\text{CH}_2, \text{cm}^{-1}$	$\nu_{\text{s}}\text{CH}_2, \text{cm}^{-1}$
Hydrocarbon	liquids	2924	2855
PCTFE-ODec		2926	2857
PCTFE-OStear		2919	2853
Hydrocarbon	solids	2918	2851



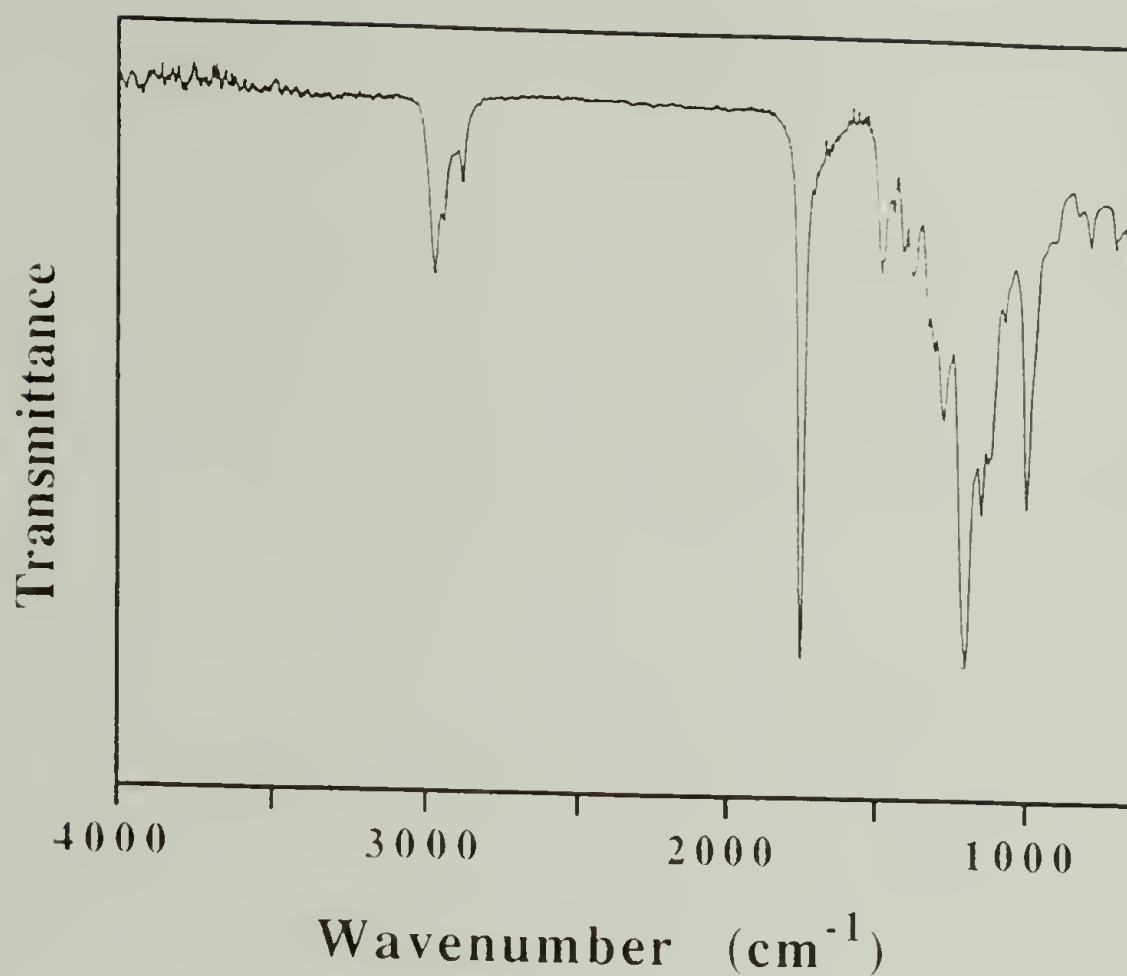


Figure 3.16. ATR-IR spectrum of PCTFE-OBuT (-15 °C initial modification).

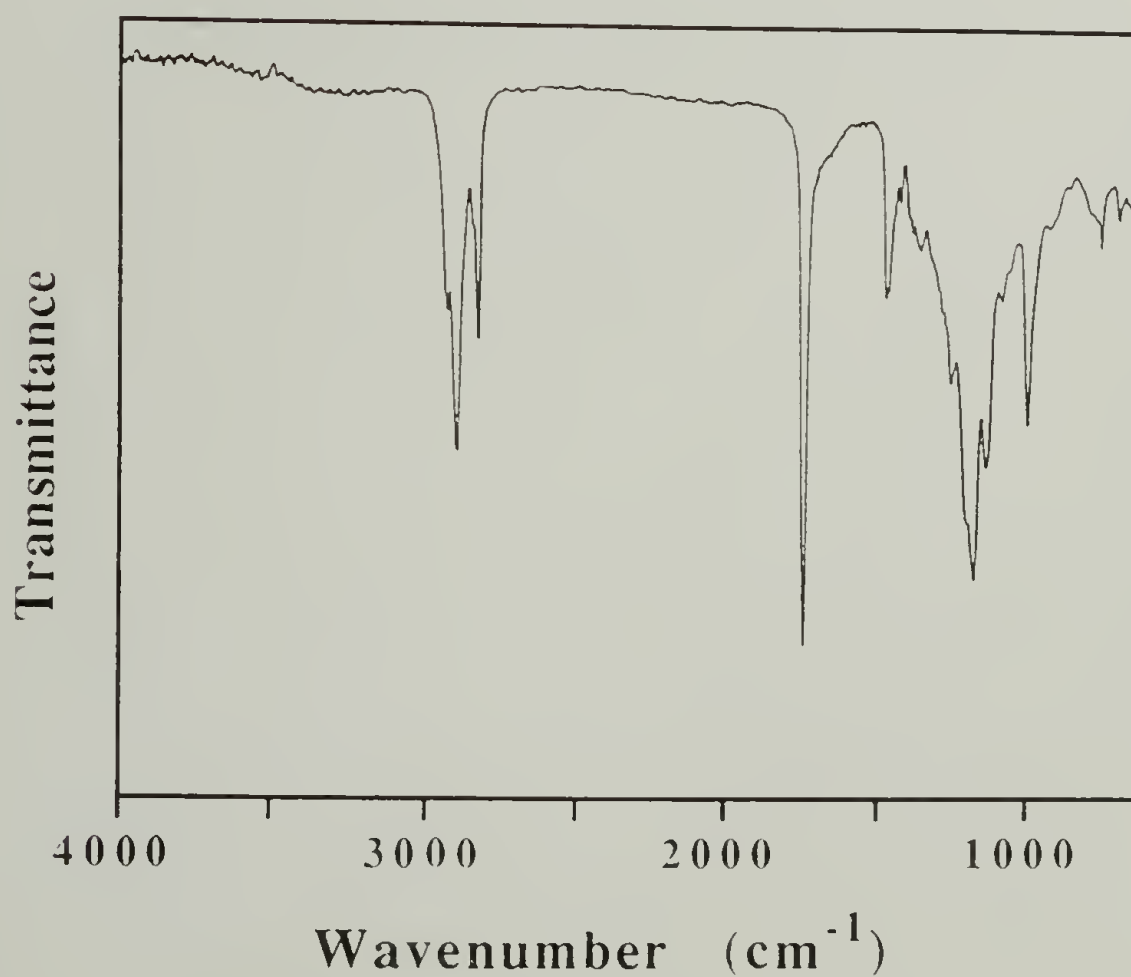
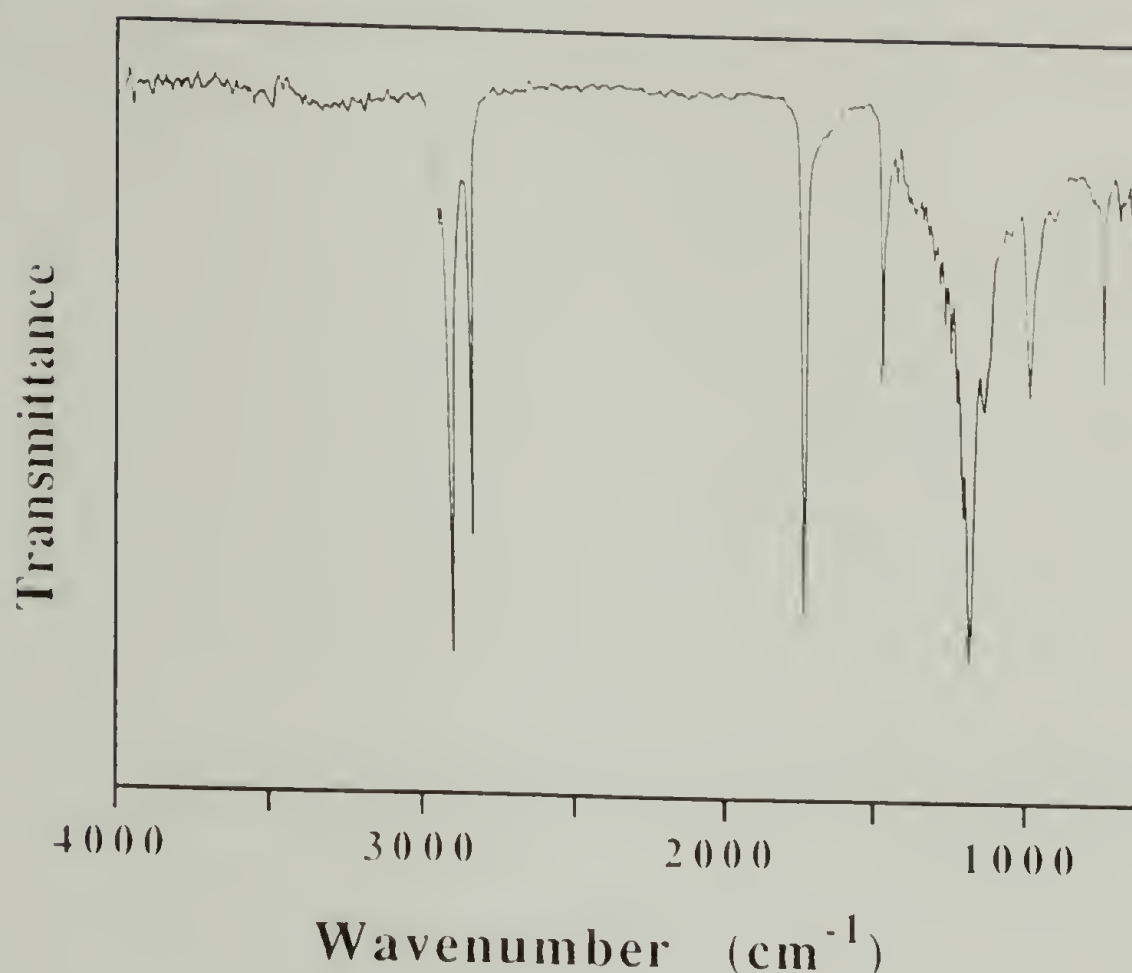


Figure 3.17. ATR-IR spectrum of PCTFE-ODec (-15 °C initial modification).



**Figure 3.18.** ATR-IR spectrum of PCTFE-OStear (-15 °C initial modification).

In the spectrum of PCTFE-OHFB (Figure 3.19), only a small amount of absorbance is observed in the methylene stretching (2990 - 2830  $\text{cm}^{-1}$ ) and bending ( $\sim 1460 \text{ cm}^{-1}$ ) regions from the propyl group located between the ester and the polymer backbone. This spectrum also contains peaks from the trifluoromethyl and difluoromethylene asymmetric and symmetric stretching in the ester tail (1350 - 1120  $\text{cm}^{-1}$ , along with the  $-\text{CF}_2-$  and  $-\text{CFCI}-$  peaks from the unreacted PCTFE). The spectrum of PCTFE-OPFDec (Figure 3.20) shows little absorbance from the methylene groups and two large peaks at 1205 and 1150  $\text{cm}^{-1}$ , which are assigned to the difluoromethylene asymmetric and symmetric vibrations of the perfluorinated ester tail.

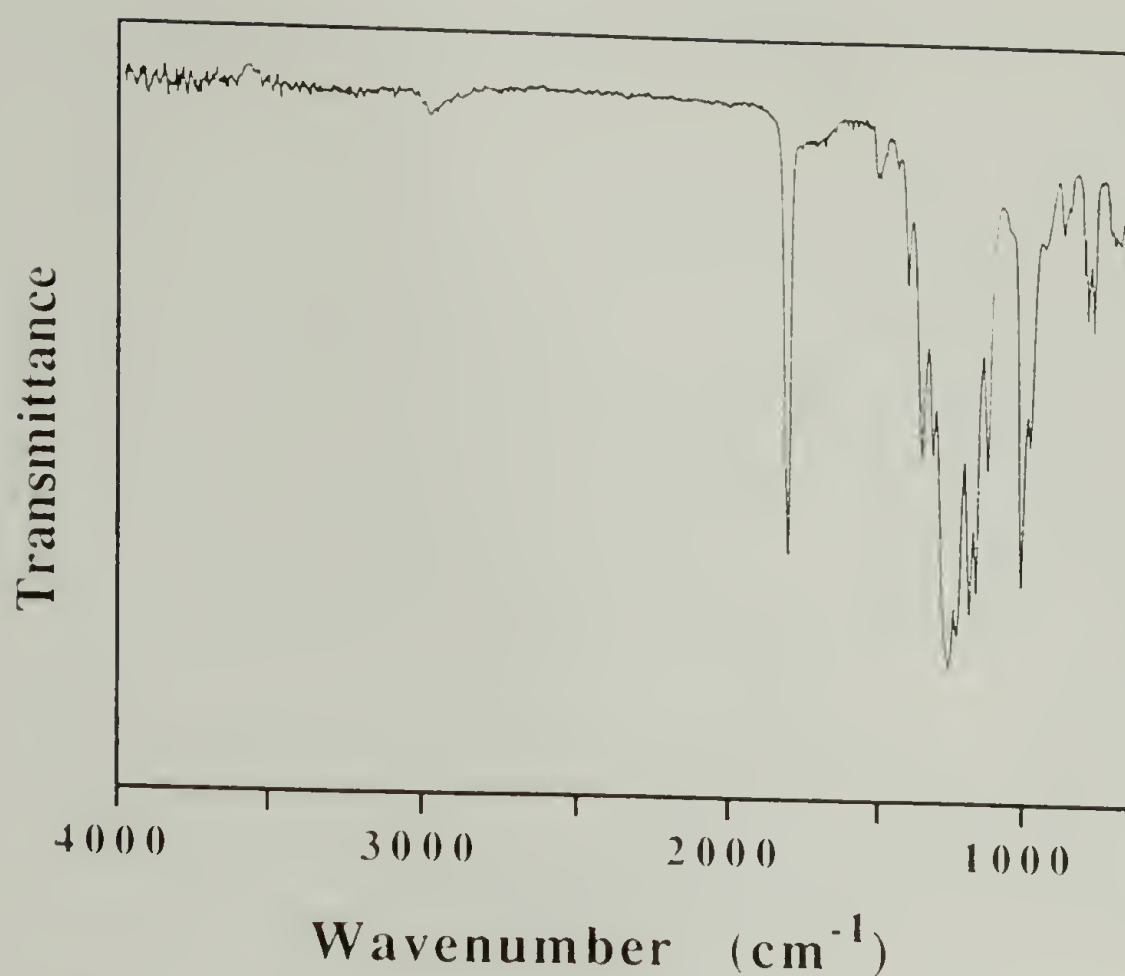


Figure 3.19. ATR-IR spectrum of PCTFE-OHFB (-15 °C initial modification).

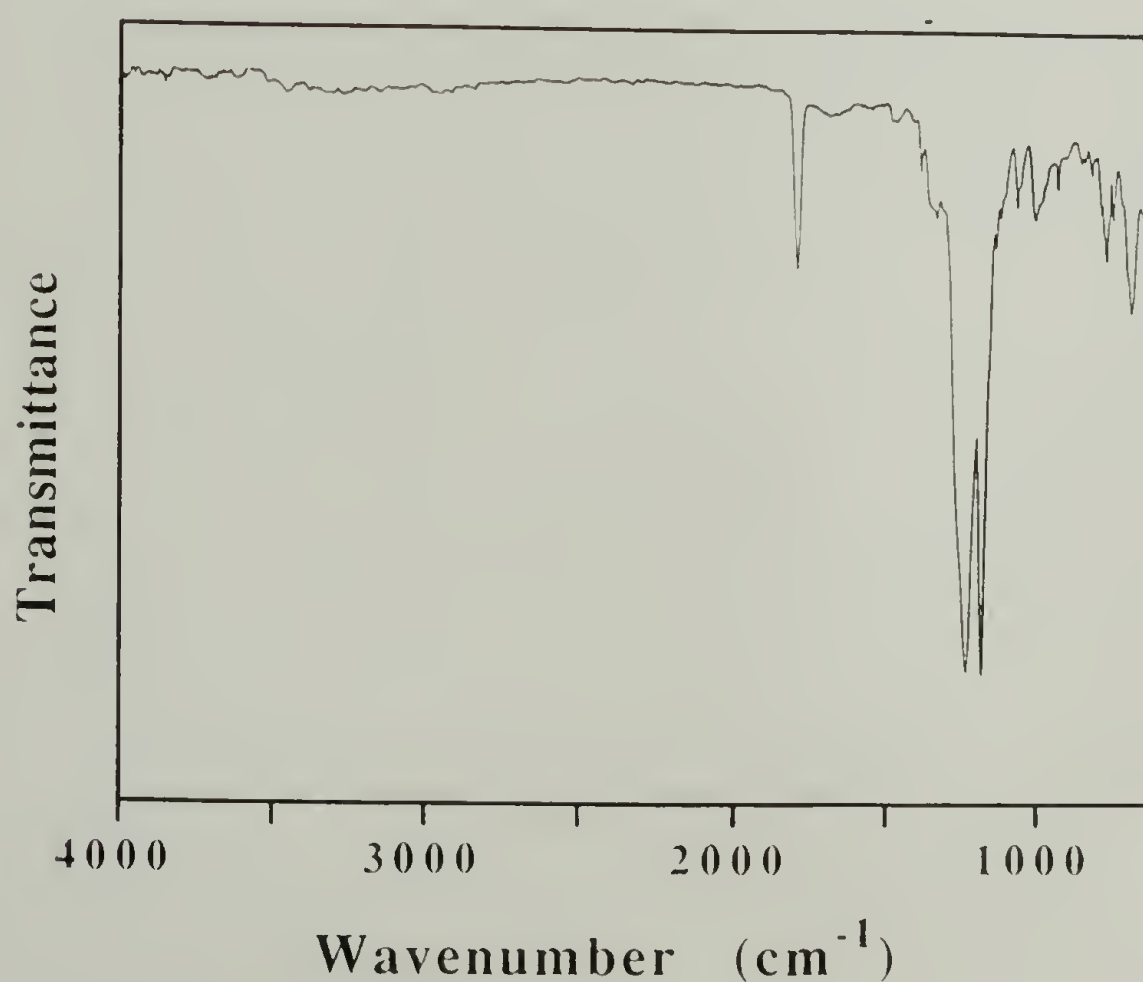


Figure 3.20. ATR-IR spectrum of PCTFE-OPFDec (-15 °C initial modification).



In the spectra of the two crosslinked surfaces (Figures 3.21 and 3.22), the absence of a hydroxyl stretching band and the sharpness of the carbonyl peak (which implies there is little carboxylic acid functionality) indicate that the di- and tri-functional acid chlorides used to prepare these surfaces have reacted multiply with PCTFE-OH. The predominance of the formation of the di- or tri-ester over the partial ester/partial acid species from a solution that has a many orders-of-magnitude excess of acid chloride (over the hydroxyl groups in the film surface) has been explained.<sup>11</sup> The rationale being that at the site of the reaction (inside the modified polymer layer), there is in fact, a large excess of hydroxyl groups. As expected the spectrum of PCTFE-O<sub>2</sub>Adip (Figure 3.21) shows only peaks arising from the methylene vibrations, while the PCTFE-O<sub>3</sub>Benz (Figure 3.22) spectrum has methylene peaks as well as bands which can be assigned to the aromatic ring stretching (1610 cm<sup>-1</sup>) and the C-H out-of-plane (741 cm<sup>-1</sup>) bending.

The ATR-IR spectra of the thinner modified surfaces (-78 and -60 °C initial modifications) show features similar to those discussed above. However, as expected, the intensities of the peaks assigned to the modified layer are significantly reduced relative to those of the unreacted bulk PCTFE (especially true for the samples initially modified at -78 °C). For comparison with the deeply modified samples, Figure 3.23 (a and b) shows the ATR-IR spectra of PCTFE-ODec initially modified at -78 and -60 °C, respectively. The corresponding spectra for PCTFE-OPFDec are shown in Figure 3.24 (a and b).

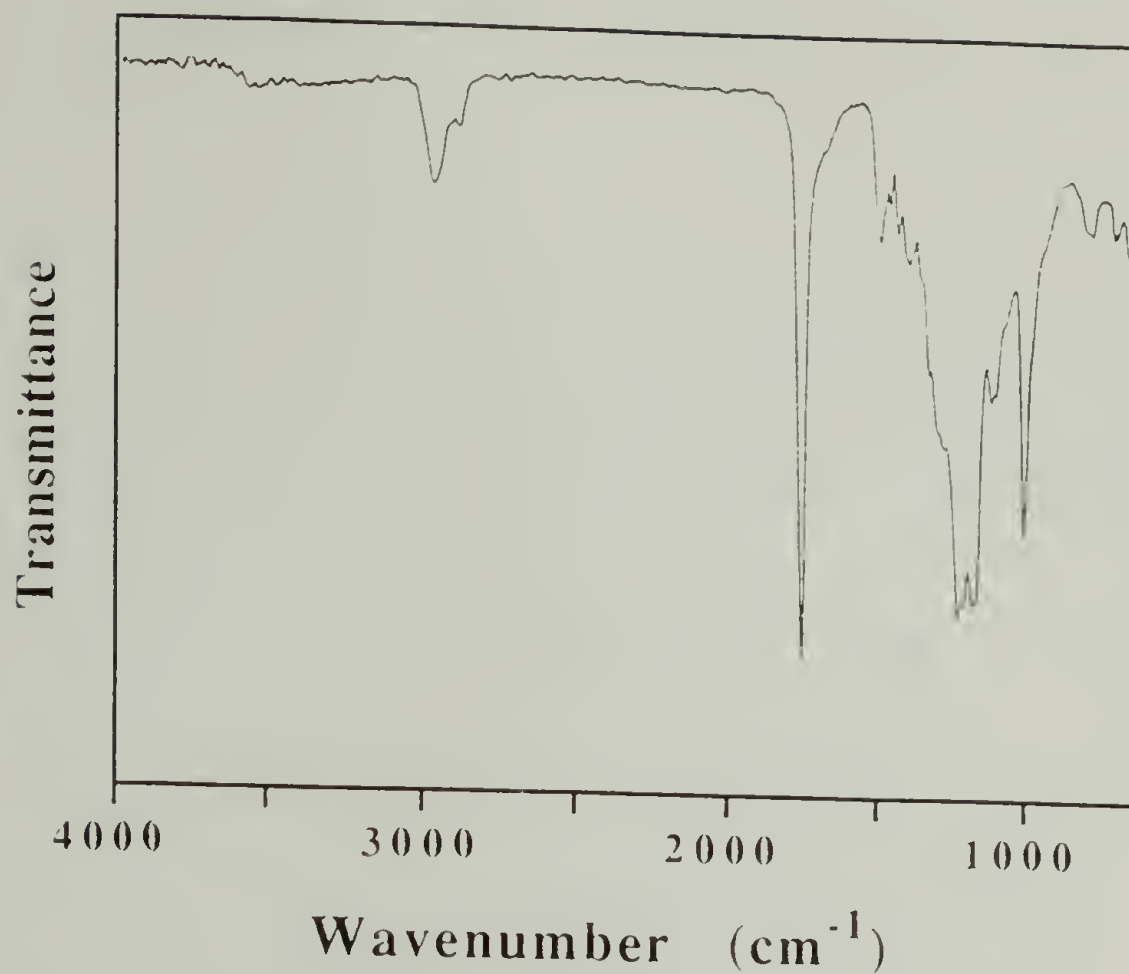


Figure 3.21. ATR-IR spectrum of PCTFE-O<sub>2</sub>Adip (-15 °C initial modification).

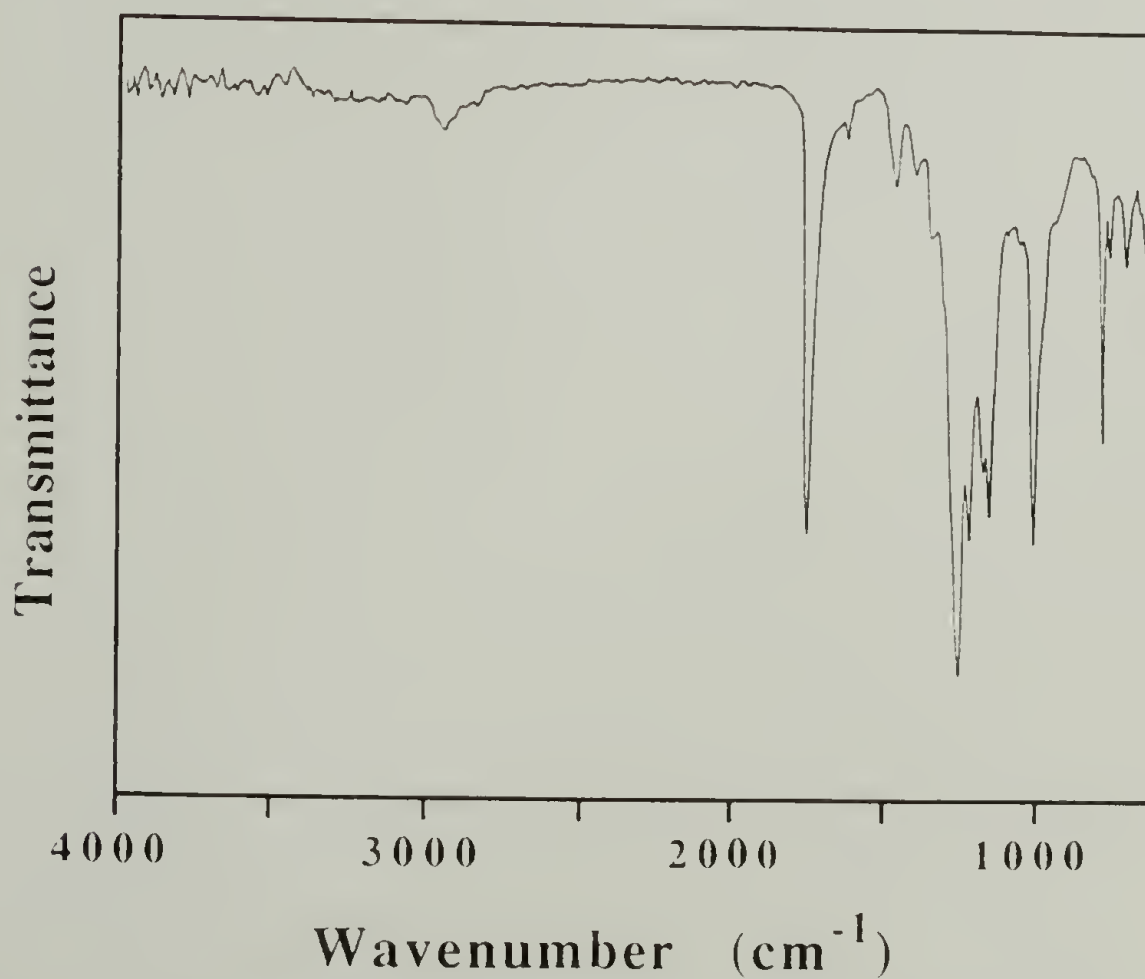


Figure 3.22. ATR-IR spectrum of PCTFE-O<sub>3</sub>Benz (-15 °C initial modification).

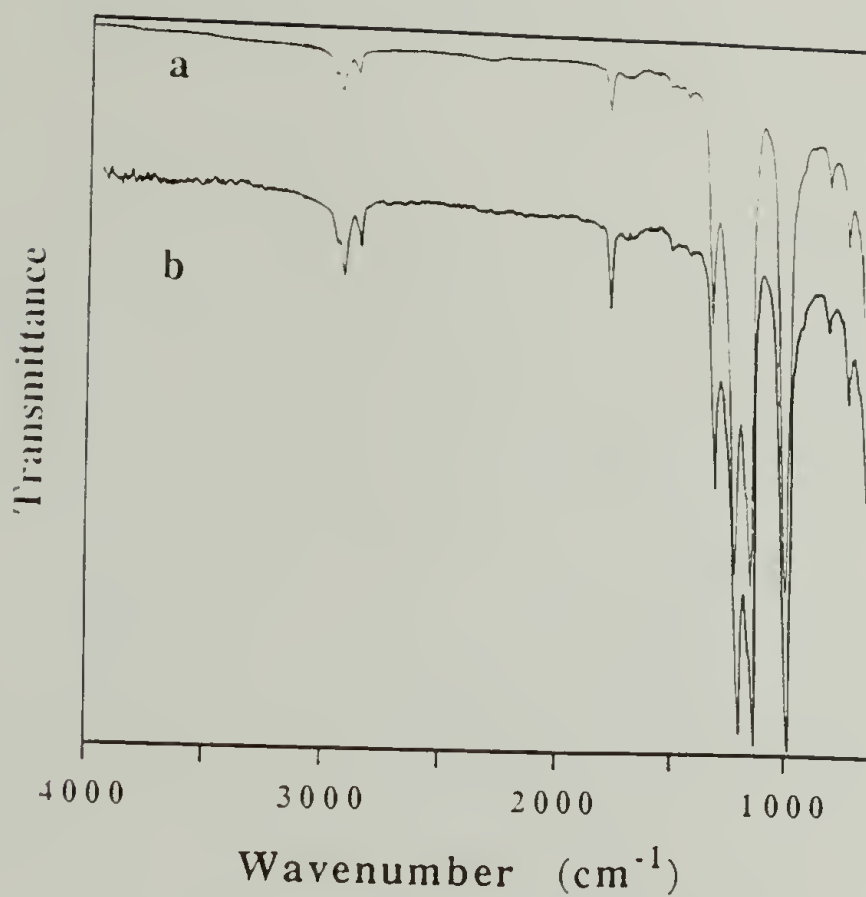


Figure 3.23. ATR-IR spectra of PCTFE-ODec: (a) -78 °C initial modification and (b) -60 °C initial modification.

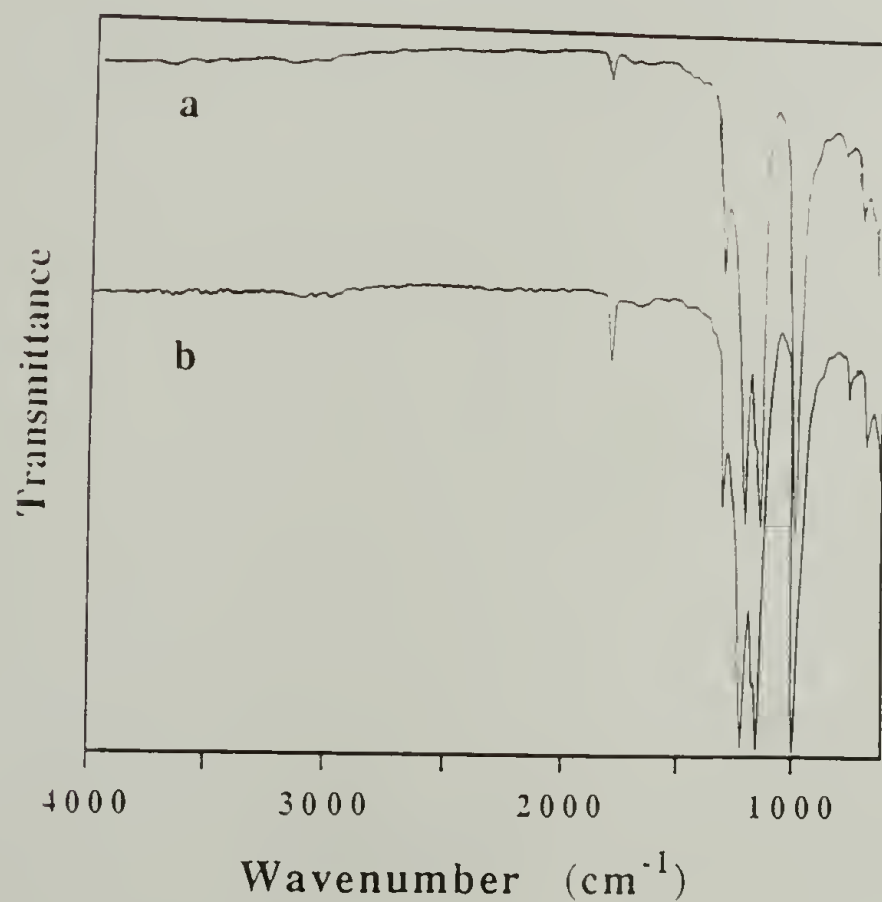


Figure 3.24. ATR-IR spectra of PCTFE-OPFDec: (a) -78 °C initial modification and (b) -60 °C initial modification.



The gravimetric thicknesses of these ester layers were measured for the samples initially modified at -60 and -15 °C. These results are shown in Table 3.3 (page 115) along with predicted values based on the measured thickness of the original acetal surface. These measured thicknesses agree with the predicted values, with the exception of PCTFE-O<sub>3</sub>Benz and PCTFE-OS<sub>tear</sub>. The values for these two surfaces indicates a lower reaction yield and/or dissolution of the modified layer during the reaction and subsequent film purification. The absence of an O-H stretching band in the ATR-IR spectra of these two esters (Figures 3.22 and 3.18, respectively) indicates that these reactions proceed in high yield, but do not necessarily indicate a quantitative reaction. The O-H stretching band is broad and has a low extinction coefficient and is thus difficult to detect in lowered concentrations. It is also likely that the residual hydroxyl groups lie deep within the film where the intensity of the evanescent infrared wave<sup>40</sup> is considerably lower than that at the polymer/germanium (the internal reflection element used in these measurements) interface. For PCTFE-O<sub>3</sub>Benz, a less than quantitative yield is the cause for the inconsistency, as it is difficult to imagine this highly crosslinked surface dissolving. Also, the intensity of the C=C double bond absorbance in the ATR-IR spectrum remains high indicating little or no dissolution. The depressed yield can be rationalized by realizing that the acid chloride must diffuse through a partially esterified and hence partially crosslinked surface before it can react with hydroxyl groups deeper within the film. As the reaction progresses, the outer surface of the film becomes more and more densely crosslinked, further inhibiting diffusion of the acid

chloride to the underlying hydroxyl functionality. It is likely that this sample consists of three layers: (1) a graduated crosslinked layer with an extremely high crosslink density at the film/air interface, (2) a layer of unreacted PCTFE-OH beneath this crosslinked surface and (3) virgin PCTFE in the bulk of the material. An autoinhibition effect can also be used to explain the inconsistencies in the gravimetric results for PCTFE-OSTear: they can be attributed to both of the factors mentioned above. The intensity of the C=C double bond absorbance is roughly the same magnitude in PCTFE-OSTear as in PCTFE-OH indicating that dissolution of the modified layer is small. However, the yield of the pyridine catalyzed reaction of PCTFE-OH (initially modified at  $-78^{\circ}\text{C}$ ) with stearoyl chloride was determined by another method<sup>41</sup> to be  $\sim 90\%$ . Thus, it is possible that as the reaction progresses the outer fully esterified regions of the film become ordered and solid-like, limiting the ability of the reagent to diffuse to the hydroxyl groups deeper within the sample.

### Conclusions and Future Work Suggestions

It was stated in the introduction to this chapter that the main objective of this portion of the dissertation was to controllably prepare a series of well-characterized surface modified samples with varying modified layer thicknesses for friction studies. The results presented in this chapter show that this objective has been met.

PCTFE film reacts with LiPEAA to incorporate the acetaldehyde propyl ethyl acetal into the polymer surface. The modified surface layer has been postulated to contain four acetals for every five

polymer repeat units with the fifth being a difluoroolefin. The depth of modification ranges from tens to thousands of angstroms and may be controlled by varying the reaction temperature. Once this initial modified surface is prepared, the acetal can be quantitatively hydrolyzed to the alcohol in a refluxing solution of aqueous HCl. ATR-IR spectra show an intense O-H stretch peak at  $3330\text{ cm}^{-1}$  for this alcohol. As expected, a decrease in the water contact angles was observed indicating that a more hydrophilic surface has been produced.

The alcohol (prepared from samples modified at  $-78$ ,  $-60$  and  $-15\text{ }^{\circ}\text{C}$ ) was esterified with a number of acylating reagents to produce a series of hydrocarbon and fluorocarbon esters and two crosslinked surfaces with various, controlled modified layer thicknesses. Contact angle results are consistent with the predicted product surfaces and indicate a significant amount of order in the stearate and perfluorodecanoate surfaces. High reaction yields were confirmed by three methods: (1) observation of the disappearance of the O-H band in the ATR-IR and the incorporation of carbonyl peaks and other absorbances consistent with the structures of the proposed esters, (2) comparison of the measured XPS atomic compositions with those predicted based on the proposed structure of PCTFE-PEAA and (3) comparison of the gravimetrically measured modified layer thicknesses with those based on that of PCTFE-PEAA.

For future research projects that use the modified surfaces discussed here for structure-property correlations, it would be desirable to put the roughnesses at the polymer/air and unmodified polymer/modified polymer interfaces on a more quantitative level.



Perhaps atomic force microscopy of the samples before and after oxidative removal of the modified layer could be used to get a physical picture of these interfaces. Relative information concerning the modified/unmodified polymer interface for samples initially modified at different temperatures could be obtained by oxidatively removing the modified layer, followed by a 5 min reaction with LiPEAA, subsequent hydrolysis and reaction with a UV label. An increase in UV absorbance with an increase in the initial modification temperature would indicate an increase in the surface area of the original modified/unmodified polymer interface.

There are a number of interesting research projects that could make use of some of the chemistry developed here. One could competitively esterify alcohol functionalized surfaces with acetyl chloride and 1,3,5-benzenetricarbonyl trichloride to control crosslink densities and thus, pore sizes for use in membrane studies. The existence of an order/disorder transition for the stearate and perfluorodecanoate esters could be investigated and utilized as a means of controlling gas diffusion through membranes that have these functional groups at their surfaces. Kinetics of esterification of deeply modified PCTFE-OH (or other densely functionalized alcohol surfaces, such polyvinyl alcohol) as a function of temperature could be followed with a combination of contact angle, XPS and ATR-IR to see if low temperature esterifications exhibit any autoinhibitive behavior (Autoinhibition would most likely be observed for PCTFE-OSTear and PCTFE-OPFDec.). These experiments could result in the formation of tri-layer surfaces (PCTFE-OEster/PCTFE-OH/PCTFE)

which may have interesting properties for studying surface reorganization phenomena or as membranes.

### References and Notes

- (1) A thorough discussion of polymer friction is presented in Chapter IV of this dissertation.
- (2) For general references see: Lee, L.H. "Advances in Polymer Friction and Wear"; Polymer Science and Technology, vols. 5A and 5B, 1974. Tabor, D. *Nature*, **1963**, *197*, 856. Bikerman, J.J. *J. Macromol. Sci.-Rev. Macromol. Chem.*, **1974**, *C11*, 1. Clark, D.T. and Feast, W.J. "Polymer Surfaces", 1978. Briscoe, B.J. *Adhesion*, **1981**, *5*, 49. Tewari, U.S., Sharma, S.K. and Vasudevan, P. *J. Macromol Sci.-Rev. Macromol. Chem and Phys.*, **1989**, *C29(1)*, 1. Cherry, B.W. "Polymer Surfaces," Cambridge University Press, Cambridge, Great Britain, 1981.
- (3) Briscoe, B.J. and Tabor, D. *Br. Poly. J.*, **1978**, *10(1)*, 74.
- (4) Erhard, G. *Wear*, **1983**, *84*, 167.
- (5) Nudel'man, Z.N., Alyabina, E.A., Prokudin, I.P., Rybalov, S.L., Tarkhava, T.P., *Kauch. Rezina*, **1969**, *28(3)*, 21.
- (6) Franchina, N.L. and McCarthy, T.J. *Macromolecules*, **1991**, *24*, 3045.
- (7) Costello, C.A. and McCarthy, T.J. *Macromolecules*, **1987**, *20*, 2819.
- (8) Bening, R.C. and McCarthy, T.J. *Macromolecules*, **1990**, *23*, 2648.
- (9) (a) Brennan, J.V. and McCarthy, T.J. *Polym. Prepr. (Am. Chem. Soc. Div. Poly. Chem.)*, **1988**, *29(2)*, 338. (b) Brennan, J.V. and McCarthy, T.J. *Polym. Prepr. (Am. Chem. Soc. Div. Poly. Chem.)*, **1989**, *30(2)*, 152.

- (10) (a) Dias, A.J. and McCarthy, T.J. *Macromolecules*, **1987**, *20*, 2068. (b) Dias, A.J. Ph.D. dissertation, University of Massachusetts, 1987.
- (11) Lee, K.-W. and McCarthy, T.J. *Macromolecules*, **1988**, *21*, 2318.
- (12) Cross, E.M. and McCarthy, T.J. *Macromolecules*, **1990**, *23*, 3916
- (13) Holmes-Farley, S.R., Bain, C.D. and Whitesides, G.M. *Langmuir*, **1988**, *4*, 921.
- (14) Troughton, E.B., Bain, C.D., Whitesides, G.M., Nuzzo, R.G., Allara, D.L. and Porter, M.D. *Langmuir*, **1988**, *4*, 365.
- (15) Morra, M. Occhiello, E. and Garbassi, F. *Langmuir*, **1989**, *5*, 872.
- (16) Holly, F.J. and Refojo, M.F. *J. Biomed. Materials Res.*, **1975**, *9*, 315.
- (17) Lee, K.-W. and McCarthy, T.J. *Macromolecules*, **1988**, *21*, 3353.
- (18) Juaristi, E.; Martinez-Richa, A.; Garcia-Rivera, A. and Cruz-Sanchez, J.S. *J. Org. Chem.* **1983**, *43*, 2603.
- (19) For a takeoff angle of  $75^\circ$  64.5% of the signal observed comes from a depth,  $t = \lambda$  while 95.5% comes from  $t = 3\lambda$  and at  $15^\circ$  64.5% comes from  $t = 0.27\lambda$  and 95.5% from  $t = 0.80\lambda$ . Where  $\lambda$  is the photoelectron's mean free path. (For C1s photoelectrons  $\lambda = 14 \text{ \AA}$ .<sup>20</sup>)
- (20) This value was measured in poly(*p*-xylylene): Clark, D.T. and Thomas, H.R. *J. Polym. Sci. Polym. Chem. Ed.* **1977**, *15*, 2843.
- (21) (a) Bee, T.G. and McCarthy, T.J. *Macromolecules*, **1992**, *25*, 2093. (b) Chapter II of this dissertation
- (22) (a) The effect of surface roughness on contact angle hysteresis was first discussed by Wenzel, R.N. in *Ind. Eng. Chem.* **1936**, *28*, 988. (b) For a general review see Chapter I of this dissertation.



- (23) See Chapter I of this dissertation for a discussion of these calculations.
- (24) This value was calculated from data presented in reference 20.
- (25) Shoichet, M.S. and McCarthy, T.J. *Macromolecules* **1991**, *24*, 982.
- (26) Kolb, B.U.; Patton, P.A.. and McCarthy, T.J. *Macromolecules* **1990**, *23*, 366.
- (27) A review of the results presented in references 10 and 26 is presented in Chapter I of this dissertation.
- (28) Based on the relative solubilities of poly(4-hydroxybutene) in the same solvents as reported by Chung, T.C.; Raate, M.; Berluche, E. and Schulz D.N. *Macromolecules* **1988**, *21*, 1903.
- (29) See Chapter V of this dissertation for other examples in which an increase in the interfacial free energy leads to reduced rates of hydrolysis.
- (30) Zisman, W. in *Contact Angle, Wettability and Adhesion*, Fowkes, F.M. Ed., Advances in Chemistry Series, No.43, 1964, 1.
- (31) (c) Johnson, R.E. and Dettre, R.H. *Surface Colloid Sci.*, **1969**, *2*, 85. (d) Neumann, A.W. and Good, R.J. *J. Colloid Interface Sci.*, **1972**, *38*, 341.
- (32) For discussion of surface reorganization in water contact angle measurements see: Andrade, J.D. *Surface and Interfacial Aspects of Biomedical Polymers. Vol. I: Surface Chemistry and Physics*, 1985.
- (33) Bain, C.D. and Whitesides, G.M. *J. Am. Chem. Soc.*, **1988**, *110*, 5897.
- (34) Ashley, J.C. *IEEE Trans. Nucl. Sci.*, **1980**, *NS-27*, 1454.
- (35) Laibinic, P.E.; Whitesides, G.M.; Allara, D.L.; Tao, Y.-T.; Parikh A.N. and Nuzzo, R.G. *J. Am. Chem. Soc.*, **1991**, *113*, 7152 and references therein.

- (36) Hare, E.F.; Shafrin, E.G. and Zisman, W.A. *J. Phys. Chem.* **1954**, 58, 236.
- (37) Banks, R.E. *Fluorocarbons and Their Derivatives*, Oldbourne Press: London, 1964.
- (38) Silverstein, R.M.; Bassler G.C. and Morrill, T.C. *Spectrometric Identification of Organic Compounds*, John Wiley and Sons: New York, 1981, p. 107.
- (39) Snyder, R.G.; Hsu, S.L. and Krimm, S. *Spectrochim. Acta, Part A*, **1978**, 34, 395.
- (40) See Chapter I of this dissertation and references therein for a discussion of ATR-IR.
- (41) See Chapter V of this dissertation.

## CHAPTER IV

# FRICTION STUDIES OF SURFACE MODIFIED POLYMER FILMS

### Introduction

As discussed earlier,<sup>1</sup> over the last decade McCarthy and coworkers have developed relatively nondestructive techniques to introduce a variety of specific functional groups into the surfaces of polymer films. The long range goal of this work is the establishment of surface structure-property relationships involving wetting, adhesion and friction. To date, only changes in the wettability of modified polymers have been correlated with changes in structure through the use of water contact angles as a surface analytical technique. Little emphasis was placed on the investigation of other structure-property relationships until suitable substrates (As discussed in Chapter I of this dissertation.) could be developed for such a study. The understanding of and the ability to manipulate and characterize surface functional group chemistry has progressed to the point where an attempt to correlate surface structure and friction behavior can now be made. The objective of this research is to study the friction behavior of the surface modified poly(chlorotrifluoroethylene) (PCTFE) films discussed earlier<sup>2</sup> and to correlate the results with the currently accepted mechanisms of polymer friction. The remainder of this introduction will focus on a



discussion of these mechanisms in the general context of their application to this research.

## Polymer Friction

### Introduction

The study of the friction of materials began almost 300 years ago with the pioneering work of Amontons<sup>3</sup> and later Coulomb.<sup>4</sup> Their observations led to the three, so-called laws of sliding friction: (1) the ratio of the frictional force,  $F$ , to the normal load,  $W$ , is a constant defined as the coefficient of friction,  $\mu$ , ( $\mu \equiv F/W$ ) that is independent of the size of the normal load; (2)  $\mu$  is not a function of the apparent area of contact between the two sliding surfaces and (3) the speed of sliding has no effect on the magnitude of  $\mu$ . For most solid materials (metals, inorganic glasses and ceramics are examples) these laws are generally valid over a wide range conditions. The processes leading to the energy losses which cause friction in these types of materials have been successfully modeled and are well understood.<sup>5</sup> In contrast, the study of friction in polymeric materials has been described as an art form.<sup>6</sup> For polymers,  $\mu$  has been found to be a function of not only the properties of the polymer under study, but also a wide variety of factors including the sliding countersurface, normal load, apparent contact area, sliding speed and ambient temperature. The ability to make accurate quantitative predictions of friction based on a knowledge of the experimental conditions and the physical properties of the sliding materials is currently impossible. The processes causing the energy losses giving

rise to friction are simply too complex to be modeled effectively with the current level of understanding. However, a consistent qualitative picture of the mechanisms of friction in polymers is reasonably well developed. It is this qualitative picture that will be discussed below.

The study of polymer friction has been exhaustively reviewed throughout the literature.<sup>5-21</sup> The currently accepted view ascribes friction to a combination of two mechanisms: (1) the ploughing or deformation mechanism and (2) the adhesion mechanism. These two mechanisms are not completely independent of one another (except under special circumstances), but it is necessary to treat them as such in order to simplify the analysis.

### Deformation Friction

The deformation mechanism of polymer friction is associated with the ploughing or grooving of the asperities on one surface through the other surface. The frictional force arises from energy losses which occur deep within the material ( $\sim 1 \mu\text{m}$ ) and is not related to surface effects. This type of friction has been closely correlated to the bulk mechanical properties of the polymer<sup>22-24</sup> and is prevalent in rolling friction, sliding friction of extremely rough surfaces and sliding friction in the presence of a lubricant under relatively large normal loads. The deformation component of friction has been effectively modeled using a simple, physical idea: energy is fed into the polymer ahead of the contact region and some of this energy is restored at the rear of the contact area. The net loss of energy is related to the input energy and the plastic and viscoelastic loss properties of the polymer at the particular temperature, contact

pressure and rate of deformation of the process causing the friction. For example, a detailed analysis for the coefficient of rolling friction,  $\mu_r$ , yields:<sup>24</sup>

$$\mu_r \approx \frac{\pi}{2} W^{1/3} R^{-2/3} (1-\nu^2)^{1/3} E^{-1/3} \tan \delta \quad (4.1)$$

where  $W$  is the applied load;  $R$  is the radius of the hard sphere used in the measurement of rolling friction and  $E$  is Young's modulus,  $\nu$  Poisson's ratio and  $\tan \delta$  the loss tangent of the polymer under study. Good agreement between the results of this type of analysis and the experimental behavior, in situations where the deformation term is thought to dominate, indicates that the majority of the energy losses occur deep within the sample and surface effects are negligible. For this reason, the experimental conditions for the research presented in this dissertation were chosen to minimize bulk deformations and thus, it is not necessary to further discuss this mechanism of polymer friction.

### Adhesive Friction

In adhesive friction, interfacial interactions lead to the formation of adhesive junctions which deform upon relative motion of the two surfaces until rupture occurs. This adhesive friction is the major cause of sliding friction in polymers. In this case, the frictional force,  $F$ , has usually been discussed in terms of the relation:

$$F = A\tau \quad (4.2)$$



where  $A$  is the true area of contact between the two surfaces and  $\tau$  is described as the interfacial shear strength. The effect that changes in the sliding countersurface, normal load, sliding speed or ambient temperature have on  $F$  (and thus,  $\mu$ ) has then been interpreted in terms of their effects on  $A$  and  $\tau$ .

The true area of contact is significantly less than the apparent area of contact due to surface roughness and depends on the deformation properties of the polymer. In the absence of an external load, two surfaces in contact with each other touch only at the tips of their asperities, thus  $A$  is very small. When a load is applied to a flexible polymer, deformation of the material at the interface will lead to a significant increase in the contact area. On the other hand, a rigid polymer will deform only slightly under similar conditions, resulting in a small increase in  $A$ .

The interfacial shear strength is primarily a function of the mechanical behavior of the weaker of the two sliding surfaces (usually chosen to be the polymer under study). Qualitatively,  $\tau$  has been described as resembling bulk polymer shear. However, quantitative agreement is poor since the interfacial shear in sliding friction typically occurs under conditions of much greater strains, strain rates and hydrostatic pressures than used in the study of bulk polymer shear. The current theories concerning  $\tau$  also do not take into account the role of the thermodynamic work of adhesion at the interface nor the different modes of failure that occur as a result of the sliding process. The location of failure depends on the relative magnitudes of the shear strength at the interface and of that in the polymer bulk. If the shear strength of the interface,  $\tau_i$ , is less than

the bulk shear strength of the polymer,  $\tau_b$ , adhesive failure occurs at the interface. If  $\tau_i > \tau_b$ , cohesive failure occurs within the polymer. The shear strength of the interface,  $\tau_i$ , depends on the strength of the adhesive junctions, which is related to the thermodynamic work of adhesion; the number of these junctions, which is related to the contact area and the deformation properties of the material at the interface. The factors that determine the shear strength of the bulk polymer are much more complicated. In this case, a detailed analysis would have to include not only the deformation properties of the polymer, but also the energy required to separate the polymer from itself. This latter energy would include contributions from the energy required to create new surfaces (the thermodynamic work of cohesion), the energy necessary to disentangle the polymer chains at the failure surface and the energy for polymer chain scissions. When cohesive failure takes place, transfer of material from the polymer to the countersurface is usually observed. As can be imagined, the energy required for adhesive failure is usually much smaller than that necessary for cohesive failure. However, failure will occur in the polymer bulk when the contact area is large and the adhesive junctions are sufficiently strong or if the bulk polymer is mechanically weak.

As discussed above, polymer friction involves the interaction of a number of variables. When each of these variables has been examined individually a number of interesting trends have been observed. While the simple analysis provided by Equation 4.2 yields poor quantitative results, it has been useful to use this relationship and a general understanding of the deformation properties of



polymers to qualitatively interpret the observed behavior. The discussions that follow will use this approach to examine how changes in some of these variables affect polymer friction.

Countersurface. Inorganic glasses, metals and a variety of polymers are examples of countersurfaces that have been utilized in the study of polymer friction. Provided that the surface shear strength of the countersurface is equal to or greater than that of the polymer under study, changes in the countersurface primarily cause changes in the work of adhesion between the countersurface and the polymer. The coefficient of friction has been measured as a function of the work of adhesion for a number of different polymer-polymer sliding combinations.<sup>25</sup> The results show that as the work of adhesion between the two surfaces increases,  $\mu$  generally increases, as would be expected. However, these studies do not consider the fact that changing the polymer sliding combination changes not only the work of adhesion, but also the deformation properties involved which may account for a significant portion of the observed changes in friction. In contrast, if the countersurface shear strength is lower than the shear strength of the polymer of interest, the friction behavior will be dominated by the properties of the countersurface.

Normal Load. The effects of variations in the applied load on the frictional force (and hence,  $\mu$ ) fall into two regimes.<sup>7</sup> At relatively high loads, it is observed that  $F$  increases linearly with increasing load and  $\mu$  is independent of load, in agreement with



Amontons' Laws. At relatively low loads, the relationship is non-linear and:

$$F = kW^m \quad \text{or} \quad \mu = kW^{m-1} \quad (4.3)$$

where  $m$  varies between 0.74 and 0.83 depending on the polymer. Thus, at low loads the coefficient of friction decreases with increasing load. These observations have generally been explained in terms of the variations of the contact area,  $A$ , with the normal load.

Contact between two surfaces initially takes place at the tips of the surface asperities. When a load is first placed on the surface, these asperities deform elastically. As the load is increased, the elastic limit is exceeded and plastic deformation occurs. The elastic limit for metals is on the order of  $10^{-5}$  to  $10^{-3}$  g for a single asperity with a radius of  $10^{-4}$  cm.<sup>26</sup> Thus, for metallic contacts, the asperities deform plastically except at extremely low loads. For polymers, the onset of plasticity occurs at a load approximately  $10^4$  times larger (for the same size asperities), because of their relatively small elastic modulus.<sup>26</sup> As a result, elastic deformation is observed if the load is not excessively large. For a single asperity undergoing purely elastic deformation, it has been calculated<sup>5</sup> that  $A \propto W^{2/3}$ , hence  $F \propto W^{2/3}$  and  $\mu \propto W^{-1/3}$ . While for plastic deformations,  $A$  is directly proportional to  $W$ , thus  $F$  is proportional to  $W$  and  $\mu$  is independent of the normal load. However, in real situations multiple asperity contacts are involved. In the case of plastic deformations the area of contact remains proportional to the load for multiple contacts and  $\mu$  is independent of the load. These results are in agreement with

Amontons' Laws and the behavior observed for metals and for polymers under relatively large loads. On the other hand, there are two distinct situations when multiple asperities deform elastically:<sup>10</sup>

1. The elastic deformation of an asperity contact increases with an increasing load, but the number of these contacts remains constant. Thus, the contact area is proportional to  $W^{2/3}$ .

2. The average area of the deformed asperities remains constant and increasing the load increases the number of these contacts proportionally. In this case,  $A \propto W$ .

In real situations where elastic deformations occur, the area of contact will reflect behavior between these two extremes and  $A \propto W^m$  and  $F \propto W^m$  where  $0.67 < m < 1.0$ , as is observed.

The true area of contact as a function of normal load has been measured for a number of polymers sliding on glass by a variety of optical techniques.<sup>27-29</sup> The results generally show that the optical area of contact varies as  $A \propto W^m$ , while the friction varies as  $F \propto W^n$ , where  $m$  is significantly less than  $n$ . The differences between the exponents  $m$  and  $n$  have been attributed to two factors. First, it is likely that the optical area of contact is not equivalent to the real contact area and the scaling exponent may not be the same for both areas. However, this explanation cannot account for all of the differences. If friction is to be explained by the relation  $F = A\tau$ , it follows from these results that the interfacial shear strength,  $\tau$ , must also increase with increasing contact pressure. The shear strength of thin polymer films as a function of contact pressure has been

measured<sup>30-34</sup> and the results show that  $\tau$  increases linearly with pressure,  $p$ , over a wide range:

$$\tau = \tau_0 + \alpha p \quad (4.4)$$

The value of  $\alpha$  is similar to that measured for the shear of bulk polymers, but  $\tau_0$  is considerably smaller.<sup>17</sup> Differences may be the result of the high degree of orientation produced in sliding or to the fact that the shear is confined to a specified plane in the thin-film experiments.

Sliding Speed. The effect of changes in the sliding speed on friction has been studied for a number of polymers.<sup>35-37</sup> At high sliding speeds significant frictional heating occurs which can melt the polymer at the interface and/or cause irreversible chemical damage. For these reasons most investigations have focused on the behavior taking place at relatively low sliding speeds. The results generally show that the effect of increasing the sliding speed varies with the class of polymers. Rigid polymers, such as thermoset resins and amorphous polymers well below their glass transition temperatures (temperature effects will be discussed), typically exhibit low coefficients of friction and show little variation in friction with sliding speed. On the other hand, the friction of semi-crystalline polymers and elastomers is generally higher and exhibits a maximum in a plot of the coefficient of friction versus sliding speed. The onset of this maximum shifts to higher sliding speeds with an increase in the ambient temperature, which discounts the possibility



of frictional heating. This time-temperature dependent behavior suggests that this maximum is closely related to the viscoelastic properties of these materials. In fact, the results of friction measurements of a number of rubbers conducted over a wide range of temperatures and sliding speeds have been superimposed on a single master curve using a Williams-Landel-Ferry transform.<sup>36,37</sup>

There have been two approaches to understanding the origins of this maximum - one microscopic and the other macroscopic.<sup>13a,14,16</sup> Both sets of theories involve the interaction of two terms, one of which increases with sliding speed and another that decreases with sliding speed, leading to the maximum. The microscopic or molecular theories of polymer friction consider that bonds are formed at the interface, strained and then broken via a rate activated process. With these theories it is generally considered that the bond strength increases with sliding speed, while the number of bonds decreases. The macroscopic theories attempt to assess the manner in which the contact area and the interfacial shear strength vary with the rate of deformation. The area,  $A$ , is thought to decrease with an increase in sliding speed, while the shear strength,  $\tau$ , increases, such that the frictional force, which equals the product of  $A$  and  $\tau$ , goes through a maximum. Both theories are in qualitative agreement with the observed behavior, but quantitative agreement is poor and other experimental evidence suggests that neither of these treatments accurately describes the processes actually occurring at the interface.<sup>14</sup> Thus, new avenues need to be explored.

Ambient Temperature. The temperature dependence of the friction of polymers also reflects their deformation properties.<sup>38,39</sup> Below the glass transition temperature of amorphous polymers, the coefficient of friction is essentially independent of the ambient temperature. However, small maxima in  $\mu$  have been observed at temperatures which correspond to the low temperature mechanical losses associated with the  $\beta$  and  $\gamma$  transitions in the polymer. At temperatures just above  $T_g$  a large maximum in  $\mu$  is observed. At  $T_g$ , the polymer begins to soften, increasing the contact area,  $A$ , while simultaneously decreasing the interfacial shear strength,  $\tau$ . As the temperature increases the magnitude of the increase in  $A$  is greater than that of the decrease in  $\tau$  and the friction increases. Eventually, any additional increase in the area is offset by the decreasing shear strength and the friction begins to decrease, thus, the resulting maximum. Finally, at temperatures far above  $T_g$  the coefficient of friction continues to decrease as the material becomes more and more liquid-like.

### Summary

From the preceeding discussion it can be seen that the friction behavior of polymers is highly dependent on the properties of the materials involved and the experimental conditions. The friction behavior reviewed above was evaluated in terms of the relation:  $F = A\tau$  (Equation 4.2). As mentioned earlier, this equation provides a good basis for qualitative understanding, but yields poor quantitative results. The energy losses that are ultimately measured arise from a complex combination of factors involving the actual area of contact,

the work of adhesion between the two surfaces and the deformation properties of the surfaces involved. Perhaps future theories may need to digress from the use of Equation 4.2 in order to obtain better quantitative agreement and develop equations that more accurately describe the processes actually occurring at the sliding interface.

The remainder of this chapter will present results of friction measurements made on the surface modified polymer films discussed in Chapter III. Specifically, a number of surface modifications have been conducted on poly(chlorotrifluoroethylene) films in order to vary the polymer surface energy, the deformation properties of the surface region and the thickness of the modified layer in a well-controlled manner without affecting the bulk polymer properties. Sliding friction measurements were then performed under conditions chosen to exaggerate the adhesion mechanism of polymer friction and, hence, emphasize the surface region of the polymer film. The goal of this research is to combine the detailed knowledge of the structure of the modified surfaces with the friction results in order to further develop the understanding of surface structure-property relationships.

## Experimental

The surface modified poly(chlorotrifluoroethylene) film samples used in these friction studies were prepared as described previously.<sup>2</sup> The poly(ethylene terephthalate) (PET) films (DuPont Mylar) used as countersurfaces were cleaned immediately before use



by rinsing thoroughly with methylene chloride and then dried (120 °C, 760 mm, 15 min).

The instrument designed and built to measure sliding friction is shown in Figure 4.1. It is based on one proposed by ASTM method D 1894-78 for the measurement of the coefficient of friction of polymer films.<sup>40</sup> It consists of a slider mounted on a linear positioner which is driven by a shunt wound motor. The motor is capable of moving the slider at speeds ranging from 0.025 to 1.5 cm/s. The polymer film to be studied is attached to the bottom of an exchangeable sled (different size sleds allow different sizes of film to be tested) which rests on top of the slider. Between the film and the sled, a layer of rigid foam is mounted to absorb deformations. Varying size loads may be applied to the top of the sled. A 0 - 10 lb high performance load cell serves as the force transducer and is outputted to a strip chart recorder. The response of the load cell was calibrated to be 0.0397 mV/g which, in the force range of interest (0 - 250 g), implies differences of  $\pm 0.5$  g can be distinguished on the chart recorder.

Friction measurements were conducted by sliding 2.0" x 2.5" pieces of the film under study over the PET countersurface under a 300 g normal load at a sliding speed of 0.10 cm/s for a distance of 25 - 30 cm.<sup>41</sup> Each film sample was slid over the same countersurface area 25 times (except where indicated). Friction forces were calculated by taking a time average of the measured voltage from the strip-chart recorder once the frictional force had decreased from its initial static value to the equilibrium kinetic friction. This voltage was then converted to a force through the use

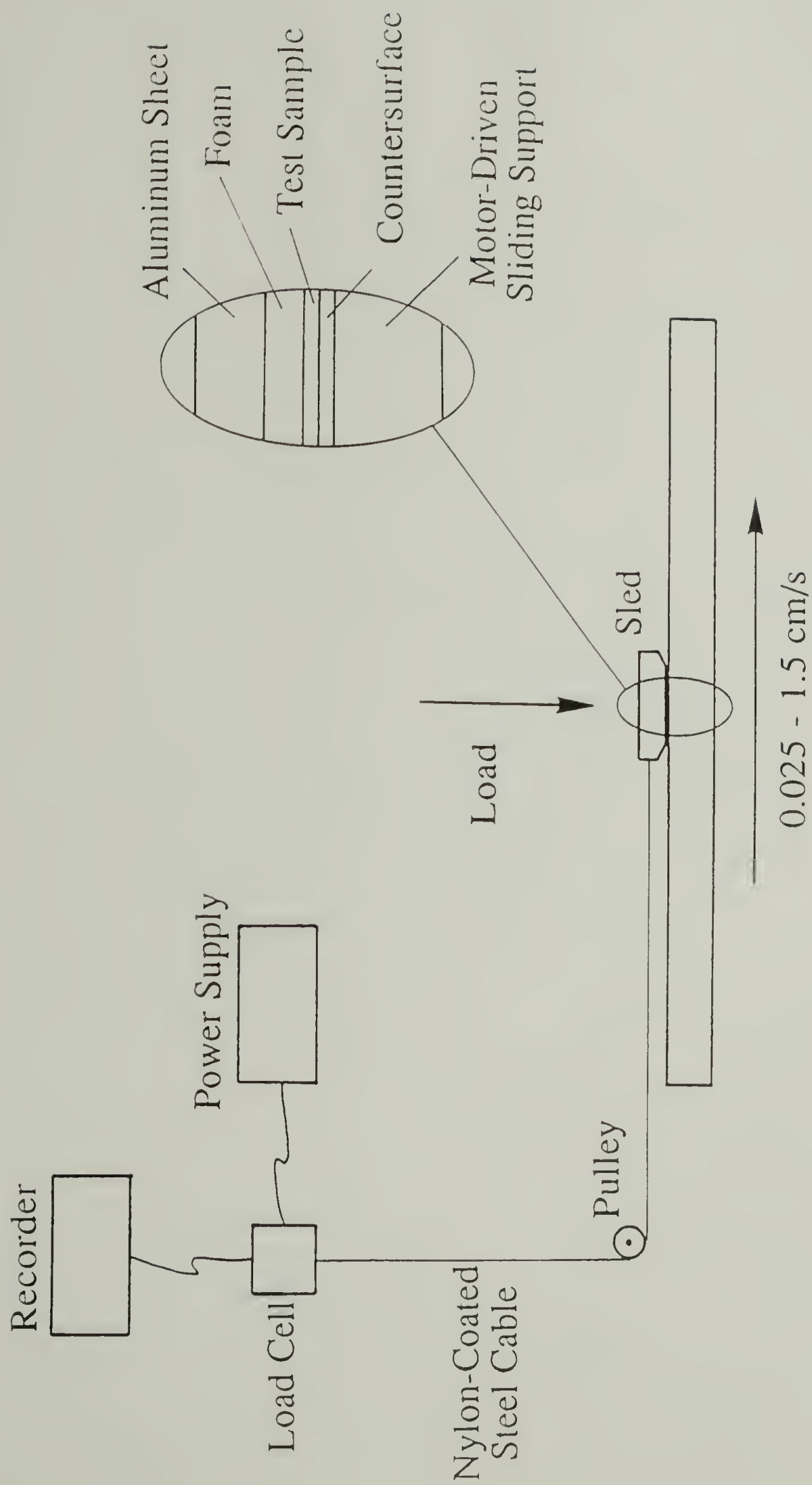


Figure 4.1. Instrument to measure coefficient of friction of polymer films.

of appropriate calibration standards. The coefficient of friction,  $\mu$ , was calculated as the measured frictional force divided by the applied normal force.

Surface imaging of the polymers before and after sliding was performed using: (1) a JEOL 35CF scanning electron microscope, (2) an Olympus BH2 optical microscope and (3) a Zygo Maxim 3D 5800 interferometric surface profilometer. X-ray photoelectron spectra (XPS) were obtained with a Perkin Elmer-Physical Electronics 5100 with Mg  $K_{\alpha}$  excitation (400 W, 15.0 kV). Binding energies shown are not corrected for sample charging. Spectra were routinely recorded at two takeoff angles ( $\Theta_T$ ):  $15^\circ$  and  $75^\circ$  (measured between the film surface plane and the analyzer).<sup>42</sup> XPS atomic composition data were determined using sensitivity factors obtained from measurements made on samples of known surface composition: F1s, 1.00; C1s, 0.225; O1s, 0.620 and Cl2p, 0.655. Dynamic advancing ( $\Theta_A$ ) and receding ( $\Theta_R$ ) water contact angles were measured with a Ramé-Hart telescopic goniometer as the probe fluid was added to ( $\Theta_A$ ) and removed from ( $\Theta_R$ ) the sample surface with a Gilmont syringe fitted with a 24 gauge flat-tipped needle. Results are reported as  $\Theta_A/\Theta_R$ .

## Results and Discussion

### Friction Behavior of Unmodified Poly(chlorotrifluoroethylene)

Figure 4.2 shows the results of a series of three friction experiments. First, virgin poly(chlorotrifluoroethylene) (PCTFE) film was slid over the same piece of poly(ethylene terephthalate) (PET)



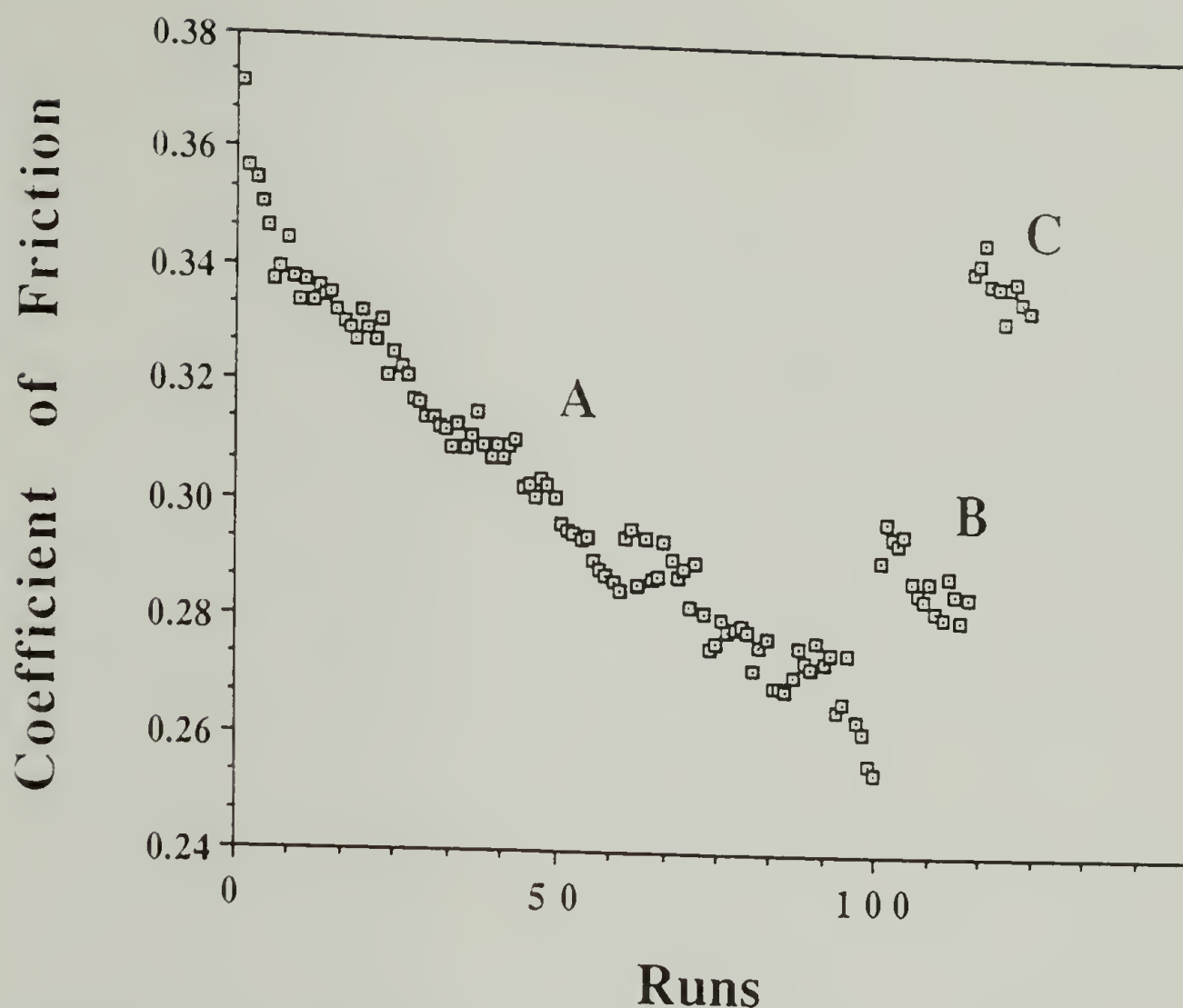


**Figure 4.2.** Coefficient of friction of virgin PCTFE sliding PET: (a) fresh PCTFE sliding on fresh PET (first 100 runs), (b) fresh PCTFE sliding on used PET (next 15 runs) and (c) used PCTFE sliding on fresh PET (last 10 runs).

film 100 times. Then a new piece of PCTFE was slid over the same PET surface 15 times. Finally, the original PCTFE film was slid over a fresh piece of PET 10 times. It can be seen from this figure that the coefficient of friction,  $\mu$ , decreases steadily with an increase in the number of times the films were slid against one another. This decrease suggests that changes are taking place in one or both of the film surfaces as a result of the sliding process. The relative increases in  $\mu$  when fresh PCTFE and PET are slid against the 100 run samples implicates changes taking place in the PET countersurface as the major source of this decrease. New PCTFE sliding on the used PET

raises the value of  $\mu$  from 0.254 to 0.291 (31.6% towards the initial value). This small increase indicates that the PCTFE has undergone some changes on sliding, but they are slight. Meanwhile, when the original PCTFE is slid over a fresh piece of PET,  $\mu$  increases from 0.254 to 0.342 (75.0%). This large increase implies that the majority of changes are occurring in the PET film. These changes may be one or more of the following: (1) transfer of polymer from or to the PET surface, (2) migration of low molecular weight material from the interior of the PET film to its surface, (3) physical roughening of the PET along the sliding direction and/or (4) orientation of the PET molecules at the surface as a result of sliding.

XPS analysis does not show any significant changes in the surface composition of either film that would indicate transfer of material from one polymer to the other. If cohesive failure had occurred in the PET countersurface, evidence of transfer would have been observed as an oxygen peak in the XPS spectrum of the PCTFE surface (PCTFE does not contain oxygen). Transfer of PCTFE to the PET would have resulted in a fluorine peak in the XPS spectrum of the PET (PET does not contain fluorine). After sliding, the absence of oxygen and fluorine in the XPS spectra of PCTFE and PET, respectively, indicates that transfer did not occur.

PET is known<sup>44</sup> to contain about 1 - 2% cyclics and oligomers which may migrate to the surface during sliding and act as a lubricant, lowering the coefficient of friction. This low molecular weight material would be indistinguishable from the bulk by XPS making its detection difficult. However, if the PET film is rinsed with methylene chloride after sliding (in an attempt to remove this low

molecular weight material) the coefficient of friction remains low when sliding is resumed. Thus, blooming of these low molecular weight molecules to the surface is not likely to be the cause of the decrease in  $\mu$ .

After 100 sliding runs both films show visual signs of wear. Each surface appears to be scratched and abraded from the sliding contact. Optical micrographs exhibit similar features and offer little insight. Scanning electron microscopy (SEM) shows some grooves and ridges in both surfaces, but they are scarce and difficult to find. It is possible that the thin ( $\sim 150$  Å), gold coating (used to prevent sample charging and damage) obscures most of the smaller features on the film surface. Surface interferometric profilometry shows the existence of several long, shallow, wide grooves and associated ridges parallel to the sliding direction. The high resolution (on the scale of angstroms) of this technique in the direction normal to the sample surface allows the observation of features that are filled in by the gold coating used in SEM. Figure 4.3 shows the interferometric surface profile of the PET surface across one of these grooves.

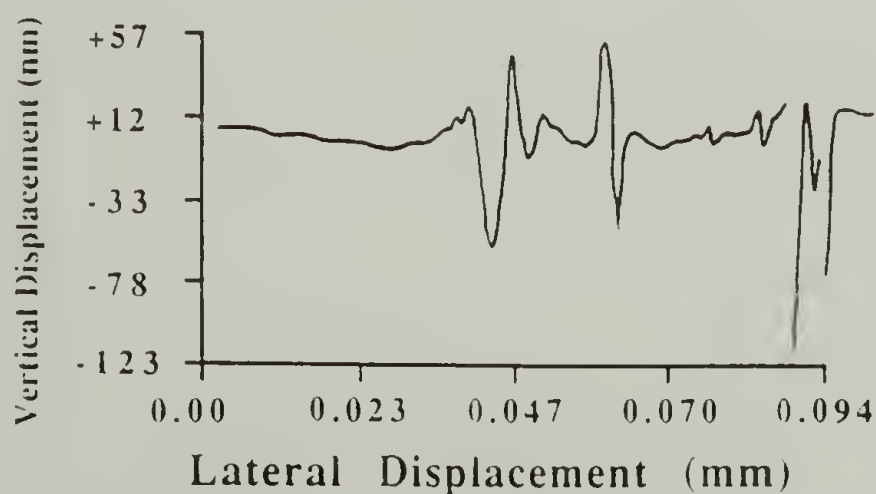


**Figure 4.3.** Interferometric surface profile of PET countersurface measured perpendicular to the sliding direction.



These furrows are observed to be on the order of  $10^2$  angstroms deep and  $10^6$  angstroms wide. Their shallowness and breadth explains the difficulty in their observation by SEM since these small abrasions are probably filled in by the gold coating.

The most interesting results come from the observed anisotropy in the water contact angle hysteresis (as shown in Figure 4.4) measured on the PET film used in the friction measurements. When the advancing and receding contact angles on the PET are measured parallel to the sliding direction, the result is the same as for fresh material ( $77^\circ/48^\circ$ ). In the direction perpendicular to the sliding, the advancing angle on the used PET increases to  $100^\circ$ , while the receding angle remains  $48^\circ$ . This increase in the hysteresis likely indicates an increase in roughness<sup>45</sup> of the PET surface perpendicular to the sliding direction, as would be expected based on the surface imaging results. The contact angles on the PCTFE ( $104^\circ/77^\circ$ ) remain unchanged in either direction.

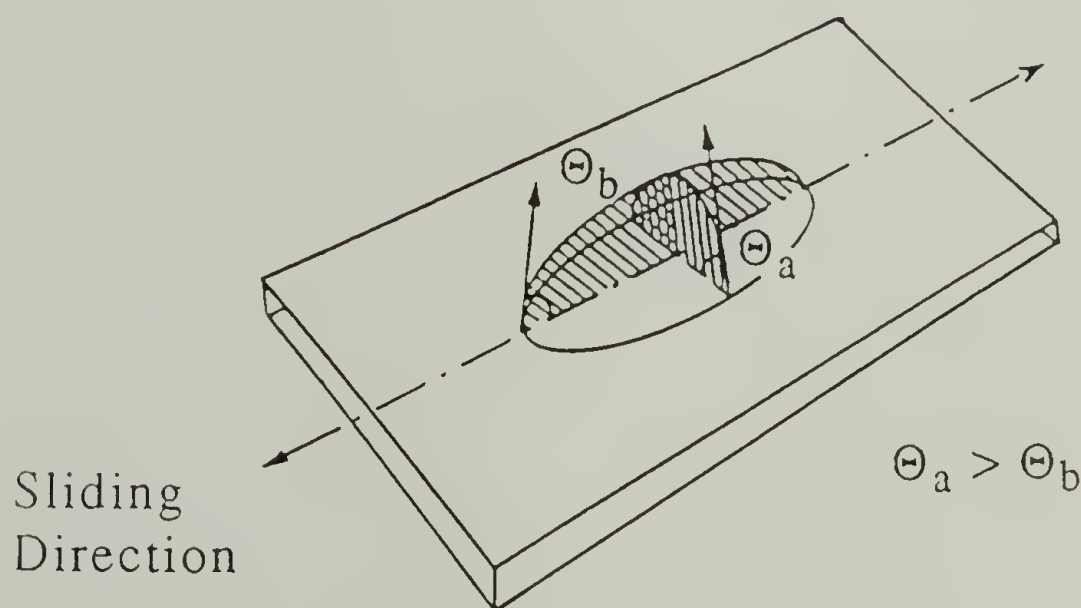


**Figure 4.4.** Measurement of contact angle anisotropy on friction surfaces.

Molecular orientation at the surface of the PET can also explain the differences in the contact angles measured perpendicular and parallel to the sliding direction. Contact angle anisotropy of this nature has also been observed on oriented polymer surfaces.<sup>46</sup> It is possible that the sliding process causes the polymer molecules at the surface to align themselves along the sliding direction. The observed decrease in friction with an increase in the number of sliding runs might also be the result of orientation of the polymer chains in the film surface. It is known<sup>8,21</sup> that when oriented polymers are slid parallel to their chain axis, the friction is lower than that of unoriented polymers. Along the same lines, the friction measured perpendicular to the chain orientation is significantly higher than that measured on an isotropic sample.

In order to further investigate the changes in the PCTFE and/or PET surfaces that result from sliding, a series of rotation experiments was performed. First, a 2" x 2.5" piece of PCTFE film was slid on a 12" x 9" PET countersurface 25 times under a 300 g load at 0.10 cm/s. As in the 100 runs experiment,  $\mu$  gradually decreased from 0.37 to 0.32. The PET was then rotated 90° and the PCTFE film slid perpendicular to the original sliding direction. A temporary increase in  $\mu$  from 0.37 to 0.39 was observed as the PCTFE crossed the original 2.5" wide sliding path. This increase in friction indicates that sliding has induced roughness perpendicular to and/or orientation parallel to the original sliding direction in the PET surface. A similar experiment was performed in which the PCTFE film was rotated 90° and slid against the PET. No change in the frictional force was

observed indicating little changes in the PCTFE surface. These results corroborate those presented above.

The effect of changes in the ambient atmosphere on friction was crudely studied by placing the friction instrument in a glove bag which was continuously purged with either nitrogen or dry,  $\text{CO}_2$  free air. The results for the friction of unmodified PCTFE sliding on PET in these two atmospheres are shown in Figure 4.5 along with the results for the friction measurement made in the laboratory atmosphere. The results show that under both the nitrogen and the dry air, the friction of PCTFE is significantly higher than when the measurement is made under a normal laboratory atmosphere. It is thought,<sup>5</sup> that when both members of the sliding contact pair are polymers, static electricity may contribute to the frictional force.

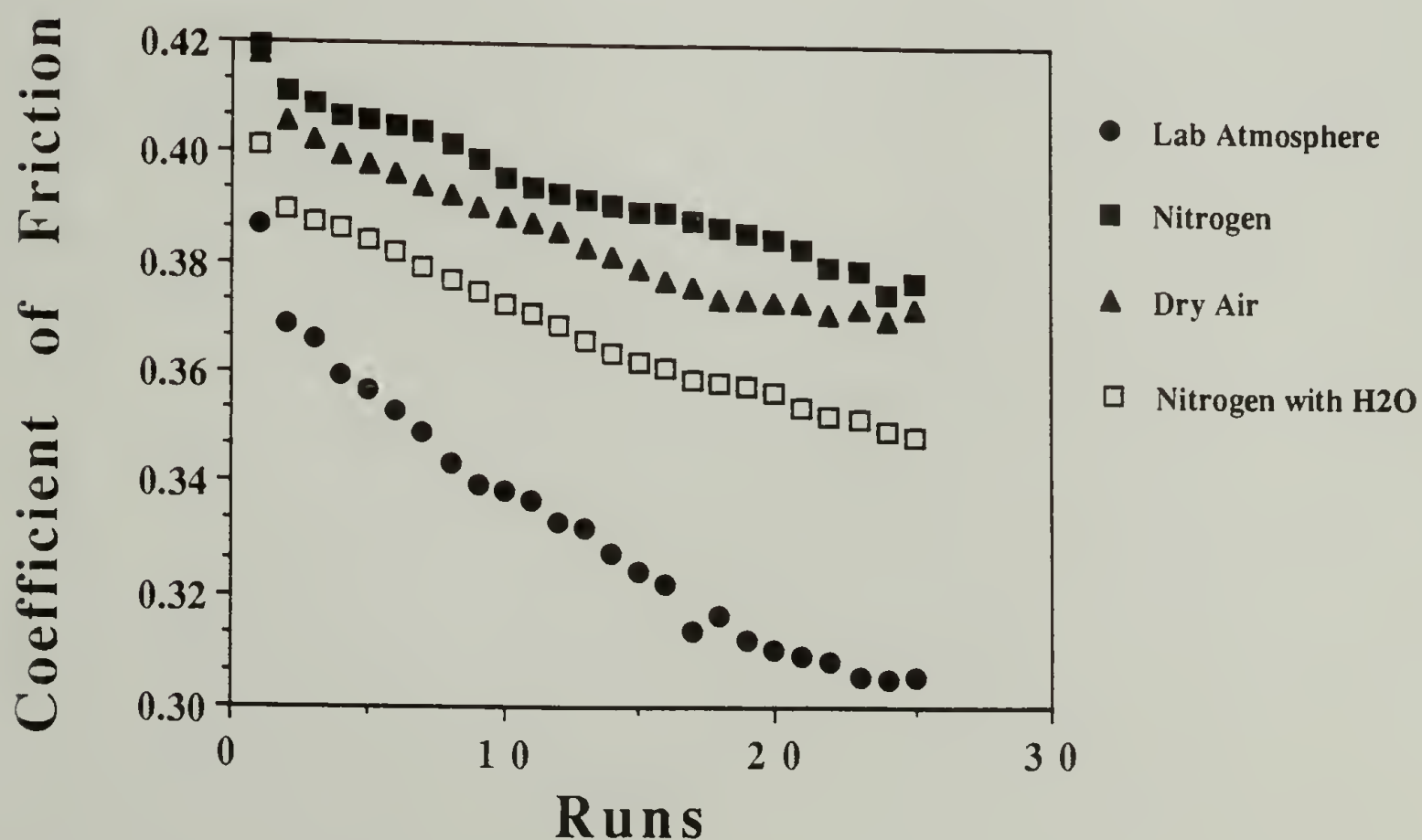


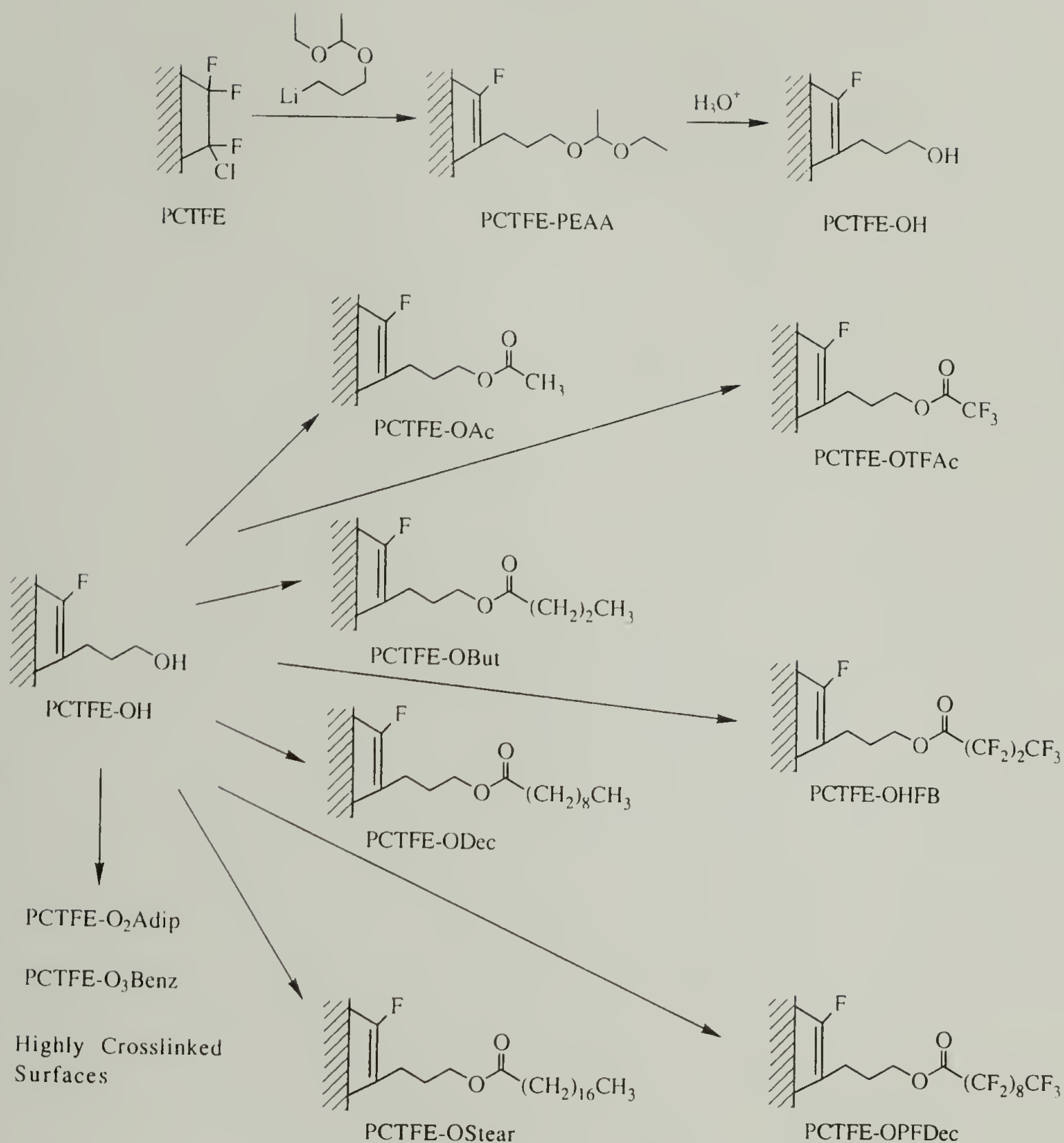
**Figure 4.5.** Friction of PCTFE measured in controlled atmospheres.



In a dry atmosphere, like those used above, dissipation of charge built up at the surface is more difficult which may cause the observed increase in friction. In an attempt to slightly increase humidity, a large crystallizing dish containing water at room temperature was placed in the glove bag. The friction was then measured under a nitrogen atmosphere. These results are also plotted in Figure 4.5 and show that a small increase in the humidity does decrease the friction slightly. While these results are interesting, the objective of the research presented in this dissertation is the study of the effects on friction of surface chemistry, not atmosphere or static electricity build up. Therefore, no further experiments were conducted in this area.

#### Friction Behavior of Modified Poly(chlorotrifluoroethylene) Surfaces

Once the friction behavior of unmodified PCTFE sliding on PET had been fully characterized, the friction of the modified PCTFE surfaces was studied. Scheme 4.1 illustrates the reactions used to prepare the surface modified films utilized in these friction studies. Briefly, PCTFE reacts with acetaldehyde 3-lithiopropyl ethyl acetal to incorporate the acetal functional group into the film surface (PCTFE-PEAA). The depth of this modification can be controlled by the reaction temperature and ranges from tens to thousands of angstroms. PCTFE-PEAA can then be hydrolyzed in high yield to produce an alcohol functionalized surface (PCTFE-OH), which can be further reacted with a number of hydrocarbon and fluorocarbon acid chlorides to create a series of ester surfaces (PCTFE-OAc, PCTFE-OTFAc, PCTFE-OBu<sub>t</sub>, PCTFE-OHFB, PCTFE-ODec, PCTFE-OPFDec and



**Scheme 4.1.** Surface modifications of PCTFE.

PCTFE-OStear). Alternatively, PCTFE-OH may be reacted with di- or trifunctional acid chlorides to prepare crosslinked surfaces (PCTFE-O<sub>2</sub>Adip and PCTFE-O<sub>3</sub>Benz). The experimental details and full characterization of the structures of these modified layers is presented in Chapter III of this dissertation.

Figure 4.6 shows results of sliding friction experiments for virgin PCTFE and the thinly ( $\sim 30 - 50 \text{ \AA}$ ) modified PCTFE surfaces sliding on a PET countersurface under a 300 g normal load at a rate of 0.10 cm/s. This plot represents an average of six measurements from different film samples for the virgin PCTFE and three for the modified surfaces. The results shown here are highly reproducible. Relative standard deviations for these measurements range from 0.5 - 2% for the different samples. Thus, a coefficient of friction for the modified samples of 0.350 with a relative deviation of 2% would have a true value of  $0.350 \pm 0.017$  at the 95% confidence level.

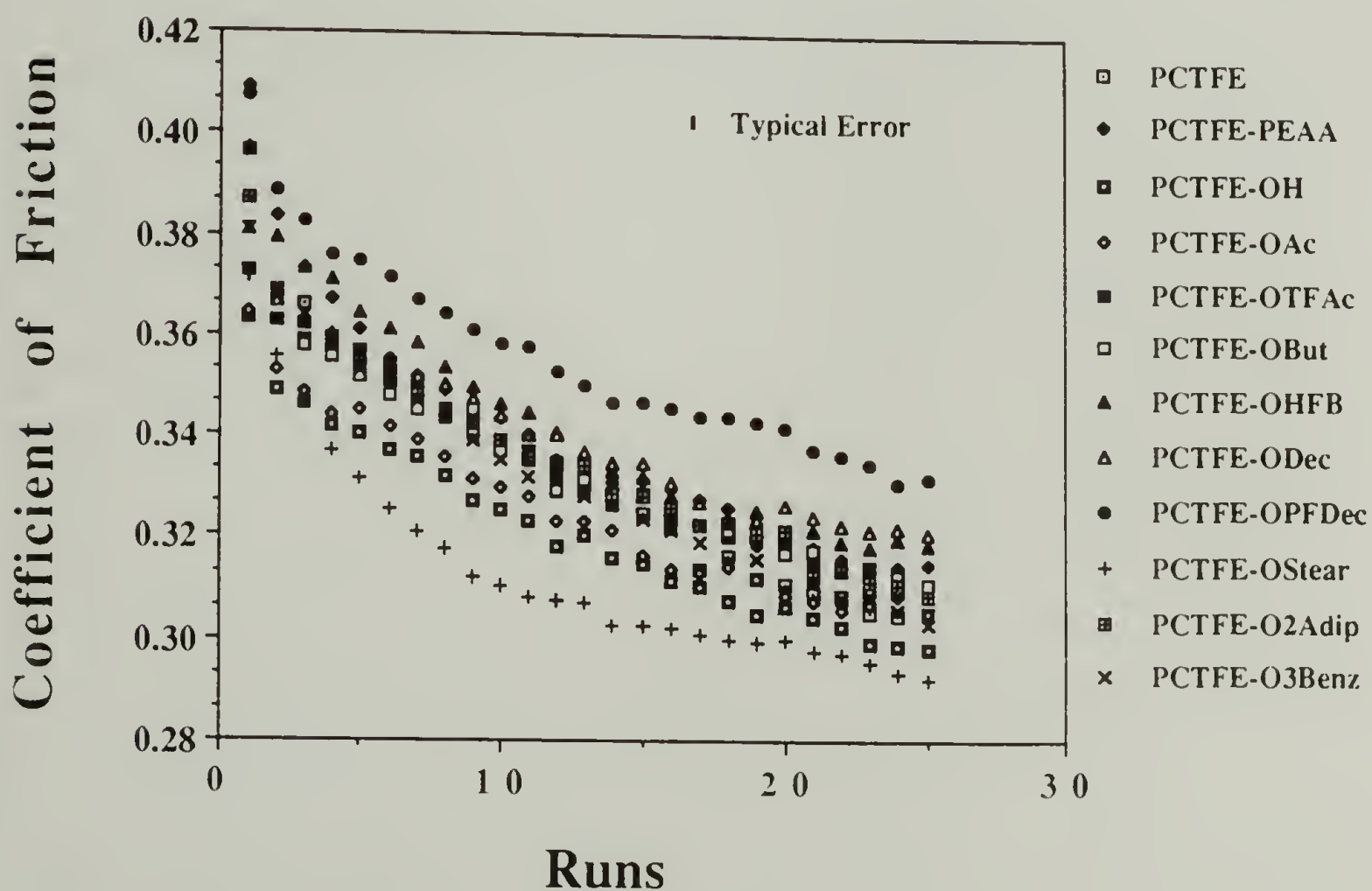


Figure 4.6. Coefficient of friction of modified polymer surfaces ( $-78 \text{ }^{\circ}\text{C}$  initial modification).



The friction results for these modified surfaces also show a decrease in the coefficient of friction with an increase in the number of sliding runs. The slope of this decrease and characterization of these surfaces after sliding show results similar to those presented above for the 100 run experiment with unmodified PCTFE. Thus, the observed decrease in friction is likely to be of similar origins. SEM micrographs show some grooves and ridges in both sliding surfaces, but again these features are small and difficult to find. Contact angle analysis yields results like those discussed earlier ---- an increase in the advancing contact angle on the PET countersurface perpendicular to the sliding direction (from  $77^\circ$  for virgin PET to  $83^\circ$  -  $87^\circ$  for the friction surfaces) and no changes in the contact angles measured parallel to the sliding direction on the countersurface nor on any of the modified surfaces in either direction. As before, XPS spectra of the PET countersurfaces do not show any evidence of transfer from the PCTFE based films. For the modified surfaces a slight increase is observed (1-2%, based on atomic composition) in the amount of chlorine, which is attributed to the unmodified PCTFE present beneath the modified layer. This change may be due to one of two factors. First, it is likely that a small amount of the modified layer is worn away during the sliding process decreasing the thickness of that layer. Also possible is the formation of a more compact layer on sliding. Calculations,<sup>47</sup> based on changes of the inelastic mean free path of electrons with changes in density coupled with a decrease in the modified layer thickness, indicate that relatively more chlorine would be seen if the modified layer were compressed.

It is observed in Figure 4.6 that there is only a small difference in  $\mu$  between these thinly modified surfaces despite contact angle analysis<sup>2</sup> showing that there are large differences in surface energy. For example, the water contact angles on the hydroxyl functionalized surface (PCTFE-OH) are 67/17°, while those on its acetate and stearate esters (PCTFE-OAc and PCTFE-OStear) are 82/46° and 108/90°, respectively. These results indicate that the work of adhesion, which is controlled by the surface energy of the two films, has little effect on the observed friction. It may therefore be concluded that it is the deformation properties of the surface region that determine the magnitude of the energy loss that results from sliding. Since these modified layers are so thin (~30 - 50 Å), the deformation properties of the PCTFE lying beneath the modified layer predominantly determine the area of contact and the interfacial shear strength. Therefore, it is expected that the friction would be essentially independent of the structure of the modified layer, as is observed.

Although Figure 4.6 does not show any substantial differences in friction between the various surfaces, subtle trends were observed. Figures 4.7a and b show that as the chain length of the hydrocarbon and fluorocarbon esters increases from 2 (PCTFE-OAc and PCTFE-OTFAc) to 4 (PCTFE-OBu and PCTFE-OHFB) to 10 carbons (PCTFE-ODec and PCTFE-OPFDec),  $\mu$  increases, except for the stearate ester (18 carbons) where a decrease in friction is observed. This behavior has also been observed in the friction of self-assembled monolayers (SAMs) on silicon wafers<sup>48</sup> and can be rationalized in terms of the deformation properties of the modified surface layers.

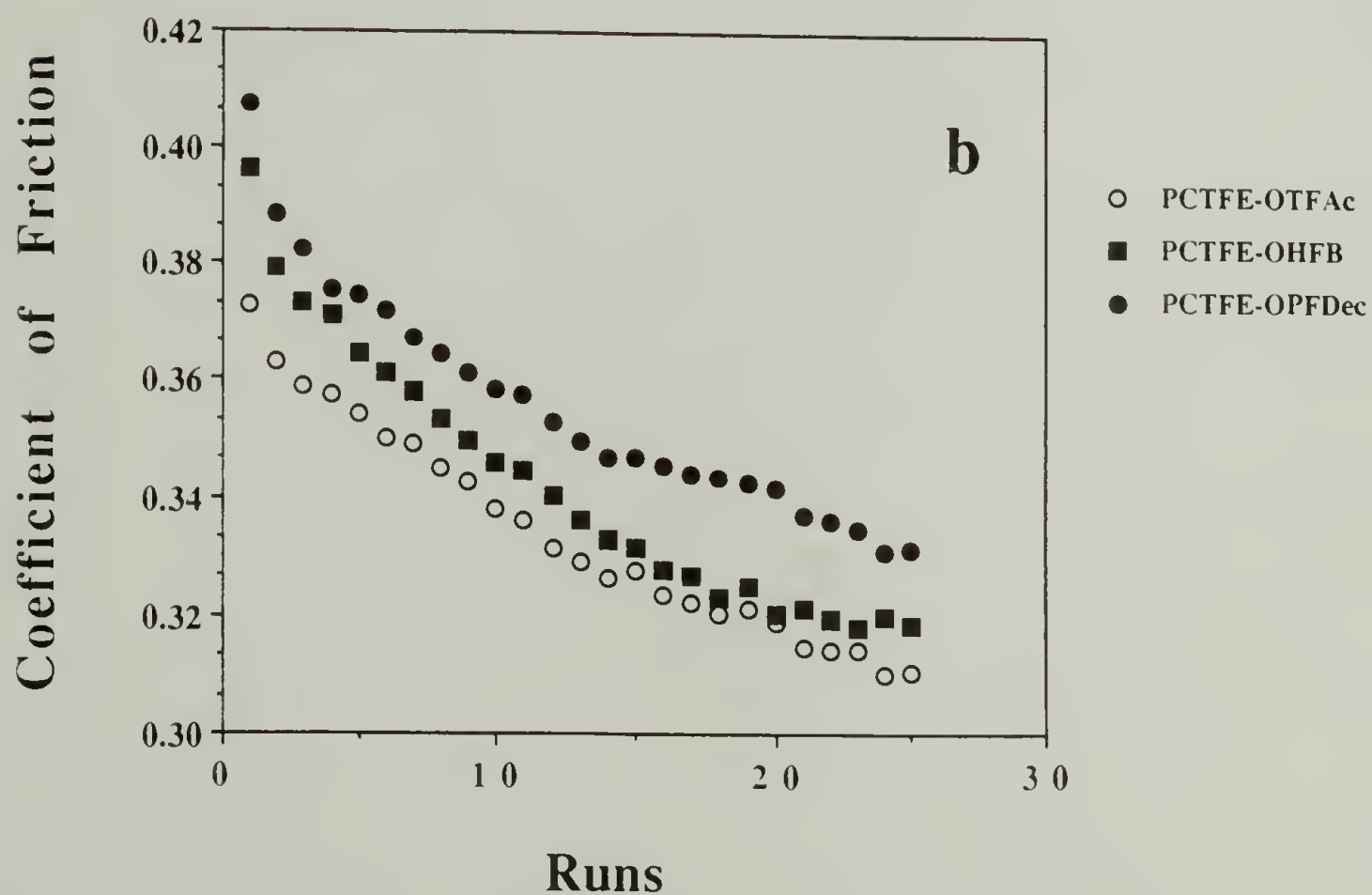
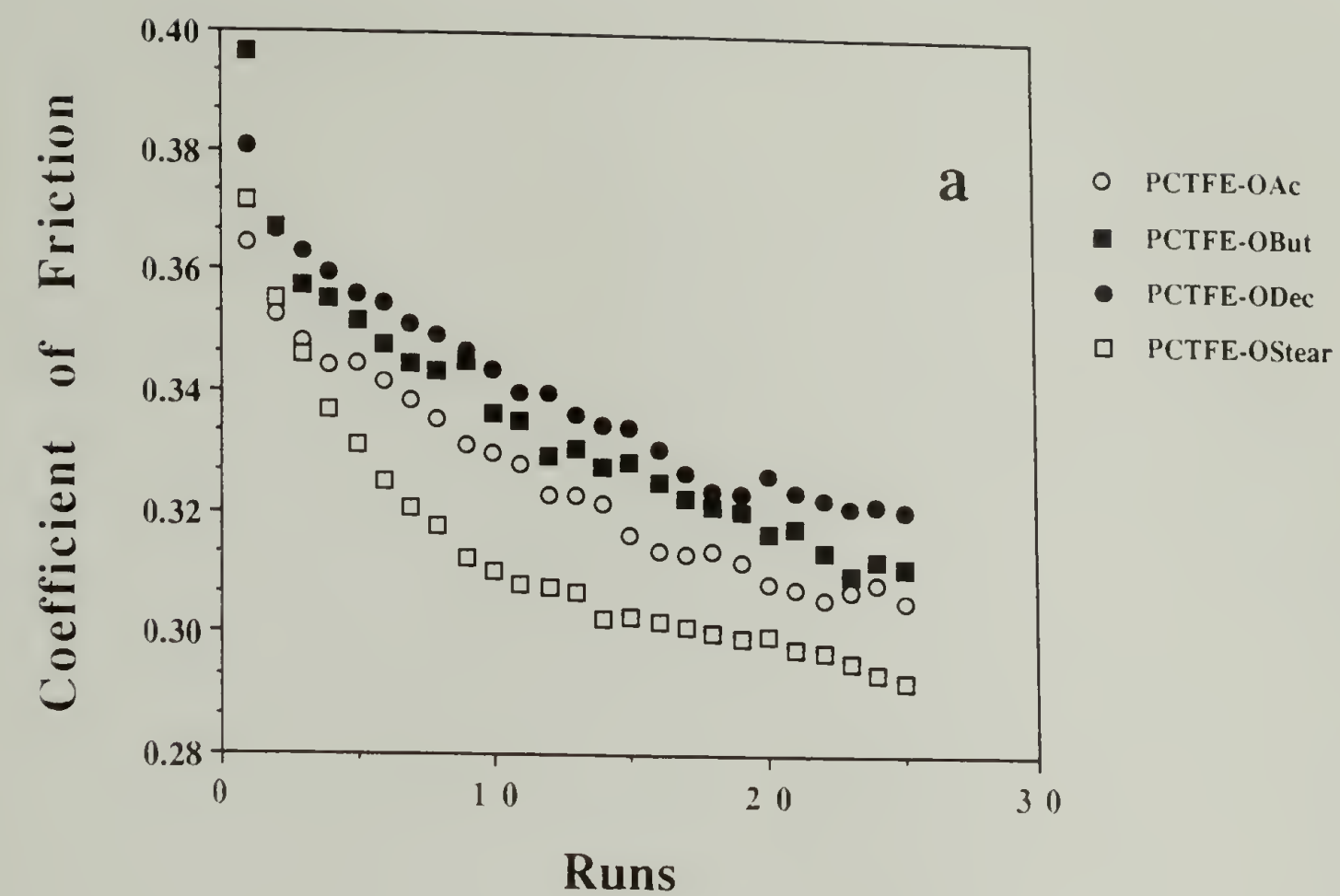


**Figure 4.7.** Coefficient of friction of: (a) hydrocarbon esters (-78 °C initial modification) and (b) fluorocarbon esters (-78 °C initial modification).



It is likely that introduction of the ester functionality into the surface causes plasticization of the polymer in the modified layer.

Lengthening the ester chain causes an increase in this plasticization, which increases the deformability of the surface, increasing the true contact area and hence, the frictional force. On the other hand, it was shown previously,<sup>2</sup> that the stearate surface is crystalline and, as such, would be expected to be reasonably rigid. This rigid surface would deform less under an applied load, resulting in a smaller contact area and a lower coefficient of friction, as is observed.

A comparison of the friction of the hydrocarbon and fluorocarbon esters is made in Figures 4.8a-c. In each case the friction for the fluorocarbon ester is greater than that of the corresponding hydrocarbon ester. The difference in  $\mu$  between the two types of surfaces also increases as the ester chain length is increased. These differences have also been observed in the friction of Langmuir-Blodgett monolayers<sup>49</sup> and SAMs<sup>48,50</sup> measured by conventional techniques and that measured on Langmuir-Blodgett monolayers using an atomic force microscope in the lateral mode.<sup>51</sup> These results are counterintuitive, as it might be expected that the lower energy perfluorinated surfaces would have the lower coefficient of friction. The reasons behind these observations are not well understood at this juncture. A consistent explanation is that upon sliding the ester chains stretch out and align themselves along the sliding direction. For this alignment to occur a number of bond rotations must take place. The energy necessary to rotate around a carbon-carbon bond is significantly larger for perfluorinated chains than hydrocarbon chains due to the greater steric hindrance of the

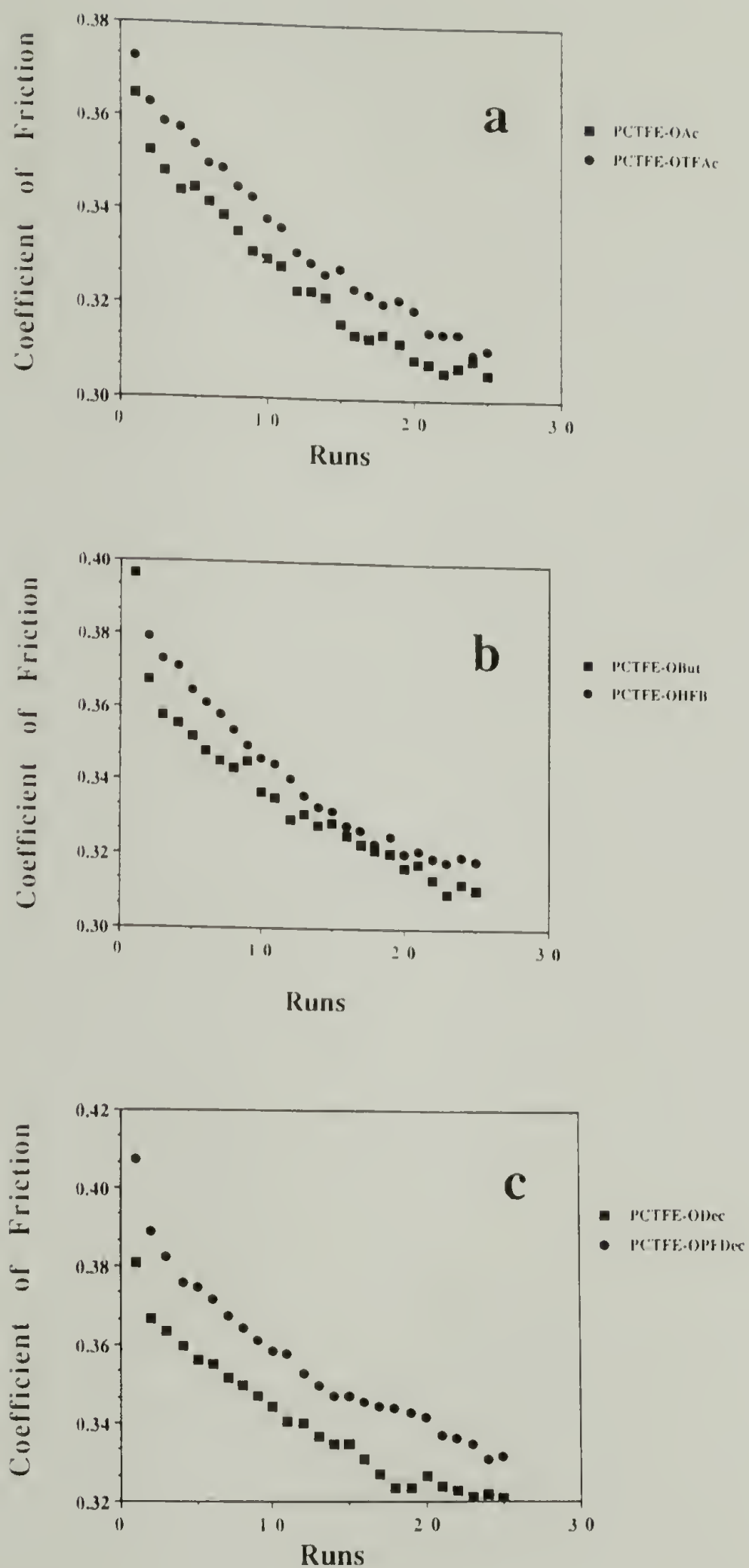


**Figure 4.8.** Coefficient of friction of: (a) hydro- and perfluoroacetate esters ( $-78^{\circ}\text{C}$  initial modification), (b) hydro- and perfluorobutyrate esters ( $-78^{\circ}\text{C}$  initial modification) and (c) hydro- and perfluorodecanoate esters ( $-78^{\circ}\text{C}$  initial modification).

fluorines. Thus, more energy would be required for sliding and a larger coefficient of friction would be the result.

Friction as a function of the modified layer thickness was first measured for the acetal surface (PCTFE-PEAA) that is formed in the initial modification (Scheme 4.1, page 169). The depth of the modification was controlled by the temperature of the reaction. Force versus sliding distance profiles for these measurements are shown in Figure 4.9. It can be seen that the thickness of the modified layer has a large effect on the friction behavior.

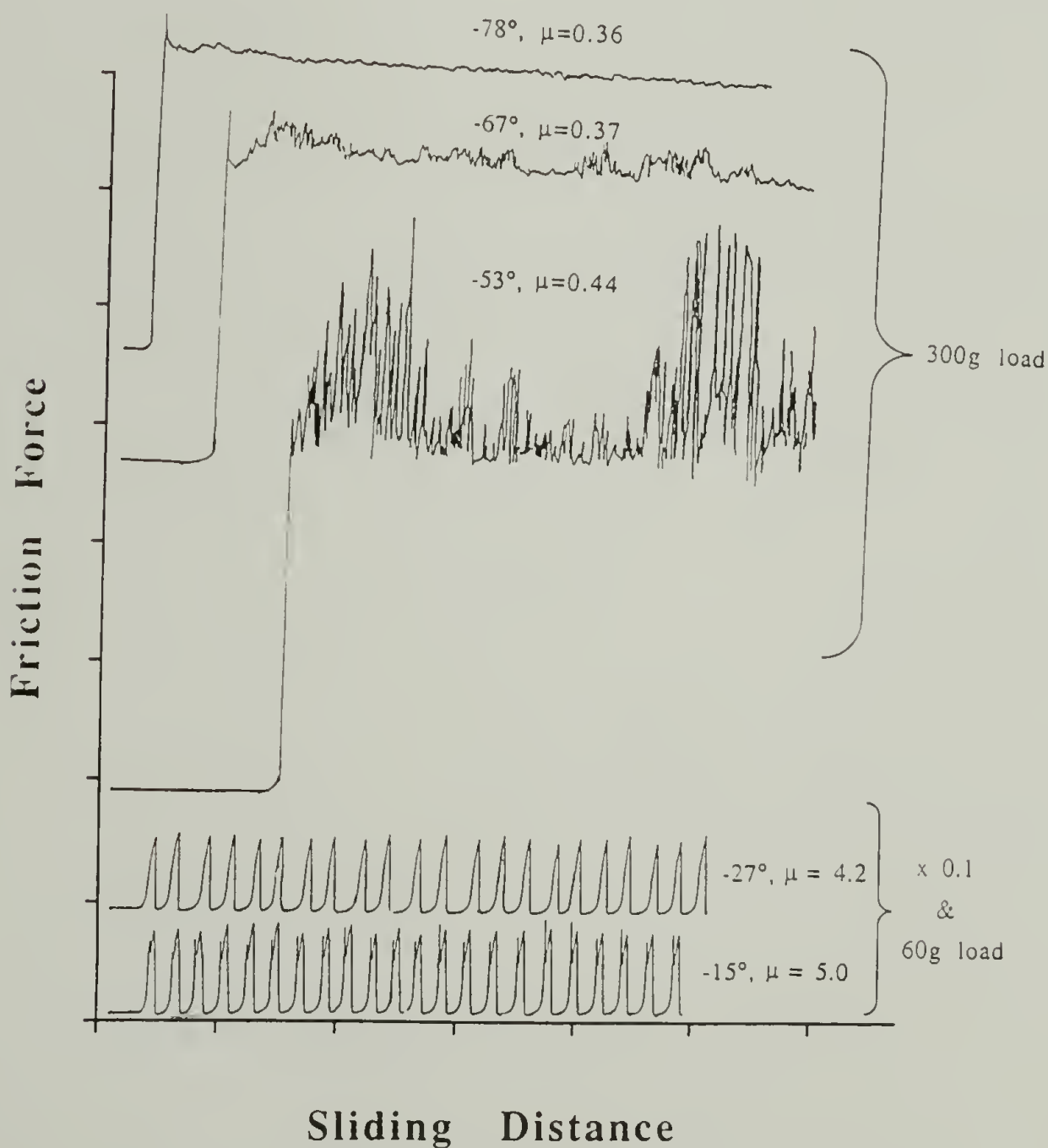


**Figure 4.9.** Raw friction data for PCTFE-PEAA as a function of modification temperature.



For the modification conducted at  $-78\text{ }^{\circ}\text{C}$  ( $\sim 50\text{ }\text{\AA}$ ), the film slides smoothly over the countersurface and yields a coefficient of friction of 0.36. When the modification temperature is increased to  $-67\text{ }^{\circ}\text{C}$  ( $\sim 140\text{ }\text{\AA}$ ), the sliding becomes rougher and  $\mu$  increases to 0.37. A  $\sim 240\text{ }\text{\AA}$  thick ( $-53\text{ }^{\circ}\text{C}$  reaction) modified surface only slides roughly across the PET and has a coefficient of friction of 0.44. For the two most deeply modified surfaces ( $\sim 1250\text{ }\text{\AA}$  and  $\sim 3950\text{ }\text{\AA}$ ,  $-27$  and  $-15\text{ }^{\circ}\text{C}$  modifications, respectively) the films would not slide at all under a 300 g load. The sled with the attached film remained stationary on the moving countersurface until enough tension built up in the cable to break the adhesive bonds formed at the interface. At this point the sled and weights jumped across the slider, spilling the weights and upsetting the sled. Thus, for the friction measurements made with these films, the load was decreased to 60 g (no attached weights). At this load, the films still did not slide across the countersurface and exhibited large-scale stick-slip behavior; however, the results were not nearly as catastrophic as for the higher load. Under these conditions only the static coefficient of friction,  $\mu_s$ , can be measured, yielding  $\mu_s = 4.2$  for the  $1250\text{ }\text{\AA}$  layer and  $\mu_s = 5.0$  for the  $3950\text{ }\text{\AA}$  thick modified surface. This increase in friction with modified layer thickness also can be explained in terms of an increase in the deformability of the surface of the polymer film. The introduction of the acetal moiety into the PCTFE surface likely increases the deformability of the film surface compared to that of the unmodified material, increasing the contact area and thus, the friction force. For the thinnest modified surface the deformation properties of the modified layer only play a small role and the

properties of the bulk PCTFE determine the friction, as discussed earlier. As the thickness of the modified layer increases, the deformation properties of this surface layer become more and more important in determining the frictional force.

For the  $-15\text{ }^{\circ}\text{C}$  acetal surface a number of qualitative friction experiments were conducted to see if this "sticking" behavior could be eliminated. Measurements were made under much higher loads (500 g) and at higher (1.5 cm/s) and lower (0.07 cm/s) sliding speeds. None of these changes decreased this type of adhesive behavior significantly.

Characterization of the three thinnest modified acetal surfaces ( $\sim 50$ , 140 and 240 Å) and their corresponding PET countersurfaces after sliding yielded results similar to those discussed earlier for the entire set of thinly modified surfaces. The two more deeply modified surfaces ( $\sim 1250$  and 3950 Å) yielded very different results. XPS spectra of the PCTFE-PEAA surfaces after sliding were identical to those recorded before sliding. However, the PET countersurfaces had a large amount (1.1% for the 1250 Å surface and 2.1% for the 3950 Å surface) of fluorine in the  $15^{\circ}$  takeoff angle spectra (Figure 4.10).

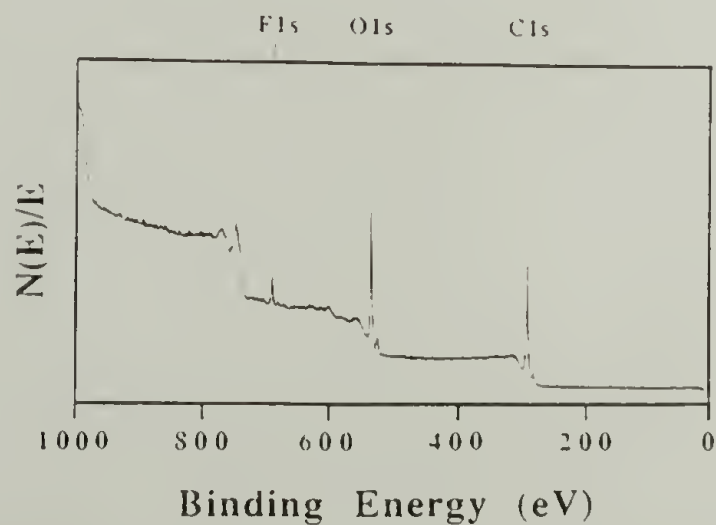


**Figure 4.10.** XPS survey spectrum ( $15^{\circ}$  takeoff angle) of PET after sliding against PCTFE-PEAA ( $-15\text{ }^{\circ}\text{C}$  modification).

This fluorine is evidence of a large amount of transfer from the PCTFE-PEAA to the PET indicating that the modified surfaces have failed cohesively. The contact angles on each of these latter two countersurfaces change after the friction measurement from  $77^{\circ}/48^{\circ}$  (virgin PET) to  $84-86^{\circ}/46-47^{\circ}$ , measured perpendicular to the sliding direction and  $84-85^{\circ}/46-48^{\circ}$  measured parallel to the sliding direction. On the corresponding PCTFE-PEAA surfaces, the parallel and perpendicular contact angles change to  $98-99^{\circ}/32-33^{\circ}$  and  $100-101^{\circ}/33-34^{\circ}$ , respectively, from the isotropic values of  $85^{\circ}/39^{\circ}$  ( $-27^{\circ}\text{C}$  modification) and  $88^{\circ}/37^{\circ}$  ( $-15^{\circ}\text{C}$  modification). These contact angle results show an increase in roughening of both sets of surfaces, both perpendicular and parallel to the sliding direction.

Figures 4.11 - 4.18 present the friction results for the more deeply modified ( $\sim 3000 - 13,000\text{ \AA}$ , based on a  $-15^{\circ}\text{C}$  initial modification<sup>2</sup>) alcohol, hydrocarbon and fluorocarbon esters and crosslinked surfaces. It is interesting to note that the deeply modified alcohol (PCTFE-OH, Figure 4.11) and crosslinked surfaces (PCTFE-O<sub>2</sub>Adip and PCTFE-O<sub>3</sub>Benz, Figures 4.12 and 4.13, respectively) all have coefficients of friction similar to their corresponding thinly modified surfaces ( $-78^{\circ}\text{C}$  initial modification). None of these three surfaces show any evidence of material transfer to the countersurface. These results strongly contrast those obtained for the acetal surface, where an increase in the modified layer thickness significantly increased the friction. The structure of each of these three surfaces makes them fairly stiff and non-deformable. As a result, an increase in the modification depth would not increase the area of contact and would have no effect on the friction.



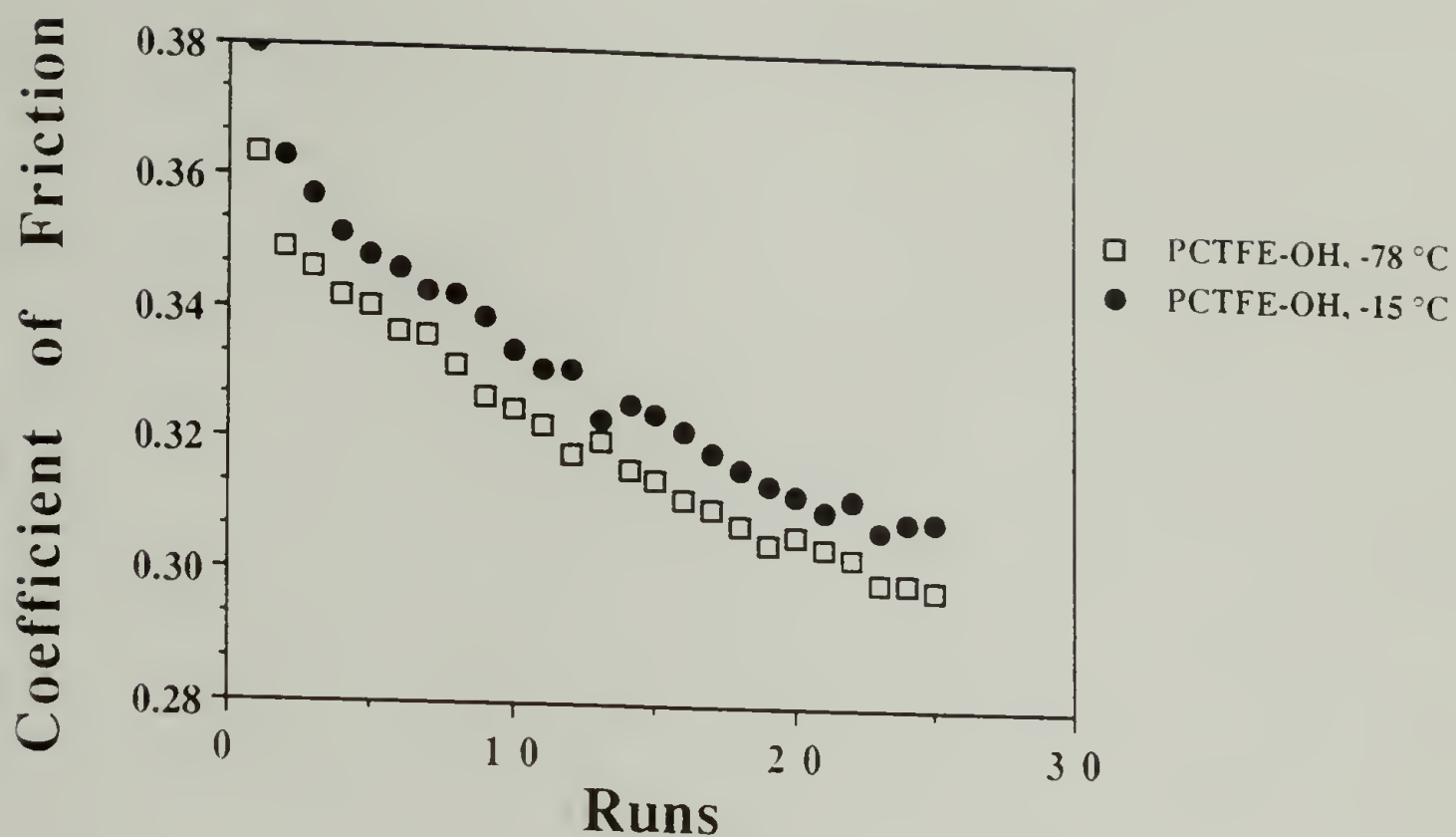


Figure 4.11. Coefficient of friction of PCTFE-OH as a function of the initial modification temperature.

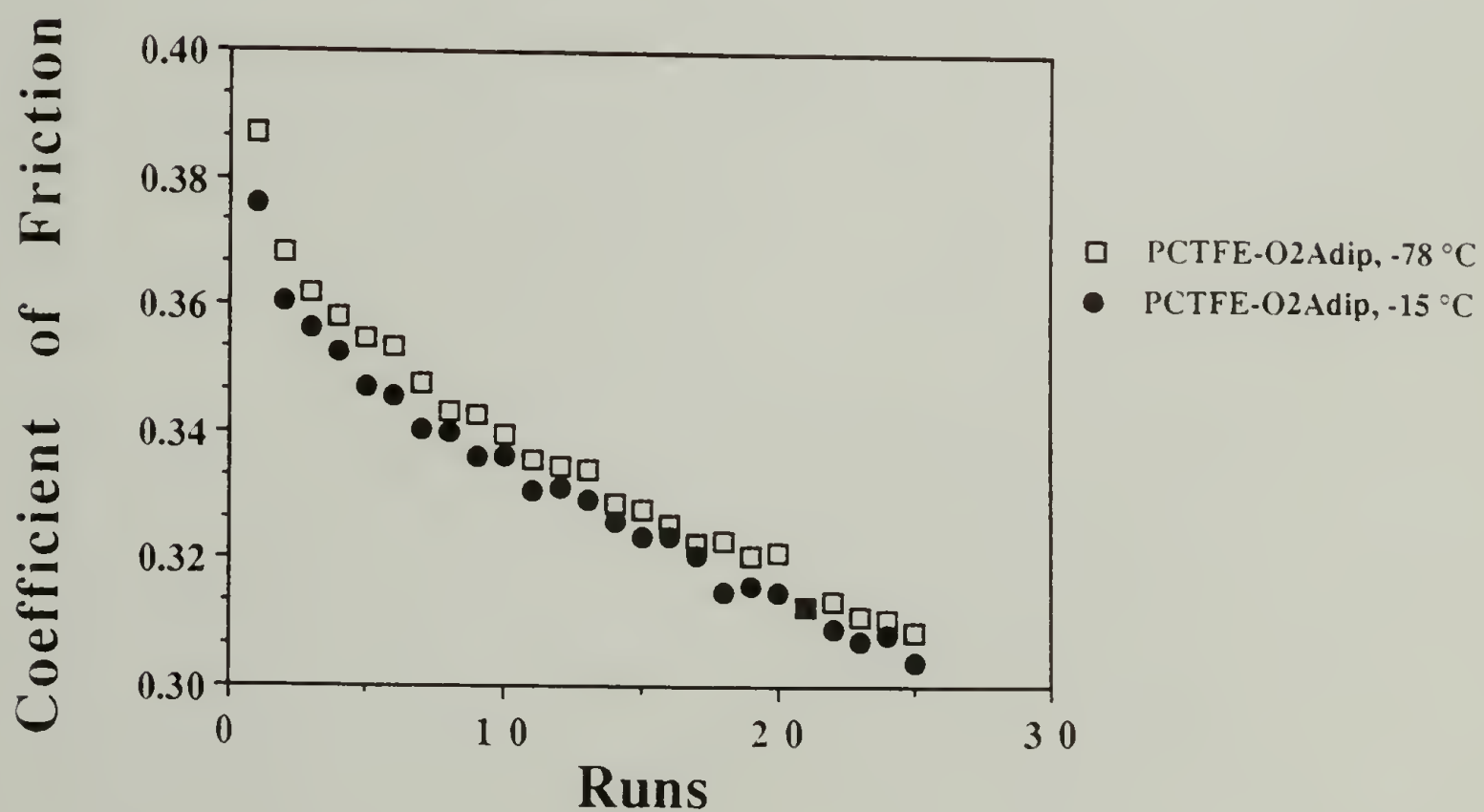


Figure 4.12. Coefficient of friction of PCTFE-O<sub>2</sub>Adip as a function of the initial modification temperature.

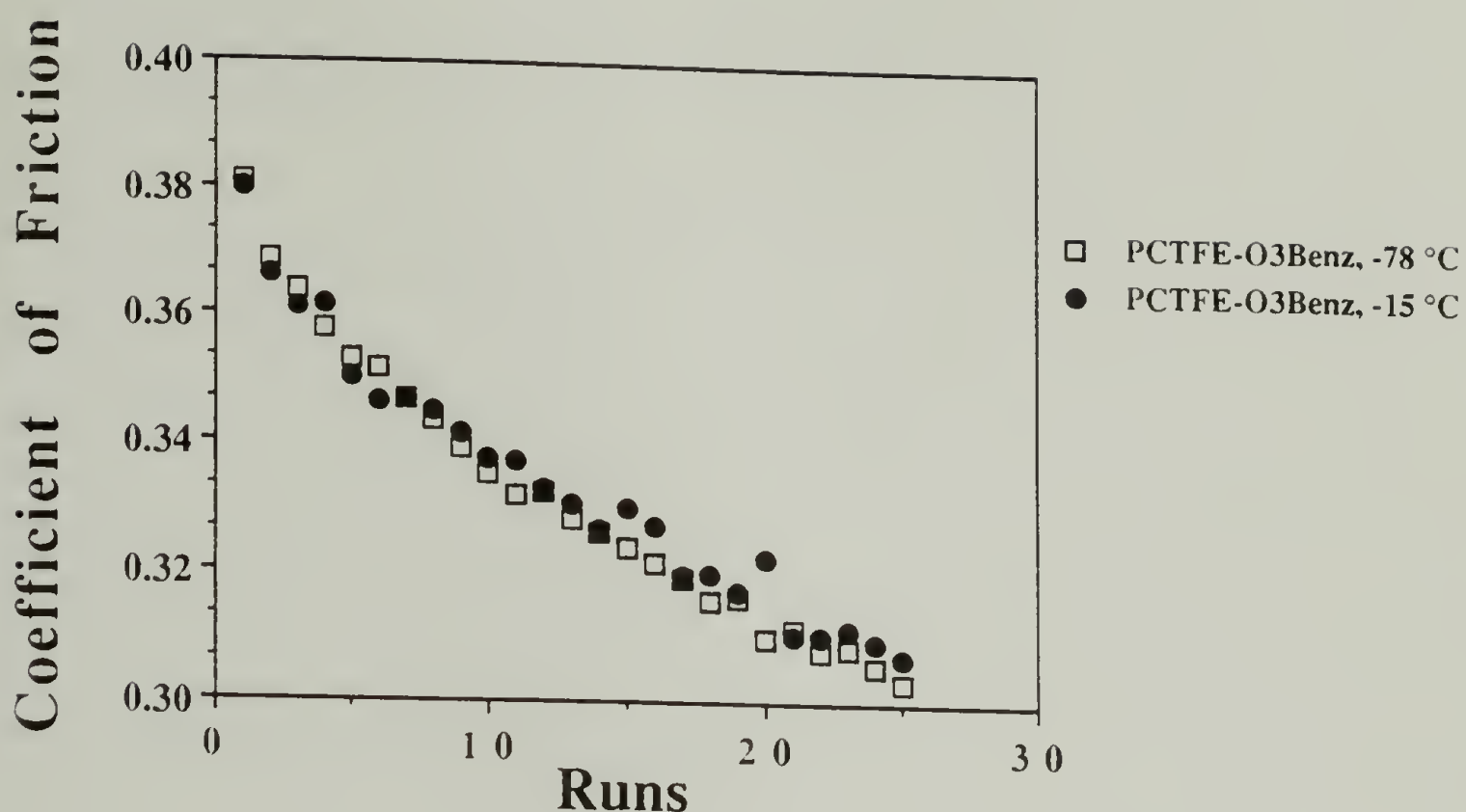


Figure 4.13. Coefficient of friction of PCTFE-O<sub>3</sub>Benz as a function of the initial modification temperature.

PCTFE-OH is likely a rigid surface due to extensive hydrogen bonding within the modified layer, while the highly crosslinked nature of the PCTFE-O<sub>2</sub>Adip and PCTFE-O<sub>3</sub>Benz surfaces explains their rigidity.

The friction of the stearate surface (Figure 4.14) is also relatively insensitive to changes in the thickness of the modified layer. The coefficient of friction of a thick (-15 °C initial modification) PCTFE-OSTear surface is higher than that of a thin (-78 °C initial modification) PCTFE-OSTear surface for the first sliding pass, but quickly decreases to a comparable value. Again, no evidence of transfer was observed. The similar values of the coefficient of friction for the thin and thick PCTFE-OSTear surfaces can also be explained in terms of the rigidity of the modified layer as

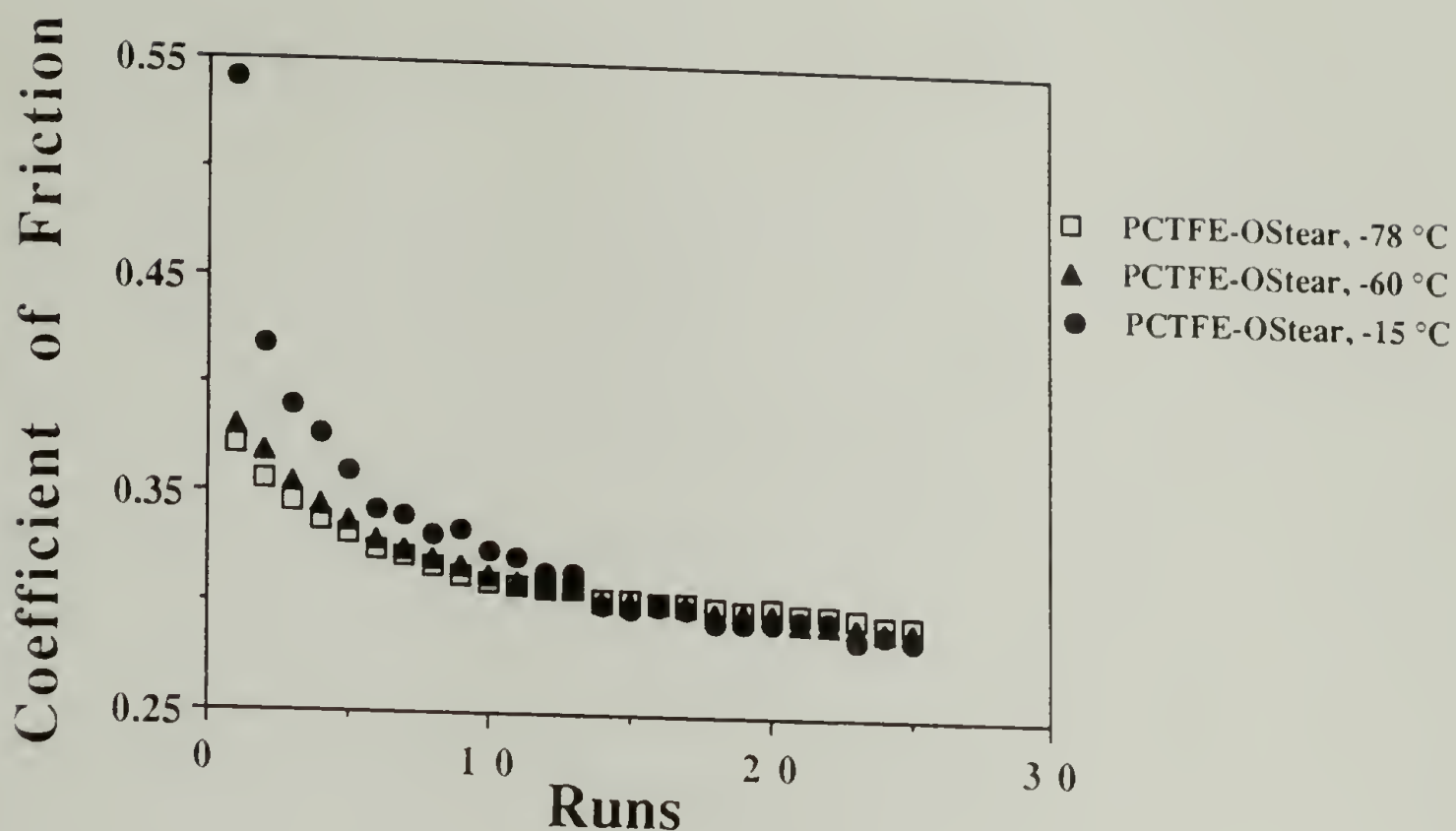


Figure 4.14. Coefficient of friction of PCTFE-OS tear as a function of the initial modification temperature.

a result of the crystallinity of this long-chain ester surface. Reasons for the initial difference in friction were not investigated, but may be related to the existence of large crystalline domains protruding from the thick PCTFE-OS tear surface.

The high deformability of the deeply modified butyrate (Figure 4.15) and heptafluorobutyrate (Figure 4.16) surfaces causes them to stick to the countersurface for the first run (like the thick acetal surface did for all runs) and then slide erratically on the countersurface with significantly higher coefficients of friction than the corresponding thinly modified surfaces. As with the deepest acetal surface, these two ester surfaces show evidence of transfer of the modified layer to the countersurface (~2 - 3% fluorine in the 15° takeoff angle XPS spectra of the PET countersurfaces).



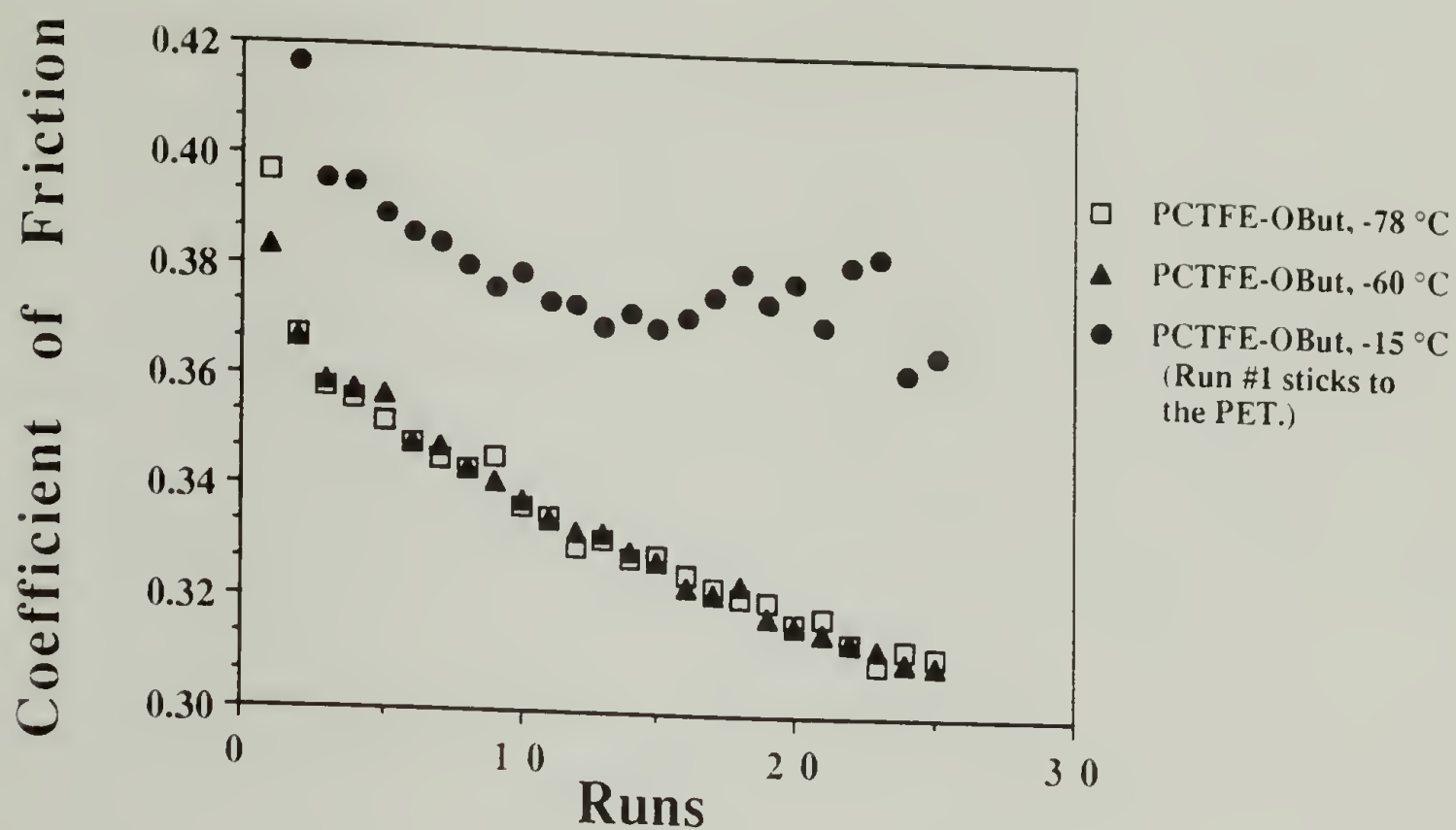


Figure 4.15. Coefficient of friction of PCTFE-OBuT as a function of the initial modification temperature.

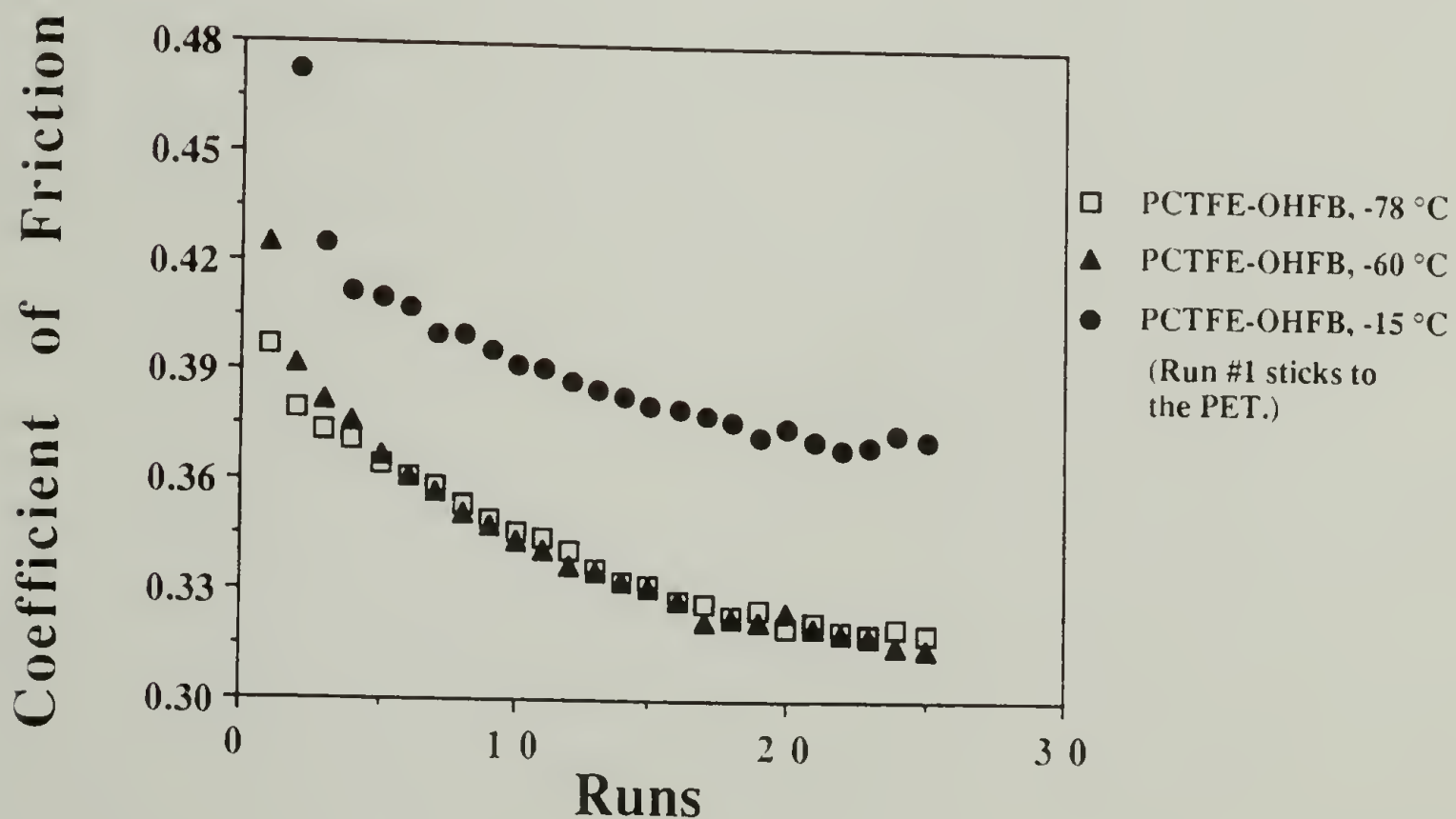


Figure 4.16. Coefficient of friction of PCTFE-OHFB as a function of the initial modification temperature.

The deeply modified decanoate (Figure 4.17) and perfluorodecanoate (Figure 4.18) surfaces stick to the countersurface for all runs, with the perfluorodecanoate surface being the tackier of the two. Both of these latter two surfaces show a large amount of transfer of the modified layer to the countersurface (Figure 4.19, page 186). Again, an increase in the deformability of these two surfaces upon introduction of the relatively short chain ester groups accounts for the high friction.

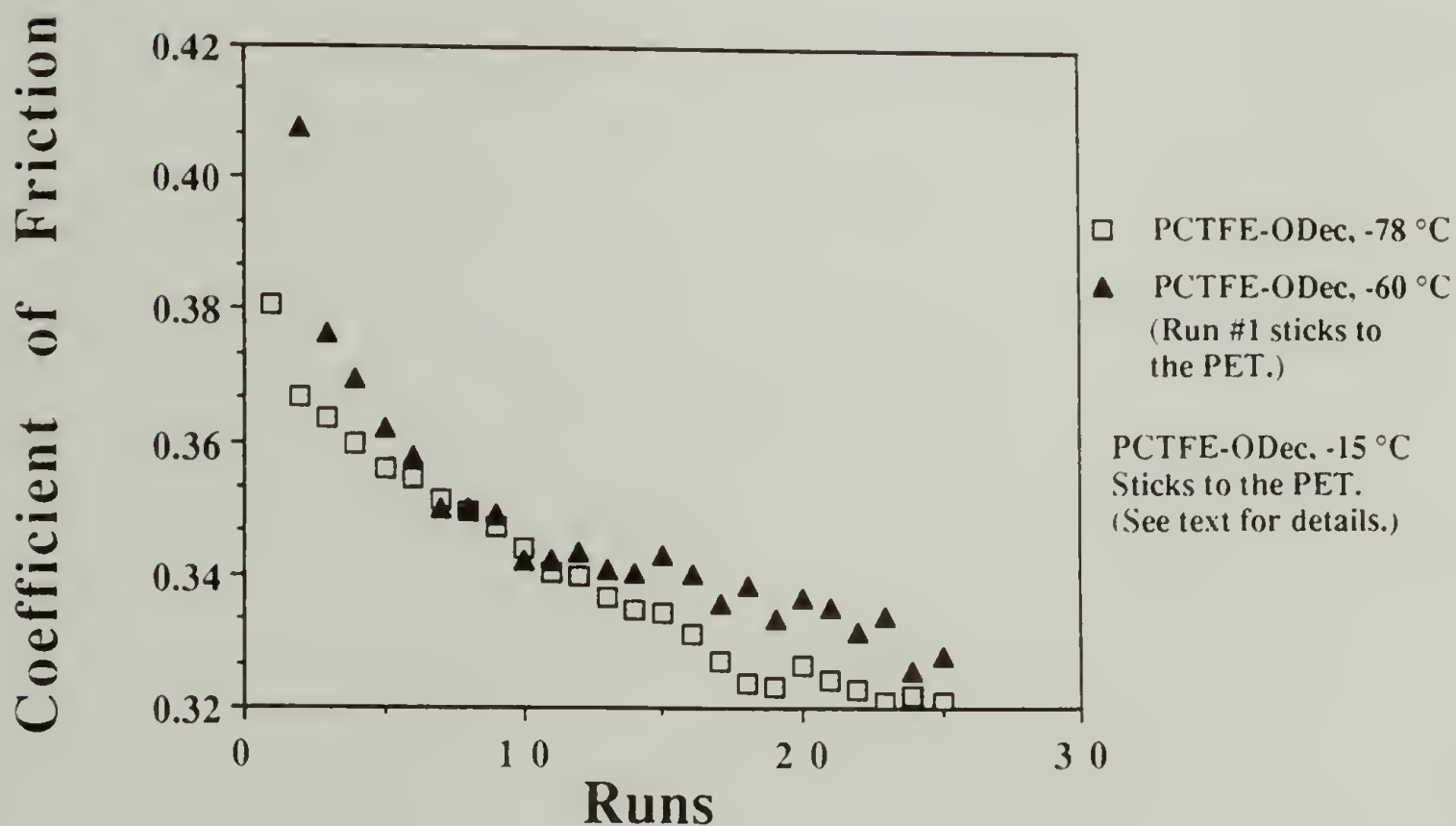


Figure 4.17. Coefficient of friction of PCTFE-ODec as a function of initial the modification temperature.

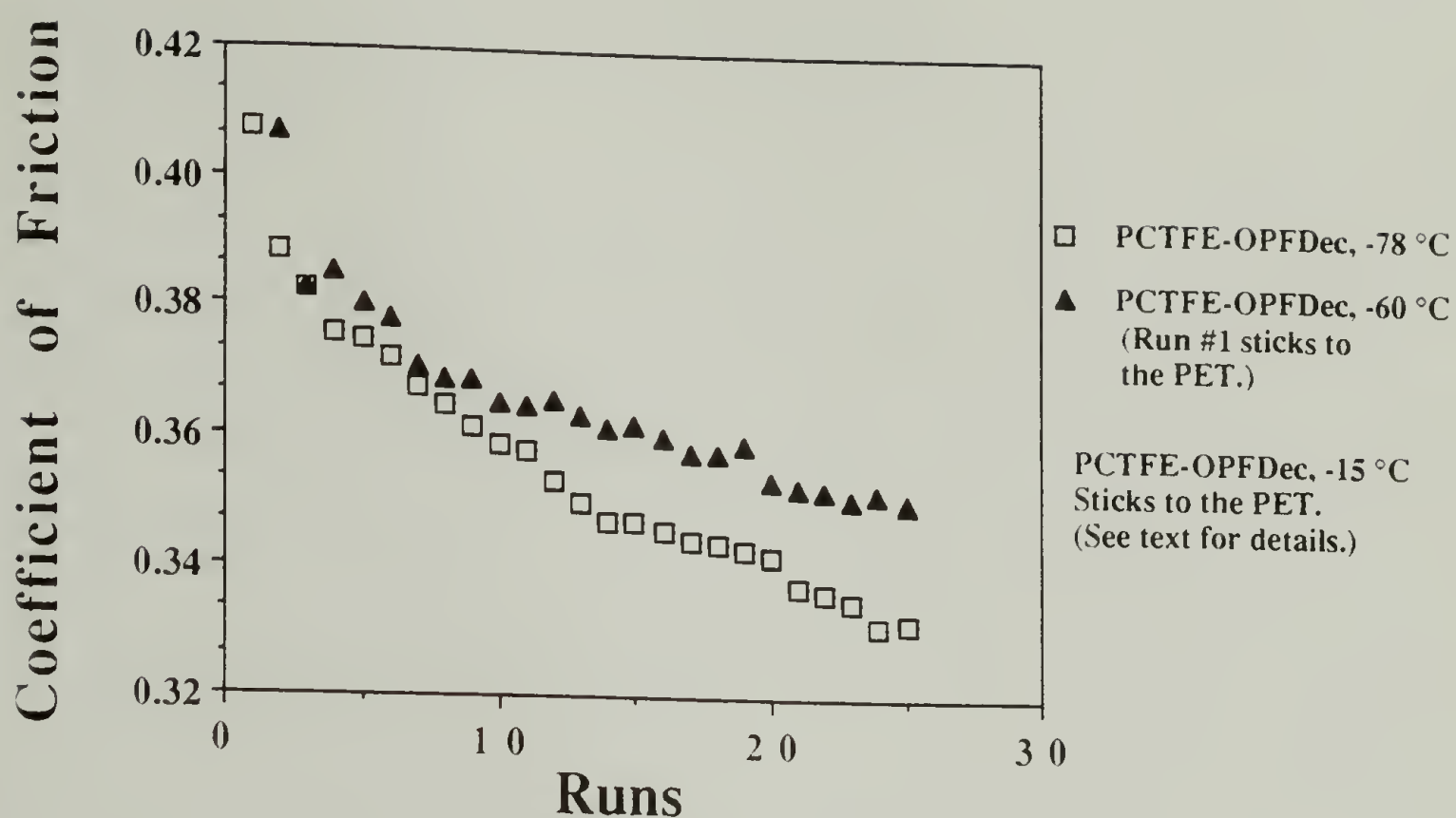
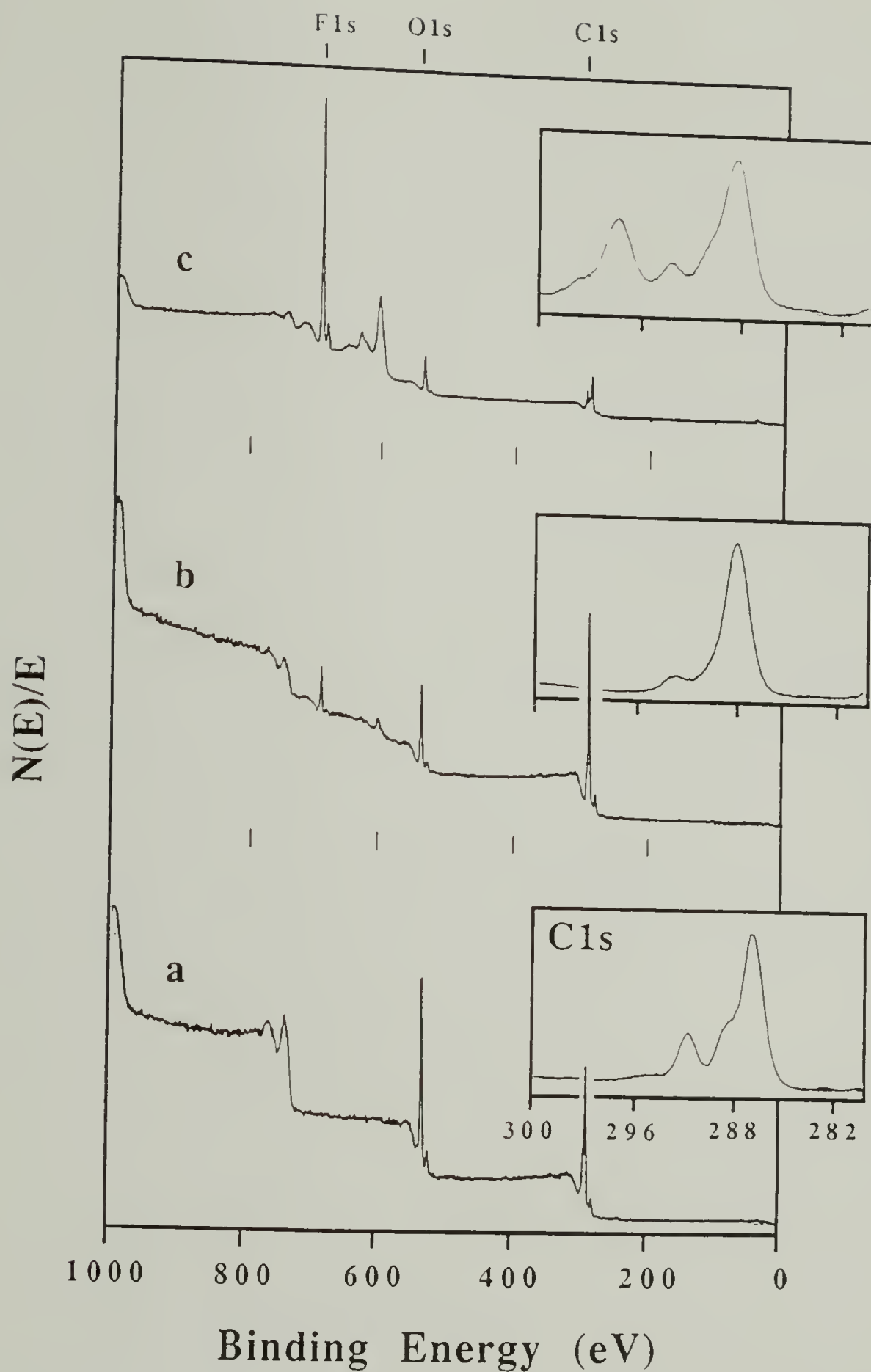


Figure 4.18. Coefficient of friction of PCTFE-OPFDec as a function of the initial modification temperature.

As expected, friction measurements made on modified surfaces with intermediate thicknesses ( $\sim 400 - 1000 \text{ \AA}$ , based on a  $-60 \text{ }^{\circ}\text{C}$  initial modification<sup>2</sup>) show intermediate results (also in Figures 4.14 - 4.18). The friction of the intermediate thickness, rigid PCTFE-OSTear surface (Figure 4.14) is comparable to that of the thin and thick modified surfaces ( $-78$  and  $-15 \text{ }^{\circ}\text{C}$  initial modifications, respectively), while the magnitudes of the coefficients of friction for the corresponding deformable surfaces (PCTFE-OBut, PCTFE-OHFB, PCTFE-ODec and PCTFE-OPFDec, Figures 4.15 - 4.18, respectively) lie between those of the thin and thick modified surface.





**Figure 4.19.** XPS survey and C1s spectra ( $15^\circ$  takeoff angle) of PET countersurface after sliding against: (a) PCTFE-OH ( $-15^\circ\text{C}$  initial modification) (b) PCTFE-ODec ( $-15^\circ\text{C}$  initial modification) and (c) PCTFE-OPFDec ( $-15^\circ\text{C}$  initial modification).

The effects of changes in sliding speed and normal load were measured on PCTFE and the thinly modified PCTFE-PEAA, PCTFE-OH, PCTFE-OBu<sub>t</sub>, PCTFE-OHFB, PCTFE-ODec and PCTFE-OSTear surfaces. A single set of measurements was made for each of the different samples under the following conditions: (1) 60 g load sliding at 0.025 and 0.10 cm/s (5 runs of each) and (2) 300 g load sliding at 0.025 (5 runs) and 1.0 cm/s (10 runs). The results are shown qualitatively in Table 4.1. As expected, a decrease in the normal load increased the coefficient of friction for all of the surfaces tested indicating that measurements were made under conditions where elastic deformations predominate. The effect of changes in the sliding speed was small or non-existent for these surfaces over the limited range studied. Thus, no conclusions can be drawn from these experiments.

**Table 4.1.** Qualitative changes in coefficient of friction,  $\mu$ , with changes in normal load and sliding speed.

<u>Surface</u>	<u>Changes in <math>\mu</math> with:</u>	
	<u>Decrease in Normal Load</u>	<u>Increase in Sliding Speed</u>
PCTFE	Increases	Slight Decrease
PCTFE-PEAA	Increases	Slight Decrease
PCTFE-OH	Increases	Increases
PCTFE-OBu <sub>t</sub>	Increases	Decreases
PCTFE-OHFB	Increases	No change
PCTFE-ODec	Increases	No change
PCTFE-OSTear	Increases	Increases

## Conclusions and Future Work Suggestions

The results of the friction studies conducted on a variety of modified PCTFE surfaces show a number of interesting features. It was observed that varying the surface energy without drastically changing the deformation behavior at the surface has little effect on friction. From these results it may be concluded that it is the deformation behavior of the surface region that determines the observed friction. It was found that the coefficient of friction could be decreased by making the surface more rigid. This was done by introducing a high concentration of hydrogen-bonding functionality into the surface, forming a densely crosslinked surface or incorporating functional groups into the surface that cause it to crystallize. Also, the coefficient of friction of a material can be increased by making the surface more deformable. This may be done by introducing functionality into the surface that plasticizes the modified layer. In this case, the depth of the modification has a large impact on friction.

It was also observed that the coefficient of friction on perfluorinated ester surfaces was higher than that measured on hydrocarbon ester surface, in contrast to the results expected from surface energy considerations. Similar behavior has been observed previously<sup>48-51</sup> and it is postulated here that the restricted carbon-carbon bond rotations present in the perfluorinated groups is the underlying cause of these observations.

There are a number of avenues which could be explored in future studies. First, friction studies of the acid and ester



functionalized surfaces presented in Chapter II of this dissertation would provide complementary results to those presented here. Next, it would be intriguing to examine the friction of the modified surfaces discussed in this chapter over a wide range of ambient temperatures (warmer for the rigid surfaces and colder for the deformable surfaces) to see if a surface-structure dependent transition from a rigid to a deformable modified layer exists. Once this temperature was identified, studies of the effects of sliding speed around this temperature could be conducted. Along the same lines, it may prove interesting to develop surface modifications that incorporate liquid crystalline moieties into the surface and study their friction behavior as a function of temperature and sliding speed. Finally, it would be desirable to be able to vary the surface functionality of the PET countersurface (or any countersurface used), so as to incorporate specific interactions (i.e. acid-base interactions) at the sliding interface and monitor the resulting friction.

### References and Notes

- (1) See Chapter I of this dissertation.
- (2) See Chapter III of this dissertation.
- (3) Amontons, G. *Memoires de l'Academie Royale*, **1699**, 206.
- (4) Coulomb, C.A. *Theories des Machines Simples*, 1785 (Memoire de Mathematique et de Physique de l'Academie Royale, Paris).
- (5) Bowden, F.P. and Tabor, D. "The Friction and Lubrication of Solids", Oxford, 1964.

- (6) Briscoe, B.J. In "Physiochemical Aspects of Polymer Surfaces, vol. 1", Plenum: New York, 1983.
- (7) Shooter, K.V. and Tabor, D. *Proc. Phys Soc.*, **1952**, B65, 661.
- (8) Pooley, C.M. and Tabor, D. *Proc Roy. Soc. Lond. A.*, **1972**, 329, 251.
- (9) Lancaster, J.K. In "Polymer Science, vol. 2", Elsevier: New York, 1972.
- (10) Tabor, D. *Surface and Colloid Science*, **1972**, 5, 245.
- (11) Lancaster, J.K. *Plastics and Polymers*, **1973**, 41, 297.
- (12) Bikerman, J.J. *J. Macromol. Sci.-Revs. Macromol. Chem.*, **1974**, C11, 1.
- (13) (a) Tabor, D. In "Advances in Polymer Friction and Wear"; *Polymer Science and Technology*, vol. 5A, 1974, 5. (b) Savdoor, A.R. In "Advances in Polymer Friction and Wear"; *Polymer Science and Technology*, vol. 5A, 1974, 69. (c) Tabor, D. In "Advances in Polymer Friction and Wear"; *Polymer Science and Technology*, vol. 5A, 1974, 149.
- (14) Briscoe, B.J. and Tabor, D. In "Polymer Surfaces", Wiley-Interscience: New York, 1978, 1.
- (15) Briscoe, B.J. and Tabor, D. *Br. Polymer J.*, **1978**, 10(1), 74.
- (16) Cherry, B.W. "Polymer Surfaces", Cambridge Univ. Press, 1981.
- (17) Briscoe, B.J. *Adhesion*, **1981**, 5, 49.
- (18) Briscoe, B.J. *Philosophical Magazine A*, **1981**, 43, 511.
- (19) Tewari, U.S. and Sharma, S.K. *J. Macromol. Sci.-Revs. Macromol. Chem.*, **1989**, C29, 1.
- (20) Briggs, D.; Rance, D.G. and Briscoe, B.J. In "Comprehensive Polymer Science, vol. 2", Pergamon Press: New York, 1989.

- (21) Yamaguchi, Y. "Tribology of Plastic Materials", Elsevier: New York, 1990.
- (22) Greenwood, J.A. and Tabor, D. *Proc. Phys. Soc.*, **1958**, 989.
- (23) Greenwood, J.A.; Minshall, H. and Tabor, D. *Proc. Roy. Soc. Lond. A*, **1958**, 245, 539.
- (24) Ludema, K.C. and Tabor, D. *Wear*, **1966**, 9, 329.
- (25) Erhard, G. *Wear*, **1983**, 84, 167.
- (26) Lincoln, B. *Br. J. Appl. Phys.*, **1952**, 3, 260.
- (27) Baily, A.I. and Courtney-Pratt, J.S. *Proc. Roy. Soc. Lond. A*, **1955**, 227, 500.
- (28) Dyson, J. and Hirst, W. *Proc. Roy. Soc. Lond. B*, **1954**, 67, 309.
- (29) Kendall, K. and Tabor, D. *Proc. Roy. Soc. Lond. A*, **1971**, 323, 321.
- (30) Briscoe, B.J.; Scruton, B. and Willis, F.R. *Proc. Roy. Soc. Lond. A*, **1973**, 333, 99.
- (31) Kraghelsky, I.V. and Sabelnikov, V.P. *Proc. Inst. Mech. Engrs. Conference on Lubrication and Wear*, 1957, 247.
- (32) Briscoe, B.J. and Tabor, D. *A.S.L.E. Trans.*, **1974**, 17, 158.
- (33) Adams, N. *J. Appl. Polymer Sci.*, **1963**, 7, 2075.
- (34) Amuzu, J.K.A.; Briscoe, B.J. and Tabor, D. *Preprint No. 76-AM-IA-3*, 31st Annual Meeting A.S.L.E., 1976.
- (35) McClaren, K.G. and Tabor, D. *Nature*, **1963**, 197, 856.
- (36) Grosch, K.A. *Nature*, **1963**, 197, 858.
- (37) Grosch, K.A. *Proc. Roy. Soc. Lond. A*, **1963**, 274, 21.
- (38) King, R.F. and Tabor, D. *Proc. Roy. Soc. Lond. B*, **1953**, 66, 728.



- (39) Bartenev, G.M. and Elkin, A.I. *J. Polym. Sci. C*, **1967**, *16*, 1673.
- (40) Annual Book of ASTM Standards, **1986**, 8.02, D1894-78, 177.
- (41) A number of different countersurfaces (PET, PVF<sub>2</sub>, PCTFE, PTFE and glass), loads (75 g, 150 g and 300 g) and sliding speeds (0.10 cm/s, 0.25 cm/s, 0.50 cm/s and 1.0 cm/s) were tested with unmodified PCTFE as a slider. The most highly reproducible results were for the conditions shown.
- (42) For a takeoff angle of 75° 64.5% of the signal observed comes from a depth,  $t = \lambda$  while 95.5% comes from  $t = 3\lambda$  and at 15° 64.5% comes from  $t=0.27\lambda$  and 95.5% from  $t = 0.80\lambda$ . Where  $\lambda$  is the photoelectron's mean free path. (For Cls photoelectrons  $\lambda = 14 \text{ \AA}$ .<sup>43</sup>)
- (43) This value was measured in poly(*p*-xylylene): Clark, D.T. and Thomas, H.R. *J. Polym. Sci. Polym. Chem. Ed.* **1977**, *15*, 2843.
- (44) Bensnoin, J.-M. and Choi, K.Y. *J. Macromol Sci.-Rev. Macromol. Chem and Phys.*, **1989**, *C29(1)*, 55.
- (45) See Chapter I of this dissertation and references therein for a discussion of the effects of roughness on contact angles.
- (46) Sung, N.H.; Lee, H.Y.; Yuan, P. and Sung, C.S.P. *Polymer Engineering and Science*, **1989**, *29*, 791.
- (47) See Chapter I of this dissertation and references therein for discussions of the dependence of the mean free path on density and how changing the modified layer thickness affects the amount of virgin material observed.
- (48) DePalma, V. and Tillman, N. *Langmuir*, **1989**, *5*, 868.
- (49) Briscoe, B.J. and Evans, D.C.B. *Proc. Roy. Soc. Lond. A*, **1982**, *380*, 389.
- (50) Levine, O. and Zisman, Z.A. *J. Phys. Chem.*, **1957**, *61*, 1068.

- (51) Overney, R.M.; Meyer, E.; Frommer, J.; Brodbeck, D.; Luthi, R.; Howald, L.; Guntherodt, H.-J.; Fujihira, M.; Takano, H. and Gotoh, Y. *Nature*, **1992**, 359, 133.

## CHAPTER V

# PREPARATION AND WETTING BEHAVIOR OF HETEROGENEOUS SURFACES

### Introduction

The vast majority of research programs studying surface structure-property relationships utilize either modified surfaces which are chemically homogeneous or those which contain a variety of functional groups in uncontrolled identities and proportions. The former studies, however, do not consider that real surfaces are usually heterogeneous in nature and that their behavior will often reflect this fact. The latter studies typically yield inconclusive results due to a lack of understanding of the true surface structure. Obviously, it would be advantageous to prepare heterogeneous surfaces of known composition in a controlled manner. Specifically, one would like to be able to dictate the types of functional groups in a surface and their relative amounts.

Recently, the wettability of controlled, heterogeneous surface structures has been studied using self-assembled monolayers of long-chain thiols on gold.<sup>1-5</sup> In cases where dispersion forces are the principal intermolecular interaction, the results appear to uphold Cassie's law,<sup>6</sup> which states that if the components of a surface act independently, then the cosine of the contact angle that a liquid drop makes when resting on a solid surface is a linear function of the



composition of that surface. In situations where specific polar interactions (hydrogen bonding, for example) predominate, strong deviations from linearity are observed. It appears that the wettability of isolated hydroxyl and carboxylic acid groups is greater than that of those in a surface containing a dense population of polar functionality. This difference may arise from intramolecular hydrogen bonding within surfaces rich in these polar functional groups.

In the research presented here, kinetic control of both the esterification of PCTFE-OH with a number of acid chlorides and the hydrolysis/methanolysis of esters of PCTFE-OH (PCTFE-Esters) have been utilized to prepare chemically heterogeneous surfaces of known composition. In general, mixed surfaces were prepared via two procedures (Figure 5.1, where R<sub>1</sub> and R<sub>2</sub> are the acid chlorides of interest): (Method 1) partial esterification with R<sub>1</sub>, followed by complete conversion of the residual hydroxyl groups with R<sub>2</sub> and (Method 2) complete esterification of PCTFE-OH with R<sub>1</sub> followed by partial ester hydrolysis and then re-esterification to complete conversion with R<sub>2</sub>. Some experiments have also been performed in which competitive reactions of R<sub>1</sub> and R<sub>2</sub> with PCTFE-OH were investigated. The wetting behavior of these mixed hydroxyl/ester and ester/ester surfaces was then studied as a function of the surface composition using water and hexadecane (also methylene iodide to a lesser extent) as probe fluids.

The objectives of this research are to: 1) controllably prepare heterogeneous surfaces of known composition via different synthetic routes and 2) determine if compositionally similar surfaces

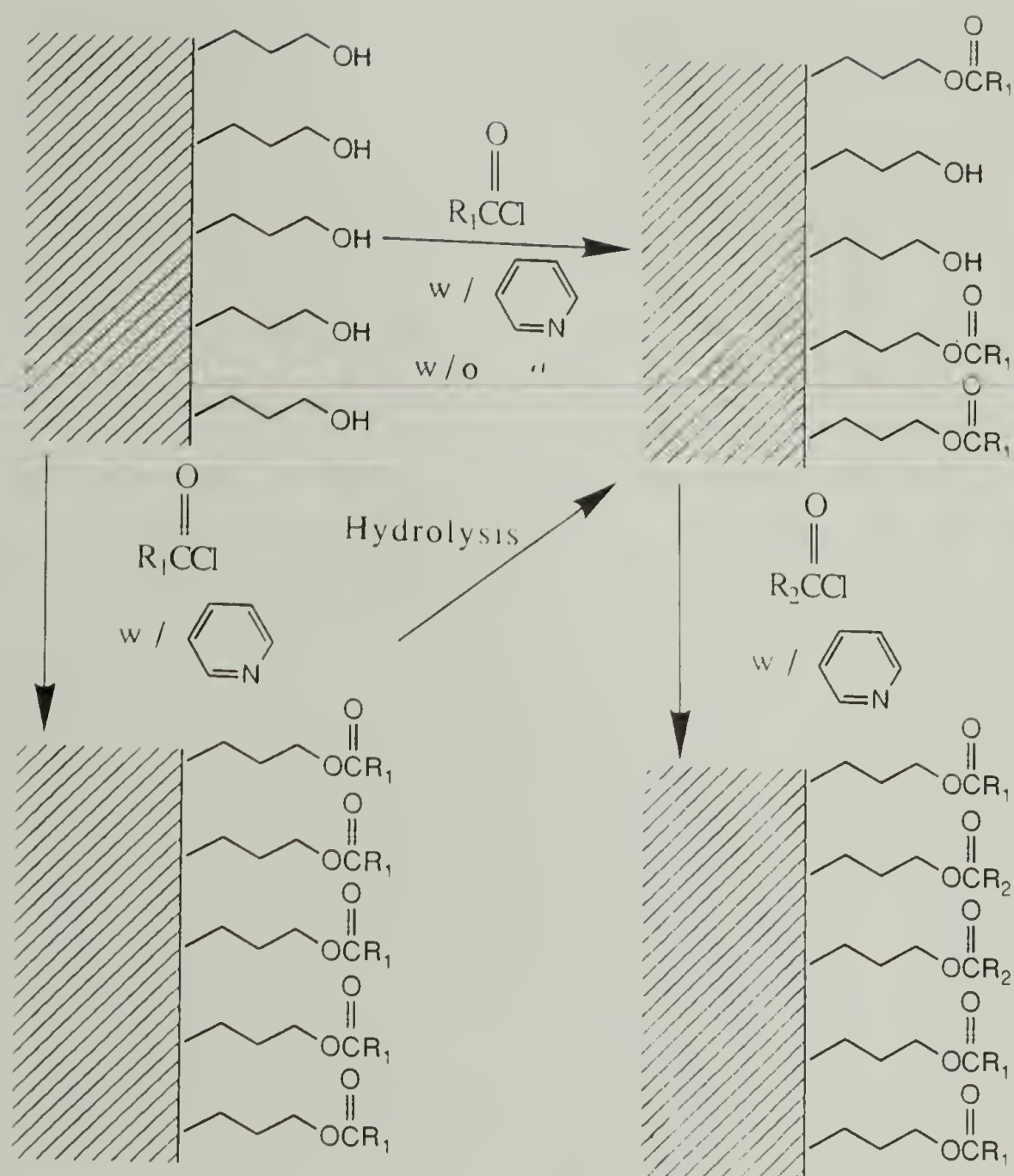


**Figure 5.1.** Preparation of mixed hydroxyl/ester and mixed ester/ester surfaces.

(as determined by XPS) prepared by different methods differ in their wetting behavior. It is conceivable that some of these methods (see (Method 1) above) could produce surfaces in which the functional groups are randomly dispersed throughout the modified layer, while others (Method 2) may result in surfaces which are "patchy" in nature. This study will also provide an improved understanding of reaction conditions and kinetics of esterification and ester hydrolysis at an interface and their impact on the ultimate surface structure.

## Experimental

### General

PCTFE-OH was prepared as described previously<sup>7</sup> from PCTFE-PEAA which was initially synthesized at -78 °C.<sup>7</sup> Tetrahydrofuran (THF) (Aldrich, anhydrous) was distilled under nitrogen from sodium/benzophenone. Pyridine (Aldrich) was distilled under nitrogen from calcium hydride. Butyryl chloride (Aldrich) was distilled and stored under nitrogen. Decanoyl chloride and stearoyl chloride (both Aldrich) were vacuum distilled and stored under nitrogen. Trifluoroacetic anhydride and heptafluorobutyryl chloride (both Aldrich) were distilled under vacuum (trap-to-trap) and stored under nitrogen. Perfluorodecanoyl chloride was prepared as described previously.<sup>7</sup> Methanol, dichloromethane (both Fisher, HPLC Grade), THF (Aldrich) and water (house distilled, redistilled with a Gilmont Still) used as wash solvents were sparged with nitrogen. Other reagents were obtained from Aldrich and used as received. X-ray photoelectron spectra (XPS) were obtained with a Perkin Elmer-Physical Electronics 5100 with Mg K $\alpha$  excitation (400 W, 15.0 kV). Spectra were routinely recorded at two takeoff angles ( $\Theta_T$ ): 15° and 75° (measured between the film surface plane and the analyzer).<sup>8</sup> XPS atomic composition data were determined using sensitivity factors obtained from measurements made on samples of known surface composition: F1s, 1.00; C1s, 0.225; O1s, 0.620 and Cl2p, 0.655. Dynamic advancing ( $\Theta_A$ ) and receding ( $\Theta_R$ ) contact angles were measured with a Ramé-Hart telescopic goniometer as the probe fluid was added to ( $\Theta_A$ ) and removed from



( $\Theta_R$ ) the sample surface with a Gilmont syringe fitted with a 24 gauge flat-tipped needle. Results are reported as  $\Theta_A/\Theta_R$ . Probe fluids used were water (purified as described above), hexadecane (vacuum distilled from calcium hydride and stored under nitrogen) or methylene iodide (vacuum distilled from  $P_2O_5$  and stored under nitrogen in the dark). (The experiments reported in this chapter can be found in Notebooks T6P139-149, T7P5-39, T8P5-149 and T9P3-39.)

Catalyzed Esterifications of PCTFE-OH (PCTFE-OB<sub>ut</sub>, PCTFE-OD<sub>ec</sub>, PCTFE-OS<sub>tear</sub>, PCTFE-OTF<sub>Ac</sub>, PCTFE-OH<sub>FB</sub> and PCTFE-OP<sub>FD</sub><sub>ec</sub>)

To a nitrogen-purged Schlenk tube containing the PCTFE-OH film, 25 mL of dry THF was added, followed by 0.71 mL of pyridine (8.8 mmole) and 8.75 mmole of the appropriate acid chloride (butyryl (But), decanoyl (Dec), stearoyl (Stear), heptafluorobutyryl (HFB) or perfluorodecanoyl (PFDec)) or anhydride (trifluoroacetyl (TFAc)). The reaction was allowed to proceed for the desired length of time after which the films were washed with THF (5x),  $H_2O$  (5x), THF (5x), methanol (5x) and then dichloromethane (5x) and dried (0.05 mm, room temp., > 24 h).

Uncatalyzed Esterifications of PCTFE-OH (PCTFE-OB<sub>ut</sub>, PCTFE-OD<sub>ec</sub>, PCTFE-OS<sub>tear</sub> and PCTFE-OH<sub>FB</sub>)

The procedure for the catalyzed esterifications was followed except pyridine was omitted from the reaction mixture.

### Acid Catalyzed Methanolysis of PCTFE-Esters

To an FEP centrifuge tube containing the PCTFE-Ester film (PCTFE-OB<sub>u</sub>t, PCTFE-OD<sub>e</sub>c, PCTFE-OS<sub>t</sub>ear and PCTFE-OHFB films were reacted), 25 mL of a solution of *p*-toluenesulfonic acid in methanol (0.025 M) was added. The tube was then capped and placed in an oil bath at 105 °C for 24 h. The film was then removed from the tube and soaked for 15 min intervals in water, methanol and then dichloromethane and dried (0.05 mm, room temp., > 24 h).

### Base Catalyzed Hydrolysis/Methanolysis of PCTFE-Esters

To an FEP centrifuge tube containing the PCTFE-Ester film (PCTFE-OB<sub>u</sub>t, PCTFE-OD<sub>e</sub>c, PCTFE-OS<sub>t</sub>ear, PCTFE-OHFB and PCTFE-OPF<sub>d</sub>ec films were reacted), 25 mL of a 0.025 M solution of potassium hydroxide in methanol:H<sub>2</sub>O (0:100, 25:75, 50:50, 75:25 or 100:0 v/v) was added. The tube was then capped and placed in an oil bath at 105 °C. After the desired reaction time, the film was removed from the tube and soaked for 15 min intervals in water, methanol and then dichloromethane and dried (0.05 mm, room temp., > 24 h).

## Results and Discussion

As stated in the introduction to this chapter, the objective of this research is to use different procedures to prepare compositionally similar surfaces which contain a variety of functional groups and to study and compare their wetting behavior. Two

synthetic routes have been utilized to prepare these mixed surfaces: 1) sequential esterification of a  $\sim 30$  Å thick, densely modified poly(chlorotrifluoroethylene) surface containing primarily hydroxyl functionality (PCTFE-OH)<sup>7</sup> to first make mixed alcohol/ester surfaces and then subsequently prepare mixed hydrocarbon ester/fluorocarbon ester surfaces and 2) partial hydrolysis of esters of PCTFE-OH (PCTFE-Esters) to form mixed ester/alcohol surfaces followed by re-esterification of the product hydroxyl groups with a second acylating agent in order to form mixed ester/ester surfaces. The competitive reaction of two acid chlorides with PCTFE-OH was also studied in one case.

In the first procedure (Method 1), the extent of reaction of PCTFE-OH with each of several acid chlorides (Figure 5.1) was kinetically controlled to prepare a series of mixed alcohol/ester surfaces with varying compositions. Butyryl (C<sub>4</sub>), decanoyl (C<sub>10</sub>) and stearoyl (C<sub>18</sub>) chlorides were chosen as acylating agents to study the effects of alkyl chain length, while heptafluorobutyryl chloride was used to compare the behavior of hydrocarbon and fluorocarbon esters. After isolation, the unreacted hydroxyl functionality in these mixed surfaces was then esterified in a second reaction (Figure 5.1) using either heptafluorobutyryl chloride (for the alcohol/hydrocarbon ester surfaces) or butyryl chloride (for the alcohol/heptafluorobutyrate surfaces) to prepare heterogeneous hydrocarbon ester/heptafluorobutyrate surfaces with varying hydrocarbon tail lengths (C<sub>4</sub>, C<sub>10</sub> and C<sub>18</sub>). The mixed hydroxyl/butyrate surface was also reacted with trifluoroacetic anhydride and perfluorodecanoyl chloride (Figure 5.1) to prepare



heterogeneous fluorocarbon ester/butyrate surfaces with varying fluorocarbon tail lengths ( $C_2$ ,  $C_4$  and  $C_{10}$ ).

In the second procedure for the preparation of heterogeneous surfaces (Method 2), kinetic control of the hydrolysis/methanolysis of homogeneous butyrate, decanoate, stearate and heptafluorobutyrate (and perfluorodecanoate to a limited extent) ester surfaces was used to prepare a series of mixed ester/alcohol surfaces (Figure 5.1). The product alcohols in these surfaces were then re-esterified with either heptafluorobutyryl chloride (used with the mixed hydrocarbon ester/alcohol surfaces) or butyryl chloride (used with the mixed heptafluorobutyrate/alcohol surface) to prepare heterogeneous hydrocarbon ester/heptafluorobutyrate surfaces.

The dynamic wetting behavior of the mixed surfaces resulting from these two methods was studied as a function of surface composition. In order to maximize wettability differences between the two types of surface components, water was utilized as a probe fluid for the mixed alcohol/ester surfaces and hexadecane for the hydrocarbon/fluorocarbon mixed ester surfaces. Water was chosen for the former group of mixed surfaces since it interacts favorably with the polar, hydrogen-bonding alcohol functionality and is repelled by the hydrophobic tails of the esters. Hexadecane, on the other hand, is attracted to the hydrocarbon esters, but repelled by the oleophobic perfluorinated groups.

As discussed previously,<sup>10</sup> the advancing contact angle provides information about the functionality present at the film/air interface while the receding contact angle yields information

concerning the functionality present at the film/probe fluid interface. As will be seen in the results discussed below, the composition of these two interfaces is usually substantially different and large contact angle hysteresis is observed. This composition difference is due to migration to the particular interface probed of whichever component in the film surface produces the lowest interfacial free energy. For the mixed alcohol/ester surfaces, the ester functionality predominates at the film/air interface, producing high advancing water contact angles. During the measurement the hydroxyl groups present in these mixed surfaces likely migrate to the film/water interface and thus, low receding water contact angles are observed. For the mixed hydrocarbon ester/fluorocarbon ester surfaces, the fluorocarbon component of the surface is present in excess at the film/air interface. Since fluorocarbons are oleophobic, high advancing hexadecane contact angles are observed. The hexadecane probe fluid induces the migration of the hydrocarbon component in these mixed surfaces to the film/liquid interface, resulting in low receding hexadecane contact angles.

The goal of this research is to obtain information about the manner in which the advancing and receding contact angles vary as the surface composition is changed from one that is wet by the probe fluid to one that is not.<sup>10</sup> Different synthetic routes for the preparation of these heterogeneous surfaces were utilized to investigate if the preparative method has an effect on the ultimate surface structure. It is expected that the procedure involving sequential esterifications (Method 1) will produce surfaces where the two functional groups are randomly dispersed throughout the

surface (Figure 5.2a). On the other hand, it is possible that the partial hydrolysis/re-esterification procedure (Method 2) will produce "patchy" surfaces. The hydrolysis/methanolysis of the ester surfaces may be inhibited initially since these hydrophobic surfaces are not sufficiently wet by the reaction solution. However, once the hydrolysis begins at some point on the surface (either at defects or some random position), that location will contain a hydroxyl group which will facilitate the transport of the reacting solution to the ester functionality surrounding the alcohol. The rate of hydrolysis at these points on the surface will then be greater than if no hydroxyl groups were present, resulting in an autoaccelerative reaction and a "patchy" surface (Figure 5.2b).

As mentioned above, both of the preparative methods for these heterogeneous surfaces involve kinetic control of an initial reaction. As a result, an added benefit of these studies is an improved understanding of the reactivity of surface-confined functional groups. For example, in Method 1, the kinetics of esterification of PCTFE-OH both with and without the use of pyridine as an acylation catalyst was studied for a number of acid chlorides. While in Method 2, the kinetics of the hydrolysis/methanolysis of the PCTFE-Esters was studied as a function of solvent composition. In each case, the reactions were monitored by following changes in the  $15^\circ$  and  $75^\circ$  takeoff angle XPS carbon/fluorine ratios (C/F) and the advancing and receding contact angles.



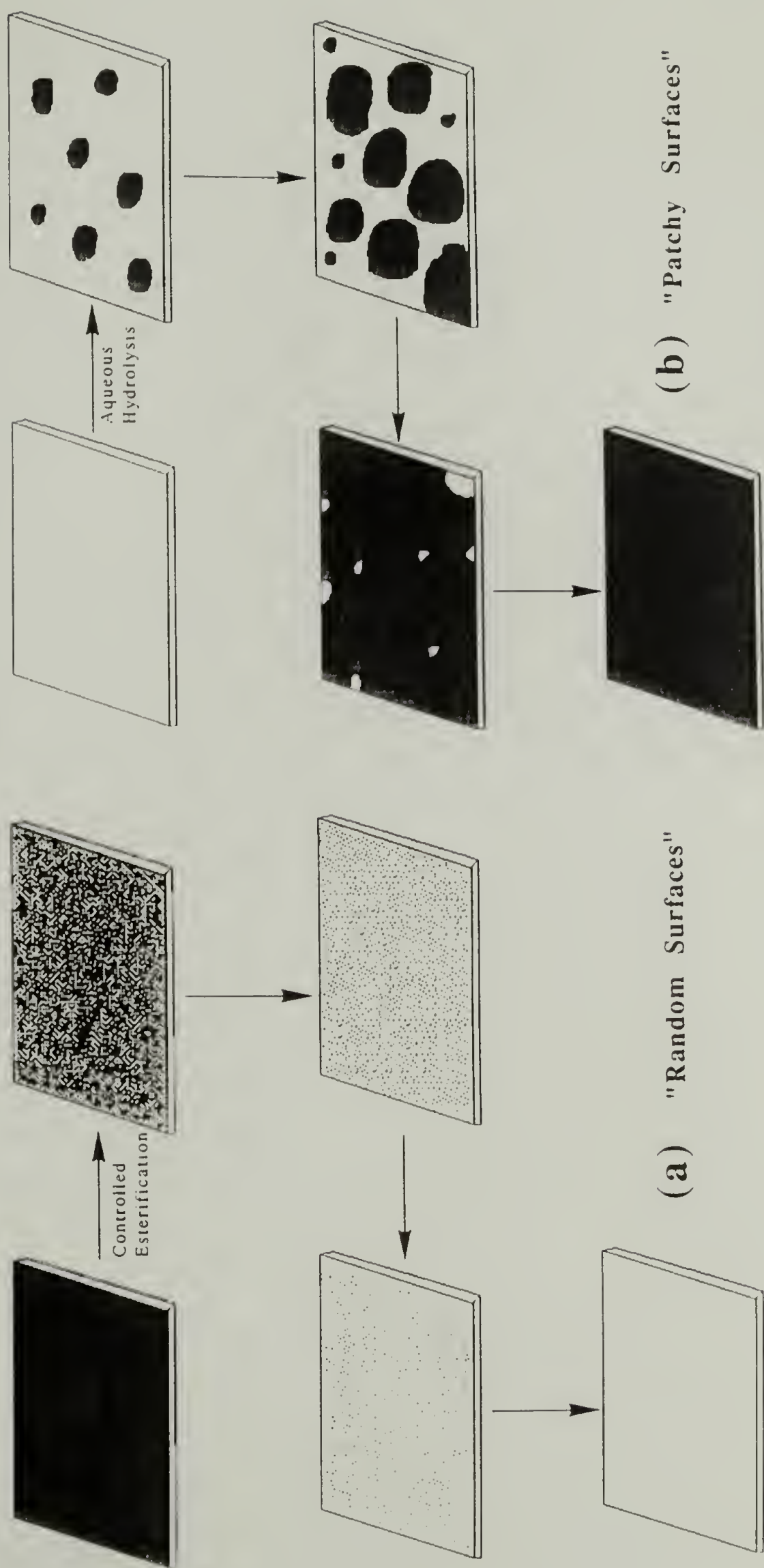


Figure 5.2. Formation of: (a) random and (b) patchy mixed surfaces.

A reference point for these studies is the characterization of the homogeneous alcohol and ester surfaces used in this research. Most of these results were thoroughly discussed in Chapter III of this dissertation and are summarized in Table 5.1. As expected, the XPS C/F ratios are high for the hydrocarbon ester surfaces and considerably lower for the fluorocarbon ester surfaces. Also, the water contact angles on the ester surfaces are greater than those on the alcohol surface and the hydrocarbon esters exhibit lower hexadecane contact angles than the fluorocarbon esters. It is these differences that will be utilized to monitor the surface reaction kinetics and to characterize the mixed surfaces discussed below.

**Table 5.1.** Characterization results for the homogeneous modified PCTFE surfaces used in this study.

<u>Surface</u>	<u>Q<sub>T</sub></u>	<u>Experim.</u> <u>C/F Ratio</u>	<u>Calculated</u> <u>C/F Ratio</u>	<u>Q<sub>A</sub>/Q<sub>R</sub><sup>H<sub>2</sub>O</sup></u>	<u>Q<sub>A</sub>/Q<sub>R</sub><sup>HD</sup></u>	<u>Q<sub>A</sub>/Q<sub>R</sub><sup>MI</sup></u>
PCTFE-OH	15 75	3.64 2.69	3.66	67/17	18/6	55/41
PCTFE-TFAC	15 75	1.60 1.76	1.67	92/51	39/24	---
PCTFE-OHFB	15 75	0.95 1.13	1.18	107/68	60/40	88/62
PCTFE-OPFDec	15 75	0.74 0.92	0.76	120/69	71/55	---
PCTFE-OBUT	15 75	5.84 5.32	6.36	89/54	10/0	62/22
PCTFE-ODEC	15 75	15.0 8.85	10.3	106/57	10/0	---
PCTFE-OSTEAR	15 75	34.4 13.3	15.5	108/90	42/35	---

## Kinetics of the Esterification of PCTFE-OH

The esterification kinetics of the reaction of PCTFE-OH with several acid chlorides were studied under two sets of conditions: (1) using pyridine as an acylation catalyst (equimolar ratio of pyridine to acid chloride) and (2) uncatalyzed. In each case, the PCTFE-OH films were reacted at room temperature with a 0.35 M solution of the acid chloride in THF. The extent of esterification as a function of the reaction time was first monitored by measuring the changes in the XPS C/F ratios and the water contact angles of the resulting mixed alcohol/ester surfaces. The residual alcohols were then labelled in a second reaction with either heptafluorobutyryl chloride or butyryl chloride under conditions known to yield quantitative esterification. The C/F ratios and hexadecane contact angles of the resulting mixed hydrocarbon ester/fluorocarbon ester surfaces were then measured. As will be shown, this labelling reaction was used not only to prepare the mixed ester surfaces, but also to facilitate the quantitative determination of the unreacted hydroxyl groups since the labelled functional group is more efficiently detected by XPS. The results are discussed below.

Pyridine Catalyzed Esterifications. In Figures 5.3 and 5.4, the XPS and contact angle results for the pyridine catalyzed reaction of heptafluorobutyryl chloride with PCTFE-OH are plotted versus the time of the initial esterification. The circles represent the data obtained after the initial reaction with heptafluorobutyryl chloride, while the squares show the results after labelling any unreacted alcohols with butyryl chloride. For comparative purposes, the data for surfaces containing only hydroxyl (PCTFE-OH),



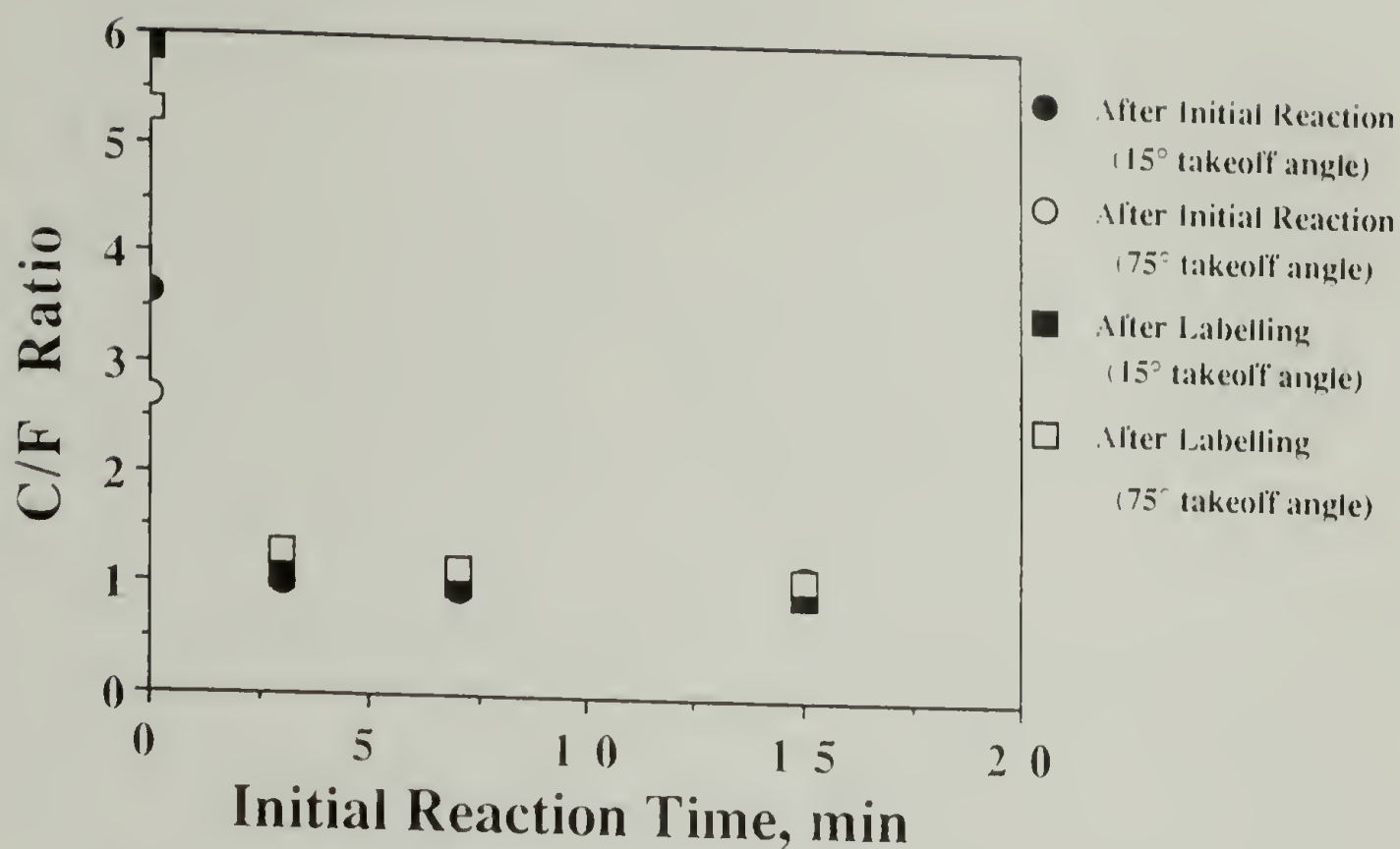


Figure 5.3. XPS results for pyridine catalyzed esterification kinetics with heptafluorobutyryl chloride.

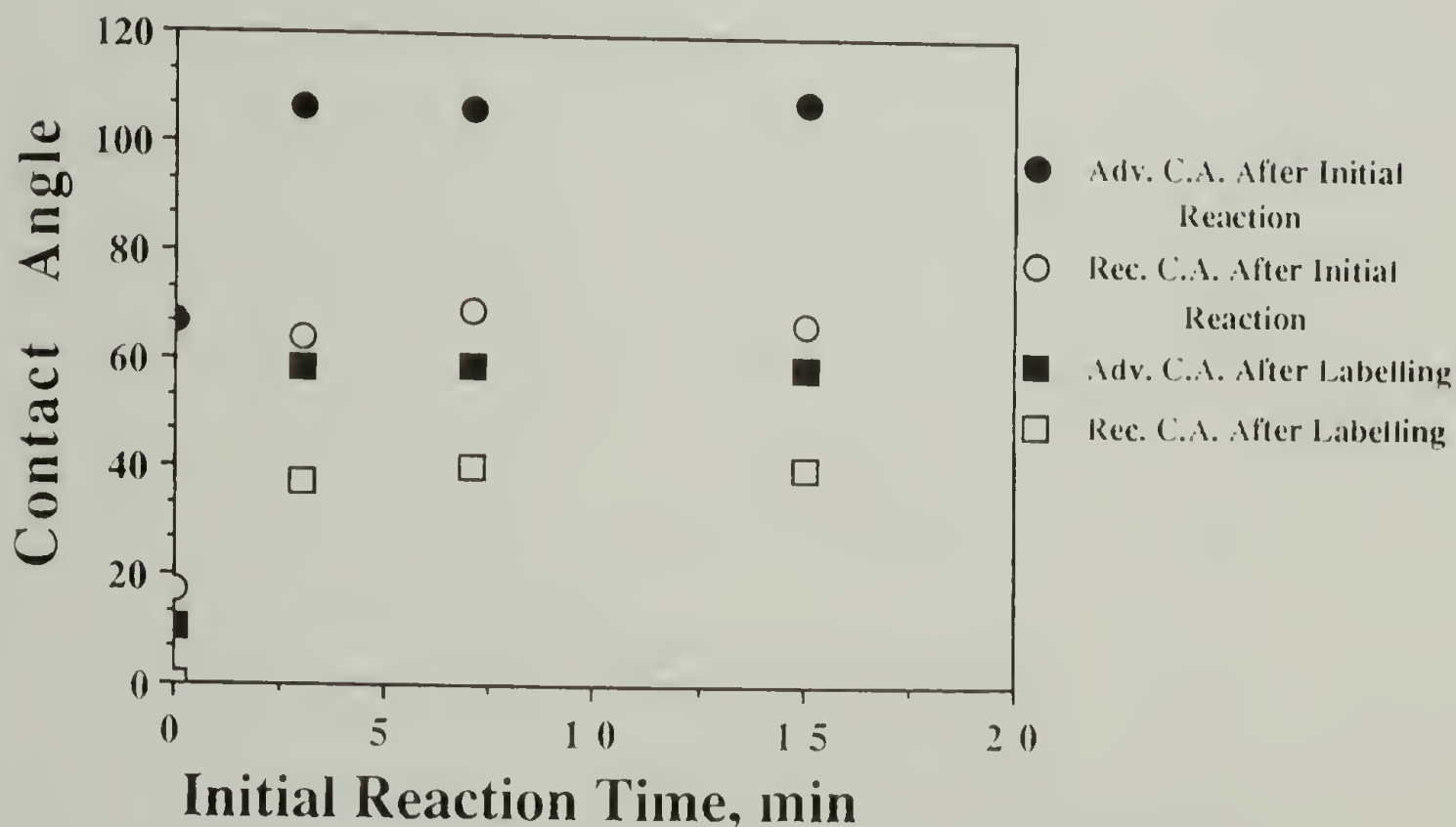
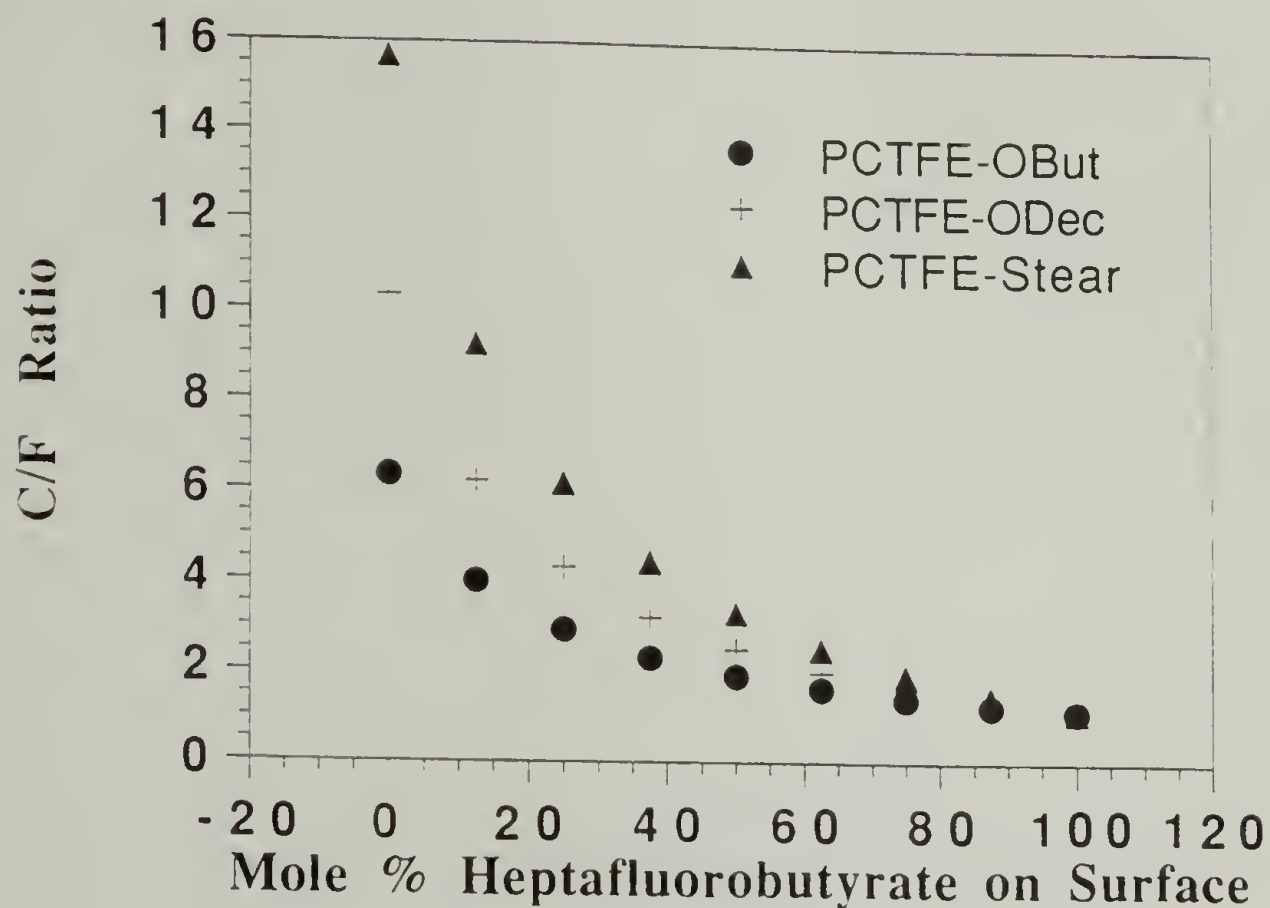


Figure 5.4. Contact angle results for pyridine catalyzed esterification kinetics with heptafluorobutyryl chloride. Water contact angles after initial reaction (circles) and hexadecane contact angles after labelling with butyryl chloride (squares).

heptafluorobutyrate (PCTFE-OHFB) or butyrate (PCTFE-OBuT) functionality are presented in Table 5.1. From these results, it is observed that this catalyzed esterification is very rapid and proceeds in high yield. After 3 min the C/F ratios have decreased from 3.64&2.59 (the values for PCTFE-OH) to 1.01&1.23 (15°&75° takeoff angle) and the water contact angles have increased from 67°/17° to 106°/64° ( $\Theta_A/\Theta_R$ ). The corresponding values for homogeneous PCTFE-OHFB are 0.95&1.13 and 107°/68°. Thus, a high percentage of the hydroxyl groups have been esterified after this short time. After 7 min, the results are essentially identical to those of homogeneous PCTFE-OHFB and the reaction is complete. When the PCTFE-OH/OHFB surface prepared in the initial 3 min reaction was treated with butyryl chloride, the C/F ratios increased to 1.06&1.30. This increase reflects the formation of butyrate esters of the unreacted hydroxyl groups present in the initially reacted surface. From the measured C/F ratio of this PCTFE-OHFB/OBuT surface and a theoretical plot of the C/F ratio as a function of the surface composition (Figure 5.5) it is estimated that approximately 15% of the ester groups in the modified layer are butyrates. Thus, approximately 85% of the hydroxyl groups in PCTFE-OH were esterified with heptafluorobutyryl chloride in the first 3 min of the initial reaction. The hexadecane contact angles on the 3 min PCTFE-OHFB/OBuT surface (58°/37°) are slightly lower than those of PCTFE-OHFB (60°/40°) confirming the presence of the butyrate groups. (A pure butyrate surface has hexadecane contact angles of 10°/0°.) The surfaces reacted in the initial esterification for 7 and 15 min show no changes in the C/F ratios (15° or 75° takeoff angle) after treatment with butyryl

chloride and exhibit hexadecane contact angles identical to those of PCTFE-OHFB. These results indicate a complete, quantitative reaction after 3 min.



**Figure 5.5.** Calculated XPS C/F ratio as a function of surface composition for mixed heptafluorobutyrate/hydrocarbon ester surfaces.

The results for the catalyzed reactions of PCTFE-OH with butyryl chloride, decanoyl chloride and stearoyl chloride are shown in Figures 5.6 - 5.11. As before, the circles represent the data obtained after the initial esterification, while the squares show the results after labelling any unreacted alcohols in a second esterification with heptafluorobutyryl chloride. Results for the surfaces containing only hydroxyl (PCTFE-OH), butyrate (PCTFE-OBuT), decanoate (PCTFE-ODec), stearate (PCTFE-OStear) or heptafluorobutyrate (PCTFE-OHFB) functionality are presented in



Table 5.1 for comparison. It can be seen from these figures that the catalyzed esterifications with the hydrocarbon acid chlorides are rapid, but slightly slower than that of the prefluorinated acid chloride. Also, as will be shown below, these reactions proceed in high yield, but are not quantitative.

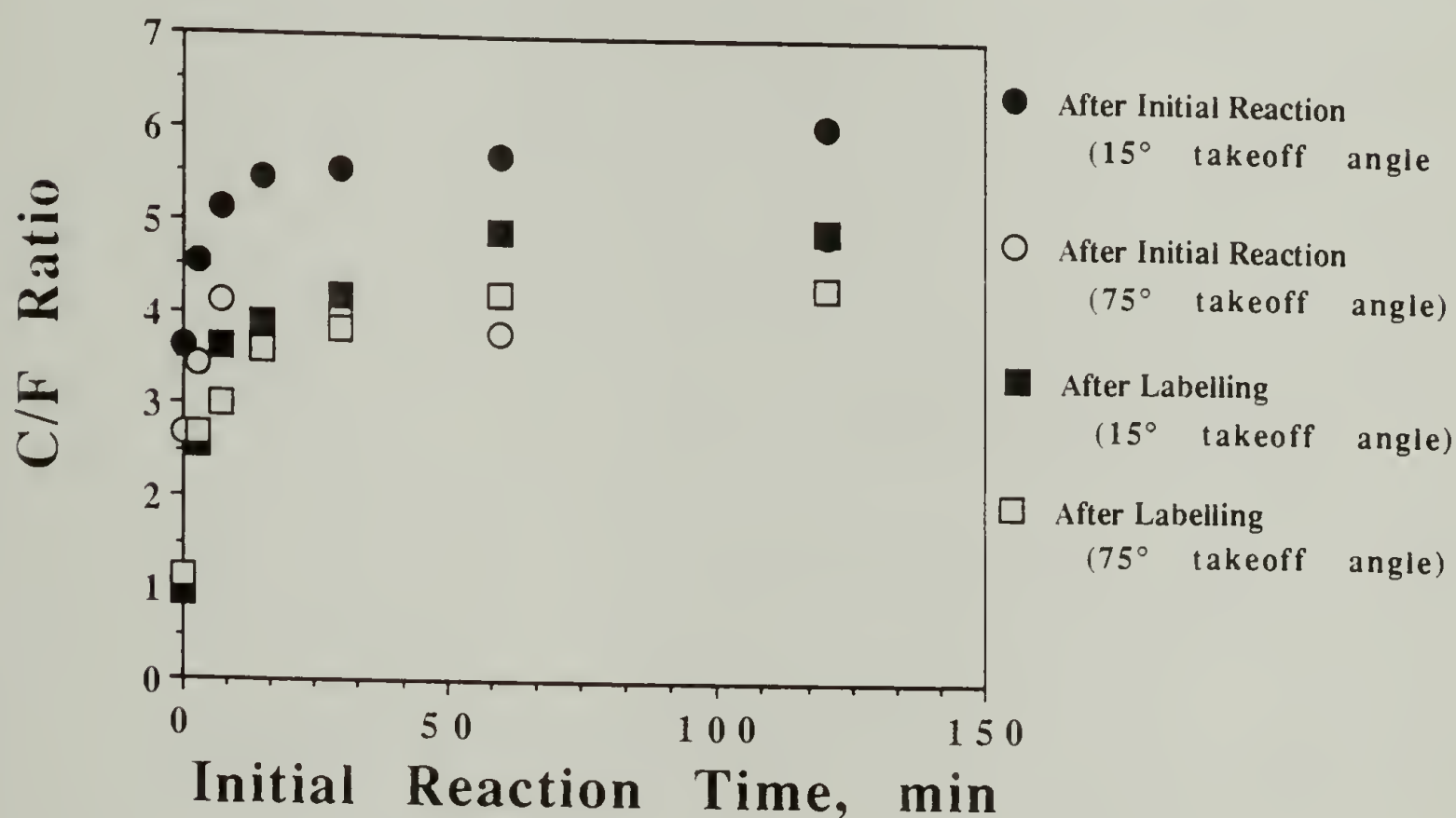
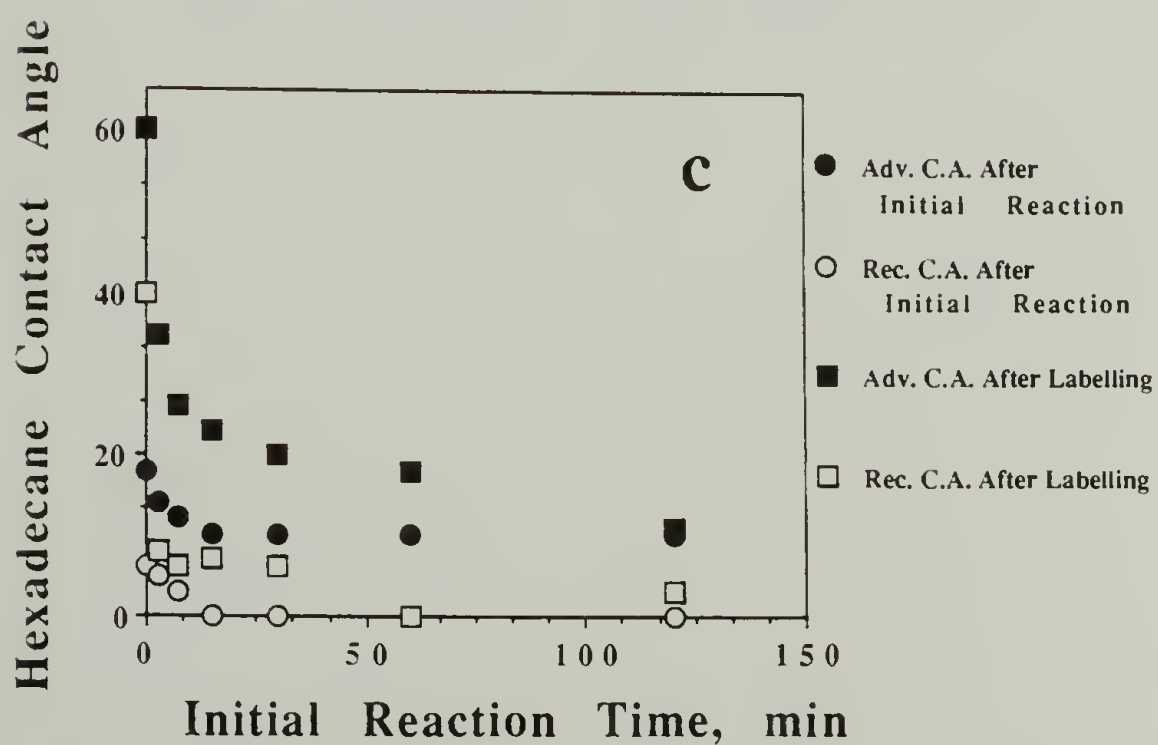
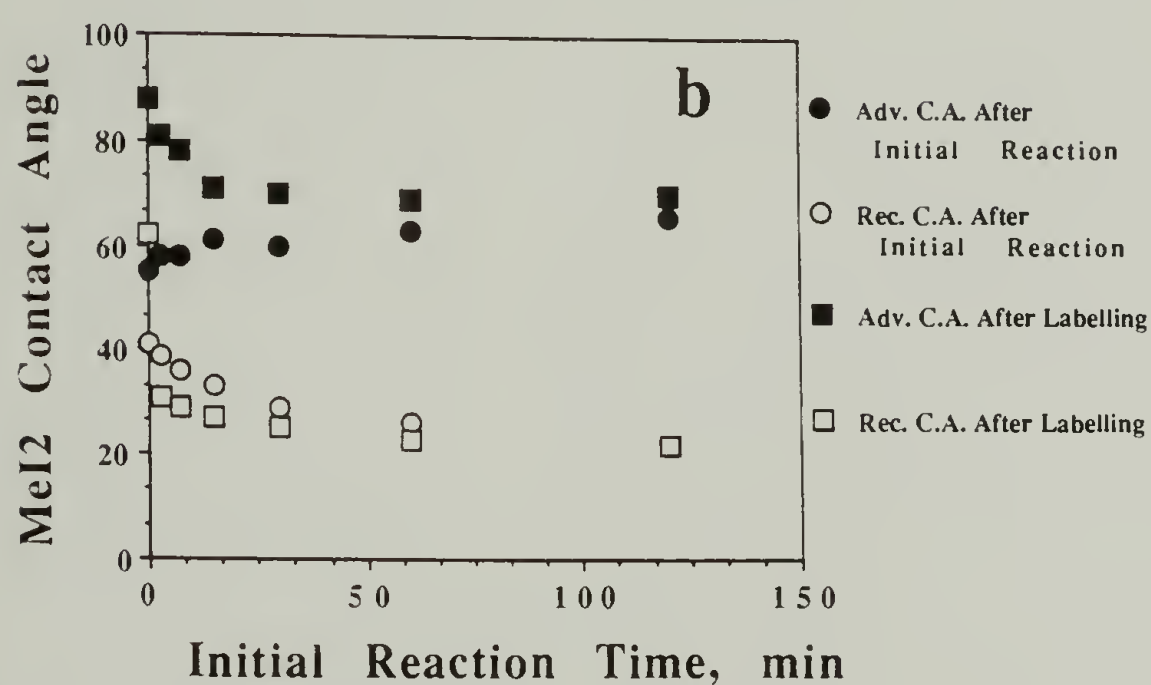
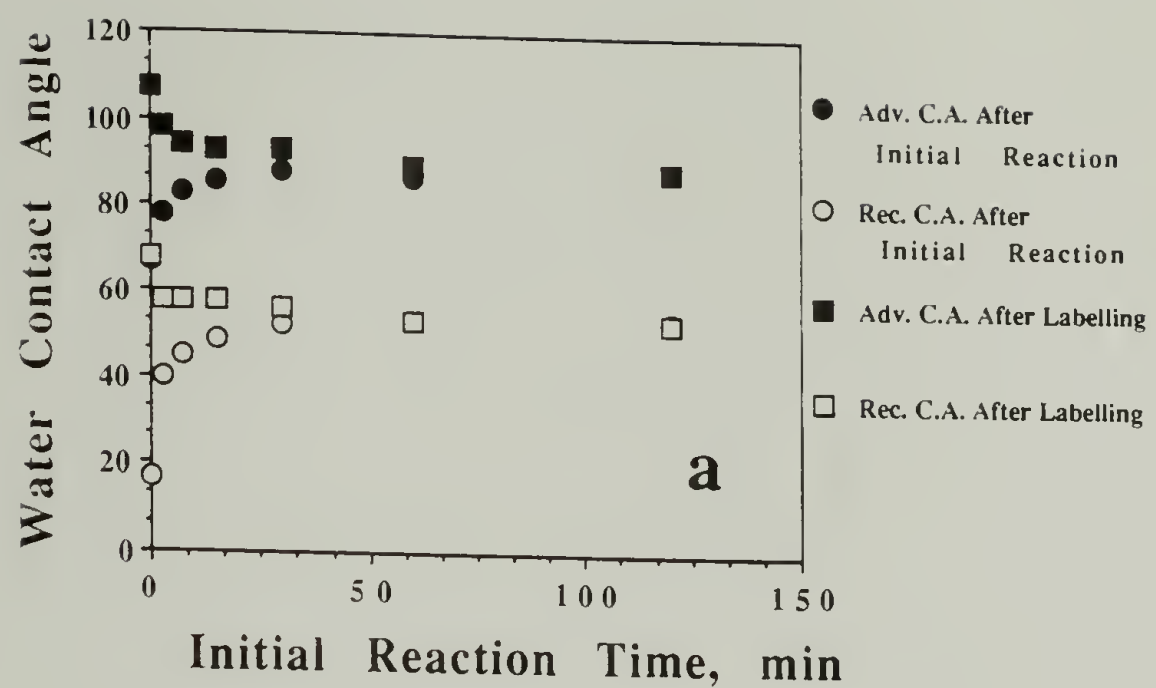


Figure 5.6. XPS results for pyridine catalyzed esterification kinetics with butyryl chloride.

XPS results for the catalyzed esterification of PCTFE-OH with butyryl chloride are shown in Figure 5.6. The data for both the initially reacted samples and after labelling these samples with heptafluorobutyryl chloride indicate that the reaction is complete in about 60 min. Unlike the esterification with heptafluorobutyryl chloride, this reaction is not quantitative. If all of the alcohol groups present in PCTFE-OH had reacted in the initial esterification, no change in the XPS C/F ratio would be observed after treatment of

these samples with heptafluorobutyryl chloride. However, the results show a decrease in this ratio due to the formation of heptafluorobutyrate esters of the unreacted alcohols. For the sample initially reacted for 2 h, the decrease in the C/F ratio after labelling indicates that the butyrate:heptafluorobutyrate ratio on this surface is 9:1. Thus, the initial reaction converts about 90% of the hydroxyl groups in PCTFE-OH to butyrate esters.

Advancing and receding contact angles on these surfaces were measured using water, methylene iodide and hexadecane as probe fluids. The results are shown in Figures 5.7 a-c and exhibit the expected behavior. For the initially esterified surfaces, the water contact angles increase from  $67^{\circ}/17^{\circ}$  for PCTFE-OH to those of PCTFE-OBu (  $89^{\circ}/55^{\circ}$  ) in the first 30 min, indicating the rapid formation of a hydrophobic surface. The hexadecane contact angles decrease from  $18^{\circ}/6^{\circ}$  to  $10^{\circ}/0^{\circ}$  in the first 15 min as the hydrocarbon content in the surface increases. Meanwhile the methylene iodide contact angles continue to change over the entire course of the reaction (from  $55^{\circ}/41^{\circ}$  to  $66^{\circ}/22^{\circ}$  ) as the concentration of butyrate groups in the surface increases. After labelling the unreacted hydroxyl groups remaining in these PCTFE-OH/OBu surfaces with heptafluorobutyryl chloride, the heptafluorobutyrate groups are detected by water contact angles for the first hour of the initial reaction and by hexadecane and methylene iodide for the first two hours (see Figures 5.7 a-c). These observations indicate that the latter two probe fluids are more sensitive to the presence of the heptafluorobutyrate groups in the mixed hydrocarbon/fluorocarbon surfaces.



**Figure 5.7.** (a) Water, (b) methylene iodide and (c) hexadecane contact angle results for pyridine catalyzed esterification kinetics with butyryl chloride.



The XPS and contact angle results for the catalyzed preparation of the decanoate ester are shown in Figures 5.8 and 5.9, respectively. Once again, the data indicate a rapid reaction. The C/F ratios for the initially reacted samples increase to 15.0&8.85 (the same as PCTFE-ODec) in the first 30 min. The decrease in these ratios after labelling indicates the formation of heptafluorobutyrate esters of the hydroxyl groups which were unreacted in the initial esterification. From the C/F ratios (measured after labelling) of the sample initially reacted for 2 h, a yield of 93% is calculated for the catalyzed esterification with decanoyl chloride. The advancing water contact angles of the initially reacted samples (PCTFE-OH/Dec) reach the maximum value ( $106^\circ$ ) in the first 7 min of the reaction. The receding contact angle, however, is more sensitive to the small quantities of the polar hydroxyl groups remaining in the surface and takes 30 min to reach its limiting value ( $57^\circ$ ). The advancing hexadecane contact angle is sensitive to the presence of the heptafluorobutyrate esters produced in the labelling of these surfaces and decreases from a value of  $60^\circ$  for a labelled sample that was not initially reacted with decanoyl chloride (i.e. PCTFE-OH) to  $18^\circ$  for a labelled which was initially reacted for 4 min. After a 30 min initial reaction, the advancing hexadecane contact angle of the labelled sample is essentially equivalent to that of PCTFE-ODec ( $10^\circ$ ) which supports the XPS data in indicating that the reaction is complete. The receding hexadecane contact angle strongly reflects the hydrocarbon functionality in the surface and as such is  $0^\circ$  for all of the surfaces reacted with decanoyl chloride.

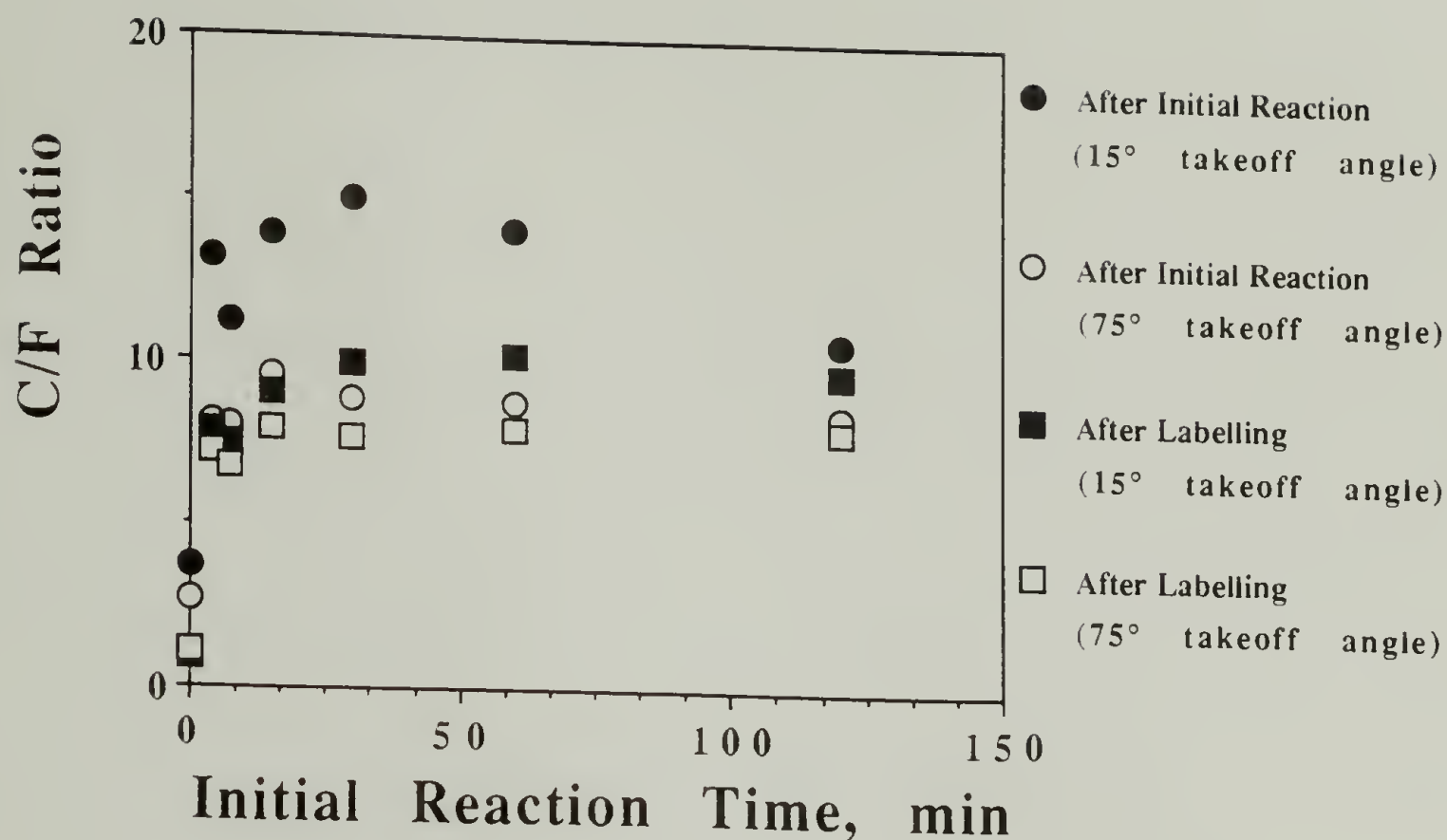


Figure 5.8. XPS results for pyridine catalyzed esterification kinetics with decanoyl chloride.

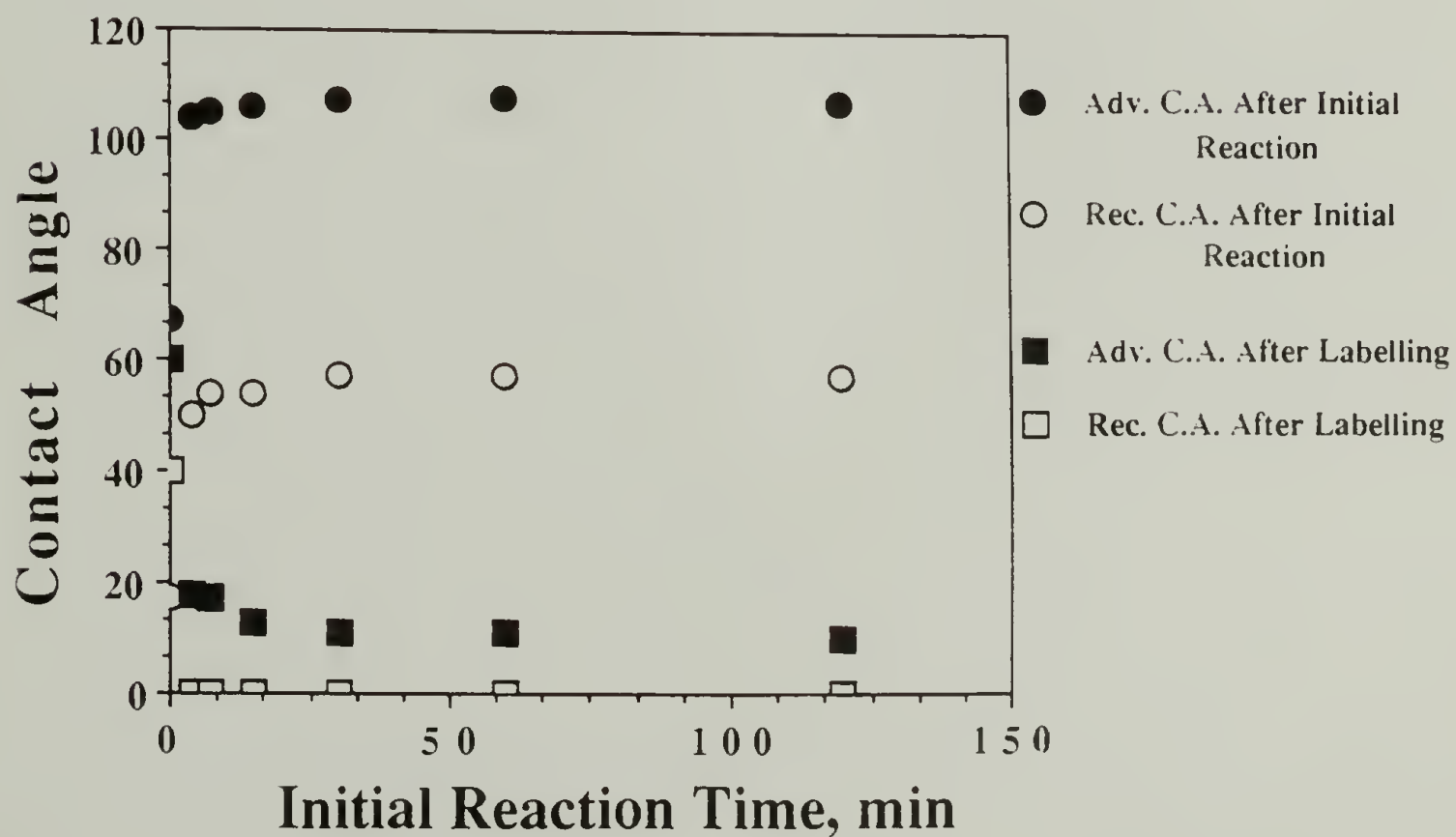
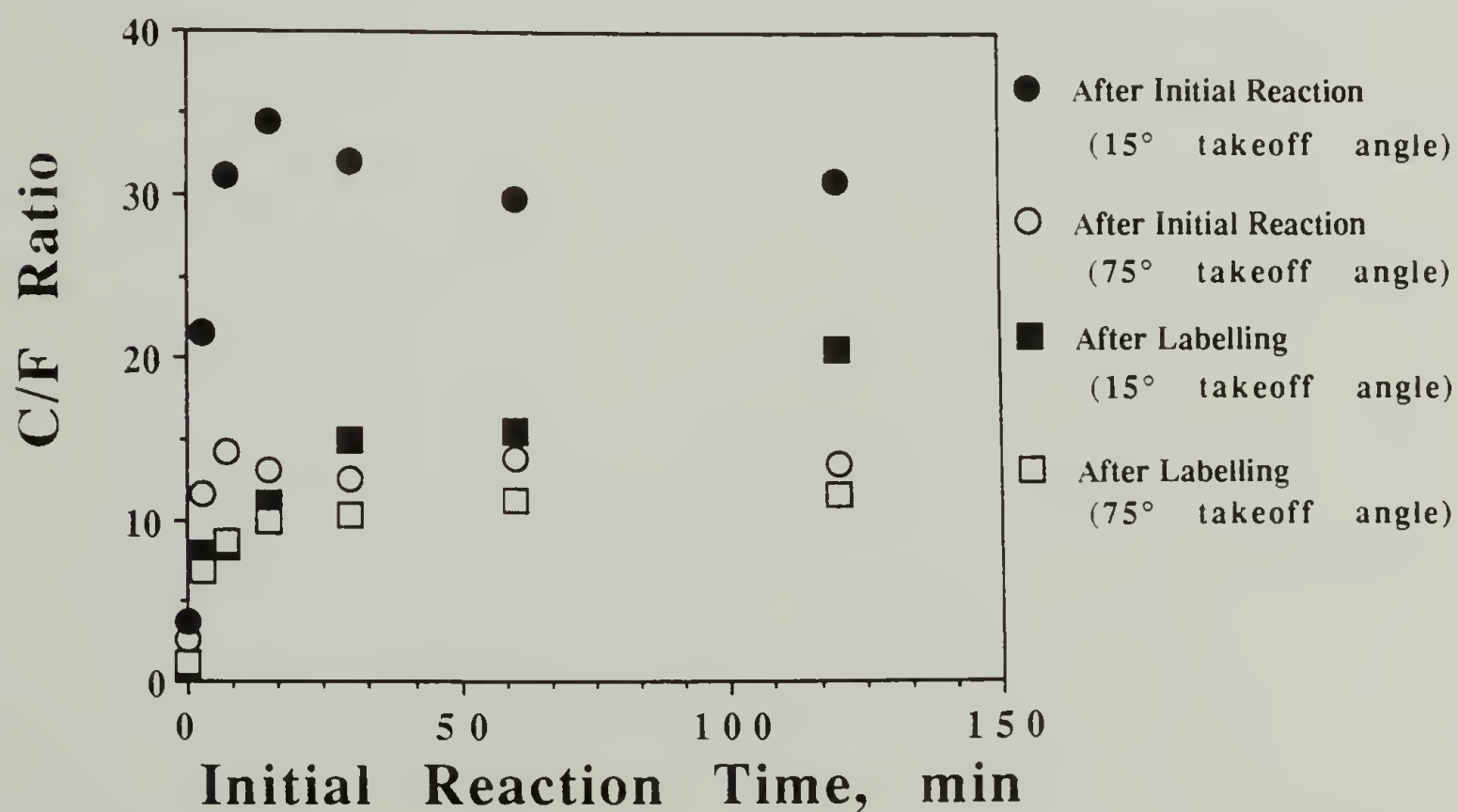


Figure 5.9. Contact angle results for pyridine catalyzed esterification kinetics with decanoyl chloride. Water contact angles after initial reaction (circles) and hexadecane contact angles after labelling with heptafluorobutyryl chloride (squares).

As discussed earlier,<sup>7</sup> the catalyzed reaction of stearoyl chloride with PCTFE-OH produces a surface containing stearate esters in an ordered array with their methyl groups located at the film/air interface. The results of the kinetic studies of this reaction illustrate the formation of this oriented surface and are shown in Figures 5.10 and 5.11. The XPS C/F ratios (circles, Figure 5.10) and the water (circles) and hexadecane (triangles) contact angles (Figure 5.11a) measured after the initial reaction indicate a rapid esterification and simultaneous ordering of the hydrocarbon chains in the surface. The C/F ratios of the initially reacted surface reach values equivalent to those of PCTFE-OS<sub>tear</sub> (34&13) in the first 7 to 15 min. The large differences between the 15° and 75° takeoff angle data are attributed to the ordered nature of the surface and were discussed previously.<sup>7</sup> In the first 7 min of the initial esterification, the advancing and receding water contact angles also increase from the values of PCTFE-OH (67°/17°) to those of PCTFE-OS<sub>tear</sub> (108°/90°) which might imply complete esterification. However, the C/F ratios after labelling this sample indicate that ~15% of the functional groups in the original 7 min esterified layer (PCTFE-OH/OS<sub>tear</sub>) are unreacted alcohols. Thus, the long, stearate tails have effectively screened these hydroxyl groups from detection by the aqueous probe fluid. Hexadecane contact angles were measured on the initially reacted surface in order to monitor the number of methyl groups present at the film/air interface (the more methyl groups, the higher the contact angle) and hence the degree of ordering in the modified layer. The results are also shown in Figure 5.11a. After a 3 min reaction these angles have increased from 18°/6° for PCTFE-OH to



29°/5° for the PCTFE-OH/OS<sub>tear</sub> mixed surface. Hexadecane contact angles of 10°/0° are expected for a surface comprised entirely of methylene groups (PCTFE-OD<sub>ec</sub> is an example), while contact angles of 42°/35° are expected for a fully esterified PCTFE-OS<sub>tear</sub> surface which contains primarily methyl groups. Thus, after 3 min the hexadecane contact angles show that some order exists in this surface. The 75° takeoff angle C/F ratio of the labelled sample (6.91) indicates that the esterification is only 78% complete at this point, but it appears that the concentration of stearate groups is high enough for ordering to begin to occur. As the reaction progresses, the degree of ordering in the surface increases (as indicated by the rise in the hexadecane contact angles) as the concentration of esters in the surface increases. After 30 min, the maximum number of methyl groups are present at the surface and the hexadecane contact angles have reached their limiting values (42°/35°).



**Figure 5.10.** XPS results for pyridine catalyzed esterification kinetics with stearoyl chloride.

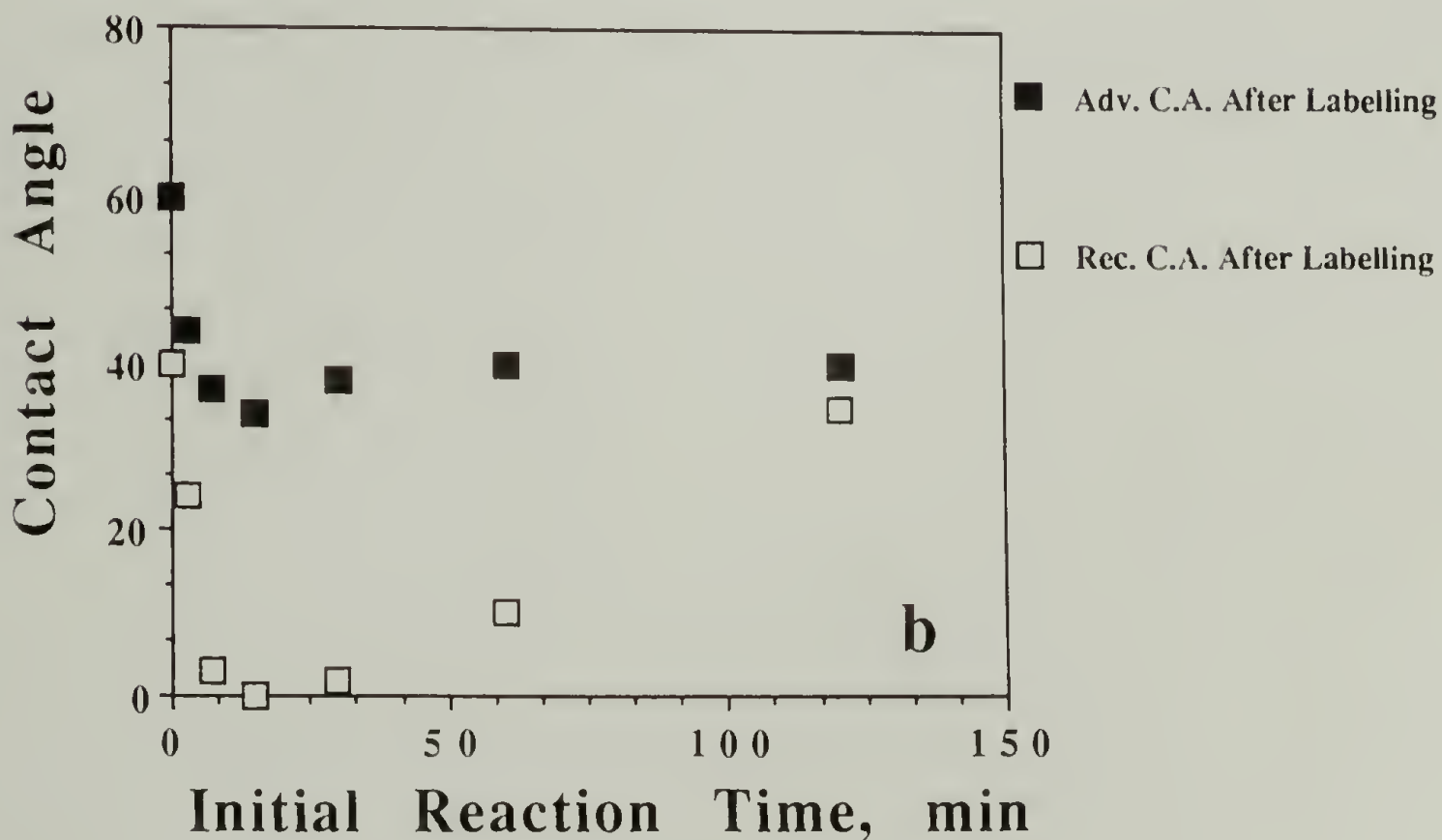
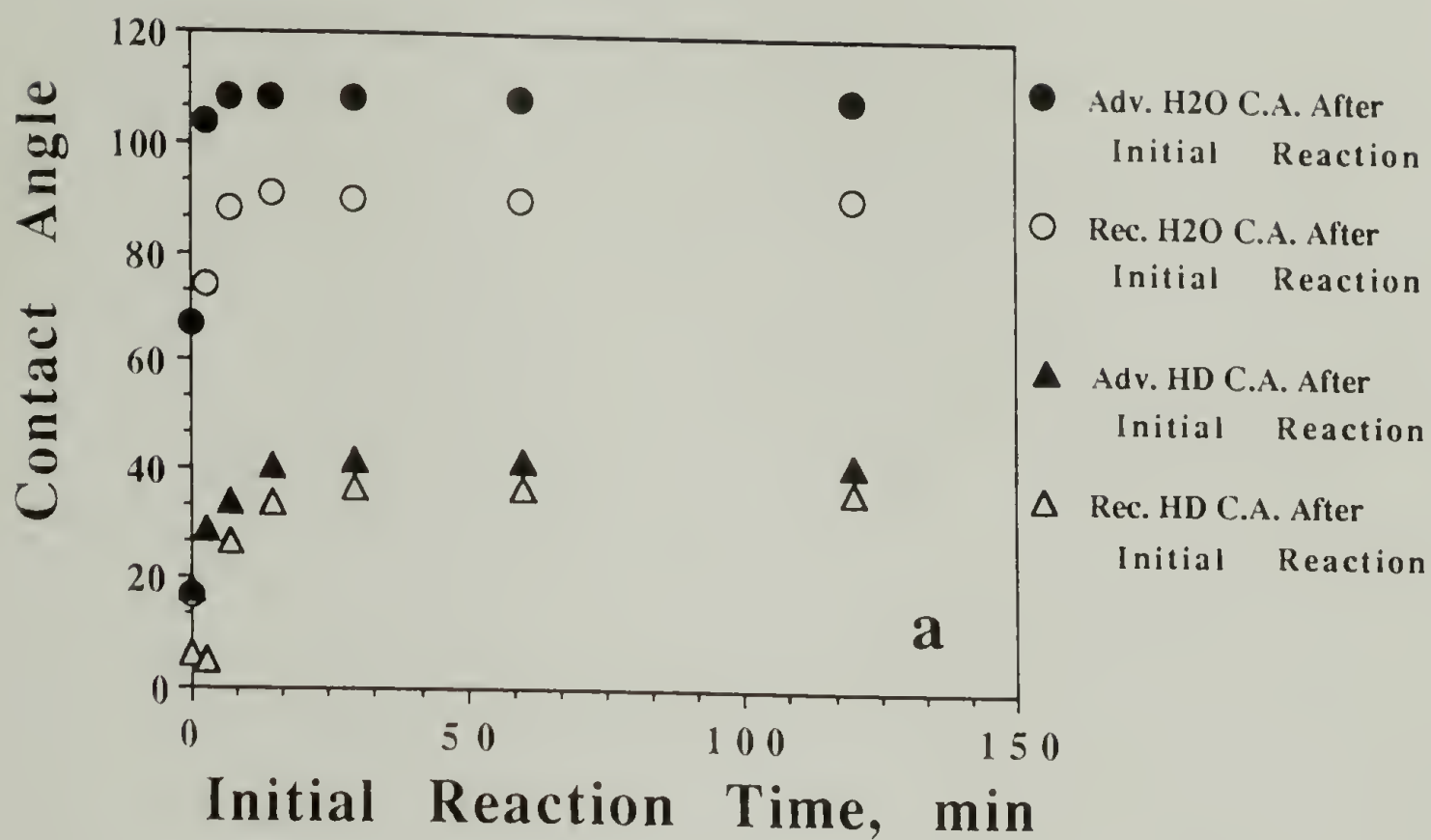


Figure 5.11. Contact angle results for pyridine catalyzed esterification kinetics with stearoyl chloride. (a) Water (circles) and hexadecane (triangles) contact angles after initial reaction and (b) hexadecane contact angles after labelling with heptafluorobutyryl chloride.

After labelling the initially reacted surfaces (PCTFE-OH/OStear), the XPS C/F ratios (squares, Figure 5.10) and the hexadecane contact angles (Figure 5.11b) both yield interesting results. The 75° takeoff angle data show a rapid increase in the C/F ratio from 1.13 to 10.1 in the first 15 min of the initial reaction as the surface composition changes from 100% heptafluorobutyrate to 89% stearate. The ratio then increases more slowly, reaching a value of 11.8 after 2 hours. This ratio indicates that the initial esterification with stearoyl chloride is ~93% complete at this time. The 15° takeoff angle ratios of the labelled samples also increase rapidly in the first 15 min of the initial reaction and are only slightly larger than those measured at 75°. The ratios then increase more slowly after this time, but the rate of the increase is substantially greater than that for the 75° data. The increasing difference between the 15° and the 75° data is a result of the significant increase in ordering of the stearate groups perpendicular to the surface as the concentration of these esters approaches its maximum value. The hexadecane contact angles reflect similar behavior. Labelling of an initially unreacted surface (PCTFE-OH) yields angles of 60°/40°, which is characteristic of PCTFE-OHFB. The contact angles of the labelled sample which was initially reacted for 3 min are 44°/24° and reflect a surface composed of mostly heptafluorobutyrate groups, along with some methylene units and possibly a few methyl groups. In the next 11 minutes of the initial reaction, the contact angles of the labelled samples decrease further to 35°/0° as the concentration of the heptafluorobutyrate groups decreases and the number of methylene and methyl groups increases. The relatively high advancing angle reflects the presence



of the heptafluorobutyrate and methyl functionalities, while the low receding angle is a result of the surface containing a significant number of methylene units. For initial reaction times greater than 30 min, the contact angles begin to increase with the time of the initial reaction. This increase is a result of the stearate groups becoming more perfectly oriented as their concentration increases, exposing more methyl groups to the interface, in agreement with the XPS results discussed above. After 2 h, the receding angle reaches a value of  $35^\circ$  which indicates a highly ordered surface.

The results discussed above and those presented in Figure 5.12 (a plot of the % esterification as a function of the reaction time for each acid chloride) show that the reaction of PCTFE-OH with an acid

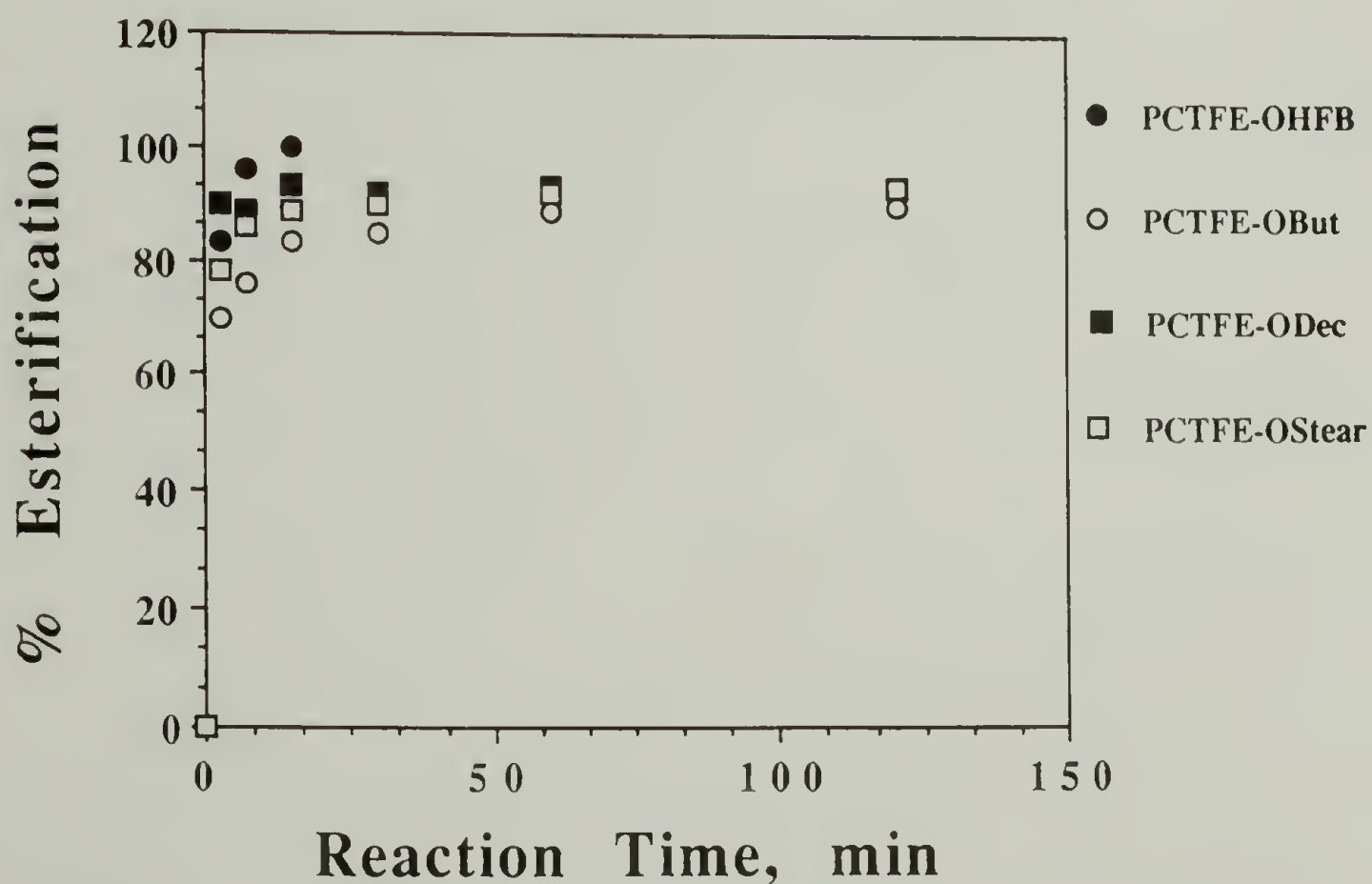


Figure 5.12. Rate of pyridine catalyzed esterifications of PCTFE-OH.

chloride in the presence of an acylation catalyst is rapid. This high rate of esterification makes it difficult to kinetically regulate the extent of reaction in order to controllably prepare heterogeneous surfaces with varying surface compositions. Thus, the study of uncatalyzed esterifications was undertaken with the hope that the reaction rate would be sufficiently slow to prepare the desired surfaces.

Uncatalyzed Esterifications. Figures 5.13 and 5.14 contain the results for the initial uncatalyzed reaction of heptafluorobutyryl chloride with PCTFE-OH and the subsequent treatment of these surfaces with butyryl chloride. The XPS results show that under these conditions the initial reaction has reached greater than 90% conversion after 15 min and is essentially complete after 30 min. The low value of the receding water contact angle after a 15 min initial reaction ( $63^\circ$  versus  $68^\circ$  for a completely esterified surface) indicates the presence of unreacted hydroxyl groups. Esterification of these hydroxyl groups in the labelling reaction introduces a small amount of butyrate esters into the surface, resulting in a lower receding hexadecane contact angle ( $28^\circ$ ) than is observed on a surface containing only heptafluorobutyrate groups ( $40^\circ$ ). Characterization (both before and after treatment with butyryl chloride) of the surfaces initially reacted for at least 30 min show results identical to those of PCTFE-OHFB indicating complete, quantitative reactions.

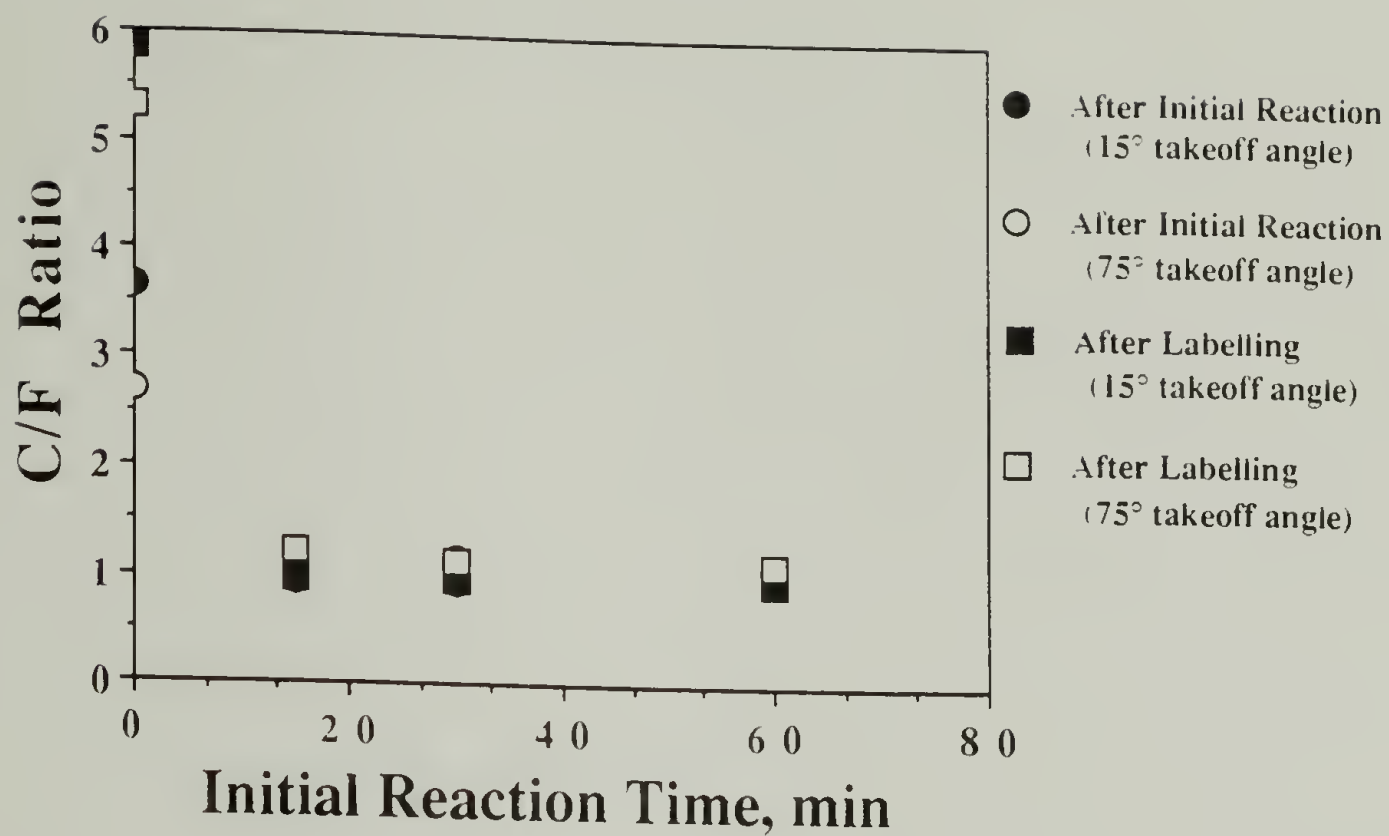


Figure 5.13. XPS results for uncatalyzed esterification kinetics with heptafluorobutyryl chloride.

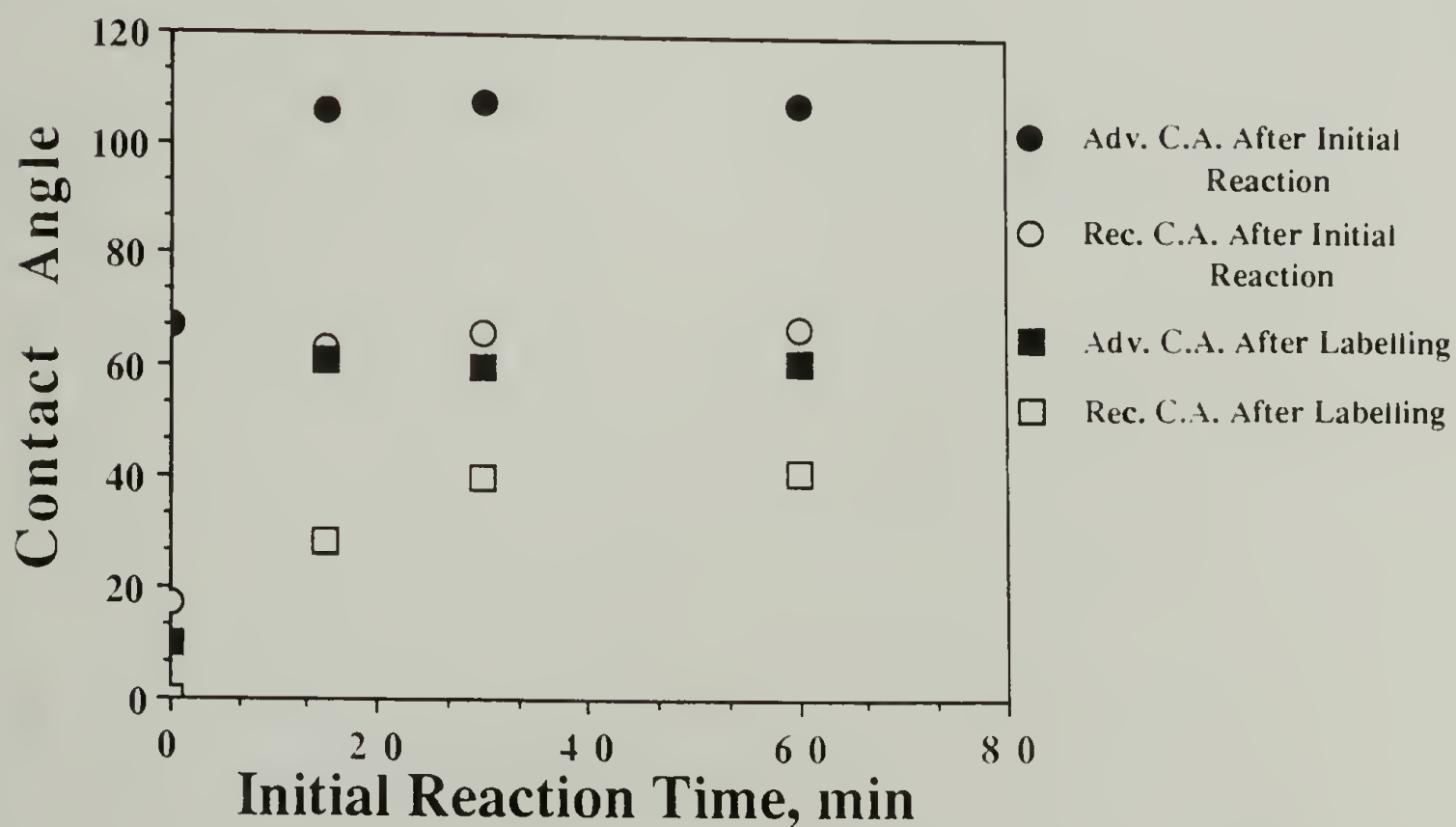
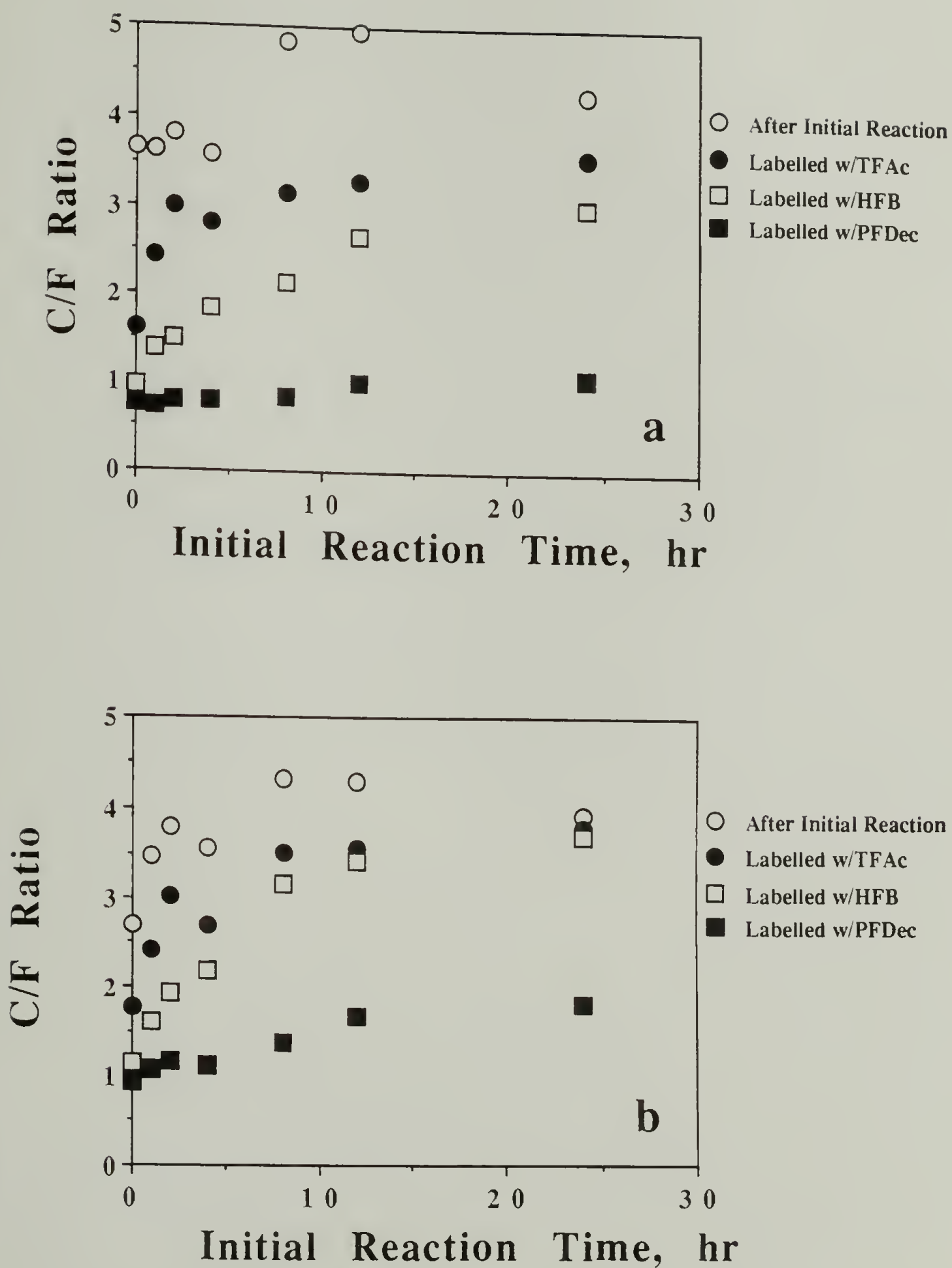


Figure 5.14. Contact angle results for uncatalyzed esterification kinetics with heptafluorobutyryl chloride. Water contact angles after initial reaction (circles) and hexadecane contact angles after labelling with butyryl chloride (squares).



Results for the uncatalyzed reaction of PCTFE-OH with butyryl chloride are shown in Figures 5.15 - 5.17. In this system, the unreacted hydroxyl groups in the PCTFE-OH/OBut surfaces were labelled with trifluoroacetic anhydride, heptafluorobutyryl chloride and perfluorodecanoyl chloride. These three reagents were chosen in order to prepare three sets of mixed hydrocarbon ester/fluorocarbon ester surfaces that contain the same relative numbers of functional groups, but vary in the size of the fluorocarbon moiety.

The XPS  $15^\circ$  and  $75^\circ$  takeoff angle data are shown in Figures 5.15a and b, respectively. The results show the expected behavior. The C/F ratios of the initially esterified and the labelled surfaces increase with the time of the initial reaction, reflecting a higher percentage of butyrate groups in the surfaces reacted for longer times. Also, the C/F ratios decrease as the number of fluorines in the labelling reagent increases. Finally, the comparatively lower C/F ratios in the  $15^\circ$  takeoff angle results (Figure 5.15a) show that the lower surface energy component (the perfluorinated group) segregates to the film/air interface<sup>8</sup> and that this effect is greatest for the  $C_9F_{19}$  ester. The  $75^\circ$  takeoff angle XPS C/F ratios of the 24 h sample after labelling with each of these reagents indicate that the yield for the initial esterification with butyryl chloride is approximately 80% which is significantly less than that of the catalyzed reaction (90%).



**Figure 5.15.** XPS results for uncatalyzed esterification kinetics with butyryl chloride. (a) 15° takeoff angle and (b) 75° takeoff angle

The water contact angle data for the initial reaction are shown in Figure 5.16. The advancing contact angle increases from  $67^\circ$  for PCTFE-OH to  $90^\circ$ , a value consistent with a surface of butyrate groups, over the first 12 h of the reaction. After the same amount of time, the receding contact angle has increased from  $17^\circ$  to  $46^\circ$  and remains at this value when the reaction time is doubled to 24 h. Since pure PCTFE-OBu has a receding water contact angle of  $54^\circ$  it can be assumed that a significant number of hydroxyl groups remain unreacted after 24 h.

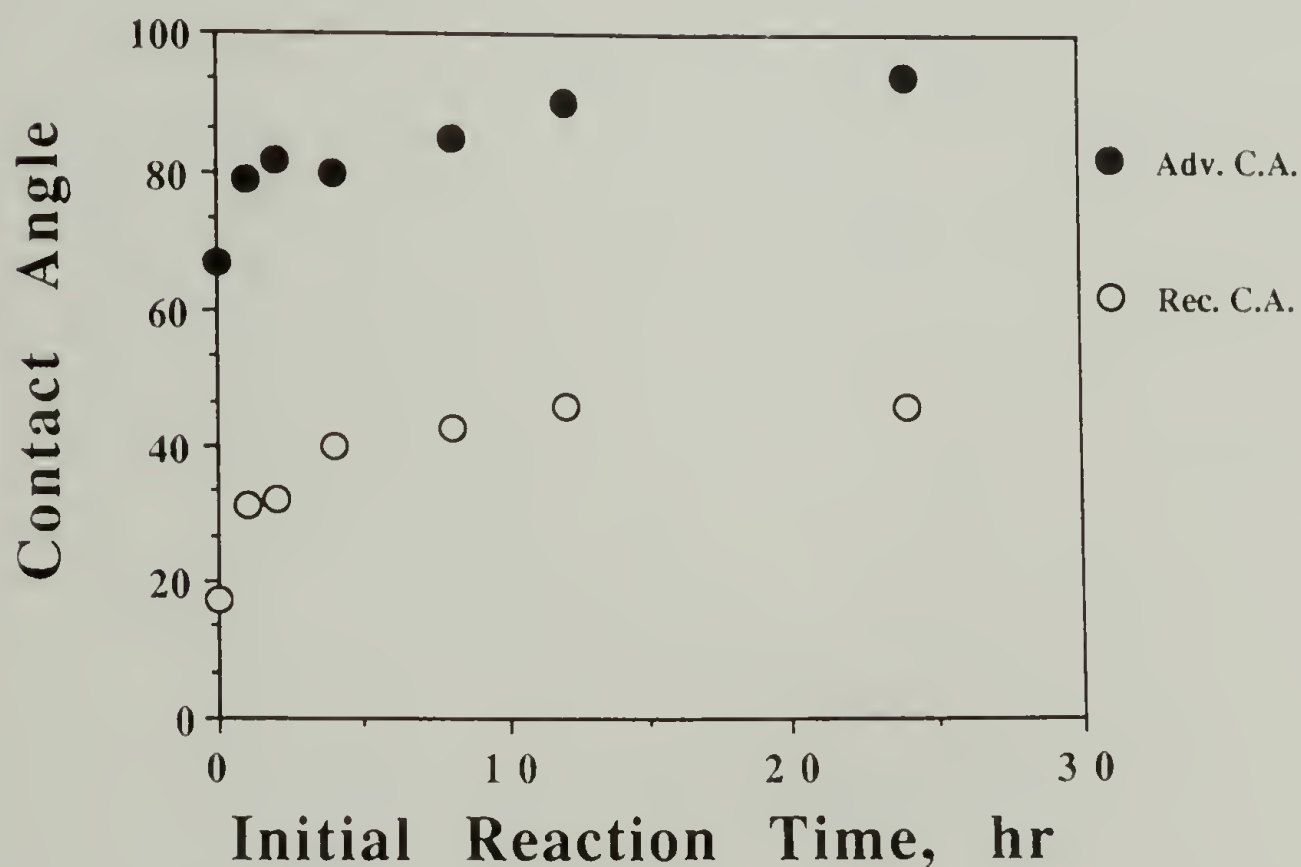


**Figure 5.16.** Water contact angle results for uncatalyzed esterification kinetics for butyryl chloride after initial reaction.



The advancing and receding hexadecane contact angles after labelling with the three perfluorinated reagents are shown in Figures 5.17a and b, respectively. As expected, the results show that the greater the amount of fluorine in the modified surface, the higher the hexadecane contact angle. These contact angle results can also be used to infer a number of interesting changes taking place in the structure of these modified surfaces. The receding contact angles of both the PCTFE-OBuT/OTFAc and PCTFE-OBuT/OHFB mixed surfaces decrease over the course of the reaction until a value ( $0^\circ$ ) consistent with a surface containing predominantly methylene units is reached. The surfaces which were labelled with trifluoroacetic anhydride reach this value sooner (8 h versus 24 h) than those labelled with heptafluorobutyryl chloride due to the lower fluorine content in the former labelling reagent. The advancing hexadecane contact angle is more sensitive to the amount of fluorocarbon in the surface and decreases more slowly for each of these mixed surfaces as the butyrate content in the surface increases. A value of  $10^\circ$ , which is consistent with that of PCTFE-OBuT is obtained for the 8 h sample which was labelled with trifluoroacetic anhydride, while the 24 h sample labelled with heptafluorobutyryl chloride is  $20^\circ$  reflecting the higher fluorine content in this surface.

As described previously,<sup>7</sup> PCTFE-OPFDec is also an oriented surface which exposes a significant fraction of trifluoromethyl groups to the film/air interface. The initial decrease (after a 1 h initial reaction) that is observed in the receding hexadecane contact angle of the mixed PCTFE-OBuT/OPFDec surface reflects partial disruption of this order. The advancing hexadecane contact angle on these

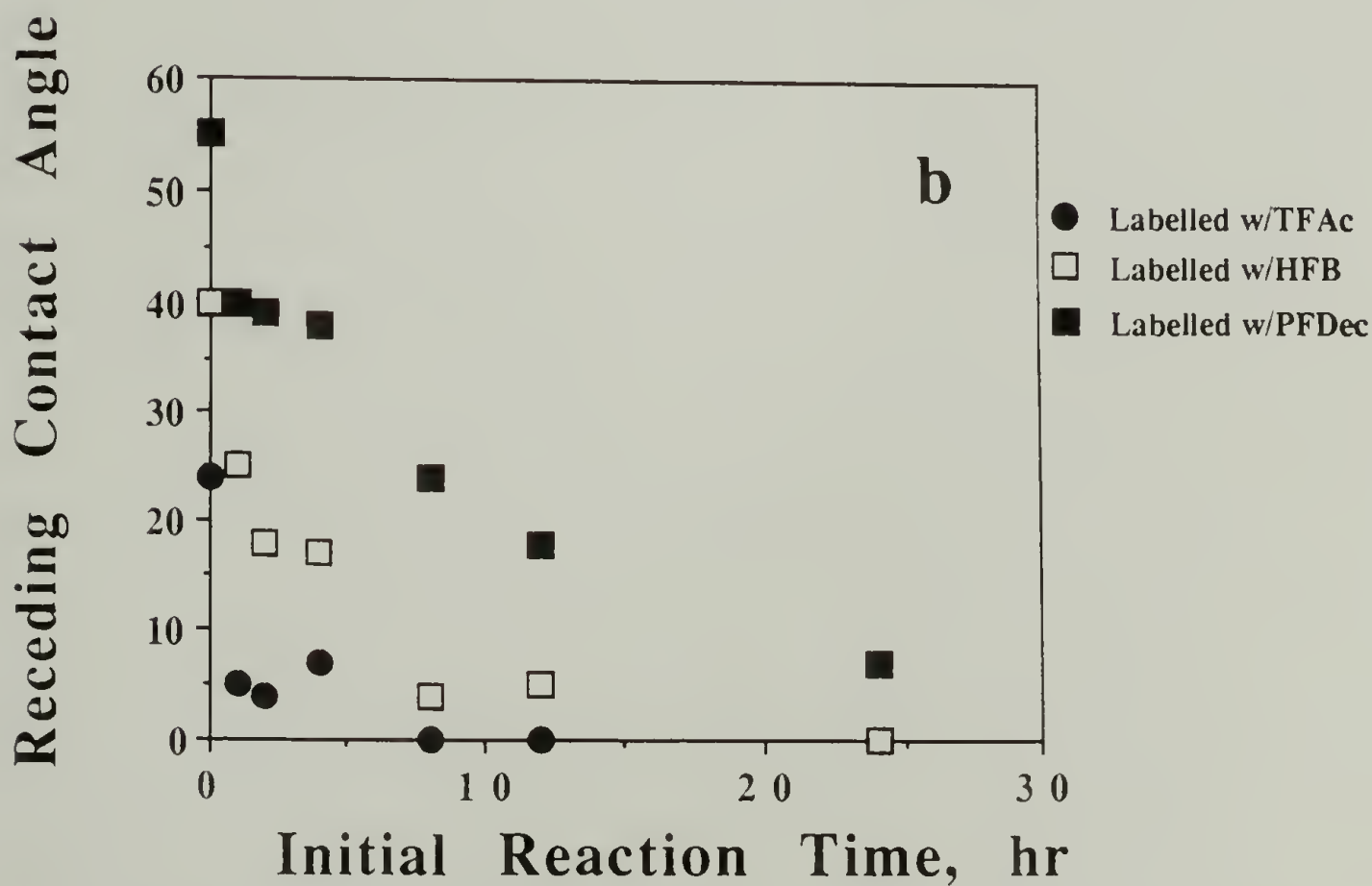
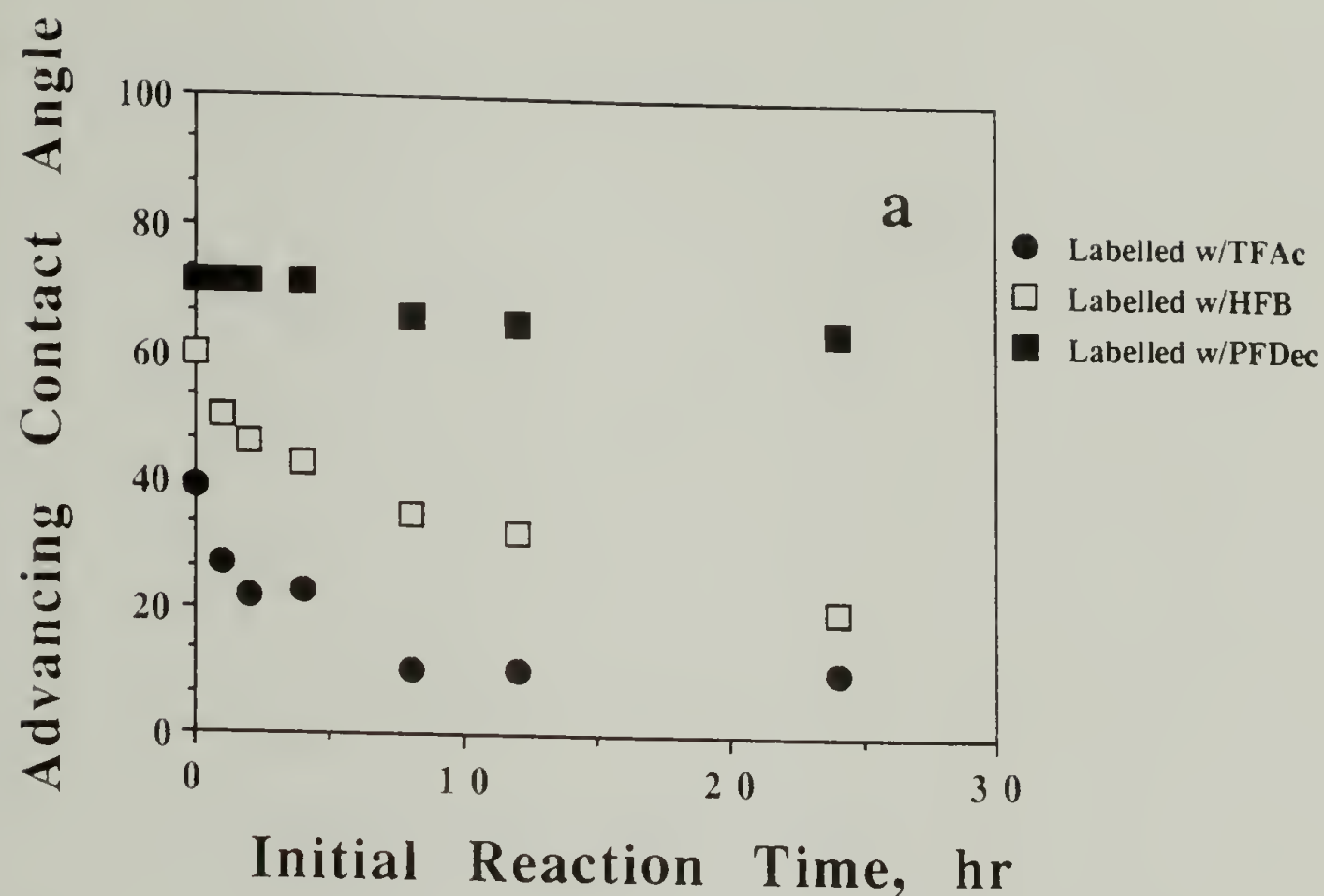
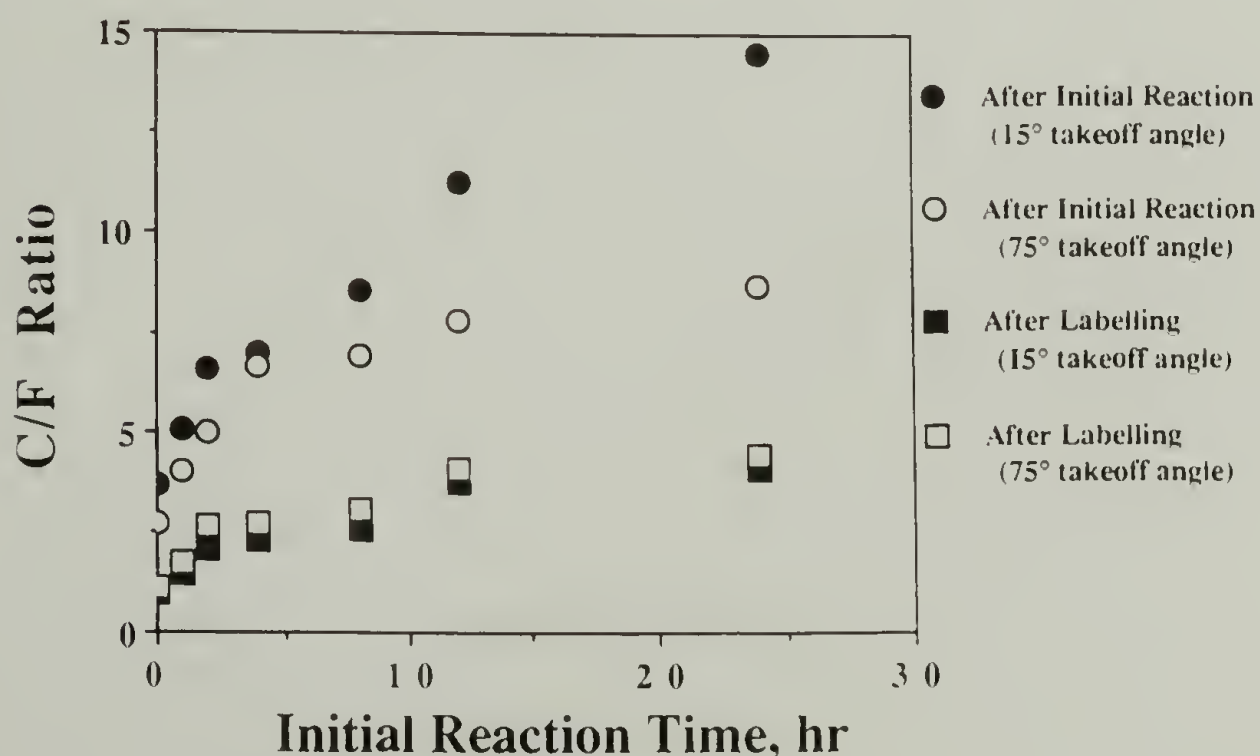


Figure 5.17. (a) Advancing and (b) receding hexadecane contact angle results for uncatalyzed esterification kinetics with butyryl chloride after labelling with perfluorinated reagents.

labelled surfaces remains constant ( $71^\circ$ ) over the first 4 h of the initial reaction indicating that most of the order is retained. Over this time the receding contact angle is consistent with a surface composed of primarily difluoromethylene groups ( $\sim 40^\circ$ ) since a significant number of the fluoroester chains remain in the surface in a random orientation. These angles decrease as the hydrocarbon content in the surface increases. After 4 h, the advancing contact angle decreases to  $66^\circ$  as the orientation is completely broken up and the surface at the film/air interface is essentially difluoromethylene. Even after 24 h, this angle is still high ( $64^\circ$ ), reflecting the high fluorocarbon content of the surface (the  $15^\circ$  takeoff angle XPS C/F ratio of this surface is 1.06).

Figures 5.18 and 5.19 illustrate the results for the reaction of PCTFE-OH with decanoyl chloride (circles) and after subsequent treatment of the initially reacted surfaces with heptafluorobutyryl chloride to label any unreacted alcohol functionality (squares).



**Figure 5.18.** XPS results for uncatalyzed esterification kinetics with decanoyl chloride.



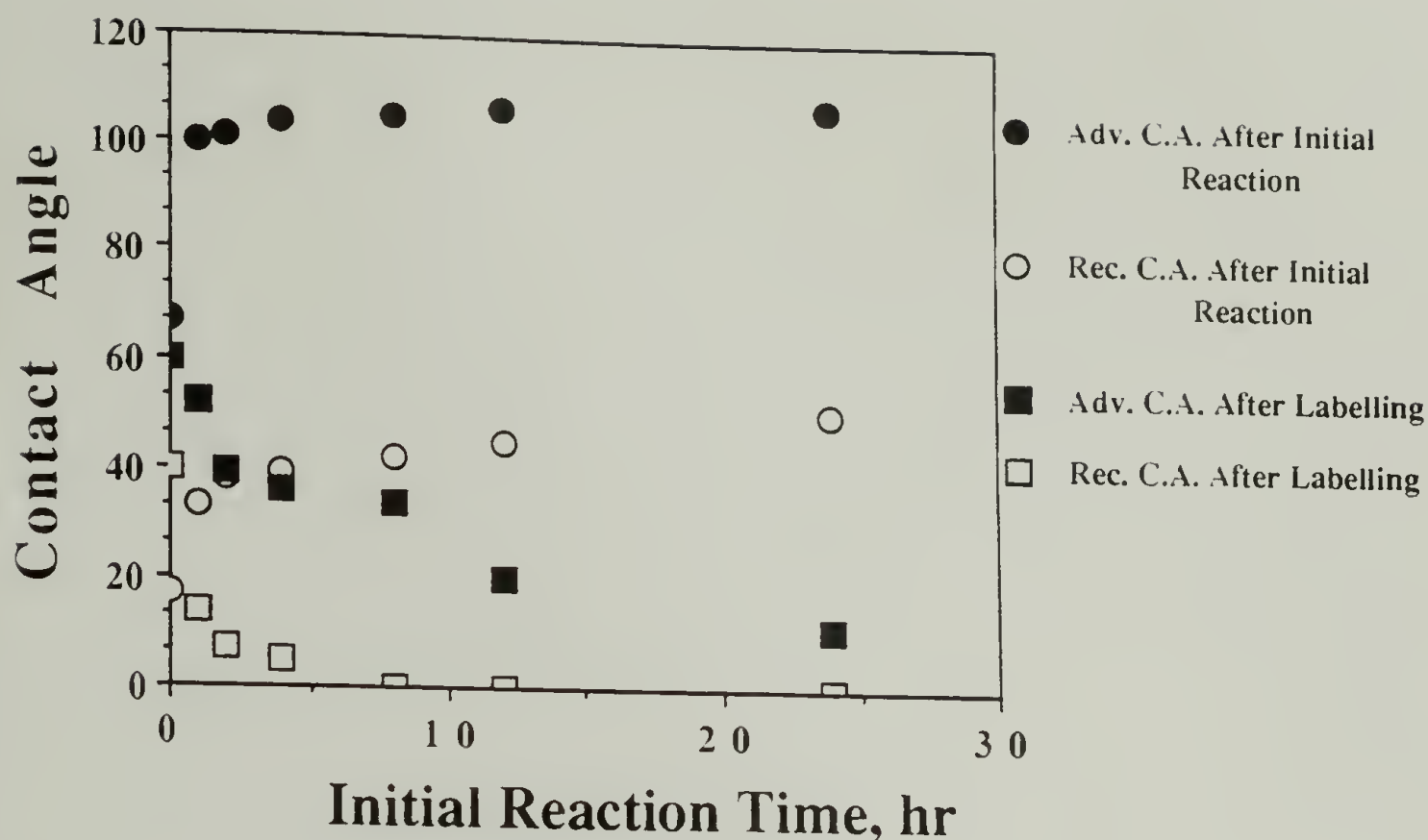


**Figure 5.19.** Contact angle results for uncatalyzed esterification kinetics with decanoyl chloride. Water contact angles after initial reaction (circles) and hexadecane contact angles after labelling with heptafluorobutyryl chloride (squares).

After 24 h, the XPS C/F ratios for the initially reacted surfaces (Figure 5.18) agree with those of PCTFE-ODec (Table 5.1, page 205) implying complete esterification. However, the receding water contact angle of this surface ( $51^\circ$ ) is slightly lower than that of PCTFE-ODec ( $58^\circ$ ) indicating unreacted hydroxyl functionality. The presence of these suspected hydroxyl groups was confirmed through labelling with heptafluorobutyryl chloride. After this second esterification, the C/F ratios of the 24 h sample decrease from 14.5&8.71 to 4.07&4.39 ( $15^\circ$ & $75^\circ$  takeoff angle values) indicating the formation of a significant number of heptafluorobutyrate esters. From this latter C/F ratio, it can be determined through Figure 5.5 (page 209) that approximately 25% of the ester groups in this surface

are heptafluorobutyrate. Thus, after 24 hours only about 75% of the hydroxyl groups in PCTFE-OH have reacted with decanoyl chloride. The advancing and receding hexadecane contact angles of the labelled samples both decrease with the time of the initial reaction as the hydrocarbon content in the surface increases.

The XPS results as a function of the initial reaction time for the uncatalyzed esterification of PCTFE-OH with stearoyl chloride and the associated labelled surfaces are shown in Figure 5.20. As in the esterifications with butyryl chloride and decanoyl chloride, these results show a relatively (compared to the catalyzed reaction) low rate of reaction and incomplete esterification even after 24 h. The XPS C/F ratios of the labelled samples indicate that after this time approximately 70% of the hydroxyl groups have been converted to stearate esters.

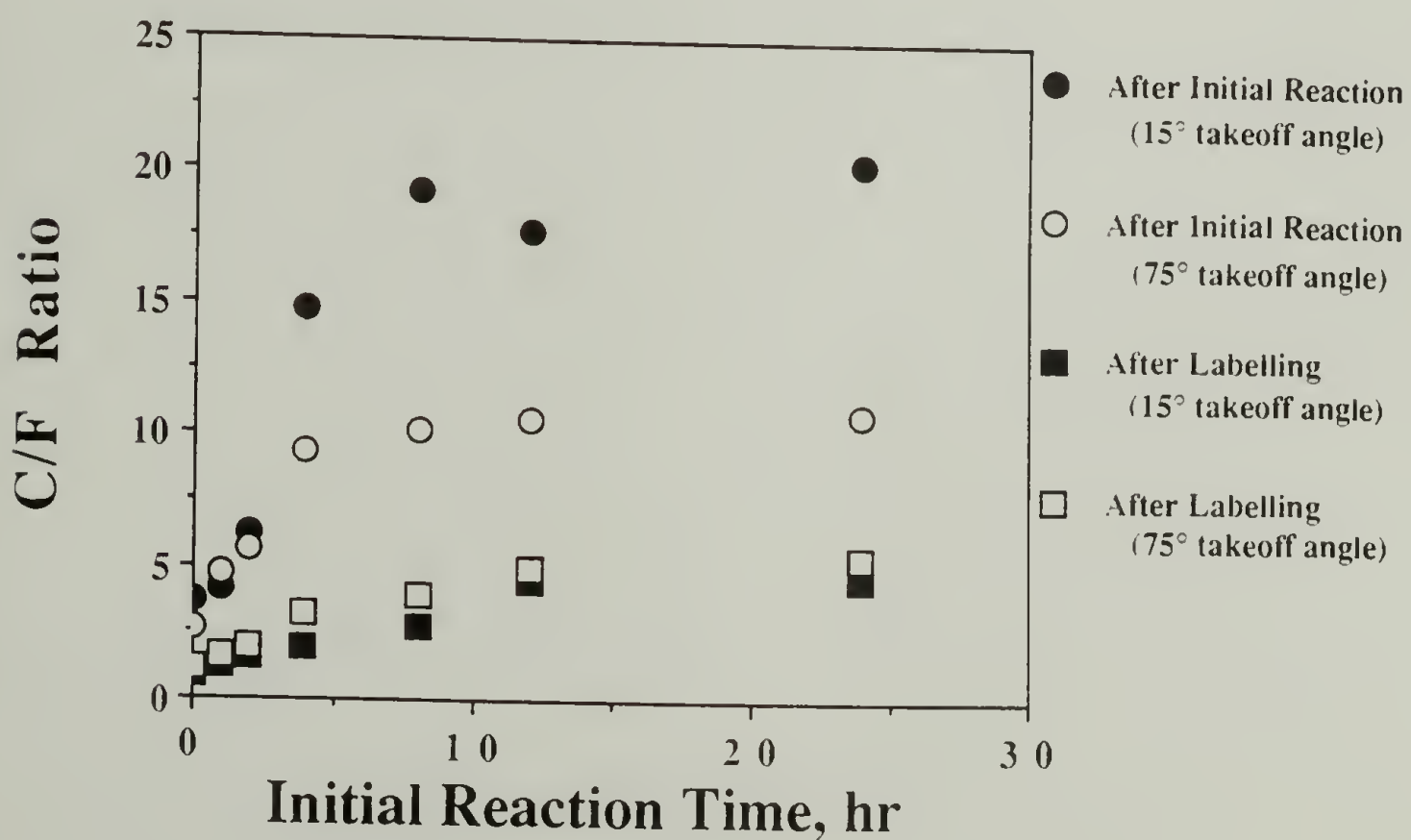


Figure 5.20. XPS results for uncatalyzed esterification kinetics with stearoyl chloride.

The water and hexadecane contact angle data for the initial stearoyl chloride esterification as a function of the reaction time are shown in Figure 5.21a. These results show a number of interesting features. After about 4 h of reaction, the advancing water contact angle, which reflects the hydrophobic functionality at the film/air interface, has increased to its maximum value ( $108^\circ$ ). On the other hand, the receding water contact angle which is more sensitive to the presence of unreacted hydroxyl groups, requires a 24 h reaction to reach its limiting value ( $90^\circ$ ). The advancing and receding hexadecane contact angles show a decrease from the initial contact angles for PCTFE-OH ( $18^\circ/6^\circ$ ) in the first hour of the reaction to  $10^\circ/0^\circ$ , followed by a gradual increase until the values of PCTFE-OSTear ( $42^\circ/35^\circ$ ) are attained. These results can be used to interpret the structure of the modified layer at different points in the reaction. In the first hour of the reaction, a relatively small number of stearate esters are formed on the surface which increases the water contact angles. The low concentration of these long chain esters makes it difficult for them to pack and orientate themselves on the surface, thus it is likely that a significant number of methylene groups are present at the film/air interface, decreasing the hexadecane contact angles. As the reaction progresses, the concentration of esters increases, as does their ability to pack together and orient themselves at the interface. The extent of this orientation is reflected by the increase in the hexadecane contact angles over the course of the reaction. The water contact angles also increase as more and more of the hydrophilic hydroxyl groups are converted to the hydrophobic esters. The difference in the rate at



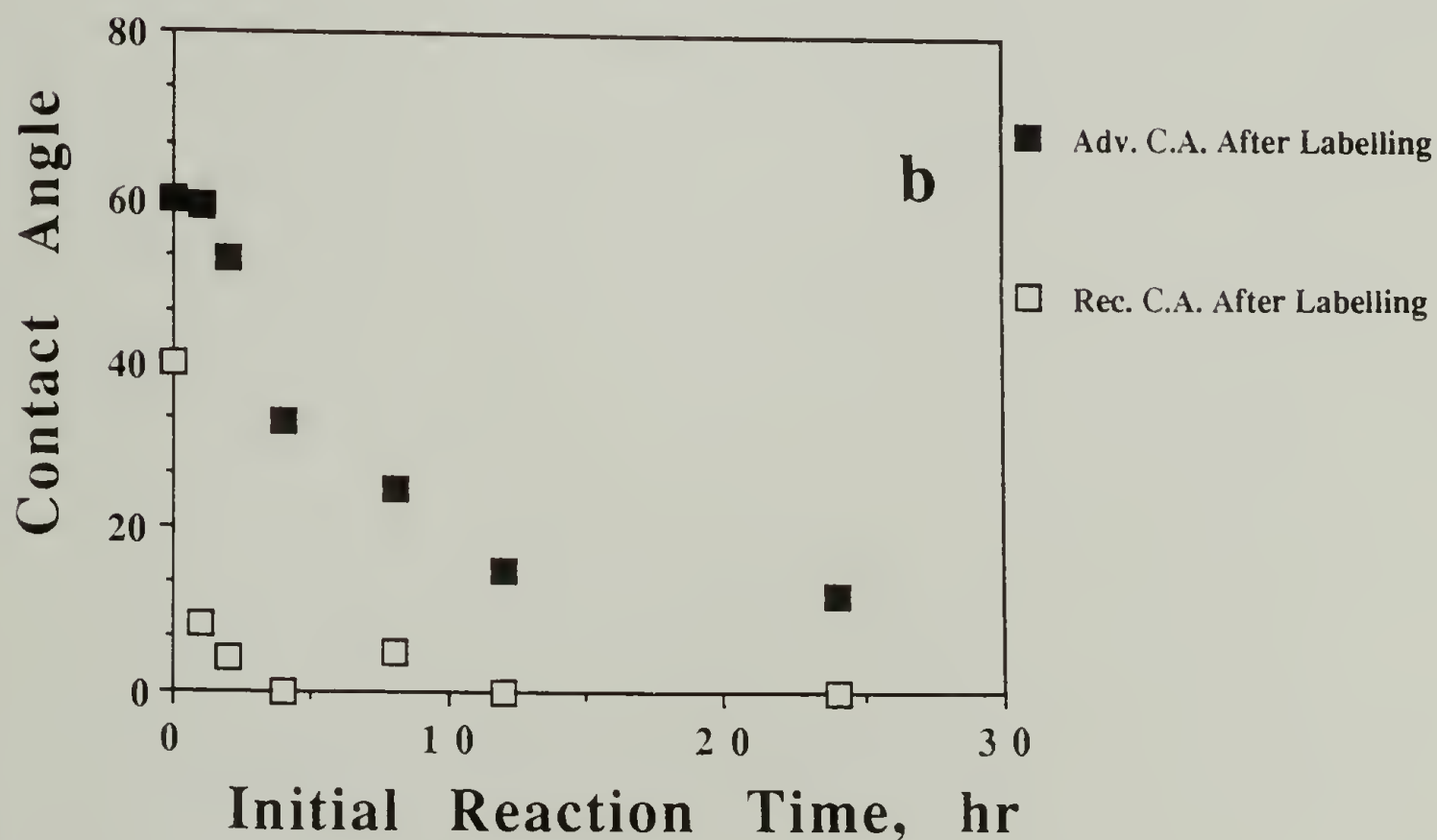
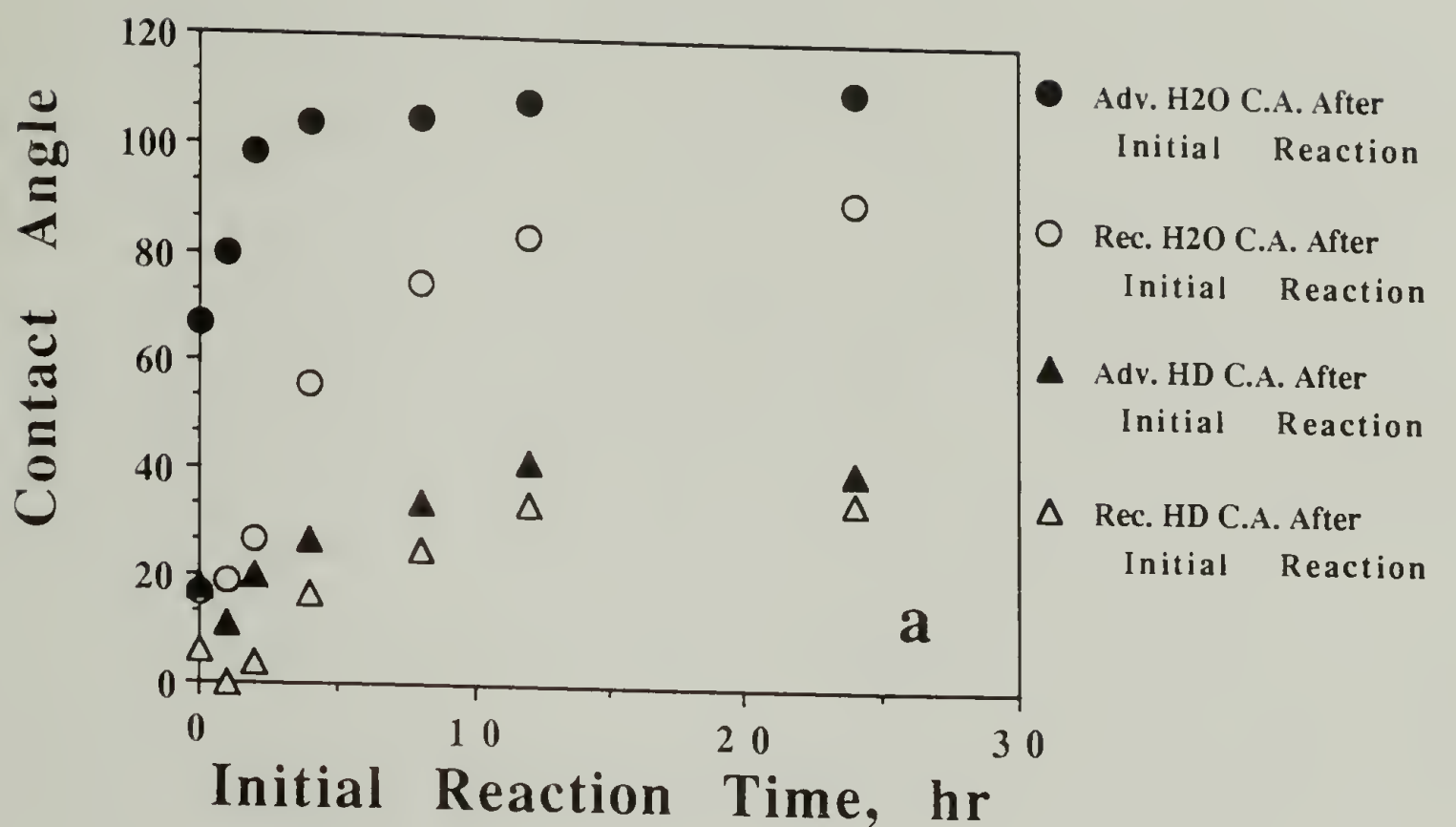


Figure 5.21. Contact angle results for uncatalyzed esterification kinetics with stearoyl chloride. (a) Water (circles) and hexadecane (triangles) contact angles after initial reaction and (b) hexadecane contact angles after labelling with heptafluorobutyryl chloride.

which the advancing and receding water contact angles reach their steady state values reflects the different structures that are probed by each measurement. As stated previously, the advancing contact angle reflects the functionality present at the film/air interface. The results show the absence of any hydrophilic functionality at this interface after 4 h of reaction. The receding contact angle is a measure the functionality present at the film/water interface and may reflect behavior resulting from water-induced surface reconstruction and/or penetration of water into the film surface. The relatively low values of the receding water contact angles for the shorter reaction times indicate that the hydroxyl groups present beneath the film/air interface are accessible to the water through one or both of these processes.

The hexadecane contact angles after labelling the PCTFE-OH/OSTear surfaces decrease as the length of the initial esterification time increases (Figure 5.21b). The advancing contact angles decrease over the course of the reaction from a value of  $60^\circ$  (for a surface containing only heptafluorobutyrate groups) to  $12^\circ$ . The receding contact angles are indicative of a surface composed of mostly methylene units, which would be expected for a disordered stearate surface. Recall that the hexadecane contact angles of the initially reacted surfaces increased with the reaction time due to ordering in the monolayer. Disruption of this ordering, caused by the heptafluorobutyrate groups that result from this reaction, accounts for this difference.

Figure 5.22 shows the reaction kinetics for the surfaces discussed in this section. The extents of reaction used in this figure

were calculated from the  $75^\circ$  takeoff angle C/F ratios of the labelled surfaces. The results show that, as expected, the uncatalyzed reactions are much slower than pyridine catalyzed acylations (compare with Figure 5.12, page 219). Also, it is observed in this figure that as the chain length of the acid chloride increases the reaction rate decreases. Finally, the perfluorinated acid chloride reacts much faster than the corresponding hydrocarbon due to an increased electrophilicity caused by the electronegative fluorines on the carbon  $\alpha$  to the carbonyl.

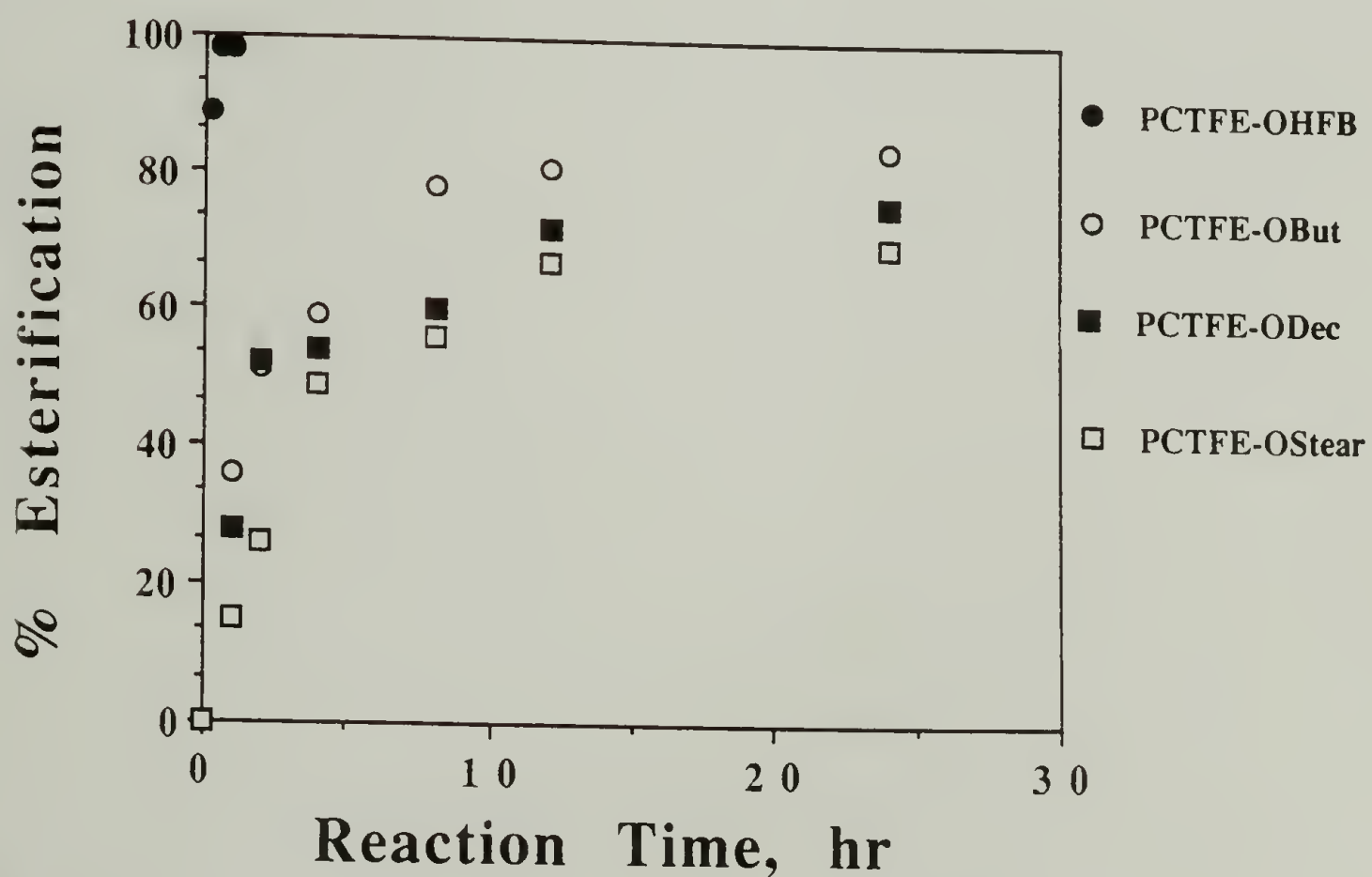


Figure 5.22. Rate of uncatalyzed esterifications of PCTFE-OH.



### Competitive esterification of heptafluorobutyryl chloride and butyryl chloride with PCTFE-OH

In an attempt to prepare mixed PCTFE-OB<sub>u</sub>t/OHFB surfaces by an alternative route, competitive esterifications of heptafluorobutyryl chloride and butyryl chloride with PCTFE-OH were conducted. The XPS C/F ratios of the resulting surfaces as a function of the solution composition used in both the catalyzed and uncatalyzed esterifications are shown in Figure 5.23 (catalyzed and uncatalyzed esterifications). These results show that even when the reacting solution is only 10% heptafluorobutyryl chloride, the surface composition is essentially 100% heptafluorobutyrate.

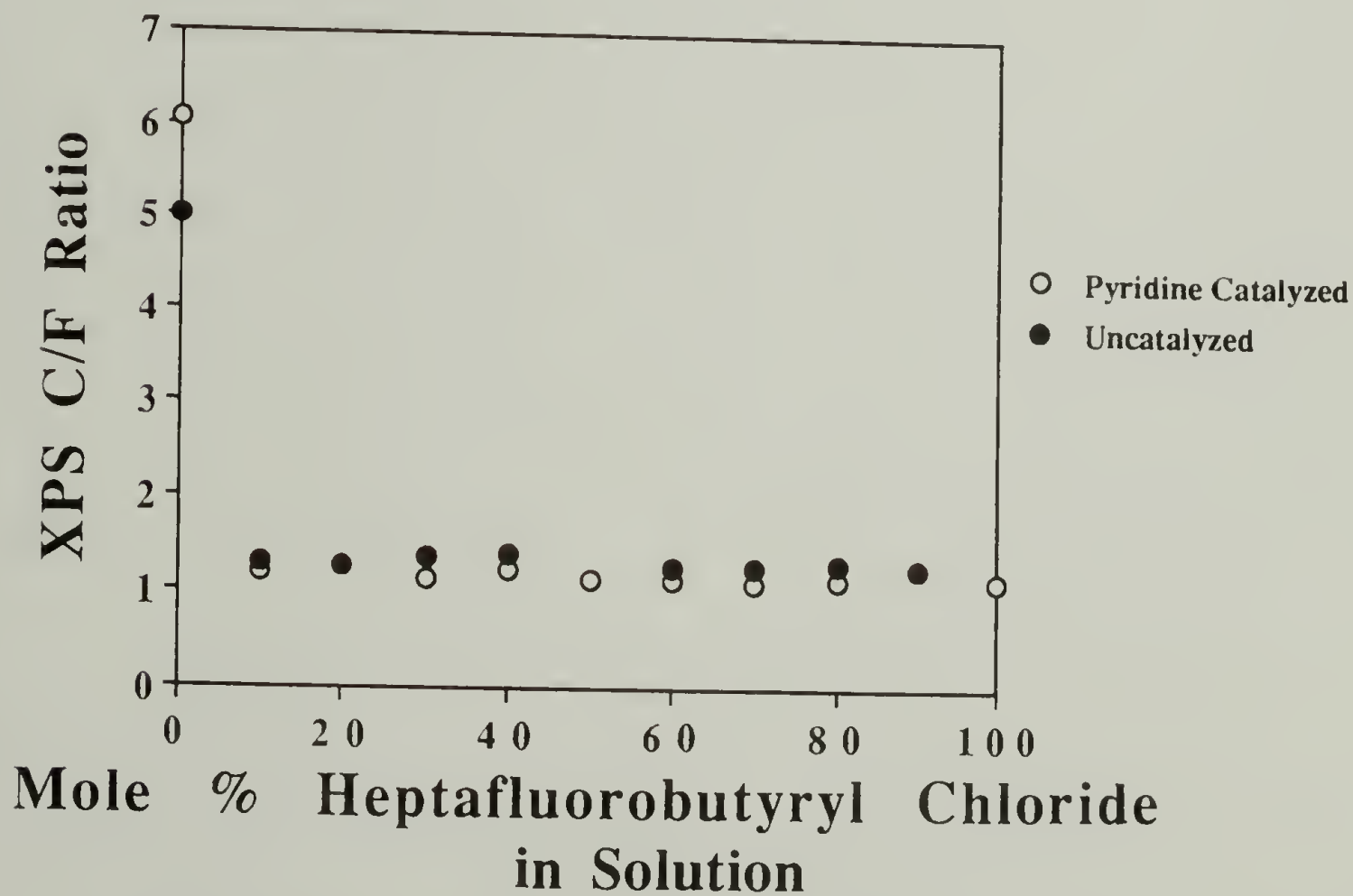


Figure 5.23. XPS results for competitive reactions of butyryl chloride and heptafluorobutyryl chloride with PCTFE-OH.

The preferential reaction of PCTFE-OH with heptafluorobutyryl chloride can be ascribed to the relatively high reactivity of the perfluorinated acid chloride over that of butyryl chloride in both the catalyzed and uncatalyzed reactions. However, contact angle results for the surface prepared from the solution containing a 1:9 ratio of heptafluorobutyryl:butyryl chloride under catalyzed conditions show that the resulting surface does contain a low concentration butyrate esters. The water, methylene iodide and hexadecane contact angles for this latter surface are  $102^{\circ}/62^{\circ}$ ,  $82^{\circ}/43^{\circ}$  and  $48^{\circ}/20^{\circ}$ , respectively. These values infer the presence of butyrate esters since they are lower than those of the other competitively prepared surfaces which all exhibit contact angles equivalent to those of PCTFE-OHFB ( $107^{\circ}/68^{\circ}$ ,  $88^{\circ}/62^{\circ}$  and  $60^{\circ}/40^{\circ}$ , respectively). This result indicates that under catalyzed conditions the reactivities of the two acid chlorides are more equivalent and butyryl chloride can begin to compete with heptafluorobutyryl chloride for the hydroxyl groups in the surface. However, the reactivity of the perfluorinated acid chloride is still much greater than that of butyryl chloride. If this method is to be used for the preparation of mixed surfaces it will likely be necessary to use very low concentrations of heptafluorobutyryl chloride or selectively catalyze the butyrate esterification.

#### Kinetics of the Hydrolysis/Methanolysis of PCTFE-Esters

The hydrolysis/methanolysis of the PCTFE-Esters (PCTFE-OHFB, PCTFE-OBu, PCTFE-ODec and PCTFE-Stear) was used as a second method of controllably preparing heterogeneous surfaces. The goal

of this portion of the research is to study the kinetics of ester hydrolysis at the film/solution interface. The methods used here for determining the reaction kinetics are the same as those used for the sequential esterifications: an initial reaction (the hydrolysis) to form a mixed alcohol/ester surface followed by esterification of the hydroxyl groups with either heptafluorobutyryl chloride or butyryl chloride to produce mixed hydrocarbon ester/fluorocarbon ester surfaces. The effects of four variables on the rate of hydrolysis were studied: (1) acid vs. base catalysis, (2) solvent composition (methanol:water), (3) fluorocarbon vs. hydrocarbon esters and (4) ester chain length. The latter three variables were specifically chosen to investigate how the ability of the solvent to wet the film surface affects the rate of the hydrolysis. Methanol is a less polar solvent than water and as such, interacts more favorably with the film surface (Table 5.2), which should increase the reaction rate. The hydrolysis of the fluorocarbon ester surfaces might be expected to be slower than the hydrocarbon ester surfaces since the former are not wet as well by the reaction solvents as are the latter (Table 5.2). However, the electron-withdrawing ability of the fluorines on the carbon  $\alpha$  to the carbonyl of the ester makes this carbonyl more electrophilic which will increase the rate of hydrolysis. The measured rate will depend on which of these effects dominate. Finally, based on their relative wettabilities, it is expected that the longer chain esters will be hydrolyzed more slowly in a given solvent than the short chain esters.



**Table 5.2.** Contact angles ( $\Theta_A/\Theta_R$ ) of the basic hydrolysis solutions on the modified PCTFE surfaces.

<u>Solution</u>	<u>PCTFE-OBut</u>	<u>PCTFE-ODec</u>	<u>PCTFE-OStear</u>	<u>PCTFE-OHFB</u>	<u>PCTFE-OPFDec</u>
100:0 <sup>a</sup>	23/0	30/0	47/28	30/0	61/0
75:25 <sup>a</sup>	26/0	61/10	n.a.	66/0	91/3
50:50 <sup>a</sup>	39/0	76/30	n.a.	82/0	103/4
25:75 <sup>a</sup>	56/4	93/39	n.a.	95/4	114/9
0:100 <sup>a</sup>	78/11	109/47	111/86	108/15	125/16
H <sub>2</sub> O <sup>b</sup>	89/54	106/57	108/90	107/68	120/69

n.a. - not available

a - methanol:water

b - Contact angles measured with pure water (no base) from Table 5.1.

Besides the expected decrease in the contact angles with an increase in the methanol content of the hydrolysis solution, the contact angles in Table 5.2 also exhibit some interesting behavior in their hysteresis. The results discussed below for the base catalyzed hydrolyses of these surfaces show that the reactivity of the surface decreases in the order: PCTFE-OHFB > PCTFE-OPFDec > PCTFE-OBut >>> PCTFE-ODec > PCTFE-OStear. The contact angles of a 0.25 M aqueous solution of KOH (0:100 solution in Table 5.2) on these surfaces reflect this reactivity trend. The contact angles measured with the basic solution on the surfaces which hydrolyze relatively fast (PCTFE-OHFB, PCTFE-OPFDec and PCTFE-OBut) show substantial hysteresis and much lower receding contact angles than when the measurement is made with neutral water. This result shows that during the time of the measurement (~1 min) some hydrolysis of these surfaces has

likely occurred. This hydrolysis introduces polar hydroxyl groups into the surface and carboxylate surfactants into the probe fluid. Both of these factors contribute to the low receding contact angles. In contrast, the two surfaces which hydrolyze more slowly (PCTFE-ODec and PCTFE-OSTear) exhibit similar contact angle hysteresis with both basic and neutral probe fluids indicating little hydrolysis.

Acid Catalyzed Methanolysis. The acid catalyzed methanolysis of PCTFE-OHFB, PCTFE-OBuT, PCTFE-ODec and PCTFE-OSTear was attempted using *p*-toluenesulfonic acid as a catalyst in methanol at 105 °C for 24 h. The results are presented in Table 5.3 and show that only PCTFE-OBuT is completely hydrolyzed under these conditions. The low water contact angles on this surface indicate the formation of a hydrophilic surface and agree with those of PCTFE-OH (Table 5.1, page 205). After labelling with heptafluorobutyryl chloride, the XPS C/F ratios and the hexadecane contact angles are comparable to those of PCTFE-OHFB, which implies that few or no butyrate esters remain in this surface after the hydrolysis. The high chlorine concentration observed in the XPS spectrum is evidence of dissolution of the alcohol functionalized surface<sup>11</sup> formed during the methanolysis and accounts for the relatively low C/F ratios in the initially reacted surface (compare to those of PCTFE-OH in Table 5.1).

The other three surfaces were barely affected under these conditions (likely due to the inability of the solution to wet and diffuse into the surface). The contact angles on the heptafluorobutyrate surface after hydrolysis and after labelling with butyryl chloride are only slightly lower than those of unreacted PCTFE-OHFB which implies little hydrolysis. The C/F ratios of this

**Table 5.3.** XPS and contact angle results for the acid catalyzed methanolysis of the modified PCTFE surfaces.

<u>Surface</u>	<u>After Initial Reaction</u>			<u>After Labelling</u>	
	$\Theta_T$	<u>C/F ratio</u>	H <sub>2</sub> O $\Theta_A/\Theta_R$	<u>C/F ratio</u>	HD $\Theta_A/\Theta_R$
PCTFE-OHFB	15	1.11	100/61	1.21	62/23
	75	1.22		1.36	
PCTFE-OB <sub>ut</sub>	15	2.16	71/14	1.05	63/35
	75	2.13		1.20	
PCTFE-OD <sub>ec</sub>	15	10.0	108/26	1.58	55/0
	75	6.94		2.31	
PCTFE-OS <sub>tear</sub>	15	18.2	111/81	5.20	26/0
	75	11.0		6.19	

surface after hydrolysis and after labelling indicate that only about 20% of the esters were removed in the hydrolysis. For the decanoate surface, the receding water contact angle after hydrolysis has decreased significantly, but the advancing contact angle is unchanged. After labelling with heptafluorobutyryl chloride, the hexadecane contact angles also show large hysteresis. These results are due to incomplete hydrolysis resulting in heterogeneous PCTFE-OH/OD<sub>ec</sub> and PCTFE-OD<sub>ec</sub>/OHFB surfaces, respectively. The yield of this hydrolysis was determined to be approximately 50% using the XPS C/F ratios of the labelled sample. The results for the stearate surface indicate the least amount of hydrolysis for the hydrocarbon



esters. The receding water contact angle after hydrolysis has decreased only slightly. The low hexadecane contact angles ( $26^{\circ}/0^{\circ}$ ) after labelling indicate little heptafluorobutyrate functionality, but do show that the order in the modified layer has been disrupted. The yield of this hydrolysis is estimated at only 30%.

Among the reaction solvents chosen for this study, pure methanol should result in the fastest reaction since it provides for the lowest interfacial free energy. The results for the reactions discussed above show that when using acid catalysis the methanolysis is very slow. Thus, these conditions are impractical as a method of preparing heterogeneous surfaces and acid catalysis was abandoned.

Base Catalyzed Hydrolysis/Methanolysis. The kinetics of the base catalyzed hydrolysis/methanolysis of PCTFE-OHFB, PCTFE-OB<sub>u</sub>t, PCTFE-OD<sub>e</sub>c and PCTFE-OS<sub>t</sub>ear (also PCTFE-OPF<sub>D</sub>ec to a limited extent) were investigated with 0.025 M solutions of potassium hydroxide in methanol:H<sub>2</sub>O (100:0, 75:25, 50:50, 25:75 or 0:100 v/v) at 105 °C. The results of these studies show that in most cases the rates of hydrolysis can be conveniently studied and some interesting behavior has been observed.

In contrast to the acid catalyzed reactions, the base catalyzed hydrolyses of PCTFE-OHFB at 105 °C are very fast. For all of the solvent conditions studied, the reaction is essentially complete in less than 15 min.<sup>12</sup> After this time, the water contact angles have decreased from  $108^{\circ}/67^{\circ}$  (PCTFE-OHFB) to values comparable to PCTFE-OH ( $67^{\circ}/17^{\circ}$ ). After labelling the 100:0, 75:25 and 50:50

(methanol:water) 15 min hydrolyzed surfaces with butyryl chloride, the low hexadecane contact angles of  $10^{\circ}/0^{\circ}$  reflect surfaces containing only butyrate functionality which is the expected result if all of the heptafluorobutyrate groups were removed in the hydrolysis. The hexadecane contact angles after labelling the 25:75 and 0:100 hydrolyzed surfaces with butyryl chloride are  $23^{\circ}/9^{\circ}$  and  $24^{\circ}/12^{\circ}$ , respectively. This result indicates a low concentration of heptafluorobutyrate groups remaining on these two surfaces. After 30 min, hexadecane contact angles of  $10^{\circ}/0^{\circ}$  show that the remaining perfluorinated esters have reacted in each of these two solvent compositions. The slightly lower rate of hydrolysis in these latter two solvent compositions is a result of the decrease in the ability of the solvent to penetrate into the surface as the water content increases.

Since the hydrolysis under these conditions is so fast (even when the reaction solvent is entirely water), control of the surface composition is difficult. In an attempt to lower the reaction rate, the effect of decreasing the reaction temperature was studied for 15 min reactions conducted in water (no methanol). Figures 5.24 and 5.25 contain XPS and contact angle data plotted as a function of reaction temperature. As expected, the results show that as the temperature is decreased, the amount of hydrolysis decreases. However, the rate is still substantial, even at  $30^{\circ}\text{C}$  where nearly 40% of the heptafluorobutyrate groups have been removed in these 15 min hydrolyses.

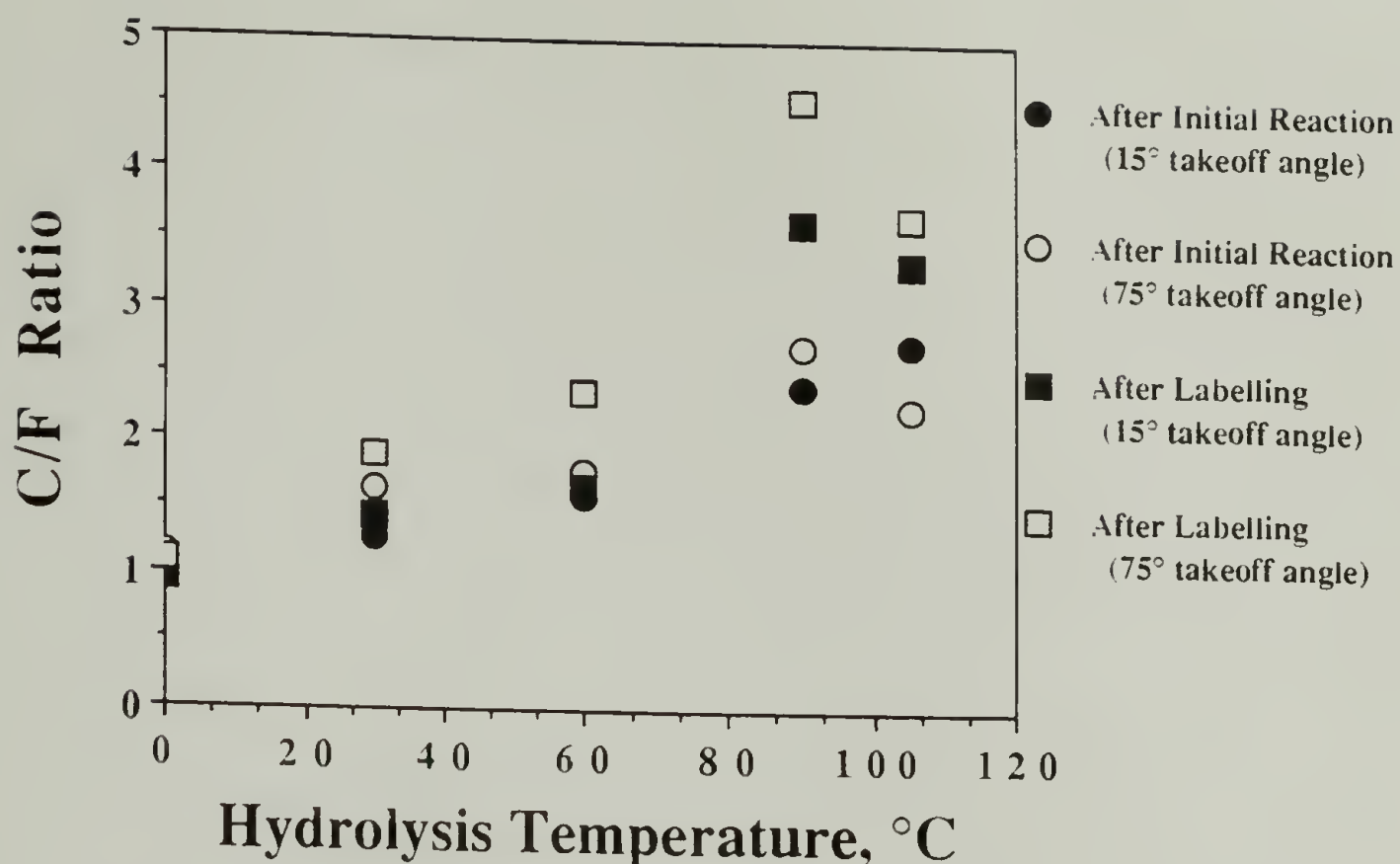


Figure 5.24. XPS results for base catalyzed aqueous hydrolysis of PCTFE-OHFB as a function of temperature (The points at 0 represent no reaction not 0 °C.)

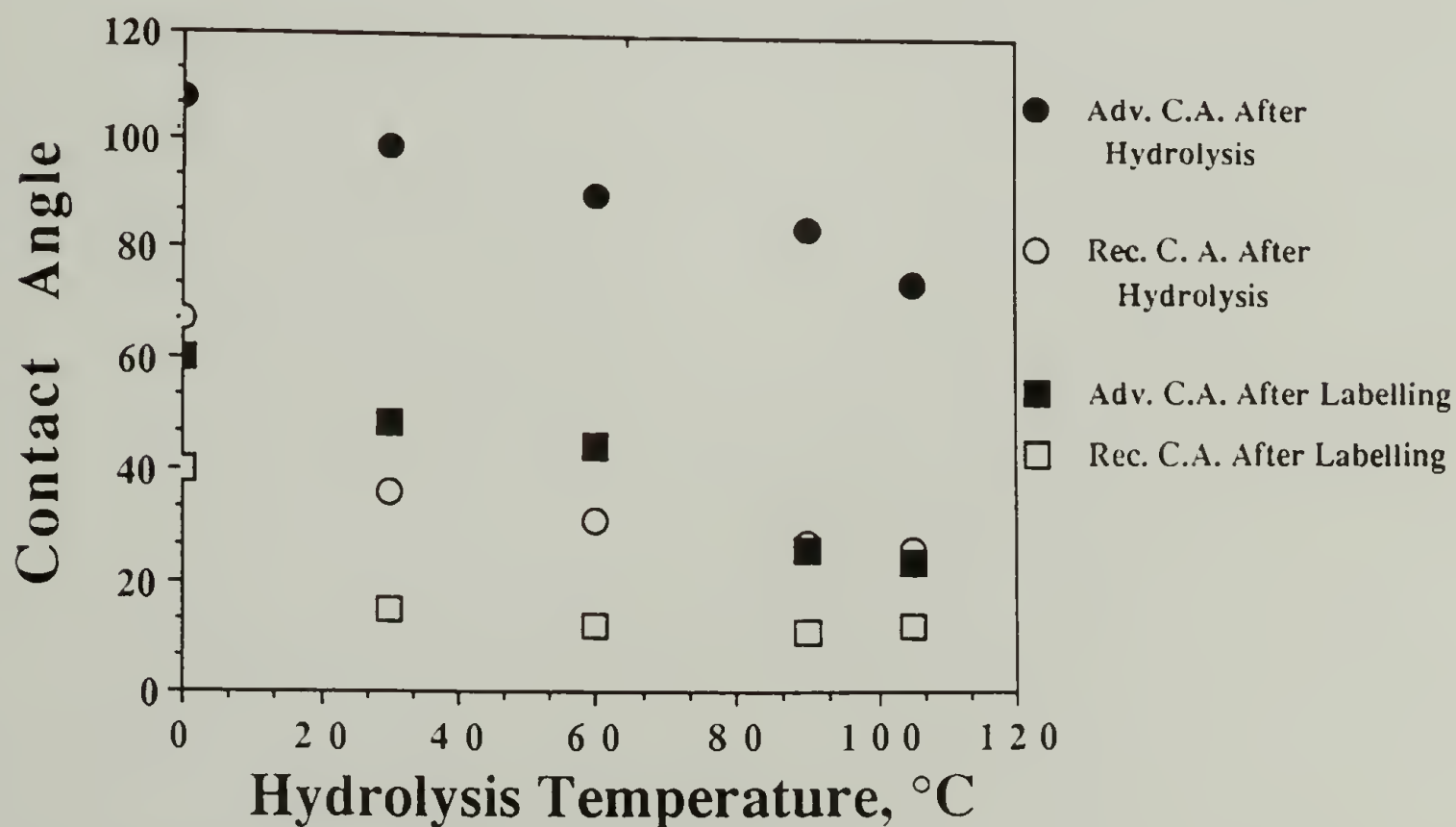


Figure 5.25. Contact angle results for base catalyzed aqueous hydrolysis of PCTFE-OHFB as a function of temperature (The points at 0 represent no reaction not 0 °C.). Water contact angles after initial reaction (circles) and hexadecane contact angles after labelling with butyryl chloride (squares).



Base catalyzed hydrolyses of PCTFE-OPFDec were conducted for 3 h in 100:0 and 0:100 methanol:water in order to roughly ascertain the reactivity of this surface. The results in pure methanol show that after the methanolysis the XPS C/F ratios have increased from 0.74&0.92 to 2.65&2.40,<sup>13</sup> while the water contact angles have decreased from 120°/69° to 71°/17°. These changes indicate that the hydrolysis has proceeded in high yield after 3 h. In the all aqueous hydrolysis, the C/F ratios after the reaction are 2.39&2.59<sup>13</sup> and the contact angles have decreased to 83°/16°, indicating that only some of the perfluoroesters remain in the surface at this point. As expected, the hydrolysis of this surface is significantly slower than that of PCTFE-OHFB due to the longer length of the ester chain increasing the interfacial free energy at the film/solution interface. However, this rapid hydrolysis does illustrate that even though this surface is initially not wet by the reacting solution, the high electrophilicity of the carbonyl group enhances the reaction rate (compare with the hydrolyses of PCTFE-ODec below).

In comparison to the fluorocarbon esters, the hydrocarbon esters hydrolyze much more slowly. Similar to PCTFE-OHFB, the hydrolyses of PCTFE-OBu<sub>t</sub> conducted in 100:0, 75:25 and 50:50 methanol:water solutions are essentially complete in the first 15 minutes of the reaction.<sup>12</sup> However, the hydrolysis of PCTFE-OBu<sub>t</sub> is considerably slower (10 h) when the solvent ratio is changed to 25:75 (methanol:water) and slower still (24 h) when the reaction is done in pure water. The results for these latter two solvent compositions are discussed below.

When the hydrolysis solution is 25% methanol the XPS results (Figure 5.26), both before and after labelling the resulting alcohols with heptafluorobutyryl chloride, show a large decrease in the C/F ratios in the first 2 h of the reaction. These results indicate that the hydroxyl group content of the surface has changed from ~10% to ~60% during this time. Over the next 8 h of the hydrolysis (10 h total reaction), the yield of the hydrolysis (as indicated by the C/F ratios of the labelled samples) increases to 78%. The behavior in the water and hexadecane contact angles reflect these kinetics.

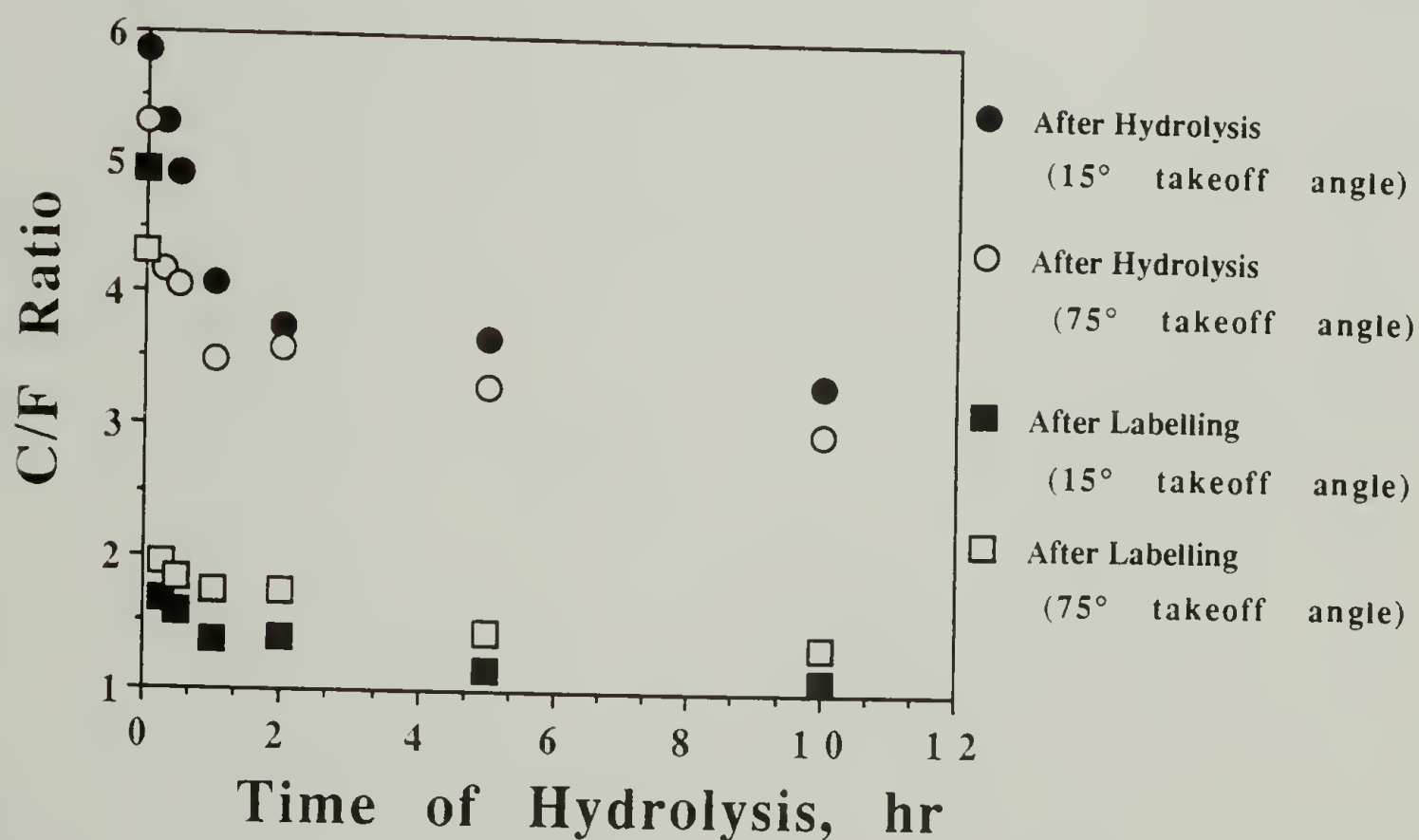
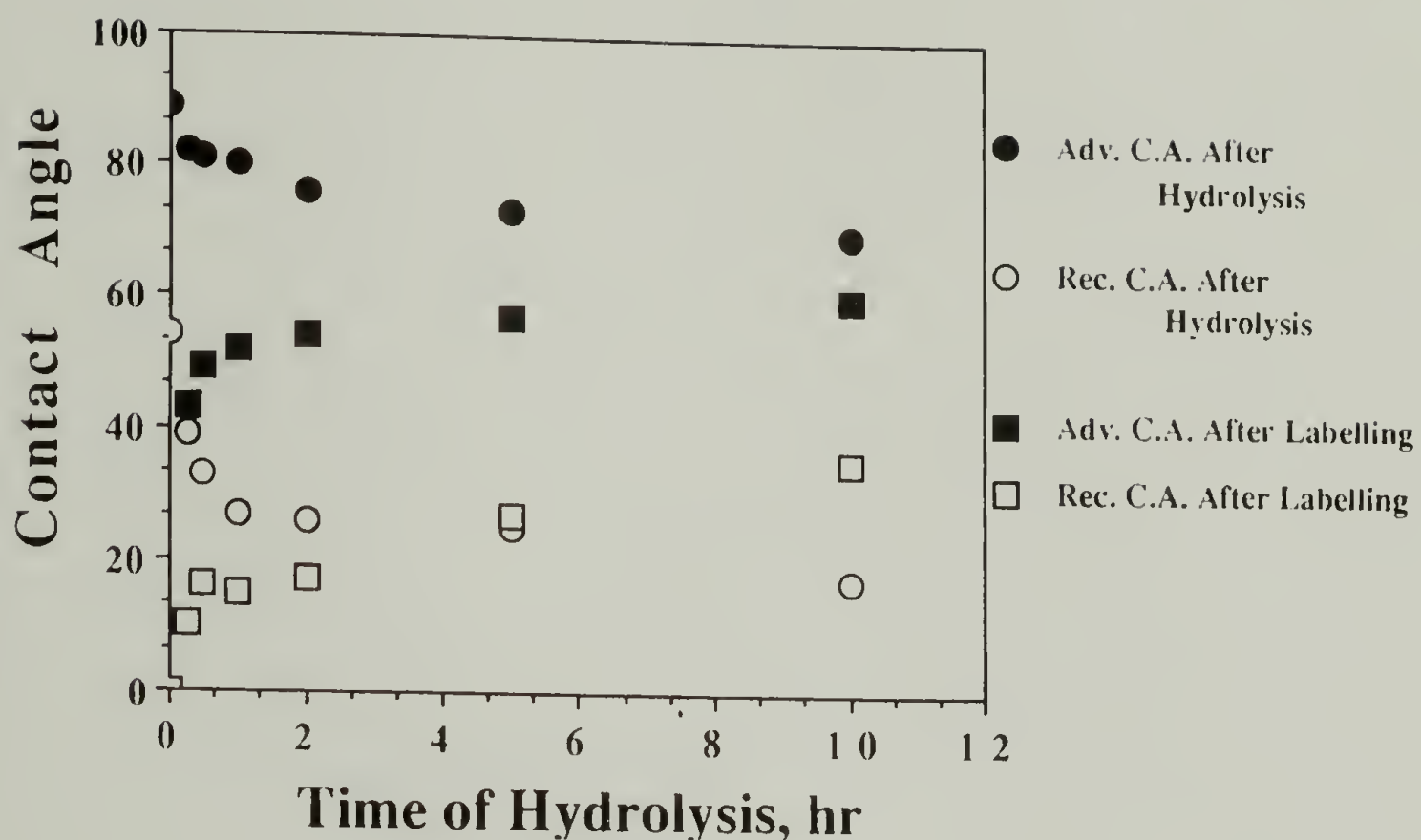


Figure 5.26. XPS results for the base catalyzed hydrolysis of PCTFE-OBuT (25:75 methanol:water).



**Figure 5.27.** Contact angle results for the base catalyzed hydrolysis of PCTFE-OBuT (25:75 methanol:water). Water contact angles after hydrolysis (circles) and hexadecane contact angles after labelling with heptafluorobutyryl chloride (squares).

During the first 2 h of the hydrolysis the receding water angles (Figure 5.27) decrease dramatically as the number of hydroxyl groups in the surface increases. Upon esterification of these hydroxyl groups with heptafluorobutyryl chloride, a corresponding rapid increase in the advancing hexadecane contact angles over the



same time period is observed. The advancing water and receding hexadecane contact angles are both sensitive to the presence of the butyrate groups in the surface and both change gradually over the course of the reaction. The low value of the receding hexadecane contact angle after labelling the sample which was hydrolyzed for 10 h ( $35^\circ$  versus  $40^\circ$  for a surface containing only heptafluorobutyrate functionality) agrees with the XPS results in showing that butyrate groups remain in the surface after this time.

For the pure aqueous hydrolysis of PCTFE-OBu the results are similar to those discussed above only the changes take place over a longer reaction time. The XPS C/F ratios (Figure 5.28) decrease over the course of the reaction and indicate that after 24 h, approximately 64% of the functional groups in the modified layer are alcohols. The receding water contact angles (Figure 5.29) after the hydrolysis and the advancing hexadecane contact angles after labelling, both change dramatically in the first 5 h of the hydrolysis, easily detecting the relatively few ( $\sim 30\%$ ) hydroxyl and heptafluorobutyrate groups present, respectively. As stated above, the advancing water contact angle and the receding hexadecane contact angle reflect the butyrate functionality in the surface and as such, change more gradually throughout the hydrolysis. Once again, the low hexadecane contact angle ( $19^\circ$ ) agrees with the XPS results in indicating that butyrate functionality remains on the surface even after a 24 h hydrolysis.

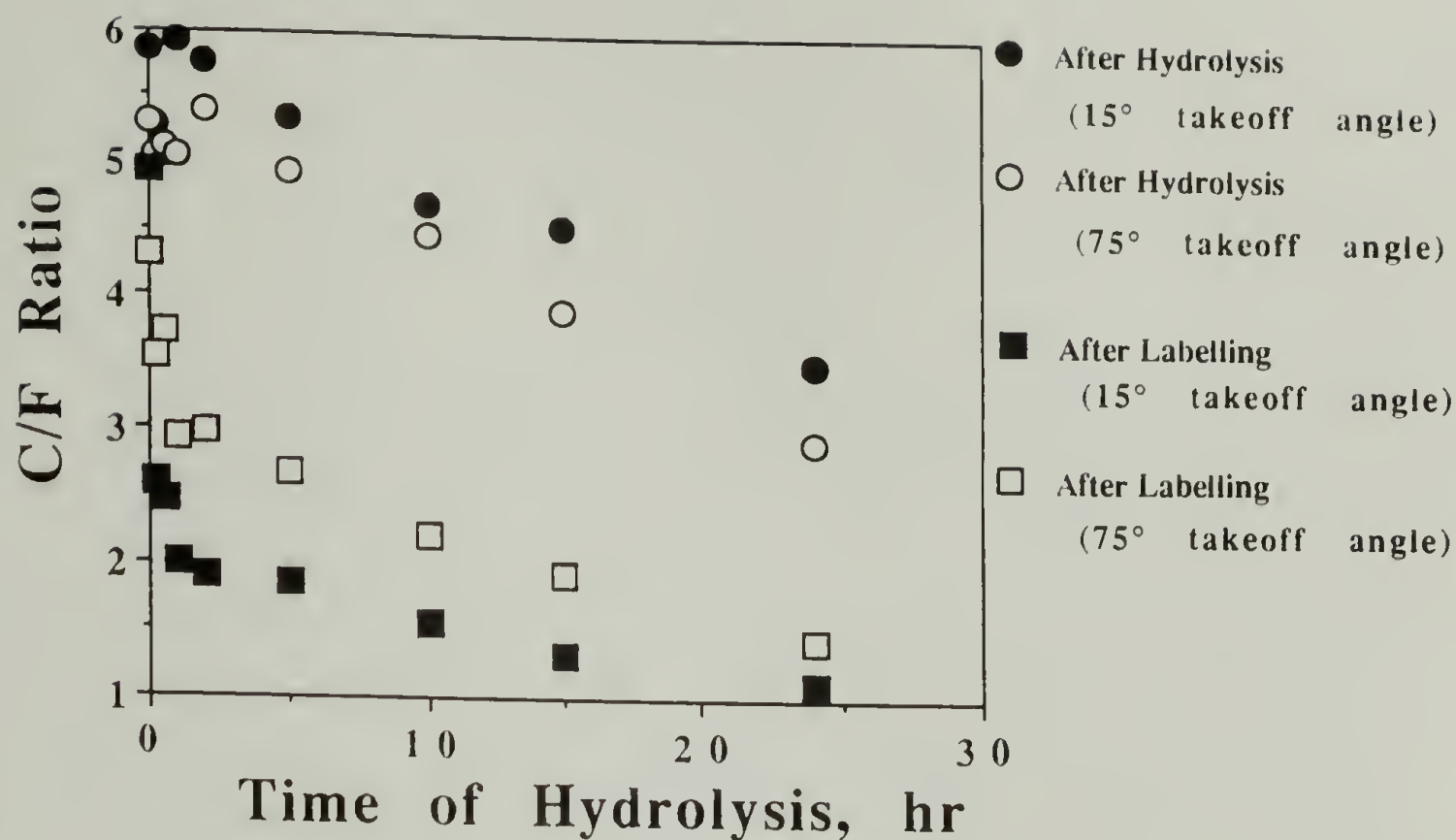


Figure 5.28. XPS results for the base catalyzed hydrolysis of PCTFE-OBuT (0:100 methanol:water).

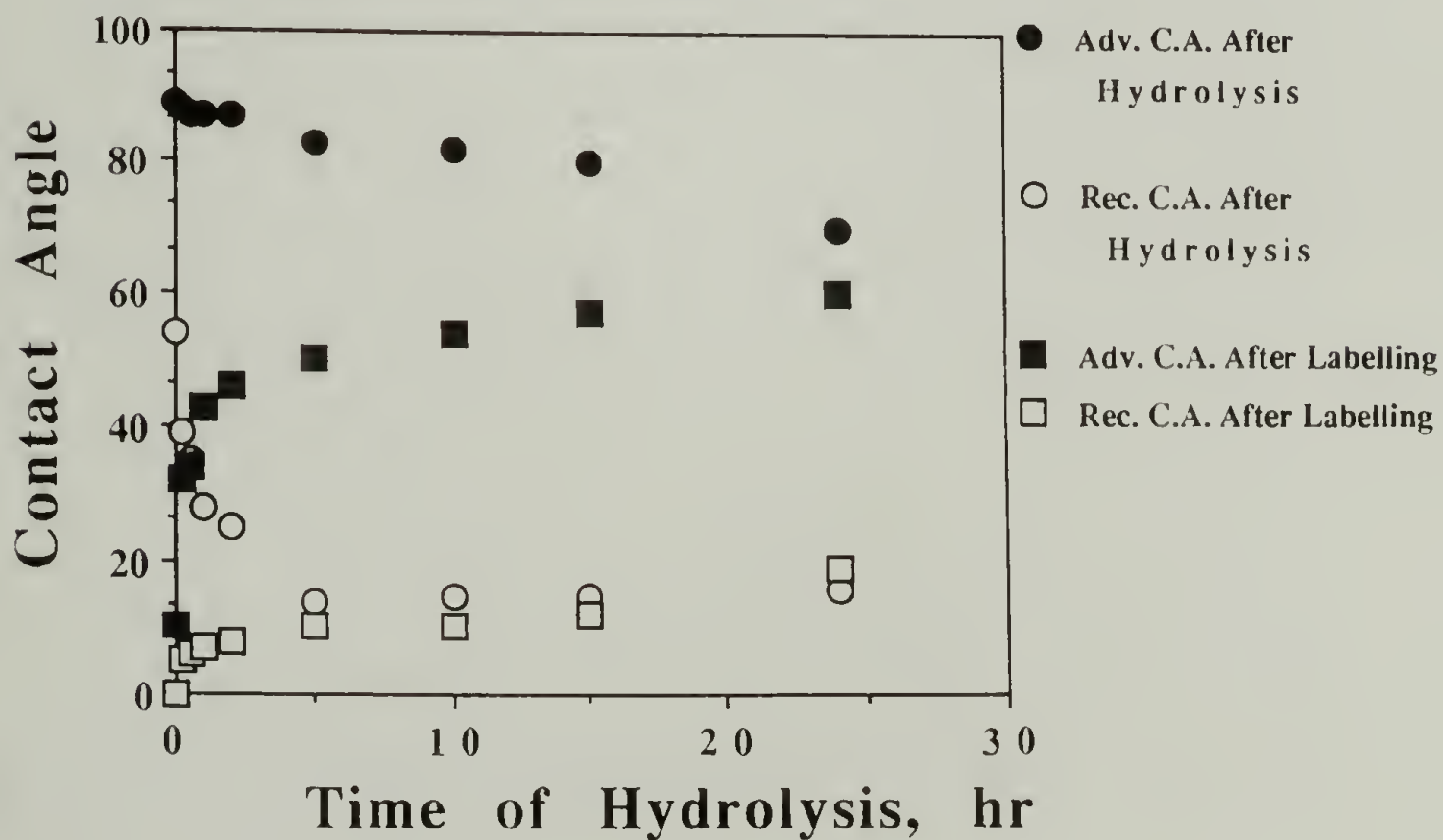


Figure 5.29. Contact angle results for the base catalyzed hydrolysis of PCTFE-OBuT (0:100 methanol:water). Water contact angles after hydrolysis (circles) and hexadecane contact angles after labelling with heptafluorobutyryl chloride (squares).

Increasing the length of the ester tail to that of PCTFE-ODec sufficiently slows the rate of hydrolysis so that the reaction conducted in pure methanol can be easily monitored. Recall that the hydrolysis of PCTFE-OBu was complete in 15 min under these conditions. The data for this methanolysis and the subsequent labelling of the resulting hydroxyl groups are displayed in Figures 5.30 and 5.31. In the first 30 min of the methanolysis, a slight decrease in the XPS C/F ratios indicates that a relatively small percentage (~30%, as calculated from the C/F ratios after labelling) of the decanoate groups have been removed. Once the modified layer contains a significant number of hydroxyl groups, the wettability of the surface is enhanced and the rate of methanolysis accelerates. Thus, in the next 15 min of the reaction, the concentration of the hydroxyl groups in the modified layer increases dramatically to 77%

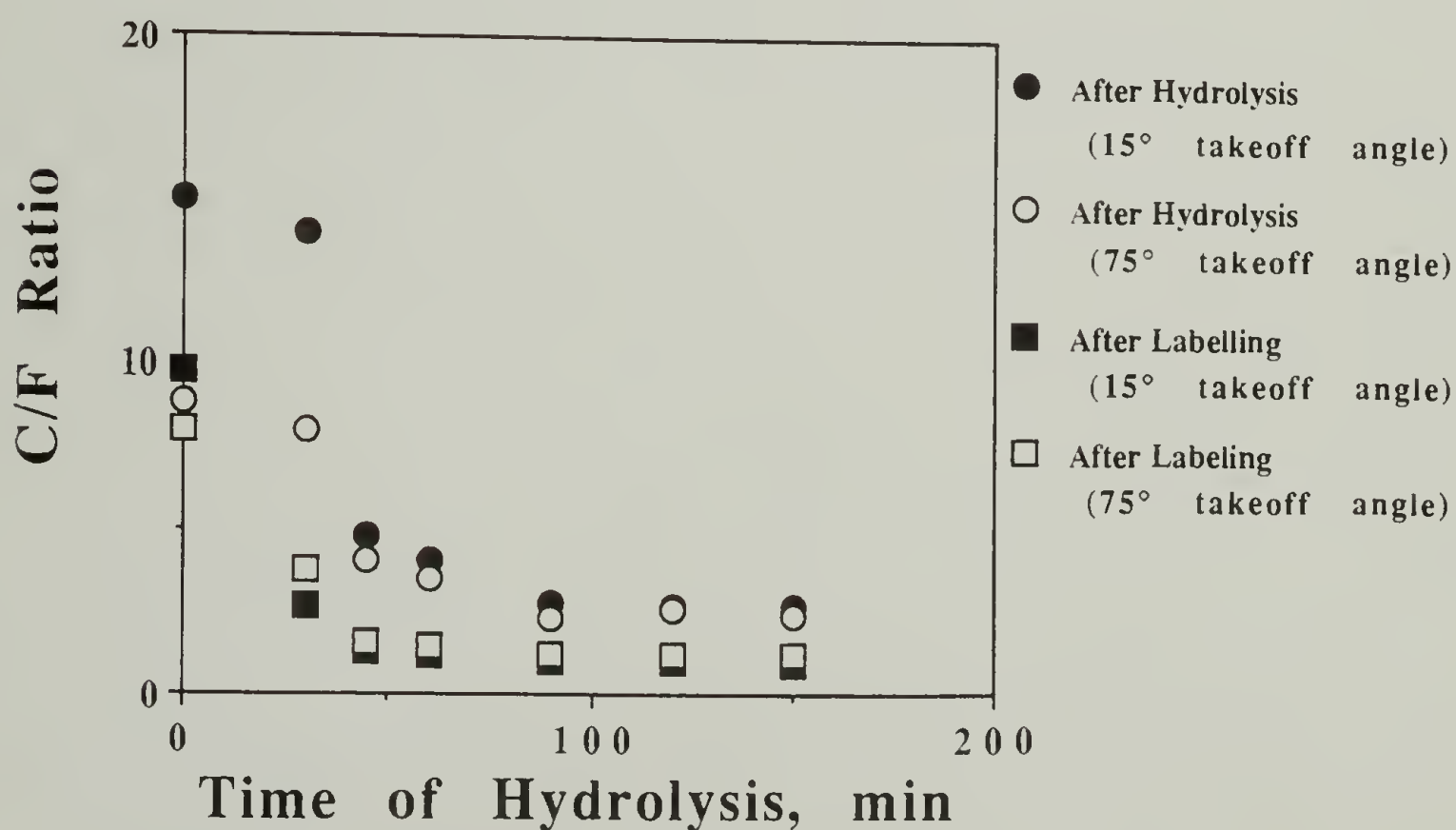
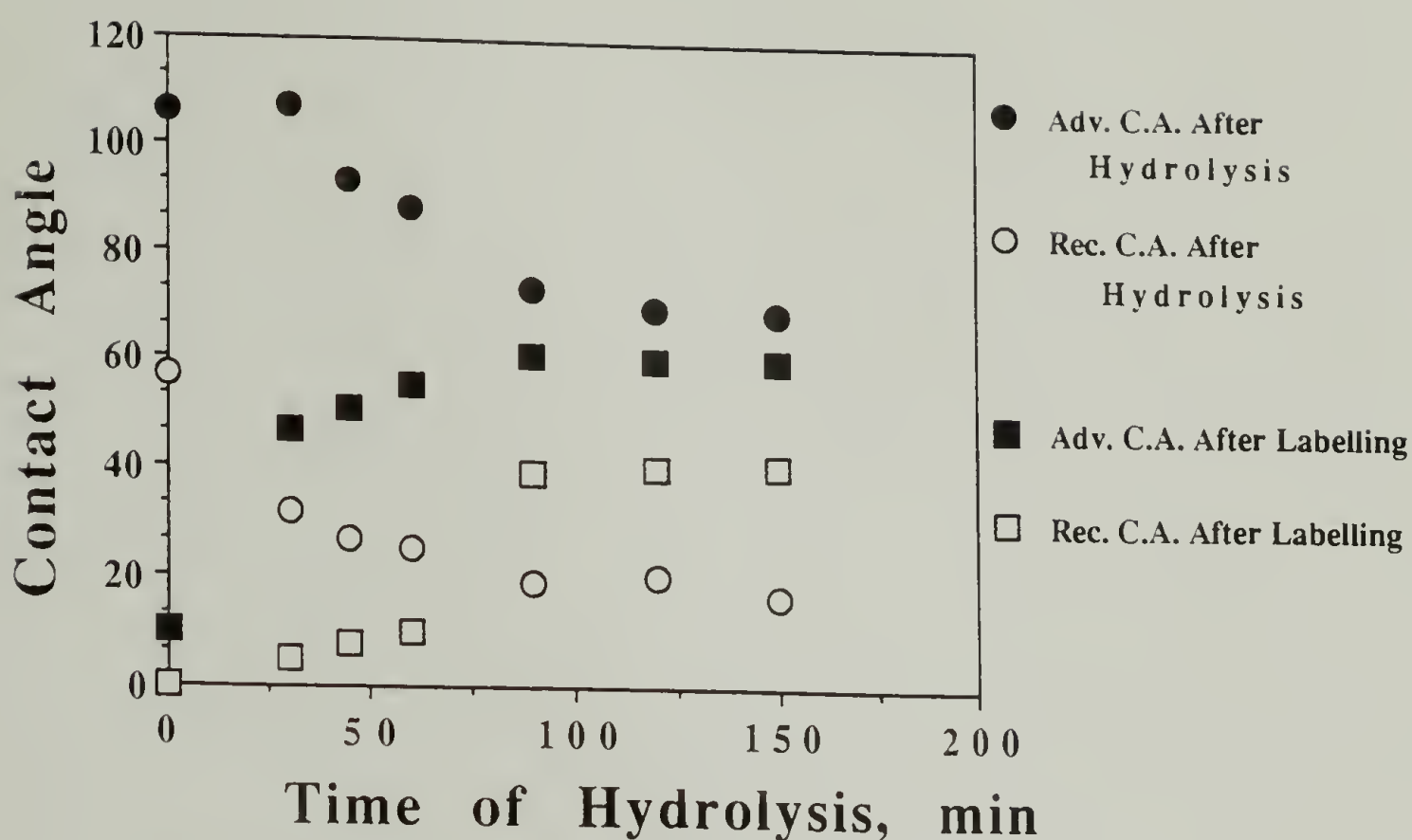


Figure 5.30. XPS results for the base catalyzed hydrolysis of PCTFE-ODec (100:0 methanol:water).





**Figure 5.31.** Contact angle results for the base catalyzed hydrolysis of PCTFE-ODec (100:0 methanol:water). Water contact angles after hydrolysis (circles) and hexadecane contact angles after labelling with heptafluorobutyryl chloride (squares).

as indicated by the rapid decrease in the C/F ratios. After this time, the rate of reaction decreases as the number of decanoate esters in the surface is depleted. The reaction is complete (96% hydrolyzed) after 90 min. The contact angle results (Figure 5.31) also reflect these changes in the surface structure. In the first 30 min, the advancing water contact angle of the hydrolyzed surface and the receding hexadecane contact angle after labelling this surface change only slightly indicating that most of the functional groups in this surface are still decanoate esters. After this point, the advancing water contact angles gradually decrease until values ( $\sim 70^\circ$ ) consistent with the structure of PCTFE-OH are obtained. The receding

hexadecane contact angle is particularly sensitive to the amount of methylene functionality in the surface and remains low for the first hour of the reaction. This angle then rapidly increases from  $10^\circ$  to  $39^\circ$  in the next 30 min as the surface composition changes from 81% to 96% heptafluorobutyrate. These results agree with those obtained from XPS in showing that the hydrolysis is complete after 90 min. In contrast, the receding water contact angle and the advancing hexadecane contact angle after labelling show large changes (from  $57^\circ$  to  $32^\circ$  and from  $10^\circ$  to  $47^\circ$ , respectively) in the first 30 min of the hydrolysis as the first few hydroxyl and heptafluorobutyrate groups begin to appear in the surface. These contact angles then slowly change until the values of PCTFE-OH ( $17^\circ$ ) and PCTFE-OHFB ( $60^\circ$ ) are obtained after a 90 min reaction.

The XPS and contact angle results for the hydrolysis of PCTFE-ODec in 75:25 methanol:water are shown in Figures 5.32 and 5.33, respectively. The data show that by introducing water into the system the resulting increase in the interfacial free energy decreases the ability of the reacting solution to penetrate into the surface which is observed as a reduction in the rate of the reaction. In the first 2 h of the hydrolysis, the concentration of the hydroxyl groups in the surface increases from 7% to 42%, based on the XPS C/F ratios of the labelled samples. During this time, the C/F ratios and the advancing water contact angles of the hydrolyzed samples and the receding hexadecane contact angles of the labelled samples show no significant changes, indicating that the modified layer is still essentially hydrocarbon. However, the dramatic decrease in the receding water contact angles of the hydrolyzed samples does reflect

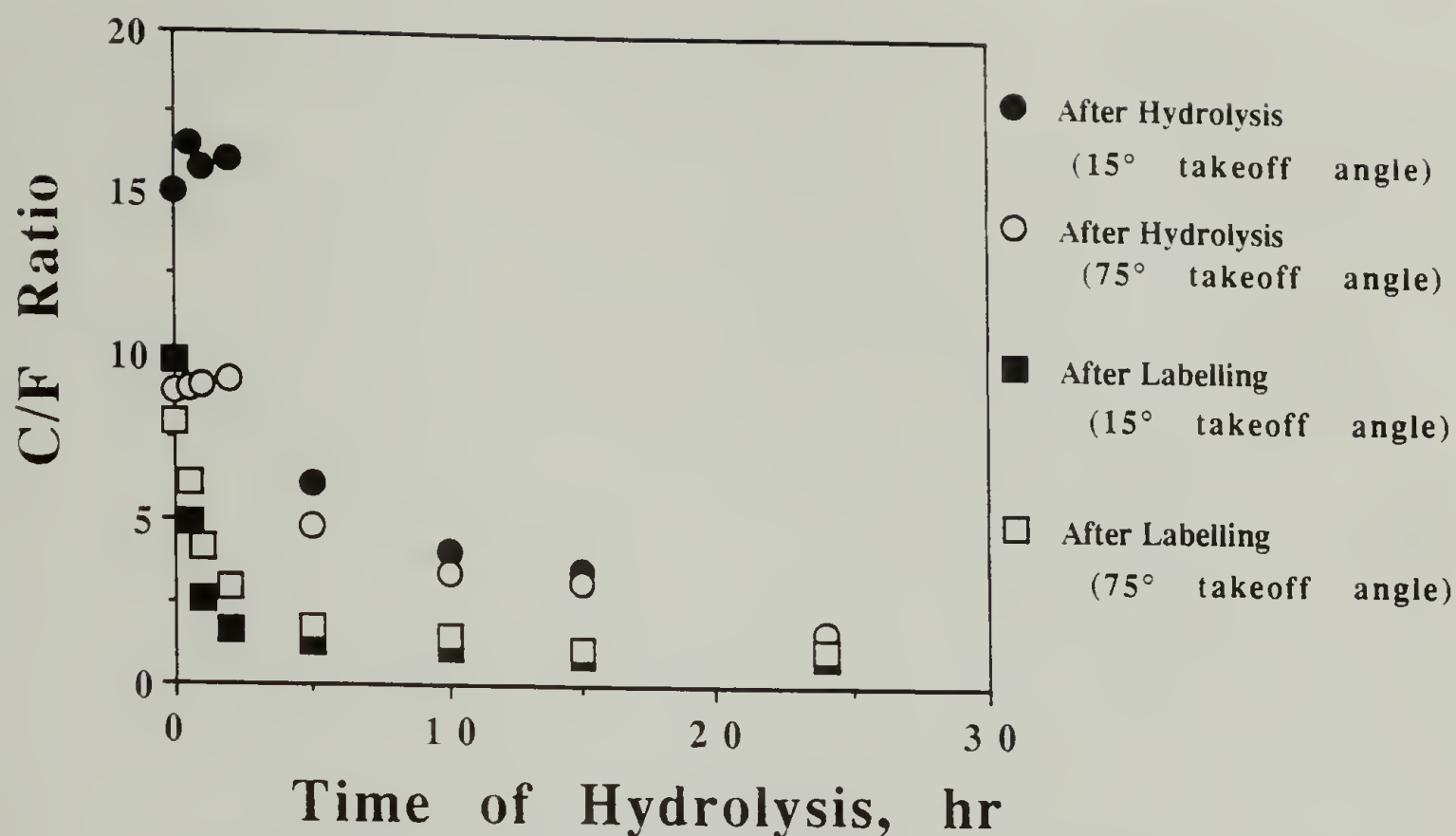


Figure 5.32. XPS results for the base catalyzed hydrolysis of PCTFE-ODec (75:25 methanol:water).

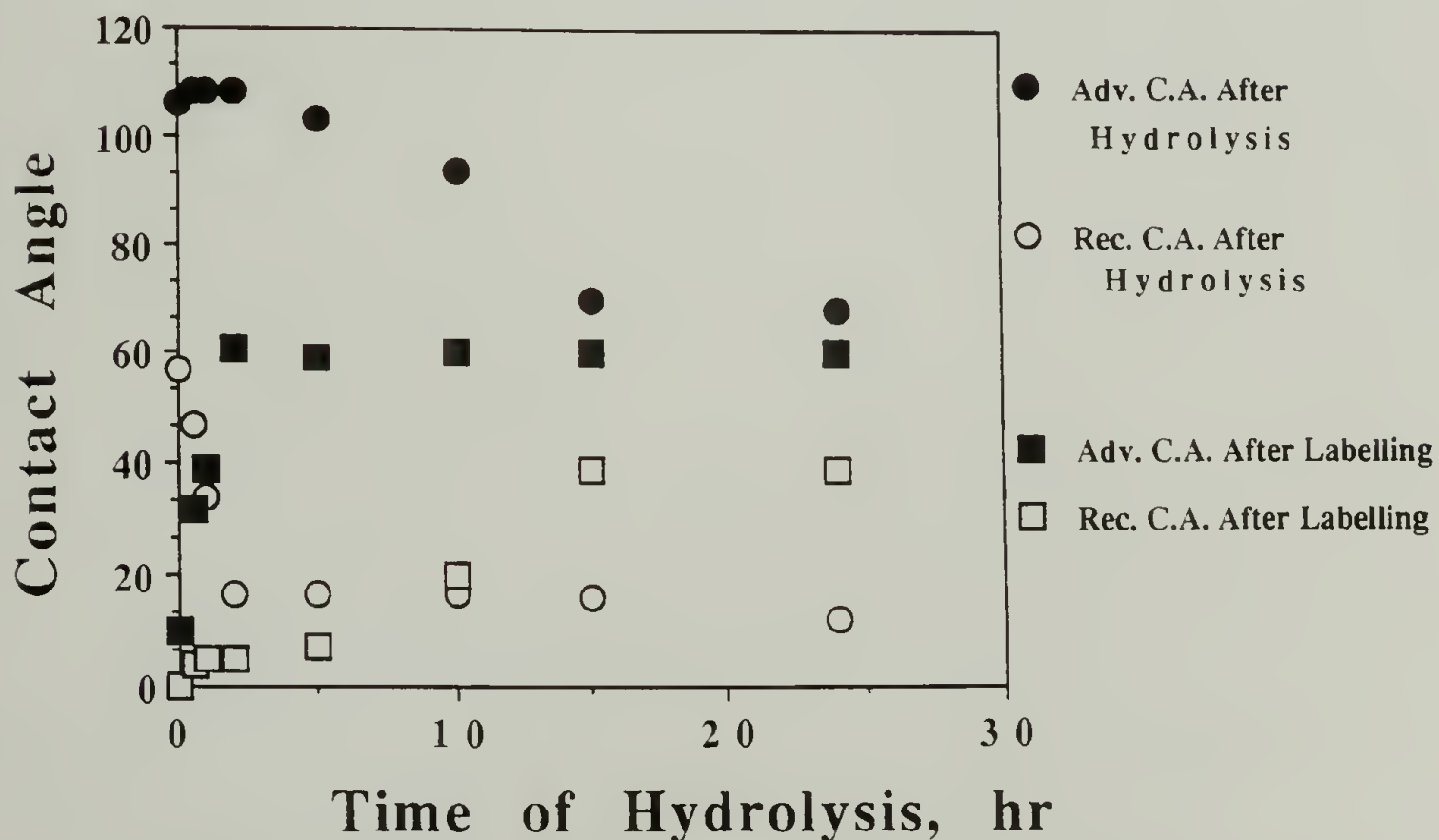


Figure 5.33. Contact angle results for the base catalyzed hydrolysis of PCTFE-ODec (75:25 methanol:water). Water contact angles after hydrolysis (circles) and hexadecane contact angles after labelling with heptafluorobutyryl chloride (squares).



the formation of a significant number of hydroxyl groups in the first 2 h. The corresponding increase in the advancing hexadecane contact angles of the labelled samples with the time of the hydrolysis indicates the formation of a number of heptafluorobutyrate esters of these alcohols.

After the first 2 h of the hydrolysis the XPS C/F ratios of the hydrolyzed samples begin to decrease more rapidly and reach values (3.52&3.16) after 15 h which are consistent with those of PCTFE-OH. The C/F ratios of the labelled samples indicate that the hydrolysis is 95% complete at this time. The further decrease in the C/F ratios of the hydrolyzed samples after 15 h is a result of dissolution of the modified alcohol containing surface as indicated by a significant amount of chlorine (~8%) in these XPS spectra. These changes in the surface compositions of the hydrolyzed and labelled samples are also measured by the advancing water and receding hexadecane contact angles on these surfaces, respectively. After the first 2 h of the hydrolysis, the advancing water contact angle on the PCTFE-OH/ODec surfaces slowly decreases over the next 8 h from 108° for a 42% hydrolyzed surface to 94° for a 83% hydrolyzed surface. This contact angle then decreases rapidly to 70° when the surface composition increases to 95% hydroxyl groups (15 h reaction). Changes in the receding hexadecane contact angle after labelling also show similar behavior. A gradual increase from 5° to 20° as the PCTFE-ODec/OHFB surface composition changes from 42% to 83% heptafluorobutyrate esters, followed by a dramatic increase to 39° for an essentially complete heptafluorobutyrate surface.

When the solvent composition for the hydrolysis of PCTFE-ODec is changed to 50:50 methanol:water, the behavior in the XPS and contact angle results after hydrolysis and after labelling is similar to that described above except it takes place over a greater length of time. The XPS C/F ratios (Figure 5.34) after the hydrolysis remain constant for the first 2 h of the reaction even though the concentration of hydroxyl groups in the surface (as indicated the C/F ratios of the labelled samples) increases from 7% to 20%. These ratios then decrease slowly for the next 48 h when the reaction is 98% complete (calculated from the C/F ratio of the labelled samples).

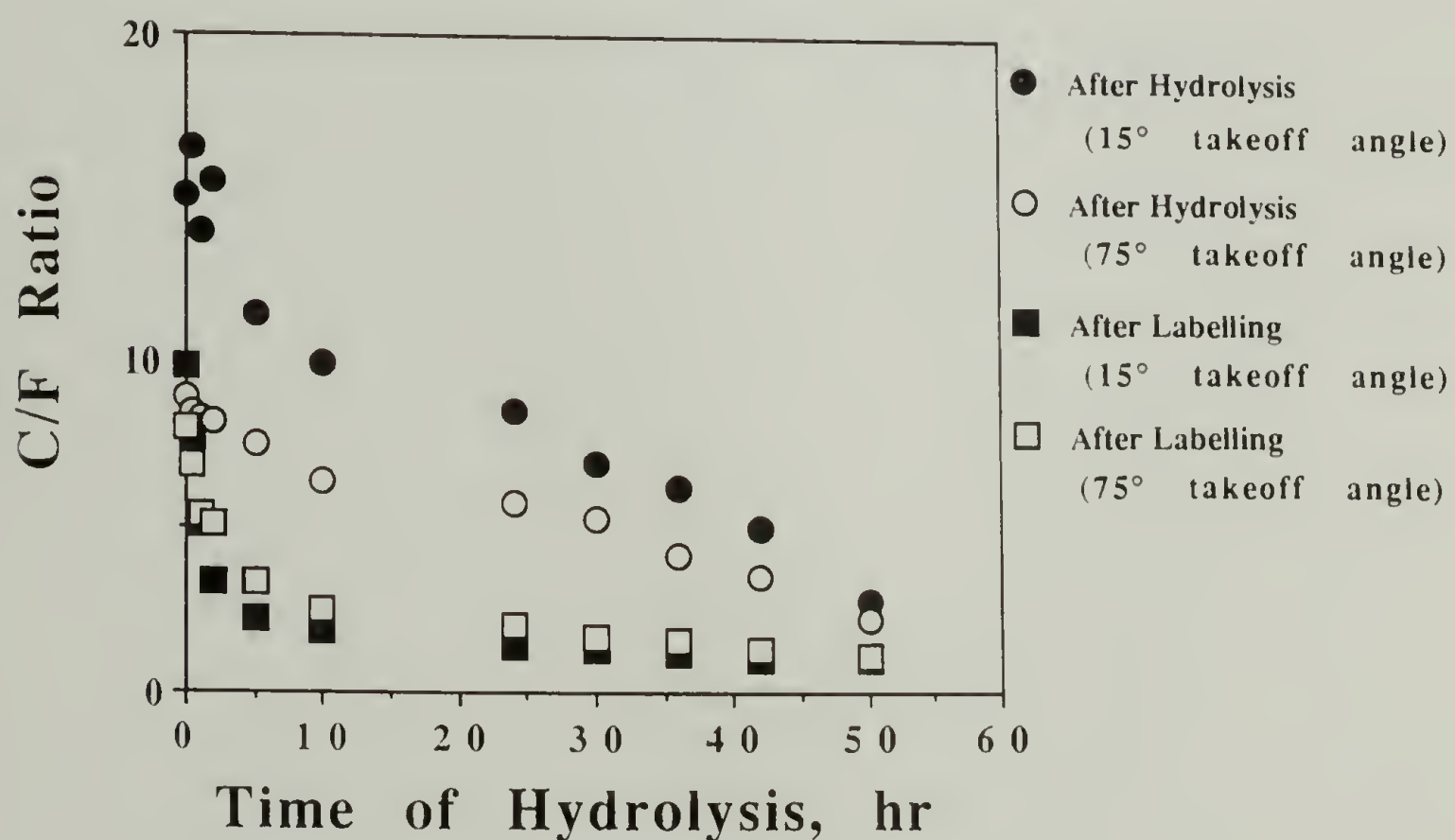
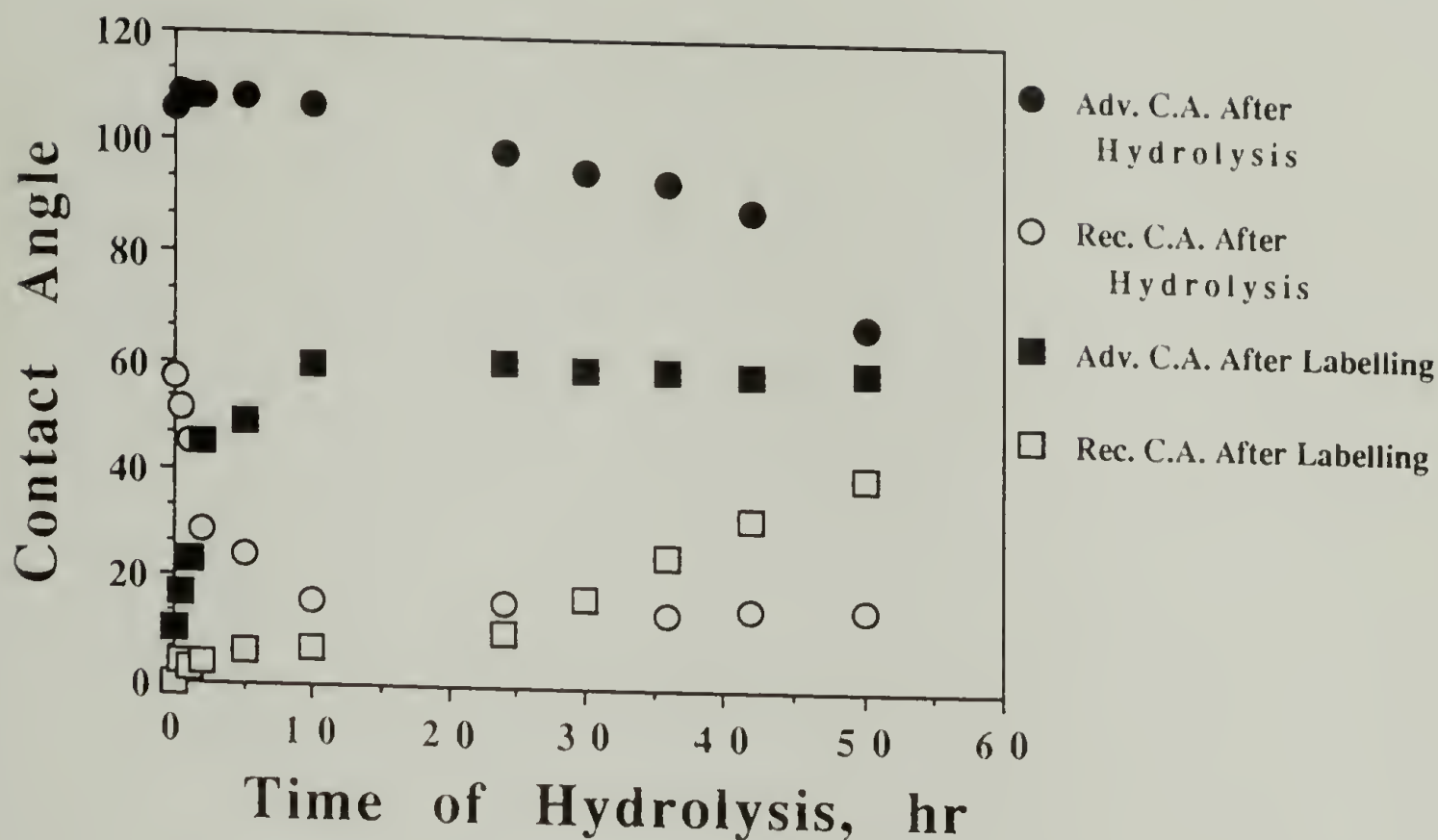


Figure 5.34. XPS results for the base catalyzed hydrolysis of PCTFE-ODec (50:50 methanol:water).



**Figure 5.35.** Contact angle results for the base catalyzed hydrolysis of PCTFE-ODec (50:50 methanol:water). Water contact angles after hydrolysis (circles) and hexadecane contact angles after labelling with heptafluorobutyryl chloride (squares).

The receding water contact angles (Figure 5.35) after hydrolysis decrease dramatically in the first 5 h of the reaction, reflecting the increase in the number of hydroxyl groups in the modified layer (from 7% to 36%). The advancing water contact angle measured on these surfaces remains constant over this composition range and begins to decrease slowly once the ratio of hydroxyl:decanoate groups exceeds 1:1 (after 10 h). Even after 42 h, where the surface is 89% hydrolyzed, the advancing water contact angle is still 89° which is considerably higher than that of homogeneous PCTFE-OH (67°). After 50 h, this contact angle decreases to 70° and the reaction is considered to be complete (98%, as determined from the XPS C/F



ratio of the labelled sample). After labelling the resulting alcohols with heptafluorobutyryl chloride, the hexadecane contact angles show the expected behavior. A rapid increase in the advancing hexadecane contact angles from  $10^\circ$  to  $60^\circ$  in the first 10 h of the reaction as the surface concentration of heptafluorobutyrate groups increases from 7% to 50% and no change thereafter with further increases in this concentration. Also, low values ( $<10^\circ$ ) for the receding hexadecane contact angles are measured on the labelled samples until the heptafluorobutyrate concentration reaches 61% (24 h). At this point, this angle gradually increases to  $40^\circ$  when the reaction is complete (50 h).

The hydrolyses of PCTFE-ODec in 25:75 and 0:100 methanol:water solutions were not attempted. It was felt that the results of the 50:50 PCTFE-ODec hydrolysis and those from the hydrolysis of PCTFE-OBu indicated that these reactions would be prohibitively long for convenient study.

The results for the hydrolysis of PCTFE-OSear conducted in pure methanol show a number of interesting features (Figures 5.36 and 5.37). In the first 30 min of the reaction, the extremely small decrease in the receding water contact angle (from  $90^\circ$  to  $87^\circ$ ) indicates that little hydrolysis has taken place. In fact, the C/F ratio of the labelled samples indicate that the hydroxyl group content in the surface has only increased from 7% to 19% in this time. For comparison, the PCTFE-OBu and PCTFE-ODec surface were hydrolyzed 87% and 30%, respectively, in the same amount of time. However, this low level of hydrolysis is sufficient to significantly disrupt the surface order of the modified layer as indicated by the

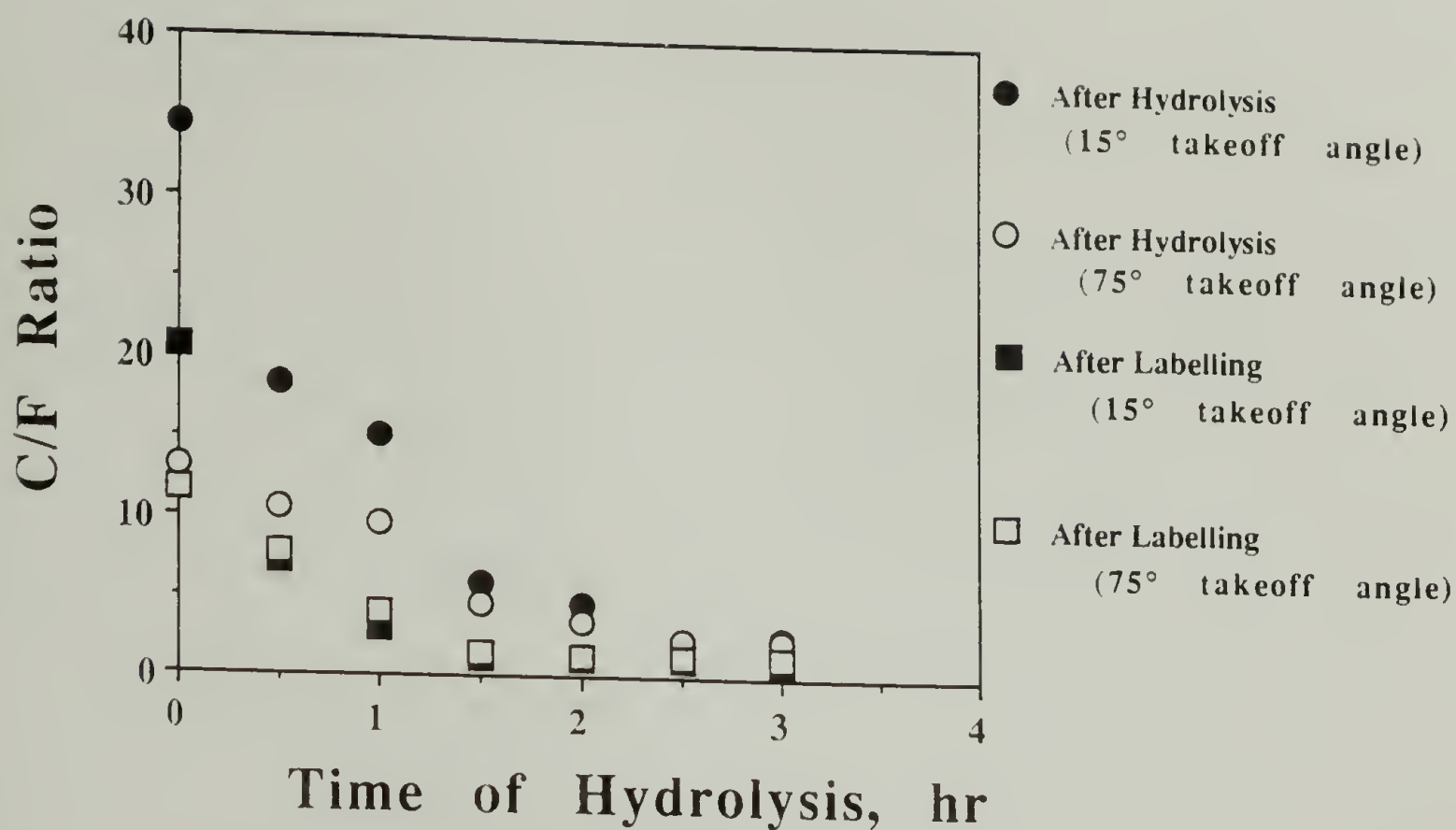


Figure 5.36. XPS results for the base catalyzed hydrolysis of PCTFE-OSear (100:0 methanol:water).

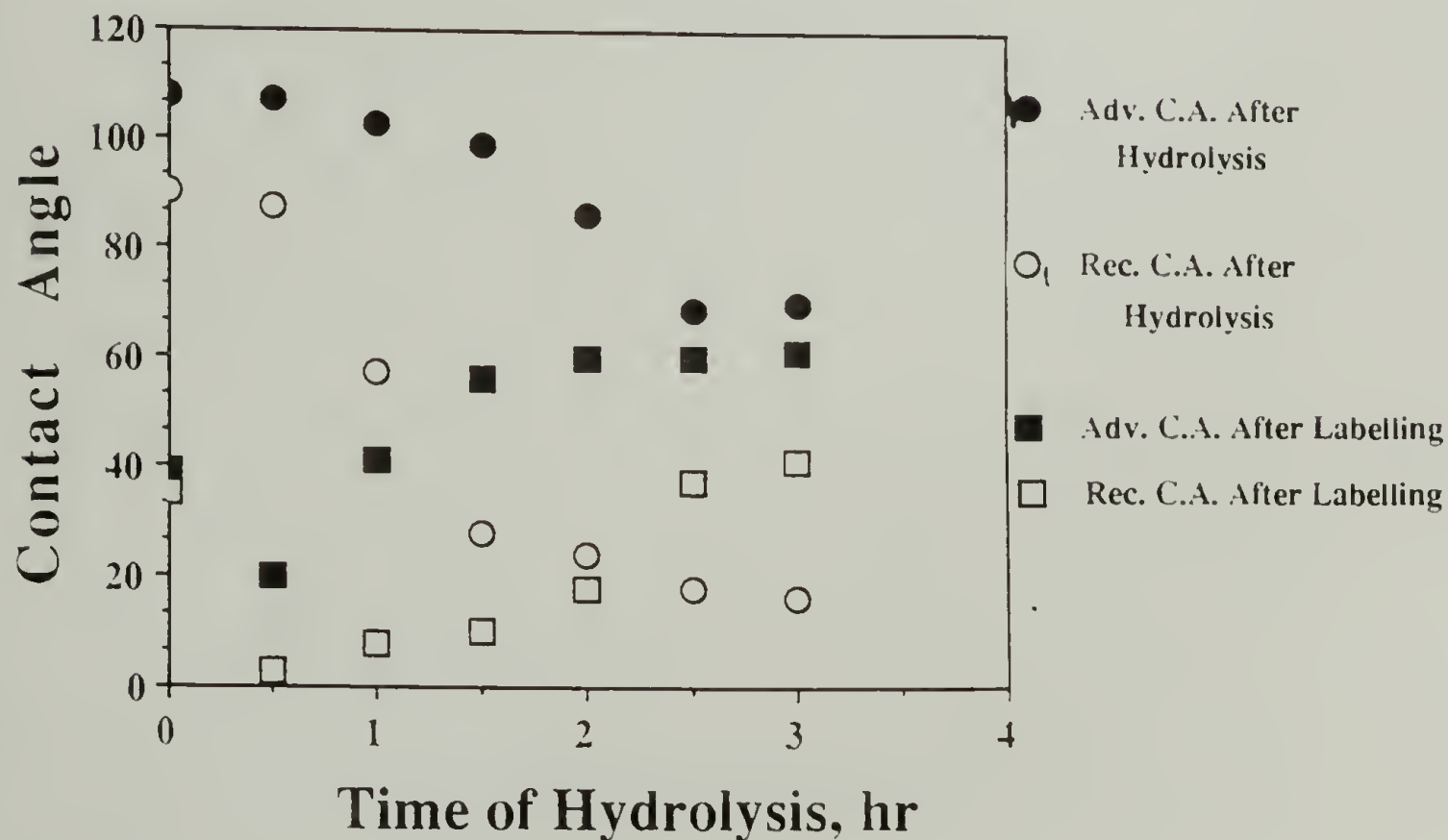


Figure 5.37. Contact angle results for the base catalyzed hydrolysis of PCTFE-OSear (100:0 methanol:water). Water contact angles after hydrolysis (circles) and hexadecane contact angles after labelling with heptafluorobutyryl chloride (squares).

pronounced decrease in the C/F ratios of the hydrolyzed sample and the decrease in the hexadecane contact angles of the labelled surfaces. A hexadecane contact angle of  $10^\circ/0^\circ$  is expected for a completely disordered surface. A relatively high value of  $20^\circ$  measured for the advancing hexadecane contact angle is inconsistent with a surface containing only 11% fluorocarbon and therefore, can only be explained if some order remains. (It is likely that the presence of the heptafluorobutyrate groups further disrupts the order in the modified layer causing lower values in the hexadecane contact angle than what would otherwise be observed on the PCTFE-OH/OStear surface.)

In the next half hour of the reaction, the XPS C/F ratios and the advancing water contact angle of the hydrolyzed surface decrease only slightly, while the receding contact angle decreases from  $87^\circ$  to  $57^\circ$ . During this time, the concentration of the hydroxyl groups in the surface has increased to 41%. At this point, the surface contains a sufficient number of hydroxyl groups to be efficiently wet by the reacting solution and the hydrolysis is very rapid. Over the next 30 min interval, the yield of the reaction rapidly increases to 90%. With this increase in the number of hydroxyl groups in the surface there is a corresponding, large decrease in the receding water contact angle to  $28^\circ$ . During this time, the advancing water contact angle has only decreased to  $99^\circ$  which illustrates the large effect that a small percentage of hydrophobic functionality has on the advancing contact angle. Both water contact angles then decrease until they reach values consistent with the structure of PCTFE-OH ( $67^\circ/17^\circ$ ) after a total of 2.5 h of hydrolysis.



After the initial decrease in the first 30 min of the reaction, the next two 30 min intervals show an increase in the advancing hexadecane contact angles on the labelled surfaces to  $41^\circ$  and then  $56^\circ$  as the heptafluorobutyrate content in the surface increases to 41% and then 90%, respectively. For the same two surfaces, the receding contact angles remain small ( $8^\circ$  and  $10^\circ$ , respectively). Even though the percent of heptafluorobutyrate groups in the surface is high (90%), the fraction of fluorocarbons (i.e. difluoromethylene and trifluoromethyl groups) in the surface remains comparatively low (61%) due to the relative lengths of the two ester chains and the receding hexadecane contact angle reflects this fact. Finally, after a 3 h hydrolysis, the receding hexadecane contact angle of the labelled sample reaches a value ( $41^\circ$ ) consistent with a surface containing only heptafluorobutyrate esters.

The XPS and contact angle results for the hydrolysis of PCTFE-OSTear conducted in a 75:25 methanol:water solution are shown in Figures 5.38 and 5.39. As expected, introducing water into the system raised the interfacial free energy at the site of the reaction and lowered the reaction rate considerably. In this case, the data show the hydrolysis to be complete after 24 h, compared to 3 h for the reaction conducted in pure methanol and 15 h for the hydrolysis of PCTFE-ODec in the same solvent. The data presented in these two figures follow similar trends as those discussed for the pure methanolysis of PCTFE-OSTear except the changes take place more slowly. For this reason, these results are not discussed in detail.

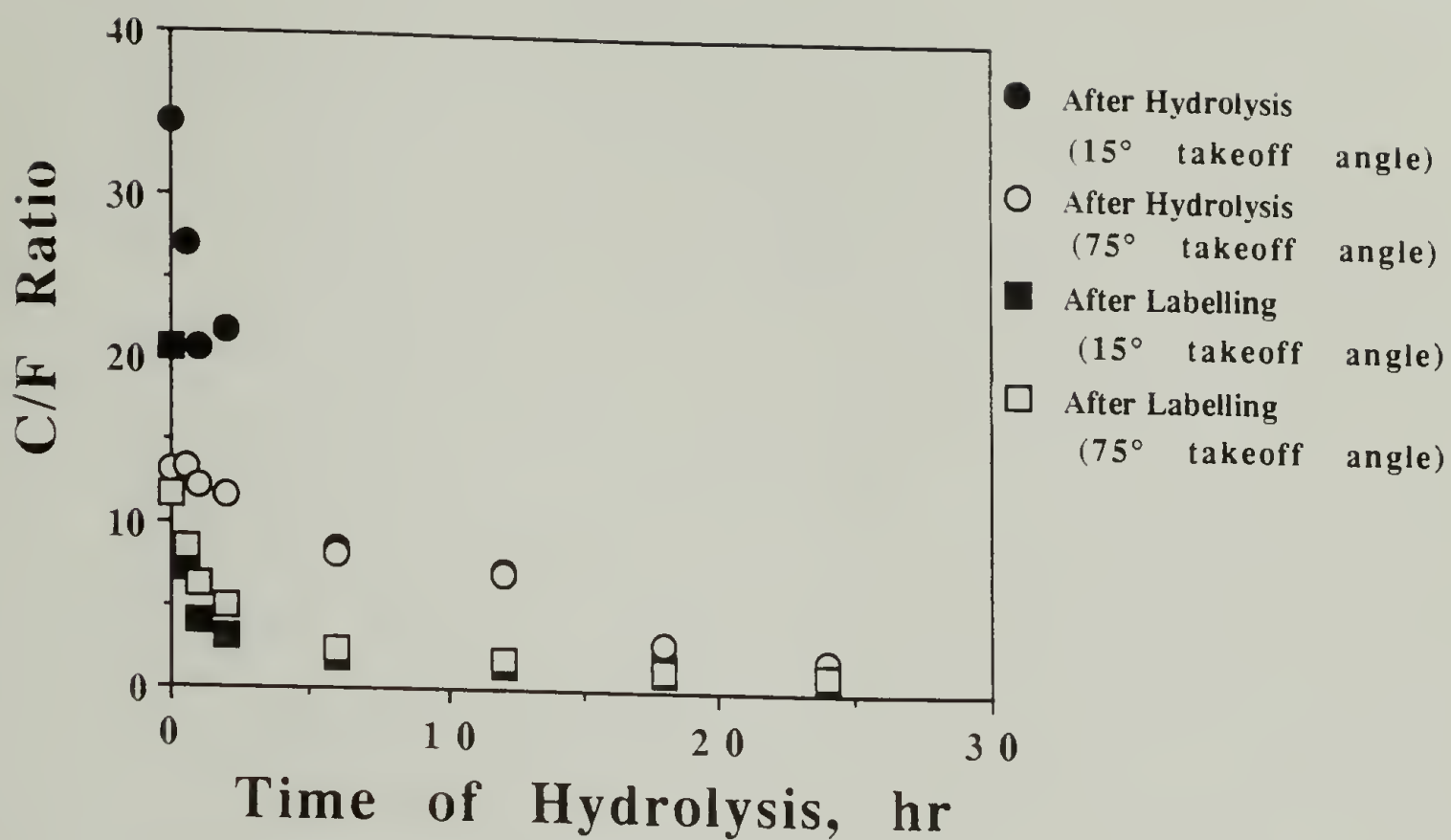


Figure 5.38. XPS results for the base catalyzed hydrolysis of PCTFE-OSear (75:25 methanol:water).

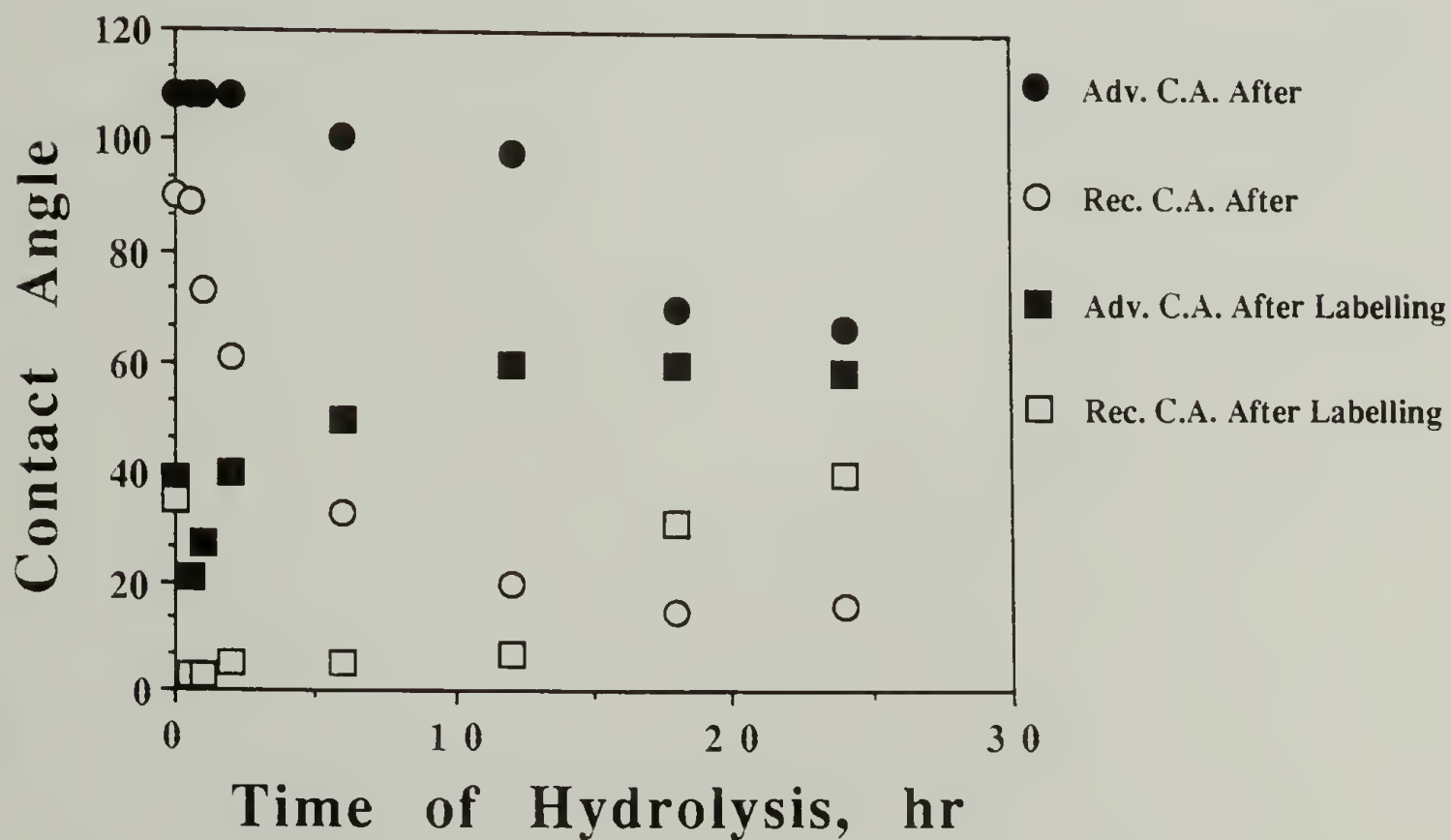


Figure 5.39. Contact angle results for the base catalyzed hydrolysis of PCTFE-OSear (75:25 methanol:water). Water contact angles after hydrolysis (circles) and hexadecane contact angles after labelling with heptafluorobutyryl chloride (squares).

The hydrolyses of PCTFE-OS<sub>tear</sub> in 50:50, 25:75 and 0:100 methanol:water solutions were not attempted because, again, it was felt that the results obtained from the hydrolysis of the other surfaces indicated that these reactions would be extremely long.

The extent of hydrolysis of PCTFE-OB<sub>ut</sub>, PCTFE-OD<sub>ec</sub> and PCTFE-OS<sub>tear</sub> as a function of reaction time is plotted in Figures 5.40 - 5.42 for each of the solvent compositions studied. These figures show that as the amount of water in the hydrolysis solution increases, the reaction rate decreases due to the increased interfacial free energy. Also, as expected, the rate of hydrolysis in a given solvent decreases as the length of the ester chain increases. Again, this effect is a result of an increase in the interfacial free energy.

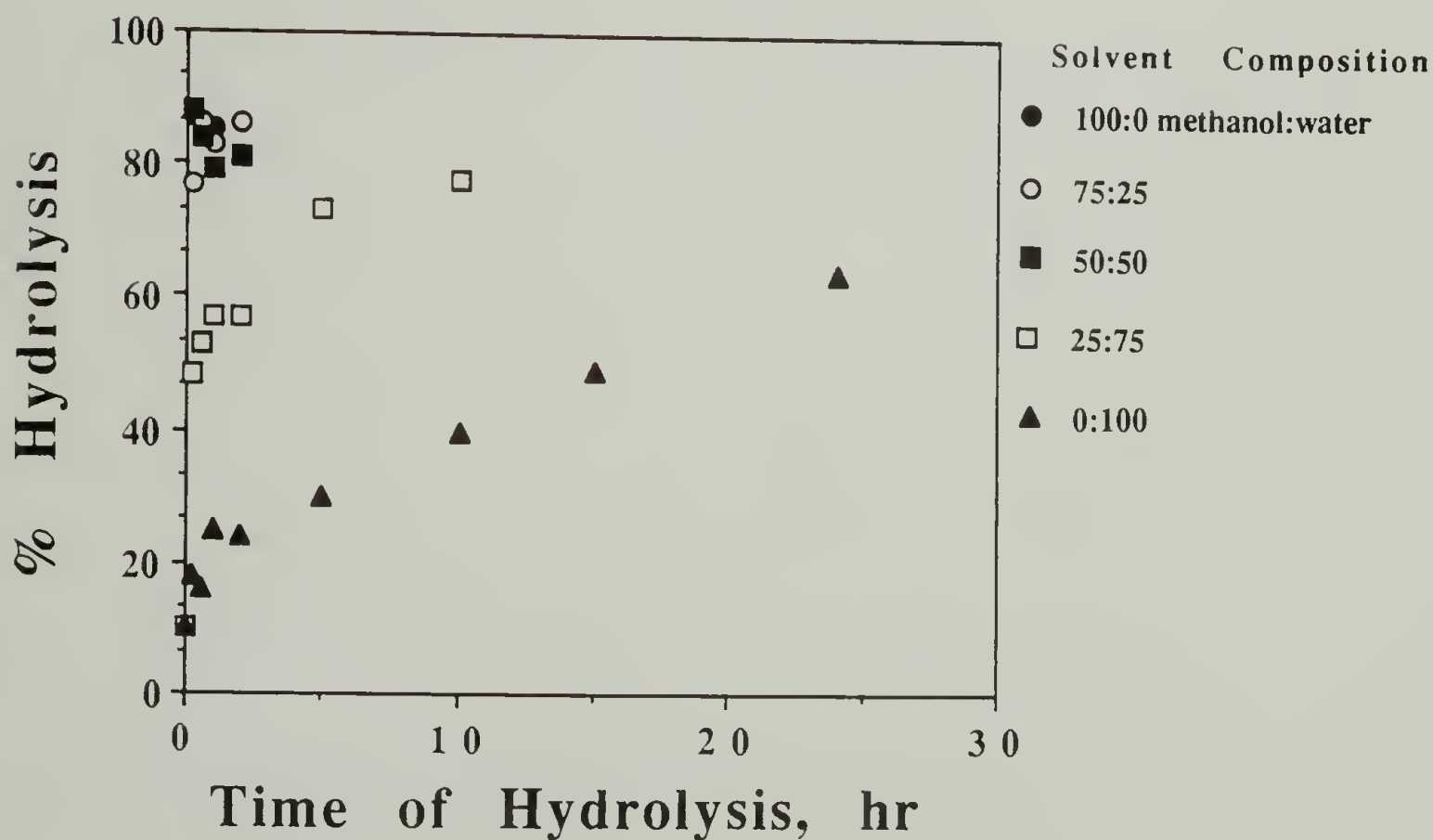


Figure 5.40. Kinetics of the base catalyzed hydrolysis of PCTFE-OB<sub>ut</sub> as a function of solvent composition.



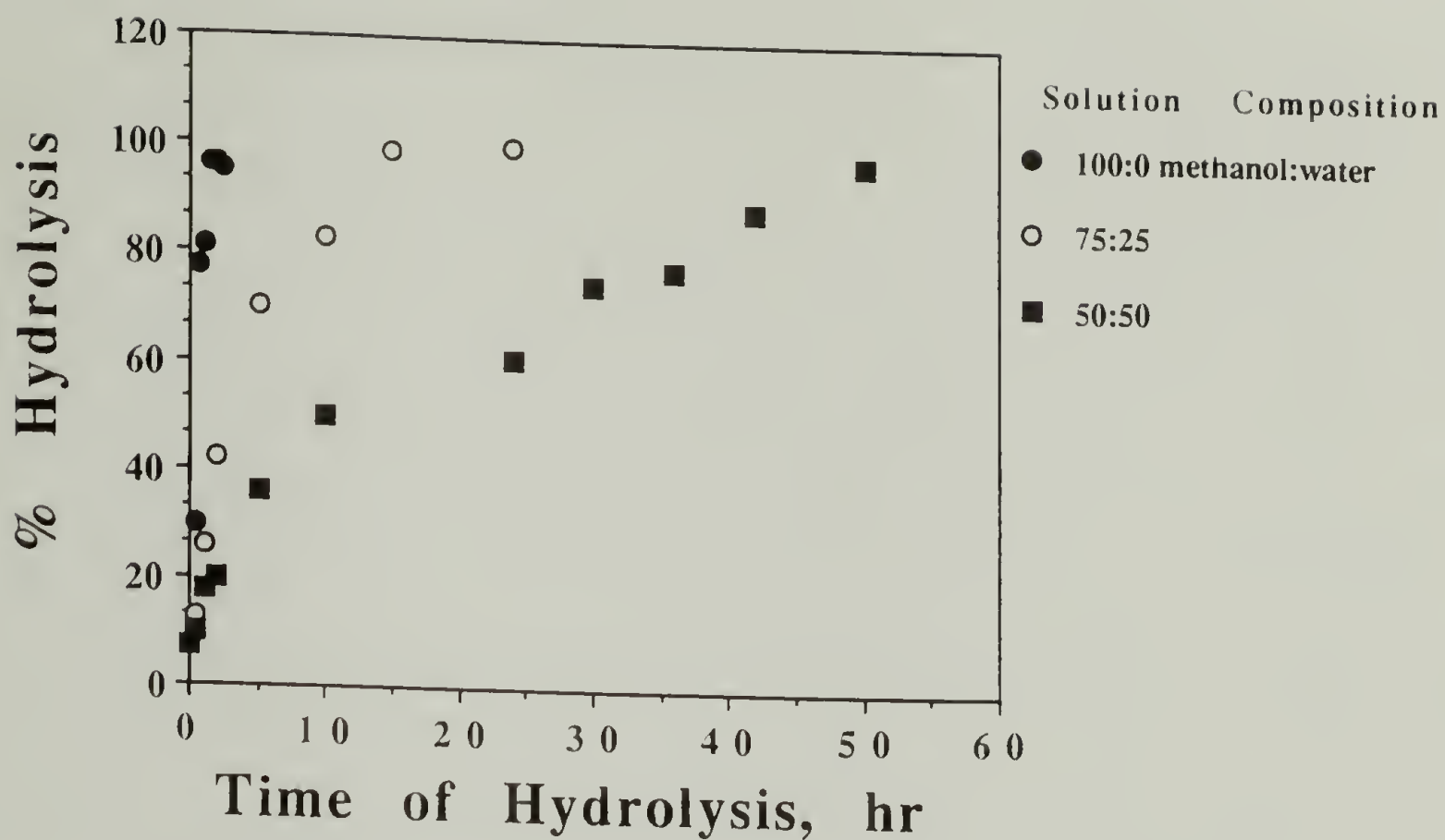


Figure 5.41. Kinetics of the base catalyzed hydrolysis of PCTFE-ODec as a function of solvent composition.

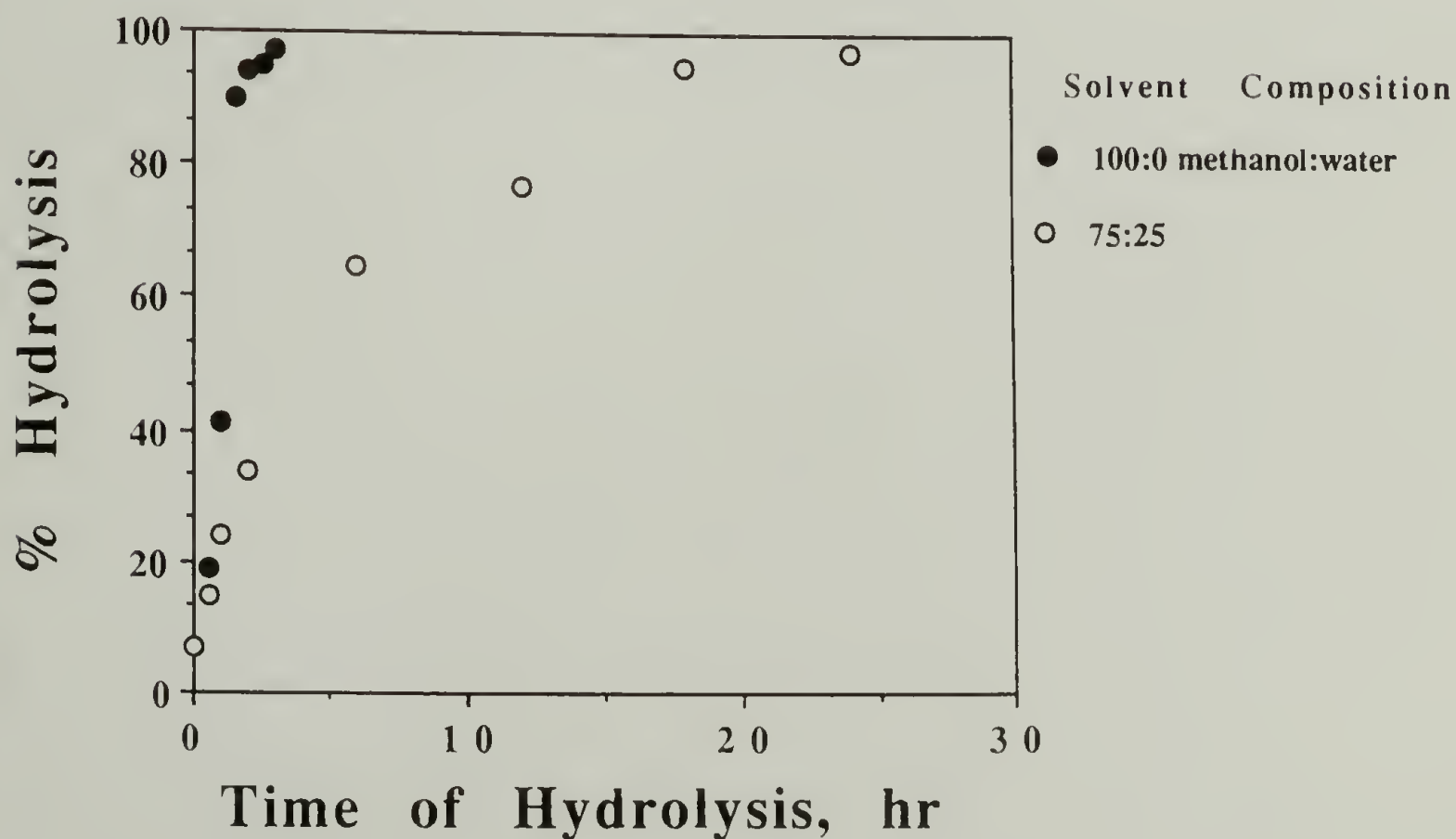


Figure 5.42. Kinetics of the base catalyzed hydrolysis of PCTFE-OSTear as a function of solvent composition.

In Figures 5.43 a and b the results for the 100:0 methanol:water methanolysis of PCTFE-ODec and PCTFE-OSTear are replotted for clarity. Each of these figures shows a relatively low rate of methanolysis initially, followed by a rapid increase in the reaction rate once the surface is sufficiently wet by the solvent.

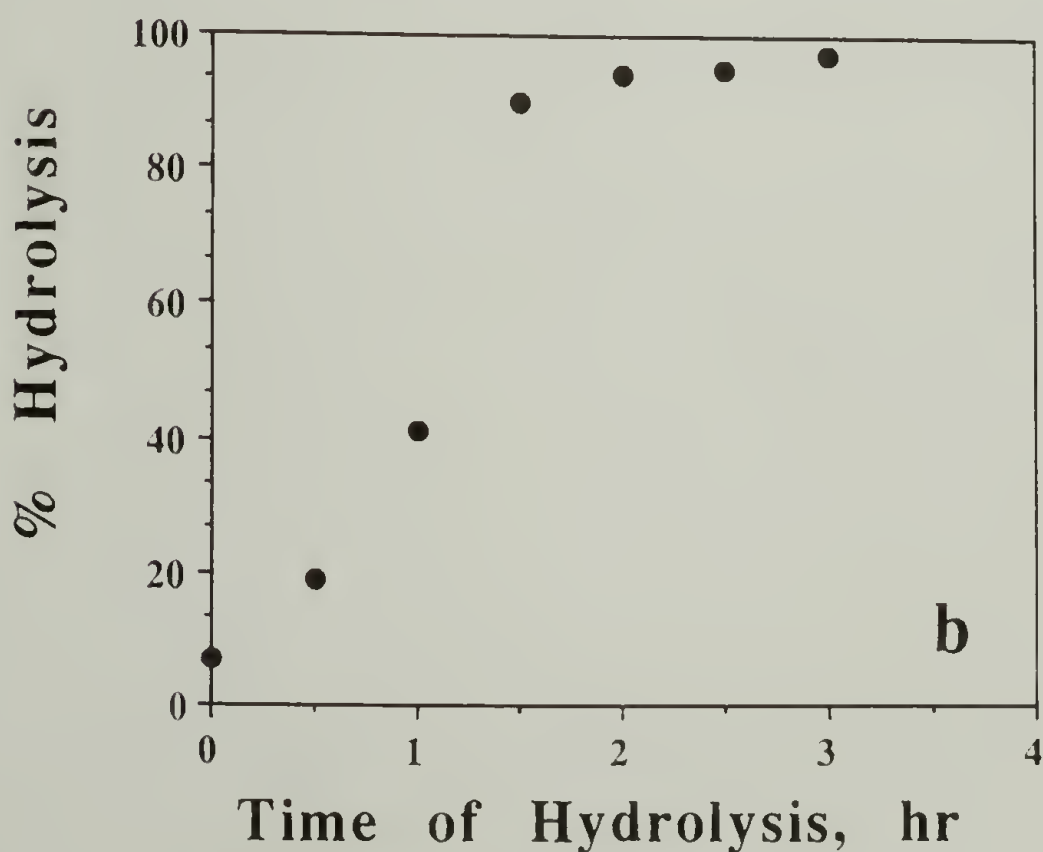
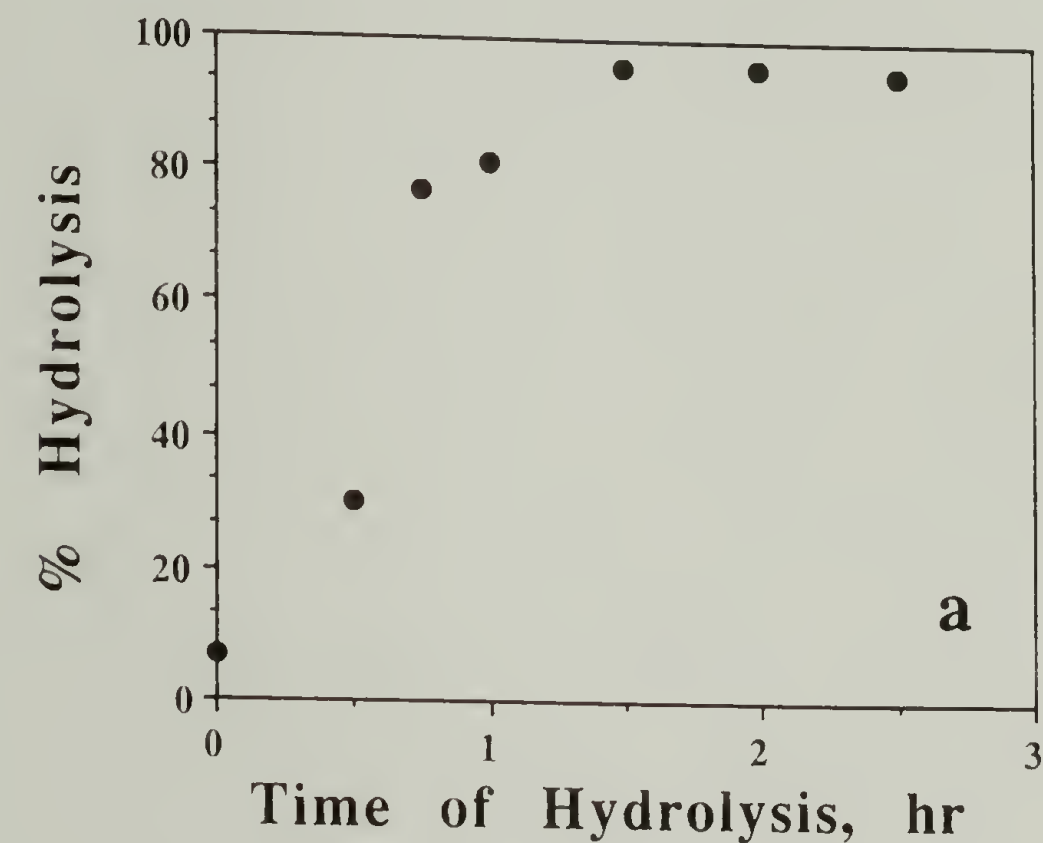


Figure 5.43. Kinetics of the base catalyzed methanolysis (100:0, methanol:water) of: (a) PCTFE-ODec and (b) PCTFE-OSTear.

## Wetting Behavior of Mixed Surfaces as a Function of Surface Composition

As stated previously, the objective of this research is to determine if the wetting behavior of compositionally similar surfaces is dependent on the method of their preparation. For this study, sequential esterifications of PCTFE-OH (Method 1) and hydrolysis/re-esterification of PCTFE-Esters (Method 2) were each used to prepare hydroxyl/ester and hydrocarbon ester/fluorocarbon ester mixed surfaces. The former set of mixed surfaces was analyzed with water contact angles, while the latter set was studied with hexadecane contact angles. These probe fluids were chosen to maximize wettability differences between the two surface components. The cosines of the advancing and receding contact angles were then plotted as a function of the surface composition.<sup>14</sup> The cosine of the contact angle is plotted since it is this value which is directly related to the surface energy (through Young's equation) and not the contact angle.<sup>10</sup> As discussed (see page 202), it is likely that Method 1 will yield surfaces where the two functional groups are randomly dispersed throughout the modified layer, while Method 2 may result in "patchy" surfaces. It is expected<sup>10</sup> that these two types of surface morphologies will differ in their wetting behavior with the latter set exhibiting greater contact angle hysteresis. In addition to studying the effect of the preparative method on wetting, the relative sizes of the surface components was also varied by changing the length of the either the hydrocarbon ester or fluorocarbon ester chain.



Figures 5.44 - 5.46 compare the water contact angle results measured on the mixed hydroxyl/ester surfaces (PCTFE-OH/OBut, PCTFE-OH/ODec and PCTFE-OH/Stear) prepared by kinetic control of the esterification of PCTFE-OH with the corresponding acid chloride (butyryl, decanoyl and stearoyl, respectively). The results for the PCTFE-OH/OBut surfaces (Figure 5.44) show that the cosines of both  $\Theta_A$  and  $\Theta_R$  change gradually over the composition range from 0.391/0.95 ( $\cos \Theta_A/\cos \Theta_R$ ) for pure PCTFE-OH to 0.017/0.588 for pure PCTFE-OBut indicating that the functional groups are dispersed randomly throughout the modified layer. The results are very different for the other two sets of mixed surfaces.

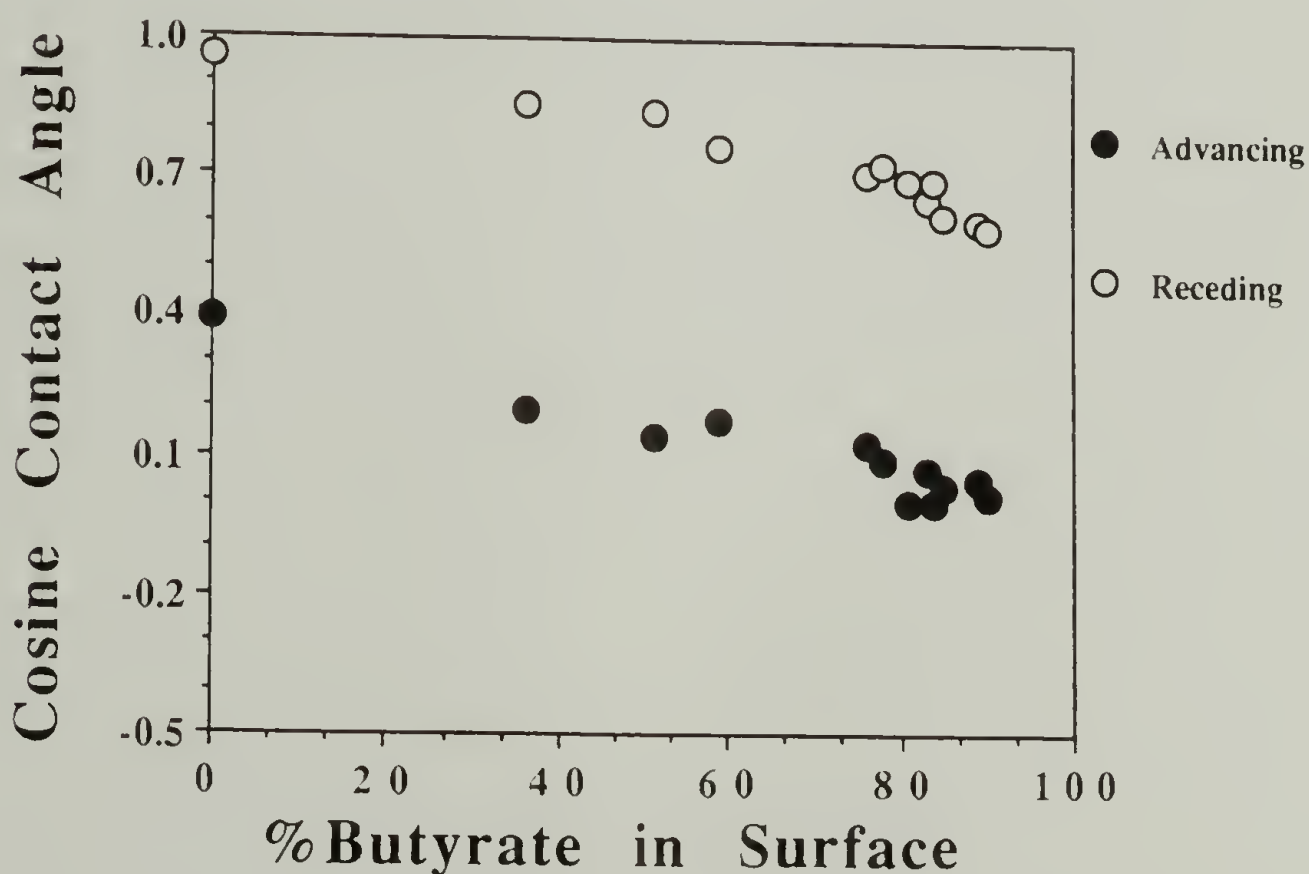


**Figure 5.44.** Cosine of the water contact angles as a function of surface composition for the mixed PCTFE-OH/OBut surfaces prepared by kinetic control of the esterification of PCTFE-OH with butyryl chloride.

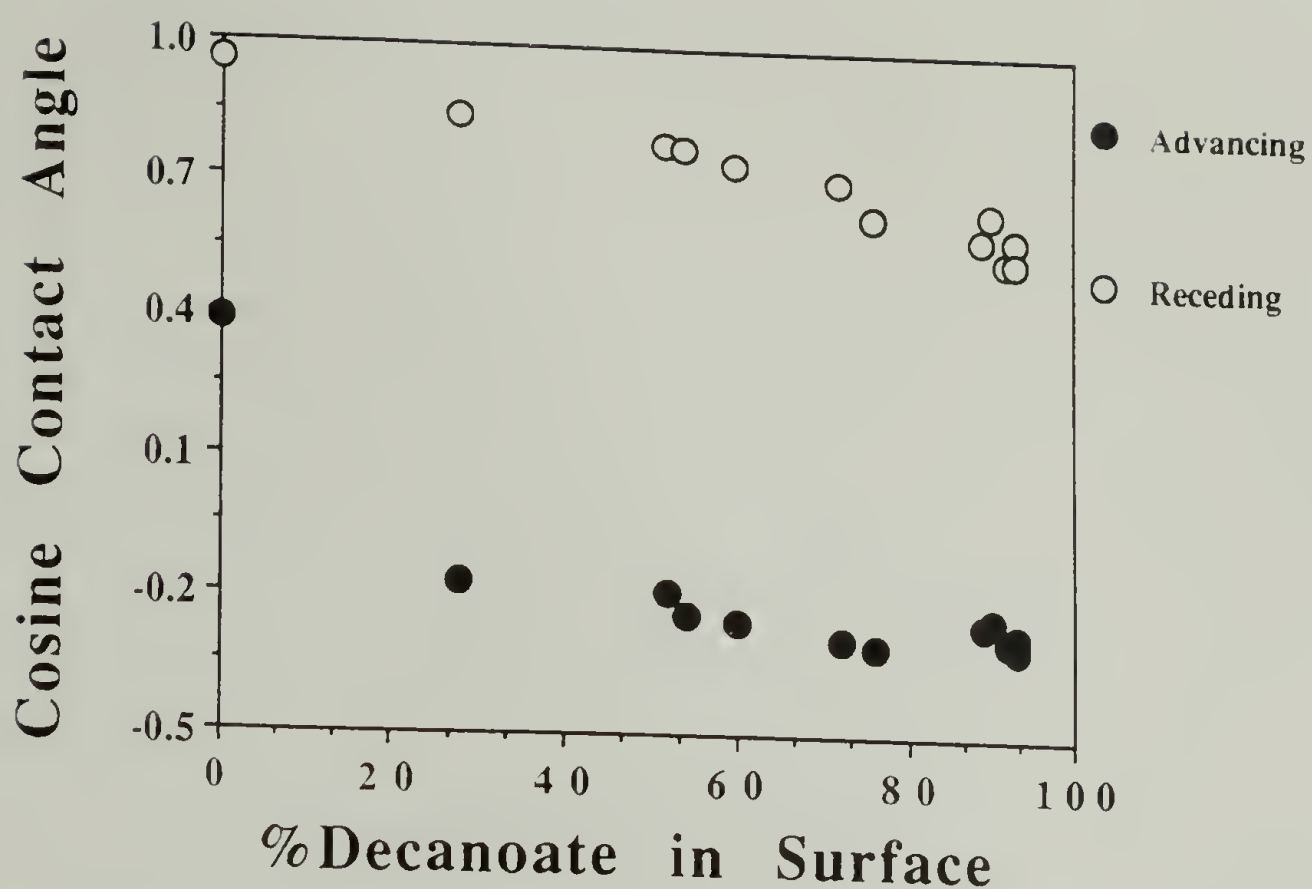


Figure 5.45. Cosine of the water contact angles as a function of surface composition for the mixed PCTFE-OH/ODec surfaces prepared by kinetic control of the esterification of PCTFE-OH with decanoyl chloride.

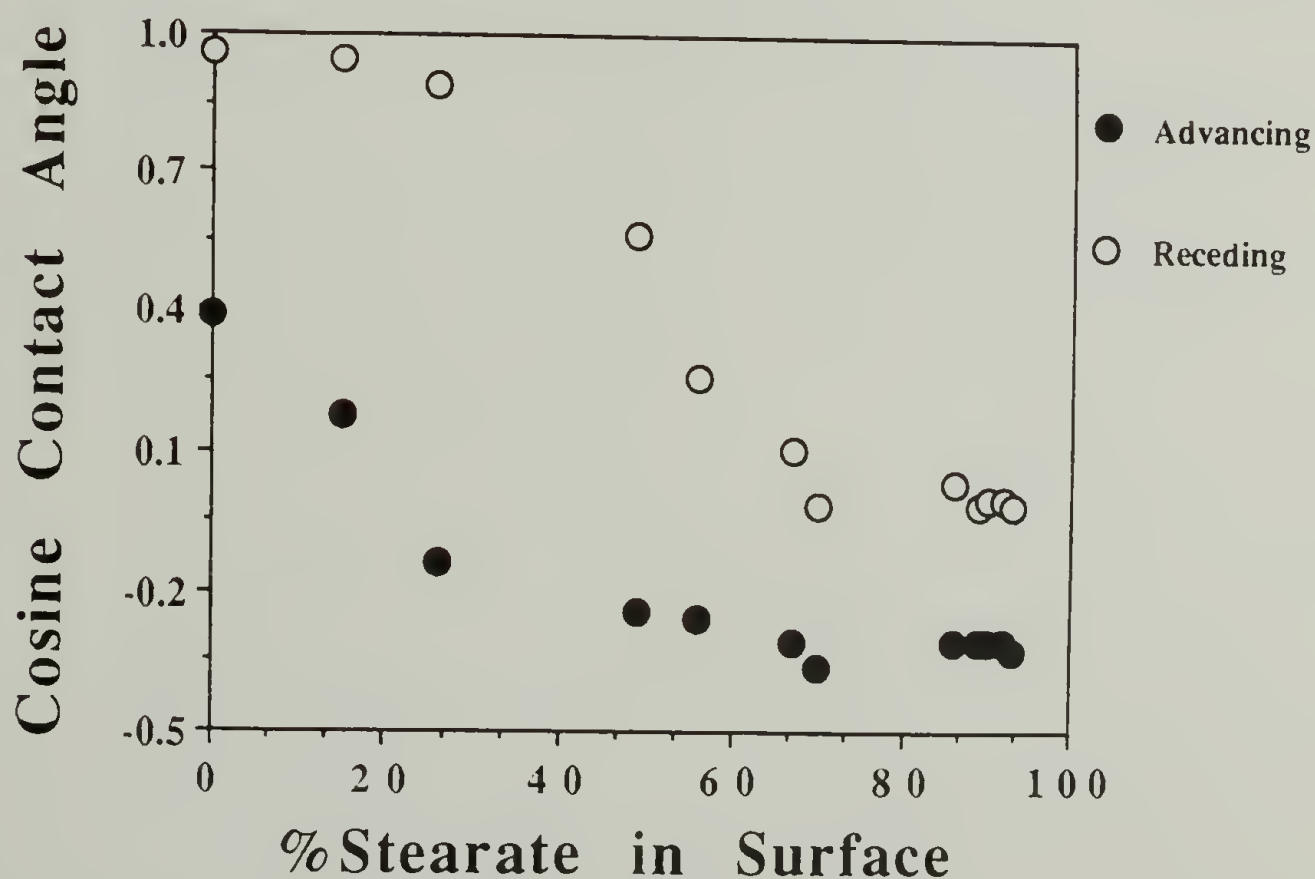


Figure 5.46. Cosine of the water contact angles as a function of surface composition for the mixed PCTFE-OH/OSTear surfaces prepared by kinetic control of the esterification of PCTFE-OH with stearoyl chloride.

$\cos \Theta_A$  for the PCTFE-OH/ODec surfaces decreases dramatically from 0.391 to -0.174 as the composition of the surface changes from 0 to 28% decanoate. After this point,  $\cos \Theta_A$  decreases slowly until a value of -0.276 for pure PCTFE-ODec is reached. This result indicates that the composition at the film/air interface (as probed by  $\Theta_A$ ) is essentially hydrocarbon once the composition of the modified layer exceeds 28% ester. On the otherhand, as with the PCTFE-OH/OBut surfaces,  $\cos \Theta_R$  for the PCTFE-OH/ODec mixed surfaces changes gradually as the surface composition changes from pure PCTFE-OH to pure PCTFE-ODec. As a result of water-induced surface reorganizations and diffusion of the probe fluid into the substrate, the hydroxyl groups in the modified layer are more effectively detected by the receding water contact angle and thus, the observed behavior.

The contact angle results for the mixed PCTFE-OH/OStear surfaces also exhibit some interesting trends. The behavior of  $\cos \Theta_A$  is similar to that of the PCTFE-ODec surfaces: a rapid decrease from 0.391 to -0.139 as the stearate content in the surface increases from 0 to 26%, followed by a gradual decrease to -0.309 for a pure stearate surface. Again, this behavior is a result of an excess of hydrocarbon at the film/air interface with a relatively low ester content in the modified layer. The behavior in  $\cos \Theta_R$  as a function of composition reflects the formation of an ordered, close-packed surface.  $\cos \Theta_R$  changes slowly from 0.956 to 0.891 as the surface composition changes from 0 to 26% stearate. The slope of this decrease is approximately the same as that for the PCTFE-OH/OBut and PCTFE-OH/ODec mixed surfaces indicating that the functional



groups at the film/probe fluid interface are similar at this point and are primarily hydroxyl and methylene. At this point, hexadecane contact angles (see page 230 and 231) show that as the concentration of esters increases, the hydrocarbon tails begin to align themselves into an ordered close-packed array, oriented perpendicular to the surface. During this orientation process, the 17 hydrocarbons in the ester tail become progressively more efficient at preventing the aqueous probe fluid from reaching the hydroxyl groups in the modified layer and  $\cos \Theta_R$  begins to decrease dramatically. When the stearate content in the modified layer reaches 70%, the ordering in this mixed surface is complete (as indicated by the hexadecane contact angles) and  $\cos \Theta_R$  remains constant at a value of 0.0.

For comparison, the water contact angle results for the same three sets of mixed surfaces prepared by hydrolysis of the corresponding PCTFE-Esters are shown in Figures 5.47 - 5.49. For each surface, the results from the different solution compositions (methanol:water) used for the hydrolyses are superimposed onto a single plot. The fact that these results are superimposable (with one exception, see below) indicates that the structure of the mixed surface that results from the hydrolysis does not depend on the composition of the solvent used in the hydrolysis. The results for  $\cos \Theta_A$  as a function of surface composition from both the 25:75 and 0:100 (methanol:water) hydrolyses of PCTFE-OBu (Figure 5.47) are similar and show the same behavior as those presented in Figure 5.44 for the PCTFE-OH/OBu mixed surfaces prepared by kinetic control of the initial esterification. In fact, although not shown,

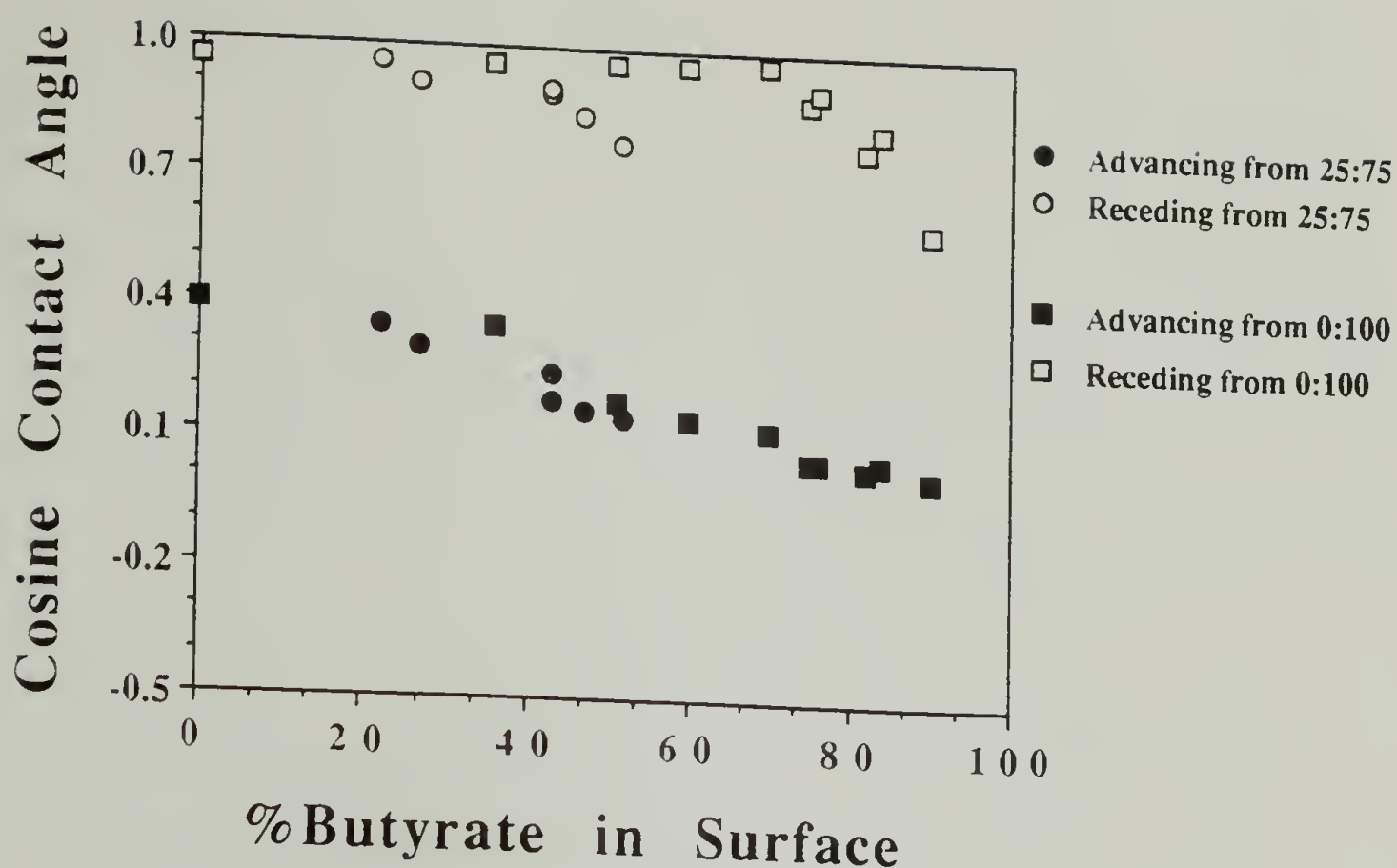


Figure 5.47. Cosine of the water contact angles as a function of surface composition for the mixed PCTFE-OH/OBut surfaces prepared by kinetic control of the hydrolyses of PCTFE-OBut.

the data for  $\cos \Theta_A$  from all three sets of experiments can be placed on a single curve which seems to indicate that the structures of the PCTFE-OH/OBut surfaces are independent of the preparative method. The values of  $\cos \Theta_R$  obtained from the 25:75 hydrolysis can also be superimposed on those from Figure 5.44 indicating that the two functional groups in this mixed surface are also likely to be distributed randomly in the modified layer. However, the  $\cos \Theta_R$  results from the 0:100 hydrolysis cannot be superimposed on those from the other two PCTFE-OH/OBut mixed surfaces indicating differences in the surface structures resulting from these preparations. The significantly greater contact angle hysteresis observed on the surfaces prepared from the 0:100 hydrolysis implies

that these surfaces are "patchy" in nature. The origin of this patchiness was described previously (see page 203) as being the result of an initially inhibited reaction (due to high interfacial free energy) to form isolated hydroxyl groups on the surface followed by an autoaccelerative hydrolysis radiating out from these points as the interfacial free energy decreases at the reacted sites. The fact that the surface structure resulting from the 25:75 hydrolysis is random indicates for this solution composition the rate of hydrolysis of a butyrate ester surrounded by other butyrate esters is comparable to that of one surrounded by hydroxyl groups.

The water contact angle results for each of the three hydrolyses (100:0, 75:25 and 50:50, methanol:water) of PCTFE-ODec to form mixed hydroxyl/ester surfaces are shown in Figure 5.48. The similarity in the data from the three reactions indicates that the three sets of mixed surface structures are essentially the same. In comparison with the data from Figure 5.45, the results for  $\cos \Theta_R$  from the hydrolyses show significantly greater contact angle hysteresis which again implies the formation of patchy surfaces. The behavior of  $\cos \Theta_A$  from these two mixed surface preparative methods are similar, but are likely to be of different origins. As discussed above, the rapid decrease in  $\cos \Theta_A$  at relatively low decanoate concentrations observed in the results from Method 1 can be attributed to an excess of the low surface energy hydrocarbon esters at the film/air interface. The  $\cos \Theta_R$  results from Method 2 indicate that these PCTFE-OH/ODec surfaces consist of patchy regions of PCTFE-OH and PCTFE-ODec. In this method (2), the observed rapid decrease in  $\cos \Theta_A$  at low decanoate concentrations can be attributed



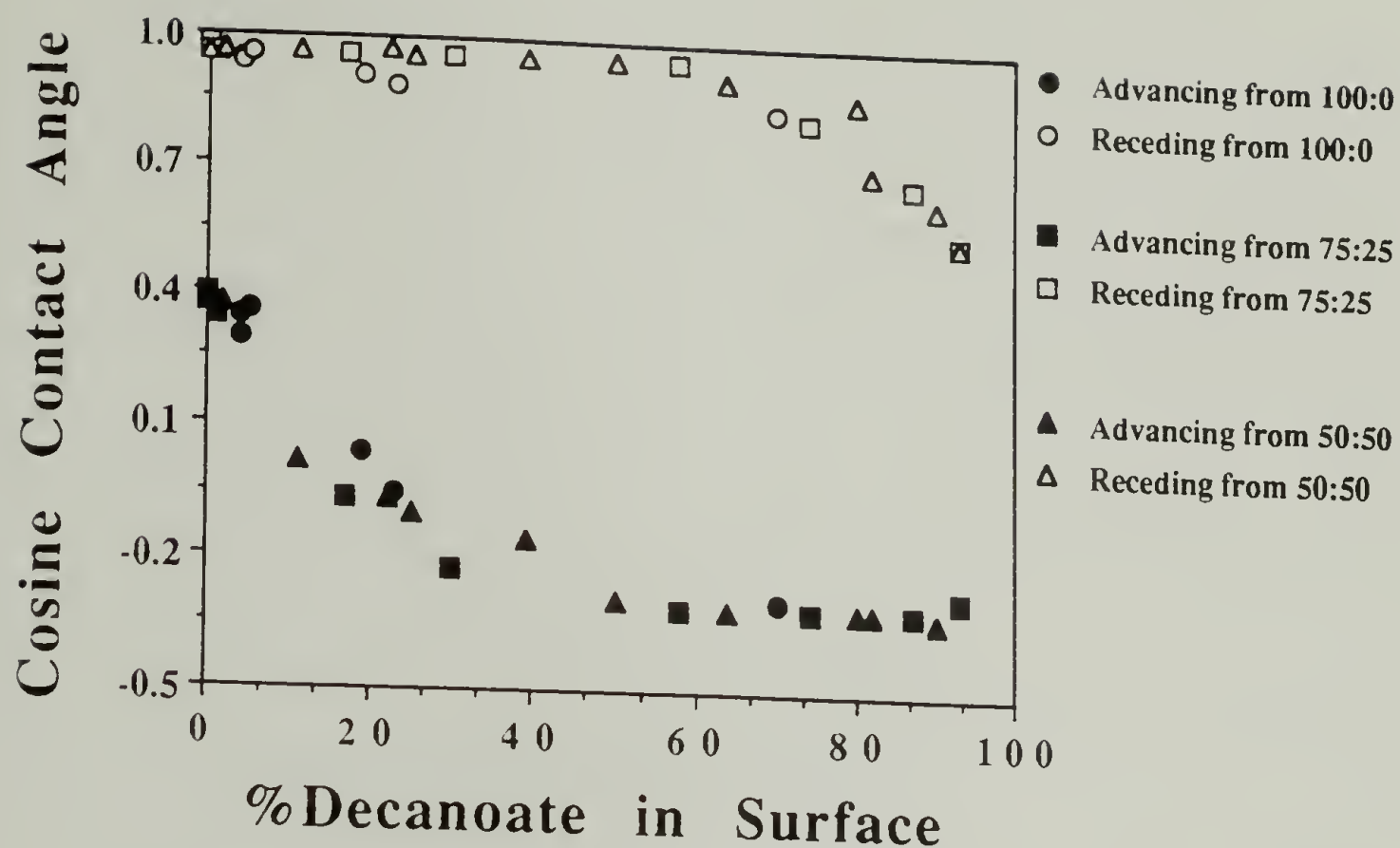


**Figure 5.48.** Cosine of the water contact angles as a function of surface composition for the mixed PCTFE-OH/ODec surfaces prepared by kinetic control of the hydrolyses of PCTFE-ODec.

to two factors. First, the purity of each of the surface phases is likely to be substantially less than 100% and thus there may be a surface excess of decanoate esters on the PCTFE-OH phase similar to that postulated for the mixed surfaces prepared by Method 1. Second, the patchy nature of the surface may force the advancing liquid contact line to be pinned at the boundary between the two surface phases. This pinning would result in an abnormally high contact angle (low  $\cos \Theta_A$ ) at relatively low decanoate concentrations, as is observed.

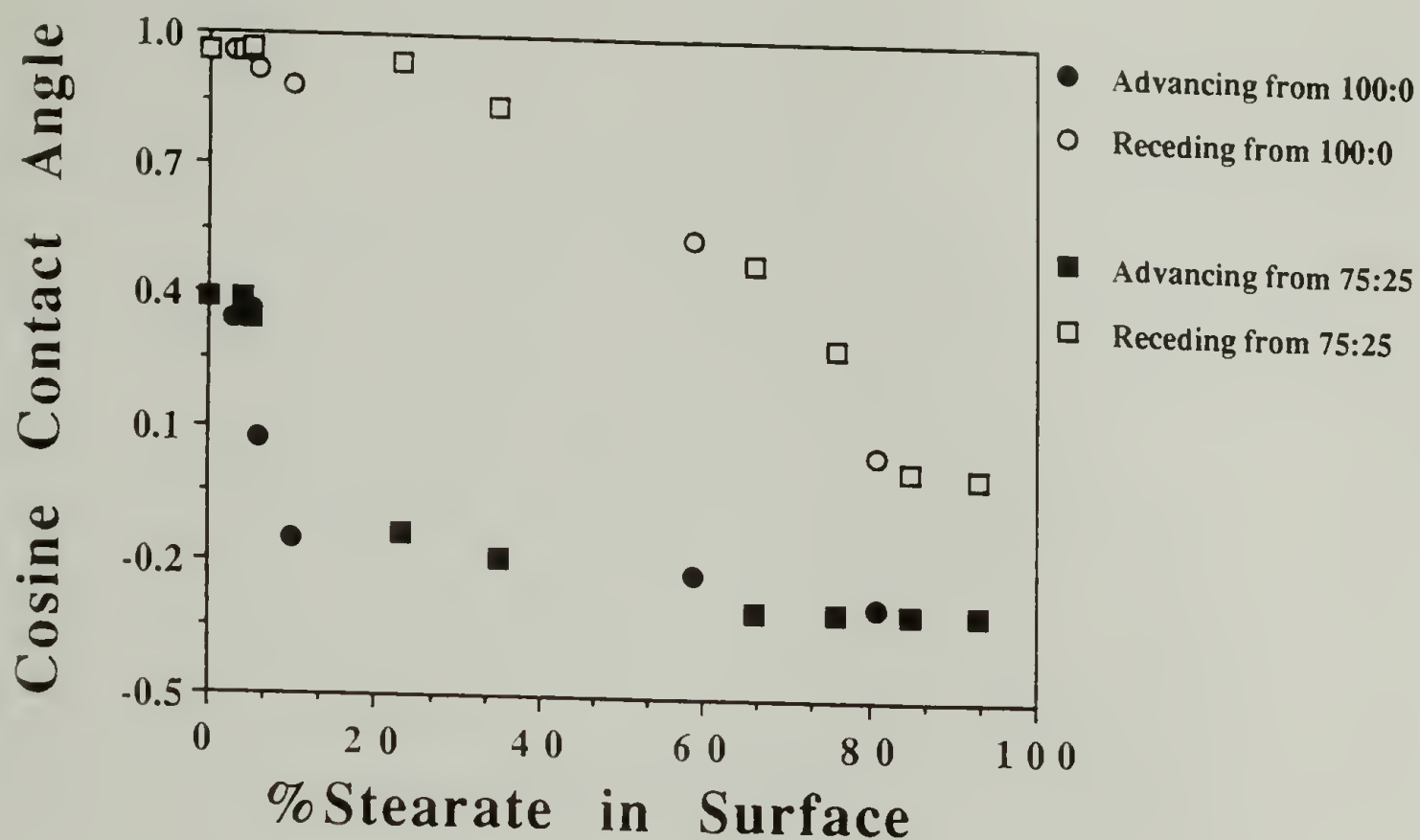


Figure 5.49. Cosine of the water contact angles as a function of surface composition for the mixed PCTFE-OH/OStear surfaces prepared by kinetic control of the hydrolyses of PCTFE-OStear.

In Figure 5.49,  $\cos \Theta_A$  and  $\cos \Theta_R$  for the hydrolyses of PCTFE-OStear are plotted as a function of the composition of the modified layer. Once again, the fact that the data from the two reactions are superimposable indicates similarity in the resulting mixed surface structures. These results should be compared with those from Figure 5.46 where the mixed PCTFE-OH/OStear surfaces were prepared by kinetic control of the esterification (Method 1). As discussed for the hydrolyses of PCTFE-OBu and PCTFE-ODec, the relatively high values of  $\cos \Theta_R$  for compositionally similar surfaces indicate the formation of patchy surfaces. In comparing the values of  $\cos \Theta_A$  between the two methods it is observed in Figure 5.49 that the initial decrease in

$\cos \Theta_A$  with increasing stearate concentration is greater than that observed in Figure 5.46. Recall from the discussion of the decanoate hydrolyses that this decrease is caused by a surface excess of esters on impure patches and contact line pinning at the patch boundaries. This larger hysteresis at low ester concentrations (compared to that observed on the PCTFE-OH/ODec prepared by both methods and the PCTFE-OH/OSTear from Method 1) indicates that the contact line pinning at the patch boundaries is the dominant factor and that the patches formed on these mixed surfaces (PCTFE-OH/OSTear from Method 2) are larger in size and/or more pure than those formed in the decanoate hydrolyses.

The hexadecane contact angle results as a function of surface composition for the hydrocarbon ester/heptafluorobutyrate mixed surfaces prepared by sequential esterifications are shown in Figures 5.50 - 5.52. For the PCTFE-OSTear/OHFB (Figure 5.50) mixed surfaces,  $\cos \Theta_A$  increases slightly from 0.500 to 0.515 as the concentration of stearates in the modified layer increases from 0 to 15% indicating that the concentration of heptafluorobutyrate esters at the film/air interface is high and remains relatively constant. At the same time,  $\cos \Theta_R$  increases from 0.766 to 0.990, reflecting a large increase in the number of methylene groups at the film/probe fluid interface. Above this modified layer concentration, the concentration of heptafluorobutyrate groups at the film/air interface begins to decrease and thus,  $\cos \Theta_A$  increases linearly with concentration to 0.966 at 67% stearate where primarily methylene groups are present at this interface.  $\cos \Theta_A$  then begins to decrease to 0.766 where the stearate content reaches 92%. This decrease is



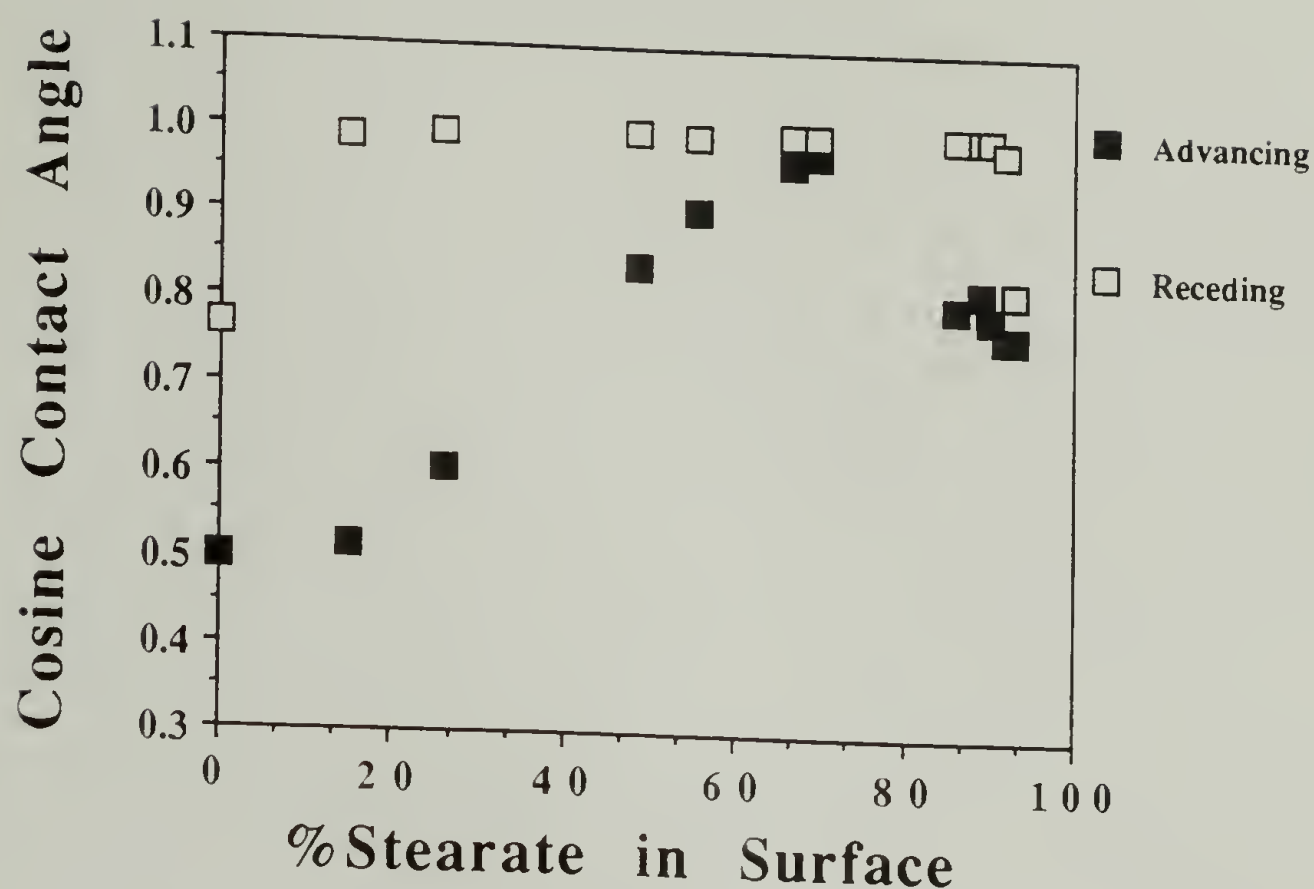


Figure 5.50. Cosine of the hexadecane contact angles as a function of surface composition for the mixed PCTFE-OSTear/OHFB surfaces prepared by sequential esterifications of PCTFE-OH.

the result of the formation of the ordered surface which presents methyl groups to the film/air interface. Above 15% stearate,  $\cos \Theta_R$  remains  $\sim 1$ , since the number of methylene groups at the film/probe fluid interface remains high. When the stearate concentration reaches 93%, a dramatic decrease in  $\cos \Theta_R$  to 0.819 is observed as the degree of ordering and hence, the number of methyl groups present at the interface, increases dramatically.

Except for the orientation behavior, the results for the PCTFE-ODec/OHFB mixed surfaces (Figure 5.51) exhibit trends similar to those discussed above. At high decanoate concentrations, both  $\cos \Theta_A$  and  $\cos \Theta_R$  remain constant at 0.98 and 1.00, respectively. When the decanoate concentration has decreased to  $\sim 76\%$ , the

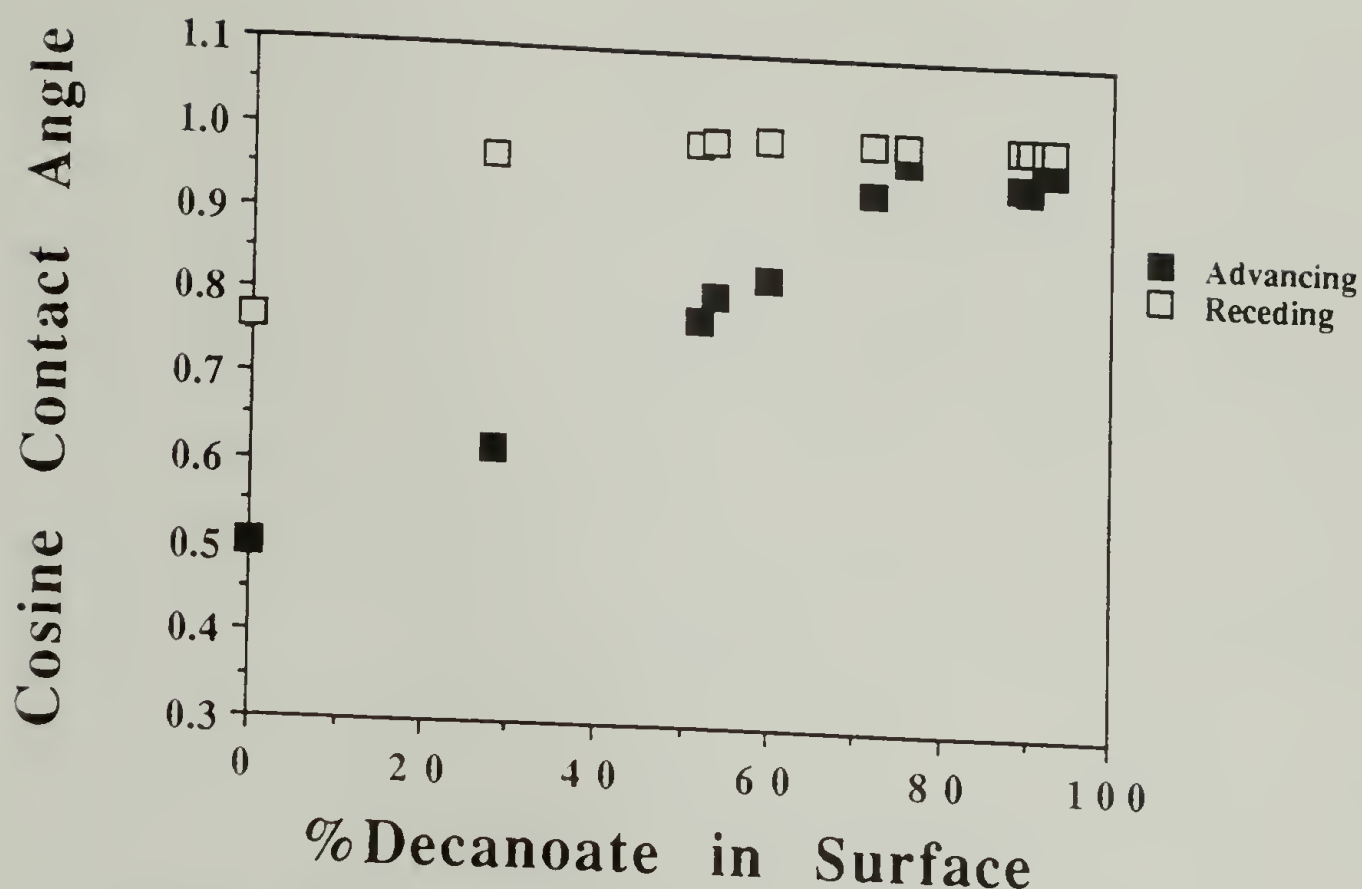


Figure 5.51. Cosine of the hexadecane contact angles as a function of surface composition for the mixed PCTFE-ODec/OHFB surfaces prepared by sequential esterifications of PCTFE-OH.

heptafluorobutyrate esters at the film/air interface begin to be observed as a decrease in  $\cos \Theta_A$ . This point occurs at slightly lower heptafluorobutyrate concentrations than was observed on the PCTFE-OSTear/OHFB mixed surfaces (67%), as would be expected based on the relative sizes of the two hydrocarbon esters. Also, the slope of the decrease in  $\cos \Theta_A$  is smaller for the PCTFE-ODec/OHFB mixed surfaces than that of the PCTFE-OSTear/OHFB surfaces for similar reasons. Unfortunately, modified surfaces with decanoate concentrations less than 20% were not prepared so the exact modified layer concentration at which the number of heptafluorobutyrate groups at the film/air interface reaches a constant, maximum value, cannot be determined. This value was

15% for the stearate/heptafluorobutyrate surfaces and would be expected to be slightly higher for the decanoate/heptafluorobutyrate mixed surfaces. In fact, the intersection of a line through the values of  $\cos \Theta_A$  between 28% and 76% decanoate with  $\cos \Theta_A = 0.50$  (a value consistent with the maximum number of heptafluorobutyrate groups at the film/air interface) comes at ~18%. As with the PCTFE-OStear/OHFB surfaces, the value of  $\cos \Theta_R$  remains high for even the lowest decanoate concentrations studied indicating a very low concentration of perfluoroesters at the film/probe fluid interface.

The hexadecane wetting behavior of the PCTFE-OBu/OHFB mixed surfaces (Figure 5.52) is similar to those of the two sets of mixed surfaces discussed above. The only differences are in the positions of the transition points in the  $\cos \Theta_A$  and  $\cos \Theta_R$  curves. Again, these differences are to be expected based on the relative sizes of the hydrocarbon ester chains. Since the sizes of the two esters in the PCTFE-OBu/OHFB mixed surfaces are comparable, the heptafluorobutyrate groups at the film/air interface are detected by  $\Theta_A$  even when the butyrate concentration is > 90%. As shown above this point occurs at 76% decanoate and 67% stearate for the other two sets of mixed surfaces.  $\cos \Theta_A$  then decreases linearly as the concentration of butyrate groups increases. Again, the slope of this decrease is less than that from the PCTFE-ODec/OHFB mixed surfaces (which is less than that of the PCTFE-OStear/OHFB surfaces) due to the smaller size of the butyrate ester. Extrapolation of this decrease to  $\cos \Theta_A = 0.50$  yields an intercept of 22% butyrate which is higher than that of the decanoate (18%) and stearate (15%) mixed surfaces, as expected. The high values of  $\cos \Theta_R$  for butyrate concentrations



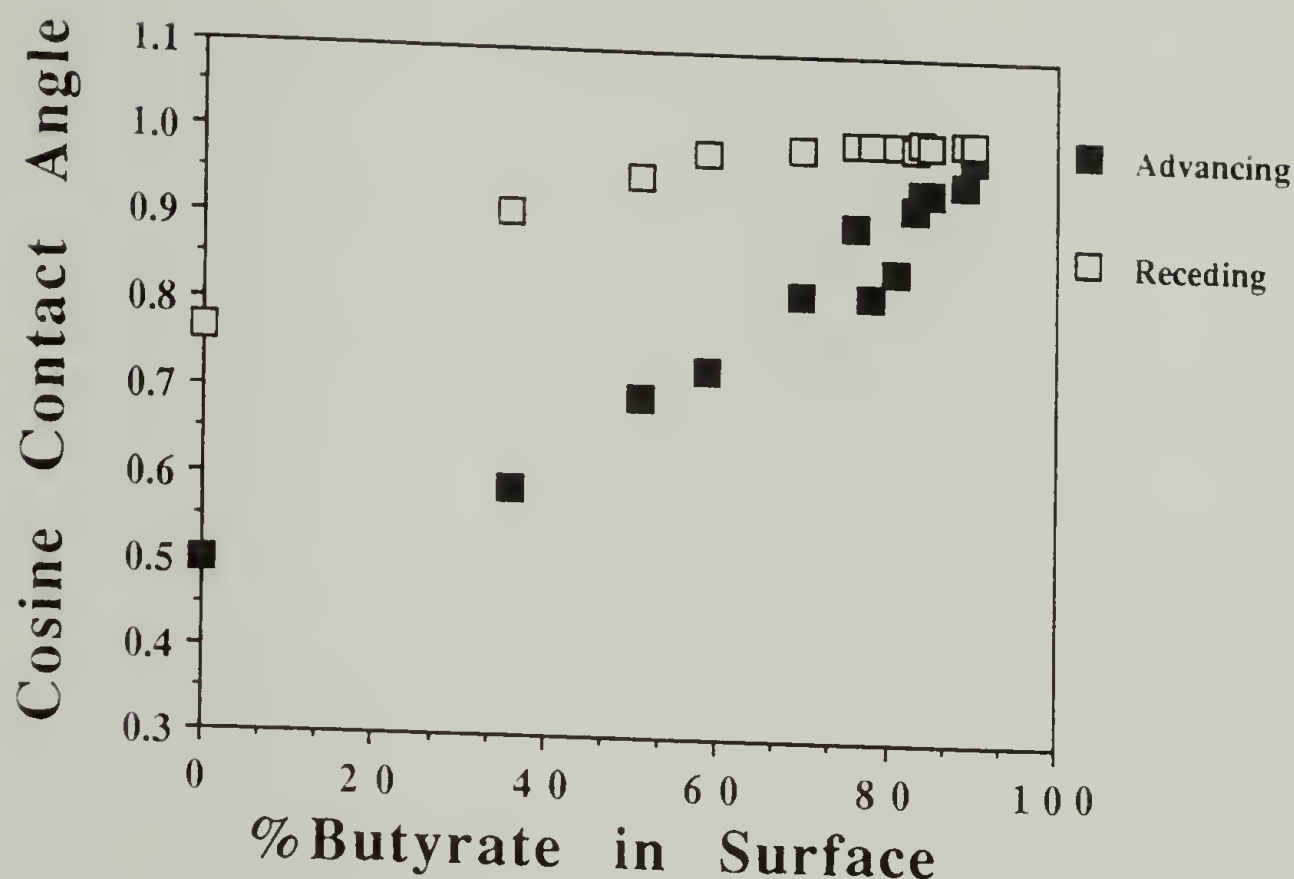


Figure 5.52. Cosine of the hexadecane contact angles as a function of surface composition for the mixed PCTFE-OBu/OHFB surfaces prepared by sequential esterifications of PCTFE-OH.

greater than 59% indicate little heptafluorobutyrate functionality is present at the film/probe fluid interface. Below this concentration, heptafluorobutyrate groups begin to be detected at this interface as indicated by decrease observed in  $\cos \Theta_R$ . It is interesting to note that this same decrease in  $\cos \Theta_R$  must also take place for the PCTFE-ODec/OHFB and PCTFE-OSTear/OHFB mixed surfaces, but it occurs below concentrations of 28% decanoate and 15% stearate which, unfortunately, were the lowest modified layer concentrations analyzed. The fact that the decrease in  $\cos \Theta_R$  is observed at a such a relatively high concentration is again a result of the similar size of the butyrate and heptafluorobutyrate moieties.

In order to study the effect of varying the perfluorocarbon ester chain length, PCTFE-OBuT/TFAc and PCTFE-OBuT/PFDec mixed surfaces were also prepared by sequential esterifications. These results are presented in Figures 5.53 and 5.54 for comparison with those from the similarly prepared PCTFE-OBuT/OHFB mixed surfaces (Figure 5.52). The results for the PCTFE-OBuT/OTFAc mixed surfaces (Figure 5.53) show differences from those for the PCTFE-OBuT/OHFB surfaces that would be expected based on the smaller trifluoroacetate group. The trifluoroacetate ester is not detected by  $\Theta_A$  until its concentration in the modified layer is greater than ~35%. Recall that the heptafluorobutyrate ester was detected at the film/air interface when its concentration was less than 10%. Also, the slope of the resulting decrease in  $\cos \Theta_A$  with decreasing butyrate concentration for the PCTFE-OBuT/TFAc surfaces is significantly less than that observed for the PCTFE-OBuT/OHFB mixed surfaces. Similarly,  $\cos \Theta_R$  on the PCTFE-OBuT/TFAc surfaces does not begin to decrease (which indicates detection of the trifluoroacetate at the film/probe fluid interface) until the concentration of perfluoroester in the modified layer is above at least 64%. As expected this value is significantly greater than that of 41% observed for the PCTFE-OBuT/OHFB surfaces. The hexadecane wetting behavior of the PCTFE-OBuT/OPFDec mixed surfaces (Figure 5.54) not only reflects changes in the surface composition, but also in the orientation of the perfluorodecanoate ester in the surface. On a pure perfluorodecanoate surface (butyrate concentration = 0%) the low values for  $\cos \Theta_A$  and  $\cos \Theta_R$  (0.326 and 0.574, respectively) indicate a high number of trifluoromethyl groups present at both the film/air

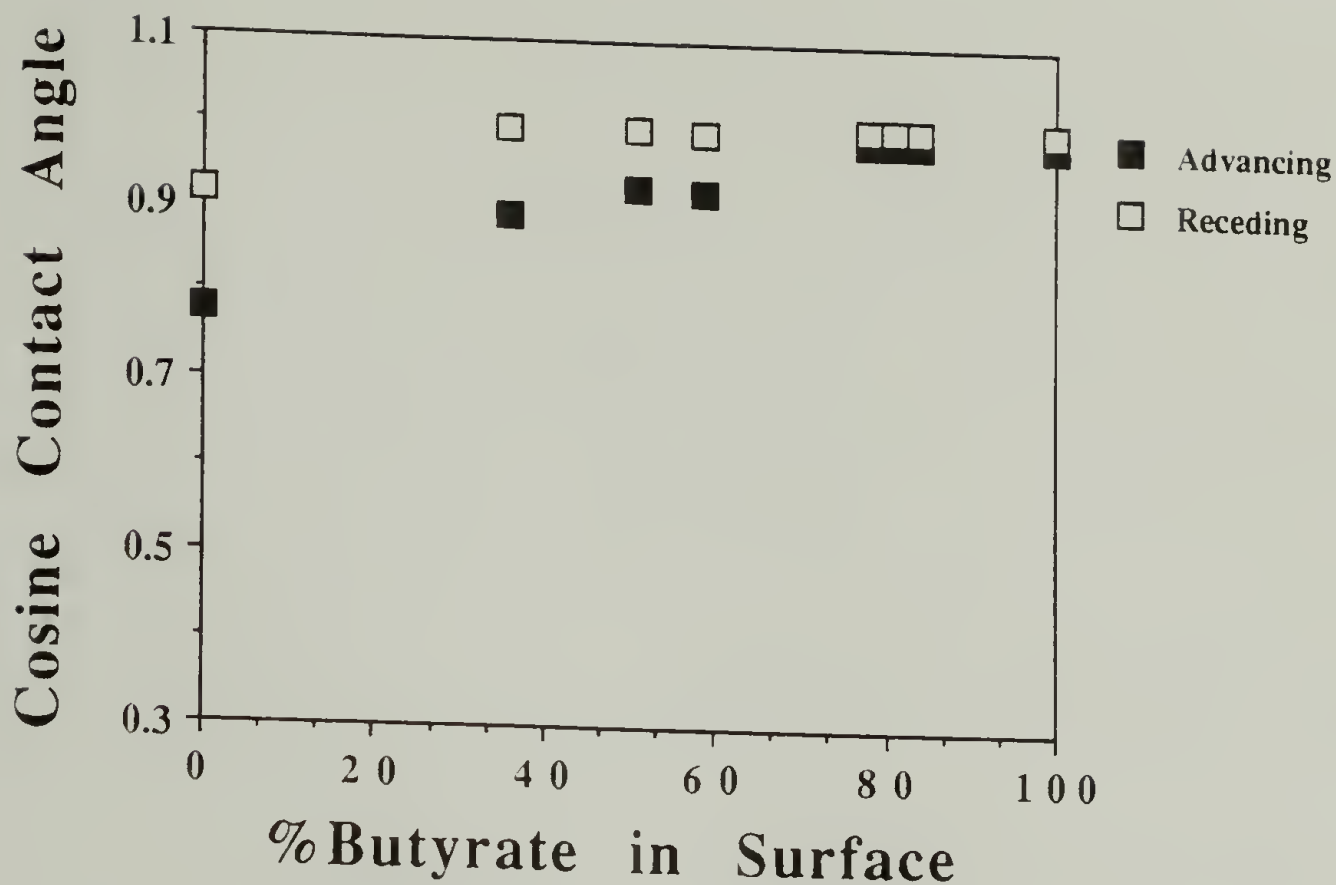


Figure 5.53. Cosine of the hexadecane contact angles as a function of surface composition for the mixed PCTFE-OBuT/OTFAc surfaces prepared by sequential esterifications of PCTFE-OH.

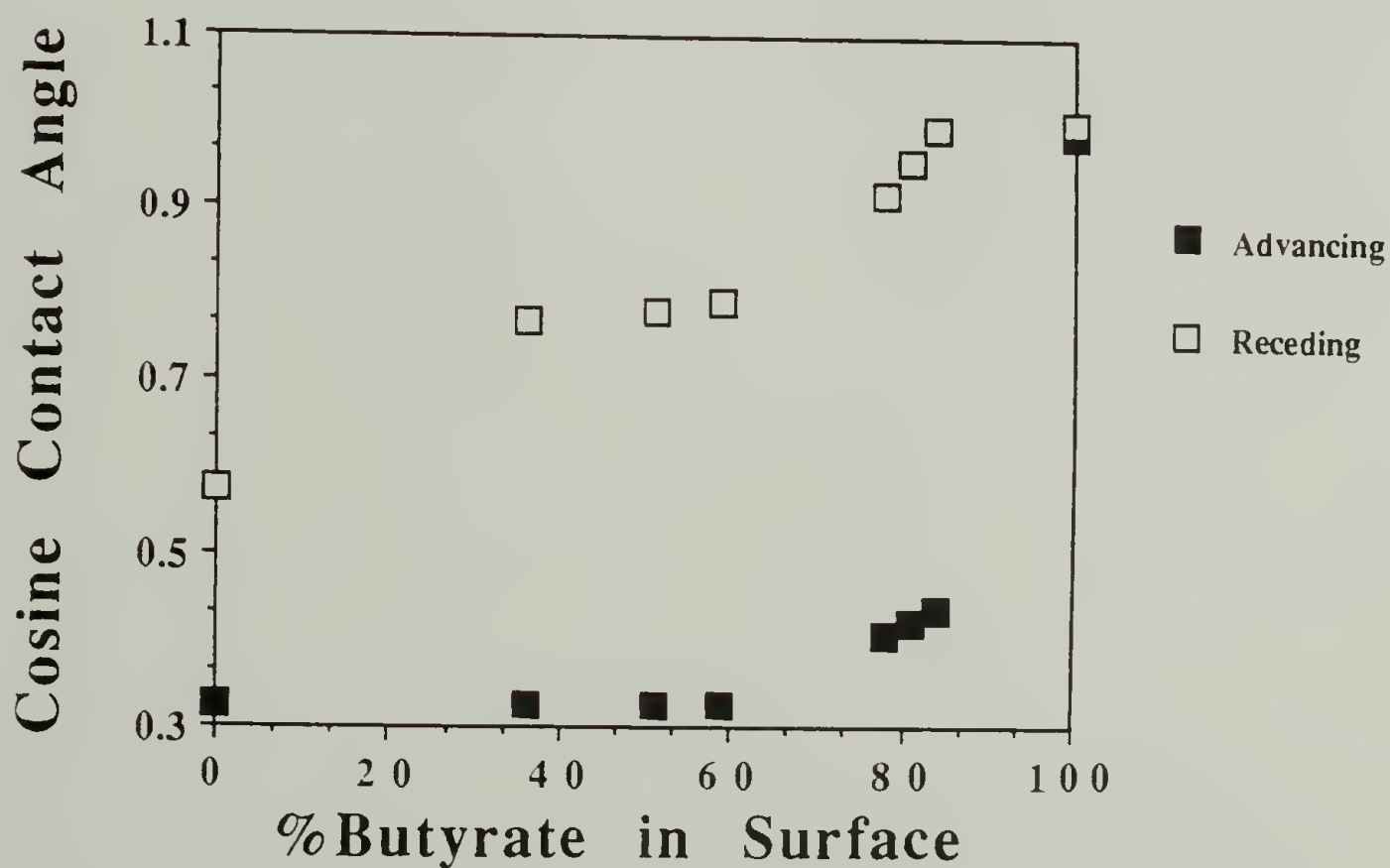


Figure 5.54. Cosine of the hexadecane contact angles as a function of surface composition for the mixed PCTFE-OBuT/OPFDec surfaces prepared by sequential esterifications of PCTFE-OH.



and film/probe fluid interfaces. When the concentration of the perfluorodecanoate esters in the modified layer decreases to 64%,  $\cos \Theta_R$  increases to 0.766 which is consistent with a high concentration of difluoromethylene groups at the film/probe fluid interface and hence disruption in the order of the perfluoroesters. However,  $\cos \Theta_A$  remains low (0.326) at this surface composition indicating that a significant number of trifluoromethyl groups remain at the film/air interface. As the amount of perfluorodecanoate in the surface decreases to 41%,  $\cos \Theta_A$  and  $\cos \Theta_R$  remain essentially constant, indicating that the compositions of the respective interfaces remain constant. Below this perfluorodecanoate concentration,  $\cos \Theta_A$  increases to 0.407 at a concentration of 22% and 0.438 at 16%. These values are consistent with a high concentration of difluoromethylene groups at the film/air interface and indicate that the order in the surface has been completely disrupted. At the same concentrations  $\cos \Theta_R$  has increased to 0.914 (22%) and 0.993 (16%) which reflects an interface composed of mostly methylene and a few difluoromethylene groups.

The hexadecane contact angle results for the mixed hydrocarbon ester/heptafluorobutyrate surfaces prepared by hydrolysis/re-esterification of the corresponding PCTFE-Esters (Method 2) are shown in Figures 5.55 - 5.57. The results from these figures should be compared with those in Figures 5.50 - 5.52 where the same mixed surfaces were prepared by sequential esterifications (Method 1). As for the mixed hydroxyl/ester surfaces prepared by Method 2, the results from the different hydrolysis conditions used are plotted in a single figure for each set of mixed surfaces. As

before, the fact that the results from the different hydrolyses used to prepare the PCTFE-OSTear/OHFB (Figure 5.55) and the PCTFE-ODec/OHFB (Figure 5.56) mixed surfaces are superimposable suggests that in these two cases the resulting surface structures are independent of the solution used in the initial hydrolysis. For both of these two sets of mixed surface the values of  $\cos \Theta_R$  can be superimposed on those from the randomly functionalized surfaces prepared by Method 1 (Figures 5.50 and 5.51). However, at high hydrocarbon ester concentrations in the modified layer, the values of  $\cos \Theta_A$  for both PCTFE-OSTear/OHFB and PCTFE-ODec/OHFB are significantly lower for the surfaces prepared by hydrolysis/re-esterification. Again, this greater contact angle hysteresis suggests that these surfaces are indeed patchy. For the mixed PCTFE-OBu/OHFB surfaces prepared by Method 2, the results for  $\cos \Theta_R$  from the two solution compositions used in the initial hydrolysis are also superimposable on themselves and on those from Figure 5.52. The results for  $\cos \Theta_A$  for the 75:25 (methanol:water) hydrolysis/re-esterification can also be superimposed on those from Figure 5.52. As discussed for the mixed PCTFE-OH/OBu, this behavior indicates that these hydrolysis conditions render randomly functionalized surfaces. However, the  $\cos \Theta_A$  results for the 0:100 hydrolysis/re-esterification show greater contact angle hysteresis which agrees with the results from the PCTFE-OH/OBu mixed surfaces in indicating that patchy surfaces have been formed.

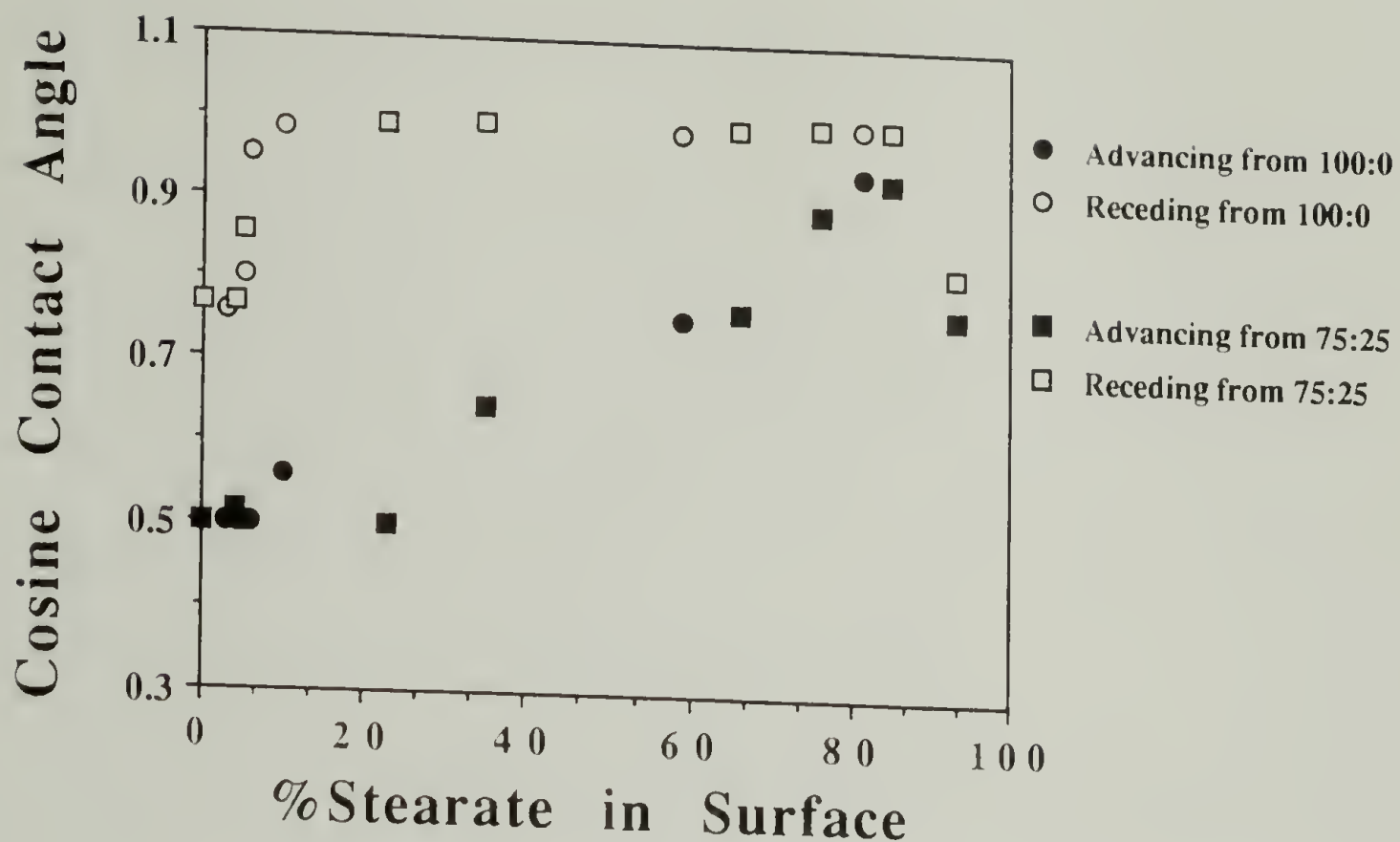


Figure 5.55. Cosine of the hexadecane contact angles as a function of surface composition for the mixed PCTFE-OSTear/OHFB surfaces prepared by the hydrolyses/re-esterification of PCTFE-OSTear.

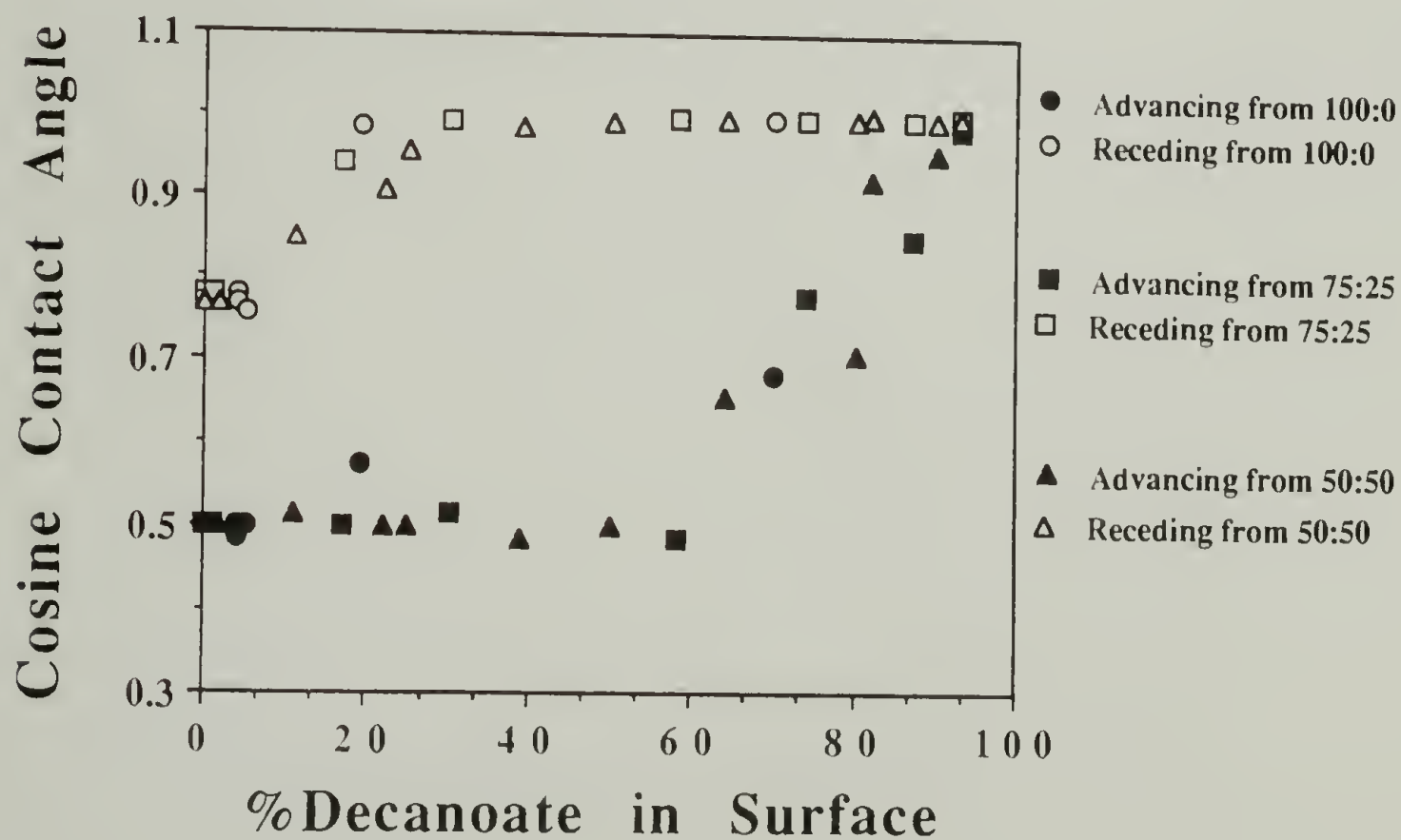


Figure 5.56. Cosine of the hexadecane contact angles as a function of surface composition for the mixed PCTFE-ODec/OHFB surfaces prepared by the hydrolyses/re-esterification of PCTFE-ODec.



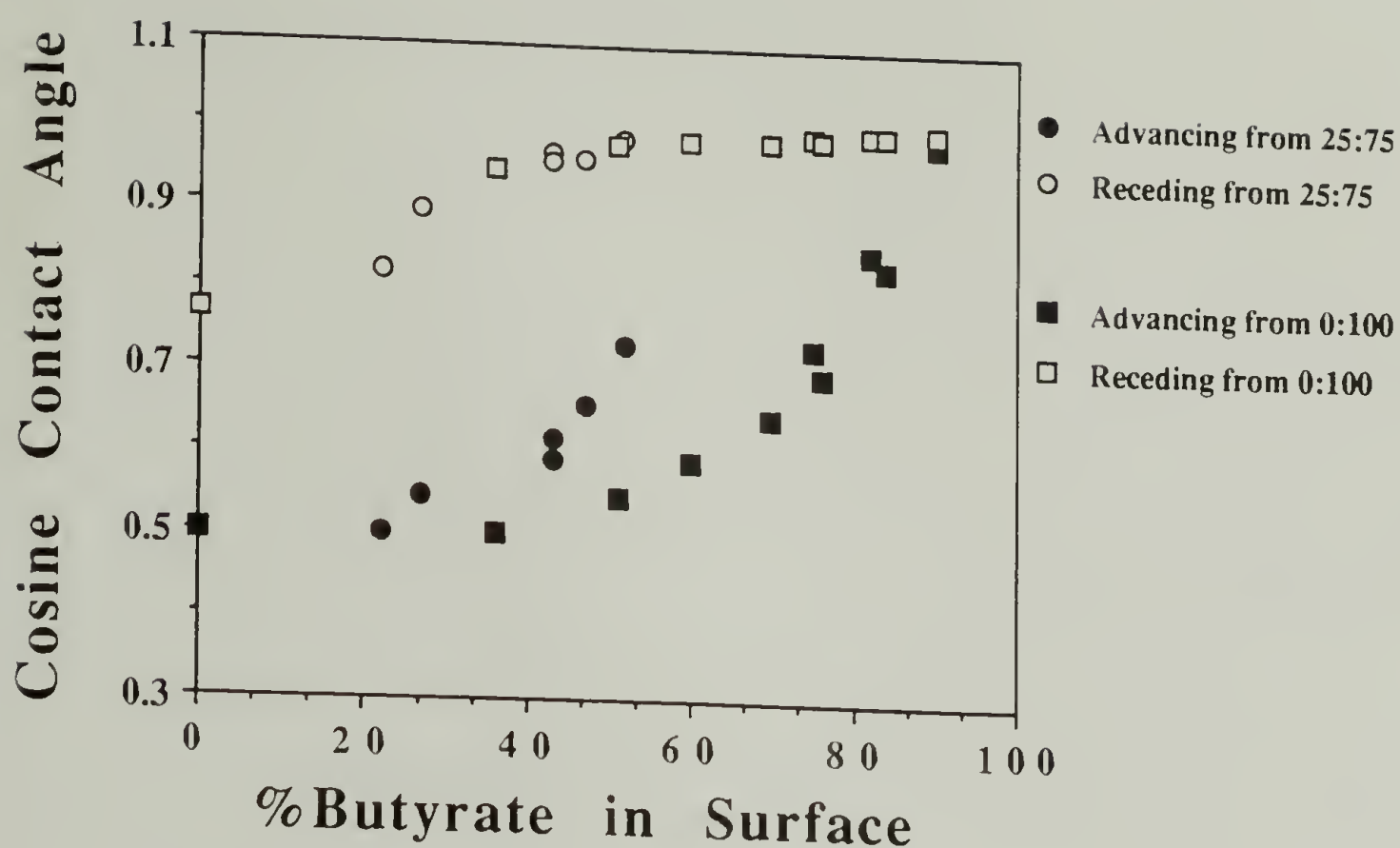


Figure 5.57. Cosine of the hexadecane contact angles as a function of surface composition for the mixed PCTFE-OBu/OHFB surfaces prepared by the hydrolyses/re-esterification of PCTFE-OBu.

### Conclusions and Future Work Suggestions

The results presented above show that the pyridine catalyzed esterifications of PCTFE-OH with a number of different acid chlorides are rapid (complete in less than 30 min) and proceed in high yield (> 90%). The uncatalyzed esterification with heptafluorobutyryl chloride was also shown to be fast and quantitative. This high reactivity made it infeasible to prepare a range of surface compositions with these reactions. On the other hand, the uncatalyzed esterifications with butyryl, decanoyl and stearoyl chlorides are substantially slower. After 24 h, the yields for these

three reactions are 84%, 76% and 70%, respectively. From these three initial esterifications a number of mixed alcohol/ester and mixed hydrocarbon ester/fluorocarbon ester surfaces were prepared. Attempts at preparing mixed PCTFE-OHFB/OBut surfaces through competitive reactions with the two acid chlorides were unsuccessful due to the high reactivity of the perfluorinated acid chloride. It was suggested that by substantially lowering the concentration of heptafluorobutyryl chloride in the reacting solution these mixed surfaces may be prepared.

A second method of mixed surface preparation utilized the hydrolysis of a number of PCTFE-Esters. The kinetics of the acid and base catalyzed hydrolyses of both perfluorocarbon and hydrocarbon esters were studied as a function of the solvent composition and the length of the ester chain. The results show that the acid catalyzed hydrolysis of these esters is very slow under conditions where the base catalyzed reaction is rapid. For the base catalyzed hydrolysis, the perfluorinated esters reacted much more quickly than their hydrocarbon analogs due to the high electrophilicity of the carbonyl in the former set of esters. Also, the rate of hydrolysis decreases as the length of the ester chain increases and/or as the solution becomes more polar. Both of these effects are the result of an increase in the interfacial free energy, which limits the ability of the reagents to penetrate into the film surface.

The wetting behavior of water and hexadecane on the mixed hydroxyl/ester and hydrocarbon ester/fluorocarbon ester surfaces, respectively, indicate that the method of the mixed surface preparation has a profound effect on the resulting surface structure.

In the mixed surfaces prepared by kinetic control of the initial esterification and a subsequent esterification the results indicate that the two functional groups are distributed randomly throughout the surface. As expected, the relatively high contact angle hysteresis on the mixed surfaces prepared by kinetic control of the hydrolysis of PCTFE-Esters and then re-esterification indicate that the two functional groups are segregated into patches on the surface.

A number of avenues for future research exist in the area of heterogeneous surface preparations. One that was not fully explored in the work presented in this dissertation concerned competitive esterifications. As discussed above, the high reactivity of perfluorinated acid chlorides would make it necessary to fully understand the effects of concentration on kinetics until mixed perfluorocarbon ester/hydrocarbon ester surfaces could be prepared by this method. It may turn out that the number of perfluorinated acid chlorides in solution will have to be less than the number of alcohols in the surface before the hydrocarbon acid chlorides can compete effectively. Alternatively, it may be possible to competitively prepare these types of mixed surfaces by selectively catalyzing the reaction with the hydrocarbon acid chloride. For example, a solution of butyryl pyridinium hydrochloride could be mixed with a solution of heptafluorobutyryl chloride. This mixture could then be added to PCTFE-OH for the competitive esterification. The same type of selective catalysis could be used in the reaction of PCTFE-OH with multifunctional reagents such as adipoyl chloride. This reagent has been shown to react multiply with PCTFE-OH producing a surface which contains few half ester/half acid species.



Using at least a two-fold excess of diacid chloride in the pyridine catalyzed reaction may result in the formation of mostly half acyl pyridinium/half acid chloride moieties. The pyridinium portion of the difunctional reagents may react so quickly with the surface that the concentration of the alcohol groups in the modified layer is depleted before the uncatalyzed portion of the molecule has time to react. This reaction would produce an acid chloride functionalized surface which could then be reacted with water or an alcohol to yield acid and ester surfaces, respectively. Alternatively, this half catalyzed difunctional acid chloride could be competitively reacted with butyryl pyridinium hydrochloride to prepare mixed acid chloride/ester surfaces.

It would also be interesting to prepare mixed stearate/acetate, stearate/butyrate and stearate/decanoate surfaces by each of the methods used in this chapter. The disruption of the order in the stearate surface by a short chain ester could then be studied as a function of the ester chain length, the surface composition and the preparative method.

Finally, it was discussed in this chapter that the hydrolysis of PCTFE-ODec and/or PCTFE-OSTear may produce surfaces which are "patchy" in nature. While "patchiness" can be inferred from the contact angle behavior, it would be desirable to image the surface by some technique in order to determine the sized of the patches and their size distribution. Perhaps the alcohols that result from the hydrolysis could be reacted with a fluorescent label, such as dansyl chloride, for fluorescence microscopy or a reagent containing an

element with a high atomic number, such as tribromoacetyl chloride, for backscattered electron imaging.

### References and Notes

- (1) Bain, C.D. and Whitesides, G.M. *J. Am. Chem. Soc.*, **1988**, *110*, 3665.
- (2) Bain, C.D. and Whitesides, G.M. *J. Am. Chem. Soc.*, **1988**, *110*, 6560.
- (3) Troughton, E.B.; Bain, C.D. and Whitesides, G.M. *Langmuir*, **1988**, *4*, 365.
- (4) Bain, C.D. and Whitesides, G.M. *Langmuir*, **1989**, *5*, 1370.
- (5) Laibinis, P.E.; Fox, M.A.; Folkers, J.P. and Whitesides, G.M. *Langmuir*, **1991**, *7*, 3167.
- (6) Cassie, A.B.D. *Discuss. Faraday Soc.*, **1948**, *3*, 11.
- (7) See Chapter III of this dissertation.
- (8) For a takeoff angle of  $75^\circ$  64.5% of the signal observed comes from a depth,  $t = \lambda$  while 95.5% comes from  $t = 3\lambda$  and at  $15^\circ$  64.5% comes from  $t = 0.27\lambda$  and 95.5% from  $t = 0.80\lambda$ . Where  $\lambda$  is the photoelectron's mean free path. (For C1s photoelectrons  $\lambda = 14 \text{ \AA}$ .)<sup>9</sup>
- (9) This value was measured in poly(*p*-xylylene): Clark, D.T. and Thomas, H.R. *J. Polym. Sci. Polym. Chem. Ed.* **1977**, *15*, 2843.
- (10) See Chapter I of this dissertation and references therein for a thorough of contact angles and dynamic wetting behavior.
- (11) The chlorine concentrations are 3.6% and 6.2% at  $15^\circ$  and  $75^\circ$  takeoff angles, respectively.
- (12) See the Data Tables in the Appendix for further information.

- (13) These C/F ratios are lower than what might be expected based on their water contact angles and reflect the detection of virgin PCTFE beneath the modified layer (Indicated by the relatively high chlorine concentrations (~5%) in the 75° takeoff angle XPS spectra).
- (14) The surface compositions were determined from the C/F ratio of the 75° takeoff angle spectra of the samples after labelling with heptafluorobutyryl chloride.<sup>8</sup>



# APPENDIX

## DATA TABLES FOR CHAPTER V

After Reaction of PCTFE-OH with Heptafluorobutyl Chloride (Catalyzed)								After Labelling with Butyryl Chloride					
Time min	$\Theta_T$	$\underline{C}$	$\underline{F}$	$\underline{Q}$	$\underline{Cl}$	$\underline{C/F}$	H <sub>2</sub> O	$\underline{C}$	$\underline{F}$	$\underline{Q}$	$\underline{Cl}$	$\underline{C/F}$	HD
							$\Theta_A/\Theta_R$						$\Theta_A/\Theta_R$
0	15	68.4	18.8	11.2	1.6	3.64	67/17	71.9	12.3	15.0	0.8	5.85	10/0
	75	61.4	22.8	10.9	4.8	2.69		70.7	13.3	14.8	1.1	5.31	
3	15	45.5	44.9	9.3	0.3	1.01	106/64	46.4	43.6	9.8	0.2	1.06	58/37
	75	49.2	40.1	9.6	1.2	1.23		50.5	38.8	9.9	0.8	1.30	
7	15	44.1	46.3	9.3	0.3	0.95	106/69	45.6	44.6	9.2	0.6	1.02	59/40
	75	48.0	41.5	9.0	1.5	1.16		47.8	41.2	8.6	2.4	1.16	
15	15	44.0	46.1	9.7	0.3	0.95	108/67	43.9	46.3	8.8	1.0	0.95	59/40
	75	47.5	41.9	9.4	1.3	1.13		46.6	42.2	8.8	2.4	1.09	

### After Reaction of PCTFE-OH with Butyryl Chloride (Catalyzed)

Time min	$\Theta_T$	$\underline{C}$	$\underline{F}$	$\underline{Q}$	$\underline{Cl}$	$\underline{C/F}$	$\underline{H_2O}$	$\Theta_A/\Theta_R$	
								$\underline{MI}$	$\underline{HD}$
0	15	68.4	18.8	11.2	1.6	3.64	67/17	55/41	18/6
	75	61.4	22.8	10.9	4.8	2.69			
3	15	69.8	15.4	13.6	1.2	4.53	78/40	58/39	14/5
	75	64.6	18.9	12.4	4.1	3.42			
7	15	70.7	13.8	14.4	1.1	5.12	83/45	58/36	12/3
	75	67.1	16.3	13.5	3.2	4.12			
15	15	71.4	13.1	14.3	1.3	5.45	86/49	61/33	10/0
	75	66.0	17.5	13.1	3.4	3.77			
30	15	72.0	13.0	14.3	1.0	5.54	88/52	60/29	10/0
	75	66.8	16.7	12.8	3.7	4.00			
60	15	71.9	12.6	14.3	1.2	5.71	87/53	63/26	10/0
	75	65.7	17.4	13.7	3.3	3.78			
120	15	72.2	11.9	15.0	0.9	6.07	89/54	66/22	10/0
	75	69.6	14.2	13.7	2.6	4.90			

After Labelling with Heptafluorobutyryl Chloride									
Time	$\Theta_A/\Theta_R$								
min	$\Theta_T$	$\underline{C}$	$\underline{F}$	$\underline{O}$	$\underline{Cl}$	$\underline{C/F}$	$\underline{H_2O}$	$\underline{MI}$	$\underline{HD}$
0	15	44.0	46.1	9.7	0.3	0.95	107/68	88/62	60/40
	75	47.5	41.9	9.4	1.3	1.13			
3	15	61.2	23.8	13.7	1.3	2.57	98/58	81/31	35/8
	75	61.1	22.6	12.9	3.4	2.70			
7	15	66.6	18.4	14.1	0.9	3.62	94/58	78/29	26/6
	75	62.4	20.7	12.9	4.0	3.01			
15	15	67.0	17.2	14.3	1.6	3.90	93/58	71/27	23/7
	75	65.5	18.2	13.3	3.1	3.60			
30	15	69.2	16.5	13.3	1.0	4.19	93/56	70/25	20/6
	75	65.7	17.2	13.6	3.5	3.82			
60	15	69.8	14.3	14.9	1.0	4.88	90/53	69/23	18/0
	75	67.4	16.0	13.6	3.1	4.21			
120	15	70.7	14.3	13.5	1.5	4.94	89/53	70/22	11/3
	75	67.7	15.7	12.7	3.0	4.31			

After Reaction of PCTFE-OH with Decanoyl Chloride(Catalyzed)								After Labelling with Heptafluorobutyryl Chloride					
Time	$\Theta_A/\Theta_R$							HD					
min	$\Theta_T$	$\underline{C}$	$\underline{F}$	$\underline{O}$	$\underline{Cl}$	$\underline{C/F}$	$\underline{H_2O}$	$\underline{C}$	$\underline{F}$	$\underline{O}$	$\underline{Cl}$	$\underline{C/F}$	$\Theta_A/\Theta_R$
0	15	68.4	18.8	11.2	1.6	3.64	67/17	44.0	46.1	9.7	0.3	0.95	60/40
	75	61.4	22.8	10.9	4.8	2.69		47.5	41.9	9.4	1.3	1.13	
4	15	84.2	6.4	8.8	0.7	13.2	104/50	79.8	10.2	9.6	0.3	7.82	18/0
	75	78.2	9.7	10.8	1.3	8.06		77.9	10.9	10.6	0.7	7.15	
7	15	82.4	7.4	9.6	0.7	11.2	105/54	79.2	10.7	9.8	0.4	7.40	17/0
	75	77.8	9.8	11.3	1.1	7.94		77.2	11.5	10.6	0.7	6.71	
15	15	84.5	6.1	9.0	0.5	13.9	106/54	81.4	9.1	9.3	0.3	8.95	13/0
	75	79.8	8.4	11.1	0.8	9.5		78.6	10.0	10.7	0.7	7.86	
30	15	84.1	5.6	10.0	0.3	15.0	107/57	82.2	8.3	9.2	0.4	9.90	11/0
	75	78.8	8.9	11.2	1.1	8.85		78.3	10.3	10.0	1.0	7.60	
60	15	83.1	5.9	10.3	0.7	14.1	108/57	82.6	8.1	9.0	0.3	10.2	11/0
	75	78.8	9.0	11.1	1.1	8.76		78.6	9.9	10.2	1.3	7.93	
120	15	82.6	7.7	9.2	0.6	10.7	107/57	82.1	8.4	9.3	0.2	9.77	10/0
	75	78.5	9.3	10.8	1.4	8.44		78.8	9.9	10.1	1.2	7.96	

After Reaction of PCTFE-OH with Stearoyl Chloride (Catalyzed)									After Labelling with Heptafluorobutyryl Chloride					
Time min	$\Theta_T$	$\underline{C}$	$\underline{F}$	$\underline{O}$	$\underline{Cl}$	$\underline{C/F}$	$\Theta_A/\Theta_R$	HD	$\underline{C}$	$\underline{F}$	$\underline{O}$	$\underline{Cl}$	$\underline{C/F}$	$\Theta_A/\Theta_R$
0	15	68.4	18.8	11.2	1.6	3.64	67/17	18/6						
	75	61.4	22.8	10.9	4.8	2.69			44.0	46.1	9.7	0.3	0.95	60/40
3	15	90.3	4.2	5.0	0.6	21.5	104/74	29/5	47.5	41.9	9.4	1.3	1.13	
	75	84.8	7.2	7.2	0.7	11.8			83.4	10.4	5.5	0.7	8.01	44/24
7	15	93.0	3.0	3.5	0.6	31.0	108/88	34/27	80.2	11.6	7.4	1.0	6.91	
	75	86.4	6.0	6.9	0.7	14.4			83.6	9.9	5.7	0.9	8.44	37/3
15	15	92.8	2.7	3.9	0.5	34.4	108/91	41/34	82.5	9.5	7.1	0.9	8.68	
	75	85.3	6.4	7.6	0.8	13.3			86.3	7.7	5.3	0.7	11.2	35/0
30	15	92.9	2.9	3.9	0.3	32.0	108/90	42/37	83.8	8.3	7.4	0.6	10.1	
	75	85.5	6.8	7.0	0.8	12.6			88.4	5.9	5.1	0.6	15.0	38/2
60	15	92.4	3.1	4.0	0.5	29.8	108/90	42/37	83.5	8.0	7.6	0.9	10.4	
	75	86.5	6.2	6.8	0.6	14.0			89.3	5.7	4.1	0.9	15.7	40/10
120	15	92.8	3.0	3.8	0.4	30.9	109/91	42/37	84.7	7.5	7.0	0.8	11.3	
	75	86.4	6.4	6.5	0.7	13.5			90.9	4.4	4.2	0.6	20.7	40/35
									85.1	7.2	7.0	0.8	11.8	

After Reaction of PCTFE-OH with Heptafluorobutyryl Chloride (Uncatalyzed)									After Labelling with Butyryl Chloride					
Time min	$\Theta_T$	$\underline{C}$	$\underline{F}$	$\underline{O}$	$\underline{Cl}$	$\underline{C/F}$	$\Theta_A/\Theta_R$	H <sub>2</sub> O	$\underline{C}$	$\underline{F}$	$\underline{O}$	$\underline{Cl}$	$\underline{C/F}$	$\Theta_A/\Theta_R$
0	15	68.4	18.8	11.2	1.6	3.64	67/17		71.9	12.3	15.0	0.8	5.85	10/0
	75	61.4	22.8	10.9	4.8	2.69			70.7	13.3	14.8	1.1	5.31	
15	15	43.6	46.2	9.8	0.5	0.94	106/63		44.7	46.8	8.3	0.3	0.96	61/28
	75	47.7	41.2	9.9	1.3	1.16			48.9	39.8	10.9	0.4	1.23	
30	15	43.5	47.1	9.2	0.2	0.94	108/66		43.4	45.7	10.7	0.2	0.95	60/40
	75	47.7	41.4	9.8	1.2	1.15			47.4	41.7	10.0	0.9	1.14	
60	15	45.6	44.9	9.1	0.4	1.02	108/67		43.7	45.9	10.1	0.3	0.95	61/41
	75	47.2	42.1	9.3	1.4	1.12			46.7	41.1	9.9	0.7	1.14	

After Reaction of PCTFE-OH with Butyryl Chloride (Uncatalyzed)									After Labelling with Trifluoroacetic Anhydride					
Time hr	$\Theta_T$	$\underline{C}$	$\underline{F}$	$\underline{O}$	$\underline{Cl}$	$\underline{C/F}$	$\Theta_A/\Theta_R$	H <sub>2</sub> O	$\underline{C}$	$\underline{F}$	$\underline{O}$	$\underline{Cl}$	$\underline{C/F}$	$\Theta_A/\Theta_R$
0	15	68.4	18.8	11.2	1.6	3.64	67/17		52.8	33.0	12.8	1.4	1.60	39/24
	75	61.4	22.8	10.9	4.8	2.69			54.3	30.9	13.4	1.4	1.76	
1	15	66.8	18.4	13.4	1.4	3.63	79/31		60.3	24.7	11.8	3.2	2.44	27/5
	75	65.7	19.0	13.0	2.3	3.46			60.2	25.0	12.8	2.0	2.41	
2	15	67.9	17.8	12.9	1.4	3.81	82/33		64.3	21.4	13.6	0.7	3.00	22/4
	75	66.9	17.7	13.1	2.3	3.78			64.0	21.2	13.3	1.6	3.02	
4	15	66.5	18.6	13.8	1.2	3.58	80/40		62.3	22.2	14.1	1.4	2.81	23/7
	75	65.1	18.3	14.2	2.5	3.56			61.4	22.7	13.3	2.6	2.70	
8	15	70.0	14.5	14.3	1.3	4.83	85/43		63.8	20.2	14.3	1.6	3.16	10/0
	75	68.4	15.8	14.2	1.7	4.33			65.7	18.7	13.8	1.8	3.51	
12	15	70.3	14.2	14.4	1.1	4.95	90/46		65.2	19.7	13.5	1.7	3.31	10/0
	75	68.6	15.9	14.2	1.3	4.31			66.0	18.6	13.6	1.8	3.55	
24	15	68.7	16.0	14.0	1.3	4.29	94/46		66.8	18.7	12.7	1.1	3.57	10/0
	75	67.2	17.1	14.3	1.5	3.93			66.9	17.7	13.5	1.9	3.78	



After Reaction of PCTFE-OH with Butyryl Chloride (Uncatalyzed)								After Labelling with Heptafluorobutyryl Chloride					
Time	H <sub>2</sub> O							HD					
hr	Q <sub>T</sub>	C	F	O	Cl	C/F	Q <sub>A</sub> /Q <sub>R</sub>	C	F	O	Cl	C/F	Q <sub>A</sub> /Q <sub>R</sub>
0	15	68.4	18.8	11.2	1.6	3.64	67/17	44.0	46.1	9.7	0.3	0.95	60/40
	75	61.4	22.8	10.9	4.8	2.69		47.5	41.9	9.4	1.3	1.13	
1	15	66.8	18.4	13.4	1.4	3.63	79/31	51.8	37.7	10.0	0.5	1.37	50/25
	75	65.7	19.0	13.0	2.3	3.46		54.3	33.9	11.0	0.9	1.60	
2	15	67.9	17.8	12.9	1.4	3.81	82/33	53.3	35.6	10.4	0.7	1.50	46/18
	75	66.9	17.7	13.1	2.3	3.78		57.4	29.6	11.5	1.5	1.94	
4	15	66.5	18.6	13.8	1.2	3.58	80/40	56.3	30.7	11.5	1.6	1.83	43/17
	75	65.1	18.3	14.2	2.5	3.56		58.7	26.9	11.9	2.5	2.18	
8	15	70.0	14.5	14.3	1.3	4.83	85/43	59.2	27.6	12.6	0.6	2.14	35/4
	75	68.4	15.8	14.2	1.7	4.33		65.1	20.6	12.9	1.4	3.16	
12	15	70.3	14.2	14.4	1.1	4.95	90/46	62.6	23.4	13.0	1.0	2.68	32/5
	75	68.6	15.9	14.2	1.3	4.31		65.9	19.2	13.6	1.3	3.43	
24	15	68.7	16.0	14.0	1.3	4.29	94/46	64.4	21.3	13.3	1.0	3.02	20/0
	75	67.2	17.1	14.3	1.5	3.93		66.6	18.0	14.2	1.2	3.70	

After Reaction of PCTFE-OH with Butyryl Chloride (Uncatalyzed)								After Labelling with Perfluorodecanoyl Chloride					
Time	H <sub>2</sub> O							HD					
hr	Q <sub>T</sub>	C	F	O	Cl	C/F	Q <sub>A</sub> /Q <sub>R</sub>	C	F	O	Cl	C/F	Q <sub>A</sub> /Q <sub>R</sub>
0	15	68.4	18.8	11.2	1.6	3.64	67/17	40.0	53.8	5.5	0.8	0.74	71/55
	75	61.4	22.8	10.9	4.8	2.69		44.6	48.4	6.1	0.9	0.92	
1	15	66.8	18.4	13.4	1.4	3.63	79/31	40.2	54.8	4.8	0.2	0.73	71/40
	75	65.7	19.0	13.0	2.3	3.46		47.7	44.3	7.1	0.9	1.08	
2	15	67.9	17.8	12.9	1.4	3.81	82/33	41.9	53.0	5.0	0.1	0.79	71/39
	75	66.9	17.7	13.1	2.3	3.78		49.4	42.3	7.5	0.8	1.17	
4	15	66.5	18.6	13.8	1.2	3.58	80/40	41.4	53.0	4.8	0.7	0.78	71/38
	75	65.1	18.3	14.2	2.5	3.56		48.0	43.0	7.5	1.5	1.12	
8	15	70.0	14.5	14.3	1.3	4.83	85/43	42.3	50.7	6.4	0.6	0.83	66/24
	75	68.4	15.8	14.2	1.7	4.33		51.7	37.8	9.2	1.3	1.37	
12	15	70.3	14.2	14.4	1.1	4.95	90/46	46.2	45.6	7.4	0.7	1.01	65/18
	75	68.6	15.9	14.2	1.3	4.31		54.9	32.7	9.9	2.5	1.68	
24	15	68.7	16.0	14.0	1.3	4.29	94/46	47.1	44.5	7.9	0.5	1.06	64/7
	75	67.2	17.1	14.3	1.5	3.93		56.9	31.4	11.1	0.6	1.81	

After Reaction of PCTFE-OH with Decanoyl Chloride (Uncatalyzed)								After Labelling with Heptafluorobutyryl Chloride					
Time	H <sub>2</sub> O							HD					
hr	Q <sub>T</sub>	C	F	Q	Cl	C/F	Q <sub>A</sub> /Q <sub>R</sub>	C	F	Q	Cl	C/F	Q <sub>A</sub> /Q <sub>R</sub>
0	15	68.4	18.8	11.2	1.6	3.64	67/17	44.0	46.1	9.7	0.3	0.95	60/40
	75	61.4	22.8	10.9	4.8	2.69		47.5	41.9	9.4	1.3	1.13	
1	15	74.3	14.7	10.0	1.0	5.05	100/33	52.8	36.9	9.6	0.6	1.43	52/14
	75	70.5	17.5	10.1	1.8	4.03		56.1	32.8	9.7	1.5	1.71	
2	15	78.4	11.9	8.8	0.9	6.58	101/38	60.7	29.1	9.5	0.8	2.09	39/7
	75	72.7	14.6	10.5	2.2	4.98		64.1	24.4	10.4	1.2	2.63	
4	15	78.2	11.2	9.7	1.0	6.98	104/39	62.5	27.7	9.3	0.5	2.26	36/5
	75	75.9	11.4	11.1	1.6	6.66		64.9	23.8	10.3	1.1	2.73	
8	15	80.7	9.4	9.1	0.8	8.59	105/42	65.0	25.1	9.5	0.5	2.59	34/0
	75	77.0	11.2	10.3	1.6	6.88		66.9	21.8	10.1	1.2	3.07	
12	15	82.3	7.3	9.8	0.6	11.3	107/45	71.2	19.0	9.5	0.4	3.75	20/0
	75	77.8	10.0	11.3	1.0	7.78		70.8	17.3	11.1	0.8	4.09	
24	15	84.3	5.8	9.4	0.4	14.5	108/51	72.5	17.8	9.1	0.6	4.07	11/0
	75	79.3	9.1	10.8	0.9	8.71		72.0	16.4	10.1	1.5	4.39	

After Reaction of PCTFE-OH with Stearoyl Chloride (Uncatalyzed)									After Labelling with Heptafluorobutyryl Chloride					
Time	H <sub>2</sub> O								HD					
hr	Q <sub>T</sub>	C	F	Q	Cl	C/F	Q <sub>A</sub> /Q <sub>R</sub>	Q <sub>A</sub> /Q <sub>R</sub>	C	F	Q	Cl	C/F	Q <sub>A</sub> /Q <sub>R</sub>
0	15	68.4	18.8	11.2	1.6	3.64	67/17	18/6	44.0	46.1	9.7	0.3	0.95	60/40
	75	61.4	22.8	10.9	4.8	2.69			47.5	41.9	9.4	1.3	1.13	
1	15	71.1	17.3	10.3	1.3	4.11	80/19	11/0	51.6	39.3	8.6	0.5	1.31	59/8
	75	71.3	15.1	10.9	2.7	4.72			54.7	35.0	9.0	1.4	1.56	
2	15	78.4	12.5	7.9	1.2	6.27	98/27	20/4	55.6	35.2	8.7	0.6	1.58	53/4
	75	74.4	13.3	9.7	2.6	5.59			59.5	30.2	8.7	1.6	1.97	
4	15	88.7	6.0	4.8	0.5	14.8	104/56	27/17	60.7	30.3	8.5	0.5	2.00	33/0
	75	82.4	8.8	8.0	0.9	9.36			69.4	21.5	8.5	0.6	3.23	
8	15	90.4	4.7	4.4	0.6	19.2	105/75	34/25	66.8	24.2	8.3	0.7	2.76	25/5
	75	82.6	8.2	8.1	1.1	10.1			72.1	18.6	8.4	0.9	3.88	
12	15	90.4	5.1	3.9	0.7	17.7	108/84	42/34	74.9	16.5	8.0	0.6	4.54	15/0
	75	83.6	7.9	7.4	1.1	10.6			75.3	15.2	8.5	1.0	4.95	
24	15	91.6	4.5	3.5	0.4	20.4	111/91	41/35	75.7	16.5	7.0	0.7	4.59	12/0
	75	84.2	7.8	7.3	0.8	10.8			77.3	14.2	7.7	0.9	5.44	

After Hydrolysis of PCTFE-OHFB (methanol:water, 100:0)								After Labelling with Butyryl Chloride					
Time	H <sub>2</sub> O							HD					
min	Q <sub>T</sub>	C	F	Q	Cl	C/F	Q <sub>A</sub> /Q <sub>R</sub>	C	F	Q	Cl	C/F	Q <sub>A</sub> /Q <sub>R</sub>
0	15	44.0	46.1	9.7	0.3	0.95	108/67	43.9	46.3	8.8	1.0	0.95	60/40
	75	47.5	41.9	9.4	1.3	1.13		46.6	42.2	8.8	2.4	1.09	
15	15	64.9	21.4	12.2	1.6	3.03	70/21	68.0	15.4	14.7	1.9	4.42	14/5
	75	62.6	21.9	11.5	4.6	2.86		67.2	16.9	13.1	2.9	3.98	
30	15	63.0	20.5	14.5	2.1	3.07	71/20	66.8	14.9	15.2	3.1	4.48	15/4
	75	61.6	21.1	12.7	4.6	2.92		64.3	18.6	13.1	4.0	3.46	
60	15	63.3	19.5	15.1	2.1	3.25	69/19	69.5	13.0	15.8	1.7	5.35	12/3
	75	61.2	21.3	12.6	5.0	2.87		67.5	15.6	14.5	2.5	4.33	
120	15	63.7	20.5	13.8	2.0	3.11	71/18	65.0	16.4	15.6	3.0	3.96	11/3
	75	59.9	21.6	12.7	5.8	2.77		62.4	19.2	13.8	4.7	3.25	

After Hydrolysis of PCTFE-OHFB  
(methanol:water, 75:25)

Time min	$\Theta_T$	$\underline{C}$	$\underline{F}$	$\underline{O}$	$\underline{Cl}$	$\underline{C/F}$	H <sub>2</sub> O $\Theta_A/\Theta_R$
0	15	44.0	46.1	9.7	0.3	0.95	108/67
	75	47.5	41.9	9.4	1.3	1.13	
15	15	64.5	21.5	12.2	1.8	3.00	70/20
	75	61.5	22.7	11.4	4.5	2.71	
30	15	64.2	19.3	14.0	2.5	3.33	72/19
	75	58.0	24.2	10.5	7.3	2.40	
60	15	64.6	21.5	11.8	2.1	3.00	70/21
	75	60.0	23.8	10.8	5.4	2.52	
120	15	61.4	21.2	14.0	3.3	2.90	73/19
	75	55.4	26.5	11.0	7.1	2.09	

After Labelling with Butyryl Chloride

$\underline{C}$	$\underline{F}$	$\underline{O}$	$\underline{Cl}$	$\underline{C/F}$	HD $\Theta_A/\Theta_R$
43.9	46.3	8.8	1.0	0.95	60/40
46.6	42.2	8.8	2.4	1.09	
70.0	12.1	16.6	1.4	5.79	10/5
69.0	14.4	14.8	1.8	4.79	
67.9	15.6	14.2	2.2	4.35	12/3
64.9	17.9	13.4	3.7	3.63	
66.8	16.4	14.2	2.7	4.07	11/0
65.8	17.8	12.4	3.9	3.70	
69.7	13.6	15.0	1.7	5.13	12/5
66.5	16.2	14.5	2.8	4.10	

After Hydrolysis of PCTFE-OHFB  
(methanol:water, 50:50)

Time min	$\Theta_T$	$\underline{C}$	$\underline{F}$	$\underline{O}$	$\underline{Cl}$	$\underline{C/F}$	H <sub>2</sub> O $\Theta_A/\Theta_R$
0	15	44.0	46.1	9.7	0.3	0.95	108/67
	75	47.5	41.9	9.4	1.3	1.13	
15	15	63.9	22.2	11.8	2.1	2.88	72/21
	75	59.0	24.6	10.7	5.7	2.40	
30	15	62.0	23.0	12.8	2.2	2.70	71/21
	75	59.9	23.1	11.4	5.6	2.59	
60	15	59.8	23.9	14.4	2.0	2.50	66/14
	75	59.2	23.2	12.6	5.0	2.55	
120	15	62.2	20.1	15.1	2.5	3.09	71/13
	75	56.6	24.2	12.8	6.4	2.34	

After Labelling with Butyryl Chloride

$\underline{C}$	$\underline{F}$	$\underline{O}$	$\underline{Cl}$	$\underline{C/F}$	HD $\Theta_A/\Theta_R$
43.9	46.3	8.8	1.0	0.95	60/40
46.6	42.2	8.8	2.4	1.09	
72.6	11.9	13.9	1.6	6.10	9/0
67.5	16.0	13.5	3.1	4.22	
67.9	15.6	14.4	2.1	4.35	14/1
66.0	17.5	13.6	2.9	3.77	
67.5	15.3	14.8	2.4	4.41	14/4
65.4	16.9	14.4	3.3	3.87	
71.4	12.0	15.4	1.2	5.95	14/0
70.0	13.7	14.8	1.4	5.11	

After Hydrolysis of PCTFE-OHFB  
(methanol:water, 25:75)

Time min	$\Theta_T$	$\underline{C}$	$\underline{F}$	$\underline{O}$	$\underline{Cl}$	$\underline{C/F}$	H <sub>2</sub> O $\Theta_A/\Theta_R$
0	15	44.0	46.1	9.7	0.3	0.95	108/67
	75	47.5	41.9	9.4	1.3	1.13	
15	15	66.4	18.9	13.4	1.3	3.51	74/27
	75	63.3	21.1	12.2	3.4	3.00	
30	15	64.6	22.7	10.9	1.7	2.85	72/21
	75	61.1	23.0	11.4	4.6	2.66	
60	15	62.6	23.7	11.0	2.7	2.64	72/18
	75	57.4	26.7	9.9	6.0	2.15	
120	15	60.2	25.6	10.5	3.8	2.35	66/15
	75	58.8	25.3	10.4	5.5	2.32	

After Labelling with Butyryl Chloride

$\underline{C}$	$\underline{F}$	$\underline{O}$	$\underline{Cl}$	$\underline{C/F}$	HD $\Theta_A/\Theta_R$
43.9	46.3	8.8	1.0	0.95	60/40
46.6	42.2	8.8	2.4	1.09	
63.2	15.6	20.2	1.0	4.05	23/9
66.1	16.4	15.7	1.7	4.03	
71.0	11.4	16.8	0.8	6.23	14/6
71.3	12.3	15.9	0.5	5.80	
64.3	20.9	11.5	3.3	3.08	13/0
58.8	24.7	0.5	5.9	2.38	
67.5	12.0	18.2	2.4	5.63	14/4
61.1	20.2	13.8	4.9	3.02	



After Hydrolysis of PCTFE-OHFB  
(methanol:water, 0:100)

Time min	$\Theta_T$	$\underline{C}$	$\underline{F}$	$\underline{O}$	$\underline{Cl}$	$\underline{C/F}$	H <sub>2</sub> O $\Theta_A/\Theta_R$
0	15	44.0	46.1	9.7	0.3	0.95	108/67
	75	47.5	41.9	9.4	1.3	1.13	
15	15	63.5	23.2	10.9	2.5	2.74	74/26
	75	57.8	25.7	11.7	4.8	2.25	
30	15	66.0	18.7	13.3	2.0	3.53	68/18
	75	64.3	19.8	12.6	3.4	3.25	
60	15	66.8	19.5	11.9	1.7	3.43	65/15
	75	61.1	22.6	11.8	4.5	2.70	
120	15	65.7	19.2	12.7	2.4	3.42	65/16
	75	60.0	23.3	11.4	5.3	2.58	

After Labelling with Butyryl Chloride

$\underline{C}$	$\underline{F}$	$\underline{O}$	$\underline{Cl}$	$\underline{C/F}$	HD $\Theta_A/\Theta_R$
43.9	46.3	8.8	1.0	0.95	60/40
46.6	42.2	8.8	2.4	1.09	
64.5	19.3	14.3	1.8	3.34	24/12
65.7	17.8	14.3	2.3	3.69	
67.5	15.3	15.4	1.7	4.41	19/6
68.2	14.6	15.4	1.8	4.67	
66.9	15.3	15.2	2.6	4.37	12/4
69.3	14.2	14.5	2.0	4.88	
65.0	17.4	14.6	3.0	3.73	10/0
63.4	18.0	14.5	4.1	3.52	

After Hydrolysis of PCTFE-OHFB  
(methanol:water, 0:100, 15 min)

Temp °C	$\Theta_T$	$\underline{C}$	$\underline{F}$	$\underline{O}$	$\underline{Cl}$	$\underline{C/F}$	H <sub>2</sub> O $\Theta_A/\Theta_R$
105	15	63.5	23.2	10.9	2.5	2.74	74/26
	75	57.8	25.7	11.7	4.8	2.25	
90	15	61.1	25.4	12.4	1.0	2.41	84/27
	75	62.2	22.8	12.6	2.4	2.73	
60	15	53.9	34.0	10.9	1.2	1.59	90/31
	75	55.3	31.1	10.6	3.1	1.78	
30	15	49.4	39.0	11.2	0.5	1.27	99/36
	75	54.1	33.0	11.9	1.0	1.64	
No react	15	44.0	46.1	9.7	0.3	0.95	108/67
	75	47.5	41.9	9.4	1.3	1.13	

After Labelling with Butyryl Chloride

$\underline{C}$	$\underline{F}$	$\underline{O}$	$\underline{Cl}$	$\underline{C/F}$	HD $\Theta_A/\Theta_R$
64.5	19.3	14.3	1.8	3.34	24/12
65.7	17.8	14.3	2.3	3.69	
65.3	18.0	15.3	1.4	3.63	26/11
68.1	14.9	15.7	1.3	4.57	
53.7	32.2	13.0	1.2	1.67	44/12
60.0	25.2	12.6	2.3	2.38	
52.3	36.5	11.0	0.3	1.43	48/15
57.0	30.1	11.2	1.6	1.89	
43.9	46.3	8.8	1.0	0.95	60/40
46.6	42.2	8.8	2.4	1.09	

After Hydrolysis of PCTFE-OBuT  
(methanol:water, 100:0)

Time min	$\Theta_T$	$\underline{C}$	$\underline{F}$	$\underline{O}$	$\underline{Cl}$	$\underline{C/F}$	H <sub>2</sub> O $\Theta_A/\Theta_R$
0	15	71.9	12.3	15.0	0.8	5.85	89/54
	75	70.7	13.3	14.8	1.1	5.31	
15	15	67.1	18.3	13.1	1.6	3.67	71/25
	75	63.5	20.5	11.7	4.3	3.10	
30	15	67.1	19.1	12.5	1.2	3.51	62/19
	75	63.7	20.1	12.3	4.0	3.17	
60	15	66.6	20.1	12.1	1.2	3.31	73/18
	75	65.2	19.2	12.9	2.8	3.40	
120	15	65.6	18.9	13.2	2.3	3.47	75/20
	75	62.0	21.1	11.5	5.4	2.94	

After Labelling with  
Heptafluorobutyryl Chloride

$\underline{C}$	$\underline{F}$	$\underline{O}$	$\underline{Cl}$	$\underline{C/F}$	HD $\Theta_A/\Theta_R$
70.7	14.3	13.5	1.5	4.94	10/0
67.7	15.7	12.7	3.0	4.31	
49.2	40.1	9.5	1.2	1.23	56/28
48.8	39.0	9.8	2.5	1.25	
47.4	42.4	9.8	0.4	1.12	57/36
49.5	38.9	10.0	1.7	1.27	
47.3	42.3	9.9	0.6	1.12	59/38
50.0	39.0	9.7	1.3	1.28	
45.3	44.6	9.4	0.7	1.02	60/41
49.3	39.0	9.5	2.2	1.26	

After Hydrolysis of PCTFE-OBuT (methanol:water, 75:25)								After Labelling with Heptafluorobutyryl Chloride					
Time min	$\Theta_T$	$\underline{C}$	$\underline{F}$	$\underline{O}$	$\underline{Cl}$	$\underline{C/F}$	H <sub>2</sub> O $\Theta_A/\Theta_R$	$\underline{C}$	$\underline{F}$	$\underline{O}$	$\underline{Cl}$	$\underline{C/F}$	HD $\Theta_A/\Theta_R$
0	15	71.9	12.3	15.0	0.8	5.85	89/54	70.7	14.3	13.5	1.5	4.94	10/0
	75	70.7	13.3	14.8	1.1	5.31		67.7	15.7	12.7	3.0	4.31	
15	15	67.2	18.2	12.4	2.3	3.69	77/29	48.9	40.1	10.3	0.6	1.22	56/22
	75	64.3	20.2	12.2	3.4	3.18		51.1	36.9	10.8	1.3	1.38	
30	15	65.7	20.9	11.4	2.0	3.14	64/16	45.7	43.9	8.7	1.7	1.04	59/35
	75	61.6	21.8	11.6	5.0	2.83		49.0	38.7	8.7	3.6	1.27	
60	15	65.8	16.9	15.7	1.7	3.89	72/17	46.9	42.8	9.5	0.8	1.10	58/37
	75	65.1	18.5	13.7	2.8	3.52		50.2	38.6	9.8	1.5	1.30	
120	15	64.2	18.0	16.0	1.7	3.57	73/19	46.4	43.5	9.8	0.3	1.07	60/39
	75	61.0	21.0	13.0	5.0	2.90		49.9	39.3	9.7	1.1	1.27	

After Hydrolysis of PCTFE-OBuT (methanol:water, 50:50)								After Labelling with Heptafluorobutyryl Chloride					
Time min	$\Theta_T$	$\underline{C}$	$\underline{F}$	$\underline{O}$	$\underline{Cl}$	$\underline{C/F}$	H <sub>2</sub> O $\Theta_A/\Theta_R$	$\underline{C}$	$\underline{F}$	$\underline{O}$	$\underline{Cl}$	$\underline{C/F}$	HD $\Theta_A/\Theta_R$
0	15	71.9	12.3	15.0	0.8	5.85	89/54	70.7	14.3	13.5	1.5	4.94	10/0
	75	70.7	13.3	14.8	1.1	5.31		67.7	15.7	12.7	3.0	4.31	
15	15	67.4	17.7	13.1	1.9	3.81	80/29	48.9	40.9	9.0	1.3	1.20	54/23
	75	63.5	20.2	11.8	4.5	3.14		48.8	39.5	9.0	2.8	1.24	
30	15	65.2	19.4	14.3	1.1	3.36	72/19	48.5	41.1	9.5	0.9	1.18	57/25
	75	62.2	21.2	13.5	3.1	2.93		50.3	38.9	9.7	1.7	1.29	
60	15	63.2	21.7	13.3	1.8	2.91	64/19	48.3	40.9	10.1	0.8	1.18	58/31
	75	61.5	21.7	12.7	4.1	2.83		50.2	37.2	10.8	1.9	1.35	
120	15	62.9	18.6	16.1	2.4	3.38	68/20	47.8	41.4	10.1	0.6	1.15	59/31
	75	61.2	20.0	14.4	4.4	3.06		50.0	37.5	10.0	2.4	1.33	

After Hydrolysis of PCTFE-OBuT (methanol:water, 25:75)								After Labelling with Heptafluorobutyryl Chloride					
Time hr	$\Theta_T$	$\underline{C}$	$\underline{F}$	$\underline{O}$	$\underline{Cl}$	$\underline{C/F}$	H <sub>2</sub> O $\Theta_A/\Theta_R$	$\underline{C}$	$\underline{F}$	$\underline{O}$	$\underline{Cl}$	$\underline{C/F}$	HD $\Theta_A/\Theta_R$
0	15	71.9	12.3	15.0	0.8	5.85	89/54	70.7	14.3	13.5	1.5	4.94	10/0
	75	70.7	13.3	14.8	1.1	5.31		67.7	15.7	12.7	3.0	4.31	
0.25	15	71.2	13.4	14.7	0.8	5.31	82/39	53.4	31.9	13.9	0.8	1.67	43/10
	75	67.4	16.2	14.4	2.0	4.16		57.1	29.1	12.9	0.8	1.96	
0.5	15	70.7	14.4	13.8	1.1	4.91	81/33	54.4	34.3	10.7	0.6	1.59	49/16
	75	67.6	16.7	13.3	2.5	4.05		56.5	30.8	11.3	1.5	1.83	
1	15	68.3	16.8	13.3	1.6	4.07	80/27	51.6	37.6	10.2	0.6	1.37	52/15
	75	65.1	18.7	12.8	3.5	3.48		55.8	31.8	11.0	1.5	1.75	
2	15	67.5	18.0	12.5	2.0	3.75	76/26	51.0	36.8	11.4	0.8	1.39	54/17
	75	64.5	20.0	12.1	3.5	3.58		55.0	31.7	11.5	1.8	1.74	
5	15	67.3	18.3	13.2	1.3	3.68	73/25	48.4	41.3	9.6	0.7	1.17	57/27
	75	64.3	19.5	12.6	3.7	3.30		51.6	35.9	9.8	2.7	1.44	
10	15	66.2	19.7	13.4	0.7	3.36	70/17	46.7	42.5	10.3	0.7	1.10	60/35
	75	63.4	21.3	13.8	1.5	2.98		50.5	37.1	10.9	1.5	1.36	

After Hydrolysis of PCTFE-OBuT (methanol;water, 0:100)								After Labelling with Heptafluorobutyryl Chloride					
Time	H <sub>2</sub> O							HD					
hr	Q <sub>T</sub>	C	F	O	Cl	C/F	Q <sub>A</sub> /Q <sub>R</sub>	C	F	O	Cl	C/F	Q <sub>A</sub> /Q <sub>R</sub>
0	15	71.9	12.3	15.0	0.8	5.85	89/54	70.7	14.3	13.5	1.5	4.94	10/0
	75	70.7	13.3	14.8	1.1	5.31		67.7	15.7	12.7	3.0	4.31	
0.25	15	70.4	13.3	15.3	1.0	5.29	88/39	61.2	23.5	14.5	0.9	2.60	32/5
	75	70.0	13.9	14.7	1.5	5.04		65.2	18.4	15.2	1.2	3.54	
0.5	15	70.2	13.9	14.7	1.3	5.05	87/35	60.1	24.3	14.8	0.8	2.47	34/6
	75	70.1	13.7	15.0	1.3	5.12		66.1	17.8	14.9	1.2	3.71	
1	15	71.7	12.1	15.6	0.6	5.93	87/28	56.7	28.3	13.7	1.3	2.00	43/7
	75	70.1	13.9	14.9	1.1	5.04		62.8	21.4	14.2	1.6	2.93	
2	15	71.0	12.3	16.1	0.6	5.77	87/25	55.1	29.0	14.8	1.1	1.90	46/8
	75	70.7	13.1	15.4	0.8	5.40		62.2	20.9	15.1	1.8	2.98	
5	15	70.5	13.2	15.1	1.2	5.34	83/14	54.9	29.5	14.3	1.3	1.86	50/10
	75	69.4	14.1	15.0	1.5	4.92		61.0	22.7	14.6	1.7	2.68	
10	15	68.6	14.6	15.3	1.5	4.70	82/15	52.0	33.4	12.5	2.1	1.56	54/10
	75	68.3	15.3	14.0	2.4	4.46		57.8	26.1	12.9	3.2	2.21	
15	15	69.8	15.4	14.0	0.8	4.53	80/15	50.7	38.0	11.1	1.1	1.33	57/12
	75	67.2	17.2	13.9	1.7	3.90		56.8	29.6	11.7	2.6	1.92	
24	15	66.8	19.0	13.5	0.7	3.52	70/16	46.8	42.3	10.4	0.7	1.11	60/19
	75	63.3	21.5	13.7	1.5	2.94		51.5	36.1	10.9	1.5	1.44	

After Hydrolysis of PCTFE-ODec (methanol;water, 100:0)								After Labelling with Heptafluorobutyryl Chloride					
Time	H <sub>2</sub> O							HD					
min	Q <sub>T</sub>	C	F	O	Cl	C/F	Q <sub>A</sub> /Q <sub>R</sub>	C	F	O	Cl	C/F	Q <sub>A</sub> /Q <sub>R</sub>
0	15	84.1	5.6	10.0	0.3	15.0	106/57	82.1	8.4	9.3	0.2	9.77	10/0
	75	78.8	8.9	11.2	1.1	8.85		78.8	9.9	10.1	1.2	7.96	
30	15	84.3	6.0	9.3	0.4	14.0	107/32	64.9	24.4	10.4	0.3	2.66	47/5
	75	78.0	9.8	10.8	1.4	7.96		69.7	18.2	11.5	0.6	3.83	
45	15	73.5	15.3	9.6	1.6	4.80	93/27	52.3	39.2	7.7	0.9	1.33	51/8
	75	69.2	16.9	11.0	2.9	4.09		54.9	34.5	9.0	1.6	1.59	
60	15	70.9	17.2	10.4	1.5	4.12	88/25	49.8	39.9	9.5	0.8	1.25	55/10
	75	67.0	19.0	10.7	3.3	3.53		53.6	35.7	9.2	1.6	1.50	
90	15	62.6	22.8	11.7	2.8	2.75	77/19	45.0	45.3	8.7	1.1	0.99	61/39
	75	58.3	25.3	10.9	5.5	2.30		48.1	40.5	8.8	2.7	1.19	
120	15	63.3	23.1	11.4	2.2	2.74	73/20	44.9	45.2	8.5	1.4	0.99	60/40
	75	60.1	23.4	11.5	5.0	2.57		48.0	40.4	9.2	2.4	1.19	
150	15	62.0	23.3	12.0	2.7	2.66	69/17	43.5	46.5	9.0	1.0	0.94	60/41
	75	59.4	24.3	11.2	5.1	2.44		48.7	40.3	9.6	1.4	1.21	



After Hydrolysis of PCTFE-ODec (methanol:water, 75:25)								After Labelling with Heptafluorobutyryl Chloride					
Time	H <sub>2</sub> O							HD					
hr	Q <sub>T</sub>	C	F	O	Cl	C/F	Q <sub>A</sub> /Q <sub>R</sub>	C	F	O	Cl	C/F	Q <sub>A</sub> /Q <sub>R</sub>
0	15	84.1	5.6	10.0	0.3	15.0	106/57	82.1	8.4	9.3	0.2	9.77	10/0
	75	78.8	8.9	11.2	1.1	8.85		78.8	9.9	10.1	1.2	7.96	
0.5	15	84.4	5.1	10.2	0.4	16.5	108/47	73.4	15.0	11.3	0.4	4.89	32/4
	75	79.3	8.8	10.8	1.2	9.01		75.8	12.4	11.1	0.7	6.11	
1	15	84.6	5.4	9.5	0.5	15.7	108/34	63.9	24.5	10.8	0.8	2.61	39/5
	75	79.4	8.7	10.9	1.0	9.12		71.0	16.9	11.0	1.3	4.20	
2	15	85.0	5.3	9.4	0.3	16.0	108/17	55.0	33.2	11.5	0.3	1.66	61/5
	75	79.5	8.6	11.2	0.8	9.24		65.5	22.2	11.4	0.9	2.95	
5	15	76.6	12.5	9.1	1.8	6.13	103/17	51.1	38.5	9.7	0.7	1.33	59/7
	75	71.9	15.0	10.5	2.7	4.79		56.7	31.9	10.1	1.4	1.78	
10	15	70.8	17.3	9.4	2.4	4.09	94/17	47.3	42.3	9.6	0.8	1.12	60/20
	75	67.0	19.3	9.9	3.8	3.47		52.2	35.9	9.6	2.2	1.45	
15	15	68.6	19.5	9.2	2.7	3.52	70/16	43.9	46.3	8.9	0.9	0.95	60/39
	75	66.0	20.9	8.9	4.2	3.16		47.5	42.0	8.4	2.1	1.13	
24	15	52.2	31.7	8.7	7.5	1.65	68/12	42.2	46.2	8.9	2.7	0.91	60/39
	75	52.0	31.4	8.4	8.3	1.66		46.1	41.1	8.6	4.2	1.12	

After Hydrolysis of PCTFE-ODec (methanol:water, 50:50)								After Labelling with Heptafluorobutyryl Chloride					
Time	H <sub>2</sub> O							HD					
hr	Q <sub>T</sub>	C	F	O	Cl	C/F	Q <sub>A</sub> /Q <sub>R</sub>	C	F	O	Cl	C/F	Q <sub>A</sub> /Q <sub>R</sub>
0	15	84.1	5.6	10.0	0.3	15.0	106/57	82.1	8.4	9.3	0.2	9.77	10/0
	75	78.8	8.9	11.2	1.1	8.85		78.8	9.9	10.1	1.2	7.96	
0.5	15	84.2	5.1	10.1	0.6	16.5	109/51	79.9	10.5	9.0	0.6	7.61	17/4
	75	78.8	9.3	10.7	1.2	8.47		77.0	11.2	10.5	1.3	6.88	
1	15	84.6	6.1	9.1	0.3	13.9	108/45	75.4	14.8	9.2	0.6	5.09	23/3
	75	78.9	9.6	10.3	1.2	8.21		74.4	13.8	10.3	1.5	5.39	
2	15	85.0	5.5	9.2	0.4	15.5	108/29	69.4	21.1	9.1	0.4	3.29	45/4
	75	78.3	9.6	10.5	1.6	8.16		74.1	14.5	11.0	0.5	5.11	
5	15	84.0	7.4	8.0	0.7	11.4	108/24	60.7	27.9	11.0	0.4	2.18	49/6
	75	78.1	10.4	10.4	1.2	7.51		68.0	20.3	10.8	0.9	3.35	
10	15	82.3	8.3	8.5	0.9	9.92	107/16	57.5	30.8	10.8	0.9	1.87	60/7
	75	75.9	11.8	10.5	1.7	6.43		62.4	25.1	10.1	2.4	2.49	
24	15	80.2	9.4	9.3	1.2	8.53	99/16	51.6	36.4	10.5	1.3	1.42	61/10
	75	74.2	13.0	10.7	2.2	5.71		59.2	28.6	10.1	2.3	2.07	
30	15	78.2	11.3	9.2	1.4	6.92	96/17	50.4	38.2	10.0	1.4	1.32	60/17
	75	72.9	13.8	10.8	2.5	5.28		54.0	33.1	9.9	3.0	1.63	
36	15	76.4	12.4	9.2	2.0	6.16	94/14	48.1	40.8	10.2	0.9	1.18	60/25
	75	69.7	16.8	10.0	3.5	4.15		53.6	34.4	10.3	1.7	1.56	
42	15	74.6	14.8	9.1	1.5	5.04	89/15	47.5	41.8	9.3	1.4	1.14	59/32
	75	68.2	19.3	10.4	2.1	3.53		49.8	37.9	10.0	2.3	1.31	
50	15	63.0	22.4	10.7	4.3	2.81	68/15	45.7	43.4	10.1	0.8	1.05	60/40
	75	57.5	25.7	8.9	7.9	2.24		47.1	41.1	10.2	1.6	1.15	

After Hydrolysis of PCTFE-OSear (methanol:water, 100:0)								After Labelling with Heptafluorobutyryl Chloride					
Time	H <sub>2</sub> O							HD					
hr	Q <sub>T</sub>	C	F	O	Cl	C/F	Q <sub>A</sub> /Q <sub>R</sub>	C	F	O	Cl	C/F	Q <sub>A</sub> /Q <sub>R</sub>
0	15	92.8	2.7	3.9	0.5	34.4	108/90	90.9	4.4	4.2	0.6	20.7	40/35
	75	85.3	6.4	7.6	0.8	13.3		85.1	7.2	7.0	0.8	11.8	
0.5	15	90.0	4.9	4.4	0.6	18.4	107/87	81.9	11.3	6.2	0.6	7.25	20/3
	75	83.4	7.9	7.5	1.2	10.6		81.2	10.5	7.8	0.6	7.73	
1	15	88.0	5.8	5.4	0.8	15.2	103/57	68.5	23.3	7.0	1.2	2.94	41/8
	75	82.5	8.6	7.7	1.3	9.59		72.9	17.9	8.0	1.2	4.07	
1.5	15	77.3	13.0	8.3	1.5	5.95	99/28	49.5	42.3	7.6	0.7	1.17	56/10
	75	72.0	15.7	10.0	2.4	4.59		52.4	37.1	8.6	1.9	1.41	
2	15	73.3	15.7	9.5	1.5	4.67	86/24	45.9	44.0	9.0	1.0	1.04	60/18
	75	66.1	18.5	11.0	4.5	3.57		49.9	38.9	9.6	1.5	1.28	
2.5	15	60.3	25.0	11.2	3.5	2.41	69/18	45.8	44.5	9.0	0.7	1.03	60/37
	75	59.2	24.9	10.7	5.3	2.38		49.6	39.2	9.5	1.7	1.27	
3	15	62.4	23.4	11.6	2.7	2.67	70/16	45.0	45.3	8.5	1.1	0.99	61/41
	75	60.2	24.0	10.9	5.0	2.51		48.6	40.1	9.4	2.0	1.21	

After Hydrolysis of PCTFE-OSear (methanol:water, 75:25)								After Labelling with Heptafluorobutyryl Chloride					
Time	H <sub>2</sub> O							HD					
hr	Q <sub>T</sub>	C	F	O	Cl	C/F	Q <sub>A</sub> /Q <sub>R</sub>	C	F	O	Cl	C/F	Q <sub>A</sub> /Q <sub>R</sub>
0	15	92.8	2.7	3.9	0.5	34.4	108/90	90.9	4.4	4.2	0.6	20.7	40/35
	75	85.3	6.4	7.6	0.8	13.3		85.1	7.2	7.0	0.8	11.8	
0.5	15	91.8	3.4	4.2	0.6	27.0	108/89	81.3	11.3	6.9	0.5	7.19	21/3
	75	85.6	6.4	7.1	0.9	13.4		82.5	9.6	7.4	0.5	8.59	
1	15	91.0	4.4	3.8	0.8	20.7	108/73	72.5	18.1	8.8	0.7	4.01	27/3
	75	85.2	6.9	7.0	0.9	12.3		78.8	12.5	7.8	0.9	6.30	
2	15	91.6	4.2	3.6	0.6	21.8	108/61	69.2	21.4	8.7	0.7	3.23	40/5
	75	84.5	7.2	7.4	0.9	11.7		76.1	15.4	7.9	0.6	4.94	
6	15	82.5	9.6	7.0	0.9	8.59	101/33	59.5	31.2	8.7	0.6	1.90	50/5
	75	80.0	9.7	9.5	0.8	8.25		62.9	26.5	9.5	1.1	2.37	
12	15	80.6	11.1	7.3	1.0	7.26	98/20	53.1	36.2	9.9	0.9	1.47	60/7
	75	79.3	11.2	8.4	1.1	7.08		58.0	31.4	9.6	1.1	1.84	
18	15	60.5	26.6	11.1	1.8	2.27	70/15	46.8	42.1	9.7	1.5	1.11	60/31
	75	63.0	21.1	12.2	3.6	2.99		49.2	39.3	10.2	1.3	1.25	
24	15	58.3	28.3	11.0	2.4	2.06	67/16	43.6	45.1	9.8	1.5	0.97	59/40
	75	57.3	27.7	10.8	4.2	2.07		47.8	39.8	10.1	2.3	1.20	

After Hydrolysis of PCTFE-OSear (methanol:water, 50:50)								After Labelling with Heptafluorobutyryl Chloride					
Time	H <sub>2</sub> O							HD					
hr	Q <sub>T</sub>	C	F	O	Cl	C/F	Q <sub>A</sub> /Q <sub>R</sub>	C	F	O	Cl	C/F	Q <sub>A</sub> /Q <sub>R</sub>
0	15	92.8	2.7	3.9	0.5	34.4	108/90	90.9	4.4	4.2	0.6	20.7	40/35
	75	85.3	6.4	7.6	0.8	13.3		85.1	7.2	7.0	0.8	11.8	
0.5	15	92.1	3.6	3.8	0.5	25.6	109/90	84.6	8.3	6.4	0.7	10.2	39/29
	75	86.0	6.6	6.7	0.7	13.0		82.5	9.4	7.5	0.7	8.78	
1	15	91.0	3.7	4.6	0.7	24.6	108/77	76.8	15.2	7.1	0.9	5.05	25/5
	75	84.4	7.6	7.0	1.1	11.1		79.5	12.4	7.4	0.7	6.41	
2	15	91.5	4.2	3.7	0.6	21.8	108/69	73.9	19.6	6.0	0.4	3.77	27/5
	75	85.8	6.6	7.1	0.6	13.0		78.7	12.8	8.3	0.3	6.15	

## BIBLIOGRAPHY

- Aclar Technical Data, Allied-Signal Chemical Corp. Morristown, New Jersey.
- Adams, N. *J. Appl. Polymer Sci.*, **1963**, *7*, 2075.
- Amontons, G. *Memoires de l'Academie Royale*, **1699**, 206.
- Amouroux, J.; Goldman, M. and Revoil, M.F. *J. Polym. Sci.: Polym. Chem. Ed.*, **1982**, *20*, 1373.
- Amuzu, J.K.A.; Briscoe, B.J. and Tabor, D. *Preprint No. 76-AM-IA-3*, 31st Annual Meeting A.S.L.E., 1976.
- Andrade, J.D.; King, R.N.; Gregonis, D.E. and Coleman, J. *Poly. Sci. Symp*, **1979**, *66*, 313.
- Andrade, J.D., Ed. *Surface and Intefacial Aspects of Biomedical Polymers, vol. 1: Surface Chemistry and Physics*; Plenum: New York, 1985.
- Annual Book of ASTM Standards, **1986**, 8.02, D1894-78, 177.
- Ashley, J.C. *IEEE Trans. Nucl. Sci.*, **1980**, *NS-27*, 1454.
- Baily, A.I. and Courtney-Pratt, J.S. *Proc. Roy. Soc. Lond. A*, **1955**, *227*, 500.
- Bain, C.D. and Whitesides, G.M. *J. Am. Chem. Soc.*, **1988**, *110*, 3665.
- Bain, C.D. and Whitesides, G.M. *J. Am. Chem. Soc.*, **1988**, *110*, 5897.
- Bain, C.D. and Whitesides, G.M. *J. Am. Chem. Soc.*, **1988**, *110*, 6560.
- Bain, C.D. and Whitesides, G.M. *Langmuir*, **1989**, *5*, 1370.
- Banks, R.E. *Fluorocarbons and Their Derivatives*, Oldbourne Press: London, 1964.



- Barker, D.J.; Brewis, D.M. and Dahm, R.H. *J. Materials. Sci.*, **1979**, *14*, 749.
- Bartell, F.E. and Shepard, J.W. *J. Phys. Chem.*, **1953**, *57*, 458.
- Bartenev, G.M. and Elkin, A.I. *J. Polym. Sci. C*, **1967**, *16*, 1673.
- Baszkin, A. and Ter-Minassian-Saraga, L. *J. Polym. Sci.: Part C*, **1971**, 243.
- Bee, T.G. and McCarthy, T.J. *Macromolecules*, **1992**, *25*, 2093.
- Bening, R.C. and McCarthy, T.J. *Macromolecules* **1990**, *23*, 2648.
- Bensnoin, J.-M. and Choi, K.Y. *J. Macromol Sci.-Rev. Macromol. Chem and Phys.*, **1989**, *C29(1)*, 55.
- Bikerman, J.J. *J. Macromol. Sci.-Revs. Macromol. Chem.*, **1974**, *C11*, 1.
- Bowden, F.P. and Tabor, D. "The Friction and Lubrication of Solids", Oxford, 1964.
- Brennan, J.V. and McCarthy, T.J. *Polym. Prepr. (Am. Chem. Soc., Div. Polym. Chem.)* **1987**, *29(2)*, 338.
- Brennan, J.V. and McCarthy, T.J. *Polym. Prepr. (Am. Chem. Soc., Div. Polym. Chem.)* **1989**, *30(2)*, 152.
- Briggs, D.; Brewis, D.M. and Konieczko, M.B. *J. Mat. Sci.*, **1979**, *14*, 1344.
- Briggs, D.; Rance, D.G. and Briscoe, B.J. In "Comprehensive Polymer Science, vol. 2", Pergamon Press: New York, 1989.
- Briscoe, B.J.; Scruton, B. and Willis, F.R. *Proc. Roy. Soc. Lond. A*, **1973**, 333, 99.
- Briscoe, B.J. and Tabor, D. *A.S.L.E. Trans.*, **1974**, *17*, 158.
- Briscoe, B.J. and Tabor, D. In "Polymer Surfaces", Wiley-Interscience: New York, 1978, 1.
- Briscoe, B.J. and Tabor, D. *Br. Polymer J.*, **1978**, *10(1)*, 74.

- Briscoe, B.J. *Adhesion*, 1981, 5, 49.
- Briscoe, B.J. *Philosophical Magazine A*, 1981, 43, 511.
- Briscoe, B.J. and Evans, D.C.B. *Proc. Roy. Soc. Lond. A*, 1982, 380, 389.
- Briscoe, B.J. In "Physiochemical Aspects of Polymer Surfaces, vol. 1", Plenum: New York, 1983.
- Cadman, P., Gossedge, G. and Scott, J.D. *J. Electron Spectr.*, 1978, 13, 1.
- Cassie, A.B.D. and Baxter, S. *Trans. Faraday Soc.*, 1944, 40, 546.
- Cassie, A.B.D. *Disc. Faraday Soc.*, 1948, 3, 11.
- Casy, G.; Furber, M.; Richardson, K.A.; Stephenson, G.R.; Taylor, R.J.K. *Tetrahedron*, 1986, 21, 5849.
- Cherry, B.W. *Polymer Surfaces*, Cambridge University Press: Cambridge, Great Britain, 1981.
- Chung, T.C.; Raate, M.; Berluche, E. and Schulz D.N. *Macromolecules* 1988, 21, 1903.
- Clark, D.T. and Feast, W.J., *J. Macromol. Sci.-Revs. Macromon. Chem.*, 1975, 12, 191.
- Clark, D.T. and Thomas, H.R. *J. Polym. Sci., Chem.*, 1977, 15, 2843.
- Clark, D.T. and Feast, W.J. *Polymer Surfaces*, Wiley-Interscience: New York, 1978.
- Clark, D.T., Thomas, H.R. and Shuttleworth, D. *J. Polym. Sci., Polym. Lett.*, 1978, 16, 465.
- Clark, D.T., Fok, Y.C.T. and Roberts *J. Electron Spectr.*, 1981, 22, 173.
- Clark, D.T. and Wilson, R. *J. Polym. Sci.: Polym. Chem. Ed.*, 1983, 21, 837.
- Clark, M.B., Jr.; Burkhardt, C.A. and Gardella, J.A., Jr. *Macromolecules*, 1989, 22, 4495.

- Collins, G.C.S.; Lowe, A.C. and Nicholas, D. *Eur. Polym. J.*, **1973**, *9*, 1173.
- Costello, C.A. and McCarthy, T.J. *Macromolecules*, **1987**, *20*, 2819.
- Coulomb, C.A. *Theories des Machines Simples*, 1785 (Memoire de Mathematique et de Physique de l'Academie Royale, Paris).
- Cross, E.M. and McCarthy, T.J. *Macromolecules*, **1990**, *23*, 3916
- Danielson, N.D.; Taylor, R.T.; Huth, J.A.; Siergiej, R.W.; Galloway, J.G. and Paperman, J.B. *Ind. Eng. Chem. Prod. Res. Dev.*, **1983**, *22*, 303.
- DePalma, V. and Tillman, N. *Langmuir*, **1989**, *5*, 868.
- Dias, A.J. and McCarthy, T.J. *Macromolecules* **1985**, *18*, 1826.
- Dias, A.J. and McCarthy, T.J. *Macromolecules* **1987**, *20*, 2068.
- Dias, A.J. Ph.D. dissertation, University of Massachusetts, 1987.
- Dwight, D.W. and Riggs, W.M. *J. Colloid Interface Sci.*, **1974**, *47*, 650.
- Dyson, J. and Hirst, W. *Proc. Roy. Soc. Lond. B*, **1954**, *67*, 309.
- Erhard, G. *Wear*, **1983**, *84*, 167.
- Evers, O.A.; Scheutjens, J.M.H.M. and Fleer, G.J. *J. Chem. Soc. Faraday Trans.* **1990**, *86(9)*, 1333.
- Fleming, R.J. and McCarthy, T.J. results to be published.
- Fowkes, F.M.. Ed. *Contact Angle, Wettability and Adhesion*, Advances in Chemistry Series, No. 43, American Chemical Society: Washington, D.C. 1964.
- Fowkes, F.M. *Ind. Eng. Chem.*, **1964**, *56*, 40.
- Franchina, N.L. and McCarthy, T.J. *Macromolecules*, **1991**, *24*, 3045.
- Gibbs, J.W. *The Collected Works of J. Willard Gibbs, Volume 1, Thermodynamics*, Yale University Press: New Haven, 1928.



- Girifalco, L.A. and Good, R.J. *J. Phys. Chem.*, **1957**, *61*, 904.
- Greenwood, J.A. and Tabor, D. *Proc. Phys. Soc.*, **1958**, 989.
- Greenwood, J.A.; Minshall, H. and Tabor, D. *Proc. Roy. Soc. Lond. A*, **1958**, *245*, 539.
- Grosch, K.A. *Nature*, **1963**, *197*, 858.
- Grosch, K.A. *Proc. Roy. Soc. Lond. A*, **1963**, *274*, 21.
- Guzonas, D.A.; Boils, D.; Tripp, C.P. and Hair, M.L. *Macromolecules* **1992**, *25*, 2434.
- Hall, S.M., Andrade, J.D., Ma, S.M. and King, R.N. *J. Electron Spectr.*, **1979**, *17*, 181.
- Hare, E.F.; Shafrin, E.G. and Zisman, W.A. *J. Phys. Chem.* **1954**, *58*, 236.
- Harrick, N.J. *Internal Reflection Spectroscopy*, Wiley Interscience: New York, **1967**.
- Holly, F.J. and Refojo, M.F. *J. Biomed. Materials Res.*, **1975**, *9*, 315.
- Holmes-Farley, S.R.; Reamey, R.H.; McCarthy, T.J.; Deutch, J. and Whitesides, G.M. *Langmuir*, **1985**, *1*, 725.
- Holmes-Farley, S.R. and Whitesides, G.M. *Langmuir*, **1987**, *3*, 62.
- Holmes-Farley, S.R.; Nuzzo, R.G.; McCarthy, T.J. and Whitesides, G.M. *Langmuir*, **1987**, *3*, 799.
- Holmes-Farley, S.R.; Bain, C.D. and Whitesides, G.M. *Langmuir*, **1988**, *4*, 921.
- Israelachvili, J.N. and Gee, M.L. *Langmuir*, **1989**, *5*, 288.
- Johnson, R.E., Jr. and Dettre, R.H. *J. Phys. Chem.*, **1964**, *68*, 1744.
- Johnson, R.E., Jr. and Dettre, R. H. In *Surface and Colloid Science*, Vol 2, Matijevic, E., Ed., Wiley-Interscience: New York, 1969.

- Juaristi, E.; Martinez-Richa, A.; Garcia-Rivera, A. and Cruz-Sanchez, J.S. *J. Org. Chem.* **1983**, *43*, 2603.
- Kendall, E.W. and McCarthy, T.J. results to be published.
- Kendall, K. and Tabor, D. *Proc. Roy. Soc. Lond. A*, **1971**, *323*, 321.
- King, R.F. and Tabor, D. *Proc. Roy. Soc. Lond. B*, **1953**, *66*, 728.
- Kolb, B.U.; Patton, P.A.. and McCarthy, T.J. *Macromolecules*, **1990**, *23*, 366.
- Kolthoff, I.M.; Sandel, E.B.; Meehan, E.J.; Bruckenstein, S. *Quantitative Chemical Analysis*, 4th ed.; MacMillan: Toronto, 1969.
- Kraghelsky, I.V. and Sabelnikov, V.P. *Proc. Inst. Mech. Engrs. Conference on Lubrication and Wear*, **1957**, 247.
- Laibinis, P.E.; Fox, M.A.; Folkers, J.P. and Whitesides, G.M. *Langmuir*, **1991**, *7*, 3167.
- Laibinis, P.E.; Bain, C.D. and Whitesides, G.M. *J. Phys. Chem.*, **1991**, *95*, 7017.
- Laibinis, P.E.; Whitesides, G.M.; Allara, D.L.; Tao, Y.-T.; Parikh A.N. and Nuzzo, R.G. *J. Am. Chem. Soc.*, **1991**, *113*, 7152
- Lancaster, J.K. In "Polymer Science, vol. 2", Elsevier: New York, 1972.
- Lancaster, J.K. *Plastics and Polymers*, **1973**, *41*, 297.
- Langmuir, I. *J. Am. Chem. Soc.* **1916**, *38*, 2221.
- Langmuir, I. *Science*, **1938**, *87*, 493.
- Lee, K.-W. and McCarthy, T.J. *Macromolecules* **1988**, *21*, 3353.
- Lee, L.H. "Advances in Polymer Friction and Wear"; Polymer Science and Technology, vols. 5A and 5B, 1974.
- Levine, O. and Zisman, Z.A. *J. Phys. Chem.*, **1957**, *61*, 1068.

- Lincoln, B. *Br. J. Appl. Phys.*, **1952**, *3*, 260.
- Ludema, K.C. and Tabor, D. *Wear*, **1966**, *9*, 329.
- March, J. "Advanced Organic Chemistry", Wiley-Interscience: New York, 1985, pp. 329 - 331 and references therein.
- McClaren, K.G. and Tabor, D. *Nature*, **1963**, *197*, 856.
- Miller, D.R. and Nikolaos, A.P. *J. Macromol Sci.-Rev. Macromol. Chem and Phys.*, **1986**, *C26(1)*, 33.
- Mirabella, F.M. Jr. *Applied Spectroscopy Reviews*, **1985**, *21(1&2)*, 45.
- Mora, M.; Occhiello, E. and Garbassi, F. *Langmuir*, **1989**, *5*, 872.
- Muller, G., Abraham, K. and Schaldach, M. *Applied Optics*, **1981**, *20(7)*, 1182.
- Neumann, A.W. and Good, R.J. *J. Colloid Interface Sci.*, **1972**, *38*, 341.
- Nudel'man, Z.N., Alyabina, E.A., Prokudin, I.P., Rybalov, S.L., Tarkhava, T.P., *Kauch. Rezina*, **1969**, *28(3)*, 21.
- O'Malley, J.J.; Thomas, H.R. and Lee, G.M., *Macromolecules*, **1979**, *12*, 996.
- Oster, G. and Shibata, O. *J. Polym. Sci.*, **1957**, *26*, 233.
- Overney, R.M.; Meyer, E.; Frommer, J.; Brodbeck, D.; Luthi, R.; Howald, L.; Guntherodt, H.-J.; Fujihira, M.; Takano, H. and Gotoh, Y. *Nature*, **1992**, *359*, 133.
- Owens, D.K. and Wendt, R.C. *J. Appl. Poly. Sci.*, **1969**, *13*, 1741.
- Parsonage, E.; Tirrell, M.; Watanabe, H. and Nuzzo, R.G. *Macromolecules* **1991**, *24*, 1987.
- Pease, D.C. *J. Phys. Chem.*, **1945**, *49*, 107.
- Pooley, C.M. and Tabor, D. *Proc Roy. Soc. Lond. A.*, **1972**, *329*, 251.



- Rasmussen, J.R.; Stedronsky, E.R. and Whitesides, G.M. *J. Am. Chem. Soc.* **1977**, *99*, 4736.
- Riggs, W. and Dwight, D.J. *J. Electron Spectr.*, **1974**, *5*, 447.
- Rossmann, K. *J. Polym. Sci.*, **1956**, *19*, 141.
- Savdoor, A.R. In "*Advances in Polymer Friction and Wear*"; *Polymer Science and Technology*, vol. 5A, 1974, 69.
- Schmidt, J.J.; Gardella, J.A., Jr. and Salvati, L., Jr. *Macromolecules*, **1989**, *22*, 4489.
- Shoichet, M.S. and McCarthy, T.J. *Macromolecules* **1991**, *24*, 982.
- Shooter, K.V. and Tabor, D. *Proc. Phys Soc.*, **1952**, *B65*, 661.
- Silverstein, R.M.; Bassler G.C. and Morrill, T.C. *Spectrometric Identification of Organic Compounds*, John Wiley and Sons: New York, 1981, p. 107.
- Snyder, R.G.; Hsu, S.L. and Krimm, S. *Spectrochim. Acta, Part A*, **1978**, *34*, 395.
- Sung, N.H.; Lee, H.Y.; Yuan, P. and Sung, C.S.P. *Polymer Engineering and Science*, **1989**, *29*, 791.
- Tabor, D. *Nature*, **1963**, *197*, 856.
- Tabor, D. *Surface and Colloid Science*, **1972**, *5*, 245.
- Tabor, D. In "*Advances in Polymer Friction and Wear*"; *Polymer Science and Technology*, vol. 5A, 1974, 5.
- Tabor, D. In "*Advances in Polymer Friction and Wear*"; *Polymer Science and Technology*, vol. 5A, 1974, 149.
- Tewari, U.S. and Sharma, S.K. *J. Macromol. Sci.-Revs. Macromol. Chem.*, **1989**, *C29*, 1.
- Thomas, H.R. and O'Malley, J.J., *Macromolecules*, **1979**, *12*, 323.
- Timmons, C.O. and Zisman, W.A. *J. Colloid Interface Sci.*, **1966**, 165.

- Troughton, E.B., Bain, C.D., Whitesides, G.M., Nuzzo, R.G., Allara, D.L. and Porter, M.D. *Langmuir*, 1988, 4, 365.
- van Oss, D.J.; Good, R.J. and Chaudhury, M.K. *Langmuir*, 1988, 4, 884.
- Ward, W.J. and McCarthy, T.J. In *Encyclopedia of Polymer Science and Engineering*, 2nd ed.; Supplement, Wiley: New York, 1989, pp.674 - 689.
- Wenzel, R.N. *Ind. Eng. Chem.*, 1936, 28, 988.
- Wu, S. *J. Adhesion*, 1973, 5, 39.
- Yamaguchi, Y. "Tribology of Plastic Materials", Elsevier: New York, 1990.
- Yamamoto, F. and Yamakawa, S. *J. Polym. Sci.: Polym. Phys. Ed.*, 1979, 17, 1581.
- Young, T. (a) *Phil. Trans.*, 1805, 95, 65 and (b) *Phil. Trans.*, 1805, 95, 82.





